



**UNIVERSITY OF
BIRMINGHAM**

**EFFECT OF FLOOR-TO-FLOOR JOINT DESIGN ON THE
ROBUSTNESS OF PRECAST CONCRETE CROSS WALL BUILDINGS**

by

MOSLEH TOHIDI

A Thesis Submitted to
The University of Birmingham
For the Degree of
DOCTOR OF PHILOSOPHY

College of Engineering and Physical Sciences
School of Civil Engineering
The University of Birmingham
August 2015

UNIVERSITY OF
BIRMINGHAM

University of Birmingham Research Archive

e-theses repository

This unpublished thesis/dissertation is copyright of the author and/or third parties. The intellectual property rights of the author or third parties in respect of this work are as defined by The Copyright Designs and Patents Act 1988 or as modified by any successor legislation.

Any use made of information contained in this thesis/dissertation must be in accordance with that legislation and must be properly acknowledged. Further distribution or reproduction in any format is prohibited without the permission of the copyright holder.

ABSTRACT

Progressive collapse of building structures typically occurs when an abnormal loading condition causes a sudden loss in the structural capacity of one or more critical members, which leads to a chain reaction of failure and ultimately a catastrophic collapse. It is well accepted that in order to prevent the progressive collapse of beams or slabs, the establishment of catenary action mechanism is crucial to attain adequate post-collapse resistance. Experimental, numerical and analytical studies have been conducted to investigate the catenary behaviour of the precast concrete slab system following the removal of their intermediate wall supports. Results indicated that specimens experiencing bar fracture failure patterns collapsed prior to the formation of the catenary action, but those specimens with the pull-out failure pattern showed clear evidence of catenary behaviour. Results also reveal that for the ties designed with inadequate embedment length, the slip and the resulting large deflection will effectively trigger the catenary action. However, the full bond will limit the development of deflection and lead to the fracture of tie bars before the catenary action is triggered. An improved TF model using numerical analyses was proposed to design the floor-to-floor joint against the progressive collapse in precast cross wall structures, which shown a close agreement with the DoD 2013 regulations.

ACKNOWLEDGMENTS

It is difficult to overstate my especial thanks to my supervisor Professor Jian Yang, for his expertise, supports and attention to the details. Also, I would like to thank my co-supervisor Professor C. Baniotopoulos for his guidance during the half of the present study.

I would like to express my gratitude to Bison Manufacturing Ltd. for their generous support by sponsoring test samples in this project. Also, I am grateful for the funding from Shanghai Pujiang Program, P.R. China (13PJ1405200).

Lastly I wish to thank my wife Dr. Aisheh and my cute daughter Karin. They supported me, and loved me; especially to my wife which she left her professional works to support me to dedicate this thesis.

Thanks are due to Mrs Janet, for her enlightened help with my academic writing as proof-reader.

TABLE OF CONTENTS

Abstract	II
Acknowledgments.....	III
Table of contents.....	IV
List of tables	X
List of figures	XI
List of symbols and abbreviations.....	XX

CHAPTER 1 - INTRODUCTION	1-1
---------------------------------------	------------

1.1	BACKGROUND	1-1
1.2	AIMS AND OBJECTIVES	1-8
1.3	RESEARCH METHODOLOGY	1-10
1.3.1	Experimental work	1-10
1.3.2	Numerical analyses	1-11
1.3.3	Analytical prediction	1-11

CHAPTER 2 - LITERATURE REVIEW	2-1
--	------------

2.1	INTRODUCTION	2-1
2.2	CROSS WALL STRUCTURES	2-1
2.3	PROGRESSIVE COLLAPSE.....	2-4
2.3.1	Definition	2-4
2.3.2	Robustness.....	2-6
2.3.3	Alternate Load Paths	2-12
2.4	CURRENT PROVISIONS FOR STRUCTURAL ROBUSTNESS.....	2-16
2.4.1	British Standard.....	2-16
2.4.2	Eurocodes Approach	2-18
2.4.3	American Society of Civil Engineering (ASCE 7-05)	2-21

2.4.4	General Services Administration (GSA) Progressive Collapse Guidelines 2003...	2-21
2.4.5	American Department of Defence (2013)	2-22
2.4.6	Summary	2-26
2.5	EFFICIENCY OF CURRENT TIE FORCE (TF) METHOD	2-27
2.5.1	Tie Force (TF) Analysis	2-30
2.6	EXPERIMENTAL STUDIES ON PROGRESSIVE COLLAPSE	2-31
2.7	NUMERICAL STUDY ON PROGRESSIVE COLLAPSE	2-46
2.8	PULLOUT BEHAVIOUR OF SINGLE BAR IN CONCRETE	2-55
2.8.1	Modes of Bond Failure.....	2-59
2.8.2	Different Factors Affecting Bond Performance	2-59
2.9	PULLOUT MODELS	2-60
2.10	EXISTING FE MODELS OF REINFORCED CONCRETE.....	2-67
2.10.1	Modelling Techniques for the Bond-slip Behaviour.....	2-69
2.10.2	Specific Finite Elements Model	2-71
2.10.3	Structural Model.....	2-72
2.10.4	Pull-out model	2-74
2.11	THE EFFECT OF LATERAL SUPPORT ON THE PROGRESSIVE RESISTANCE	2-77
2.11.1	Membrane actions	2-77
2.11.2	Compressive membrane actions.....	2-79
2.12	OVERALL SUMMARY	2-87

CHAPTER 3 - EXPERIMENTAL STUDIES3-1

3.1	INTRODUCTION	3-1
3.2	MATERIAL PROPERTIES.....	3-2
3.2.1	Reinforcing Steel.....	3-2
3.2.2	Concrete	3-3
3.2.3	Precast Concrete Floor Slabs.....	3-5
3.3	PULLOUT TEST	3-6
3.3.1	Geometry and properties of test specimens.....	3-6

3.3.2	Pullout test results and evaluation	3-10
3.4	FULL SCALE FLOOR-TO-FLOOR EXPERIMENTS	3-25
3.4.1	Geometry and properties of test specimens	3-26
3.4.2	Test setup and instrumentation	3-31
3.4.3	Validation of the present loading method resembling the sudden removal of support wall	3-33
3.4.4	Instrumentation	3-34
3.4.5	Test results	3-36
3.4.6	Summary	3-55
3.5	OVERALL SUMMARY	3-56
 CHAPTER 4 - FINITE ELEMENT MODELLING		4-1
4.1	INTRODUCTION	4-1
4.2	PROPERTIES OF REFERENCE TEST SPECIMENS	4-3
4.2.1	Pullout Test Specimens	4-3
4.2.2	Full Scale Floor Joint Test Specimens	4-4
4.3	FINITE ELEMENT MODELS	4-5
4.3.1	Bond model	4-6
4.3.2	Embedded Element	4-6
4.3.3	Friction	4-6
4.3.4	Spring Element	4-7
4.3.5	Translator	4-8
4.4	MODELLING OF BAR-CONCRETE INTERFACE	4-10
4.5	MESH DESCRIPTION	4-11
4.6	BOUNDARY CONDITIONS	4-15
4.7	MATERIAL PROPERTIES	4-18
4.7.1	Concrete and Steel	4-18
4.7.2	Concrete Damage Plasticity (CDP)	4-18
4.7.3	Plotting Stress- Inelastic Strain Curve	4-19
4.7.4	Damage Parameters of d_t and d_c	4-21
4.7.5	Translator Property	4-27

4.8	ANALYSIS SOLUTION STRATEGY	4-28
4.9	VERIFICATION OF MODELS	4-29
4.9.1	Performance of Pullout Models.....	4-29
4.9.2	Performance of Floor-to-Floor Model.....	4-33
4.9.3	Performance of RC Beam Model.....	4-45
4.10	SUMMARY	4-46

CHAPTER 5 - NUMERICAL PARAMETRIC STUDY5-1

5.1	INTRODUCTION	5-1
5.2	DESCRIPTION OF THE SELECTED STRUCTURE	5-2
5.2.1	Floor-to-floor joint analysis using longitudinal ties.....	5-3
5.2.2	Floor-to-floor system using longitudinal and transverse ties	5-3
5.3	FINITE ELEMENT MODELING TECHNIQUE.....	5-5
5.3.1	Boundary condition	5-5
5.3.2	Material properties	5-7
5.3.3	Translator properties	5-9
5.3.4	Analysis solution strategy	5-10
5.4	WALL SUPPORT REMOVAL ANALYSIS.....	5-10
5.4.1	Floor-to-floor system using longitudinal ties	5-10
5.4.2	Floor-to-floor joint analysis using longitudinal and transverse ties.....	5-15
5.5	SUMMARY	5-41

CHAPTER 6 - GENERAL ANALYSIS AND DESIGN GUIDELINE6-1

6.1	INTRODUCTION	6-1
6.2	DESIGNS FOR PROGRESSIVE COLLAPSE	6-1
6.2.1	Overall Structural Concept.....	6-2
6.2.2	Detailed Provisions	6-2
6.3	IMPROVED TF METHOD	6-3
6.3.1	Bar Fracture Failure Mode	6-4
6.3.2	Pullout Failure Mode.....	6-7
6.4	ALTERNATE LOAD PATH METHOD (ALP)	6-8

CHAPTER 7 - APPROXIMATE ANALYTICAL APPROACH	7-1
7.1 INTRODUCTION	7-1
7.2 MODELLING OF FLOOR-TO-FLOOR SYSTEM UNDER CATENARY ACTION	7-2
7.3 ULTIMATE DEFORMATION FOR CATENARY ACTION FOR THE TF METHOD	7-5
7.4 PULLOUT LOAD-DISPLACEMENT SIMULATION	7-7
7.4.1 Four/Five-Linear Bond-slip Model	7-8
7.4.2 Governing Equations for Bond	7-10
7.4.3 Bonded (Elastic) Stage	7-12
7.4.4 Elastic-softening Stage	7-14
7.4.5 Elastic- debonding Stage	7-18
7.4.6 Debonding Stage	7-20
7.4.7 Pullout Load-Slip Calibration	7-22
7.5 ANALYSIS OF FLOOR-TO-FLOOR SYSTEM WITH LONGITUDINAL TIES. 7-28	
7.5.1 Pullout failure mode (group A)	7-29
7.5.2 Bar fracture failure mode (group B).....	7-34
7.5.3 Effect of compressive membrane action	7-34
7.5.4 Verification.....	7-35
7.6 APPROXIMATE ANALYSIS OF FLOOR-TO-FLOOR SYSTEM USING LONGITUDINAL AND TRANSVERSE TIES	7-39
7.6.1 Strength of system provided by transverse ties	7-40
7.6.2 Pull-out failure mode.....	7-46
7.6.3 Bar fracture failure mode	7-47
7.7 SUMMARY	7-49
CHAPTER 8 - RECOMMENDATIONS FOR FUTURE WORK	8-1
8.1 INTRODUCTION	8-1
8.2 APPLIED ELEMENT METHOD (AEM)	8-4
8.3 THE SPECIMENS WITH THREE STOREYS ERROR! BOOKMARK NOT DEFINED.	
8.4 USING MODIFIED PULLOUT FAILURE MODE.....	8-2

8.5	USING DISTRIBUTED TRANSVERSE TIES.....	8-3
APPENDIX 3A: GAUGE PREPARATION AND VALIDATION.....		345
APPENDIX 3B: DETAILS OF THE FULL SCALE TEST STRUCTURE.....		350
APPENDIX 3C: BEHAVIOUR OF THE FULL SCALE SPECIMENS		355
APPENDIX 4A: CONCRETE MODELLING		365
APPENDIX 5A SAP 2000 MODELLING.....		380
REFERANCES		384

LIST OF TABLES

Table 2-1	The percentage of increase of the line load with the number of storey (α) (BS 8110-11(1997)).....	2-15
Table 2-2	Building class and solution strategies (BS EN 1991-1-7:2006).....	2-20
Table 2-3	Code approaches to design structures for progressive collapse (Nair, 2003).....	2-28
Table 2-4	Adequacy of codes to prevent progressive collapse (Nair, 2003).....	2-28
Table 2-5	Bond-slip model presented in the different FE codes (Johnson, 2006).....	2-74
Table 3-1	Pullout test data with 8 mm diameter rebar.....	3-12
Table 3-2	Pullout test data with 10 mm diameter rebar.....	3-14
Table 3-3	Pullout test data with 12 mm diameter rebar.....	3-17
Table 3-4	Pullout test data with 16 mm diameter rebar.....	3-20
Table 3-5	Average bond stress along effective embedment length.....	3-21
Table 3-6	Details of test components	3-28
Table 3-7	Applied load and middle joint deflection at critical points	3-39
Table 4-1	Specimens' properties for reinforcement bar into keyways	4-3
Table 4-2	Details of variables in the floor-to-floor system	4-5
Table 4-4	Mesh properties for pullout models -reinforcement bars	4-13
Table 4-5	Mesh type for various parts in the full scale specimens.....	4-15
Table 4-6	Materials' Properties	4-18
Table 5-1	The properties of specimens for bar fracture failure mode	5-4
Table 5-2	The properties of specimens for pullout failure mode	5-5
Table 5-3	Materials' Properties [13]	5-8
Table 5-4	Longitudinal and transverse tie force with relevant maximum strength.....	5-29
Table 5-5	Tie force based on pullout failure mode.....	5-40
Table 6-1	Tie force based on bar fracture failure mode	6-4
Table 6-2	Tie force based on pullout failure mode.....	6-7
Table 6-3	Pullout specification of different reinforcement bars.....	6-8
Table 7-1	Bond stress-slip properties for three different specimens, $f_c = 20MPa$, $\alpha = 0$	7-25
Table 7-2	Comparison between experimental study and analytical model	7-35
Table 7-3	The property and strength of a floor-to-floor system with longitudinal	7-48
Table 7-4	Longitudinal and transverse tie force with relevant average strength-bar fracture failure mode.....	7-48

LIST OF FIGURES

Figure 2.1	Examples of precast concrete wall construction (Courtesy of Bison Concrete)	2-2
Figure 2.2	Isometric view of typical large panel concrete structure (PCA 1975-1979).....	2-2
Figure 2.3	Typical arrangement of structural wall panel in large panel building systems (PCA 1975-1979)	2-3
Figure 2.4	Typical ties arrangement in precast concrete cross wall structure	2-3
Figure 2.5	Failure modes of Ronan Point collapse (PCA, 1975-1979).....	2-4
Figure 2.6	Ronan Point building progressive collapse (16 May 1968)	2-7
Figure 2.7	Schematic diagram of robustness design process	2-8
Figure 2.8	Residual resistance beyond point of maximum (Starossek, 2007b).....	2-10
Figure 2.9	Section view of a precast cross wall building subjected to the wall damage.....	2-13
Figure 2.10	Precast floor-to-floor systems of a cross-wall building	2-14
Figure 2.11	Catenary mechanisms facilitated by longitudinal ties.....	2-15
Figure 2.12	Tie force in frame structures (DoD, 2013).....	2-23
Figure 2.13	Determination of L_1 for one-way load-bearing wall construction (DoD, 2013)	2-25
Figure 2.14	3D view of 5 stories concrete structure (Abruzzo et al., 2006).....	2-29
Figure 2.15	Load vs. deflection at the location of removed column (Abruzzo et al., 2006).....	2-29
Figure 2.16	Two floor-to-floor test specimens (PCA, 1975-1979)	2-32
Figure 2.17	Middle reaction support vs. middle joint deflection (PCA, 1975-1979).....	2-33
Figure 2.18	The details of the joints (Regan, 1975)	2-34
Figure 2.19	Catenary behaviour of specimen (Regan, 1975)	2-34
Figure 2.20	Applied load vs. middle joint deflection for different specimens (Regan, 1975)	2-34
Figure 2.21	Reinforcement detailing of a two spans reinforcement beam (Sasani and Kropelnick, 2007)	2-35
Figure 2.22	Applied load vs. middle joint deflection (Sasani and Kropelnick, 2007)	2-35
Figure 2.23	The layout of test specimen (Orton, 2007)	2-37
Figure 2.24	Specimen with no continuous bars (Orton, 2007).....	2-37
Figure 2.25	Specimen with continuous bars (Orton, 2007).....	2-38
Figure 2.26	details of model frame and instrumentation layout (Yi et al., 2008)	2-39
Figure 2.27	Reaction support on the jack under middle column (N) versus middle joint deflection (Yi et al., 2008)	2-39

Figure 2.28	Details of test specimens (He and Yi, 2008).....	2-40
Figure 2.29	Applied load versus middle joint displacement for different specimens (He and Yi, 2008)	2-41
Figure 2.30	The layout of test specimens; seismic load resisting system (Trung et al. 2010)	2-41
Figure 2.31	Applied load vs. middle joint deflection (Trung et al. 2010).....	2-42
Figure 2.32	The detailing and Layout of beam-column sub-assemblages (Yu and Tan, 2010).....	2-43
Figure 2.33	Applied load vs. middle joint deflection (Yu and Tan, 2010)	2-44
Figure 2.34	Pushover, capacity, and load curve (Powell et al., 2003)	2-47
Figure 2.35	Typical composite floor in tall buildings (Rahmani and Moazami, 2003)	2-47
Figure 2.36	The 20 stories steel structure model considering various column removal scenarios (Fu, 2009)	2-48
Figure 2.37	The three stories RC structure model (Shi et al., 2010)	2-50
Figure 2.38	Analysis result of the structure based on three different methods (Shi et al., 2010)...	2-50
Figure 2.39	FE model of the entire building Kwasniewski (2010)	2-51
Figure 2.40	Applied gravity load to the slab versus time (Kwasniewski, 2010).....	2-52
Figure 2.41	The time history of maximum deflection (Kwasniewski, 2010).....	2-52
Figure 2.42	Modelling concept using the AEM method (Salem et al., 2011).....	2-53
Figure 2.43	Shear and normal springs between two adjacent elements in AEM method (Salem et al., 2011)	2-53
Figure 2.44	Progressive collapse of the five-story reinforced concrete building (Salem et al., 2011)2-54	
Figure 2.45	Typical pullout specimen (Radlofl, et al., 1991; Amleh, 2006).....	2-56
Figure 2.46	Modified pullout test. Type 1&2 (Radlofl et al., 1991), and type (3, 4) (Salmons and McCrat 1977)	2-57
Figure 2.47	The distribution of bond and steel stress along embedment length (Radlofl, 1991; Leonhardt, 1964)	2-58
Figure 2.48	Typical bond stress-slip laws (CEP-FIP, 2000) and (Girard and Bastien, 2002).....	2-59
Figure 2.49	Assumed pullout load versus slip.....	2-60
Figure 2.50	Assumed interfacial bond stress for cases (a) $P \leq P_{crit}$ (b) $P \geq P_{crit}$ and (c) Normal force distribution (Naaman et al. 1991)	2-61
Figure 2.51	Alternative interfacial shear stress versus slip with frictional decay	2-61
Figure 2.52	Typical pullout test subjected to various type of loading (Abrishami and Mitchell, 1996)	2-63

Figure 2.53	Free body diagram of single bar into concrete (Abrishami and Mitchell, 1996).....	2-64
Figure 2.54	Bond model for splitting failure (Abrishami and Mitchell, 1996)	2-64
Figure 2.55	Assumed bond-slip model-Tri-linear (Ren et al., 2009)	2-66
Figure 2.56	Assumed interfacial shear stress Ren et al. (2009)	2-66
Figure 2.57	Finite element idealization: (a) coordinate system, (b) finite element idealization	2-69
Figure 2.58	Axis symmetric representation of the slip layer (Reinhardt et. at. 1984).....	2-70
Figure 2.59	Bond modelling at interface between steel and concrete (Keuser and Mehlhorn, 1988). 2-71	
Figure 2.60	Various possible spring models (Hemmaty et al., 1991)	2-72
Figure 2.61	(a) Pullout test specimen; and (b) concrete and steel substructures (Darwin and McCabe 1994)	2-73
Figure 2.62	RILM pullout test (Nardin et al., 2005)	2-75
Figure 2.63	Numerical model for pull-out specimen (Nardin et al., 2005).....	2-75
Figure 2.64	Pull-out force vs. slip- ANSYS influence of the FKN (Nardin et al., 2005)	2-76
Figure 2.65	Pull-out force vs. slip using various confinement pressure (P) and friction coefficients- ABAQUS (Nardin et al., 2005).....	2-76
Figure 2.66	Load vs. slip using ABAQUS (Gálvez et al., 2010)	2-77
Figure 2.67	Arching action (Rankin and Long, 1997)	2-78
Figure 2.68	Load vs. middle joint deflection considering compressive membrane and catenary action (Park and Gamble, 1980).....	2-79
Figure 2.69	Idealized masonry wall (MacDowel et al., 1956)	2-80
Figure 2.70	Equivalent three-hinged arches (Ranking and Long, 1997).....	2-82
Figure 2.71	The effect of lateral stiffness on the arch capacity (Rankin and Long, 1997)	2-85
Figure 2.72	Plastic hinges of beams with the elastic lateral supports (Park and Gamble, 1980)..	2-86
Figure 2.73	Load vs. deflection for a beam with rigid support	2-86
Figure 3.1	Stress-strain for different bar sizes used in the four full scale specimens.....	3-3
Figure 3.2	Test equipment.....	3-4
Figure 3.3	Stress-Strain curves for concrete grout	3-5
Figure 3.4	Precast concrete slabs for pullout tests	3-6
Figure 3.5	Details of a typical pullout specimen	3-7
Figure 3.6	Test setup for a pullout test, series PT and ST.....	3-10
Figure 3.7	Precast and prism specimens for pullout tests.....	3-11

Figure 3.8	Pullout load versus pullout displacement for 8 mm diameter bar and different embedment lengths; $f_c = 30MPa, \alpha = 0$	3-13
Figure 3.9	Pullout load versus slip for 8 mm diameter bar	3-14
Figure 3.10	Pullout load versus pullout displacement for bar size of 10mm and different embedment lengths and under straight and inclined force.....	3-16
Figure 3.11	Pullout load versus pullout displacement for bar size of 12 mm and different embedment	3-19
Figure 3.12	Pullout load versus pullout displacement for bar size of 16 mm and different embedment	3-20
Figure 3.13	Cone failure at the loaded end of precast and prism specimens - pullout failure mode	3-21
Figure 3.14	Bond strength for bar size of 10, 12, and 16 mm with the same compressive strength..	3-23
Figure 3.15	Bond model.....	3-24
Figure 3.16	Constant embedment length to provide constant pullout force.....	3-25
Figure 3.17	Plane view of the test assembly	3-27
Figure 3.18	Cast-in-suit concrete grout in the floor joint gaps.....	3-28
Figure 3.19	Precast concrete floor units used in the full scale test specimens (courtesy of Bison Ltd.)	3-29
Figure 3.20	Device for applying initial force to remove any rigid slip between the bars and anchor bolts	3-29
Figure 3.21	Marked points on the bar at the middle joint to measure permanent elongation	3-29
Figure 3.22	Plastic tube at the bar end	3-30
Figure 3.23	Typical arrangement of strain gauges (Appendix 3A).....	3-31
Figure 3.24	Floor joint test specimens (Appendix 3B)	3-32
Figure 3.25	Tie force- vertical deflection under various loading applications (Appendix 3C).....	3-34
Figure 3.26	Instrumentation	3-35
Figure 3.27	Layout and labelling of strain gauges	3-36
Figure 3.28	Strain gauges on the bracing support	3-36
Figure 3.29	3D view test assemblies	3-37
Figure 3.30	Applied load versus middle joint deflection	3-38
Figure 3.31	Horizontal reaction support force in side bracing vs. middle joint deflection	3-40
Figure 3.32	Failure pattern at the middle and sides joints for FT2	3-41
Figure 3.33	Failure pattern at the middle and ends joints for FT5	3-41

Figure 3.34	Typical strain-deflection relationship in the bar fracture failure mode.....	3-43
Figure 3.35	Strain development over embedment length (1MR of FT5 as indicated in Fig. 3.45). 3-44	
Figure 3.36	Stress vs. strain of tie bars used in the floor joint tests	3-44
Figure 3.37	Layought of stain gauges-FT1	3-45
Figure 3.38	Stresses versus mid-joint deflection for FT1	3-45
Figure 3.39	Elongation and yield length of bars at the middle joint of FT1	3-46
Figure 3.40	Layought of stain gauges - FT2	3-47
Figure 3.41	Stress versus middle joint deflection of FT2	3-48
Figure 3.42	Layought of stain gauges-FT3	3-49
Figure 3.43	Stress versus mid-joint deflection –of FT3	3-49
Figure 3.44	Cone failure around the middle bar (taken near 1MR in FT3) at deflection of 347mm .. 3-49	
Figure 3.45	Layought of stain gauges (FT4 & FT5)	3-50
Figure 3.46	Stress versus vertical deflection (FT4).....	3-51
Figure 3.47	Stress versus vertical deflection (FT5).....	3-52
Figure 3.48	Calculation model for the catenary action mechanisms.....	3-53
Figure 3.49	Load versus middle joint deflection based on test result of FT5	3-54
Figure 4.1	Illustrative diagram of the pullout test	4-3
Figure 4.2	Illustrative diagram of the full scale floor joint tests with the layout of strain gauges . 4-4	
Figure 4.3	Frictional behaviour in ABAQUS ABAQUS, 2006).....	4-7
Figure 4.4	Linear and nonlinear spring element (ABAQUS 2006).....	4-8
Figure 4.5	Translator type of connector (ABAQUS 2006)	4-9
Figure 4.6	Partitions can make a part structured meshable (ABAQUS 6-10-1, 2006)	4-11
Figure 4.7	Finite element mesh pattern	4-12
Figure 4.8	Convergences' analyses for pullout model; $\phi=12\text{mm}$, $L_d=250\text{ mm}$	4-13
Figure 4.9	Effect of the translator pattern on the analyses result for pullout model; $\phi=12\text{mm}$, $L_d=250\text{ mm}$	4-14
Figure 4.10	End boundary condition in finite element model for pullout and full scale model.....	4-17
Figure 4.11	Properties of materials in CDP and plastic model	4-21
Figure 4.12	Damage parameters for CDP model (Appendix 4A)	4-25
Figure 4.13	Stress vs. strain using various damage parameter and dilation angle (Appendix 4A) 4-26	
Figure 4.14	Translator properties used in the modelling process.....	4-28

Figure 4.15	Pullout load-displacement based on present experimental and FE results.....	4-30
Figure 4.16	Pullout and failure mode of specimen, ϕ 12mm $L_d=350, 400\text{mm}$	4-31
Figure 4.17	Slip over embedment length for reinforcement bars-ST42.....	4-32
Figure 4.18	Bond stress over embedment length of steel into concrete	4-33
Figure 4.19	Floor-to-floor behaviour for bar fracture failure mode	4-35
Figure 4.20	Floor-to-floor behaviour for pullout failure mode-FT3	4-37
Figure 4.21	Load-middle joint deflection relationship for pullout failure mode-FT4.....	4-38
Figure 4.22	Behaviour of the middle bar at the cracked section-FT1	4-39
Figure 4.23	Stress versus middle joint deflection at the location of strain gauges-FT1	4-40
Figure 4.24	Stress-middle joint deflection at the location of strain gauges- Right bar-gauge 5R-FT2	4-41
Figure 4.25	Post yielding length of ties for bar fracture failure mode-FT1 and FT2	4-41
Figure 4.26	Stress versus middle joint deflection at the location of strain gauges-FT3.....	4-42
Figure 4.27	Stress/pullout versus middle joint deflection at the location of strain gauges-FT4	4-44
Figure 4.28	Stress versus middle joint deflection at the location of strain gauges-FT5.....	4-45
Figure 5.1	Floor-to-floor system facilitated by longitudinal ties.....	5-3
Figure 5.2	Floor-to-floor system facilitated by longitudinal and transverse ties.....	5-4
Figure 5.3	Boundary condition.....	5-6
Figure 5.4	Stiffness of shear walls, $L=2, 4$ and 6m - $H=3.5\text{ m}$	5-7
Figure 5.5	Properties of materials in CDP and plastic model (Appendix 4A)	5-8
Figure 5.6	Damage parameters for CDP model	5-9
Figure 5.7	Bond-slip relationship to define translator property [13].....	5-9
Figure 5.8	Bar fracture Failure mode	5-11
Figure 5.9	Load vs. middle joint deflection considering various slab lengths	5-11
Figure 5.10	Load vs. middle joint deflection considering slab length of 6 m with 2 and 3 ties at the joints.....	5-12
Figure 5.11	Floor-to-floor joint with top and bottom tie bars	5-13
Figure 5.12	Load versus middle joint deflection for slab length of 2 m using tie bars at the top and bottom and only tie bar at the bottom of joints	5-13
Figure 5.13	pullout failure mode behaviour of floor-to-floor system for various slab lengths and ties at the joints	5-15
Figure 5.14	Failure mode of specimen-LFT1.....	5-16

Figure 5.15	Load versus middle joint deflection using longitudinal and transverse ties - LTF1...	5-17
Figure 5.16	Reaction supports versus middle joint deflection - LTF1	5-17
Figure 5.17	Failure procedure in the longitudinal and transverse ties; strain in different ties at middle joint deflection of 365-LFT1	5-18
Figure 5.18	Load versus middle joint deflection using longitudinal and transverse ties - LTF2 ...	5-19
Figure 5.19	Reaction supports versus middle joint deflection - LTF2	5-19
Figure 5.20	Failure mode of LFT3 specimen	5-20
Figure 5.21	Load versus middle joint deflection using longitudinal and transverse ties - bar fracture failure mode - LTF3	5-21
Figure 5.22	Failure process of LFT3	5-22
Figure 5.23	The layout of longitudinal and transverse ties indicating progressive failure procedure	5-23
Figure 5.24	Strain versus middle joint deflection-LFT4	5-23
Figure 5.25	Reaction supports versus middle joint deflection - bar fracture failure mode - LTF4	5-24
Figure 5.26	Load versus middle joint deflection for using longitudinal and transverse ties - bar fracture failure mode - LTF4	5-25
Figure 5.27	Load versus middle joint deflection for various slab lengths using longitudinal and transverse ties - bar fracture failure mode - LTF5	5-26
Figure 5.28	Reaction supports versus middle joint deflection -LTF5	5-27
Figure 5.29	Failure mode of LFT3 specimen, $\delta_s / l_b = 8\%$	5-27
Figure 5.30	Failure mechanism of specimen, $\delta_s / l_b = 8\%$ -LFT5	5-28
Figure 5.31	Load versus deflection for different stiffness	5-30
Figure 5.32	Failure mode of specimen	5-31
Figure 5.33	Failure process of longitudinal and transverse tie at deflection of 745 mm	5-31
Figure 5.34	Strain versus deflection in longitudinal and transverse ties-LFP1	5-32
Figure 5.35	Load versus middle joint deflection for various slab lengths using longitudinal and transverse ties - bar fracture failure mode – LTP1	5-33
Figure 5.36	Load versus middle joint deflection using longitudinal and transverse ties - bar fracture failure mode - LTP1	5-33
Figure 5.37	Bond behaviour of tie bars-LFP1	5-34
Figure 5.38	Load versus middle joint deflection using longitudinal and transverse ties - bar fracture failure mode - LTP2	5-35
Figure 5.39	Failure mode of specimen LFP3	5-36

Figure 5.40	Failure mechanism of specimen LFP3 at deflection of 475mm	5-37
Figure 5.41	Load versus middle joint deflection using longitudinal and transverse ties - bar fracture failure mode - LFP3	5-37
Figure 5.42	Load versus middle joint deflection using longitudinal and transverse ties - bar fracture failure mode - LTP4.....	5-38
Figure 5.43	Failure mode of specimen LFP5	5-39
Figure 5.44	Reaction support versus middle joint deflection using longitudinal and transverse ties - pullout failure mode - LTP5.....	5-39
Figure 5.45	Load versus middle joint deflection using longitudinal and transverse ties - LTP5 ..	5-40
Figure 5.46	Behaviour of specimen LFP3 under instantaneous load of $7.5 \text{ kN} / \text{m}^2$	5-41
Figure 6.1	Tie-Force versus slab length	6-5
Figure 6.2	Axial force in longitudinal ties based on the proposed method and the FE method.....	6-6
Figure 6.3	Axial force in transverse ties based on the proposed method and an FE approach	6-7
Figure 6.4	Location of external and internal load bearing wall removal (BS EN 1991-1-7:2006)..	6-10
Figure 7.1	Catenary action facilitated by longitudinal ties.....	7-3
Figure 7.2	Catenary mechanism for unequal span	7-5
Figure 7.3	Catenary system idealized as a free body	7-6
Figure 7.4	Interfacial bond stress distribution along embedment length. (a) Bonded phase; (b, c) elastic–softening phase; (d) elastic–debonding phase; (e) debonding phase	7-9
Figure 7.5	Analytical bond-slip model.....	7-10
Figure 7.6	Free-body diagrams of pullout specimen.....	7-11
Figure 7.7	Typical non-dimensional pullout load-slip cure	7-13
Figure 7.8	Analytical bond-slip model-two branch in the ascending stage.....	7-21
Figure 7.9	Comparison between pullout load-displacement based on analytical and pullout test results	7-24
Figure 7.10	Bond stress versus pullout displacement for three specimens	7-25
Figure 7.11	Comparison of pullout load-displacement between analytical and pullout test results ..	7-27
Figure 7.12	Pullout load-displacement relationship for three different reinforcement bars based on an analytical model	7-28

Figure 7.13	Pullout load-displacement relationship for bar size of 12 mm with different embedment lengths based on an analytical model	7-28
Figure 7.14	Floor-to-floor system facilitated by longitudinal ties.....	7-28
Figure 7.15	Assumed tie force-deflection relationship	7-29
Figure 7.16	Deflection mode of full scale tests.....	7-31
Figure 7.17	Tie force-deflection relationship based on analytical and experimental study	7-36
Figure 7.18	Applied line load – displacement relationship according to experimental and analytical study-FT4	7-37
Figure 7.19	Tie force and vertical deflection-FT4; $w=2.35 \text{ kN/m}^2$, $P=17.1 \text{ kN}$	7-37
Figure 7.20	Load vs. middle joint deflection -FT5	7-38
Figure 7.21	Load vs. middle joint deflection relationship-bar fracture failure mode.....	7-39
Figure 7.22	Floor-to-floor system facilitated by longitudinal and transverse ties.....	7-40
Figure 7.23	Catenary action behaviour of transverse ties (Astaneh et al., 2001).....	7-40
Figure 7.24	Model of the cables laced in the floor slab of a typical structure	7-41
Figure 7.25	FE analysis of a specimen with 5 span lengths of 7.2 m and bar size of 30mm	7-42
Figure 7.26	FE analysis of a specimen with 5 spans lengths of 7.2 m, bar size of 30mm with fixed boundary condition at side supports.....	7-43
Figure 7.27	Floor-to-floor joint facilitated by longitudinal ties and transverse ties-free body diagram of half system	7-44
Figure 7.28	Free body diagram of half transverse tie.....	7-45
Figure 8.1	Illustrative diagram of the modified pullout test with a support outside of grouted keyway	8-2
Figure 0.2	Proposed alternative for transverse and longitudinal ties.....	8-3
Figure 0.3	Applied element model (AEM).....	8.4

LIST OF SYMBOLS AND ABBREVIATIONS

LP	Large Panel
PCA	Portland Cement Association
PCI	Precast Concrete Institute
AD-A	Approved Document A
AD-B	Approved Document B
ASCE	American Society of Civil Engineers
DoD	Department of Defense (USA)
GSA	General Services Administration (USA)
IStructE	Institution of Structural Engineers
CDP	Concrete Damage Plasticity
ALP	Alternate Load Path
TF	Tie Force
BS	British Standard
BRE	Building Research Establishment
RC	Reinforced Structures
EC2	EuroCode 2
w	Uniformly distributed load (dead load and imposed loads)
b_p	Spacing of ties
l_b	Floor span
F_l	Force in the longitudinal tie joining adjacent slabs
δ_s	Vertical displacement at the middle wall support
q	Line load exerted by the upper wall
α	Percentage increase of the line load considering the number of storeys (see Table 2.1)
$(g_k + q_k)$	The sum of the characteristic dead and imposed floor loads (in kN/m ²)
F_t	The lesser of $(20 + 4n_o)$ or 60 kN/m, where n_o is the number of storeys
l_r	The greater of the distances (in metres) between the centres of the columns,

	frames or walls supporting any two adjacent floor spans in the direction of the tie under consideration
Z	<p>The lesser of two terms:</p> <ul style="list-style-type: none"> 5 times the clear storey height H (m), or the greatest distance in metres in the direction of the tie, between the centres of the column or vertical load-bearing members whether this distance is spanned by: <ul style="list-style-type: none"> - a single slab or - by a system of beams and slabs
L^{ASCE}	Load to be considered for the key element, (ASCE 7-05)
D	Dead Load
L	Live Load
S_n	Snow Load
W	Wind Load
L^{GSA}	Load to be considered for the key element, (GSA)
F_i	Tie strength (kN)
w_F	Floor load (kN/m^2); $w_F = 1.2D + 0.5L$
L_l	<p>L_L = Greater distance between two adjacent wall supports in the longitudinal direction,</p> <p>L_T in transverse direction which is lesser of:</p> <ul style="list-style-type: none"> - $5h_w$; h_w = clear story height (m) - Width of structure in the transverse direction (m)
L^{DoD}	Load to be considered for the key element, (DoD)
L_i, L_j	the span length of beams at the left and right of the removed column
F_Q	Maximum tie strength
Δ_Q	Maximum slip
r_b	The radius of bars
d_c	The distance between mean steel surface and cracks

τ_c	Bond stress
L_d	Embedment length
u	nominal bond stress (psi)
d	Local slip (in)
$F(x)$	The force in the bar at distance x from the free end of the bar
τ	The local interfacial shears stress between the bar and grout
C	The perimeter of the bar
κ	Bond modulus
A_m, E_m	The area and elastic modulus of grout
A_f, E_f	The area and elastic modulus of bar
P	Pull-out force
τ_{\max}	Maximum shear stress
τ_f	Bond stress in the frictional stage
u	Debonded length
$\nu_m \nu_f$	Poisson's ratio in grout and steel
s	Slip
f_{ck}	the compressive strength of concrete (MPa)
A_s	The area of reinforcement bar
f_s	Stress in the reinforcement bar
A_c	The area of concrete
f_c	Stress in the concrete
E_b	Bond modulus in ascending stage
E_d	Bond modulus in descending stage
$T(x)$	Force in the bar
δ_l	Slip at maximum bond strength
δ_f	Slip at frictional stage
P_u	The resultant force of the compressive stress on the contact area

M_{arch}	The arch bending moment capacity
r_u	The lever
\bar{y}	Distance between centre of stress distribution to the bottom of the element
ϵ_m	Strain along the contact area at y from bottom
ϵ_{mc}	The ultimate crushing strain
ϵ_{co}	Plastic strain of the concrete
L_{rig}	The span of rigid restrained slab strip
h	The overall depth of the cross section
h_1	The depth of the arching section
f'_c	The compressive strength of concrete
ρ	The positive reinforcement ratio
ρ'	The negative reinforcement ratio
f_{sy}	The yield strength of the reinforcement
d	The effective depth of the cross section
L_e	The span of the laterally restrained strip
E_c	The elastic modulus of the concrete
S	The stiffness of the lateral spring restraint
A	The area of the arch leg
b	The width of the section
w_{mecc}	The mechanism load = $k_o (M_{y2} + M_{y1})$
ω_{arch}	The arching load = $k_o M_a$
k_o	A static moment coefficient (for a uniformly distributed load $k_o = 8 / L^2$)
M_{y1}	The positive yield moment
M_{y2}	The negative yield moment
n	Numbers of ties at the joints
ϕ	Reinforcement bar diameter
d_b	Bar diameter

f_{cu}	Compressive strength of concrete cube specimen (MPa)
τ_{ave}	Average bond stress (MPa)
μ	The coefficient of friction
F_N	The normal force
$\bar{\varepsilon}_c^{in}$	Inelastic compressive strain
$\bar{\varepsilon}_t^{ck}$	Cracking strain
E_{cm}	Secant modulus of elasticity of concrete (MPa)
f_{cm}	Mean value of concrete cylinder compressive strength (MPa)
d_c, d_t	Damage parameters
ε_t	Total tensile strain
ε_{ot}^{el}	Strain corresponding to undamaged material
$\bar{\varepsilon}_t^{pl}$	Tensile plastic strain
σ_t	Tensile stress at the failure point
E_o	Elastic stiffness of the concrete
$\bar{\varepsilon}_C^{pl}$	Tensile plastic strain
σ_c	Compressive stress of concrete
σ_{cmax}	Maximum compressive strength
f_t	Tensile strength of concrete
k	Stiffness of springs
l_b	Span length in longitudinal direction
l_b	Span length in transverse direction
P_l	Required longitudinal tie force at joints (kN)
P_t	Required transverse tie force at joints (kN)
δ_{ls}	Extension at the side joint
δ_{lm}	Extension at the middle joint
δ_l	Increase in the length of each floor slab

l_1, l_2	Floor span length in the first and second span, respectively
δ_1	Slip corresponding to maximum bond strength
δ_2	Slip at descending stage
δ_3	Slip at the beginning of the frictional stage
κ_b	Bond modulus in the ascending stage
κ_d, κ_c	Bond modulus in the descending stage
τ_d	Frictional bond strength
Δ	Loaded end slip
P_{crit}	The force at the initiating of the partial debonding stage which induces τ_{max}
l_{db}	Basic anchorage length
Δ_c	Slip at the descending stage
Δ_d	Slip at the beginning of the frictional stage
T	Tensile force in transverse ties
k_s	Stiffness of transverse ties
k_{sp}	Stiffness of transverse ties corresponding to plastic strain
A_{st}	Cross section of transverse ties
w_t	Progressive resistance of system corresponding to transverse ties

Chapter 1

INTRODUCTION

1.1 BACKGROUND

The Large Panel (LP) building system was developed in France for the first time by Raymond Camus and Eduard Coignet in the 1950s. This system soon became popular in former Soviet Union and Eastern European countries, and millions of apartments have been constructed by using this type of system in the last three decades (Ned, 2008). It has maintained its fundamental principle despite many novel changes such as the details of construction.

As is defined by the Portland Cement Association (PCA Report 1, 1976), the term “large-panel” concrete structure is used to describe a building system consisting of vertical wall panels together with precast concrete floor and/or roof slabs. Large panel buildings are featured as wall panels being used as the load-bearing structure. In the conventional general arrangement, a wall that is perpendicular to the longitudinal axis of a structure is referred to as the cross wall and that is parallel to the longitudinal axis is termed as the spine wall. In the cross wall system, floors/roofs are typically made of one way hollow core precast concrete slabs and only cross walls carry the floor loads. The typical spans of floor slabs are between 5 and 13.0 m, and the unit width is around 1.2 m.

The behaviours of multi-storey buildings using the precast concrete cross wall constructions have been subjected to limited research and attention in the last two decades as compared with the cast-in-situ ones. According to literature review, due to the shortage of research data in the field, many design guidelines for preventing progressive collapse are lack of adequate

theoretical supports or rational explanation. Although the issue of progressive collapse is frequently studied in the general structural area, the research literature on the analysis and design of connections in precast concrete cross wall buildings is rather limited (Ellingwood et al., 2007)

In the early development of cross wall system, only the gravity and wind loads were considered and the abnormal loads such as those caused by gas/bomb explosion or vehicular collision were rarely included in the design of these structures (Ned, 2008; Ellingwood et al., 2007; PCA Report 2, 1976). However, a gas explosion at Ronan Point apartment in London in 1968 has triggered intensive attentions on the importance of abnormal loads on the safety of the cross wall structures (Moor, 2002; Ned, 2008, Li et al., 2011). Although these loads occur infrequently, they pose serious threat on the safety of the buildings and occupants, as they initially involve only local damages, but they can precipitate additional damage. The damage is almost entirely disproportionate to the significance of the initiating cause; and as it can progress in horizontal and vertical directions, it has become known as “progressive collapse.” The concept of progressive collapse is defined as the chain reaction of failures following the damage to only a small portion of a structure (PCA, 1979).

A gas explosion in the Ronan Point apartment, a 22-storeys precast concrete cross wall building, blown away the load bearing precast concrete walls located in the 18th floor; this initiated a progressive collapse upward to the roof and downward to the ground level. A UK government inquiry report concluded that the pressures produced by explosion were of 21 to 83 kN/m². This is within the normal range of gas explosion, and it should not be considered as exceptional violence (Griffiths et al., 1968; Pearson, 2005). Also the inquiry found that the progressive collapse following the initial structural damage caused by the explosion was mainly due to its design and it was not the result of any deficiencies in the manufacture of the factory-build units, workmanship or in the erection on site (Merola, 2009). Furthermore, as

there were no codes or standards at the time to prevent progressive collapse especially for large concrete panel buildings, this report also suggested serious deficiencies in the building regulation.

The attendances in a three-days workshop regarding the progressive collapse of structures was held in November (1975) at the University of Texas concluded that if the Ronan Point building had been designed in accordance with CEB-FIP recommendations (Recommendations for the Design and Construction of Large-panel Structures), the disproportionate collapse might have not occurred (Breen, 1975). The workshop proposed the complete necessity of effectively tying together various elements of the structure in order to prevent the large panel building from behaving as a house of cards by using horizontal, peripheral and internal ties.

Following the Ronan Point apartment incident, the British Standards for concrete structures started to incorporate provisions to deal with the problem of progressive collapse (Starossek, 2007; Ned, 2008). In 1976, the U.K. building regulation required that all buildings must be designed to resist disproportionate failure by tying together building elements, adding redundant members, and providing sufficient strength so that structures are strong, ductile and capable of redistributing loads (Ellingwood et al., 2007). The Fifth Amendment of British Standard has introduced two important concepts for the first time: “*Key Element Design*” and “*Alternate Load Path*”. These two concepts have been employed by the current British standard and many other International Codes (Rudi, 2009).

The Portland Cement Association conducted a series of comprehensive investigations to form an underpinning knowledge basis supporting the stipulated minimum detailing requirements to ensure the development of an alternative load path (ALP) in the event of any local damage

(PCA, 1975-1979). The aim was to provide minimum provisions for designing LP concrete structure to sustain abnormal loads.

After a series of terrorist attacks on buildings in the world, several U.S. government agencies (GSA 2003, DoD 2005/2013) have published their own design requirements for preventing progressive collapse. As each agency has adopted different performance objectives for buildings subjected to abnormal loads, the design methods for the progressive collapse have not been standardized through these documents. Furthermore, because the progressive collapse can affect a considerable part or even the entire structure with different collapse patterns, any specific design method has not been developed yet. However, in order to prevent progressive collapse, most codes and standards emphasized on two methods, i.e. indirect method such as tie force (TF) method and direct one such as "the alternate load path (ALP) " method (British Standard BS 8110-11, 1997; DoD 2005/2013; BS EN 1991-1-7:2006).

TF is one of the main design approaches for preventing progressive collapse, in which an indeterminate structure is analyzed manually through assuming a failure mode for a structure which is usually determinate. To establish the catenary action and prevent the progressive collapse, the TF method was established in the BS8110-1:1997 for the first time in the world after the Ronan Point event. Eurocodes then employed quite similar method and DoD 2005 has directly employed the provision of the British Standard. By performing further investigation and accumulating new knowledge related to the progressive collapse, DoD (2013) has undertaken a significant revision to TF method in its latest version (DoD,2005).

This method, which is mainly of a prescriptive nature, requires the inclusion of internal, peripheral and vertical ties to provide different new loading mechanisms, e.g. catenary, cantilever, vertical suspension and diaphragm actions, in the event of the loss of underlying wall supports. These prescriptive tie requirements may have proven adequate in engineering

practice but are not fully scientifically justified, so substantial efforts are still needed to improve the understanding, at a fundamental level, of how the mechanism of post-collapse resistance is developed through these tie provisions. This need has also been supported by a number of researchers in the last decade.

According to the results of two building cases under an abnormal load, Moore (2002) concluded that the UK provisions can improve the resistance of progressive collapse effectively. Dusenberry (2002) indicated the necessity of a better understanding of the mechanism by which the progressive collapse can be resisted. The UK Building Research Establishment (BRE) has conducted a series of quarter-scale tests to verify the adequacy and reliability of the tie force method (Moore, 2002). Nair (2003) also performed an evaluation on three well known collapsed building cases based on five current codes of practice or standards. Results revealed that all three studied structures are susceptible to progressive collapse. Abruzzo et al. (2006) has also indicated the inadequacy of the TF method to prevent progressive collapse of structures. The necessity of developing an improved TF method has also been recommended by the US Department of Defence (DoD, 2005). Based on the analytical study on single-span beams, Rudi (2009) suggested that the tie rules are effective for progressive collapse when the Class C steel is used. To investigate the efficiency of the TF design method, Li et al. (2011) also conducted comprehensive numerical studies on two reinforced concrete (RC) structures of 3 and 8 stories, respectively; results were verified by the experimental work of Yi et al. (2006). The numerical results revealed that the current tie force method cannot provide a safeguard to progressive collapse for all RC structures that have a different number of stories and experience damage in different locations; accordingly, an improved TF method was proposed. This conclusion has been further confirmed by the latest edition of DoD design criteria published in 2013, in which the required tie force has been increased significantly compared to the previous recommendations quoted in DoD (2005), British standard (BS 8110-1, 1997) and BS EN1991-1-7 (2006). Based on numerical assessment results of the disproportionate collapse, Gerasimidis et al. (2013) suggested that a

structure could respond better if damage was distributed in two adjacent elements rather than only in one element.

Another criticism of the TF method has been recently raised by several researchers who believe that the TF method does not take into account the overall behaviour of the structure as a whole, particularly for the structures susceptible to buckling failure, e.g., steel frame structures (Yan et al., 2013; Spyridaki et al., 2013; Ettouney et al., 2006). In addressing this issue, they proposed that a global analysis of the progressive collapse should be performed by considering the loss of stiffness in the local regions. However, in order to do so, the key step is to characterise the real behaviours of the local regions, such as joints, during the progressive collapse.

Through the review of the TF method, it has also been found that this method has not taken into account the effect of bond behaviour between tie bars/strands and the surrounding grout. Such behaviour is influenced by many factors, such as bar/strand-grout interface characteristics, shear stress-slip relationship, the material properties, the bar diameter, the interfacial modulus and the embedment length of tie bars/strands. This type of lacking may also attribute to the abovementioned inadequacy and will be addressed in this study. With regards to the subject of the bond behaviour of steel bars in concrete, although a large body of research work has been available in the published literature, most of this was related to the crack damage analysis and the pre-bond-failure performance of concrete reinforced members (Shen et al., 2014, Kwasniewski, 2010, Ren, et al., 2010, Hao, 2008; CEB FIP, 2000;).

Compared with the experimental studies on the catenary action of steel structures, limited experimental studies are available on assessing the catenary action in RC structures (Jun and Kang, 2010; He and Yi, 2008; Ellingwood et al., 2007). This is particularly the case for the multi-storey precast concrete cross wall buildings (Pekau, 2006). PCA's (1975-1979) experimental studies and Regan (1975) are the only published work on the performance of

cross wall structures in terms of the catenary action and the progressive collapse by considering the floor joint behaviour. The previous research on the progressive behaviour of precast cross wall structures mostly focused on the behaviour of walls during the progressive collapse (Pekau, 2006; Scaloni and Kianoush; 1988). The experimental study conducted by PCA (1975-1979) indicates that the catenary action can be achieved through the pullout failure mode by using appropriate embedment length, strand size and grout strength. As the only recorded data were the tie force against the middle joint deflection relation, the actual progressive collapse resistance of the floor assembly system were not exhibited through these full scale tests.

Most experimental studies on the progressive resistance of RC structures indicated that the specimens detailed in compliance to the seismic design rules are capable to establish the effective catenary action with the ultimate strength higher than the yield capacity. Although it was found that the resistance significantly varies with different boundary conditions, most tests almost resulted into the same range of deflection/span ratio, i.e. $17 \leq \delta_s/l_b \leq 21$. However, there are noticeable discrepancies amongst the abovementioned experimental studies regarding the behaviour of progressive collapse. Sasani and Kropelniki (2007) concluded that the resistance of a two-span beam developed in the catenary stage was slightly less than the resistance due to the yield failure. By using almost the same properties of specimens, Yu and Tan (2010), Yi et al. (2008), He and Yi (2008) obtained the catenary/yield resistance ratios of 1.75, 1.35 and 2.0, respectively. Meanwhile, Trung et al. (2010) stated that the progressive collapse resistance of specimens with the rebar detailing in compliance with the seismic design rule is more than twice that of specimens without seismic detailing; while Yi et al.'s. (2008) experimental study indicates that there is no obvious difference between these two specimens. It is without doubt that there are significant discrepancies in evaluating the progressive collapse resistance of RC structures. Furthermore, unlike the other studies, Orton (2007) argued that specimens with continuous reinforcement bars could not develop the

catenary action, while the specimens without continuous bars are capable of developing catenary action through stirrups, which is in contradiction to the other studies.

Literature survey reveals that there is a deficiency in studies, in particular, from the experimental perspective, on the evaluation of progressive collapse resistance at the catenary action stage. Even these limited number of experimental study also showed discrepancy. For instance, those experiments adopting almost the same properties lead to considerably different result.

The above analysis reveals that an evident knowledge gap exists which has potentially prohibited the development of rational design approaches. This type of knowledge gap can be classified as follow:

- Limited experimental and numerical studies on progressive behaviour of precast cross wall system have been performed ;
- The prescriptive tie requirements may have proven adequate in engineering practice but are not fully scientifically justified, so substantial efforts are still needed to improve the understanding, at a fundamental level, of how the mechanism of post-collapse resistance is developed through these tie provisions
- The studies in this filed rarely examined the impact of ductility of the floor system on the progressive resistance of the floor joints in cross wall structures

1.2 AIMS AND OBJECTIVES

Current design practice in the UK and most other countries has employed descriptive method e.g. TF approach, to specify the tie strength in order to address the progressive collapse problem in the precast concrete cross wall construction. This method is widely used in industries. Although these designs method have proved to work effectively, the real

performance after the localized failures has not yet been fully understood. The initial goal of the project is to address this knowledge gap.

Developing and validating numerical and analytical models will be the second principal aim of this study. The models will focus on various levels of details, which include the bond failure modelling for the tie bars, the post-bond failure behaviour analysis of the floor connections and the behaviour of a typical building unit. The model validation was carried out by comparing the corresponding data with the counterpart lab test results.

This PhD research focuses on the evaluation of the tie design of the joints in cross wall buildings by using the direct method. The work carried out provided a first-hand test dataset of post-collapse-failure behaviour of precast floor joints. They were used as the benchmark cases for the subsequent modelling, analysis and design improvements of the floor connection against the progressive collapse. As an outcome of the study, a rational floor to floor joint design was developed to reduce the risk of progressive collapse due to the sudden loss of a vertical load bearing wall. The design procedure was supported by appropriate experimental tests and numerical nonlinear analyses.

In summary, the aim of this research is to investigate post-collapse behaviour of precast floor-to-floor joint following wall removal, develop an FE approach to simulate the pullout and the floor-to-floor joint in order to establish an analysis method to design connections between slabs to prevent progressive collapse in the event of removing underlying wall support in the precast concrete cross wall structures and, also, examine the adequacy of the codified provisions for the longitudinal ties in the codes of practice. This was achieved by carrying out a series of pullout and full scale floor-to-floor joints tests that are followed by a systematic numerical simulations to inform the best practice of designing ties for this type of construction following the removal of a support wall. The objectives of present study can be summarised as follow:

- To carry out a series of experimental study to understand the pullout behaviour of ties into keyways of precast slabs, and investigate the strength, ductility, and robustness of floor slab joints;
- To perform numerical simulations to reproduce the laboratory tests of pullout and full scale floor-to-floor joint tests;
- To perform parametric numerical studies to propose general analysis and design guidance.

1.3 RESEARCH METHODOLOGY

In order to evaluate the behaviour of the catenary action mechanism through the floor to floor joint system and examine the adequacy of the provisions of longitudinal ties at the floor joints, a combined experimental-numerical-analytical- research methodology was adopted and the following research work was completed: (1) Carrying out two series of laboratory tests, i.e. pull-out and floor-to-floor joint tests using reinforcement bars within the keyways; (2) Developing nonlinear numerical model to analyze the floor system which were validated by the test results (3) Performing extensive parametric analysis once the model is validated; (4) Formulating an approximate analytical model to predict the behaviour of full scale tests, (5) Proposing design guidance based on the research findings. The details of experimental studies are classified in the three main categories as follow.

1.3.1 Experimental work

Experimental work consists of two phases:

1.3.1.1 Pullout test of tie bars

- To evaluate the pullout behaviour, in particular, the post-bond-failure behaviour of grout specimens containing tie bars of various sizes, embedment lengths, concrete strengths, and mould shapes,
- To provide an experimental dataset for FE and analytical approaches,
- To evaluate the pullout behaviour under inclined loads.

1.3.1.2 Full scale floor-to-floor joint tests

- To examine the strength, ductility and robustness of the floor-to-floor joints and to characterise the behaviour of catenary action mechanism with various tie design details;
- To study the effect of bar size, the embedment length within the slab keyways and the number of longitudinal ties at joints on the catenary action mechanism.

1.3.2 Numerical analyses

To perform numerical simulations using finite element software to reproduce the laboratory tests of pullout and full scale floor-to-floor joint tests and to perform the parametric numerical analyses to propose the general analysis and design guidance.

1.3.3 Analytical prediction

Predicting the behaviour of full scale specimens prior to performing the tests and proposing an approximate analytical model to predicate the progressive resistance of the floor-to-floor joints at the catenary stage

Chapter 2

LITERATURE REVIEW

2.1 INTRODUCTION

In this chapter, an in-depth review of the progressive collapse, robustness, experimental and numerical analysis of the progressive collapse resistance of an RC structure is presented. A short description of precast concrete cross wall structure and the general regulations for progressive collapse is presented in Section 2.2. The definition of progressive collapse and the factors that affect the robustness of structures are discussed in Section 2.3. A summary of the international code regulations with regards to the design for progressive collapse has been presented in section 2.4. Through experimental and FE study conducted in the last decade, the efficiency of the current tie force method is discussed in section 2.5. The recent experimental and FE study on progressive collapse in RC structures with extensive discussion is presented in section 2.6 and 2.7, respectively. A review of pullout behaviour and an analytical simulation of steel bars into concrete are presented in sections 2.8 and 2.9. Numerical modelling of the bond-slip of steel bars in the concrete and a relevant application is presented in section 2.10. A review of analytical approach to define progressive collapse resistance of RC structure is discussed in section 2.11. A summary of the literature review is discussed in section 2.12.

2.2 CROSS WALL STRUCTURES

Cross wall structures is one of the modern construction methods and well adopted for high-rise housing (Fig. 2.1). As most building components are pre-fabricated in factories, they are

precisely engineered and can facilitate a fast-track construction. This method of construction has been developed for residential buildings such as multifamily housing, hotels, and student residences. As is defined by the Portland Cement Association (PCA, 1975-1979), the term “large-panel” concrete structure is used to describe a building system consisting of vertical wall panels together with the precast concrete floors and/or roofs (Fig. 2.2). In the usual arrangement, a wall that is perpendicular to the longitudinal axis of a structure is referred to as the cross wall and a wall that is parallel to the longitudinal axis is termed as the spine wall. In the cross wall system, the floor/roof slabs are typically one way hollow core precast concrete slabs and only the cross walls carry the floor loads (Fig. 2.3).

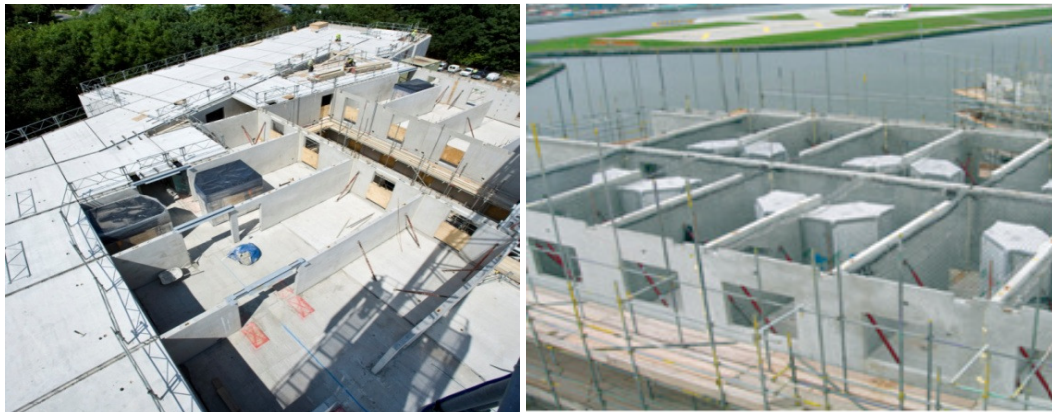


Figure 2.1 Examples of precast concrete wall construction (Courtesy of Bison Concrete)

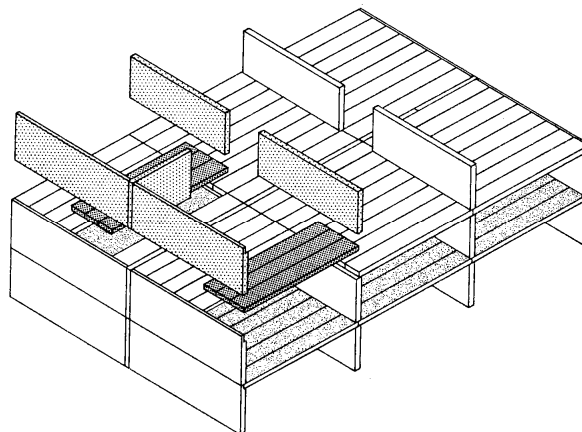
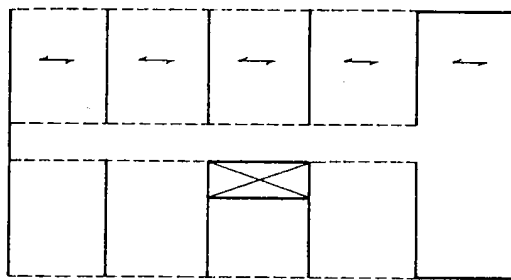
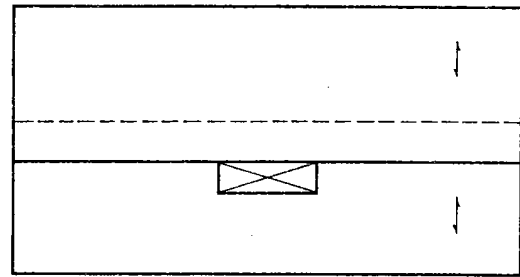


Figure 2.2 Isometric view of typical large panel concrete structure (PCA 1975-1979)

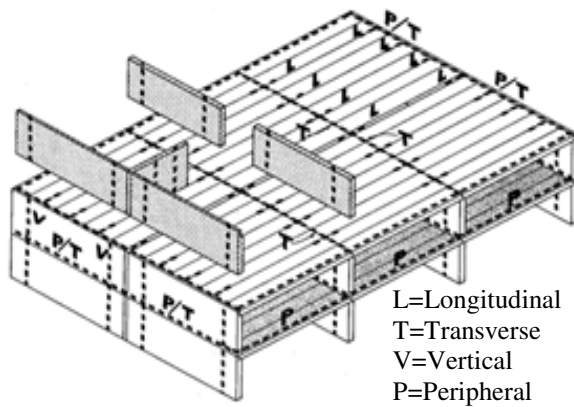


(a) Cross Wall System



(b) Spine Wall System

Figure 2.3 Typical arrangement of structural wall panel in large panel building systems (PCA 1975-1979)



(a) Overall tie requirements (PCA 1979)



(b) Examples of longitudinal ties (Courtesy of Bison Concrete)

Figure 2.4 Typical ties arrangement in precast concrete cross wall structure

The construction method employs a series of transverse, vertical and longitudinal ties, designed to meet the criteria against progressive collapse based on provisions of building codes (Fig. 2.4a). These ties allow cantilever behaviour and beam actions for wall panels, membrane/catenary actions and horizontal suspension actions for floors and vertical suspension actions for wall/floor junctions (Burnet and Hanson, 1977; PCA, 1979; Ellingwood et al., 2007).

2.3 PROGRESSIVE COLLAPSE

2.3.1 Definition

The concept of progressive collapse emerged in the codes after the well-known collapse of the Ronan Point apartment in London in 1968 (Pearson and Delatte, 2005). Although the apartment did not collapse completely, the volume of damage was entirely disproportionate to the initial damage (Fig. 2.5). “The degree of ‘progressivity’ is defined as the ratio of total collapsed area or volume to area or volume of local or initial damage. In the case of the Ronan Point the ratio was approximately 20” (Ellingwood et al., 2007).

Progressive collapse in buildings typically occurs when abnormal loading conditions cause the loss of structural capacity (not necessarily removal) of one or more critical members. In the progressive collapse process, the damage is mostly disproportionately greater than the local failure. PCA defines progressive collapse as a “chain reaction of failures following damage to only a small portion of a structure ” (PCA 1975-1979).

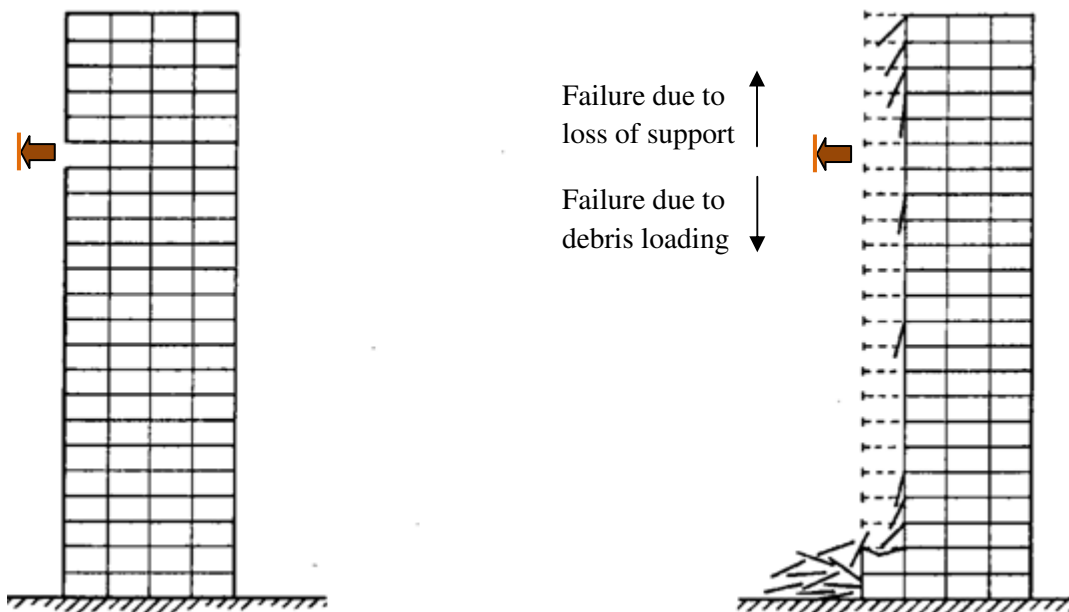


Figure 2.5 Failure modes of Ronan Point collapse (PCA, 1975-1979)

British Standards have not employed explicitly the terminology of progressive collapse, but they require that measures should be taken to avoid the collapse of a large part of a structure in the event of the local damage to the structure or the failure of a single element; as can be seen in BS 8110-1:1997 (BSI, 1997). Although the Eurocodes do not have a specific definition of progressive collapse, they provide provisions for designing buildings to prevent progressive collapse due to local failure from an unspecified cause without disproportionate collapse in BS EN 1991-1-7:2006.

The ASCE Standard defines progressive collapse as “the spread of an initial local failure from element to element resulting, eventually, in collapse of an entire structure or disproportionately large part of it” (ASCE 7-05, 2006). The American Department of Defence document (DoD, 2005), has used the same definition as ASCE. The General Services Administration (GSA, 2003) defines progressive collapse as “a situation where local failure of a primary structural component leads to the collapse of adjoining members which, in turn, leads to additional collapse, hence the total damage is disproportionate to the original cause”.

The situation that failure of one member results in a much larger-scale collapse than the initial damage is called disproportionate collapse. Thus, the “progressive collapse” is a type of progressive failure which the total damage is not proportionate to the local failure. In some countries, the term “disproportionate collapse” is used to describe this type of collapse. The term of progressive collapse and disproportionate collapse are conceptually different. Meacham and Matthew (2006) stated that “progressive collapse describes the spreading of a collapse of one part of the structure to areas that were initially not touched by the damage event, such as fire or blast”. While, a “disproportionate damage occurs when the consequence of an event is far greater than expected”. In general, progressive collapse is a kind of disproportionate collapse but inverse, disproportionate is not necessarily progressive collapse. Due to various triggering events, Starossek (2007) implied that “progressive collapse is

characterized by a disproportion in size between a triggering event and resulting collapse” and according to this definition six types of progressive collapse were defined;

Pancake type collapse, where an upper part of the structure fails and starts to move downward accumulating kinetic energy.

Zipper type collapse, the failure of a load bearing member generates an alternative load path which overloads the adjacent members

Domino type collapse, where a member of the structure fails and overturns in an angular rigid-body motion around the bottom edge pushing on the upper edge of an adjacent member.

Section type collapse, where a part of a cross section of a member fails and the internal forces transmitted by this part are redistributed into the remaining cross section.

Instability type collapse, stabilizing elements fail generating the destabilization of load carrying members that fail with a small deflection. As a result, other members of the structure are involved in the failure process.

Mixed type collapse, which is a combination of two or more collapse types discussed above.

2.3.2 Robustness

In the Ronan Point event, the damage of one member set off a chain reaction failure so that the total damage was extremely disproportionate to the significance of the initiating case (Fig. 2.6). This failure clearly highlighted the importance of “robust” structures. Subsequently, most codes adopted rules to introduce some measure of robustness into all new structures. The current structural design codes mainly take into account the failure modes to design

structural members and the main aim is to provide basic provisions to ensure sufficient structural safety by using suitable and cost effective materials (Fig. 2.7). Although, most modern structural design codes have provided some general provision for robustness, the issue remains unclear for many engineers; so incorporating robustness and complying with provisions is still a challenge. It clearly indicates the importance of further studying the concept of robustness (Banu, 2011). It is worth noting that no engineers can design a structure to prevent total collapse if the initiating case is big enough, but a robust structure can assure that the total damage is not disproportionate to the local failure.



Figure 2.6 Ronan Point building progressive collapse -16 May 1968 (Nair, 2005)

Mann et al. (2010) stated that “The robustness topic does not yet lend itself to academic precision. Indeed, the rules we have now are a pragmatic balance between cost and perceived risk which is nevertheless judged to be reasonably effective in restricting the extent of failure when put to the test”.

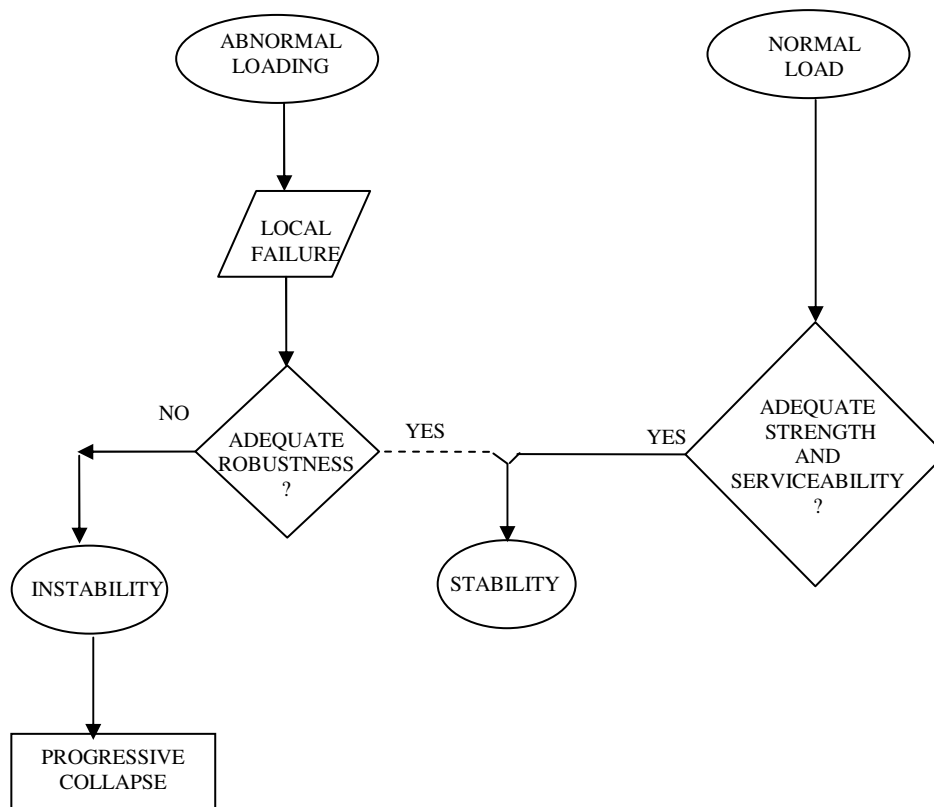


Figure 2.7 Schematic diagram of robustness design process (PCA, 1979)

It has been argued that in practical designing of structures the major risk is not dependent on an inadequate safety factor, but it mainly lies on inadequate robustness. In the robust structures, there is no organic relationship between the probability of local failure and a high safety level against local damage with robustness; which is a property of a structure (Banu, 2011). The implicit regulation to design a structure for robustness adopted in the codes is mainly not explicit, thus it will be left up to professionalism and good practice (Mann et al. 2010).

2.3.2.1 Concept of Robustness

To define robustness, various terms such as structural integrity, prevention of disproportionate collapse and structural robustness have been used; while most definitions are relatively similar, especially those provided by the modern design codes. BS EN 1990 2.1 (Section 2.1

Basic requirements) has defined robustness as “a structure shall be designed and executed in such a way that it will not be damaged by events such as explosion, impact, and the consequences of human errors, to an extent disproportionate to the original cause”. According to the British Standard BS 8110-1:1997, structures that are not susceptible to the effects of an accidental load are robust. It is obvious all of these requirements are relatively general and do not provide a clear guideline on achieving structural robustness. GSA (2003) defines robustness as an “ability of a structure or structural components to resist damage without premature and/or brittle failure due to events like explosions, impacts, fire or consequences of human error, due to its vigorous strength and toughness”.

Beeby (1997) defines robustness as “the capacity of buildings to sustain abnormal loads without disproportionate collapse”. The Institution of Structural Engineers (IStructE, 2002) defines the concept of robustness as “the ability of an engineered structure or system that enables it to survive a potentially damaging incident or extreme event without disproportionate loss of function”. For a robust structure to survive a circumstance or unforeseen event it must be capable of providing a reserve capacity to stand up during or after the event; i.e. a robust system has therefore:

$$\text{Residual capacity} > \text{Residual demand} \quad (2.1)$$

It is obvious that the term of capacity can be related to the strength of the system, but it is also related to the ductility, deformability, stability or stiffness; where, depending on the event, one of these properties may play a critical role. The term of residual is related to the situation where the event has taken place. Finally, we can define robustness as the criteria of structural design. Under an abnormal loading, a degree of damage to structures may be acceptable, but with adequate robustness, they should survive unusual or unforeseen circumstances so that evacuation and repair at a reasonable cost is possible.

2.3.2.2 Design for Robustness

It is generally accepted that the current regulation is mainly reliant on a level of redundancy (alternate load path) and continuity to provide robustness to bridge over the load from damaged areas to the remaining undamaged elements; but in intensive overload e.g. gas explosion or bomb attack, the more alternate load path that exists the better. Spare capacity as a second level of redundancy should be taken into account in any further discussions on robustness (Banu, 2011).

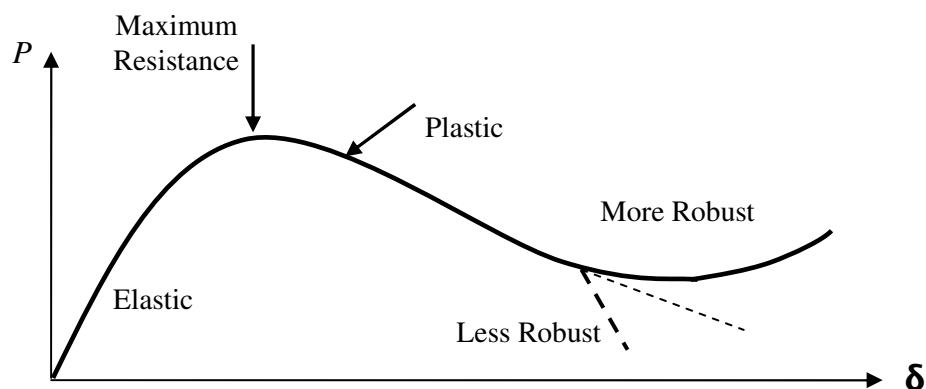


Figure 2.8 Residual resistance beyond point of maximum (Starossek, 2007b)

The current design method is more or less based on strength and stiffness against applied loads. This process does not take into account such important factors as global stability, global stiffness and insensitivity to the inevitable errors or minor alterations (Mann et al. 2010). These properties can be classified as the quality of robustness. A robust structure will present a resistance against loads that will continue after reaching the maximum strength of its structure or elements; although with a decrease in resistance (Fig. 2.8). Robust structures will endure damage and they will not collapse. Additional strength to the key element, multiple load paths, second line of defence and design only in deformation controlled situations, would enhance robustness (BSI, 1997; BS EN1991-1-7, 2006; Ellingwood, et al., 2007; Knoll and Vogel, 2009; Franz and Thomas, 2009). To enhance the robustness of structures and reduce

the risk of progressive collapse when one vertical support is ineffective, the following structural traits should be considered in the design:

1. **Strength:** Providing strength, beyond the minimally needed strength based on a conventional design method, is the most economical approach to improve the robustness,
2. **Second line of defence:** The ability of a structure to develop much more resistance following an initial failure through a second load path,
3. **Redundancy:** Providing different alternate load paths for loads resulting from local damage of structural elements. This concept resembles a second line of defence, but in this case the loads are transferred through more load paths so that if one element fails, the rest may be able to sustain the load,
4. **Ductility:** The capability to maintain the strength through large deformation or load redistribution so that it can absorb significant strain energy without rupture or collapse. The ductility plays a critical role in second line of defence and redundancy and is defined as maximum deformation / maximum elastic deformation,
5. **Continuity:** the capability of bridging to transfer loads over collapsed element,
6. **Ties:** To prevent progressive collapse the system requires the transfer of the load throughout the structure (vertically and horizontally) through alternative load paths. The continuity between adjacent members can enhance the ability of a structure to redistribute or transfer loads along these load paths,
7. **Over-strength:** Using an enhanced factor of safety in order to design key elements subjected to abnormal loading.

In comparison with conventional structures, connections in the LP structures can be identified as weak links due to the lack of continuity through the joints. Although existence friction can develop a degree of resistance for stability under gravity load, such a connection cannot

provide sufficient strength to sustain abnormal loads. Thus, a degree of continuity and ductility across the connection must be established to provide general structural integrity. Continuity is necessary to bridge loads over the removal of a load bearing wall (alternate load path) and ductility is essential to redistribute the load, sustain vertical deflection demand and provide energy absorption under the dynamic effect of abnormal loads in the event of the loss of a supporting wall (PCA 1976, Koncz, 1995, Ellingwood et al. 2007, Ned 2008).

It can be concluded that to design robust structures an alternate load path should be considered as the most significant factor, hence it will be discussed in more detail in the following section.

2.3.3 Alternate Load Paths

In conventional structures, the normal load will transfer safely from the point of application to the foundations through an established load path. Following the removal of a wall support in the precast cross wall structure due to an abnormal loading, a new load path must be provided and is defined as an “alternate load path”. The new load path should be capable to bridge over loads from the damaged elements or area, to the remaining undamaged structure, to prevent progressive collapse. In the precast cross wall structures this can be achieved through tying the whole structure together in both horizontal and vertical directions. An alternate load path can be established through the “catenary action of floor-to-floor system, cantilever and beam action of wall panels, vertical suspension of wall panels, and diaphragm action of the floor plans”. Catenary action mechanism is the first step of the transferring of a load through a load path. In the present study, based on the catenary action mechanism, a numerical and analytical simulation to design a longitudinal tie will be performed, hence it will be discussed in details.

2.3.3.1 Catenary Action Mechanism

Reinforced concrete structures can sustain disproportionate collapse through a different mechanism, i.e. catenary action (cable action), membrane action in the floor slab, compressive arch action and contribution from infill walls. Catenary and membrane action can sustain gravity loads through tensile force in the ties while the structural elements are carrying excessive deflection. In precast cross wall structures, when an underlying wall support is suddenly removed due to an abnormal load (Fig. 2.9), to bridge out the loads exerted by the upper walls and retain structural integrity, continuity at the floor-to-floor joints must be provided so that an alternate load path can be found. Unlike under normal service conditions, a much larger deformation in the affected zone is allowed. Therefore, the ductility of these connections must be sufficient to satisfy the deformational demand.

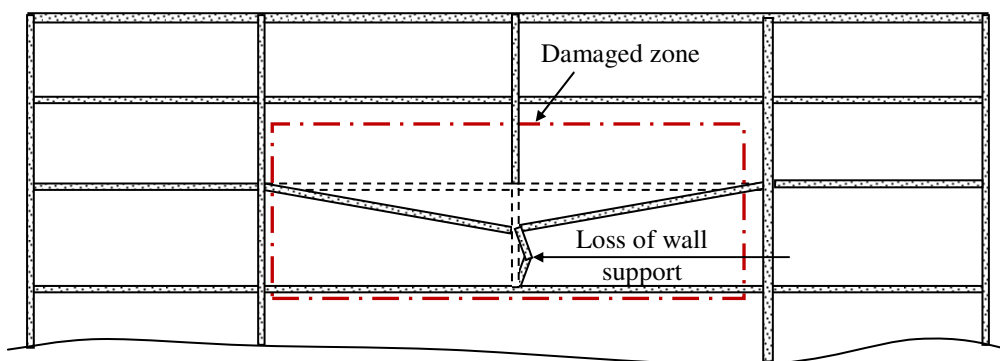


Figure 2.9 Section view of a precast cross wall building subjected to the wall damage

In precast cross-wall constructions, these requirements can be facilitated by longitudinal ties embedded in the cast in-situ grout placed in the keyways and the end gap of floor slabs (Fig 2.10). It is generally accepted that through the catenary mechanism the applied load is sustained by tensile force along the elements. Although so far, there is no clear definition for the starting point of catenary action, but obviously it can be defined as the point which axial force in the elements turns from compression to tension (Sasani, 2007). Furthermore, the rebounding point to the second-ascending phase has been defined as the starting point of catenary action by some researchers (Yun, 2010). In the frame structures, initially beam

action (beam-end moment) sustains the applied load and then following the developing plastic hinges at a small vertical deflection, catenary action (axial force) will carry loads at a large deformation. McNamara and Salvia (2003) state that “catenary action is considered as the first defence of a structure to mitigate progressive collapse, provided that the remaining structure after an initial damage can develop alternate load paths and a large deformation has occurred in the affected beams and slabs. As a result, catenary action requires high continuity and ductility of joints”.

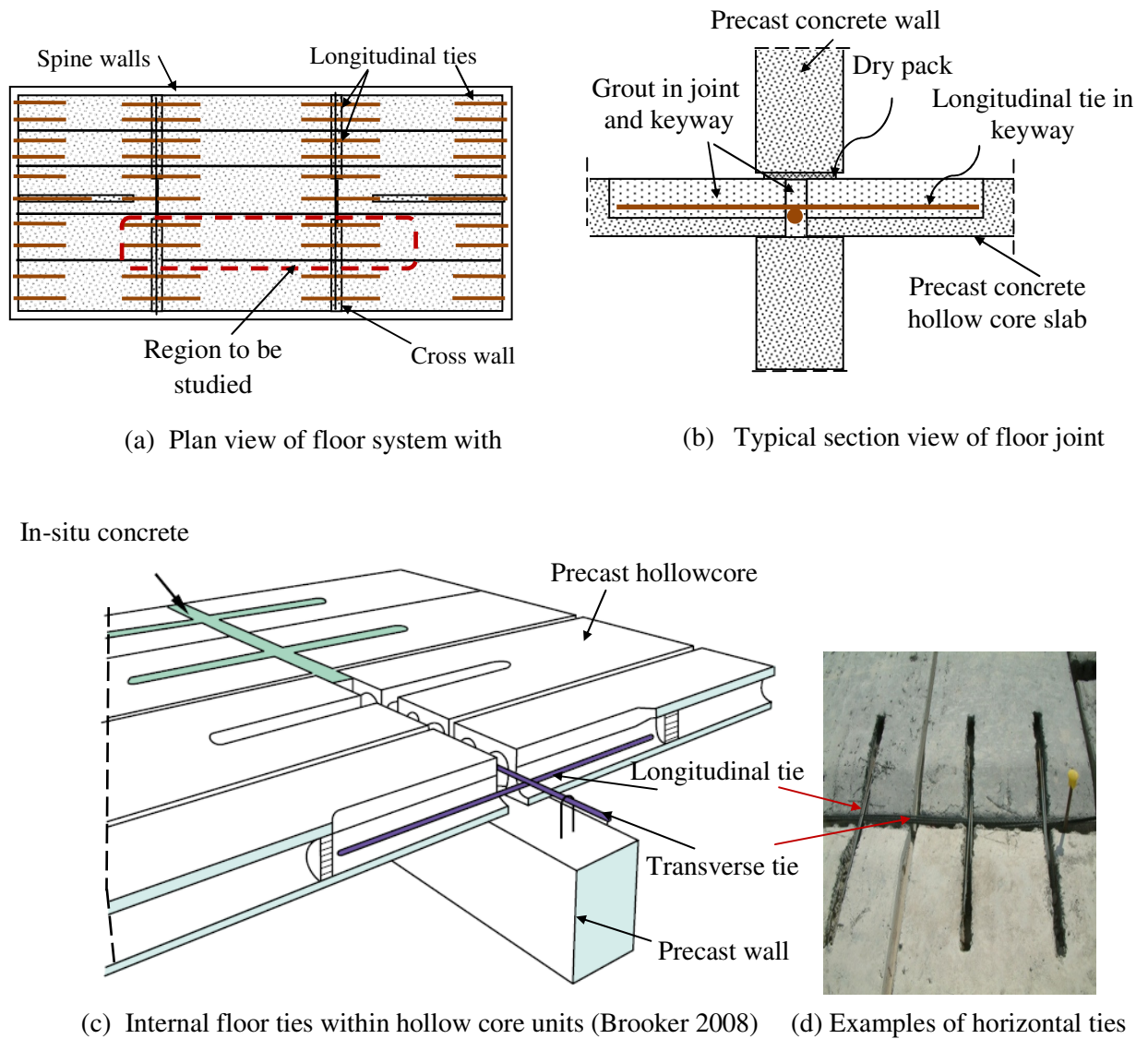


Figure 2.10 Precast floor-to-floor systems of a cross-wall building

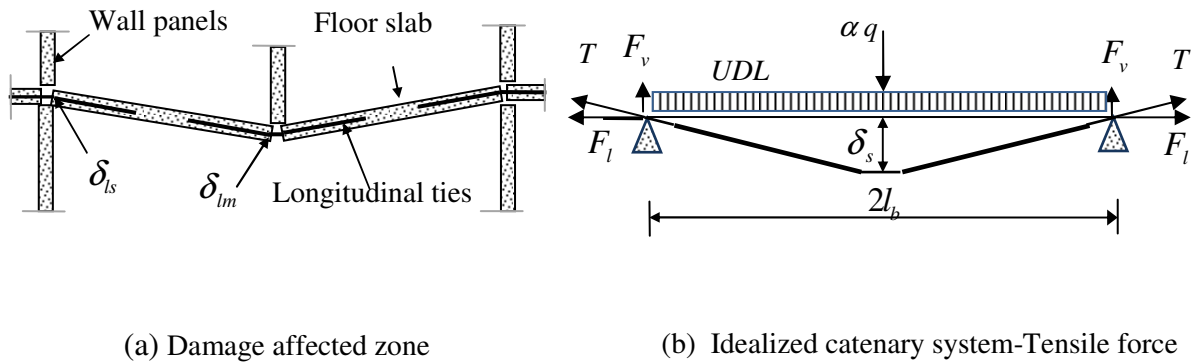


Figure 2.11 Catenary mechanisms facilitated by longitudinal ties (PCA, 1979)

An equilibrium equation of the catenary system can be derived by taking moments about the side support in the free body diagram of the half system as shown in Fig. 2.11b (PCA, 1979):

$$F_l = \frac{wb_p l_b^2}{2\delta_s} + \frac{\alpha q b_p l_b}{2\delta_s} \quad (2.2a)$$

$$\text{Let } q = wl_b, \quad F_l = (1 + \alpha) \frac{wb_p l_b^2}{2\delta_s} \quad (2.2b)$$

where:

- w = Uniformly distributed load (dead load and imposed loads)
- b_p = Spacing of ties
- l_b = Floor span
- F_l = Force in the longitudinal tie joining adjacent slabs
- δ_s = Vertical displacement at the middle wall support.
- q = Line load exerted by the upper wall
- α = Percentage increase of the line load considering the number of storeys (see Table 2.1)

Table 2-1 The percentage of increase of the line load with the number of storey (α) (BS 8110-11(1997))

storey	1	2	3	4	5	6	7	8	9	10
$\alpha\%$	0	17	33	50	67	83	100	117	133	150

2.4 CURRENT PROVISIONS FOR STRUCTURAL ROBUSTNESS

Due to the significant consequences related to the collapse of various types of buildings, the issues associated with robustness have been taken into consideration by many national and international codes. The fundamental design regulations in these codes are associated with the design and ability of each element, connection or structural component to provide sufficient robustness. Since the Ronan Point catastrophic collapse, most standards and codes have attempted to deal with the issue of progressive collapse in different types of buildings. Most of them have only utilized an indirect method and prescriptive provision. The codes mainly have focused on enhancing the overall structural integrity by minor changes in the amount, location, and detailing of member reinforcement and in the detailing of the connection hardware. The regulations to prevent progressive collapse adopted in various codes are discussed in the following section.

2.4.1 British Standard

Immediately after the collapse of Ronan Point apartment, British Standards adopted useful provisions to deal with progressive collapse. The Building Regulations (HMSO, 1976) required that all structures (five storeys and over) should be designed so that they can provide minimum structural integrity by the tying of different structural elements of a LP building together, to provide sufficient continuity and ductility. Ties can enhance the strength of connections to prevent the blowing out of a wall panel in the event of an explosion and also the ability of a structure to transfer load over a lost support. The UK's Building Regulations provide three levels of design for progressive collapse to ensure minimum robustness following the removal of a wall support. These regulations have been adapted in different British Standard Material Codes i.e. BSI, 2000; BSI, 1985; BSI, 1978, AND BS5950 (Moor, 2002).

2.4.1.1 Tying

With this method, different ties are used to increase redundancy of structures and develop various alternate load paths. To design structures against progressive collapse, BS8110-1:1997 defines three kinds of ties (Fig. 2.4), i.e. internal ties, peripheral ties, and vertical ties.

Internal ties: “These ties should be at each floor and roof level in two directions approximately at right angles. They should be effectively continuous throughout their length and should be anchored to the peripheral ties at each end (unless continuing as horizontal ties to columns or walls.” The internal ties in the two directions should be designed to carrying a tensile force of P (in kN/m width) equal to the greater of:

$$P_1 = \frac{(g_k + q_k) l_r}{7.5} \frac{F_t}{5} \quad \text{kN / m} \quad (2.3a)$$

$$P_2 = F_t \quad \text{kN / m} \quad (2.3b)$$

Where:

$(g_k + q_k)$ is the sum of the characteristic dead and imposed floor loads (in kN/m²) ;

F_t the Basic Strength , which is the lesser of $(20 + 4n_o)$ or 60 kN/m, where n_o is the number of storeys;

l_r is the greater of the distances (in metres) between the centres of the columns, frames or walls supporting any two adjacent floor spans in the direction of the tie under consideration

The Basic Strength F_t is a function of the number of storeys, which, according to Burnett 1975 “reflects that the probability of occurrence and magnitude of an abnormal loading increases with building height”.

2.4.1.2 Bridging

In this method, an element is notionally removed, one at a time. The requirements specified that the structures should be designed so that if any load bearing element is removed, the structural failure should be limited to the storeys above and below the removed element. However, the structural failure should not exceed 70 square metres or 15% of the area of the storey in the horizontal plane, whichever is less.

2.4.1.3 Key Element

In this approach whenever the effect of the removal of any single column or beam carrying a column would result in the collapse of any area greater than 70 m² or 15% of the area of the storey, that member should be designed as a key element. The key elements can be designed for an accidental loading not less than 34 kN/m², or the notional load imposed by authorities.

2.4.2 Eurocodes Approach

Eurocodes are a series of modern codes adopted by many European countries that may also be supplemented with a national annex. In addition to providing general design guidelines to avoid progressive collapse, such as selection of a good structural layout, Eurocodes also recommend tying the building together and define quantities for the tie forces. Buildings can be assigned to one of three safety classes, with only the two highest classes requiring consideration of progressive collapse. The Eurocodes provision gives rules and methods for designing buildings to sustain an extent of localised failure from an unspecified cause without disproportionate collapse. Adopting these provisions should provide a building with sufficient robustness to survive a reasonable range of undefined accidental actions.

A comparison between introduced classes shows that the building classes in BS EN 1991-1-7:2006 are practically the same as the UK Approved Document A-2004 (Merola, 2009). In

addition, according to BS EN 1991-1-7: 2006, strategies for preventing of progressive collapse will be provided by using one or more of the following methods:

1. Designing key elements by using accidental loads specified in the codes directly i.e. $34 \text{ kN} / \text{m}^2$ for structures.
2. Designing the structures so that following local damage e.g. removal of one element, the stability of the structure would be provided and any failure area does not exceed 100 m^2 or 15 % of the floor area whichever is less.
3. Applying prescriptive design rules in 3D order

A summary of building class and relevant solution strategies is presented in the Table 2.2.

In the prescriptive design method, the internal tie force in the two directions should be the greater of P (in kN/m width):

$$P_1 = \frac{(g_k + q_k) z}{7.5} F_t \quad \text{kN} / \text{m} \quad (2.4a)$$

$$P_2 = F_t \quad \text{kN} / \text{m} \quad (2.4b)$$

Where:

$(g_k + q_k)$ is the sum of the characteristic dead and imposed floor loads (in kN/m^2) ;

F_t is the lesser of $(20 + 4n_s)$ or $60 \text{ kN}/\text{m}$, where n_s is the number of storeys;

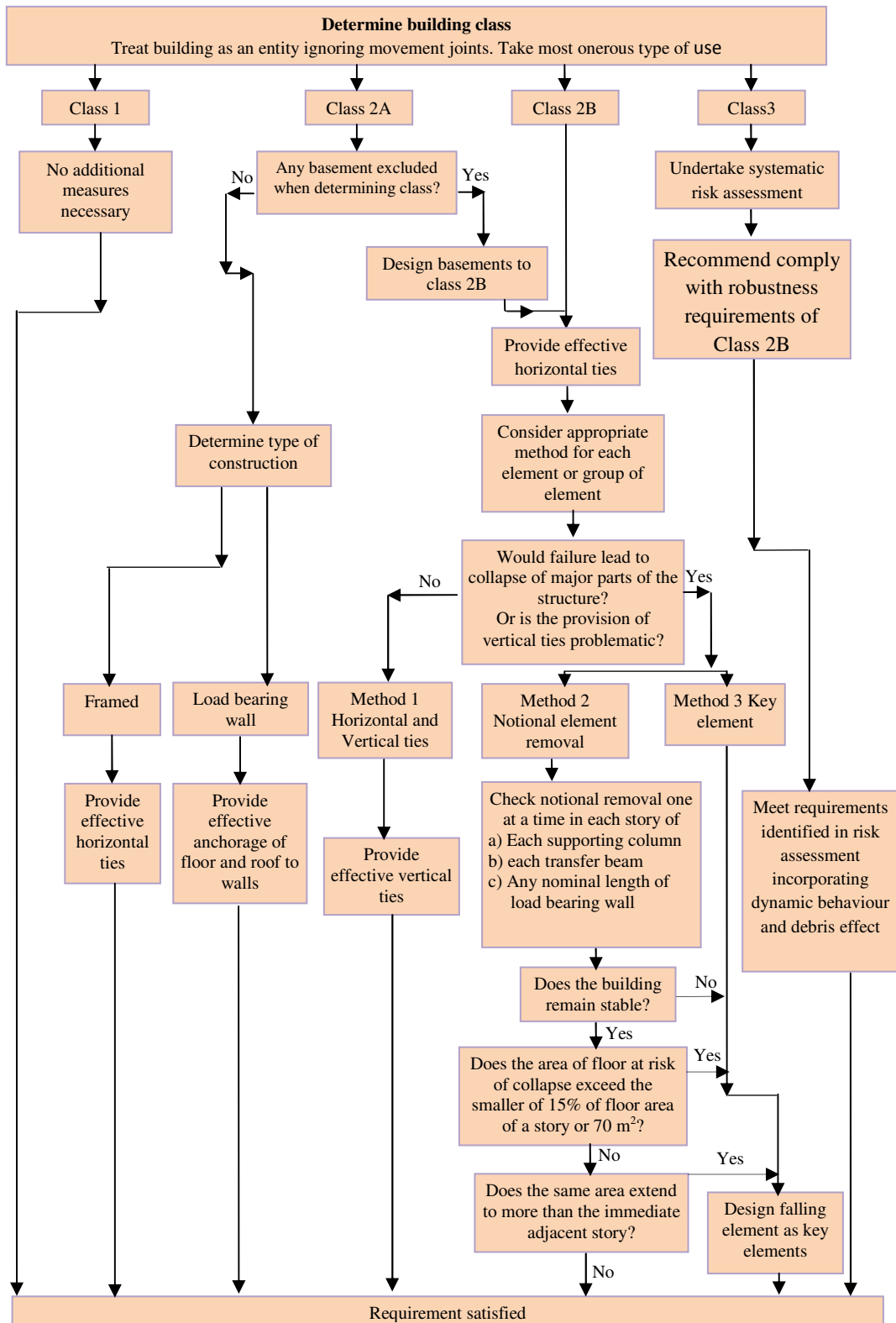
Z is the lesser of:

5 times the clear storey height H (m), or

the greatest distance in metres in the direction of the tie, between the centres of the column or vertical load-bearing members whether this distance is spanned by:

- a single slab or
- a system of beams and slabs.

Table 2-2 Building class and solution strategies (BS EN 1991-1-7:2006)



2.4.3 American Society of Civil Engineering (ASCE 7-05)

The American Society of Civil Engineering (ASCE 7-02) mainly focuses on redundancy and alternate load paths, without any specific mention of degree of redundancy, and requirements are entirely threat-independent. ASCE 7-05 considers two methods to prevent progressive collapse as follows:

Direct design method: in this method, the resistance of a structure to prevent progressive collapse is considered explicitly in the design process through the following approaches:

- a) Alternate load path method: it provides alternate load paths to bridge over localized damage and prevents progressive collapse.
- b) Specific local resistance method: it provides sufficient strength in the key element to prevent failure from accidental loads. In this method any local failure is not allowed.

According to ASCE in the first stage one load bearing element is removed and then the remaining structure should be capable of sustaining the following load:

$$L^{ASCE} = (0.9 \text{ or } 1.2) D + (0.5L \text{ or } 0.25 S_n) + 0.2W \quad (2.5)$$

Where:

D, L, S_n , W, are dead, live, snow, and wind load, respectively.

Indirect Design: in this prescriptive method, the minimum levels of strength, continuity, and ductility are provided.

2.4.4 General Services Administration (GSA) Progressive Collapse Guidelines 2003

GSA guidelines mainly provide rules for analysis and design of new federal office buildings. To reduce the effect of progressive collapse, the GSA publication employs a threat independent approach. It introduces a process to determine the necessity of a design to prevent progressive collapse considering the type of building without any reference to level of

threat, but focuses on redundancy as GSA 2000. The overall recommendation is that in case of removal of one column or wall, the failure should be smaller than the bay adjacent to the removed elements or:

- 330 m² at the floor directly above and below interior removed element, and
- 170 m² at the floor directly above and below exterior removed element.

It can be seen that the GSA limits for local damage are much relaxed than the British Standard and BSEN 1991-1-7 (2006). The GSA provision stipulates the alternate load path to prevent progressive collapse and has recognized the use of linear analysis (for buildings of 10 or less storeys) or nonlinear analysis (for buildings of more than 10 storeys) to evaluate the structure after notional removal of a vertical load bearing wall or column support. The factored load combinations recommended are:

Static analysis to apply to entire structure:

$$L^{GSA} = 2.0(D + 0.25L) \quad (2.6)$$

Dynamic analysis to apply to entire structure

$$L^{GSA} = D + 0.25L \quad (2.7)$$

Where D = Dead Load, and L = Floor Live load.

2.4.5 American Department of Defence (2013)

Due to recent test data and analytical models related to design for progressive collapse of concrete, steel and wood structures, DoD 2005 UFC 4-023-03 was updated in 2013. These updates show a significant change to the 25th January 2005 version. The magnitude and location of tie forces has been greatly revised. The current TF method has been revised based on the catenary action mechanism. The location and size of load-bearing walls has significantly been changed. Generally, resistance to progressive collapse is considerably greater since the DoD 2005 version or BS 8110-1:1997 and BS EN 1991-1-7:2006; hence the

relevant costs will be significantly greater due to the increased force requirement, while for the APL method there is not a considerable difference between the two versions.

According to DoD (2013) UCF 4-023-03, all structures of three storeys or more should be designed for progressive collapse. It is notable that this limitation in BS 8110-1:1997 is five storeys. DoD (2013) uses the design approach of ASCE 7, which defines two main methods to design a structure for progressive collapse or reducing the disproportionate collapse. To provide different levels of resistance to progressive collapse, according to the Occupancy Category (OC), three structural response modes are defined. (1) Tie force facilitating catenary response and (2) Alternate load path, through which structures should be capable to bridge over removed elements. (3) Enhanced local resistance, in which the capacity of perimeter walls or columns are increased to reduce the probability of local failure. A significant portion of the design guidelines and criteria in the UFC are based on the British Standards approach. Furthermore, DoD 2013 states “for load-bearing wall structures, the Alternate Path approach will often be the most practical choice”.

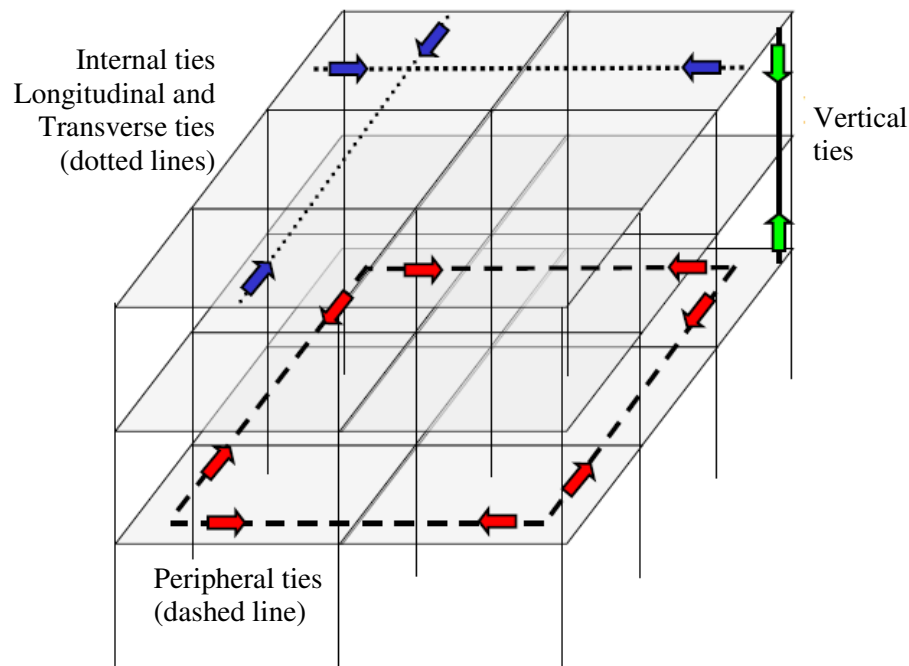


Figure 2.12 Tie force in frame structures (DoD, 2013)

2.4.5.1 Indirect Design Approaches (Tie Force Method)

In this method, minimum levels of continuity, ductility and redundancy are provided by specifying the minimum strength needed to tie the whole structure together. Although this method is similar to the British Standard and the current provision in the Eurocode, while the tie force requirement is significantly greater than those codes. With this approach, the whole structure is mechanically tied together using four different ties i.e. transfer, longitudinal, peripheral and vertical ties (Fig. 2.12). DoD (2013) states “Unless the structural members (beams, girders) and their connections can be shown capable of carrying the required longitudinal, transverse, or peripheral tie force magnitudes while undergoing rotations of 0.20-rad (11.3-deg), the longitudinal, transverse, and peripheral tie forces are to be carried by the floor and roof system”. The precast concrete floor plank with concrete topping with a effective mechanical connection, cast-in-place concrete and composite deck, have been recognised by DoD (2013) to carry the load following local damage.

To apply the TF method, the frame and two-way load bearing structures need to have at least four bays in each direction. Furthermore, for the structures with a one-way load bearing wall, a minimum of four bays must be provided in the direction of the one-way slabs. The length of load bearing walls must be $4h_w$ or greater where h_w is the clear storey height. The tie force requirement for the frame and the load bearing wall is more or less similar. For a one-way floor system, the required tie strength in longitudinal and transverse directions is

$$F_i = 3w_F L_i \quad (2.8)$$

Where

F_i = Tie strength (kN)

w_F = Floor load (kN / m²); $w_F = 1.2D + 0.5L$; D = Dead load (kN / m²), L = Live load (kN / m²)

L_i = L_L = Greater distance between two adjacent wall supports in the longitudinal direction,

L_T = the distance in transverse direction which is lesser of:

- $5h_w$; h_w = clear story height (m)

- Width of structure in the transverse direction (m)

The definition of L_1 is shown in Figure 2.13.

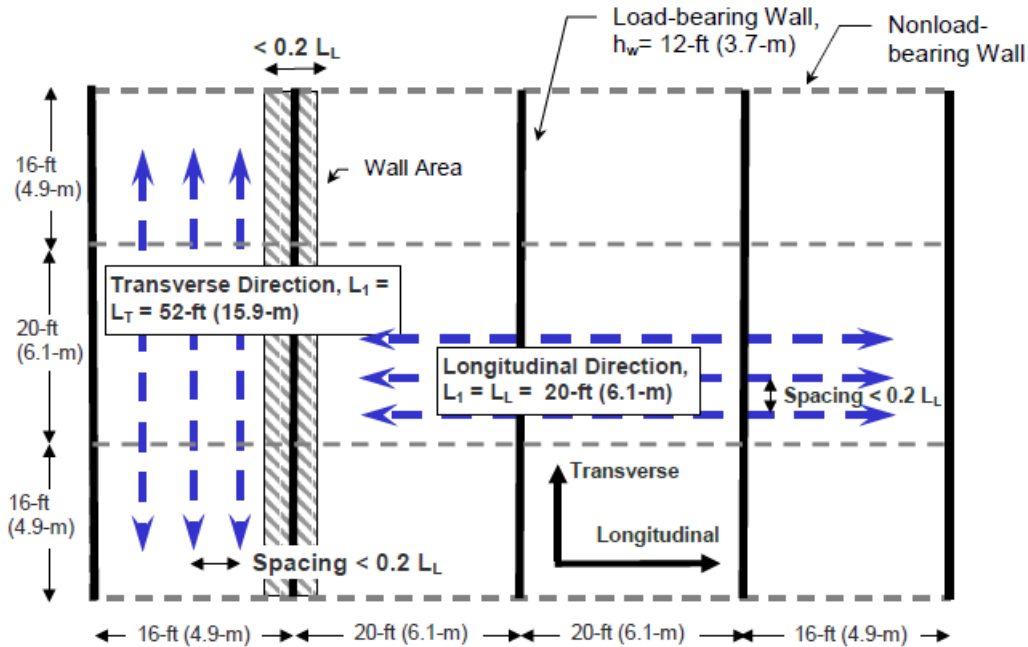


Figure 2.13 Determination of L_1 for one-way load-bearing wall construction (DoD, 2013)

2.4.5.2 Direct Design Approaches

This method includes “explicit consideration of resistance to progressive collapse during the design process” (DoD, 2013) and it can be categorised in 1) the Alternate Load Path (AP) method, in which a structure must be capable to bridge over the load from the damaged part to the remaining undamaged part; and 2) the Specific Local Resistance (SLR) method, which requires that a certain element or part of structure must be able to resist a specific load and threat (key element).

2.4.5.3 Alternate Load Path Method

This method is mostly based on LRFD philosophy of ASCE 7-02 by using a new load factor combination to consider intensive loading and a resistance factor to introduce a design factor.

DoD 2013 recommends 3-dimensional models to analyze a structure to eliminate any negative effect of simplifications. Three different analysis approaches have been defined by DoD 2013 as follows:

Linear static: the behaviour of material is considered as linear elastic and the geometric formulation is developed through assuming a small deformation. In this method, load will be applied at one time and hinges in some areas are accepted.

Nonlinear static: the geometry and material are treated as non-linear. With knocking out a load-bearing wall, a full factored load is applied to the structures. In this case, the following factored load combination should be applied to the adjacent bays to the removed wall support and all floors above the removed element:

$$L^{DoD} = 2[1.2 D + (0.5L \text{ or } 0.2S)] \quad (2.9)$$

Nonlinear dynamic: both geometry and material are treated as non-linear and the following gravity load combination should be applied to the entire structure:

$$L^{DoD} = 1.2 D + (0.5L \text{ or } 0.2S) \quad (2.10)$$

where:

D , L , and S are Dead, Live, and Snow load, respectively (in kN/m^2).

2.4.6 Summary

The rules to prevent progressive collapse emerged in the codes following the partial failure of the Ronan Point apartment in 1968. The British Regulation (Fifth Amendment) 1970 developed the provisions for alternate load path, key element, and tie force method. Following the UK standards, most national codes have adopted these three rules to prevent progressive collapse, e.g. the American Department of Defence (DoD 2005), the Eurocodes (EN 1992 1-1:2004), American Society of Civil Engineering (ASCE 7-05) and the General Service

Administration (GSA:2003). According to the above discussion on the various codes and standards, it can be concluded that all codes follow the same concept, but it is obvious that the most comprehensive provisions have been adopted in the DoD (2013).

Although in some cases, these provisions have proven successful in sustaining buildings against remarkable damage, but they have been subjected to numerous criticisms. Most reviewers imply that these rules are not well documented over the time. On the other hand, it is generally agreed that ductility and continuity are the two most important factors to prevent progressive collapse; however, the TF method, more or less, are based on strength rather than ductility.

2.5 EFFICIENCY OF CURRENT TIE FORCE (TF) METHOD

The tensile tie force (TF) method is one of the main design approaches for preventing progressive collapse; whereby an indeterminate structure is analyzed statically through assuming a failure mode for a locally simplified determinate structure. To establish catenary action and prevent progressive collapse following removal of a load bearing wall, the TF method was established in the BS8110-1:1997 for the first time after the well known Ronan Point event (Li, 2011). The tie force approach provides a mechanism that allows slabs to span over a removed load bearing wall support. It is emphasised that there is no theoretical justification in which the tie force method can enable elements to bridge over removed wall supports in all circumstances. Hence, a number of theoretical approaches should be developed to address this concern, although some difficulties will exist during justifying the efficiency of ties following removal of a corner wall. On the other hand, although the tie force method's requirements are given by codes of practice, there is no specific provision to provide ductility; hence further difficulties might exist again in relying on catenary and membrane action (Mann et al., 2010).

These prescriptive tie requirements may have proven adequate in engineering practice, but are not fully scientifically justified; therefore substantial efforts are still needed to improve understanding at a fundamental level of how the mechanism of post-collapse resistance is developed through these tie provisions. This need has also been supported by a number of researchers in the last decade. Dusenberry (2002) indicated the necessity of a better understanding of the mechanism by which progressive collapse can be resisted. To show adequacy of five current codes and standards, an evaluation on three famous collapsed buildings was performed by Nair (2003).

Table 2-3 Code approaches to design structures for progressive collapse (Nair, 2003)

	ASCE 7-02	ACI 318-02	GSA PBS 2000	GSA PBS 2003	GSA PBS Guidelines
Redundancy	*		*		*
Local resistance					
continuity		*			
Threat-dependent analysis				*	

Table 2.3 shows the approaches to preventing collapse which are used in five discussed codes by Nair. Table 2.4 indicates that approximately all three studied structures are susceptible to progressive collapse. Accordingly, Nair (2003) concluded that the discussed codes and standards might not provide sufficient strength, ductility and continuity to prevent progressive collapse in those structures (Table 2.4)

Table 2-4 Adequacy of codes to prevent progressive collapse (Nair, 2003)

	ASCE 7-02	ACI 318-02	GSA PBS 2000	GSA PBS 2003	GSA PBS Guidelines
Ronan Point	?	Y	?	N	N
Murrah Building	N	?	N	Y	N
WTC 1&2	N	N	N	N	N

Y=yes, N=no, ?=maybe

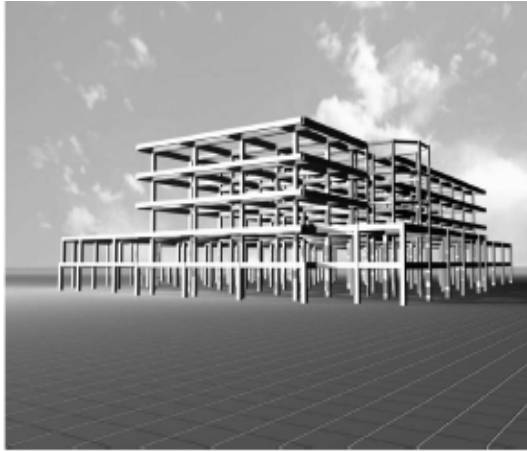


Figure 2.14 3D view of 5 stories concrete structure (Abruzzo et al., 2006)

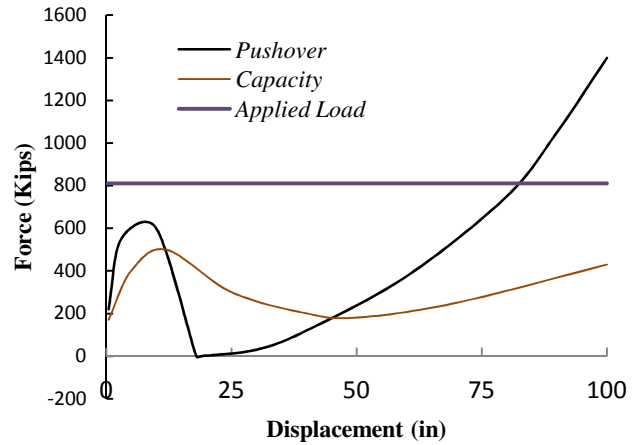


Figure 2.15 Load vs. deflection at the location of removed column (Abruzzo et al., 2006)

Abruzzo et al. (2006) conducted a nonlinear dynamic analysis on a five storey concrete building which met the ACI's integrity requirement and DoD 2005 tie force provision (Fig. 2.14 and 2.15). The result indicated that those regulations significantly underestimated the tie strength requirement and the structure was remarkably susceptible to progressive collapse following removal of one column support.

To evaluate the adequacy of the tie strength method, Li et al. (2011) conducted a numerical study on two different frame structures of three and eight storeys by considering normal seismic load, the DoD alternate load path method (AP) and the TF design method. The susceptibility of the two structures in the case of normal seismic design and current tie strength design was quite identical. The numerical results revealed that the current tie force method cannot provide a safeguard to progressive collapse for all RC structures with different number of storeys and experience damage in different locations; accordingly, an improved TF method was proposed.

$$F_i > \beta q L_i L_j / \delta_s \quad (2.11)$$

Where $\beta = 0.67$ is the internal force modification factor; q in the uniformly distributed load acting on the elements; L_i and L_j are the span length of beams at the left and right of the removed column; and $\delta_s = L/5$. Eq. (2.11) indicates significant revision to the TF method

adapted in BS8110-1:1997, BS EN 1991-1-7:2006, DoD 2005 while it is relatively close to the DoD 2013 TF requirement.

This conclusion has been further confirmed by the latest edition of the DoD (2013) design criteria published in 2013, in which the required tie force has been increased significantly compared to the previous recommendations quoted in the DoD (2005) and the British Standard. Another criticism of the TF method has been recently raised by several researchers who believe that it does not take into account the behaviour of the structure as a whole (Yan et al. 2013; Spyridaki et al. 2013; Ettouney et al. 2006). In addressing this issue they proposed that, a global analysis of progressive collapse should be performed by considering the loss of stiffness in local regions.

2.5.1 Tie Force (TF) Analysis

The current tie force method has been developed in terms of tie strength F_t , which is the minimum tensile tie force to prevent progressive collapse. In real structures, loads are distributed in a 3-D manner, while the current TF method considers a 2-D catenary model for calculating the basic tie strength; hence the effect of the spans in a different direction is not taken into account and the tie forces are calculated individually (Mann et al., 2010). According to current codes and standards, the basic tie strength is the less of $20+4n_o$ and 60 kN/m, where n_o is the number of storeys of the building; which indicates that buildings with more storeys would be more vulnerable to progressive collapse. The first magnitude is empirical without any theoretical verification (Li et. al. 2011) and the second value can be defined based on the catenary action mechanism or the limit state failure mode. Considering this assumption, the structure can be considered as a determinate system instead of a complex indeterminate structure. It is assumed that in the catenary behaviour under a limited vertical deflection, tensile tie strength will be provided so that collapse is avoided. In Eq. (2.2a), by equating F_t to F_t and for a one storey building we have:

$$F_t = \frac{wb_p l_b^2}{2\delta_s} \quad (2.12)$$

Where, F_t is the total tensile force at the mid-support. By considering $b_p = 1m$, $\delta_s = l_b / 5$ and $w = (D+L/3) = 4.8 \text{ kN} / m^2$, the basic tie strength can be calculated i.e. $F_t = 60 \text{ kN} / m$ (DoD 2005). The above calculation indicates that the required basic tie strength has been developed considering a one storey building, while the term of $20+4n_o$ provides the same value considering a 10 storey building, which needs to be clarified. Furthermore, the above calculation clearly indicates that the effect of the impact factor has not been applied. However, applying the required basic tie strength and impact factor of 2 to the TF method in the British Standard or Eurocode leads to relatively the same result as of DoD 2013:

$$P = 3.2(g_k + q_k)l_b \quad \text{kN} / m \quad (2.13)$$

The numerical study conducted by Li et al. (2011) shows if the number of storeys above the removed column increase, the redundancy of the remaining structure is higher due to various alternate load paths which exist to transfer the applied loads to the undamaged part of the structure. In other words, in structures with more storeys resistance against progressive collapse is increased, thus demand for progressive collapse is decreased; while based on the empirical magnitude of the tie strength $F_t = 20+4n_o \text{ kN} / m$, the progressive design demand is increased with the higher number of storeys. It is important to note that the basic tie strength $F_t = 20+4n_o \text{ kN} / m$ underestimates tie force demand for low rise and higher storeys in a high rise building, accordingly the imperial term was not taken into account by Li et al. (2011).

2.6 EXPERIMENTAL STUDIES ON PROGRESSIVE COLLAPSE

Compared with the experimental studies on the catenary action of steel structures, limited experimental studies are available on the study of the catenary action in RC structures (Yun,

2010). This is especially the case for the multi-storey precast concrete cross wall buildings (Pekau and Cui, 2006). PCA's experimental studies and Regan (1975) are the only published work on the performance of cross wall structures in terms of developing the catenary action and mitigating the progressive collapse considering the floor joint behaviour. The recent research mostly focused on the behaviour of walls during progressive collapse (Pekau and Cui, 2006; Scanlon and Kianoush, 1988).

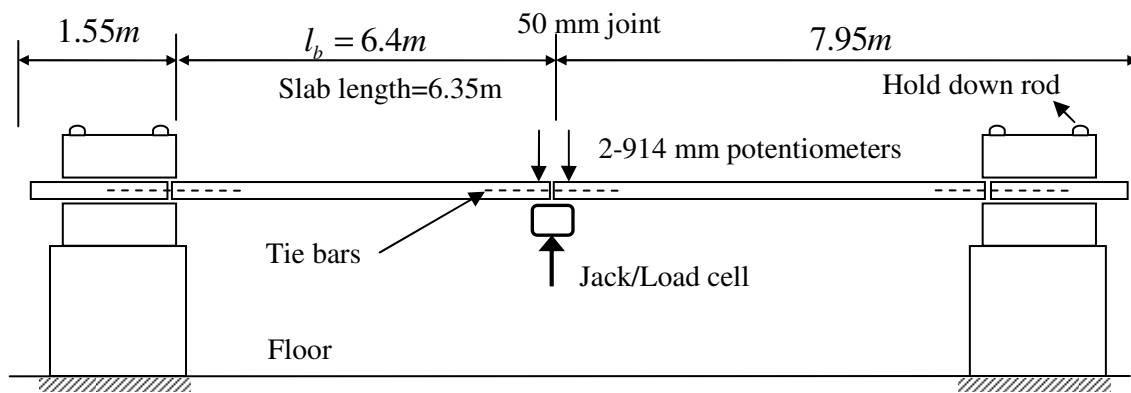


Figure 2.16 Two floor-to-floor test specimens (PCA, 1975-1979)

In order to evaluate the catenary action mechanism in precast cross wall structures' floor system; examine the feasibility of providing longitudinal ties in the key ways; and the performance of short lengths of 7-wire high tensile pre-stressing strand; an experimental study on four full scale two-span slab systems was undertaken by PCA (1975-1979). In each test, the partial loss of support due to some abnormal loading was simulated by slowly lowering the middle support. In this study, the longitudinal ties were placed in the keyway between adjacent floors, where the distance between ties was one metre in three tests and in the last test it was 600 mm (Fig.2.16). In all the tests dead load i.e. 63 lb/sq.ft (3.1 kN/m²) plus 50% of live load i.e. 20 lb/sq.ft (1 kN/m²) was applied on the floors i.e. D+0.5L. Variation of the middle support reaction/original reaction ratio with vertical deflection is shown in Fig 2.17,

where zero percent shows the complete catenary action of the floor system. The result indicated that the catenary action system was developed in none of the tests. PCA (1975-1979) attributed this unexpected result to incorrect length, size of ties and especially boundary condition.

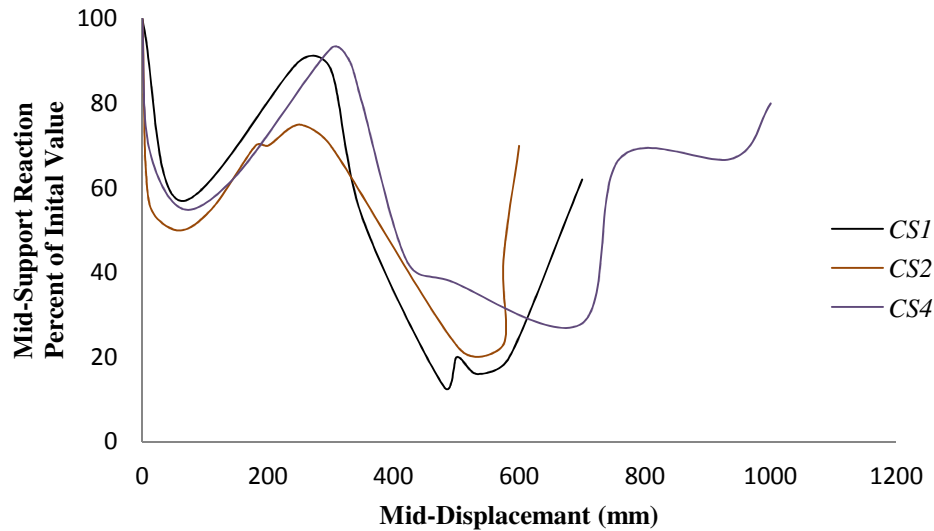


Figure 2.17 Middle reaction support vs. middle joint deflection (PCA, 1975-1979)

Based on pullout and full scale tests, PCA have proposed that to provide effective catenary action δ_s / l_b should be more than 5% and less than 15%. This limit was defined as a safe region to design longitudinal ties. It is notable that, considering the DoD's 2005 recommendation and the laboratory test conducted by Yi et al. (2008) regarding to the fracture limit for RC frame structures, Li et al. (2011) proposed an ultimate deformation of 0.06L and 0.2L for beam and catenary action, respectively.

To study the possibility of developing a catenary action, several tests on two spans of precast floor strips were carried out by Regan (1975) at the Imperial College in London. The specimens were two 9ft slabs with a joint between them representing the removed wall support and 14 in. to 28in. wide. The 2in. cast-in-place topping was used at the top of a 2in. thick precast slab (Fig. 2.18).

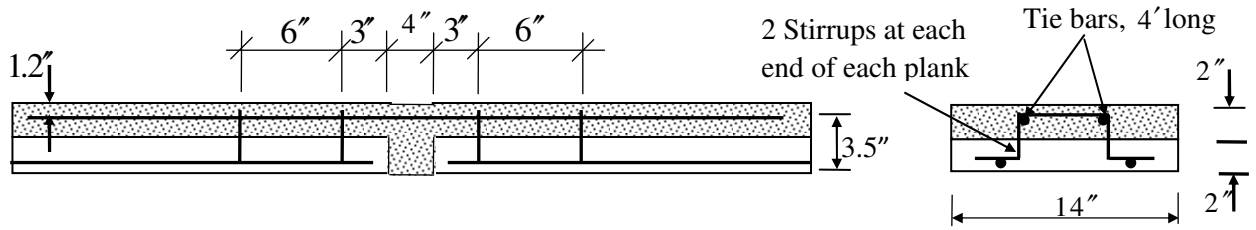


Figure 2.18 The details of the joints (Regan, 1975)

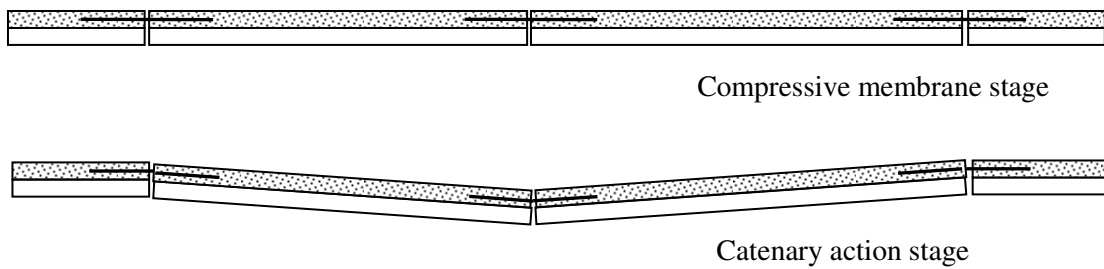


Figure 2.19 Catenary behaviour of specimen (Regan, 1975)

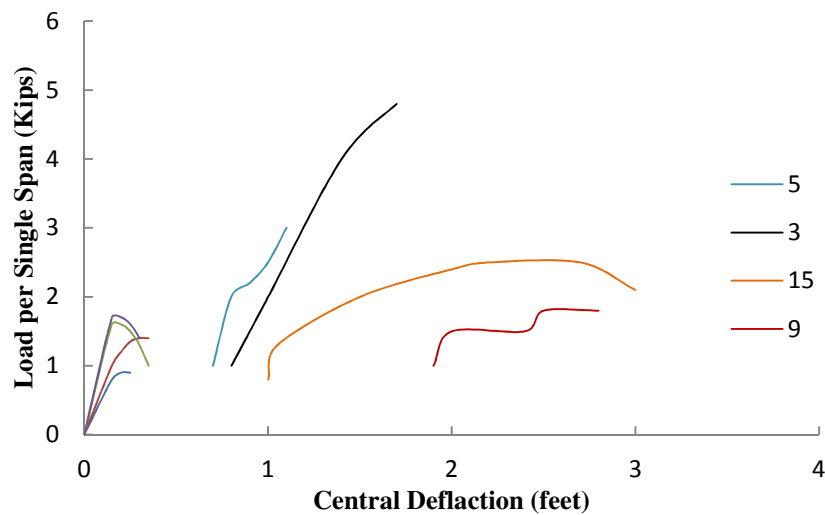


Figure 2.20 Applied load vs. middle joint deflection for different specimens (Regan, 1975)

The results indicated that for all specimens there were two different stages i.e. the compressive arch phase and the catenary action mechanism (Fig. 2.19/2.20). It was observed that the majority of specimens failed due to the fracture of the bottom bars at the middle joints at a deflection of 10-13% of slab length (Specimen 5, Fig. 2.20); while only a few specimens failed due to yield in the side bars before yielding of the bottom bars (Specimen 3, Fig. 2.20), which provided higher catenary load and ultimate deflection was around 20% slab length.

According to the test result, Regan (1975) stated “successful development of a catenary action requires that the members in question possess not only tensile strength but also ductility, which is largely determined by the detailing of the longitudinal reinforcement.”

To investigate the behaviour of the perimeter beam in RC structures following the removal of a column, an experimental study on 3/8 scaled model of two spanning RC beams representing a seven storey building (Fig. 2.21) was carried out by Sasani and Kropelniki (2007). The structure was designed based on ACI 318, 2002. The result indicated that, in spite of bottom reinforcement bars at the one side of the removed column fracturing, the beam had significant remaining capacity and the catenary action was established through the top bars (Fig. 2.22). The result indicates that the ultimate capacity in the catenary stage at a deflection/span ratio of 17.38% is less than in the plastic phase (Fig. 2.22).

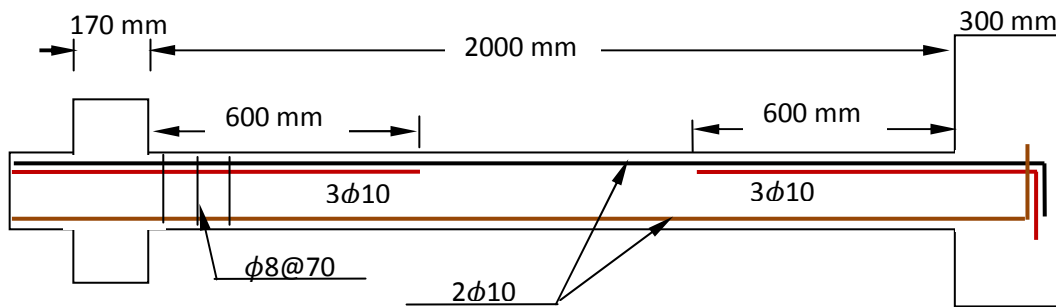


Figure 2.21 Reinforcement detailing of a two spans reinforcement beam (Sasani and Kropelnick, 2007)

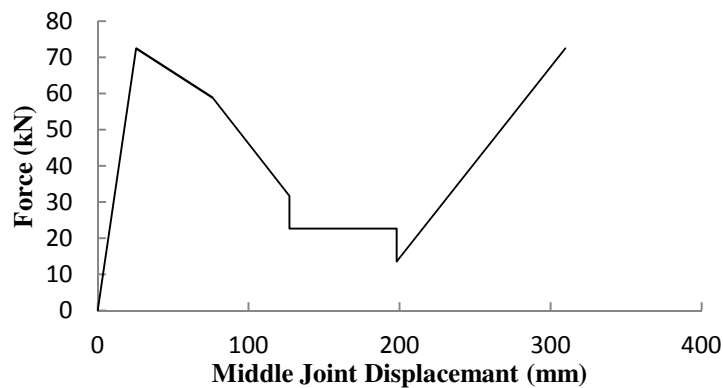
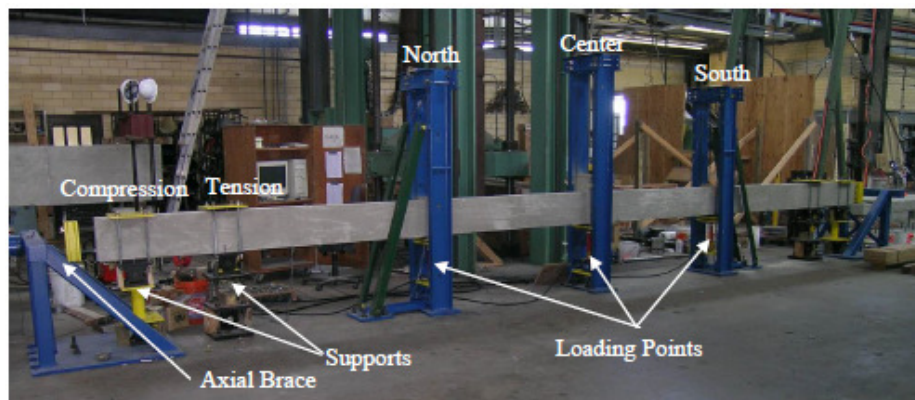
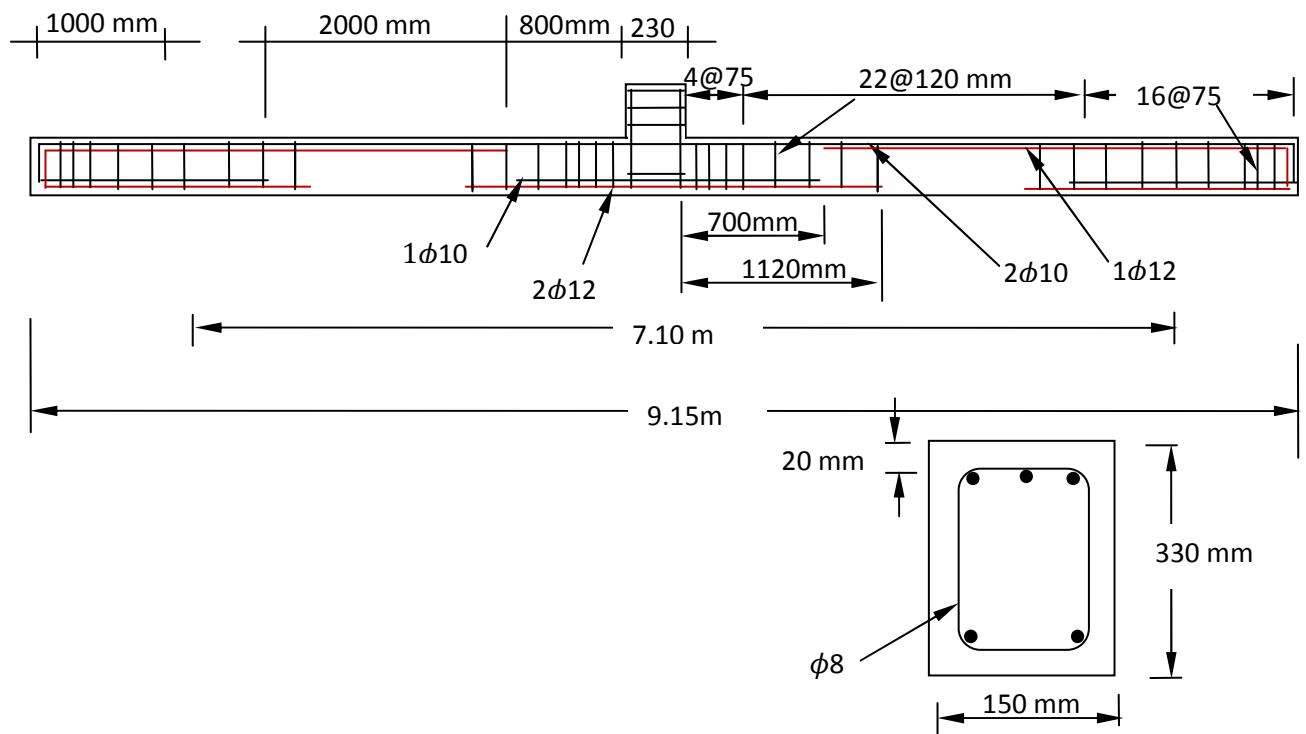


Figure 2.22 Applied load vs. middle joint deflection (Sasani and Kropelnick, 2007)

To study the effect of CFRP on progressive collapse resistance of existing RC structures, an experimental investigation on eight continuity beam tests with no contiguous bars, with contiguous bars and with CFRP to provide continuity at the top and bottom of the beam close to the column, was carried out by Orton (2007) (Fig. 2.23). It was found that the specimen without a continuous bar was capable of active catenary action through transferring tension force from the positive to the negative reinforcement bars (Fig. 2.24); while the specimen with the continuous bars failed to reach the catenary action stage (Fig. 2.25). As the hinge develops at the location of the maximum bending moment, it is expected that following the initial hinge the continuous bars contribute to the catenary action mechanism and active catenary more effectively than the specimens without contiguous reinforcement bars. There is no discussion to highlight the reasons for this behaviour, which is in contrast to all the other experimental work reported herein. Also it is important to note that all experimental studies reported herein clearly indicate the importance of continuous bars to establish catenary action mechanism.

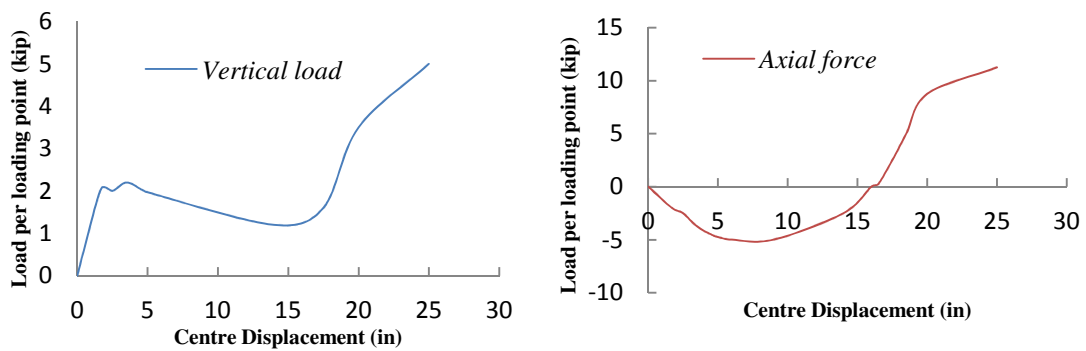


(a) Photo of the test setup



(b) Reinforcement details of beams

Figure 2.23 The layout of test specimen (Orton, 2007)



(b) Applied load vs. middle joint deflection

Figure 2.24 Specimen with no continuous bars (Orton, 2007)

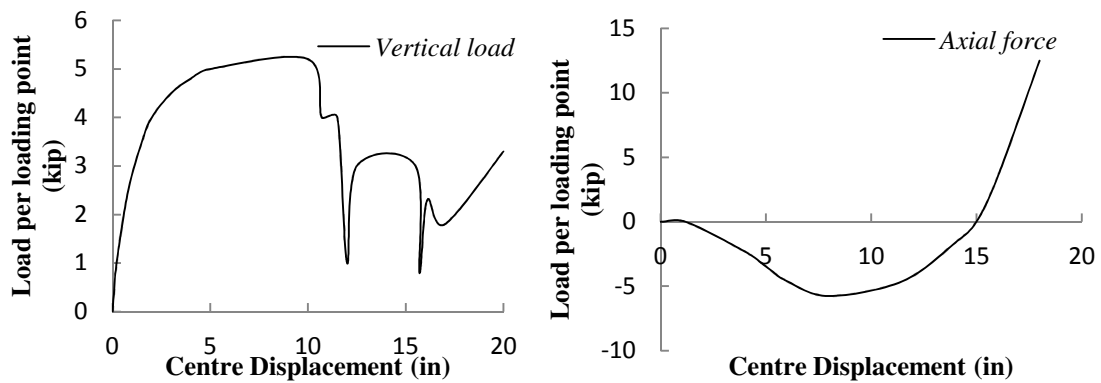


Figure 2.25 Specimen with continuous bars (Orton, 2007)

To study progressive failure behaviour of an RC structure, Yi et al. (2008) conducted an experimental investigation on a one-third scale model of three storeys (Fig. 2.26) representative of an eight storey building designed based on ACI 318-02 code of practice. The beam dimension of 100x200 mm with two 12 mm bar size was used in all beams. They concluded that the conventional code design requirements were capable of providing sufficient collapse resistance to reinforcement structures, while there is no clear comparison between code requirements to prevent progressive collapse with the experimental result. Also, the result indicated that the beam experienced elastic, plastic and catenary stages and the capacity of the structure considering a plastic mechanism was 70% of the total strength of the system at the failure point in the catenary stage at the ultimate deflection/span ration of 16.8% (Fig. 2.27).

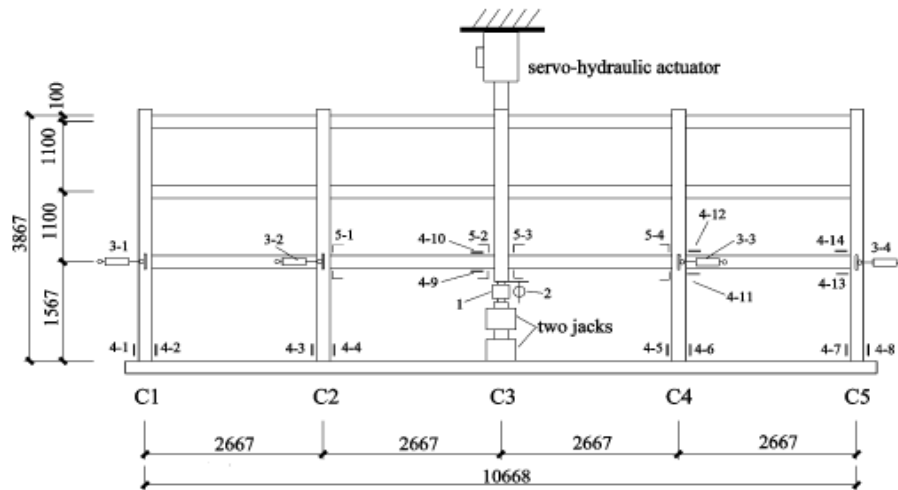


Figure 2.26 details of model frame and instrumentation layout (Yi et al., 2008)

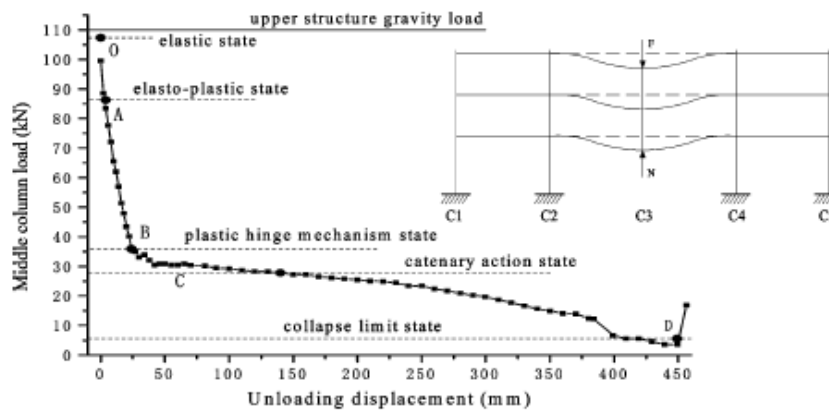
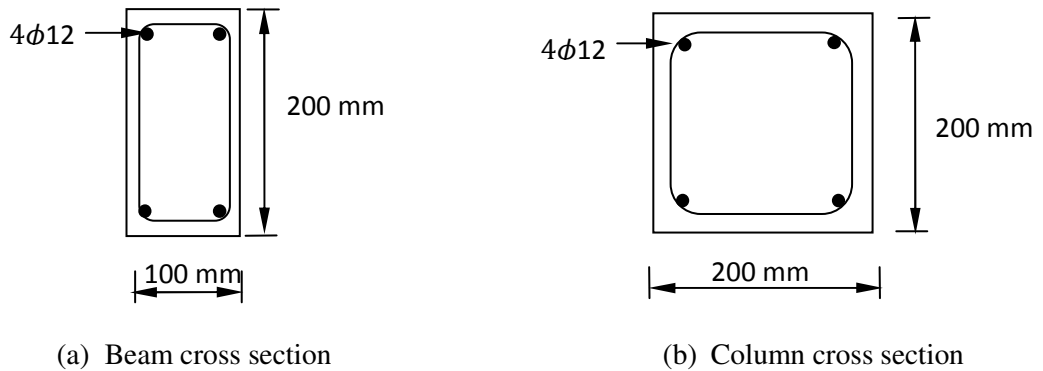


Figure 2.27 Reaction support on the jack under middle column (N) versus middle joint deflection (Yi et al., 2008)

To study the ability of RC structures in resisting disproportionate collapse, an investigation on five simple support RC beam-column-resistance sub-structures with different arrangements of steel bars (Fig. 2.28) was conducted by He and Yi (2008). The specimens were designed

based on different steel ratios i.e. 0.7% and 1.4% using various yielding capacity of reinforcement bars i.e. 400, 335, 235 MPa with compressive strength of 30MPa.

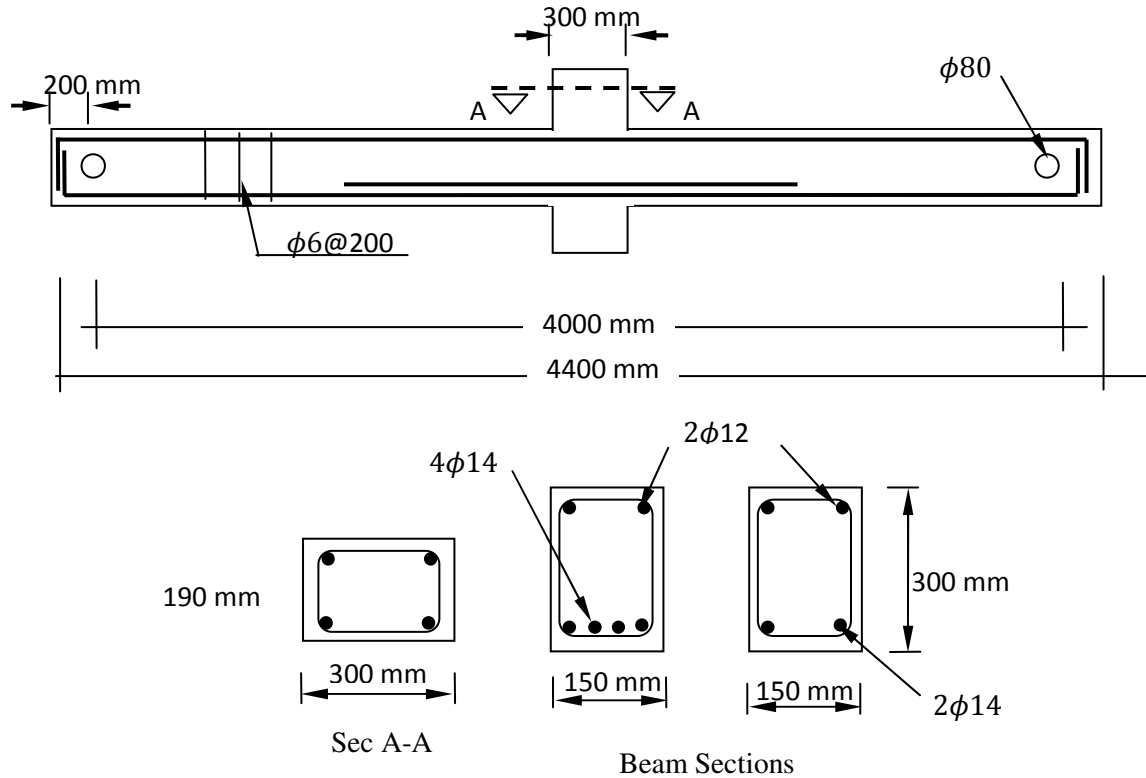


Figure 2.28 Details of test specimens (He and Yi, 2008)

The result indicates that collapse occurred at middle joint deflection/ span ratio around 21.6% which is slightly more than the result obtained by Li et al. (2008), Yi et al. (2008), Sasani (2007), and Orton (2007). Also, the result shows that the ultimate capacity in the catenary stage was about twice as much as in the plastic mechanism (Fig. 2.29); while Yi et al. (2008) stated that it increased by only 30%. It was found that the catenary action strength greatly relies on elongation and the strength of the tie bars. Furthermore, due to in the practical design the cross section of the top bars at the connection are much more than the bottom bars; assuming the cross section of the top bars only 30% of the bottom bars led to meaningful errors in the findings. Furthermore, due to assuming a simple support the collapse mechanism

followed a totally different load-deflection relationship to the result obtained by Sasani and and Kropelniki (2007) and Orton (2007).

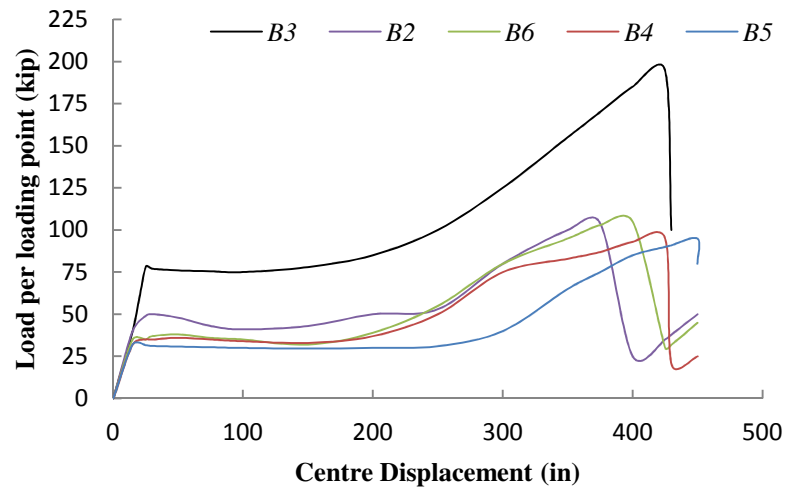


Figure 2.29 Applied load versus middle joint displacement for different specimens (He and Yi, 2008)

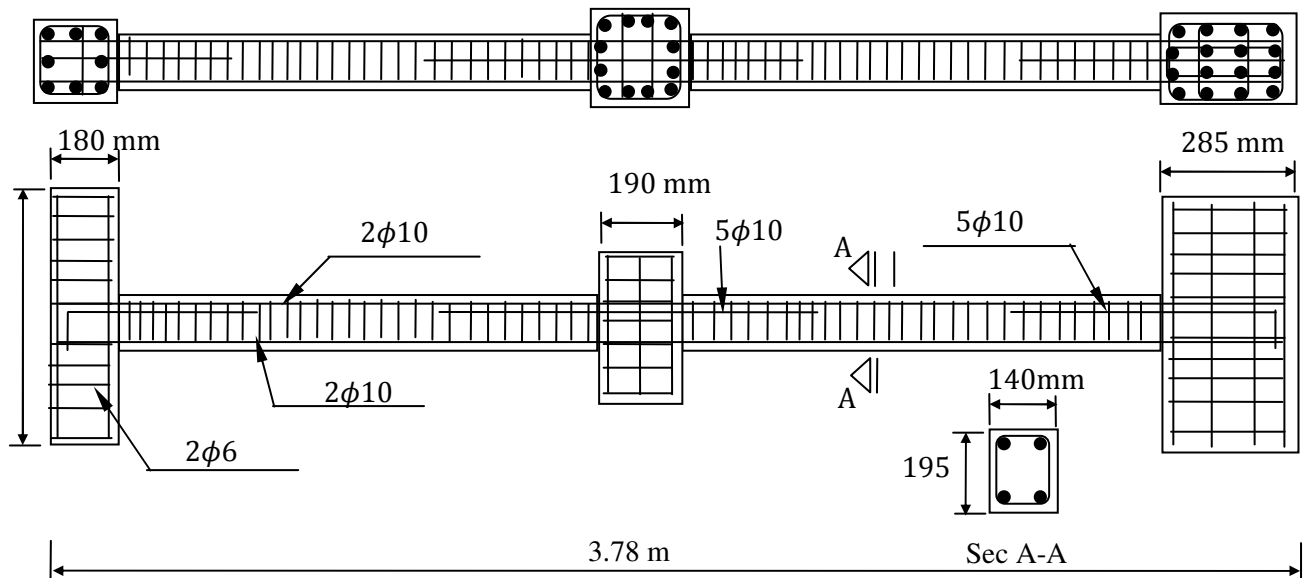
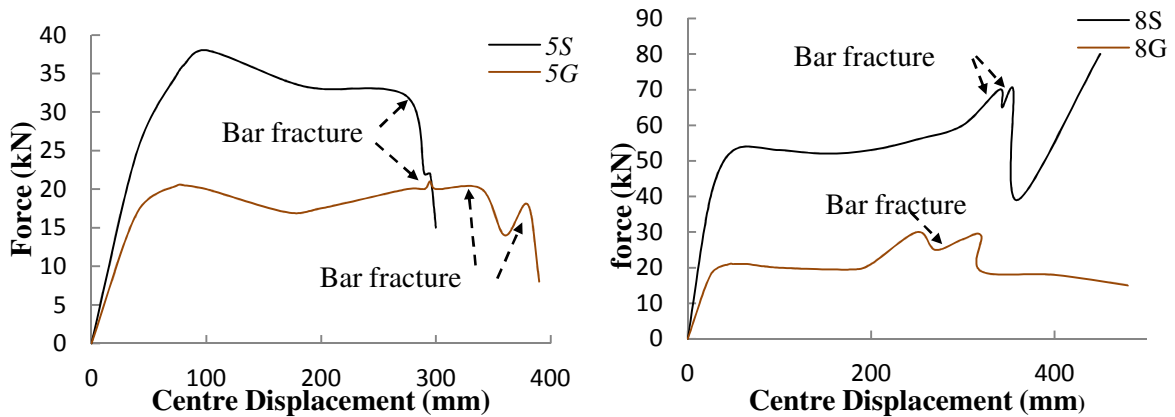


Figure 2.30 The layout of test specimens; seismic load resisting system (Trung et al. 2010)

To study the progressive collapse capacity of RC beam-column sub assemblages following removal of a supporting column, a scaled experimental investigation on four specimens using

different concrete compressive strength and re-bar detailing was carried out by Trung et al. (2010). The scales of the specimen's representative of five and eight storeys were 37% and 35%, respectively (Fig. 2.30). The specimens were designed in two levels of seismic (S) and non-seismic detailing (G) based on ACI 2005. The results indicated that the progressive collapse resistance of specimens designed for seismic load was two times of specimens without seismic detailing (Fig. 2.31); while Yi et al. (2008) experimental work shows only a 30% increase for the same concept. Furthermore, it was observed that in specimens with lower compressive strength i.e. 17MPa due to concrete crushing at the beam-column joint, catenary action was not established. They concluded that only specimens with a high compressive strength and seismic reinforcement bar detailing are capable to activate the catenary action mechanism.



(a) Sub-assembly of 5-story structure,

$f_{ck}=17$ MPa

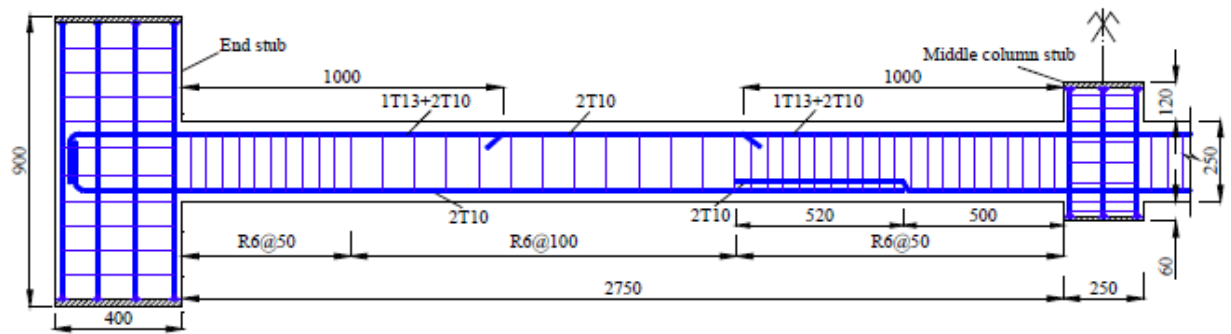
(b) Sub-assembly of 8-story structure,

$f_{ck}=30$ MPa

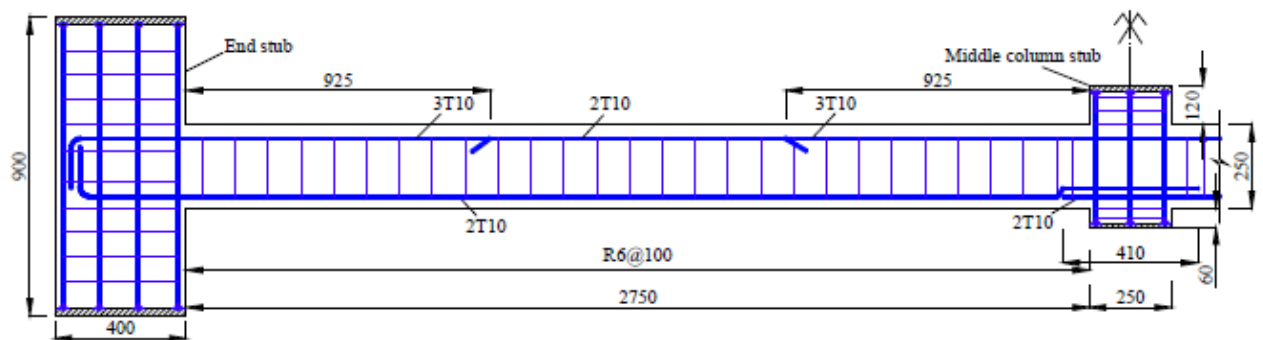
Figure 2.31 Applied load vs. middle joint deflection (Trung et al. 2010)

Yu and Tan (2010) conducted an investigation on two one-half scaled beam-column sub-assembly specimens with three spans and actual bar arrangement of a bar at the top and bottom of the RC beams designed according to ACI 318-05 (Fig. 2.32). Considering various reinforcement ratios at the top and bottom of the RC beams overcame the deficiency of Yi et

al. (2008) work and using a column with a fixed boundary condition overcame the weakness of the study conducted by He and Yi (2008).



(a) Seismic specimen S1



(b) Non-Seismic specimen S2



(a) Test Specimen

Figure 2.32 The detailing and Layout of beam-column sub-assemblages (Yu and Tan, 2010)

The results indicate that the current ACI 318-05 regulation is capable of establishing catenary action. It was found that the strength of catenary action is more than the capacity of a plastic

mechanism by 76.2% and 65.5% for the specimens with non-seismic and seismic detailing, respectively (Fig. 2.33). This result is more than two times higher than the result obtained by Yi et al. (2008) and it is 87% of the ultimate capacity provided by the experimental study of He and Yi (2008). The result also indicated that the maximum deflection/span length ratio at the collapse was 21.81%, which is slightly more than the previous works. Furthermore, it was found that the failure was not controlled by a bar fracture of the top bars at the middle joints, but it is bar fracture of the beam ends which controls the failure of the specimen; which is totally in contrast with He and Yi's (2008) conclusion while confirms the results obtained by Trung et al. (2010). Figure 2.33 clearly indicates that it is tie strength and deflection which affects the capacity of specimens rather than the detailing provided based on seismic and non-seismic requirements, while Trung et al. (2010) experimental study indicated that the catenary strength of specimens with the seismic detailing is twice that of the non-seismic reinforcement requirement.

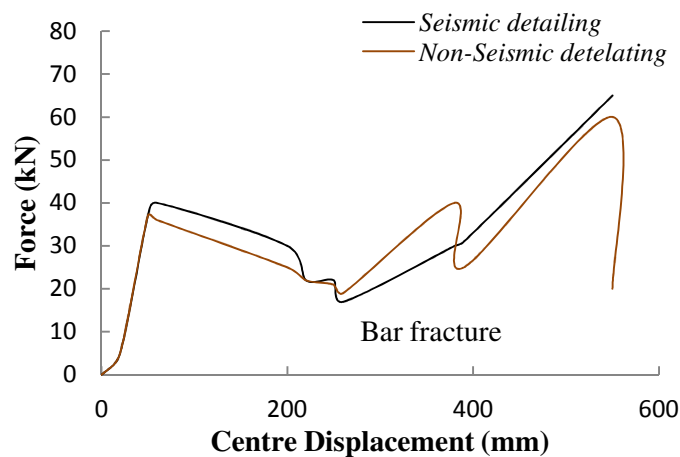


Figure 2.33 Applied load vs. middle joint deflection (Yu and Tan, 2010)

Discussion

The experimental study conducted by PCA (1975-1979) indicates that catenary action can be achieved through pullout failure mode by using proper embedment length, strand size and grout strength. As only tie force-middle joint deflection had been recorded, the strength of the

system had been obtained using catenary action behaviour i.e. Eq. (2.2), hence the actual progressive collapse resistance of a floor-to-floor system through these full scale tests cannot be monitored. Furthermore, all specimens failed due to boundary condition errors; hence the real performance and efficiency of pullout failure mode to develop catenary action cannot be evaluated using the test results. The experimental study conducted by Regan (1975) indicate that most of the specimens failed due to bar fracture at the middle without any obvious catenary action, while the specimens with fracture at the side bars showed clear evidence of catenary action.

The majority of experimental study on the progressive resistance capacity of RC structures indicates that the specimens with seismic detailing of the reinforcement bars are capable of establishing effective catenary action with ultimate strength more than the plastic phase. It was found that maximum strength significantly varies with different boundary conditions, while the majority of specimens approximately resulted in the same deflection/span ration i.e. $17 \leq \delta_s/l_b \leq 21$. However, there are remarkable discrepancies between the abovementioned experimental studies. While Sasani and Kropelniki (2007) concluded that the strength of a two spans beam in the catenary stage is slightly less than in the plastic phase, with roughly the same properties of specimens, Yu and Tan (2010), Yi et al. (2008), He and Yi (2008) obtained catenary/plastic strength ratios of 1.75, 1.35 and 2.0, respectively. On the other hand, Trung et al. (2010) state that strength of specimens with seismic re-bars detailing is more than two times that of specimens with no seismic detailing; while Yi et al. (2010) indicate that there is no meaningful difference between two specimens, which can be considered as a significant discrepancy. Furthermore, Orton (2007) argues that specimens with continuous reinforcement bars cannot activate catenary action, which is totally in contrast to all other experimental studies. Finally, the main deficiency of the experimental studies is that they have not established any comparison between applied loads considering the impact factor and load combination provided by GSA (2003) or DoD (2005) with progressive resistance collapse of the specimens. Also, the results clearly indicate that the progressive collapse resistance of RC

structures still has not been standardized and the phenomenon remains hazy which needs further and comprehensive investigation to obtain actual progressive behaviour of structures with various re-bars detailing.

2.7 NUMERICAL STUDY ON PROGRESSIVE COLLAPSE

To design a safe and economical structure against progressive collapse due to any abnormal loads, developing comprehensive progressive analysis seems to be essential. Due to unforeseeable consequences of disaster, any type of progressive analysis needs to be reliable and able to provide concise and accurate methodology to reproduce the actual behaviour of a structure. Thus, to develop efficient, straightforward and reliable methods a great deal of effort has been put into researches conducted in the last decades. A review of recent numerical studies of progressive collapse indicates that the commercial nonlinear FE programmes of ABAQUS (Usmani, 2003; Lee et al., 2009), ADAPTIC (Izzuddin et al., 2008; Vlassis et al., 2008), FEAP (Hartmann et al., 2008; Moller, et al., 2008), LS-DYNA (Khandelwala et al., 2009; Moller et al., 2008), and SAP2000 (Marjanishvili, 2004; Bae et al. 2008) have been used in most of the works (Kwasniewski, 2010). Beam element dominated most of the modelling strategy and most consideration was based on a 2D subsystem using numerous simplifications.

To develop a quantitative measurement of the potential for progressive collapse, an energy balance method was presented by Powell (2003). Progressive collapse was considered as a single degree of freedom system with a concentrated mass and nonlinear spring. Based on the proposed procedure, a six-story reinforced concrete building designed based on ACI 318 and was analysed using nonlinear static analysis method. As shown in Figure 2.34 due to the capacity curve is relatively less than load curve, the 2D frame is highly susceptible to progressive collapse, which indicates that code regulation is not able to meet the progressive

collapse demand. To obtain the capacity curve, the energy under the pushover curve is divided by the corresponding deflection.

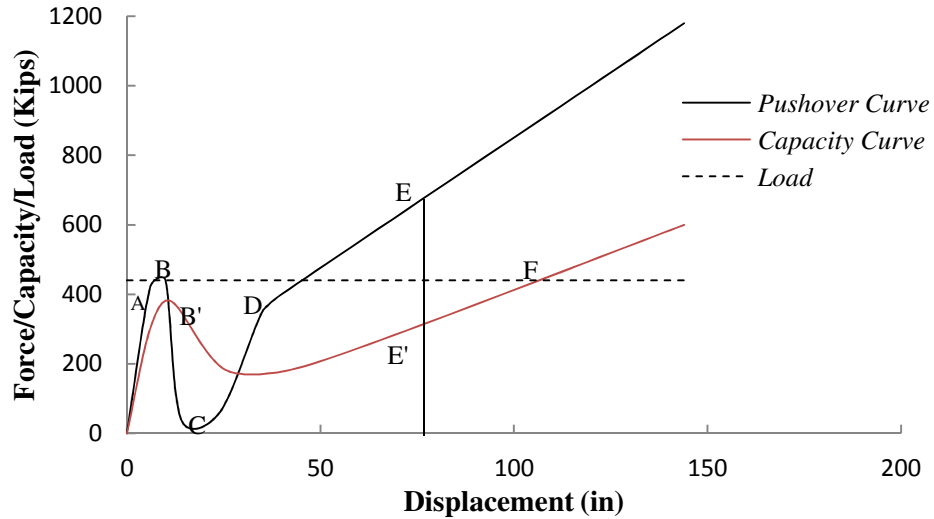


Figure 2.34 Pushover, capacity, and load curve (Powell, 2003)

To improve the structural integrity of a high rise building, a 3D nonlinear analysis considering material and geometrical nonlinearity was carried out by Rahmani and Moazami (2003) using LARSA (LARSA Integrated Linear and Non-linear Finite Element Analysis and Design) computer program. A typical composite floor with the relevant beams and columns was analysed using pushover analysis to study the behaviour of the system following various column removal scenarios (Fig. 2.35).

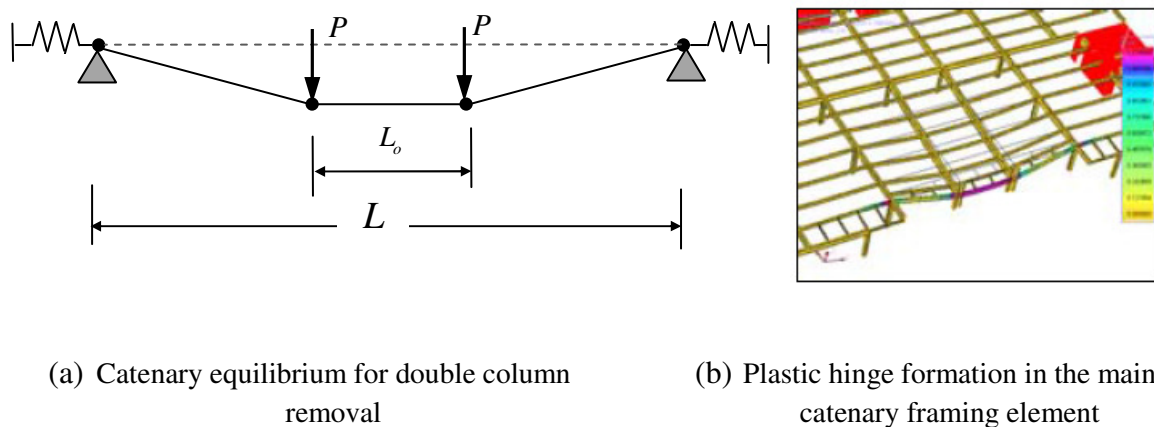


Figure 2.35 Typical composite floor in tall buildings (Rahmani and Moazami, 2003)

The results do not clearly show the relationship between the applied load and deflection and the result presented in terms of stress and strain on the floor. They concluded that to develop catenary action the beams need to be designed to provide full plastic capacity. Furthermore, it was observed that the combination of floor, beams and columns in a 3D system is able to develop catenary action and redistribute the loads in all directions.

To study the progressive behaviour of a high-rise building following sudden loss of a supporting column, a numerical analysis was carried out by Fu (2009) with reference to a 20 storey steel structure using a 3D finite model developed by ABAQUS (Fig. 2.36). The beam, column and bracing elements were simulated using a Beam element. The shear walls and slab floors were simulated by a Shell element. The material property of steel was modelled using an elastic-plastic model in ABAQUS library and a concrete damage plastic model (CDP) was used to model concrete material.

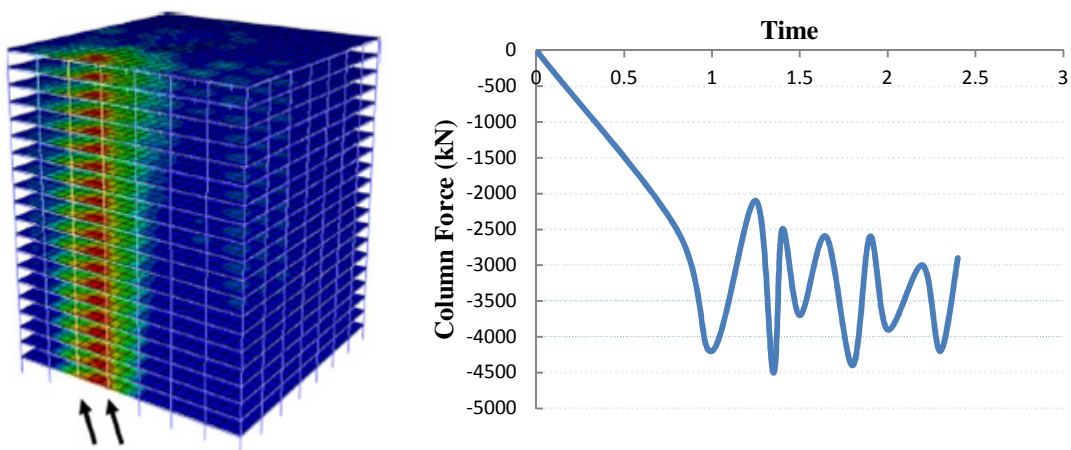


Figure 2.36 The 20 stories steel structure model considering various column removal scenarios (Fu, 2009)

The results indicate that, following column removal the axial force in a column is increased twice as much as static analysis; hence he concluded that all elements and relevant connections need to be designed to at least twice of $1.0DL+0.25LL$, which confirms the relevant provision suggested by GSA (2003) and DoD (2013). Furthermore, the result indicated that removing a column at higher storeys led to greater joint deflection than a column removal at the ground floor. It can be attributed to the more alternate load path provided in the ground floor which is in contrast with the imperial value of the TF method given by BS 8110-11(1997) or BS EN1991-1-7 (2006). This result agrees well with the conclusion made by Li et al. (2011).

As stated, to perform progressive analysis the current provision and most investigations use the alternate load path method and zero initial condition. Shi et al. (2010) argue that initial damage and condition has a remarkable effect on the behaviour of RC structures; hence a new method to take account of the effect of initial damage to the adjacent element and initial condition on the performance of a structure following a blast was proposed. The non-zero initial condition was defined as the displacement and velocity of the adjacent members at the beginning of the dynamic response of a structure, or following total loss of the key supporting column; which also can be considered as the beginning of the progressive collapse defined by the DoD or GSA. As the displacement at the blast duration is relatively small, it was ignored and only the initial velocity was considered in the proposed method. Shi et al. (2010) applied the FE LS-DYNA to develop a new method to analyze RC structures for progressive collapse.

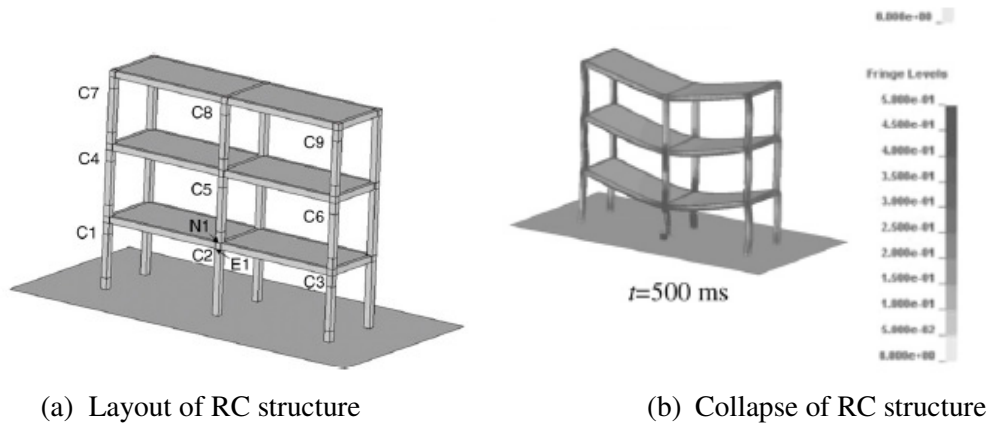


Figure 2.37 The three stories RC structure model (Shi et al., 2010)

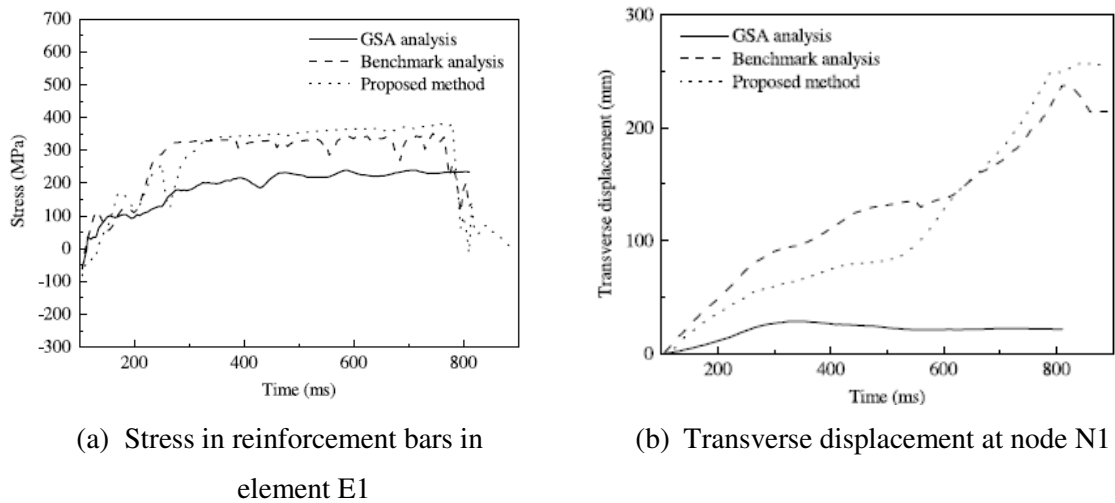


Figure 2.38 Analysis result of the structure based on three different methods (Shi et al., 2010)

To show the reliability of the proposed method to analyze an RC structure for progressive collapse, first a series analyses considering direct blast load were carried out, followed by analysis of the same structure using the alternate load path and the proposed method. The numerical analysis on a three storey RC structure (Fig. 2.37) considering the proposed method indicated that the current alternate load path method (DoD, 2013; GSA, 2003) underestimates the stress and displacement (Fig. 2.38). The result indicates that the initial condition do not have effect considerable on the collapse resistance (Fig. 2.38).

To identify the main factors affecting the behaviour of a steel structure following removal of a supporting column in a different location, a nonlinear dynamic finite element study using the GSA (2003) guide line was conducted by Kwasniewski (2010). The eight-storey steel frame structure designed for a full-scale fire test in the UK was selected as a representative example of a modern structure which meets most British and European code provisions (Fig. 2.39). The gravity loads recommended by GSA (2003) i.e. Eq. (2.7) were applied in all analyses. The designed dead and live load were assumed to be 3.65 and $3.5 \text{ kN} / \text{m}^2$, respectively. The applied load versus time is shown in Figure 2.40. The additional load was considered to define the safety margin. It was assumed that the column is removed at second 2 of simulation and the gravity load increased after 4 seconds following the column removal. The global analysis was performed considering notional column removal at the corner, near the middle of the long side of the structure and an interior supporting column. The result indicates that the structure collapses at the gravity load of 1.5 times of defined load by GSA (2003) (Fig. 2.41). Load factor in the Figure 2.41 was defined as the ratio of applied load/GSA reference load ratio i.e. $\text{DL}+0.25\text{LL}$. Furthermore, the results show that the steel structures designed by British or European codes are not susceptible to progressive collapse.

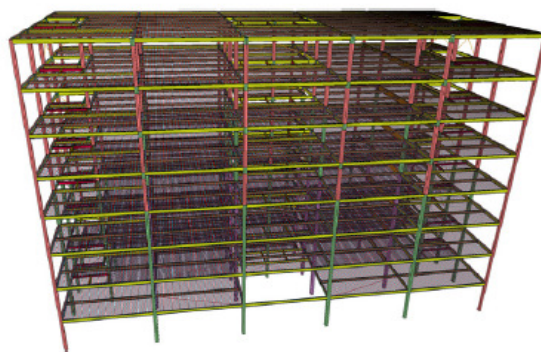


Figure 2.39 FE model of the entire building (Kwasniewski, 2010)

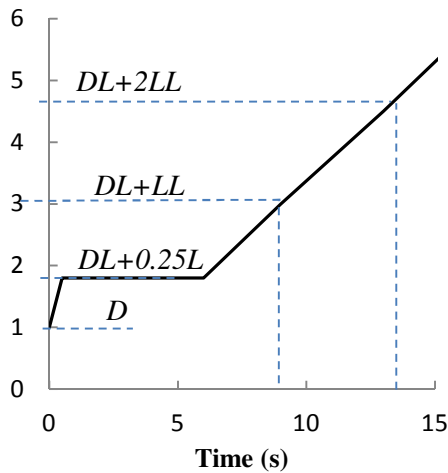


Figure 2.40 Applied gravity load to the slab versus time (Kwasniewski, 2010)

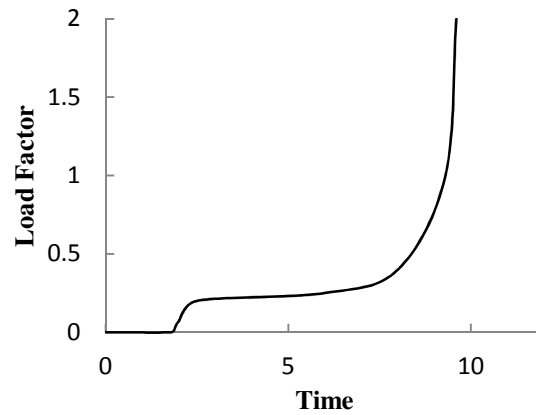


Figure 2.41 The time history of maximum deflection (Kwasniewski, 2010)

Although it is generally accepted that FE is a robust structural analysis approach, the separation, collision with other elements and falling simulation would be relatively difficult and the analysis cannot follow the procedure to entire collapse. To simulate the real behaviour of RC structures following removal of one or two supporting columns, the Applied Element Method (AEM) was used by Salem et al. (2011). This method is capable of applying dynamic analysis, to allow falling and separation of different elements of structures. This method can be considered as an efficient method using the discrete cracking concept (Salem et al., 2011; Sasani, 2008; Meguro and Tagel-Din, 2002; Meguro and Tagel-Din, 2001). In the AEM method, the various elements of structures are virtually divided and then their surfaces are connected together using a set of shear and normal springs (Fig. 2.42 and Fig. 2.43). The contact points are distributed on the face of the elements and two adjacent elements are separated if the normal or shear springs are ruptured. In this study, the Extreme Loading for Structures (ELS) software was used to simulate total progressive collapse following the removal of one and two adjacent columns.

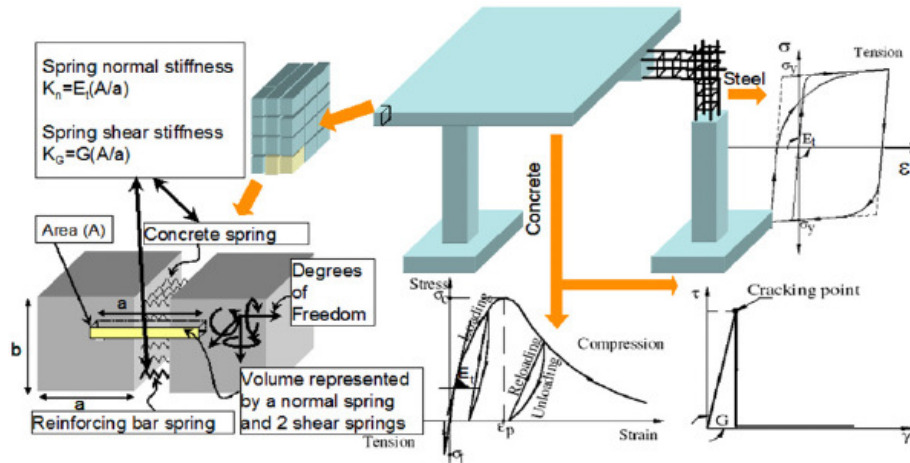


Figure 2.42 Modelling concept using the AEM method (Salem et al., 2011)

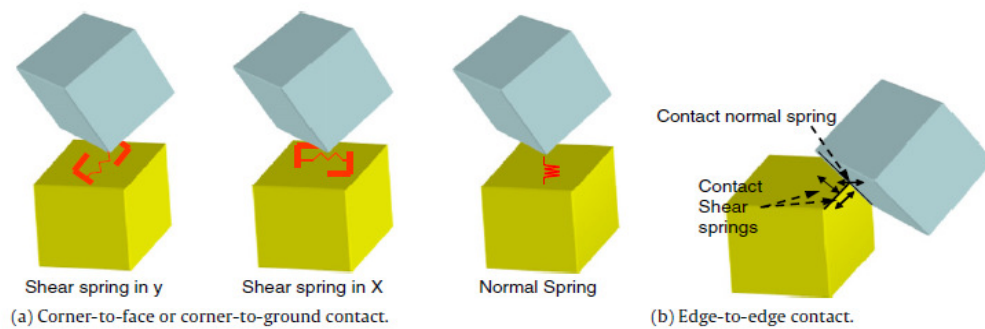


Figure 2.43 Shear and normal springs between two adjacent elements in AEM method (Salem et al., 2011)

The results of progressive analyses on a five storey RC structure indicated that the buildings designed based on ACI 318-08 with one column removal are not susceptible to progressive collapse; while collapse of two ground columns results in a progressive collapse of 30% of the structure (Fig. 2.44). They argue that the AEM is more accurate and efficient to simulate progressive collapse of RC structures and it is more economical by 50% compared to the FEM method.

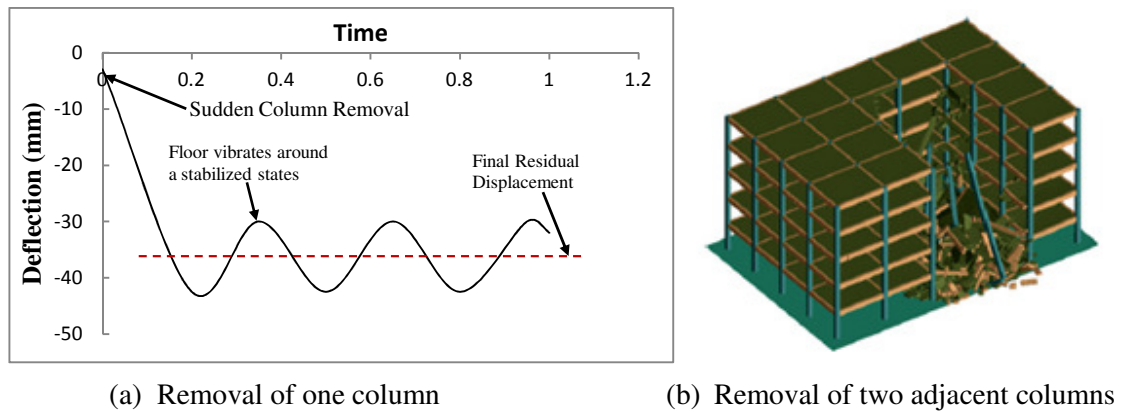


Figure 2.44 Progressive collapse of the five-story reinforced concrete building (Salem et al., 2011)

Discussion

The FE results indicate that the progressive collapse phenomenon can be successfully simulated using the FE commercial software. As progressive collapse is a many-faceted phenomenon, the FE analyses have not led to a consistent result. However, some of FE studies on RC structures concluded that current provision underestimates the stress and deflection, which indicates that these provisions are not able to provide the required robustness in the structures to prevent progressive collapse, while some other studies concluded opposite result, which indicate further research is needed to minimize the discrepancies.

The results of analyses on various structures with different properties show that the internal force or displacement is increased twice as much as static analysis, which confirms the reliability of the relevant regulation in DoD (2013) and GSA (2003). Furthermore, the result indicated that removing a column at higher storeys leads to greater joint deflection than a column removal at the ground floor. It can be attributed to the more alternate load path provided in the ground floor which is in contrast with imperial value of the TF method given by BS 8110-11(1997) or BS EN1991-1-7 (2006).

The recent studies on progressive collapse imply that initial damage and condition affect the behaviour of RC structures; hence the column or wall support needs to be removed during the analysis and not at the beginning of the process, which is required by most of the codes and standards. Due to deflection at the removal wall support being relatively small, the velocity needs to be considered to take account of the effect of the initial condition. Generally, the initial condition increases stress and vertical deflection of structure.

Although the conventional FE analysis is considered as a robust structural analysis approach, from the progressive collapse point of view, simulation of separation and entire collapse would be relatively difficult. As in progressive collapse the main attention is on general collapse, the Applied Element Method (AEM) can be considered as a comprehensive solution. This method applies dynamic analysis to allow falling and separation of the different elements of structures. This method can be considered as an efficient method using the discrete cracking concept. It is argued that the AEM is more accurate and efficient to simulate progressive collapse of RC structures and it is more economical by 50% compared to the FE method.

2.8 PULLOUT BEHAVIOUR OF SINGLE BAR IN CONCRETE

In modern structural design, performance-based criteria requires considering the bond design of RC structures using a more reliable prediction of bond to design accurate development/anchorage length. It is generally accepted that minimum development lengths calculated by the designer will provide a fully bonded or anchored structure, while in practice some bar slip has been observed in experimental studies (McCabe and Pantazopoulou, 1998). Recent studies on the bond behaviour of steel in concrete provide the basic knowledge to improve our understanding about the effect of various parameters such as material properties,

spacing and confinement on the bond. In conventional design of RC structures, design for bond is considered to provide adequate anchorage length of bar into concrete to develop yield force.

To study bond characteristics of bars in concrete at the interface between two materials, different test methods have been developed and proposed in the last four decades. The test methods can be summarized in two groups (Nawy 1996): pullout tests i.e. both the concentric and the eccentric, and beam test i.e. the National Bureau of Standards beam, the University of Texas beam. A useful review of the different approaches to determine bond strength can be found in FIB (2000), MacGregor (1997), ACI Committee 408 (1992), Ferguson et al. (1988), Park and Paulay (1975). The main aim of a bond test is to investigate different parameters which affect transferring stress between concrete and steel and vice versa.

This section mainly focuses on the pullout test results of reinforcement bonded in concrete or grout. Due to its simplicity, the pullout test is well known and widely used by researchers. In some cases for comparison, results from different bond conditions are also included. Single-bar tests provide upper bound on the bond performance and the results are important, so they can present basic principles to evaluate test result of multi-bar cases.

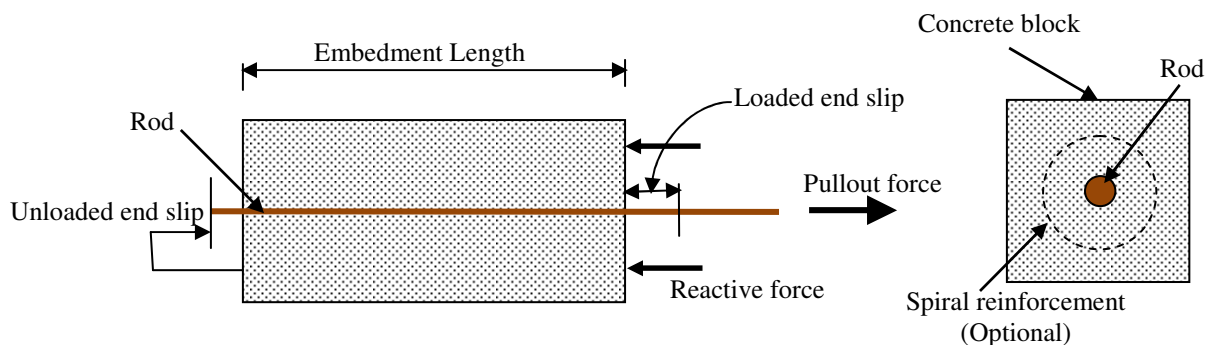


Figure 2.45 Typical pullout specimen (Radlofi et al., 1991; Amleh, 2006)

In the typical bond pullout test, the steel is placed in a grout or a concrete block (Fig. 2.45). The specimen is held by suitable supports at the loaded end. According to the result of a pullout test on normal reinforcement Radloff et al. (1991) implies that confining of the reactive compression force has considerable effect on the pullout response. To reduce or eliminate this negative effect, the modified pullout specimens are shown in Fig. 2.46.

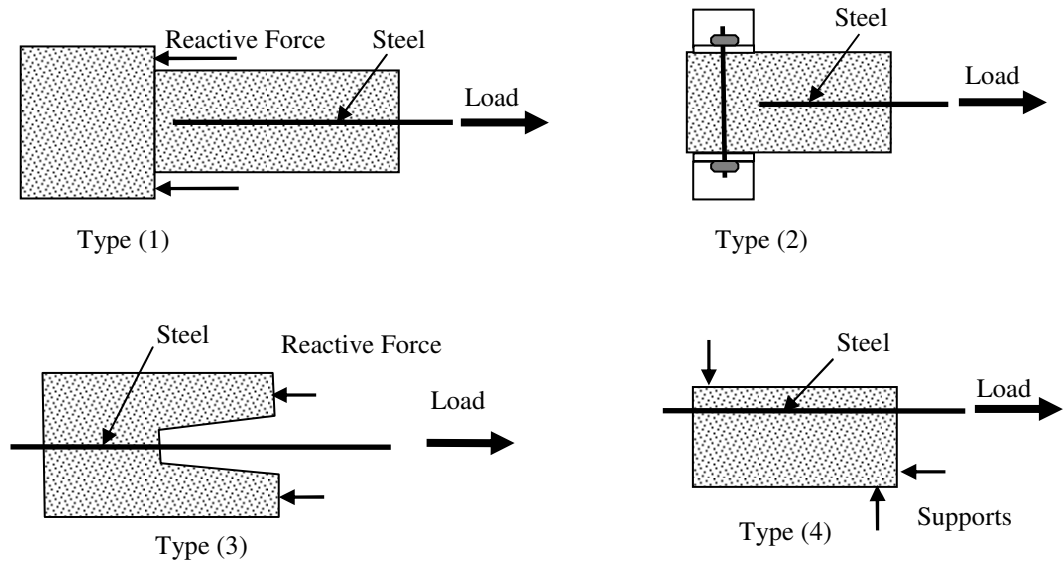


Figure 2.46 Modified pullout test. Type 1&2 (Radloff et al., 1991), and type (3, 4) (Salmons and McCrat 1977)

As concrete is in a compressive state and bar is in a state of tension, the remarkable differential strain produces slip at the loaded end. Mostly relative slip at the loaded (live) end and free (dead) end is measured. While the tensile force is increased, slip is propagated at the loaded end towards the free end. The sufficient and measurable slip at the loaded end load is defined as slip. However, this method is efficient when load versus pullout displacement is studied rather than real bond resistance (Ferguson 1988), which is the case in the present study.

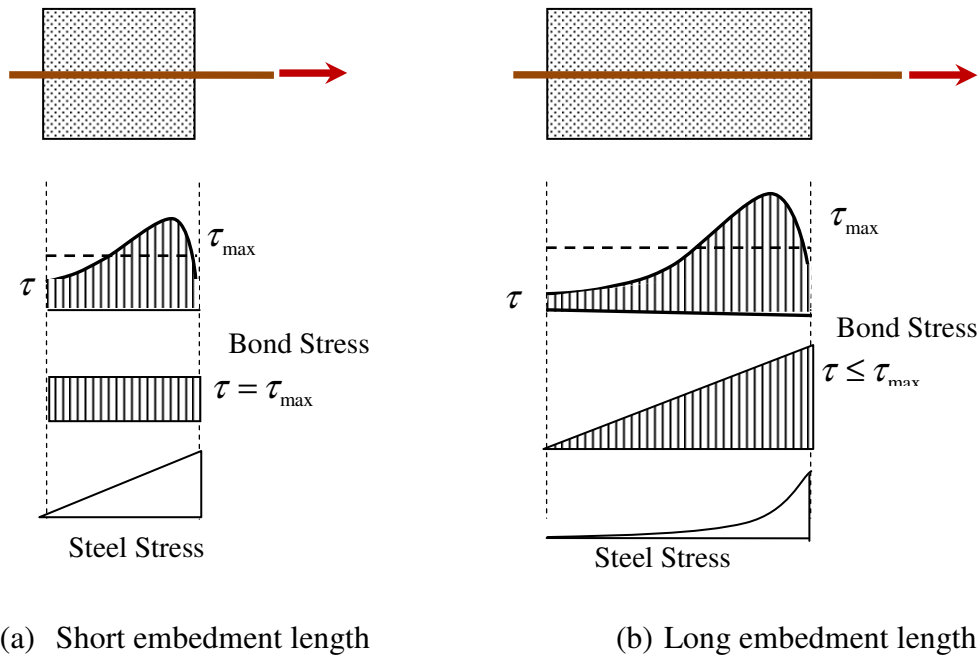


Figure 2.47 The distribution of bond and steel stress along embedment length (Radlofl, 1991; Leonhardt, 1964)

However, the variation in the stress is commonly clear for long embedment length and low load. Accordingly, in the shorter length and higher loads the bond stress would be uniform. Researches have shown that the distribution of bond stress and the corresponding slip between steel and concrete along the embedment length is nonlinear (Abrishami and Mitchel, 1996; Radlofl, 1991; Leonhardt, 1964). Mostly the uniform bond stress is taken into account or in some cases it has been assumed linear varying from zero at the free end to maximum at the loaded end (Fig. 2.47). According to the magnitude of the embedment length, two types of failure might occur. For long embedment length, the bond strength will be greater than the tensile strength of the bar; hence bar fracture occurs. If the embedment length is relatively short and peak pullout force is less than the tensile strength of the bar; pullout governs the failure mechanism. For pullout failure case, longitudinal splitting occurs due to concrete cracking.

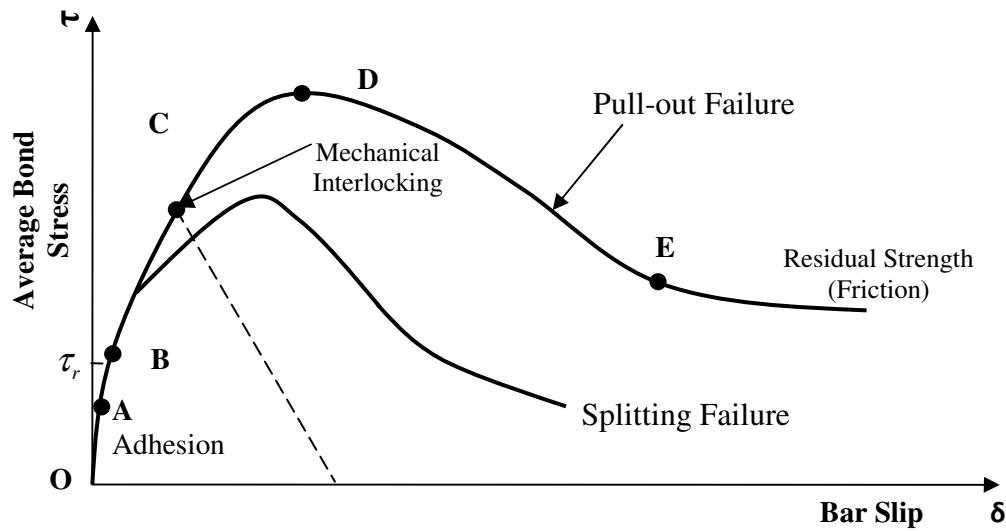


Figure 2.48 Typical bond stress-slip laws (CEP-FIP, 2000) and (Girard and Bastien, 2002)

2.8.1 Modes of Bond Failure

Based on the crack propagation, two failure modes can be defined. In the case of small diameter bar embedded in a large concrete block, heavy confinement, and if the ratio of concrete cover to bar diameter is more than three (Cairns and Abdullah, 1996), pullout is induced due to shearing off of the concrete between the bar lugs. Also, if the ratio of concrete cover to bar diameter is less than three (Cairns and Abdullah, 1996) splitting occurs accompanied by slip on the rib face. The pullout load-slip relationship representing splitting and pullout failure mode can be summarized in Figure 2.48 (CEB – FIP, 2000). Figure 2.48 shows that the bond-slip relationship can be divided into three stages: the uncracked (OB), partially cracked (BD), and the fully debonding stage (DE).

2.8.2 Different Factors Affecting Bond Performance

Bond stress depends on several factors, which refer to the concrete, steel unit (bar, strand, and tendon), and the stress state in both the surrounding concrete and reinforcing bar.

Nevertheless, a few technological factors come into play too; such as geometry of the reinforcement bar, steel and concrete strength, concrete cover, bar size, embedment length, bar spacing, and stirrups. However, since the scope of this research is not intended to be state-of-the-art work on bond, only the analytical model for pull-out is discussed in detail.

2.9 PULLOUT MODELS

A comprehensive literature review about the relationship between pullout load and slip between fibre and its surrounding matrix has been conducted by Naaman et al (1991). Based on existing literature, they found that no complete analytical study of the mechanics of pullout has been performed. However, they developed a mathematical model which describes the response of straight smooth fibres embedded in a cementitious matrix and subjected to a pullout load. It was assumed that the relationship between pullout load and slip is such as the bond-shear-stress-slip for bars in reinforced concrete or strand in pre-stressed concrete employed by Edwards and Yannopoulos (1979); Eligehausen et al. (1983); Nilson (1972). The pullout versus slip curve was divided into three zones (Fig. 2.54). In zone I, a perfect bond exists between steel and grout; thus the behaviour can be assumed elastic. In phase II, the debonding is initiated at P_{crit} and it continues till P_b where full debonding occurs and influence of friction increases. Mechanical interlocking and friction provide bond resistance in the debonding phase.

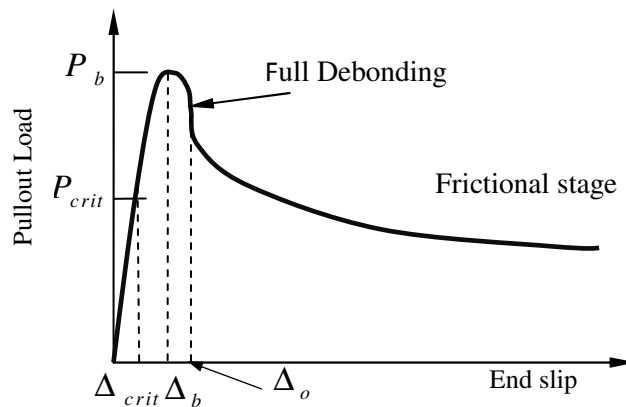


Figure 2.49 Assumed pullout load versus slip

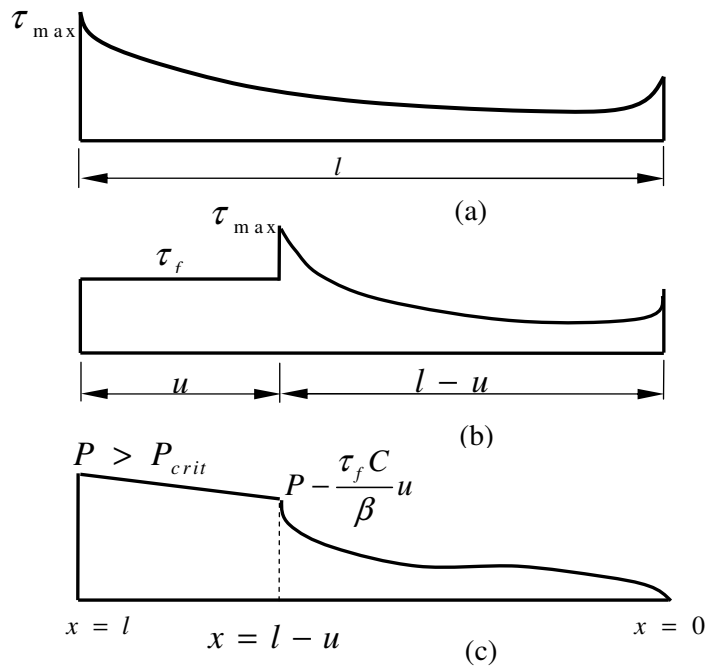


Figure 2.50 Assumed interfacial bond stress for cases (a) $P \leq P_{crit}$ (b) $P \geq P_{crit}$ and (c) Normal force distribution (Naaman et al., 1991)

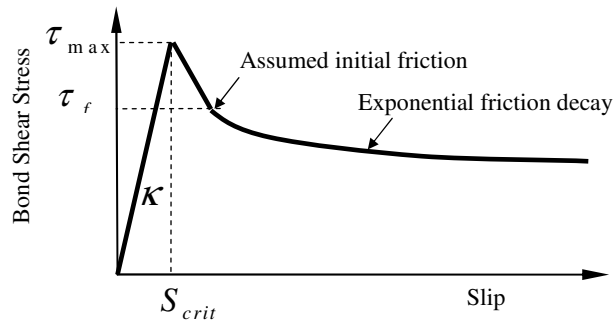


Figure 2.51 Alternative interfacial shear stress versus slip with frictional decay (Naaman et al., 1991)

Assuming bond stress distribution (Fig. 2.50), bond-slip curve (Fig. 2.51) and pullout load-slip relationship (Fig. 2.50), Neman et al. (1990) developed three equations corresponding to the three different phases

Fully Bonded Stage:

$$F(x) = A'e^{\lambda x} + B'e^{-\lambda x} + \frac{P}{Q} \quad (2.14)$$

$$A' = \frac{P}{1 - e^{-2\lambda l}} \left[\left(1 - \frac{1}{Q}\right)e^{-\lambda l} + \frac{1}{Q}e^{-2\lambda l} \right] \quad (2.15)$$

$$B' = \frac{P}{1 - e^{-2\lambda l}} \left[-\left(1 - \frac{1}{Q}\right)e^{-\lambda l} - \frac{1}{Q} \right] \quad (2.16)$$

$$\frac{P}{\Delta} = \frac{\lambda A_m E_m}{(Q - 2)} \left(\frac{1 + e^{-\lambda l}}{1 - e^{-\lambda l}} \right) \quad (2.17)$$

Partial Debonding Stage :

$$P = \tau_f u + \frac{\tau_{\max}}{\lambda} \frac{1 - e^{-2\lambda(l-u)}}{\frac{2}{Q}e^{-\lambda(l-u)} + \left(1 - \frac{1}{Q}\right)(1 + e^{\lambda(l-u)})} \quad (2.18)$$

$$\Delta = \frac{P(Q-1)u - \frac{\tau_f u^2}{2}(Q-2) + \left(P - \tau_f u\right) \left(\frac{1 - e^{-\lambda(l-u)}}{1 + e^{-\lambda(l-u)}} \right) \frac{Q-2}{\lambda} - \tau_f ul}{A_m E_m} \quad (2.19)$$

Full Debonding Stage:

$$P = \left(1 - \exp \left\{ \frac{-2\mu v_f x}{E_f r_f \left[\frac{(1 + v_m)}{E_m} + \frac{(1 - v_f)}{E_f} \right]} \right\} \right) \frac{\delta E_f \pi r_f}{v_f} \quad (2.20)$$

Where

$$Q = 1 + \frac{A_m E_m}{A_f E_f}, \quad \lambda = \sqrt{KQ}, \quad K = \frac{C \kappa}{A_m E_m}$$

$F(x)$ The force in the bar at distance x from the free end of the bar

τ The local interfacial shears stress between the bar and grout

C The perimeter of the bar

κ	Bond modulus
A_m, E_m	The area and elastic modulus of grout
A_f, E_f	The area and elastic modulus of bar
μ	The coefficient of friction between bar and grout
P	Pull-out force
τ_{\max}	Maximum shear stress
τ_f	Bond stress in the frictional stage
u	Debonded length
ν_m and ν_f	Poisson's ratio in grout and steel

To develop a pullout load-slip-relationship, with forces acting on a pullout specimen with the length of d_x and equilibrium conditions for a bar of length of d_x (Fig. 2.53), Abrishami and Mitchell (1996) proposed a comprehensive model for slip, bond stress and pullout slip relationship for both pullout and split failure considering pullout, push-in, and a combination of the pullout and push-in tests (Fig. 2.52).

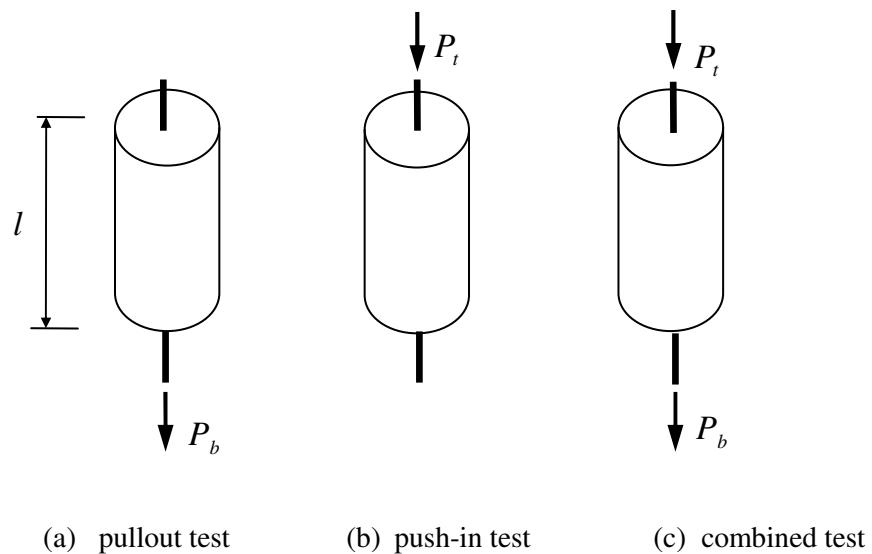
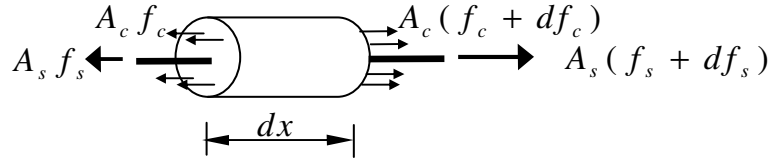
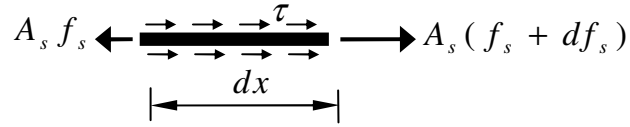


Figure 2.52 Typical pullout test subjected to various type of loading (Abrishami and Mitchell, 1996)



(a) force acting on the concrete and reinforcing bar



(b) bond stress and forces action on the reinforcing bar

Figure 2.53 Free body diagram of single bar into concrete (Abrishami and Mitchell, 1996)

To predict the response of a specimen subjected to axial force, a mathematical model was assumed as shown in Figure 2.54 which can be summarized as follows:

$$\tau = E_b u \quad 0 < u < u_s \quad (2.21a)$$

$$\tau = E_d u + E_b u_s - E_d u_s \quad u_s < u < u_f \quad (2.22)$$

$$\tau = \tau_f \quad u > u_f \quad (2.23)$$

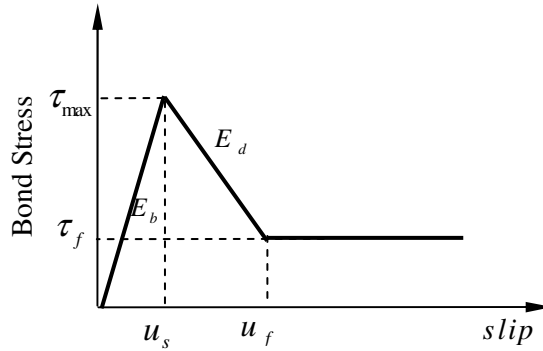


Figure 2.54 Bond model for splitting failure (Abrishami and Mitchell, 1996)

Where $E_b = \tau_{\max} / u_s$ and $E_d = (\tau_f - \tau_{\max}) / (u_f - u_s)$. Equilibrium in Fig. 2.53 and solving relevant differential equation, the pullout load-slip relationship for the ascending and descending stage is given as follows:

$$P_b = \left[\frac{2\kappa(e^{\kappa l} - e^{-\kappa l})}{2 + e^{\kappa l} + e^{-\kappa l}} \left(\frac{E_s A_s}{1 + n\rho} \right) \right] u_{av} \quad 0 < u < u_s \quad (2.24)$$

where u_{av} = average slip of top and bottom of specimens, $\kappa = \sqrt{k_s E_b}$, $\rho = A_s / A_c$, $\kappa_s = 4(1 + n\rho) / (d_b E_s)$, and, $n = E_s / E_c$

$$P_d = \left[\frac{-2\kappa \sin(\kappa l)}{1 + \cos(\kappa l)} \left(\frac{E_s A_s}{1 + n\rho} \right) \right] (u_{av} + m) \quad u_s < u < u_f \quad (2.25)$$

where $\kappa = \sqrt{-k_s E_d}$, $\kappa_s = 4(1 + n\rho) / (d_b E_s)$, $m = u_s (E_b / E_d - 1)$

The results shows that pullout-slip relationship based on proposed model agree extremely well with pullout test result.

An analytical method to predict the full-range mechanical behaviour of grouted rock bolt in tension based on an idealized tri-linear bond-slip model (Fig. 2.55) considering residual bond stress at the interface between bolt and grout was developed by Ren et al. (2009). To develop the pullout-slip relationship, five distinct stages i.e. elastic stage, elastic-softening stage, elastic-softening-debonding stage, softening-debonding stage, and debonding stage were taken into account (Fig. 2.56). For each stage interfacial bond shear stress and pullout load-slip relationships were developed. To validate the analytical approach, two pullout tests were conducted. The results of the proposed method were found to be very close to those pullout test results. All parameters in Figure 2.56 were calibrated using pullout test results. The assumed bond model was mathematically expressed as follows:

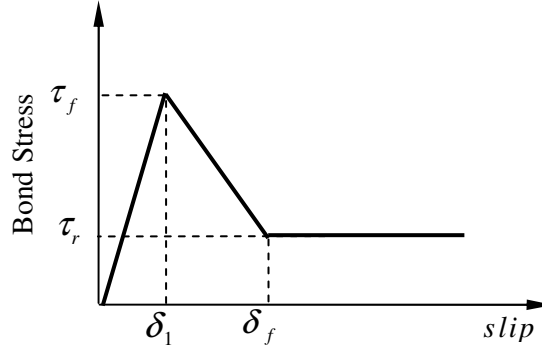


Figure 2.55 Assumed bond-slip model-Tri-linear (Ren et al., 2009)

$$\frac{\tau_f}{\delta_1} \delta \quad 0 \leq \delta \leq \delta_1 \quad (2.26)$$

$$\frac{k\tau_f(\delta - \delta_1) + \tau_f(\delta_f - \delta)}{\delta_f - \delta_1} \quad \delta_1 \leq \delta \leq \delta_f \quad (2.27)$$

$$k\tau_f \quad \delta \geq \delta_f \quad (2.28)$$

Where $k = \tau_r / \tau_f$.

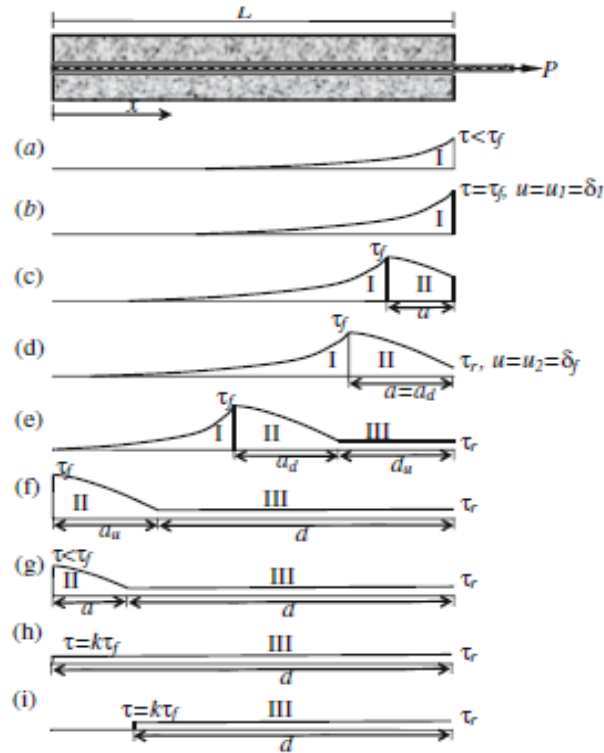


Figure 2.56 Interfacial shear stress based on the analysis (Ren et al., 2009)

Discussion

Different approaches to simulate bond stress at the interface between steel and surrounding concrete have been reviewed. As real behaviour of steel in concrete has not been standardized, various models have been developed. Although all models have their own advantages, in practice and from a design point of view the optimum model should be easy to use while all influencing factors are taken into account. The developed model by Ren et al. (2009) can be considered as the most comprehensive analytical simulation; which can predict pullout displacement and slip along the embedment length, bond stress distribution along the embedment length of bar into concrete, and finally the pullout load-displacement relationship at a fundamental level.

However, even though there are a lot of uncertainties in the progressive behaviour of a structure following the removal of a wall support, the extra accuracy obtained using Ren et al's (2009) model does not provide more safety factors in the designing of structures for progressive collapse. Due to its consideration of nonlinear bond stress distribution and slip along the embedment length, the proposed model by Abrishami and Mitchell (1996) can be taken into account as the most practical model; especially as the relation between pullout load and displacement have explicitly been developed. It can be concluded that Abrishami and Mitchell's (1996) can be considered as an adequate model in the analytical analyses of catenary action mechanism to design floor-to-floor joints following removing a wall support.

2.10 EXISTING FE MODELS OF REINFORCED CONCRETE

Reinforced concrete consists of two materials with totally different properties; which, by working together, they sustain various types of loadings. However, prediction of bond-slip behaviour of reinforced concrete elements using FE analysis is somewhat complex. To simulate reinforced concrete elements three different models of FE analysis are used: distributed, embedded, and discrete models.

For the distributed modelling technique, it is assumed that reinforcement is smeared into every element of concrete. In this model reinforced concrete is considered as a homogeneous material, in which the rebar has been transferred to an equivalent amount of concrete. For this model perfect bond is assumed. In the embedded technique, the reinforcement is considered as a longitudinal element which is connected into the concrete and the concrete and rebar have the same displacement. As perfect bond again is assumed, the two materials work together exactly like a unit. When using the discrete technique, to simulate reinforced concrete behaviour subjected to different types of loading comprehensively, three distinct elements need to be considered. In this model a special element is used to simulate concrete, rebar, and interface between bar and concrete, respectively. Note that, steel and concrete are two totally independent elements.

All the three mentioned models have their own advantages. Due to simplicity of implementation, the distributed model is mainly used in practical analysis and design. As the bars are smeared into concrete, internal force of reinforcement cannot to be quantified. According to the definition, the bond-slip relationship only can be modelled by using the discrete technique. It is obvious, although this model is more complex, for modelling of reinforcement concrete an accurate discrete technique would be the only alternative. By considering the implementation and complexity, the embedded technique can be placed between the discrete and distributed model.

The current finite element software packages such as ABAQUS, ANSYS, NASTRAN, and ADINA have their own special element to simulate concrete and rebar. The reinforced concrete models can be developed by a combination of concrete and rebar with adding advanced material properties into the models e.g. cracking, fracture and bond-slip behaviour. To defined bond-slip various element and technique has been proposed in literature; a summary of these models are discussed in the following sections.

2.10.1 Modelling Techniques for the Bond-slip Behaviour

Since bonding is the key factor in the analysis and design of RC structures and it governs most RC performances, not just progressive collapse, seeking a technically reliable and economically viable bond modelling technique remains a challenging issue. To date, numerous research papers have been published which study the bond-slip behaviour between the tie and the surrounding grout; a large proportion of which were carried out by numerical modelling. In this section, a wide range of modelling techniques to simulate such behaviour is presented. The early studies on FE models were conducted by Ngo and Scordelis (1968), Bresler and Berto (1968), and Nilson (1968); they considered both linear and nonlinear spring for bond modelling and suitable boundary layers. However, from the mid-eighties onwards FE modelling has widely been used; in which they employed the results of research that was carried out in the seventies and was published in the state-of-art report by ASCE (1982). Furthermore, CEB-FIP (2000) has presented a comprehensive literature review regarding to FE modelling of bond in reinforced concrete elements.

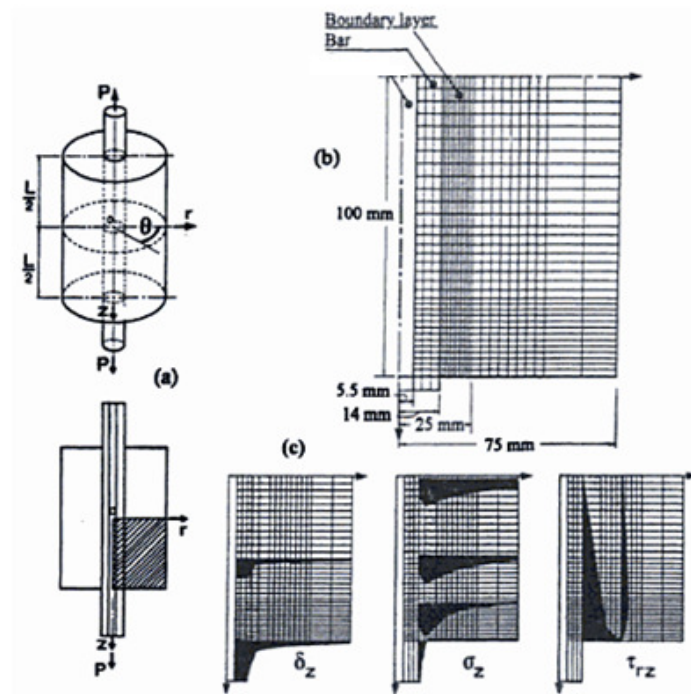


Figure 2.57 Finite element idealization: (a) coordinate system, (b) finite element idealization, and (c) diagrams of the longitudinal displacement and normal stress (Bresler and Bertero, 1968)

Bresler and Bertero (1968) first introduced a layerwise model. Since bond only occurs in the concrete zone near the reinforcement surface, to differentiate the inelastic deformation and fracture damage in this zone from the bulk concrete, the concrete is divided into two zones, i.e. an inner boundary layer and an outer layer (Fig. 2.57). It was assumed that both zones have a linearly-elastic isotropic behaviour, but with different material properties. In this study elastic modulus, thickness and Poisson's ratio of the boundary layer was assumed to be $0.06E_c$, 0.4 times of the bar diameter, and $2.5\nu_c$, respectively. The boundary layer was assumed as a homogenized material, with the capability of transferring stress and displacement from steel to concrete.

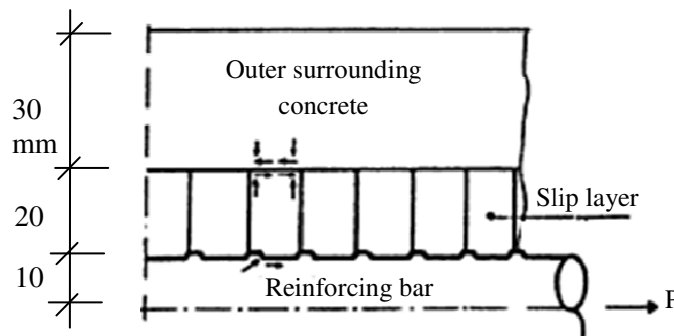


Figure 2.58 Axis symmetric representation of the slip layer (Reinhardt et. at. 1984)

Reinhardt et al. (1984) later introduced a “slip layer”, which was divided into two layers, one with a thickness equal to the bar diameter and the other equal to the outer zone of concrete (Fig. 2.58). The steel bar was assumed to be elastic. The nonlinearity of the concrete layer was described by an elastic-softening constitutive law in the tension zone and an elastic-plastic law in the compression zone. The chosen element for the steel bar can represent exactly the shape of a ribbed bar. The concrete closest to the bar can slip and once the slip-layer elements have been calibrated, modelling of the bond problem by FE analysis can be established.

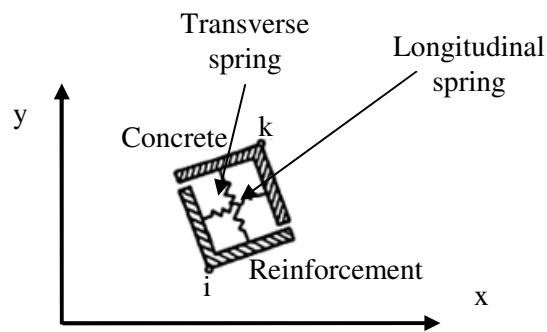


Figure 2.59 Bond modelling at interface between steel and concrete (Keuser and Mehlhorn, 1988)

2.10.2 Specific Finite Elements Model

From the 1980s onwards, varieties of new types of FE element emerged and were applied successfully to simulate the bond-slip relationship. A useful review was presented by CEB-FIP 2000. An alternative treatment to model the interfacial zone is to assume a negligible thickness of the interface layer, which transfers the bond problem into a category of “contact issue”. A useful review was presented by Keuser and Mehlhorn (1987) in respect of this type of work, in which the normal stress between the steel bar and the concrete and the bond-slip behaviour, was modelled by using a double spring with one movement in the longitudinal axis and the second in the perpendicular direction (Fig. 2.59). These two springs transfer normal and shear force between concrete and selected nodes. The spring does not have dimension and the relevant stiffness is calculated based on the bond-slip characteristics. It is to be noted that in this method a discontinuous or continuous connection between the two materials has been accepted. However, CEB-FIP (2000) states that “Assuming a contact element with a linear displacement function seems to be the best in terms of good fitting of test results and computational efficiency”.

To model bond-slip, various analyses by framework of the FE code ANSYS were conducted by Hemmaty et al. (1991). In this model the bond-slip curve introduced by Tassions with some modifications was used; it took into account the initial cohesive behaviour of bond.

Then to simulate the interface layer closest to steel, “bond-zone models ” (similar to the layer introduced by Reinhardt et al., 1984, thickness $\phi/2$ in the FE code DIANA), and a “spring model ” was introduced. In this model, the contact between steel bars and concrete was defined by a unidirectional spring element (Fig. 2.60, ANSYS element 39), characterized by a nonlinear generalized force-displacement capability (CIB-FIP 2000).

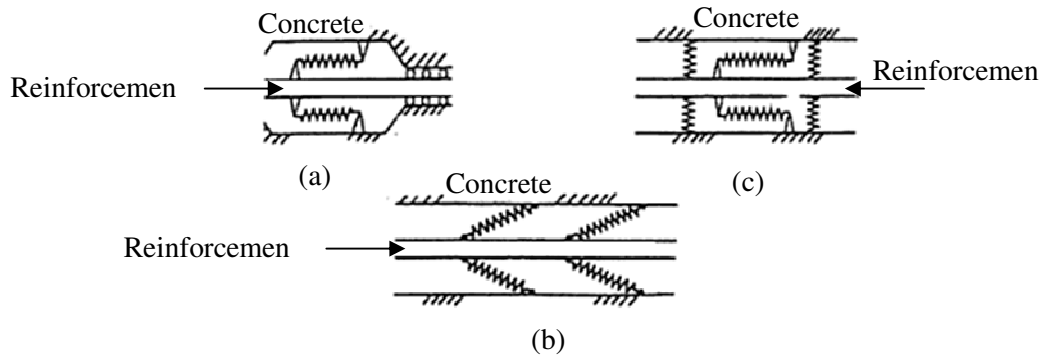


Figure 2.60 Various possible spring models (Hemmaty et al., 1991)

2.10.3 Structural Model

The bond strength is a structural behaviour rather than just a material property; thus recent modelling of full-size RC structures have been taken into consideration to determine the effect of concrete tensile strength, cover, development length, confinement and the properties of ribs. In this regards, Darwin and McCabe (1994) proposed a full scale reinforced concrete model and simulated the interface layer by using a 3D interface link, which acts as a contact-slip element (Fig. 2.61). To define this element cohesion, $c=1.7$ MPa and the coefficient of friction, $\mu=0.3$ were assumed. The results show that the effect of rib height on bond strength prior to the partial debonding stage is negligible; while it would be a key factor after the peak of the bond-slip curve. The developed model in the present study uses model type (a) suggested by Hemmaty et al., (1991) and structural model proposed by Darwin and McCabe (1994) simultaneously.

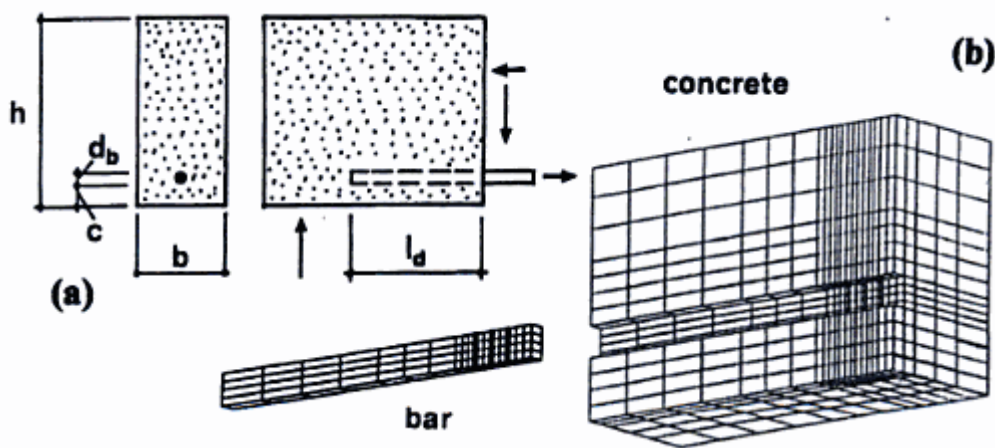
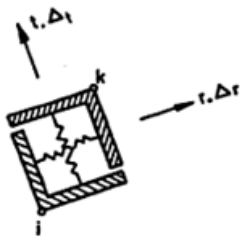


Figure 2.61 (a) Pullout test specimen; and (b) concrete and steel substructures (Darwin et al., 1994)

In a recent EU project, FE packages ABAQUS, ANSYS, DIANA, GEFDEN, AND LUSAS have been used and a comparison of various packages has been provided by Jefferson et al. (2005). It has been shown that the nonlinear control parameters have an extensive effect on the result of highly nonlinear problems. It was concluded that in most cases, ABQAUS is capable of providing efficient result for complex nonlinear problems, especially while it is accompanied with calibration (Jefferson et al., 2005).

A state-of-the-art literature review regarding to the capabilities of various software packages to model reinforcement concrete considering non-linear finite element methods has been conducted at the University of Illinois (Johnson, 2006). In this study approaches used by ABAQUS, ADINA, ATENA, DIANA, OpenSees, VECTOR2, and ZEUS-NL to model reinforced concrete and bond slip have been presented in detail. There are various methods to simulate bond between concrete and steel. In the discrete technique, the bond can be modelled as a contact surface between two different materials. Some elements have been suggested in earlier research and they have been widely used by the above commercial FE software. Specifically, the bond-slip relationship has been presented in ABAQUS, ATENA, and DIANA using a specific element (Table 2.5). Johnson (2006) states that the bond-slip in ABAQUS can be successfully simulated using a special connector i.e. translator.

Table 2-5 Bond-slip model presented in the different FE codes (Johnson, 2006)

	ABAQUS	ADINA	ATENA	DIANA	OpenSees	VecTor2	ZeusNL
	✓		✓	✓			

2.10.4 Pull-out model

To simulate the static behaviour of a pullout test i.e. the bond-slip behaviour, a discrete RC model using the FE ABAQUS code was developed by Li (2007). In this model, due to its flexibility to consider linear and nonlinear of the bond-slip relationship, a spring-like translator element for modelling the bond behaviour was used. This connector element is able to model the whole bond-slip relationship by adding elasticity and damage behaviour. In this study it was assumed that the bond-slip relationship between steel and concrete is constant and splitting failure will not happen. A numerical approach to simulate pullout behaviour of bar into concrete using ABAQUS and ANSYS was conducted by Nardin et al. (2005). A 10 mm reinforcing bars and concrete with compressive strength of 30MPa in a RILEM pull-out test was used (Fig. 2.62). In this study, a contact surface was used to simulate interface between steel and concrete and nonlinear material properties was applied to define material properties of steel and concrete (Fig. 2.62).

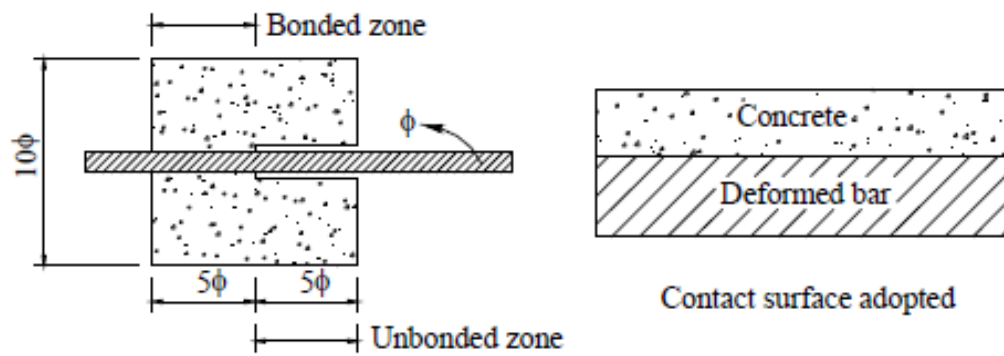


Figure 2.62 RILM pullout test (Nardin et al., 2005)

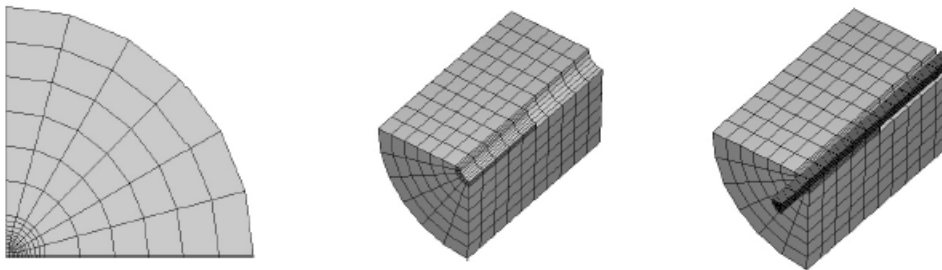


Figure 2.63 Numerical model for pull-out specimen (Nardin et al., 2005)

In ABAQUS modelling contact surface with friction coefficient and confinement pressure was used to simulate bond between steel and concrete. The bonded contact behaviour was used in ANSYS using normal contact stiffness i.e. FKN from 1 to 10 and sliding contact stiffens factor i.e. FKT was assumed 1.0. The results indicate that, the developed model is effectively able to simulate pull-out behaviour in the ascending stage while it fails to model descending phase of pull-out behaviour of steel in concrete.

Numerical analyses using ABAQUS provide relatively the same result. To show the effect of friction and confinement pressure, the specimens was analyses assuming various combinations of both parameters (Fig. 2.78). The results indicates that, both set of analyses

agree well with pull-out test result in the ascending stage, while they are not able to simulate descending stage (Fig. 2.77).

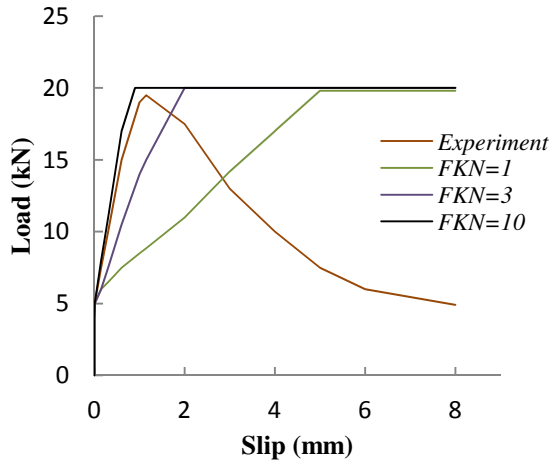


Figure 2.64 Pull-out force vs. slip- ANSYS influence of the FKN (Nardin et al., 2005)

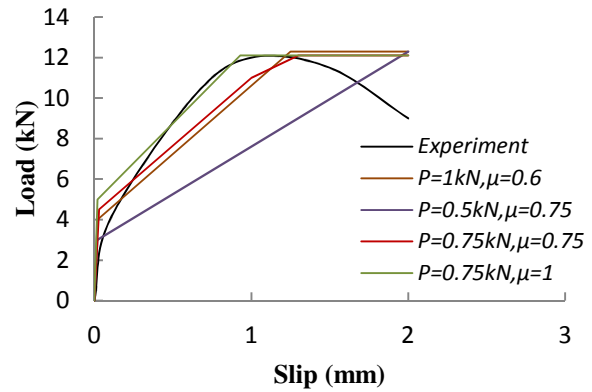


Figure 2.65 Pull-out force vs. slip using various confinement pressure (P) and friction coefficients- ABAQUS (Nardin et al., 2005)

A numerical procedure to define cohesive-frictional model for bond and splitting action of prestressing wire was developed by Gálvez et al. (2010) using finite element code ABAQUS. To improve bond between steel and concrete, intended bar was used. To take account the radial component of the prestressing, the Poisson's effect was increased. The cohesive model for simulation of radial cracks was introduced using non-linear springs. Similar to the previous models, this model is able to predict pull-out force-slip relationship in the ascending stage while fails to simulate the descending behaviour of bar into concrete (Fig. 2.66). To overcome the above mentioned deficiencies, in the present study a specific model to simulate full pull-out behaviour of steel into concrete will be developed in detail.

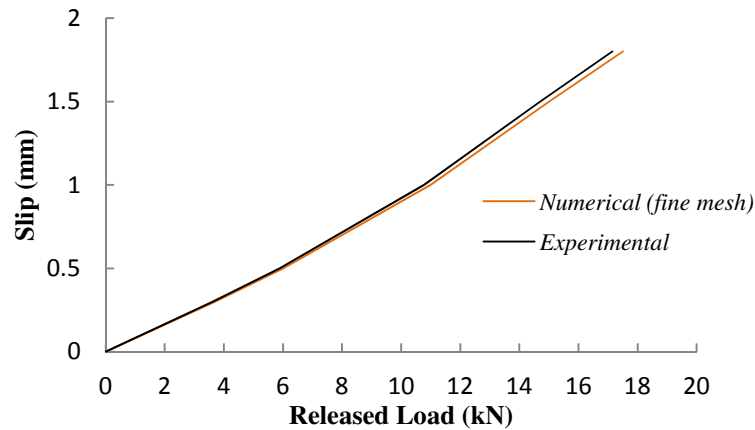


Figure 2.66 Load vs. slip using ABAQUS (Gálvez et al., 2010)

Discussion

Different methods to simulate bond-slip have been presented, each considering the reinforced concrete element and small slip. These models can successfully be used to analyze elements with bar fracture failure mode, while they are not be able to simulate the entire pullout behaviour of bar into concrete. It can be concluded that, for the structures with pullout failure mode with large slip and precast concrete structures, a spring-element model seems to be the best approach. Since bond is the key factor in analysis and design of RC structures and it governs most RC performance, bond modelling still would be a challenging issue in the future.

2.11 THE EFFECT OF LATERAL SUPPORT ON THE PROGRESSIVE RESISTANCE

2.11.1 Membrane actions

It is generally accepted that, boundary condition affects the compressive and catenary behaviour of the beams which may increase the strength of system. The compressive forces increases the capacity of beam in plastic zone and catenary action at the large deflection, also, will improve the load bearing resistance. Figure 2.67 indicates that, the end of beam tend to

move outward, the reaction on the side supports will induce the compressive membrane action. These compressive forces tend to enhance the load bearing capacity of beam following flexural capacity. With the increase of vertical deflection the compressive force will be reduced due to the beam ends tend to move inward, in which at the large deflection the compressive force changes to tensile forces.

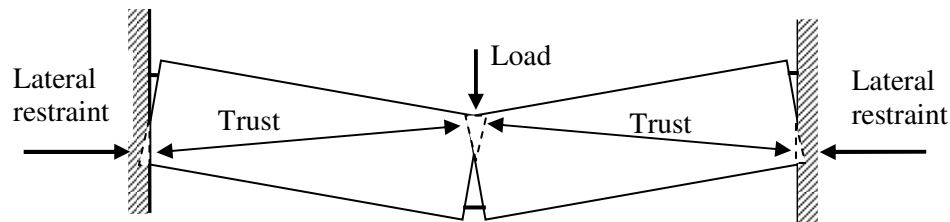


Figure 2.67 Arching action (Rankin and Long, 1997)

Figure 2.68 displays a typical load-deflection showing both compressive and tensile membrane action for a concrete beam subjected to uniform load (Park and Gamble, 1980). From A to B, the behaviour of beam is elastic, followed by yielding at the point B. The load bearing capacity is increased from B to C due to effect of compressive membrane forces. The plastic hinges will induce at the point C, followed by a considerable reduction in load capacity of beam. At the large deflection i.e. point D, the load is sustained by catenary action mechanism. The beam is able to carry more loads up to bar fracture at the point E.

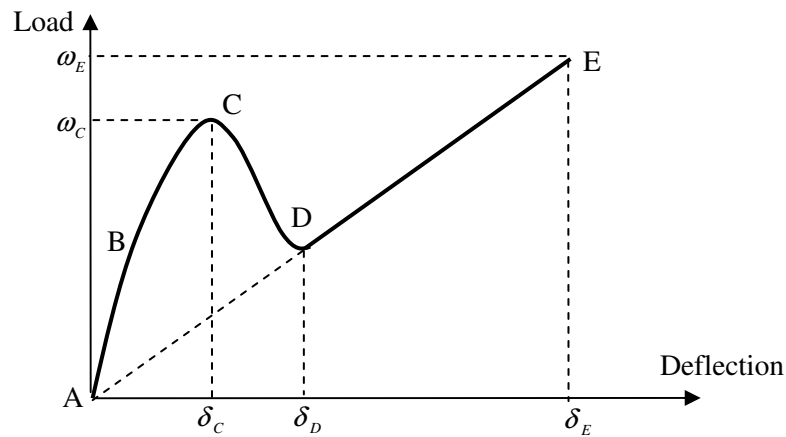
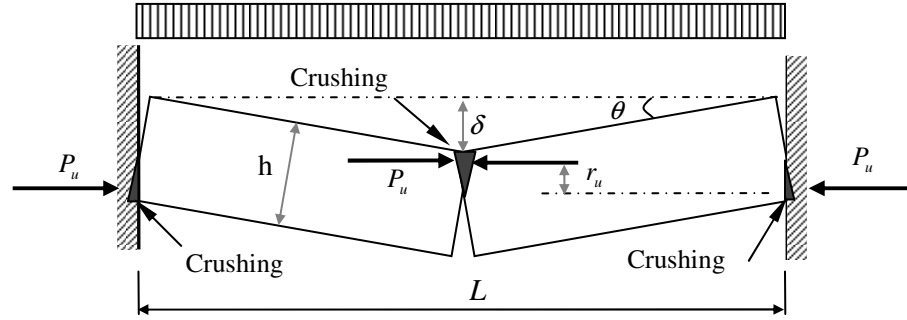


Figure 2.68 Load vs. middle joint deflection considering compressive membrane and catenary action (Park and Gamble, 1980)

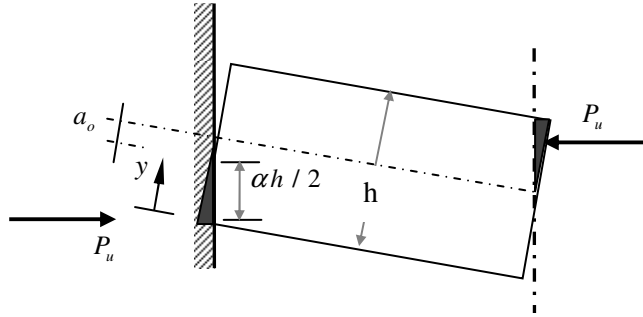
2.11.2 Compressive membrane actions

Literature review indicates that, the majority of studies on compressive membrane action are performed on membrane action in the slabs (Merola, 2009). The positive effect of lateral supports on the load bearing capacity of concrete panels was studied and verified by Ockleston (1955). According to three test result, Ockleston (1958) found that, the maximum capacity of panels is more than three time compare with yield line theory, which is attributed to the effect of compressive membrane forces. Since that time several analytical and experimental studies have been conducted on the effect of lateral support on the capacity of reinforcement concrete elements. (Park and Gamble, 1980; Eyre, 1990 and 2000; Rankin and Long, 1997; Taylor et al., 2001). A comprehensive literature review regarding to the analytical approaches has been provided by Merola (2009). An arch action theory was developed by McDowell et al. (1956) considering masonry walls (Fig. 2.69). They considered a beam constrained between two rigid supports. It was assumed that, half of the element rotates about the outer edge of contact surface with the supports at the depth of $\alpha h / 2$ from the first point of contact. Applying horizontal equilibrium in Fig. 2.84a McDowell et al. (1956) showed that

$$a_o = \frac{L(1 - \cos \theta)}{4 \sin \theta} \quad (2.29)$$



(a) Deflection



(b) Support geometry

$$\alpha = \frac{1 + (n^* u)^2}{1 - (n^* u)^2} \left(1 - \frac{u}{2}\right)$$

$$n^* = h / L$$

$$u = \delta_s / L$$

Figure 2.69 Idealized masonry wall (MacDowell et al., 1956)

where a_o and θ are shown in Fig. 2.69. Also, from Fig. 2.69a MacDowell et al. (1956) showed that the middle joint deflection can be give by

$$\delta = \frac{L(1 - \cos \theta)}{\sin \theta} \quad (2.30)$$

Comparing Eq. (2.29) and Eq. (2.30) results

$$a_o = \frac{\delta}{4} \quad (2.31)$$

Assuming P_u as the resultant force of the compressive stress on the contact area, the arch bending moment capacity, M_{arch} can be obtained

$$M_{arch} = P_u r_u \quad (2.32)$$

where the r_u is the lever arm and shown in Fig. 2.694a. Considering the geometry, r_u determined by McDowell et al. (1956)

$$r_u = h(1 - u - \frac{2\bar{y}}{h}) \quad (2.33)$$

where \bar{y} is the distance between centre of stress distribution to the bottom of the element.

McDowell et al. (1956) also defined the strain distribution along the contact area as

$$\frac{R\epsilon_m}{\epsilon_{mc}} = u(1 - \frac{2y}{h} - \frac{u}{2}) \quad (2.34)$$

where

ϵ_m is strain along the contact area at y from bottom,

ϵ_{mc} is the ultimate crushing strain

$R = \frac{\epsilon_{mc} L^2}{4h^2}$ is a non-dimensional variable

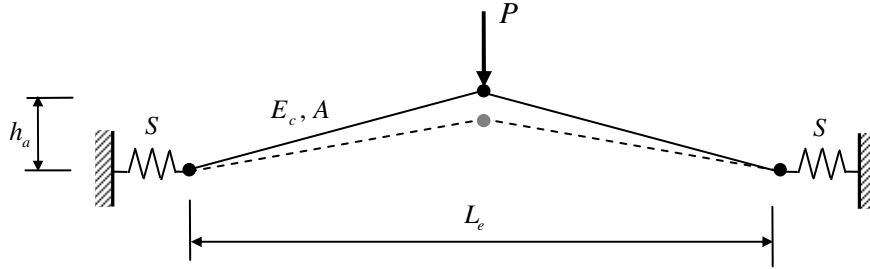
$u = \frac{\delta_s}{h}$ is the non-dimensional deflection

The relationship between load capacity and deflection is obtained by equating Eq. (2. 32) to the bending moment equation

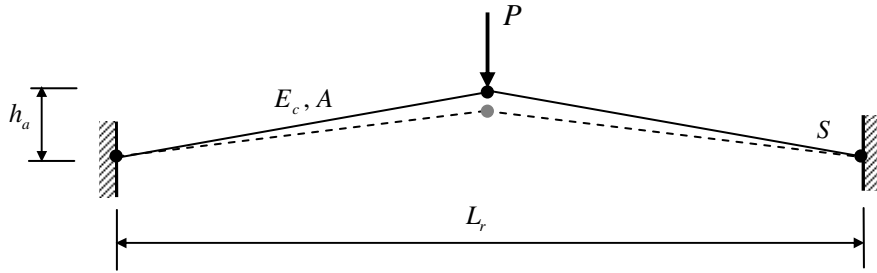
$$M_{rach} = \frac{w_{arch} L^2}{8} \quad (2.35)$$

The ultimate compressive membrane force i.e. P_u and bending moment i.e. M_u applying various values of R and u was determined by McDowell et al. (1956). The results was presented in terms of dimensionless parameters of M_r and P_r which were based on R and u . To study the behaviour of concrete elements considering lateral restrain (Fig. 2.70), Rankin and Long (1997) modified the theory developed by McDowell et al. (1956). The bending

moment and arching load strength were obtained separately to calculate the total load sustained by the elements.



(a) Elastic lateral support



(b) Rigid lateral support

Figure 2.70 Equivalent three-hinged arches (Ranking and Long, 1997)

By differentiating McDowell et al's equations for M_r with respect to u , Rankin and Long (1997) determined relationship between dimensionless arching moment ratio of M_r and R .

$R > 0.26$

$$M_r = \frac{0.3615}{R} \quad u = 0.31 \quad (2.36)$$

$0 < R < 0.26$

$$M_r = 4.3 - 16.1\sqrt{(3.3 \times 10^{-4} + 0.124R)} \quad u = -0.15 + 0.36\sqrt{8.18 + 5.6R} \quad (2.37)$$

where

$$R = \frac{\epsilon_{co} l_{rig}^2}{4h_1^2} \quad (2.38)$$

$$u = \frac{\delta_s}{h_1} \quad (2.39)$$

where ϵ_{co} is plastic strain of the concrete and $\epsilon_{co} = (-400 + 60f'_c - 0.33f'^2_c) \times 10^{-6}$

L_{rig} is the span of rigid restrained slab strip

h is the overall depth of the cross section

δ_s is the central deflection

h_1 is the depth of the arching section, see equation 2.41

f'_c is the compressive strength of concrete

The maximum bending moment in the compressive membrane action can be calculated, when arching bending moment ratio corresponding to the relevant R is known

$$M_{ra} = \frac{M_r 0.85f'_c h_1^2}{16} \quad (2.40)$$

where h_1 is the depth of the arching section

$$h_1 = h - (\rho + \rho') \frac{f_{sy} d}{0.85f'_c} \quad (2.41)$$

with:

h is the overall depth of the cross section

ρ is the positive reinforcement ratio

ρ' is the negative reinforcement ratio

f_{sy} is the yield strength of the reinforcement

d is the effective depth of the cross section

To study the effect of lateral restrain on the capacity of the slab strips, Rankin and Long extend their method by applying springs on the supports. They concluded that, elements with

elastic spring on the supports, Fig. 2.70a, and assuming rigid supports, Fig. 2.70b provides the same the load-deflection response if Eq. (2.42) is used to calculate arch span corresponding to rigid support. Also, it was found that the relationship between maximum arching bending moment assuming elastic and rigid support can be given by Eq. (2.43)

$$L_{rig} = L_e \left[\frac{E_c A}{S(l_b / 2)} + 1 \right]^{1/3} \quad (2.42)$$

$$M_a = M_{ar} \frac{l_e}{L_{rig}} \quad (2.43)$$

where:

L_e is the span of the laterally restrained strip

E_c is the elastic modulus of the concrete, $E_c = 4730\sqrt{f'_c}$, Mpa

S is the stiffness of the lateral spring restraint

A is the area of the arch leg, $A = 0.5h_1b$

b is the width of the section

The effect of lateral stiffness on the arching capacity is shown in Figure 2.71. Rankin and Long (1997) showed that for the lateral stiffens equal to the slab strip stiffness the arching capacity is between 50 and 80% of arching moment assuming rigid supports. The arching moment for the restraint stiffness is increased to 75 and 90%, if the stiffness is increased three time of arching stiffness of the strip slab. The maximum load sustained by the elements corresponding to the compressive membrane action can be obtained following calculating of the maximum arching moment

$$W = W_{mecc} + W_{arch} \quad (2.44)$$

where:

W_{mecc} is the mechanism load $= k_o (M_{y2} + M_{y1})$

W_{arch} is the arching load $= k_o M_a$

k_o is a static moment coefficient (for a uniformly distributed load $k_o = 8 / L^2$)

M_{y1} is the positive yield moment

M_{y2} is the negative yield moment

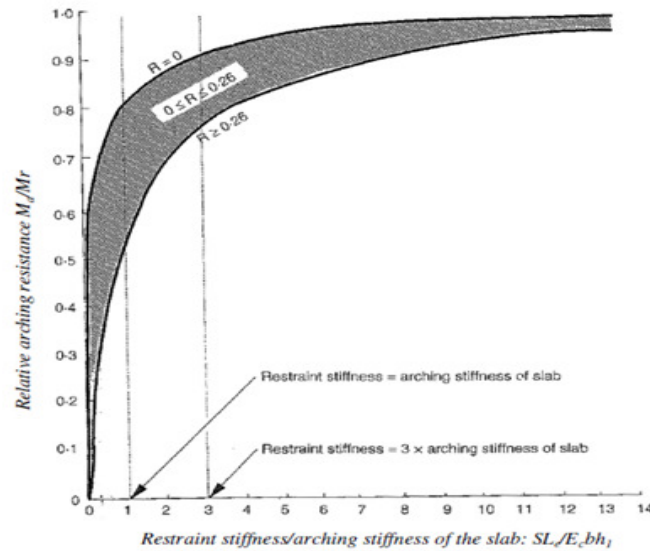


Figure 2.71 The effect of lateral stiffness on the arch capacity (Rankin and Long, 1997)

A comprehensive analytical model considering geometry of failure mechanism and section properties was developed by Park and Gamble (1980). It was assumed that the end supports is restrained against rotation and vertical deflection, but to consider the effect of lateral stiffness an elastic support with stiffness of S was applied at the ends as shown in Fig. 2.72. To develop the model the top steel at the both side assumed to be identical and at the each plastic hinge the steel is yielded. As in the present study only one hinge will be induced, the result of this method cannot be applied to study the behaviour of floor-to-floor slabs following removal wall panels.

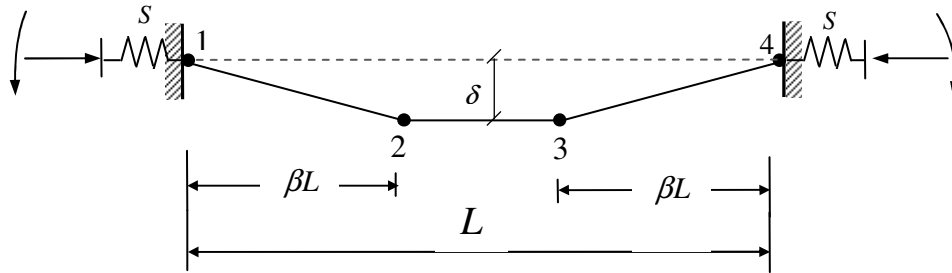


Figure 2.72 Plastic hinges of beams with the elastic lateral supports (Park and Gamble, 1980)

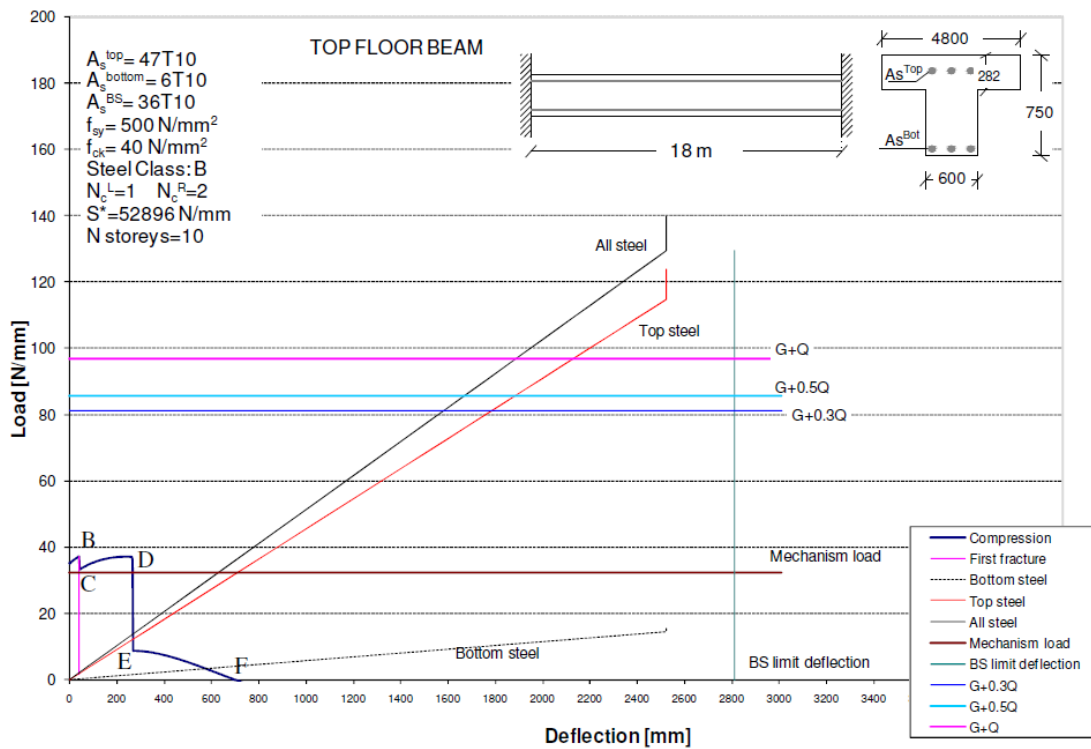


Figure 2.73 Load vs. deflection for a beam with rigid support (Merola, 2009)

Merola (2009) developed Park's (1964, a, b) model by identifying bar fracture failure during the compressive membrane action stage. In this model total strain suggested by Park (1964) was adopted to identify the point of bar fracture (Fig. 2.73). The developed model only is able to predict behaviour of RC beams in plastic stage without any obvious catenary action identified by Fig.2.68.

Discussion

Generally speaking almost the same concepts are used by the all three above models, while various failure mechanisms have been adopted. Total strain and deformation was considered by Rankin and Long's and Park's. Although the lateral elastic support was taken into account, but various approaches has been used. Also, Rankin and Long (1997) determined only maximum capacity, which can be considered as simplified model compare to the model developed by McDowell et al., as in later case complete load-deflection was proposed. The main deficiency of McDowell et al's model is that, it is not able to consider the elastic lateral support. In order to determine the maximum capacity corresponding to compressive membrane action, the model suggested by Rankin and Long (1997) is the best for the present study. In this model the effect of lateral support has been explicitly indentified. As in the present study only bottom steel exist, the overall depth in the Rankin and Long's model is assumed to be 30 mm more than effective depth of section.

2.12 OVERALL SUMMARY

To design structure for progressive collapse the prescriptive approach is used. These prescriptive tie requirements may have proven adequate in engineering practice but are not fully scientifically justified and have been subjected to numerous criticisms; so substantial efforts are still needed to improve the understanding, at a fundamental level, of how the mechanism of post-collapse resistance is developed through these tie provisions. This need has also been supported by a number of researchers in the last decade and the DoD 2005. Also, most reviewers imply that these rules are not well documented over the time. Furthermore, the provisions adapted in the British Standard and Eurocode show that the tie force needs to be accompanied by an extremely high vertical deflection in the event of removal of the wall supports i.e. in all cases more than storey height. However, according to

PCA tests or other experimental/FE studies on progressive behaviour of RC structures, the maximum deflections at the collapse are less than 20% of the span length.

According to recent test data and analytical models related to design for progressive collapse on concrete, steel and wood structures, the DoD 2005 UFC 4-023-03 was updated in 2013. These updates show a significant change to the 25 January DoD 2005 version, BS 8110-11:1997 and BS EN 1992 1-1:2004. The magnitude and location of tie forces has been remarkably revised. It clearly indicates that analysis and design approach to prevent progressive collapse has not yet been standardized.

In precast cross-wall constructions, requirements to prevent progressive collapse can be facilitated by the tie bars/strands embedded in the cast in-situ grout placed in the keyways and the end gap of floor slabs. After a removal of an underlying wall support, the grout will soon be crushed under the increased loads and these ties will immediately experience tensile forces and develop a large deflection for the floor slabs. This process forms a catenary mechanism. The catenary mechanism can be defined as the ability of a structure to sustain gravity loads through tension while the structural elements are withstanding excessive deflection. Stability of this mechanism heavily relies on bond-slip behaviour of the interface between steel bars and grout.

The pullout and bond-slip relationship of reinforcement bars/strands embedded in concrete and grout were reviewed. Pullout behaviour of a steel bar in concrete has been subjected to excessive investigation both analytically and experimentally in the last three decades; but research with regard to bond-slip simulation between steel bars and its surrounding grout in entire stages is relatively limited. According to the literature review, to date, analytical work for the full-range pullout process of reinforcement bars and the analytical/numerical analysis

of the catenary action mechanism in precast concrete cross wall structures have not been taken into account in previous work.

Compared with the experimental studies on the catenary action of steel structures, limited experimental studies are available on assessing the catenary action in RC structures. This is especially the case for the multi-storey precast concrete cross wall buildings. PCA's and Regan's experimental studies are the only published work on the performance of cross wall structures in terms of the catenary action and the progressive collapse by considering the floor-to-floor joint behaviour. The previous research mostly focused on the behaviour of walls during the progressive collapse.

The experimental studies indicate that the progressive resistance of RC structures varies extremely with boundary condition and reinforcement detailing. However, most studies concluded that RC structures with reinforcement detailing for seismic zones are capable of developing catenary action following removal of a column support. In some cases for the same beam dimension and reinforcement bars' detailing, the result of investigation on progressive collapse resistance shows a significant discrepancy, so that in notable cases the differences are meaningful. Furthermore, although, progressive collapse of RC structures has been successfully simulated using various softwares, the focus was mostly on simulation of the catenary action mechanism and progressive collapse resistance of RC structures; while the efficiency of codified provision has been subjected to limited attention.

Chapter 3

EXPERIMENTAL STUDIES

3.1 INTRODUCTION

This chapter presents the results of an experimental study to investigate a mechanism which can be used to prevent progressive collapse, due to the removal of a wall support in a precast concrete cross wall structure in the event of explosion or bombing attack. The concept that was studied and verified is based on the recommendation of Bison and Coltman Ltd, which is used in the current cross wall structures' industry. To prevent progressive collapse a catenary action mechanism should be provided to bridge up the load from the damaged area to the rest of the undamaged structure. In other words, an alternate load path should be established to limit the scope of the progressive collapse. To this end, longitudinal ties must be placed in the floor-to-floor joints. Accordingly, an experimental investigation programme studying the pre- and post-bond failure performance of floor-to-floor connections with longitudinal ties is carried out. To develop a reliable criterion for the catenary behaviours two types of experimental tests are performed i.e. pullout tests and full-scale floor-to-floor tests.

This chapter presents a study on the bond behaviour of reinforcement bars in normal strength concrete considering the bar size, embedment length, concrete type and the direction of the applied pullout force. The other aim of this study is to study the abilities of ribbed tie bars to develop a catenary mechanism in a typical floor-to-floor joint. Developing a firsthand data set for finite element analysis and analytical modelling of a floor-to-floor system can also be considered as one of the aims of the present experimental study.

The test specimens were a full-scale representation of a precast hollow core slab of typical cross wall structures for both pullout and full scale floor-to-floor tests. The test set-up was designed, fabricated and installed by the researcher. In the pullout test, the size of the specimens was selected according to the required embedment length of the steel in the concrete. According to literature and due to some limitations in the laboratory, two floors slabs with a length of two metres and of full width were chosen for the full scale floor-to-floor joint tests.

Through the pullout results, the tie force versus pullout displacement relationship was established and the ultimate bond force and post-bond failure behaviour was recorded. The floor-to-floor system consists of a full scale two-span floor slab assembly including connections with grout, keyways and longitudinal ties. In this system, a precast concrete slab manufactured by Bison Ltd, cast-in-situ grout and steel bars in keyways were used. The strain in the tie and the vertical deflection at the middle joint is recorded by pre-instrumented sensors, e.g. strain gauges and LVDTs.

3.2 MATERIAL PROPERTIES

3.2.1 Reinforcing Steel

In the UK's precast concrete industry, to design for the progressive collapse, most tie bars are specified as 10 or 12 mm in size in accordance with the current TF method. In this study, bar sizes of 8 mm, 10 mm and 12 mm were selected. The reinforcement bars were of the UK type C, with a characteristic yield stress of 500 MPa. To characterise the actual tensile behaviour of the reinforcement bars, three standard tension tests were performed for the steel bars used in each test; from which the stress-strain curves were recorded. The actual yield stress was 530, 515 and 547 MPa for bar sizes of 8 mm, 10 mm and 12 mm respectively. The ultimate tensile strength for the same bar sizes were 635, 615 and 675 MPa respectively. Figure 3.1

shows an average stress-strain curve for the different bar sizes used in four full scale tests. Each curve is the average of four specimens.

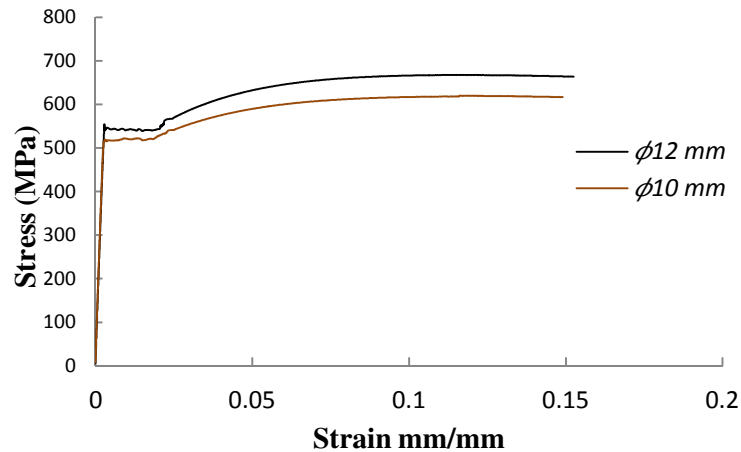


Figure 3.1 Stress-strain for different bar sizes used in the four full scale specimens

3.2.2 Concrete

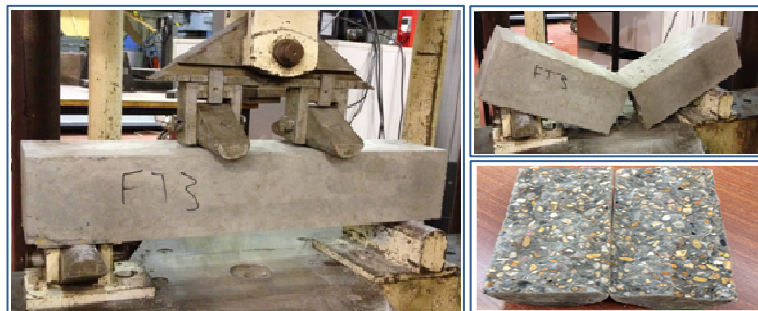
The concrete mix was designed for a targeted compressive strength of 20, 25 and 30MPa at 28 days. The compressive strength for the different specimens in pull-out test experiments are presented in Tables 3.1, 3.2 and 3.3. Due to the limited space in the keyways, the most challenging aspect of the pull-out and full scale floor joints' tests was developing a concrete mix which could satisfy both workability and strength requirements. The measured slump was required to be between 100 and 125. The grout mix consisted CEM2, aggregate with a size of up to 10 mm. In order to develop an efficient concrete mix design which could meet the requirements during different castings, six trial batches were mixed. According to these results, three design mixes which could provide a concrete strength of 20, 25, 30 MPa were developed. The manufactureinge, quality, placement and curing of the grout in the keyways and transverse joints was chosen to be the replication of practice. To provide concrete with different strengths, in this study the amounts of aggregate and cement were chosen based on

"Design of Normal Concrete Mixes" (Teychenné et al., 1997). The compression test specimens for the concrete were the cube with side lengths of 100 mm or a standard cylinder.



(a) Test machine for cube and cylinder compressive test

(b) Slump Test



(c) Tensile test on prism and cylinder specimens

Figure 3.2 Test equipment

The average compressive strength of the cube or cylinder and the tensile strength of the prism were calculated based on the three specimens $\phi 150 \times 300$ mm cylinder or $100 \times 100 \times 100$ mm cube specimens on the days of the tests. The slump of concrete was between 90-110 mm on the day of the placements, which was in the range of the design limit (Fig. 3.2). The stress-strain curves for the concrete grout in full scale tests are shown in Fig. 3.3.

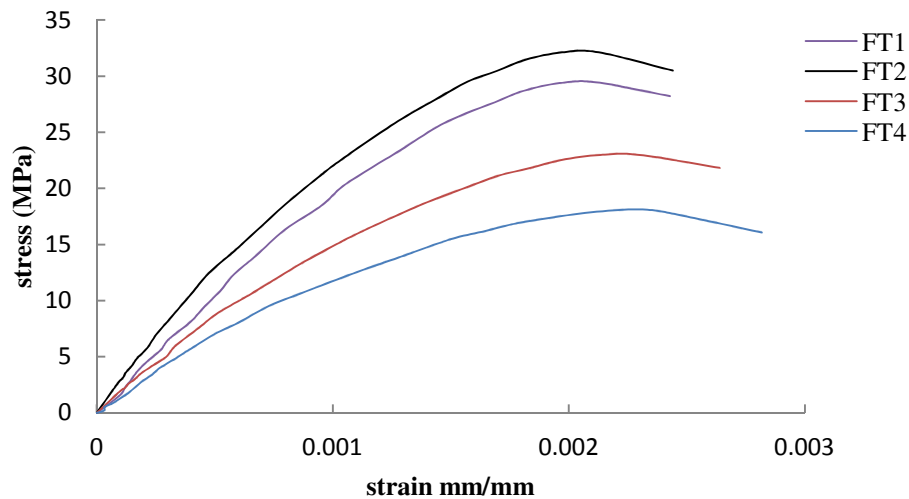


Figure 3.3 Stress-Strain curves for concrete grout

3.2.3 Precast Concrete Floor Slabs

Precast hollow core plankS up to 1.2 m in width are usually used as a floor member in the precast cross wall building. For the present research, 97 precast concrete specimens designed and provided by Bioson Ltd were used; among which, 85 short precast slabs were allocated for pullout and 12 full scale slabs were for the full scale tests (Fig. 3.4). In all specimens one open trough was provided to facilitate various embedment lengths (Fig. 3.4b).



(a) 97 precast slab specimens provided by Bison Ltd



(b) Providing open
through

(c) 85 short precast slabs used as pullout test
specimens

Figure 3.4 Precast concrete slabs for pullout tests

3.3 PULLOUT TEST

3.3.1 Geometry and properties of test specimens

This present study was carried out with the aim of studying the behaviour of ribbed bar in grouted keyways of a precast slab, using actual embedment length and developing the bond-slip criteria to design a floor-to-floor joint in precast concrete cross wall structures. The influences of concrete type, embedment length, bar size and slope of applied load were examined. The specimens were designed to create the pullout and bar fracture failure modes requirements. As has been shown in some research works, the assumptions of a uniform stress along the bonded length is valid only for an infinitesimally small embedment length of bars (Engstrom et al., 1996; Abrishami and Mitchel, 1992). In practice, a bonded length of finite value had to be adopted and thus, this assumption is no longer true. Accordingly all pullout tests are performed using full scale slabs along with an actual embedment length.

In present study 57 pullout tests were performed. The steel bars were placed in grouted keyways milled in the short length of precast concrete slabs or into prisms. Concrete type, direction of pullout load, diameter and embedment of steel bars were considered as significant

variables. The details and dimension of the pullout test specimens are shown in Fig. 3.5, which due to its high efficiency is designed to meet type three or four experiments presented in Chapter 2. The blocks were cut from the precast hollow core slabs and had the following dimensions: 400 mm in width, 150 mm in height and a variable length, with an aim to study the effect of the embedment length. The number of specimens and corresponding variables in the pullout tests are illustrated in Tables 3.1 to 3.4. It is important to note that to confirm the reliability of the rig, the first 17 tests were used to calibrate the test rig and other equipment, whose results are not included in the discussion.

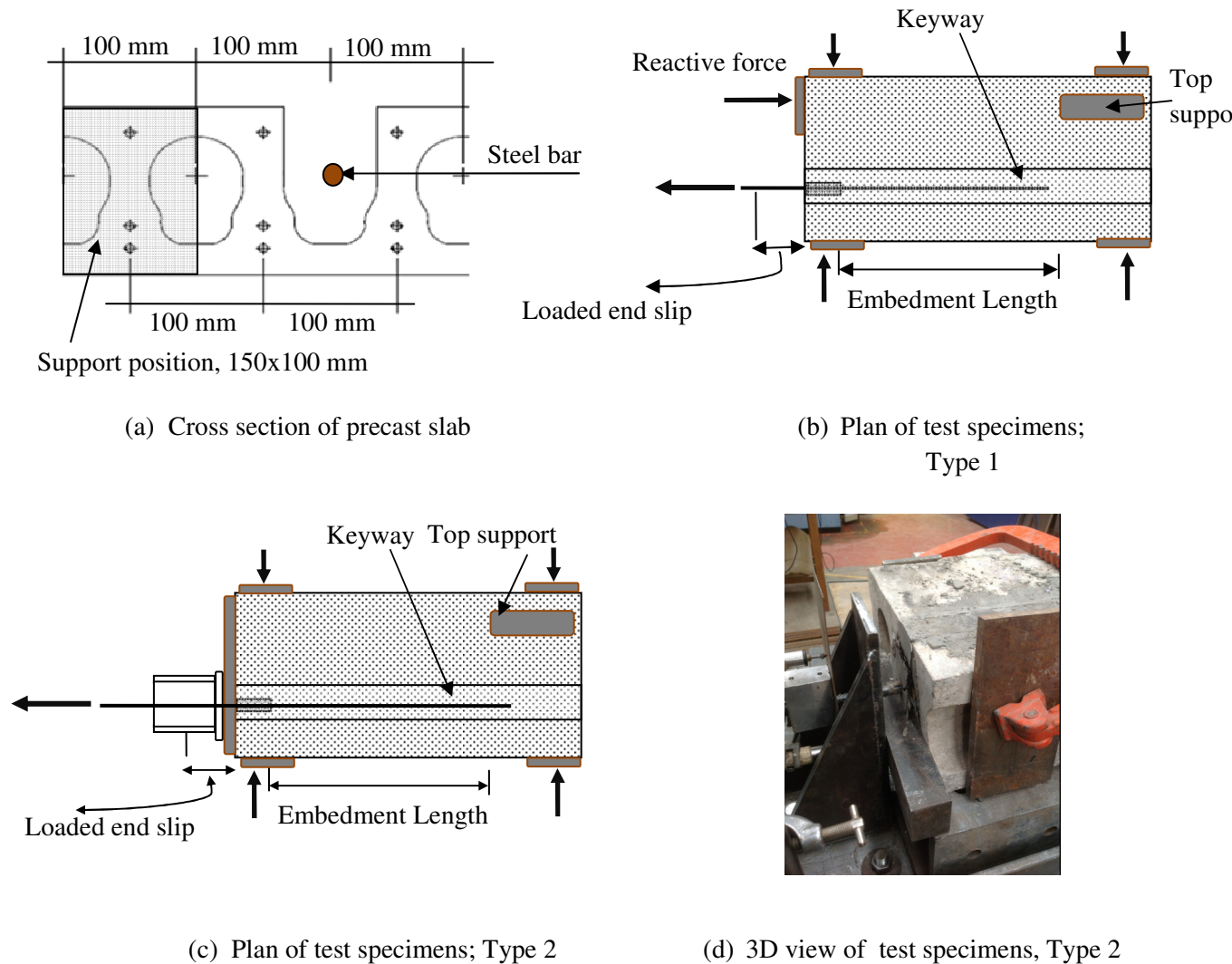
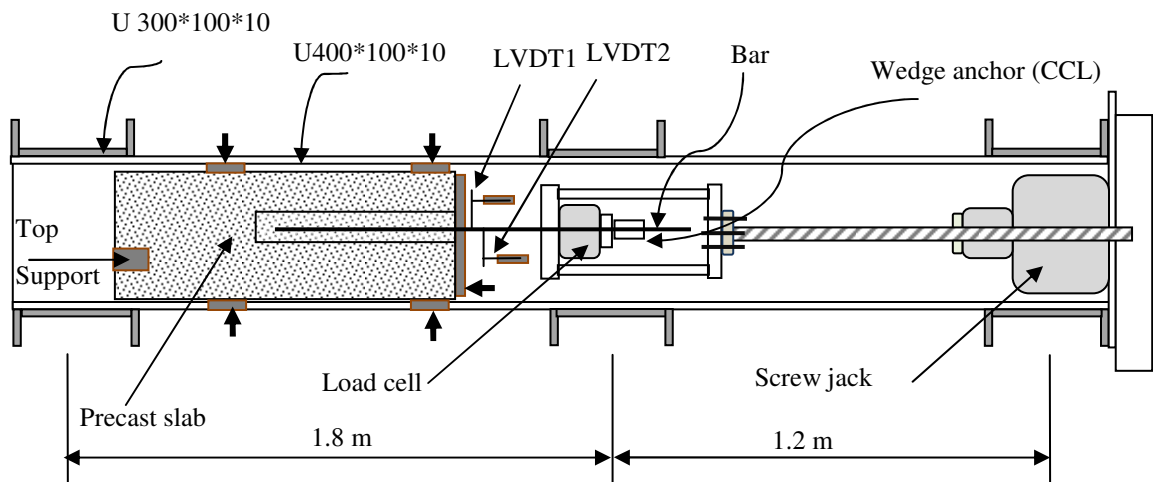


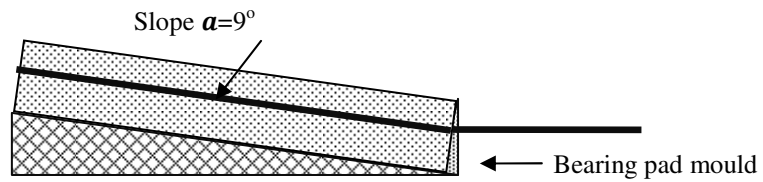
Figure 3.5 Details of a typical pullout specimen

The test set up for both types of specimens, i.e. precast slab and prisms, is shown in Figure 3.6. Due to the relatively large dimensions of the specimens and an expected maximum pullout load up to 100 kN, a frame structure consisting of U300x10 and L100x100 was analyzed and designed. Each column was connected to a strong floor. Due to the eccentricity of the applied load in type 1, in addition to the front support, four supports at the sides and one support at the top of the specimens were applied. Following trial tests, it was found that there is not obvious difference between type 1 and 2 test rigs, hence type 2 was chosen for the pullout tests (Fig. 3.5c, d, and Fig. 3.6a).

To apply tensile force a screw jack with a capacity of 200 kN was used and a load cell measured the relevant applied load. Displacement of the steel bars at the pulled end was measured by LVDTs through a data logger connected to the PC. To study the pullout behaviour of the steel bars in the concrete, load versus pullout displacement was plotted for all specimens. A 30 mm plastic tube bond breaker was placed on the steel at the loaded end of the specimen to reduce the effects of confinement. The bond breaker reduces the effects of confinement on the steel bond. The results reveal that the tubes do not affect the relationship between the pullout load and displacement remarkably. The concentrically cast steel was pulled at a rate of 0.35 mm /min. A synchronized graph of applied load and relative displacement was monitored through Squirrel software. Initially to take up any slack in the apparatus and attachment, a force of around 2% of the expected ultimate load (BS 5080-1:1993) was applied. Pull-out test on the specimens were carried out when the concrete had reached compressive strength of f_c MPa \pm 3 MPa.



(a) Plan of pullout test rig



(b) Pull out test under inclined load

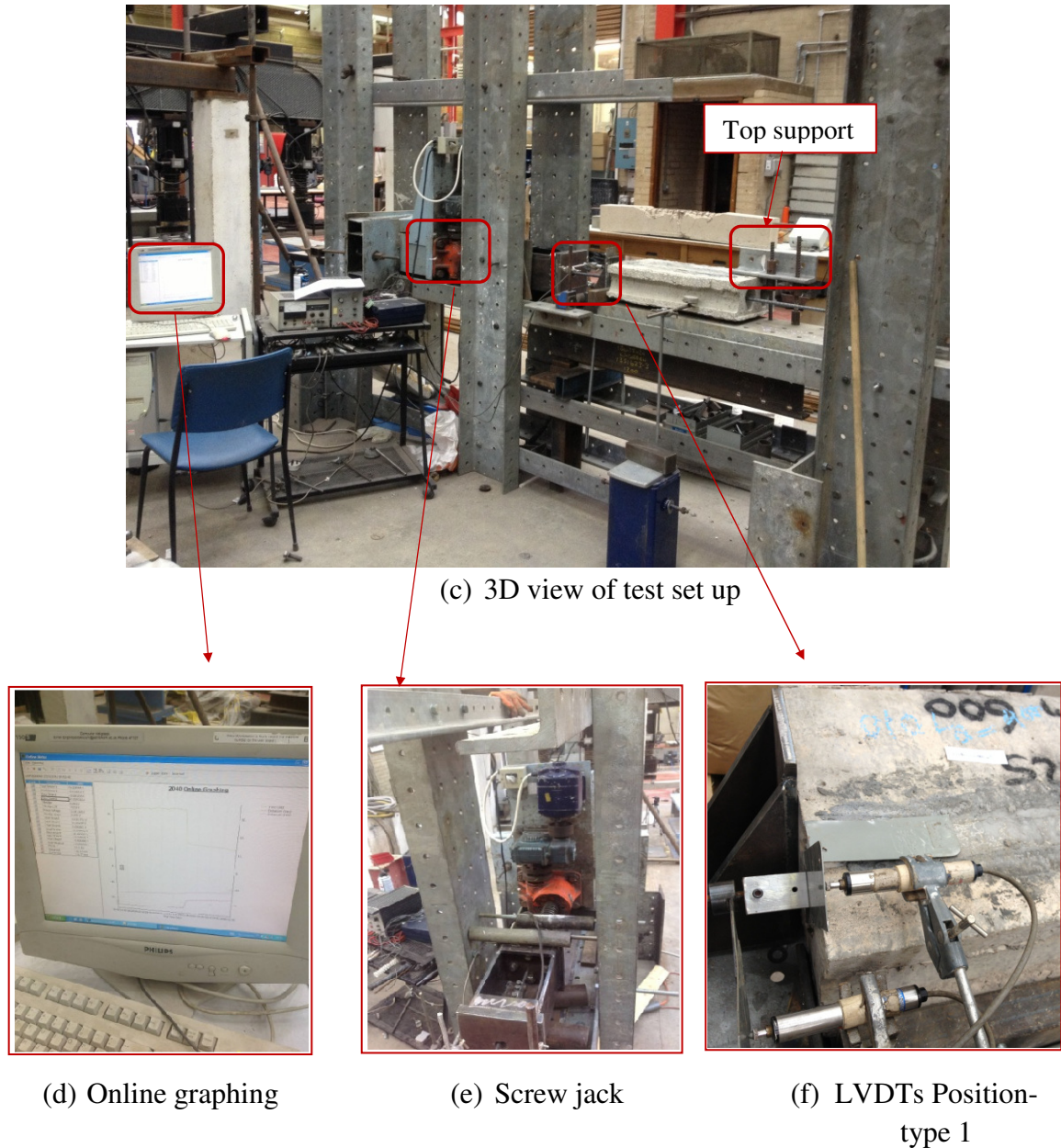
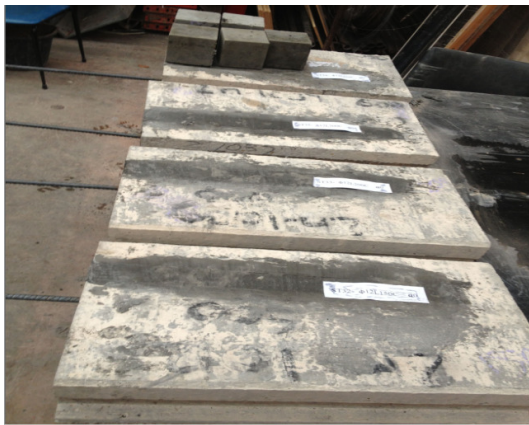


Figure 3.6 Test setup for a pullout test, series PT and ST

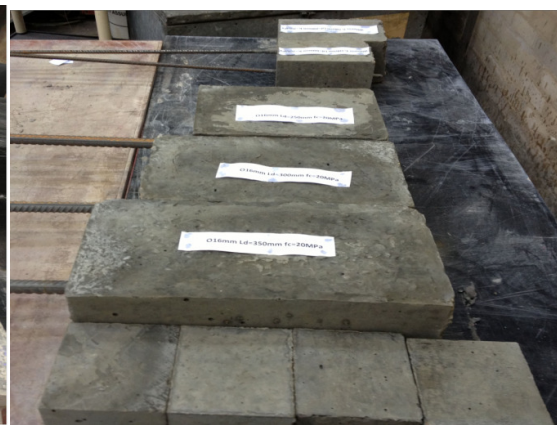
3.3.2 Pullout test results and evaluation

It is obvious that the possible failure may occur: (a) in the bar, (b) in the concrete, (c) in the slab, (d) at the bar-concrete interface, (e) at the concrete-keyway and precast slab interface, (f) or a combination of these failure modes. This study was concerned with the bar-concrete interface failure, which is the most common failure mode. As the deformation of the

surrounding concrete is often negligible, it can be assumed that the bar will be under uniaxial tension and the bar-concrete interface layer will experience interfacial shear slip only (Ren et al., 2000). Specimens with steel bars cast into the keyways of the precast slabs are referred as ST, steel bars cast in a prism is called as PT and they were all numbered from 1 to 57 followed by four numbers. The first number indicates bar size, the second number indicates embedment length; the third number shows the compressive strength of the specimens and fourth number shows the angle of applied load (Tables 3.1-3.4).



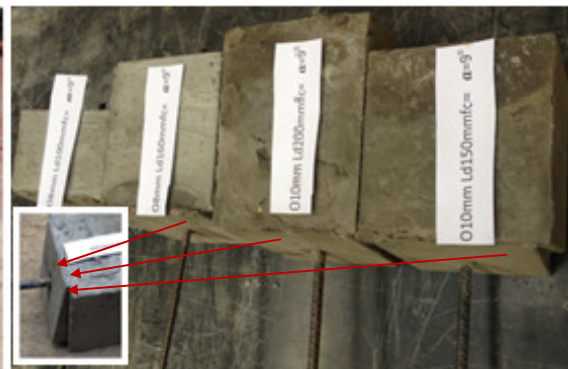
(a) Precast specimens, $\alpha=0^\circ$



(b) Prism specimens, $\alpha=0^\circ$



(c) Precast specimens, $\alpha=9^\circ$



(d) Prism specimens, $\alpha=9^\circ$

Figure 3.7 Precast and prism specimens for pullout tests

Forty-seven pullout specimens were subjected to horizontal loads (Fig. 3.7a, b) and ten specimens were subjected to an inclined load (Fig. 3.7c, d). To show any possible difference between the behaviour of the tie in the grouted keyways in the precast element and the prisms, 13 specimens were made on prisms (Fig. 3.7b, d). Bar size and embedment lengths were the principal variables in both series of tests. In addition, other variables included compressive strength of concrete, inclination angle of pulling load and shape of moulds. Due to the current factory requirements for the properties of cast-in-situ concrete in the keyways, the first three series of tests were made on 8 mm, 10 mm and 12 mm bar sizes with an average compressive strength of 30, 35 and 31 MPa, respectively.

Table 3-1 Pullout test data with 8 mm diameter rebar

Mark	Type	L_e/d_b	Pullout angle (deg)	Concrete strength (Mpa)	Embedded length (mm)	Maximum pullout force (kN)	Note*
ST1-φ8L160C30 a 0	S	20	0	30	160	27.1	Keyway rupture
ST2-φ8L250C30 a 0	S	31	0	30	250	24.0	Bar fracture
ST3-φ8L400C30 a 0	S	50	0	30	400	27.3	Bar fracture
ST4-φ8L160C18 a 0	S	20	0	18.3	160	18.9	Bar fracture Bar fracture Bar fracture
ST5-φ8L200C18 a 0	S	25	0	18.3	200	25.8	
ST6-φ8L250C18 a 0	S	31	0	18.3	250	25.3	
ST7-φ8L300C18 a 0	S	37.5	0	18.3	300	26.3	
ST8-φ8L160C24 a 0	S	20	0	24.5	160	23.1	
ST9-φ8L200C24 a 0	S	25	0	24.5	200	24.5	
ST10-φ8L160C20 a 9	S	20	9	20	160	20.4	Bar fracture
ST11-φ8L200C20 a 9	S	25	9	20	200	24.1	
Prisms							
PT12-φ8L200C18 a 0	P	25	0	18	200	23.3	Bar fracture Bar fracture
PT13-φ8L250C18 a 0	P	31.25	0	18	250	25.5	
PT14-φ8L300C18 a 0	P	37.5	0	18	300	26.9	

*Pullout unless otherwise noted

The experimental results for the 8 mm reinforcement bar as a preliminary investigation are summarized in Table 3.1. Figures 3.8 and 3.9 show the experimentally determined relationship between pullout force and slip at the loaded end for the bar size of 8 mm, considering various embedment lengths and compressive strength of the concrete. The results

indicate the difference between the response of specimens displaying fracture failure and pullout failure mode. All specimens with a compressive strength of 30 MPa at 28 days and an embedment length of more than 160 mm experienced bar fracture failure mode (Fig. 3.8).

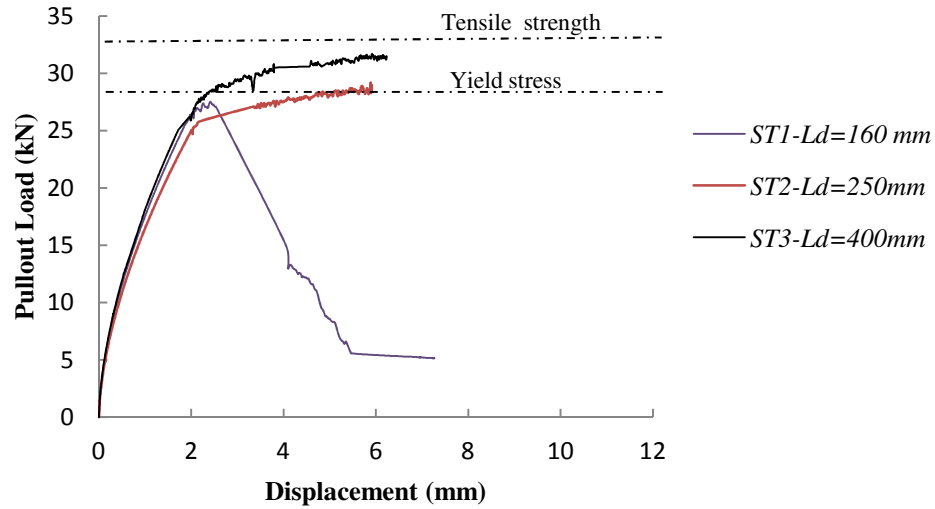


Figure 3.8 Pullout load versus pullout displacement for 8 mm diameter bar and different embedment lengths; $f_c = 30\text{MPa}$, $\alpha = 0$

In line with the above results, the next sets of specimens were designed considering a compressive strength of 18, 20 and 24 MPa. However, only specimens with a compressive strength less than 25 MPa and an embedment length less than or equal to 160 mm led to pullout failure mode (Fig. 3.9). Pullout failure mode with remarkable strength and large displacement occurred for an embedment length less than 20 diameters and compressive strength of 20MPa, i.e. $l_d / \phi \leq 20$. Extraordinary damage of the concrete around the reinforcement bar occurred at pullout. In the pullout failure mode, concrete at the interface sheared off along the embedment length in a cylindrical pattern. However, Figure 3.9 displays that following the peak pullout force there is still considerable constant pullout force. This residual pullout strength is due to the fact that concrete is capable of transferring bond stress across the rough crack along the interface between the steel and the concrete. It is to be noted that in Tables 3.1, 3.2 and 3.3, maximum pullout load in the case of the bar fracture mode was recorded based on yielding force and not ultimate tensile capacity.

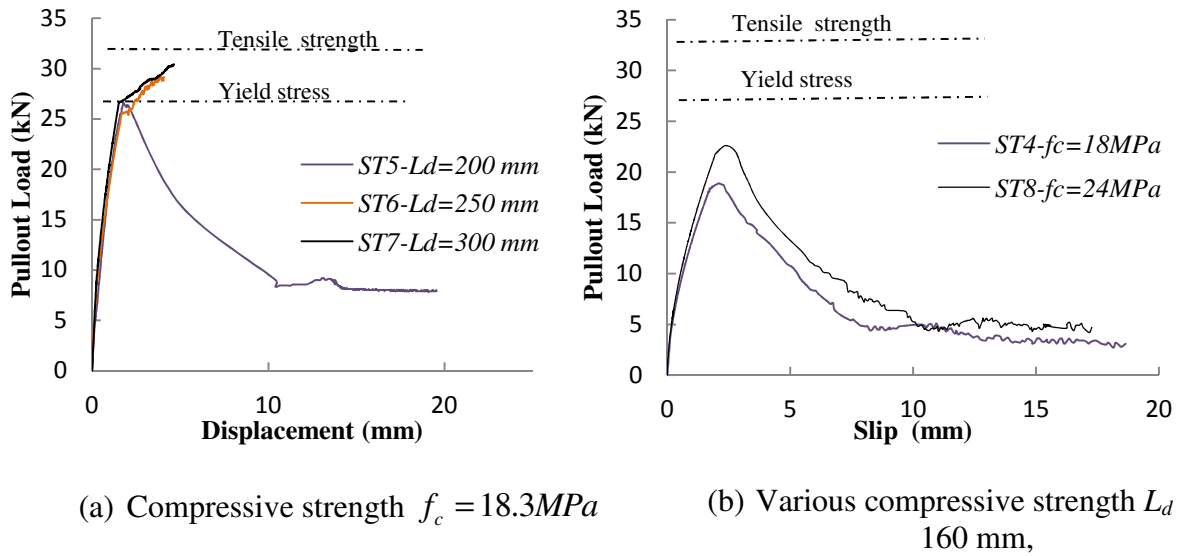


Figure 3.9 Pullout load versus slip for 8 mm diameter bar

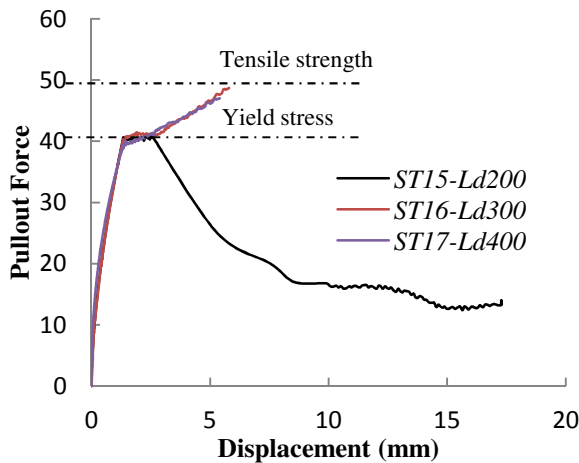
Table 3-2 Pullout test data with 10 mm diameter rebar

Mark	Type	L_d / d_b	Loading angle (Deg)	Grout strength (Mpa)	Embedded length (mm)	Maximum pullout force (kN)	Note *
ST15- $\phi 10\text{L}200\text{C}35\text{a}0$	S	20	0	35	200	40.9	Keyway fracture**
ST16- $\phi 10\text{L}300\text{C}35\text{a}0$	S	30	0	35	300	41.3	Bar fracture
ST17- $\phi 10\text{L}400\text{C}35\text{a}0$	S	40	0	35	400	39.3	Bar fracture
ST18- $\phi 10\text{L}210\text{C}19\text{a}0$	S	21	0	19.2	210	36.6	
ST19- $\phi 10\text{L}200\text{C}25\text{a}0$	S	20	0	25	200	37.92	Bar fracture
ST20- $\phi 10\text{L}300\text{C}25\text{a}0$	S	30	0	25	300	39.10	Bar fracture
ST21- $\phi 10\text{L}400\text{C}25\text{a}0$	S	40	0	25	400	41.3	Bar fracture
ST22- $\phi 10\text{L}150\text{C}20\text{a}0$	S	15	0	20.3	150	26.2	
ST23- $\phi 10\text{L}200\text{C}20\text{a}0$	S	20	0	20.3	200	34.4	
ST24- $\phi 10\text{L}250\text{C}20\text{a}0$	S	25	0	20.3	250	42.3	Bar fracture
ST25- $\phi 10\text{L}300\text{C}20\text{a}0$	S	30	0	20.3	300	40.1	Bar fracture
ST26- $\phi 10\text{L}150\text{C}21\text{a}9$	S	20	9	21	150	32.3	
ST27- $\phi 10\text{L}200\text{C}21\text{a}9$	S	25	9	21	200	37.3	
Prisms							
PT28- $\phi 10\text{L}200\text{C}18\text{a}0$	P	20	0	18	200	32.1	
PT29- $\phi 10\text{L}300\text{C}18\text{a}0$	P	30	0	18	300	35.3	Split failure
PT30- $\phi 10\text{L}400\text{C}18\text{a}0$	P	40	0	18	400	42	Bar fracture

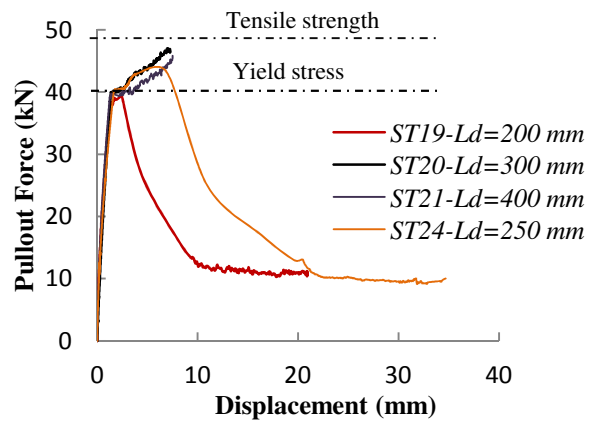
*Pullout unless otherwise noted

** Keyway fracture happened while bar was in the middle of plastic zone

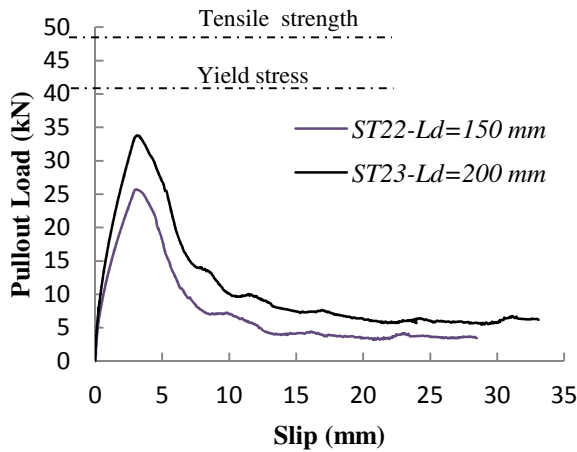
Data for 10 mm reinforcement bar is presented in Table 3.2. To investigate the respective requirements for pullout and bar fracture failure modes, various embedment lengths and compressive concrete strength were taken into account. The pullout force-slip relationship considering both failure modes is shown in Figure 3.10. The results indicate that the pullout strength of the specimens is increased with the increasing of the embedment length and the compressive strength of the concrete. Figures 3.10 (a), (b) and (c) clearly indicate that a wide range of embedment lengths and compressive strength led to the bar fracture mode of failure. The specimens with embedment lengths more than 20 diameters and a compressive strength of 35 and 25 MPa led to bar fracture failure mode (Figs. 3.10 a, b). Although it is generally accepted that reinforcement bars with an embedment length more than the anchorage length are fully bonded and they will not experience any slip, the results show that at the yielding, steel bars experience considerable slip at the loaded end.



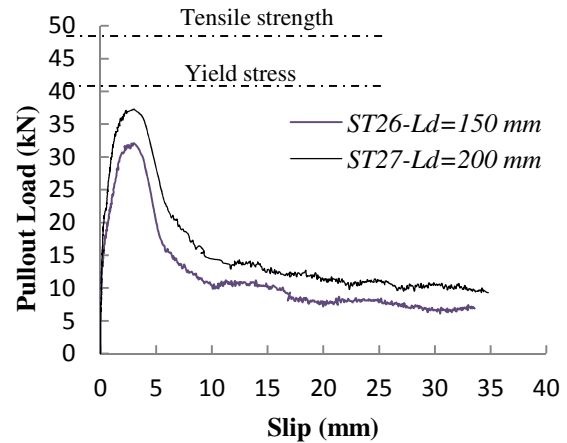
(a) Compressive strength
 $f_c = 35 \text{ MPa}, \alpha = 0$



(b) Various compressive strength and
embedment length



(c) Compressive strength $f_c = 20\text{MPa}$



(d) Compressive strength $f_c = 21\text{MPa}, \alpha = 9^\circ$

Figure 3.10 Pullout load versus pullout displacement for bar size of 10mm and different embedment lengths and under straight and inclined force

Pullout failure mode with suitable tensile strength at a relatively high pullout displacement occurred at embedment lengths of less than 20 diameters and compressive strength of less than 25 MPa, i.e. $l_d / \phi \leq 20$. Figures 3.10 (c) and (d) show the different behaviours of pullout load against slip. It can be seen that both show a similar pattern except 9° loading inclination angle will increase the ultimate bond load as well as the residual pullout strength. The results show that slip at the peak load for all specimens was almost identical and both around 2.77 mm. Figures 3.10 (c) and (d) display remarkable constant residual pullout strength up to pullout displacement of 35 mm, which will play a crucial role in the catenary action mechanism in the precast cross wall structure following the removal of wall supports due to any abnormal loads.

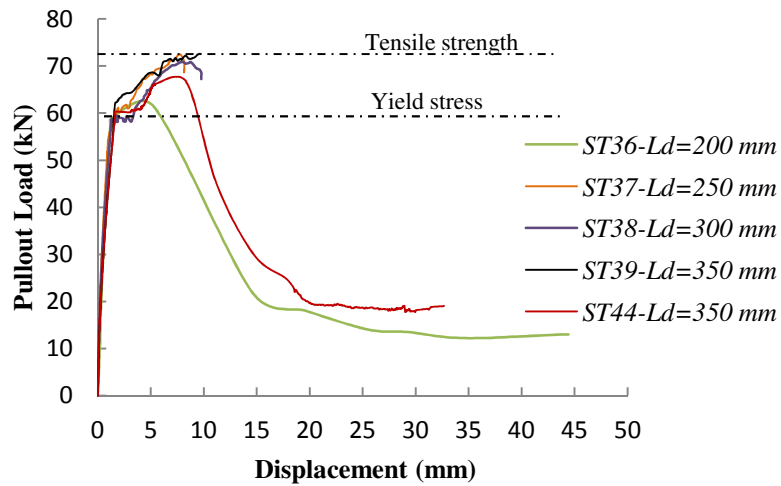
Table 3-3 Pullout test data with 12 mm diameter rebar

Mark	Type	L_d/d_b	Pullout angle (Deg)	Grout strength (MPa)	Embedded length (mm)	Maximum pullout force (kN)	Note*
ST31- ϕ 12L240C31a0	S	20	0	31	240	47.1	Slab separated Unrestrained
ST32- ϕ 12L300C31a0	S	25	0	31	300	49.6	Slab separated-Unrestrained
ST33- ϕ 12L360C31a0	S	30	0	31	360	50.9	Slab separated-Unrestrained
ST34- ϕ 12L420C31a8	S	35	0	31	420	53.3	Slab separated-Unrestrained
ST35- ϕ 12L480C31a0	S	40	0	31	480	62.2	Bar fracture—Restrained
ST36- ϕ 12L200C35a0	S	16.7	0	35	200	61.8	Bar Fracture-Pullout
ST37- ϕ 12L250C35a0	S	20.8	0	35	250	61.1	Bar Fracture
ST38- ϕ 12L300C35a0	S	25	0	35	300	59.5	Bar Fracture
ST39- ϕ 12L350C35a0	S	29.2	0	35	350	61.8	Bar Fracture
ST40- ϕ 12L150C20a0	S	12.5	0	19.9	150	31.5	Bar Fracture
ST41- ϕ 12L200C20a0	S	16.7	0	19.9	200	41.0	
ST42- ϕ 12L250C20a0	S	20.8	0	19.9	250	47.9	
ST43- ϕ 12L300C20a0	S	25	0	19.9	300	55.6	
ST44- ϕ 12L350C20a0	S	29.2	0	19.9	350	59.2	
ST45- ϕ 12L250C20a9	S	20.8	9	20	250	53.4	
ST46- ϕ 12L300C20a9	S	25	9	20	300	61.95	
Prisms							
PT47- ϕ 12L200C22a0	P	16.7	0	22	200	43.8	Bar fracture
PT48- ϕ 12L250C22a0	P	20.8	0	22	250	48.9	
PT49- ϕ 12L300C22a0	P	25	0	22	300	68.4	
PT50- ϕ 12L200C21a9	P	16.7	9	21	200	48.07	
PT51- ϕ 12L200C21a9	P	20.8	9	21	250	56.6	

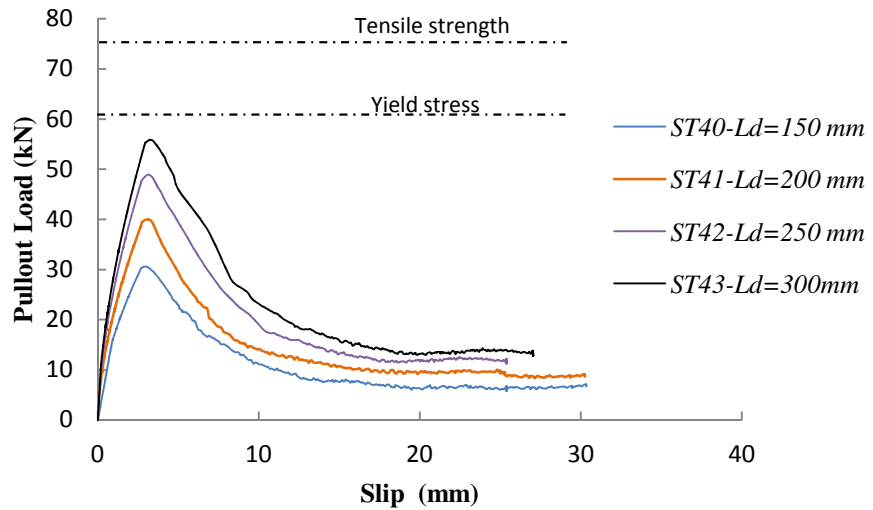
*Pullout unless otherwise noted

The geometric and material properties and their test results for bar size of 12 mm are shown in Table 3.3. . Slab-keyway rupture or slab separation occurred for all embedment lengths with a compressive strength of 35MPa without lateral support. Similar to previous pull-out tests, in the specimens with lateral support, small, small anchorage length and low compressive strength i.e. 20 MPa, pullout failure mode occurred while the steel bar was in the elastic range. For low compressive strength, bar fracture happened for an embedment length of more than 25 diameters; while for higher compressive strength, i.e. 31 MPa, bar fracture occurred in the specimen with smaller embedment length, i.e. 17 diameters. The pullout force versus slip curves are shown in Figure 3.11. The results show that pullout capacity increases

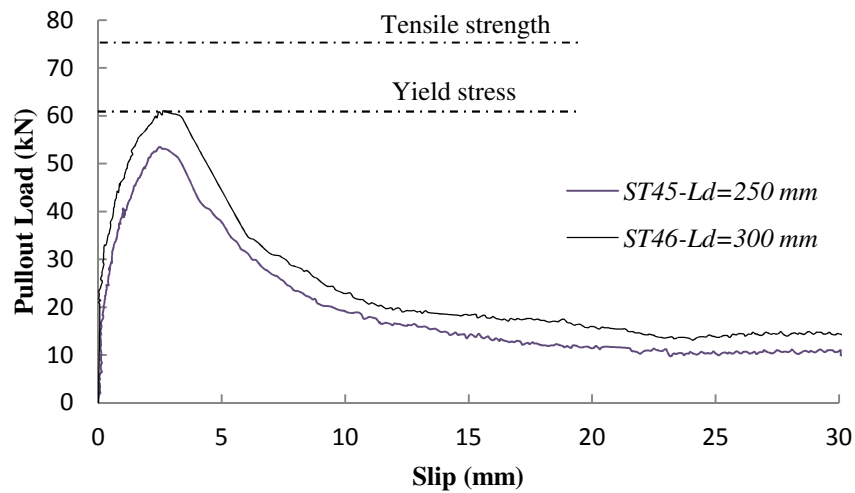
proportionally to embedment length. Furthermore, for specimens with embedment lengths slightly less than anchorage length, proposed by EC2, following the plastic zone pullout failure mode occurs. The same result was obtained the pull-out tests undertaken by Engstrom et al. (1998).



(a) Bar fracture failure mode



(b) Pullout failure mode , $f_c = 20\text{MPa}$, $\alpha = 0$



(c) Pullout failure mode, $f_c = 20\text{MPa}$, $\alpha = 9$

Figure 3.11 Pullout load versus pullout displacement for bar size of 12 mm and different embedment

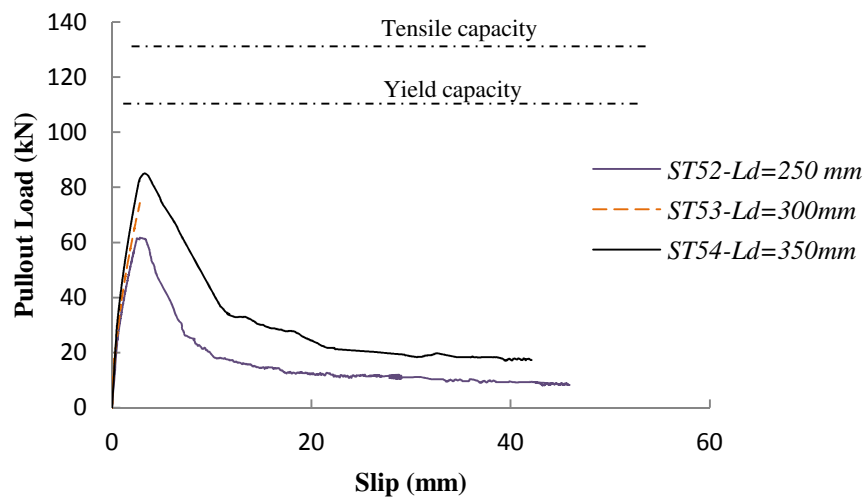
In specimens with inclined pullout load, inclined force resulted in increased strength and friction. Figure 3.11c shows the effect of pull angle on pullout behaviour. Furthermore, pull angle allowed remarkable pullout displacement before the descending phase.

Data for the tie bar of 16 mm are shown in Table 3.4. According to the results of 8, 10, and 12 mm bar size, only low compressive strength and an embedment length/bar size ratio of less than 20 were chosen. For low compressive strength, bar fracture again happened for an embedment length of more than 20 diameters. Tie force versus pullout displacement curves are shown in Figure 3.12. Also, note that, following the pull-out failure a in some specimens along the keyway of precast a small longitudinal crack was observed, which may resulted a relatively sharp descending phase.

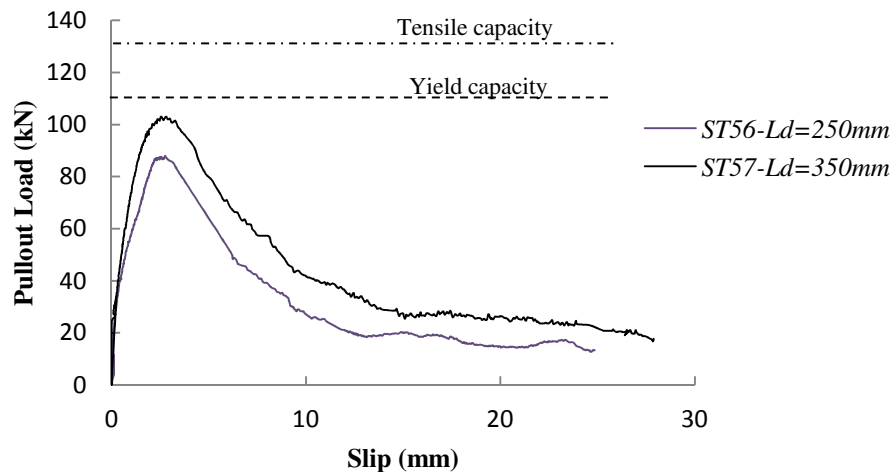
Table 3-4 Pullout test data with 16 mm diameter rebar

Mark	Type	L_d/d_b	Pullout angle Deg	Grout strength (Mpa)	Embedded length (mm)	Maximum pullout force (kN)	Note*
ST52- $\phi 16$ L250C20a0	S	15.6	0	19.7	250	62.7	Pullout- Support failure Bar fracture-Jack broke
ST53- $\phi 16$ L300C20a0	S	18.75	0	19.7	300	75.7	
ST54- $\phi 16$ L350C20a0	S	21.9	0	19.7	350	83.5	
ST55- $\phi 16$ L500C20a0	S	31.25	0	19.7	500	114.5	
ST56- $\phi 16$ L250C25a9	S	15.6	9	25	250	85.1	
ST57- $\phi 16$ L350C25a9	S	21.9	9	25	350	102.78	

*Pullout unless otherwise noted



(a) Pullout failure mode, $f_c = 20\text{MPa}$, $\alpha = 0$



(b) Pullout failure mode, $f_c = 20\text{MPa}$, $\alpha = 9$

Figure 3.12 Pullout load versus pullout displacement for bar size of 16 mm and different embedment

Discussion

In the short precast slab specimens with suitable lateral supports to simulate full precast slab, three different modes of failure were observed. For the specimens with a small embedment length of bars in the keyways i.e. $l_d / \phi \leq 20$ and in low compressive strength i.e. $f_c \leq 20 \text{ MPa}$, pullout failure mode occurred. For the same compressive strength, specimens with higher embedment lengths i.e. $l_d / \phi = 30$, the stress in the steel bar exceeded the yield stress and the reinforcement bars fractured. For the intermediate embedment length i.e. $l_d / \phi = 25$, in some specimens the yield stress of the reinforcements is reached, but at the hardening stage pullout failure mode occurred with considerable plastic deformation experienced by the steel bars. The same result obtained by Engstrom et al. (1998). Based on pullout test results on cylindrical specimens, they concluded that 16 mm reinforcement bar with an anchorage length of 300 in concrete with a compressive strength of 29 MPa, led to the bar fracture failure mode; while an embedment length of 250 mm led to pullout failure mode.



Figure 3.13 Cone failure at the loaded end of precast and prism specimens - pullout failure mode

In the pullout failure mode, it was observed that reinforcement bars slid in a cracked circular plan around the steel bars and concrete was left between the ribs. For the well confined specimens no splitting crack was observed; while a cone failure at the loaded end of the bars

was formed. This concrete remained bonded to the reinforcement bars while the steel bars were pulled out from the specimens (Fig. 3.13). In the specimens with a compressive strength of 20MPa, the average depth of cone failure was 14, 18, 21, and 27 mm for bar size of 8, 10, 12 and 16 mm, respectively; which can be defined as 1.75 times the bar diameter. There was not a remarkable difference between the average depths of cone failure in specimens with different compressive strengths. Comparing pullout test results for various bar sizes, indicates that pullout capacity in pullout failure mode is increased proportionally to the increasing of the embedment length of the bar in the keyways. It was found that this relationship is approximately linear. Table 3.5 shows the average bond stress in pullout failure mode for various bar sizes with effective embedment length.

Table 3-5 Average bond stress along effective embedment length

Bar Diameter (mm)	Test specimen	Concrete strength f_{cu} (MPa)	Effective* embedment length (mm)	Maximum pullout force (kN)	Average bond stress τ_{ave} (MPa)	$\frac{\tau_{ave}}{\sqrt{f_{ck}}}$	$\frac{\tau_{ave}}{f_{ck}}$
$\phi 8mm$	ST4	18.3	146	18.9	5.16	1.34	0.28
	ST8	24.5	146	23.1	6.29	1.42	0.26
	ST18	19.2	208	36.6	5.6	1.54	0.29
$\phi 10mm$	ST22	20.3	148	26.2	5.63	1.56	0.28
	ST23	20.3	198	34.4	5.53	1.48	0.27
	ST40	19.9	129	31.5	6.48	1.62	0.32
$\phi 12mm$	ST41	19.9	179	41.01	6.08	1.52	0.30
	ST42	19.9	229	47.9	5.55	1.39	0.28
	ST43	19.9	279	55.6	5.28	1.32	0.26
$\phi 16mm$	ST52	19.7	222	62.7	5.62	1.41	0.28
	ST53	19.7	272	75.7	5.54	1.39	0.28
	ST54	19.7	322	86.5	5.34	1.34	0.27
Average						1.45	0.28

*the embedment length mines depth of cone failure

** $f_{ck} = 0.8f_{cu}$

It was found that on considering actual embedment length, the relationship between the average bond strength and the square root of compressive strength can be assumed approximately linear. The average bond strength was found to be $\tau_{ave} = 1.45\sqrt{f_{ck}}$ or $\tau_{ave} = 0.29f_{ck}$ which shows very close agreement with previous work (Engstrom et al., 1998; CEB-FIP, 2000). Based on pullout test results on various embedment lengths of 16 mm steel bar in concrete with an average compressive strength of 28 MPa and well confinement, Engstrom et al. (1998) suggested $\tau_{ave} = 1.43\sqrt{f_{ck}}$ and $\tau_{ave} = 0.27f_{ck}$. The results of this study were then confirmed through state-of-the-art research on bond mechanism in both pullout and splitting failure modes conducted by CEB-FIP (2000). It can be concluded that, the pullout behaviour of a single bar into keyway of a precast slab shows approximately the same behaviour of bar in prism with well confinement condition.

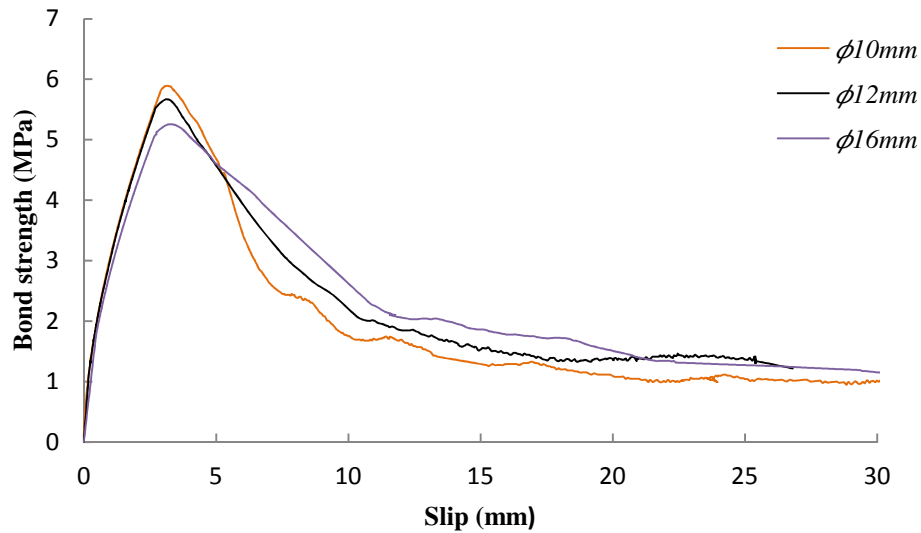


Figure 3.14 Bond strength for bar size of 10, 12, and 16 mm with the same compressive strength

The results indicate that, assuming the actual embedment length for the same compressive strength, the specimens with smaller bar size resulted in more bond stress (Table 3.5 and Fig. 3.14), while Table 3.5 indicate that assuming effective embedment length result approximately the same bond strength. Furthermore, for the specimens with similar compressive strength and various embedment lengths, it was found that the magnitude of slip at the maximum bond stress were approximately similar. Figure 3.14 indicates that the average slip corresponding to peak bond stress is 2.0-3.0 mm, which shows good agreement with MC90 (1190) and the CEP-FIP (2000) bond model.

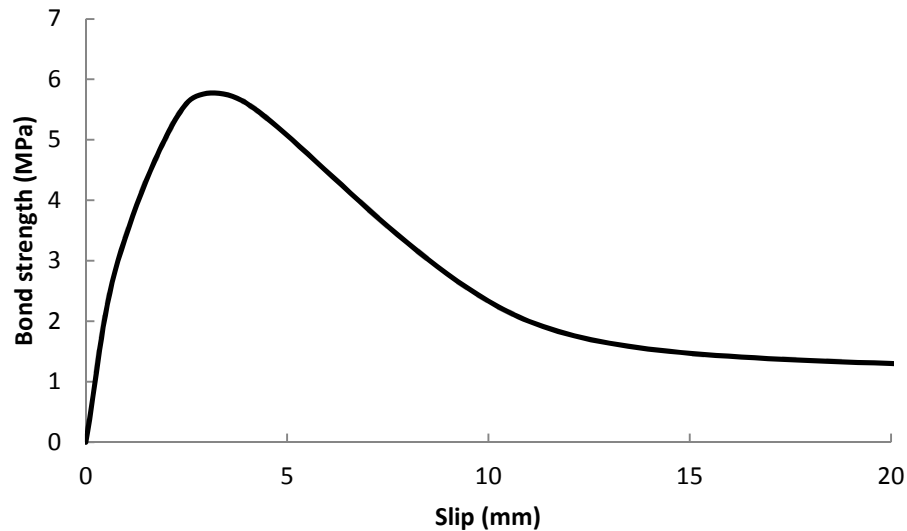


Figure 3.15 Bond model

The bond model developed in the present study was found to be in good agreement with the schematic bond model in MC90 (1990) or CEP-FIP (2000), except for the frictional stage. MC90 (1990) assumed a constant frictional strength about $\tau_f = 0.15\tau_{\max}$, while the present model led to frictional strength of $\tau_f = 0.19\tau_{\max}$. Furthermore, the Model Code suggested a constant frictional strength; while it was found that the bond stress is decreased approximately

linearly with the increasing of slip (Fig. 3.15). Furthermore, pullout test results clearly indicate that the descending stage needs to be modelled into three branches.

As stated previously, catenary action will be established while reinforcement bars experience the frictional stage assuming pullout failure mode. As strength of the system in catenary stage is proportional to the product of tie force and vertical deflection, constant tie force will provide considerable strength. The bond model in MC90 was developed considering a short embedment length i.e. 2.5 times the bar diameter; while the bond model in the present study was established considering the actual embedment length. It can be concluded that in the case of providing constant embedment length constant bond stress will be established. Accordingly, in the full scale test specimens a constant bond mode will be applied using a plastic tube to isolate the reinforcement bar from the surrounding concrete (Fig. 3.16). However, a constant bond stress can be considered in FE modelling, as well.

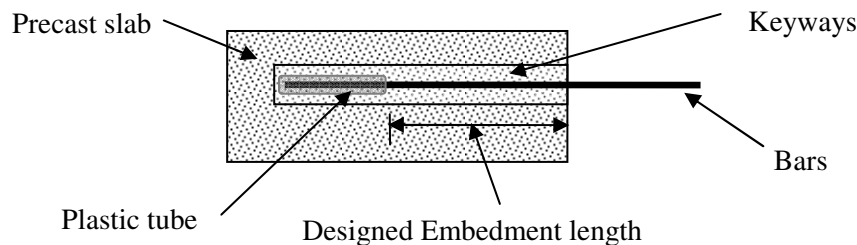


Figure 3.16 Constant embedment length to provide constant pullout force

3.4 FULL SCALE FLOOR-TO-FLOOR EXPERIMENTS

This section presents the results of the experimental study on the mechanism of preventing the progressive collapse in the precast concrete cross wall structures under an accidental event such as an explosion or bombing attack. The concept that was studied is based on the TF method specified by the BS Standard which is commonly used in the current cross wall

structures design in the UK. The key to TF method is to develop the catenary action mechanism that is expected to dissolve the energy arose from the accidental event and divert the loads to the undamaged structure.

In multi-story precast concrete cross wall structures, the applied load is sustained by one way precast slabs simply supported on vertical wall panels. In the case of damage from the supporting walls, the floor joint above the removed wall is the most critical element which can redistribute the applied loads to the undamaged parts of the system. Immediately after the removal of the joint support, the axial restraints at both sides will introduce a compressive arch action which can enhance the resistance of the system (Jun, 2010, Sasani and Kropelnicki, 2007, Yi, 2008). This arch action soon disappears and the system turns into flexural action once the deflection develops at the mid-joint. Under flexural action, the joint grout soon fails due to its low strength. While the deflection continues increasing, the system will develop a catenary action with the presence of axial restraints at both ends, and tie bars mainly experience axial forces.

3.4.1 Geometry and properties of test specimens

Test assemblies were designed to represent a portion of the floor system that is affected by the loss of wall support. It includes one pair of floor units spanning across two adjacent spans in the longitudinal direction (Figs. 3.17), and consists of two hollow-core planks with dimensions of 2000 x 1200 x 150mm. This assembly provides two or three keyways, where straight steel bars can be placed as ties (Fig. 3.17). The precast floor slabs used in the test were provided by Bison Ltd. with a standard size in their product range.

In the test assembly, the adjacent floors and walls were replaced by two braced steel frames (Fig. 3.17 and 3.24). The lateral stiffness of the support system has been chosen to represent the stiffness of a typical cross wall structure. In the test, two possible failure modes of tie bars

are expected to attain, i.e. the bar fracture and the pull-out failure. FT1 and FT2 (group A) were designed to develop the bar fracture failure mode, while FT3, FT4 and FT5 (group B) were designed to establish the pullout failure mode. To consider this, two target grout strengths, i.e. 30MPa (group A) and 20MPa (group B), were adopted. In addition, based on the pullout test results conducted in the present study, appropriate embedment length of tie bars l_d for two bar diameters d_b were selected to introduce these two failure modes (Table 3.6). The tie ratio is calculated by the cross-sectional area of ties divided by that of the precast concrete slab. The mean compressive strength of cube f_{cm} and the flexural tensile strength of prism f_{ctm} were measured for the grout concrete based on the corresponding standard material tests from three specimens on the days of tests (Table 3.6). In order to study the contribution of the concrete grout at the joint gaps during the loading process, the FT4 specimen was specially designed without any cast-in-situ concrete grout in the gaps, while the remaining specimens were fully grouted as presented in Fig. 3.18. Amongst all five specimens, only FT2 uses three tie bars, and the remainder use two.

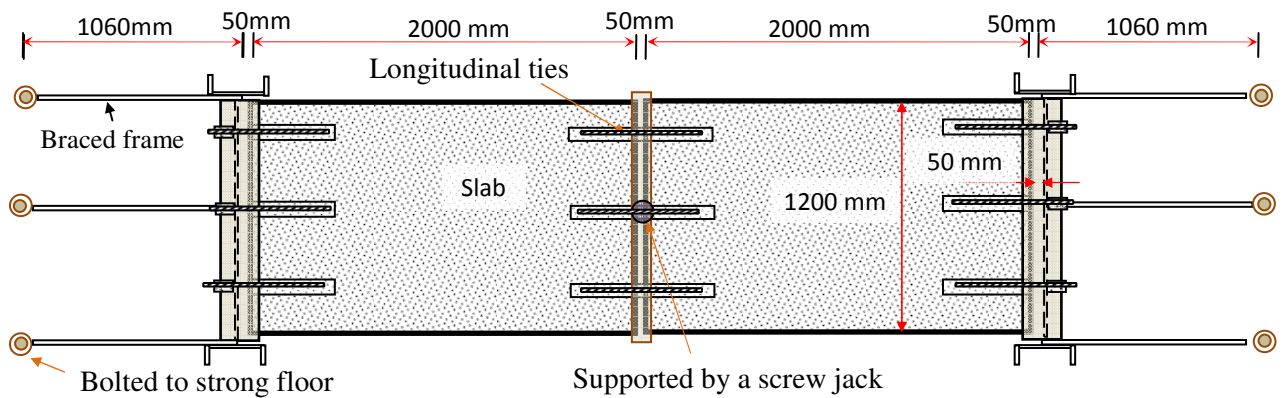


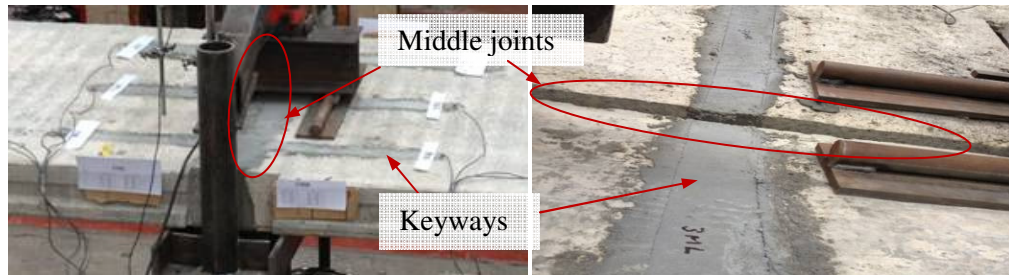
Figure 3.17 Plane view of the test assembly

Table 3-6 Details of test components

Group	Tests	Steel Ties							Tie No.	Grout	
		d_b (mm)	l_d	L_d/d_b	Tie Ratio (%)	Fracture strain %	Yield stress (MPa)	Tensile strength (MPa)		Compressive strength f_{cm} (MPa)	Flexural strength f_{cm} (MPa)
A	FT1	$\phi 10$	350	35	0.087	14.13	515	616	2	30	4.07
	FT2	$\phi 10$	350	35	0.087	14.36	515	614	3	32	4.53
B	FT3	$\phi 12$	200	16.7	0.126	15.98	545	667	2	23	3.14
	FT4	$\phi 12$	250	20.8	0.126	16.40	545	671	2	18	---*
	FT5	$\phi 12$	250	20.8	0.126	16.98	545	671	2	17	2.55

* Specimen without grout at the joints

The slump of concrete, which was between 90-110 mm, falling into the range of the normal specifications. The material properties of the tie bars, such as the fracture strain, the yield stress and the tensile strength are also listed in Table 3.6 under the general heading of ties.



(a) Concrete grout used at the joint gaps and keyways of FT1, FT2, FT3 and FT5 (b) Cast-in-suit concrete grout in the keyways of FT4

Figure 3.18 Cast-in-suit concrete grout in the floor joint gaps

Tie bars were placed into keyways 65-75 mm above the bottom surface of the slab or 25-40 mm above the lower surface of keyways (Fig. 3.19). To remove any rigid slip between the bars and anchor blots at the side support, prior to placing the tie bars into keyways, an axial

force of 5 kN for 10 mm bars or 8 kN for 12 mm bars was applied using the hydraulic jack (Fig. 3.20). Spacers were employed to locate the bars in the designated positions during casting and vibrating. To measure the permanent elongation, steel bars were marked at two points with the spacing of 50 mm at the middle joint gap (Fig. 3.21). For all specimens, the gap width was 50 mm.

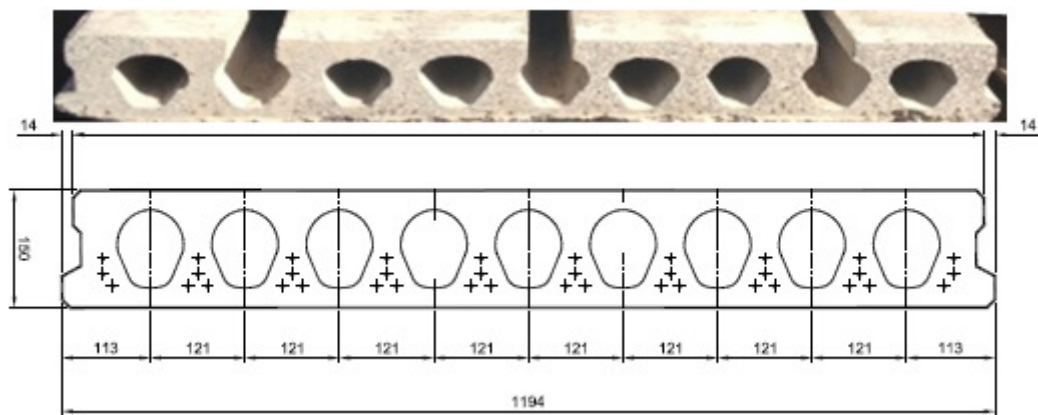


Figure 3.19 Precast concrete floor units used in the full scale test specimens (courtesy of Bison Ltd.)

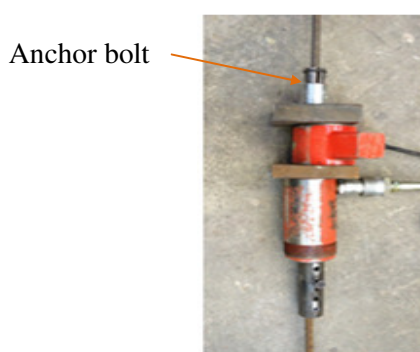


Figure 3.20 Device for applying initial force to remove any rigid slip between the bars and anchor bolts



Figure 3.21 Marked points on the bar at the middle joint to measure permanent elongation

In devising the test programme, it is anticipated that group B that will experience the pull-out failure mode will develop the catenary action more efficiently. To introduce the pull-out failure mode, two 12mm steel bars are placed in the grout of both middle and side joints with the embedment length (i.e. 200mm and 250mm), less than the anchorage length. The pull-out test results indicated that the bond resistance will decline at the frictional stage, i.e. during the fully debonding stage, due to the gradual reduction in the embedment length. In this study, plastic tubes were used to cover the free end of the steel bars to provide a constant embedment length so that the pullout resistance will remain approximately in a constant level (see Fig. 3.22).



Figure 3.22 Plastic tube at the bar end



(a) Middle tie bars



(b) Side tie bars

Figure 3.23 Typical arrangement of strain gauges (Appendix 3A)

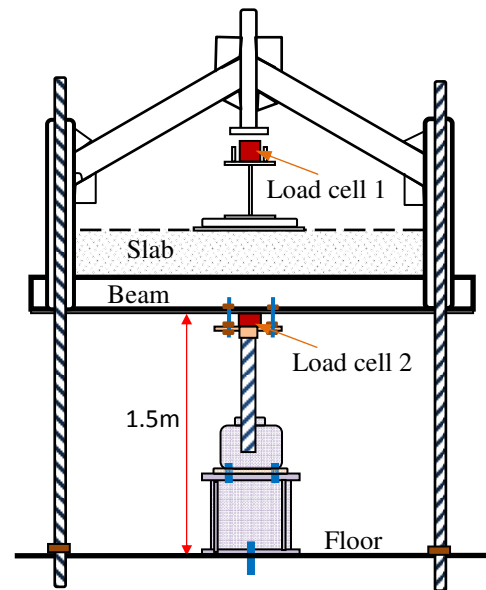
To capture the strain, two or three strain gauges were attached on the middle tie bars (see Fig. 3.23a). In the bars at the side joints only one strain gauge was applied at the top of the bars or at the defined location (see Fig. 3.23b).

3.4.2 Test setup and instrumentation

Fig. 3.24 shows the overview of the test setup and loading devices. A braced steel frame consisting of beam supports, two columns and three bracings provides the axial and vertical restraints at the slab ends. As shown in Fig 3.24, the precast slabs rest on the steel beam and are horizontally restrained at both ends by anchoring tie bars to the supporting frame. The loading device is so designed to resemble the scenario that an underling support wall is gradually removed (Appendix 3B). In practice, on the loss of the supporting wall, the floor may experience an impact line load from the upper wall. This will then lead to a chain reaction of damage to the upper floors. The resulting damage and the load path diversion occur within an extremely short duration and hence are of a dynamic nature. In this study, the dynamic effect is not considered, but a quasi-static case was examined to reveal the failure process and its mechanisms. The whole loading process involved two stages: the gradual reduction in the reaction to the gravity load of the middle support, followed by a downward line load acting from the top.



(a) Perspective view of the test set-up



(b) Loading device used in the test

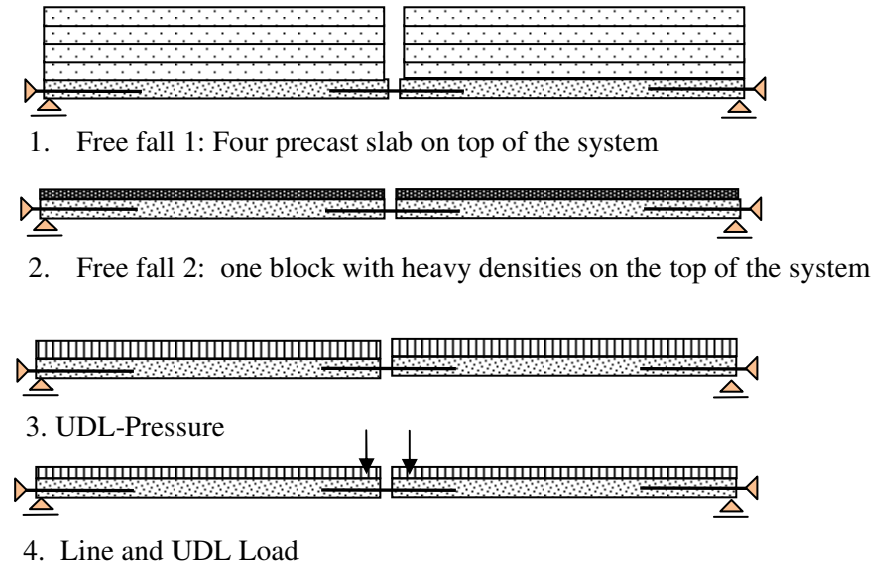
Figure 3.24 Floor joint test specimens (Appendix 3B)

To introduce the collapse in a slow manner, a screw jack is considered to support the slabs at the middle joint so that it can be moved down to mimic the removal of the wall support in a slow manner (Fig. 3.24b). Astaneh-Asl et al. (2002) used the same approach to simulate the column removal in a steel frame structure, dividing the middle supporting columns into two parts so that lower section can be pulled down. As only the gravity load due to the self-weight of slabs was present in the full scale tests, applying imposed and finishes load in the UDL form presented a challenge. A line load was then applied at the middle joint instead. This loading arrangement is similar to that adopted in the previous studies (PCA, 1979; Yi et al., 2008; He, 2008; Jun, 2010,). A loading device was designed to facilitate this type of action in this testing programme, involving the use of a screw jack with a stroke length of 600mm (Fig. 3.24b). The load was applied using a displacement control method up to bar fracture or pull-out. When the screw jack initially moved down, the central support reaction was reduced; with the jack continuing lowering to the point of zero contact with the slab, the top loading unit touched the upper loading mechanism and started to exert a downward load

onto the slab. This process was continued until the failure of the test assembly. The loads and the deflection were recorded by the load cell and the LVDT during the process.

3.4.3 Validation of the present loading method resembling the sudden removal of support wall

The jack can apply a downward load by moving with a constant velocity of 5mm/minute. Assuming that under an accidental event, the floor joist experiences a free fall impact action, the main concern is whether the tie force and the joist deflection would be the same as the case where the system is subjected to steady movement, in particular, for the relationship between the tie force and the deflection of the joint. To examine this, a series of finite element analyses were performed for the test designs, considering various loading cases including the free fall action, the UDL load and the line load applied by the screw jack at the middle joint[Fig. 3.25(a)]. ABAQUS software was used for the numerical analysis). The results clearly show that using a screw jack to pull the slabs down produces the same tie force in the reinforcements at the mid-joint as occurs in a free fall drop [Fig. 3.25(c)]. A similar observation was obtained by Astaneh-Asl et al. (2002) in their study on the composite floor for the progressive collapse resistance.



(a) Four types of loading to verify sudden removal of support wall (Appendix 3C)

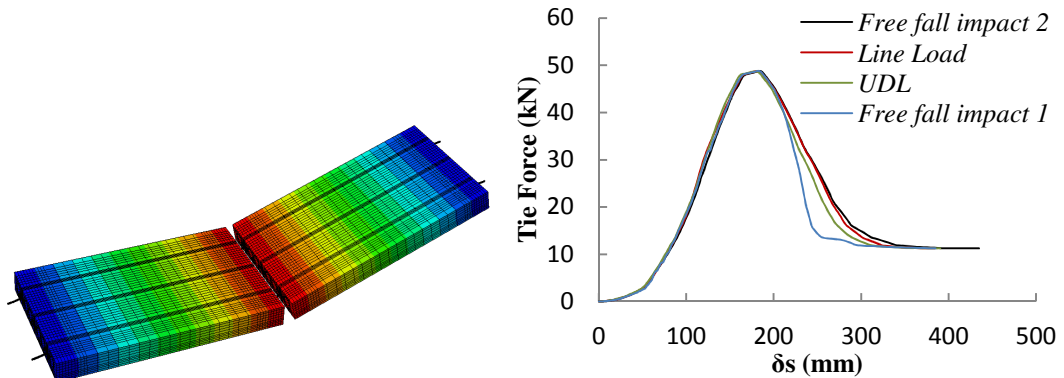


Figure 3.25 Tie force- vertical deflection under various loading applications (Appendix 3C)

3.4.4 Instrumentation

To monitor the tie force and vertical deflection in the floor system tests, several instruments were placed at the carefully chosen critical locations in the specimens. As illustrated in Fig. 3.26, strain gauges were pre-glued on the bar surfaces at designated places before they were placed in grout (Appendix 3A). To show efficiency of strain gauges setup, prior the full scale tests, 4 strain gauges attached on the 12 mm and 10 mm reinforcement bar in a standard

pullout test considering pullout and bar fracture failure mode. In both pull-out and bar fracture failure mode, the pull-out load or stress calculated from strain gauges is found very close to that observed using load cell results (Appendix 3A). A linear variable differential transformer (LVDT) was used to measure the vertical deflection at the mid-span point of the specimen (Fig. 3.26).

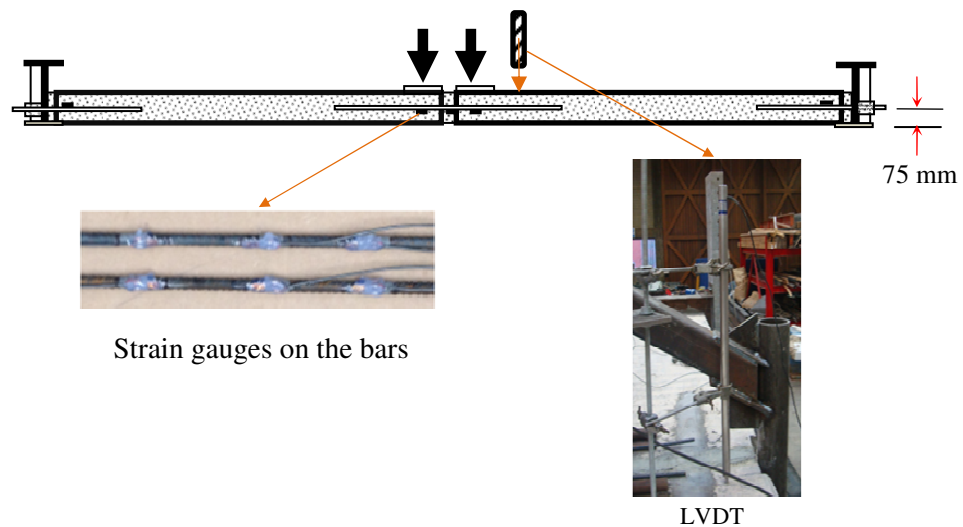


Figure 3.26 Instrumentation

The details, locations and labelling of instruments are presented in Fig. 3.27. To monitor the restraining forces at the side supports due to the large vertical deflection, in FT2 and FT3 specimens, strain gauges were also used to measure the forces in the bracing (Fig. 3.28). The applied load was measured by two load cells as shown in Fig. 3.24b.

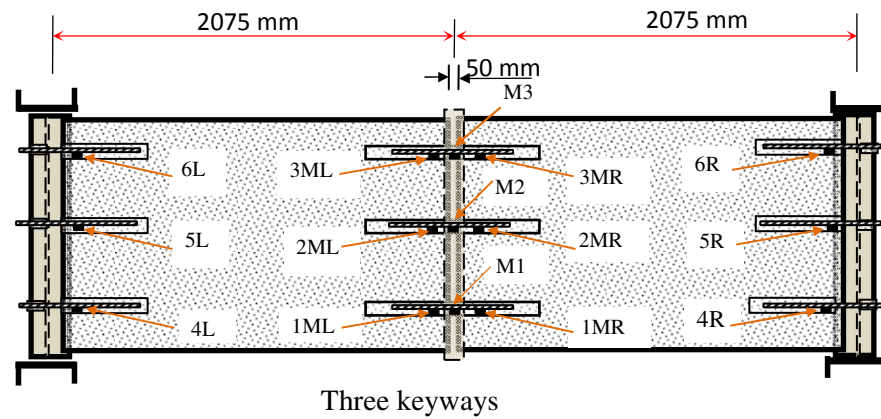


Figure 3.27 Layout and labelling of strain gauges

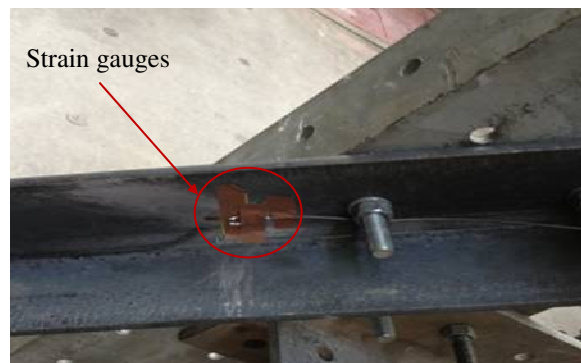


Figure 3.28 Strain gauges on the bracing support

3.4.5 Test results

Test results are presented at two levels, i.e., at the floor units and the reinforcement bars.

3.4.5.1 Results at the floor units level

A total of five full scale floor system tests were performed considering the variables of bar size, embedment length, compressive strength and the number of ties at joints. The group A specimens (FT1 and FT2) were tested to investigate the behaviour of the system using an embedment length of more than the required anchorage length to introduce the bar fracture failure mechanism, and the effect of the number of ties at the floor joints was examined. The group B specimens (FT3, FT4 and FT5) were used to investigate the behaviour of the system

concerning the pull-out failure mechanism. The general behaviour of floor-to-floor system immediately following removing wall support at the middle joint is discussed in Appendix 3C).



(a) Prior to loading



(b) Failure pattern

Figure 3.29 3D view test assemblies

The screw jack was lowered at a constant rate until the tie bars at the middle joint fractured in FT1 and FT2 or were pulled out in FT3 to FT5. The final deflection patterns of all specimens were very similar (Fig. 3.29). In FT1 and FT2, the observed fracture failure pattern is

different from those observed in the continuous RC beams, where the failure usually occurred in the end bars (Li et al., 2011; Yi et al., 2008). In this study, no bar fracture was observed at the end supports (Appendix 3C).

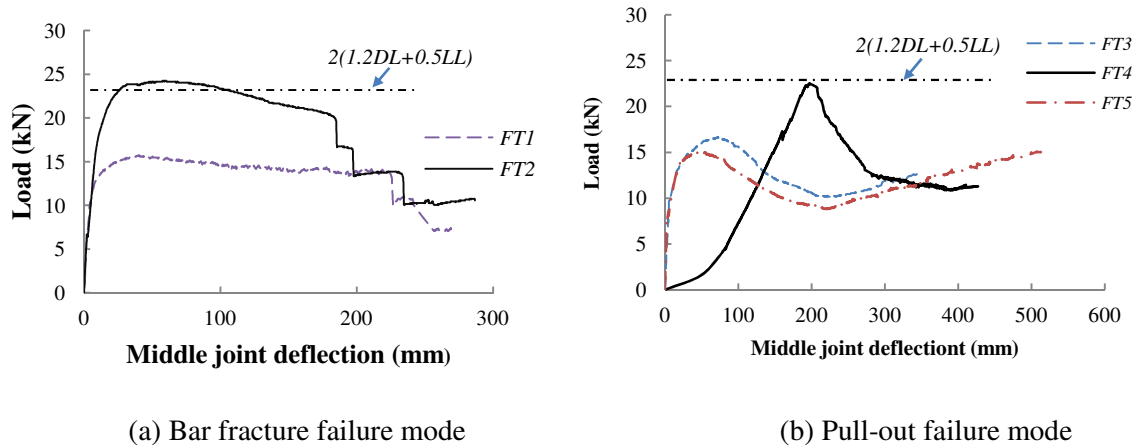


Figure 3.30 Applied load versus middle joint deflection

Fig. 3.30 presents the applied load vs. the middle joint vertical deflection for all five specimens. Test results reveal the key differences in the two specimen groups. The failure patterns of FT1 and FT2 are approximately same. The middle bars fractured at the deflection around 200-230 mm, (i.e. 11% of span length) and the rotation of the slabs was 6.3° . For specimens FT3 to FT5, no bar fracture failure was observed even at the deflection of around 500 mm, i.e. 20% of span length (Fig. 3.30b). In the case of RC beams studied in other research work, even very well detailed RC beams would have failed at this level of deflection (Li et al., 2011; Yi et al., 2008). Fig. 3.30(b) also shows an obvious trend of the second increase after the fall in all three specimens, which indicates the establishment of the catenary mechanism in the specimens with pullout failure mode. The test was terminated due to the jack reaching its maximum travel in Group B specimen; otherwise, it is expected that the loading resistance can be further increased in the catenary phase.

In Fig. 3.30a, the sudden drops in the applied load as observed in FT1 and FT2 are due to the bar fracture in sequences. The applied load and corresponding displacement at the critical points of curve are listed in Table 3.7. During the initial loading stage, a combination of flexural and compressive membrane action governs the behaviour of system. As expected, this phase was short-lived and followed by the visible crack at the mid and the side supports. From Fig. 3.30(a), it can be seen that FT2 /FT1 strength ratio is 1.62, which indicates that the strength of system is roughly proportional to the area of tie placed in the joint.

Table 3-7 Applied load and middle joint deflection at critical points

Test	Deflections at the middle joint (mm)				Loading resistance		
	At the first peak	1 st rebar fracture	2 st /3 rd rebar fracture	2nd increase in loading resistance	Ultimate bending moment resistance (kN.m)	Peak load due to flexural action (kN)	Peak load due to catenary action (kN)
FT1	40	227	241	-	6.14	15.7	-
FT2	33	185	198/225	-	9.15	24.15	-
FT3	77	-	-	270	5.98*	16.65	13.62**
FT4	198	-	-	380	-	22.47	11.45**
FT5	50	-	-	240	8.4*	14.9	15.02**

*Considering the maximum pull-out force.

**Due to the head of screw jack reaching the maximum travel, the test was stopped in the catenary phase.

To measure the horizontal reaction of specimens during the loading process, strain gauges were attached on the inclined bracing angles in two specimens (FT2 and FT3). Results indicate that the maximum horizontal support reactions are close to the total yield force of the relevant ties in FT2 (i.e. 121 kN) and total pullout force of bar into keyways in FT3, (i.e. 86 kN) (Fig. 3.31). Furthermore, results also show that, for the pull-out failure mode, the reaction force will rise after a decline, which again confirms the establishment of the catenary mechanism (Fig. 16b).

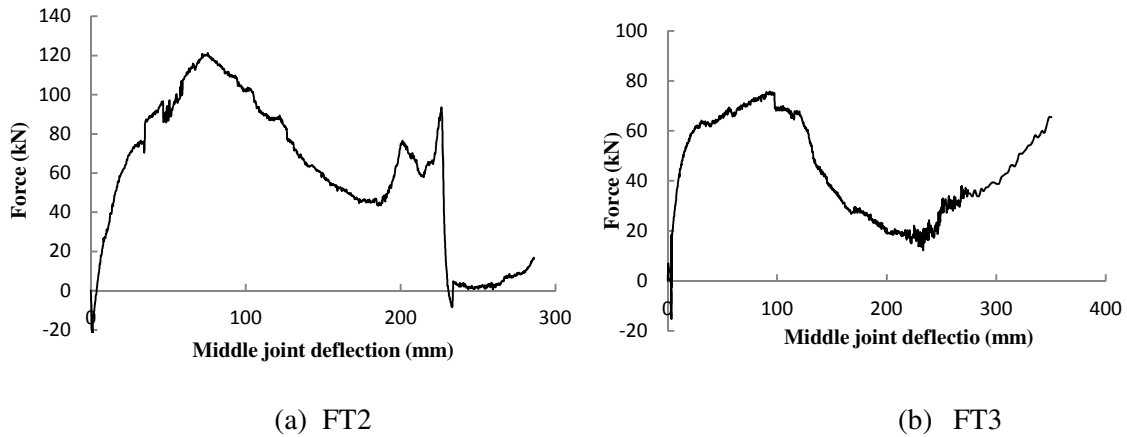


Figure 3.31 Horizontal reaction support force in side bracing vs. middle joint deflection

Figure 3.32 and 3.33 illustrates the typical ultimate failure patterns near the middle and side joints for FT2 and FT5, representing the two typical failure modes, respectively. It is interesting to observe that, in all specimens, only one major crack developed at the interface between the precast slab and cast in-situ grout at the middle joint gap, which widened very rapidly with the increase in deflection (Figs. 3.32 and 3.33). This has suggested that the tie bars reaches the yield point at a very early stage, i.e. at the deflection around 1-2% of slab length. Also, one tension cracks in the lower grout were observed at the side supports at the vertical deflection of 5.16 and 3.25 mm for FT2 and FT5, respectively.

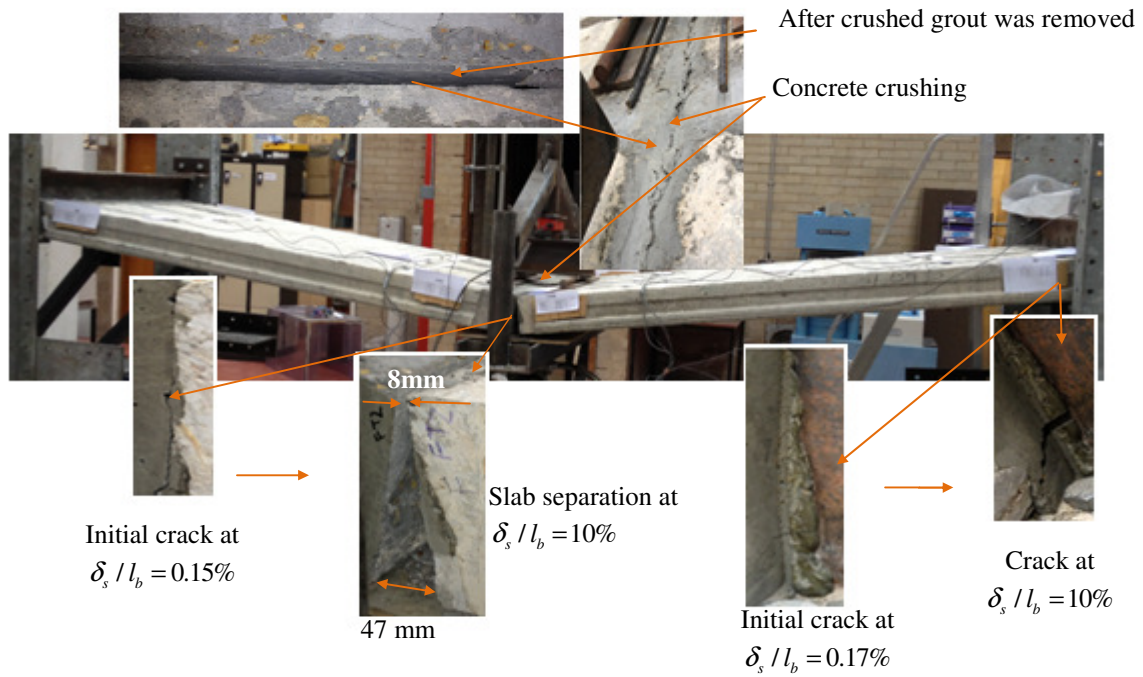


Figure 3.32 Failure pattern at the middle and sides joints for FT2

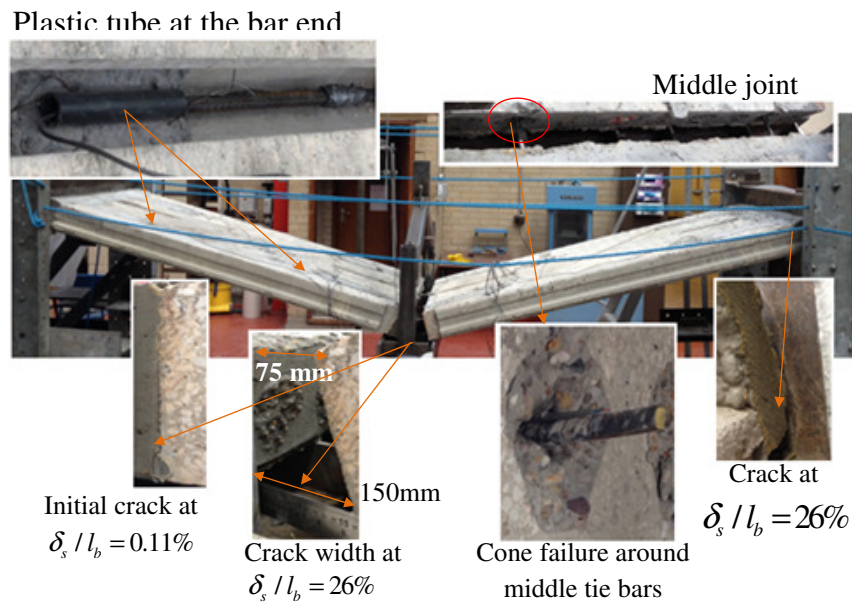


Figure 3.33 Failure pattern at the middle and ends joints for FT5

The failure patterns indicate that following the initial crack at the middle joint, floor slabs act as two rigid bodies connected by tie bars at the joints as shown in Figs. 3.32 and 3.33. Fig. 3.32 shows that, in FT2, the grout is crushed up to a depth of 4-5 mm and then the middle tie bars fractured and a very wide crack penetrated through the entire slab depth. Slabs rotate as rigid elements without experiencing much flexural deformation. Comparing FT2 and FT5, it was observed that the two slab units separated at the middle joint under different vertical deflections. Specimen FT1/FT2 separated at the deflection around 200mm (Fig. 3.32); whereas no visible separation was observed in FT3/FT5 at the same deflection level. This difference can be attributed to the fact that, following the peak load, the components of the applied force acting in parallel to the slab surface tend to push the slab units in the pull-out failure mode toward the middle joint, and this tendency becomes more obvious with an increase in the deflection. FE analyses results indicate that the slip of the middle tie bars following the peak pull-out force decreases with an increase in vertical deflection, but it increases at the side joints (Chapter 5).

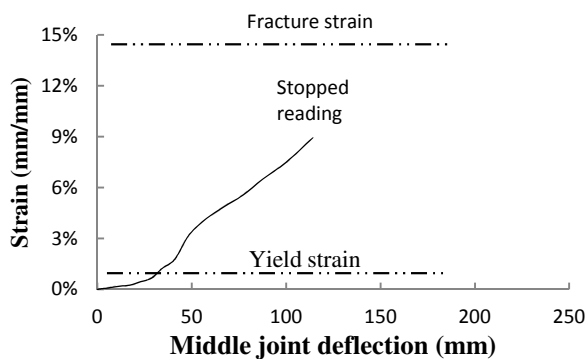
It is generally accepted that, the catenary action will be established at a relatively large deflection. In the specimens with the bar fracture failure mode, due to the bar fractures at the deflection around 10% of the span length, they failed to develop the second increase in the loading capacity (Table 3.7) or the catenary action (Fig. 3.30a).

As expected, the behaviour of the FT4 specimens exhibited a remarkable discrepancy compared with the remaining tests. The test results of FT4 indicate that the peak load occurred where $\delta_s / l_b \approx 10\%$, while for the other specimens it was around 1-3% (Fig. 3.30). The results in Table 3.7 show that the peak load of FT4 due to flexural action is similar to that of FT2 with the same area of steel in the keyways. Based on the pull-out test result, the ultimate bond force for the tie bars in FT2 is 148kN (governed by the tension failure), which is 39% higher than that in FT4 (106kN due to the pull out failure). This provides strong

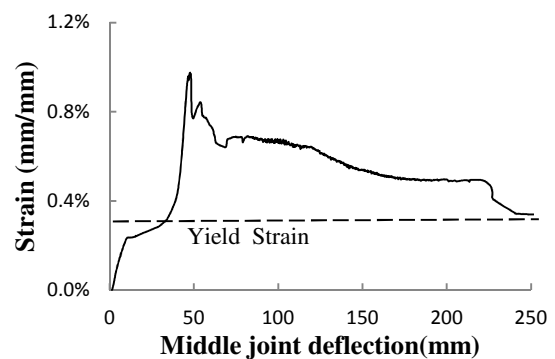
evidence suggesting that the loading capacity of floor systems such as FT4 is a combined result of the ultimate bond force of the tie bars and the middle joint deflection in catenary stage.

3.4.5.2 Results at the reinforcement bar level

The strain results for the reinforcement bars exhibited three types of development pattern in various bar locations or specimens. In the group A specimens, following the initial yield of the tie bars, the strain gauges located in the cracked section measured a constantly increasing strain until the bar fractured (Fig. 3.34a), while for the gauges along the embedment length, following the initial yield of tie bars, the strain started to fall but remained above the yield point (Fig. 3.34b). In group B specimens, the strain gauges on the cracked section showed the same behaviour as those along the embedment length of group A specimens (Fig. 3.34b), and the strain in the embedment length showed a classic pull-out behaviour (Fig. 3.35). The measured strains were converted to stresses by using stress-strain curves taken from the standard bar tests (Fig. 3.36), and will be presented for further discussion below.



(a) Strain development at the middle joints
(M1 of FT1 as indicated in Fig. 3.37)



(b) Strain development over embedment
length (1MR of FT1 as indicated in Fig. 3.37)

Figure 3.34 Typical strain-deflection relationship in the bar fracture failure mode

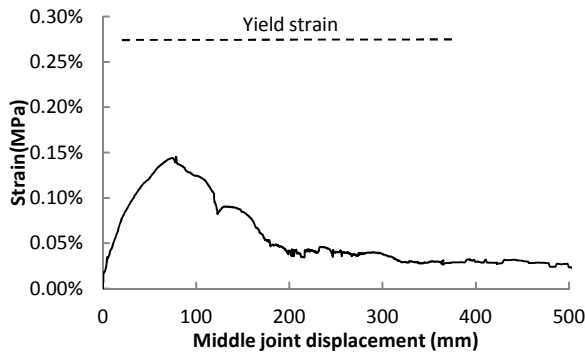


Figure 3.35 Strain development over embedment length (1MR of FT5 as indicated in Fig. 3.45)

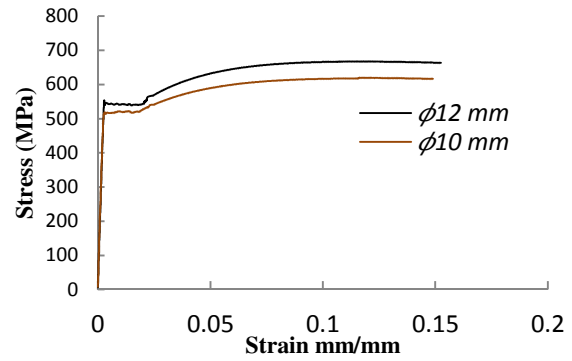
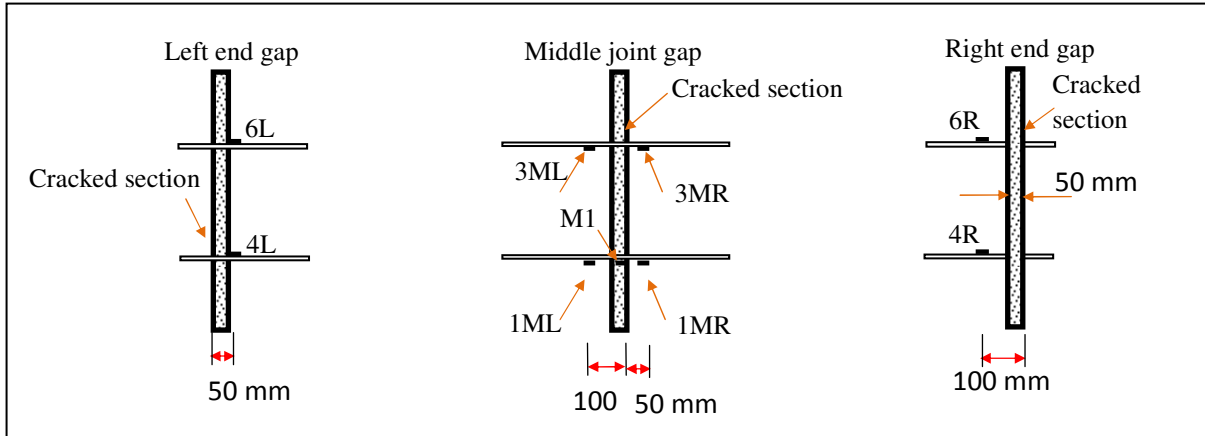


Figure 3.36 Stress vs. strain of tie bars used in the floor joint tests

FT1: In the specimen FT1, only one strain gauge was attached in the middle joint gap (M1). The yield strain of the steel bar was 0.28%. As indicated in Fig. 3.37, the locations of gauges 1ML/3ML and gauges 1MR/3MR are respectively 100 mm and 50 mm, respectively from the cracked section in the middle joint gap. The location of strain gauges 4L/ 6L and 4R/ 6R are 50 mm from the end gaps, and 100 mm from cracked section, respectively. The tensile stresses in the tie bars for group A specimens are represented by converting the strain results from FT1 test, and are shown in Fig. 3.38. In Figure 3.38, the comparison of the stresses between 1MR/3MR and 4L/6L, both 50 mm away from the cracked section, indicates that the middle ties yielded at the deflection around 18 mm; while the side ties yielded at the deflection around 140 mm. The horizontal sections of the stress curves of 1MR/3MR (Fig. 3.38a) and 4L/6L (Fig. 3.38b) indicate that, at those measurement locations, tie bars reached the yield stress but did not enter the hardening phase. At the deflection of 230 mm, one of the middle ties in FT1 fractured at the strain of 14.13% as indicated by M1 curve in Fig. 3.38, and the longitudinal ties at the side supports did not fail but experienced the plastic deformation (Fig. 3.38b).

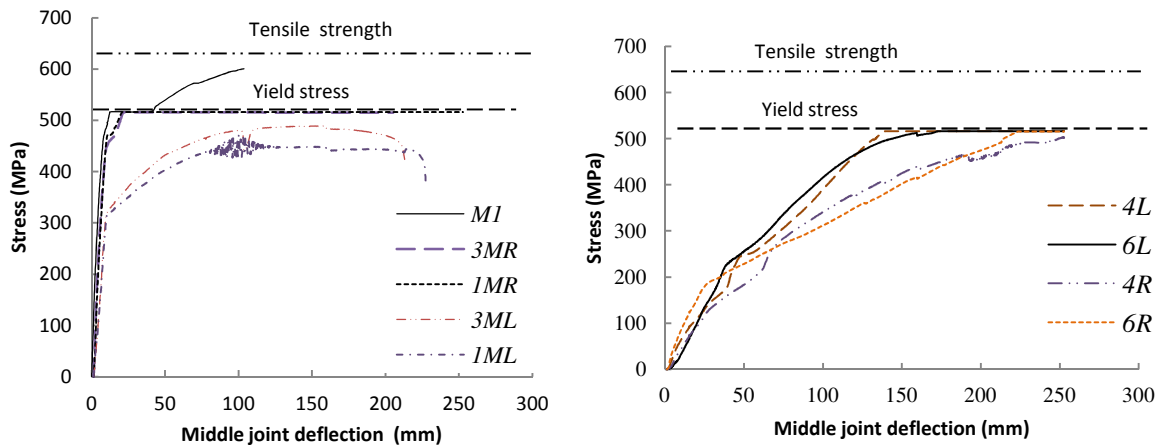


(a) Left ties

(b) Middle ties

(c) Right ties

Figure 3.37 Layout of stain gauges-FT1



(a) Stresses at the middle joint

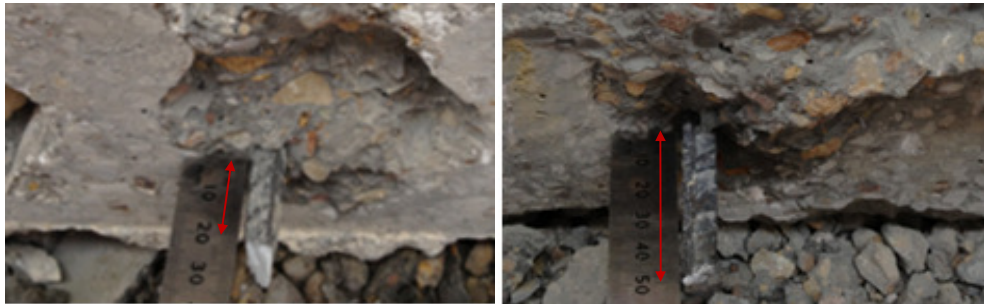
(b) Stresses at the right and left joints

Figure 3.38 Stresses versus mid-joint deflection for FT1

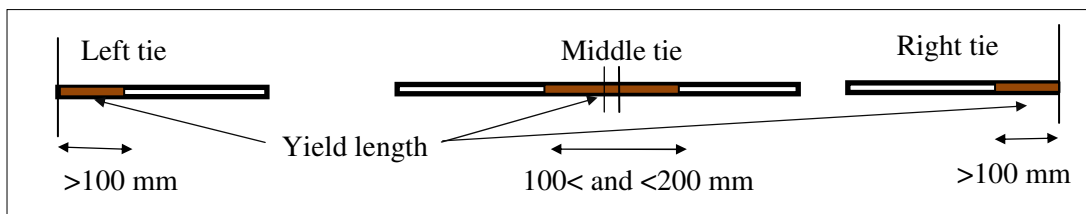
The results show that, prior to developing the crack at the interface between the grout and precast slab, 1MR/3MR and 1ML/3ML gauges experienced almost the same stress. This would be expected, given the symmetrical nature of the test system. After the occurrence of

the visible crack at the middle joint at 5 mm deflection, the 1MR/3MR and the 1ML/3ML gauges showed different behaviour (Figs. 3.38a). This can be attributed to the various distances of the gauges from the cracked section where bond stress is distributed in a non-uniform fashion along the bond length.

By analysing the results, as shown in Fig. 3.38, it can be seen that, at collapse, the side tie bars yielded at a length greater than 100mm from the end of the side joint gap. Such a length is referred to as the yield length (see Fig. 3.39b). For the middle ties, the stress-deflection curves for 1MR/3MR and 1ML /3ML indicate that the yield length is greater than 100mm but less than 200mm (see Figs. 3.39b). After collapse, the measured tie bar length between slab ends at the middle joint was 70 mm, which revealed a 20 mm elongation. Considering the average non-recovery strain at fracture to be 14% (Fig. 3.21), the total yield length of middle bars can be derived as 143mm which is in agreement with the prediction shown in Fig. 3.39b.



(a) Length of tie bars between end slabs at the middle joint at collapse



(b) Yield length over embedment length at the collapse

Figure 3.39 Elongation and yield length of bars at the joint of FT1

FT2: To study the effect of the number of ties, three 10mm ties were used in this specimen. To capture the maximum stress and strain, the location of the strain gauges on the side bars was moved to the middle of the side gaps, and the strain gauges at the middle-joint were in a similar position to those on specimen FT1 (see Fig. 3.40). Figure 3.41 presents the stress against deflection curves converted from the strain gauge readings. The floor joint system collapsed at a deflection of 190mm by the bar fracture in the middle joint at a strain of 14.36%. The result indicates that, although the distance of middle strain gauges (e.g. 1MR) from the cracked section is more than side strain gauges (e.g. 5L/5R), the middle bars yield at a deflection of 18mm, while the side bars reach the same stress at a deflection of more than 50mm, which again confirm this fact that collapse will be induced by middle bar fracture. Furthermore, the strain gauges located 100mm from the cracked section, i.e. 1ML, 2ML and 3ML, did not yield, while 1MR and 2MR, which were 50mm from the crack, yielded at the very beginning. It is also worth noting that the elongation of the middle tie at collapse was the same as in FT1. Figures 3.38 and 3.41 show that stress-deflection curve at the middle joint of FT2 is very close to that of FT1. These results indicate that middle joint is the most critical point in the floor joint system.

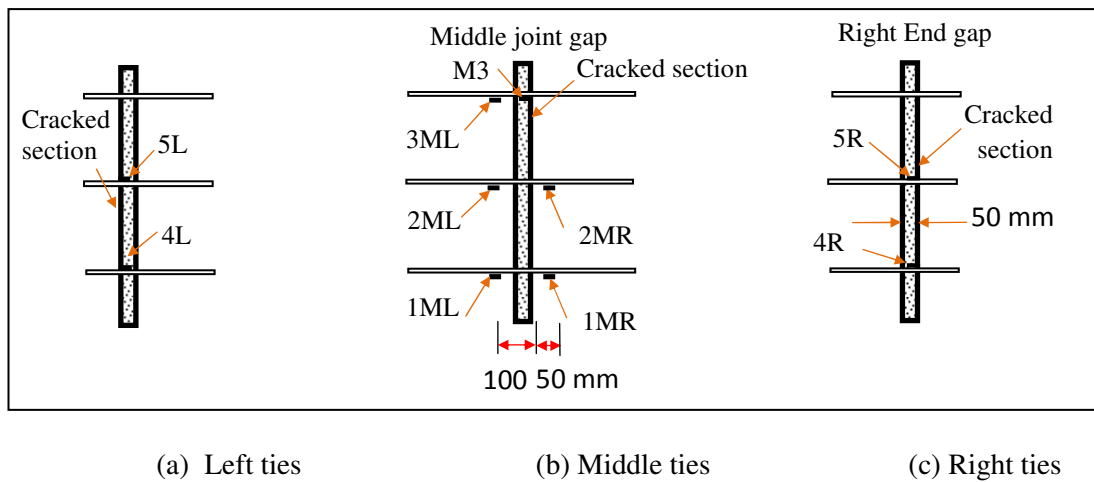


Figure 3.40 Layought of stain gauges - FT2

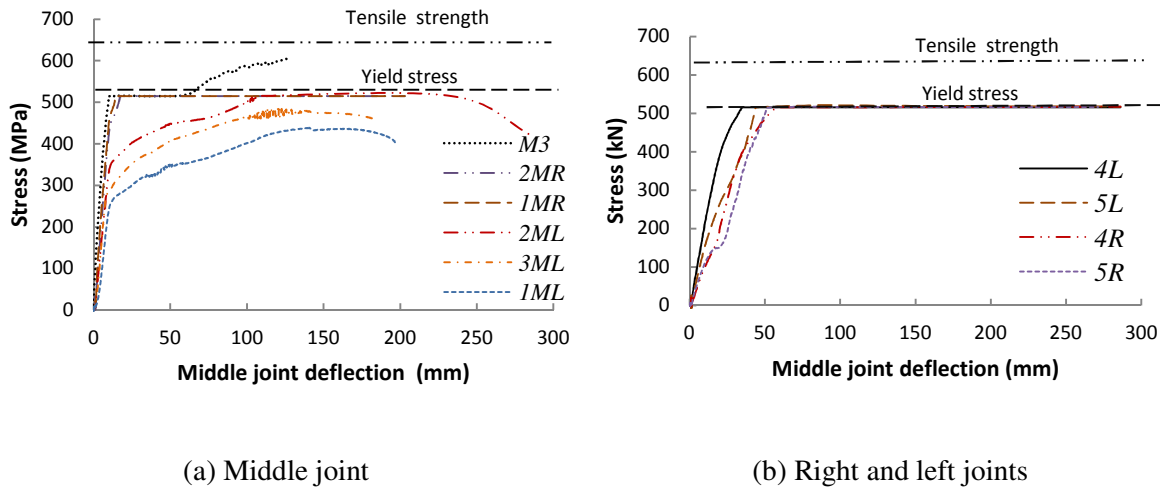


Figure 3.41 Stress versus middle joint deflection of FT2

FT3. To study the behaviour of the floor joint system, in particular pull-out behaviour, FT3 was designed with an embedment length of 200mm and grout strength of 25MPa. The test was carried out at a grout compressive stress of 23MPa. To compare the result with the pullout experiments and to capture the maximum pull-out force, the 1ML, 3ML, 1MR, and 3MR gauges were moved to the end of the slabs at the middle joints, and the other gauges remained the same as for FT2 (Fig. 3.42). It is worth noting that as the strain gauges are attached at the bar surfaces, the strains captured including both the axial strains and those due to the bending of tie bars. The bending effect is particularly significant near the cracked sections. This is reflected in the stress-deflection curves shown in Fig. 3.43, where an early yield is noticed. The following statements confirm that FT3 experienced the pull-out failure mode: (1) the embedment length of the bars was less than the basic anchorage length; (2) at a vertical deflection of 347mm the system still sustained the load without bar fracture, while FT1 and FT2 collapsed at the deflection around 200mm (Fig. 3.30 a, b); (3) the cross sectional area of the ties in FT3 was equal to FT2 specimens but has a lower peak resistance than FT2 (Fig. 3.30a and b); (4) considerable cone failure around the middle ties indicates the pull-out failure mode (Fig. 3.44).

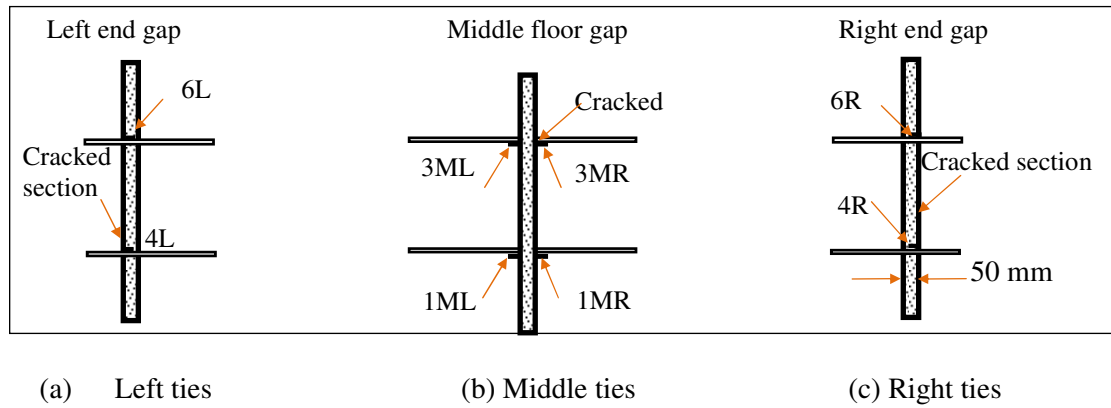


Figure 3.42 Layout of strain gauges-FT3

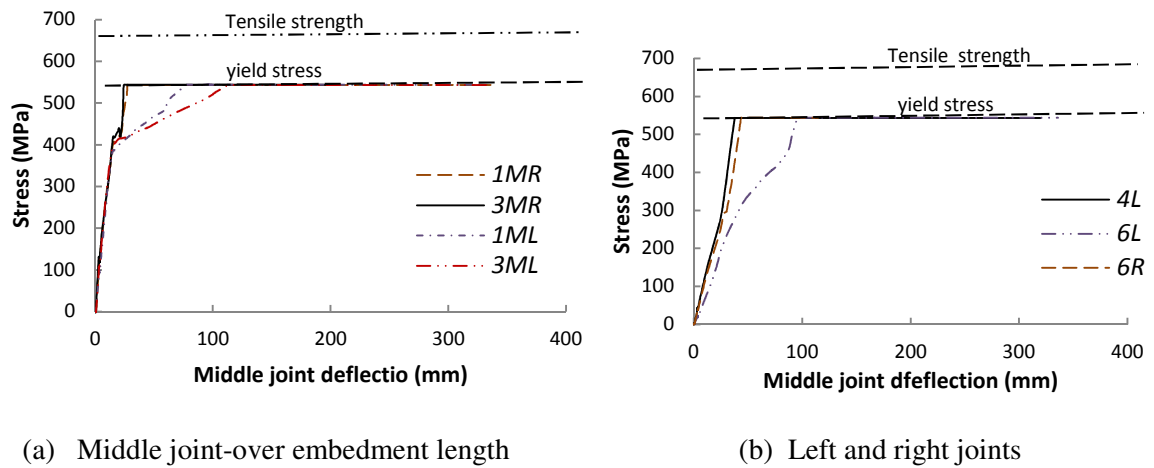


Figure 3.43 Stress versus mid-joint deflection –of FT3



Figure 3.44 Cone failure around the middle bar (taken near 1MR in FT3) at deflection of 347mm

FT4. To study the effect of grout at the joint gaps on the behaviour of a floor system, concerning the pull-out failure mode, the FT4 specimen was designed so that grout was only cast in the keyways. The gaps at the joints were left without concrete. To capture the variation in the tie force along the tie bars, a new arrangement of strain gauges was applied (Fig. 3.45). Strain gauges were attached to the bottom surface of the middle ties at the gap centres (M1 and M3) and two gauges (1MR/3MR) were attached 80 mm away, and other two (1ML/3ML) were 150 mm away. Three gauges, 4L, 6L, and 6R were attached to the top surface of the side ties 50 mm from the gap edge, and only one gauge, 4R, was attached to the lower surface of the side tie to identify the maximum stress near the end support. To ensure that the specimen went through the pull-out failure mode, FT4 was designed, in accordance with the pull-out test results, with an embedment length of 250mm and grout strength of 25MPa. The test was carried out at grout strength of 18MPa.

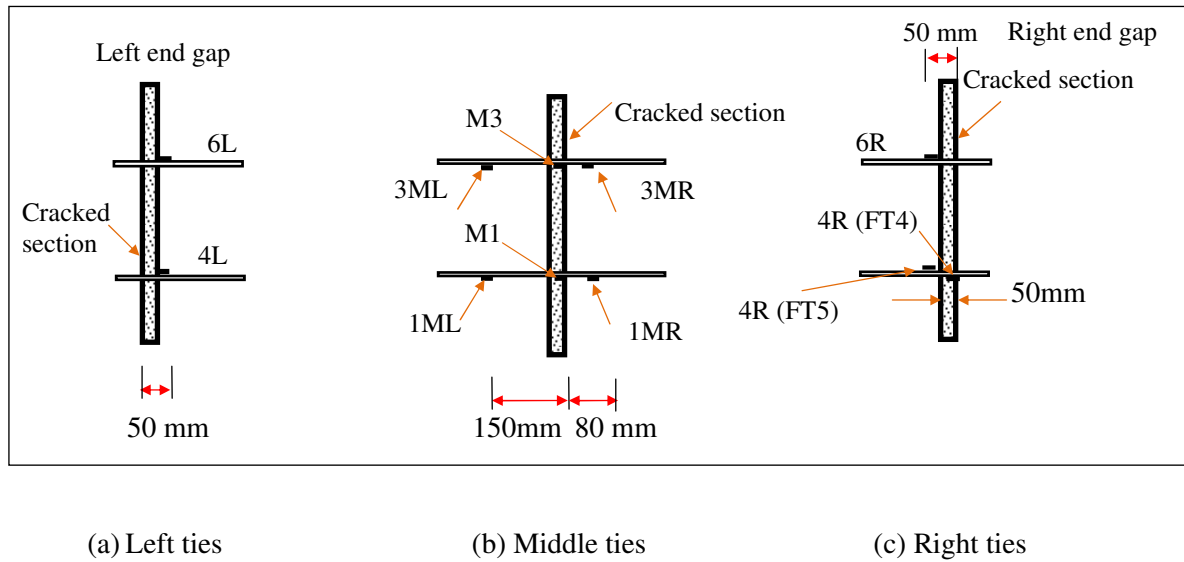


Figure 3.45 Layout of strain gauges (FT4 & FT5)

Figure 3.46 shows the stress-deflection curves for FT4. The results indicate that the stress-deflection relationship follows the pull-out behaviour of the tie bars into the keyways. Due to

the absence of grout in the joint gaps, M1 and M3 yielded primarily due to bending action. The ties did not experience yield on the embedment length. The strain in the middle joint gap and over the embedment length behaved differently. The stress from M1 and M3 increased from the very beginning of the test due to bending action at the middle joint and the stress-mid-joint-deflection curve remains almost linear up to a deflection of 50mm, where the screw jack released the slab and the catenary action was developed. In the catenary phase, the entire load was carried by the middle bars which led to a dramatic increase in the gradient up to the yield point.

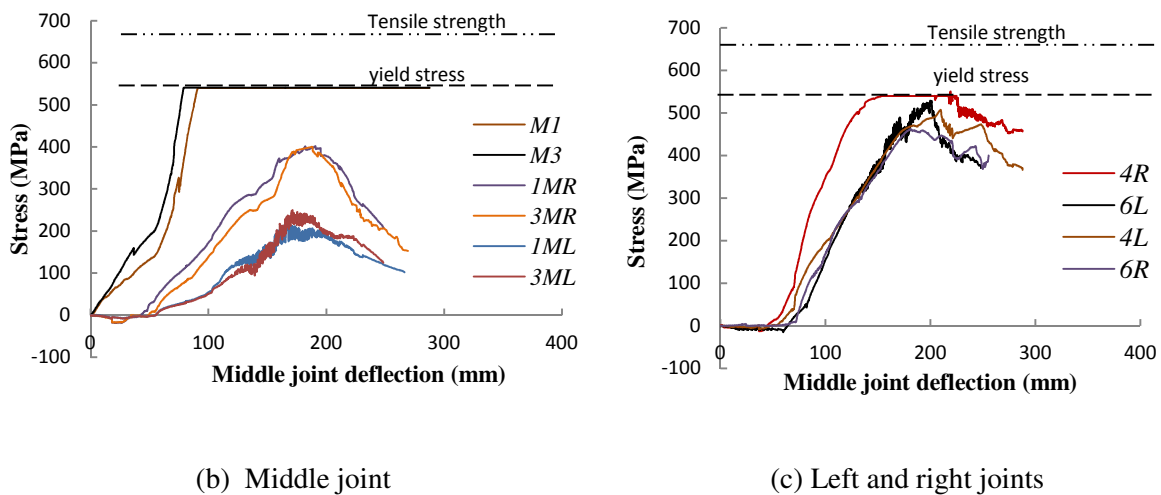


Figure 3.46 Stress versus vertical deflection (FT4)

However, for the stress measured from strain gauges 1MR, 3MR, 1ML and 3ML, prior to the catenary action, the stress was relatively small, followed by a linear increase up to the maximum stress at a deflection of 200mm. Prior to the development of the catenary action, the load only caused a bending action which was sustained by the middle ties alone. The axial action was minimal up to this point. Accordingly, the tensile force over the embedment length of the bars was negligible. With the increase in load, the axial action picked up and hence the tensile force was increased.

The tie stresses in 4L, 6L, and 6R show that the maximum stress from the strain gauges attached to the side ties shows a similar trend to the maximum tie stress from the pull-out test results of the inclined specimen (Fig. 3.11). This suggests that the pull-out behaviour of the reinforcement bars in the keyway dominates the floor system behaviour. Figure 3.46 shows that 4R yielded at a deflection of 120mm, which again confirms that, in the specimens with the pull-out failure mode, the tie bars close to the cracked section experienced yield.

FT5: Specimen FT5 was designed with the same gauge arrangements as FT4 (except for gauge 4R) but was cast with grout in the joint gaps. The tie stress-deflection relationship is similar to that of FT4. As was discussed for FT4, Figure 3.47a, b clearly indicates that pullout failure mode govern the behaviour of the floor system. Figure 3.47a shows a relatively constant tie force at the post-bond failure stage, which confirms the efficiency of maintaining a constant embedment length through the plastic tube beyond the designed embedment length. The attached gauges on the lower surface of the bars at the middle joint and the top of bars at the right support reached the yield capacity, while the gauges over the embedment length at the middle and sides showed typical pull-out behaviour (Fig. 3.47). Due to the crack developing at the right side of the slab-grout interface of the middle joint, the ties at the right support carry a higher force than those at the left support [Fig. 3.47(b)].

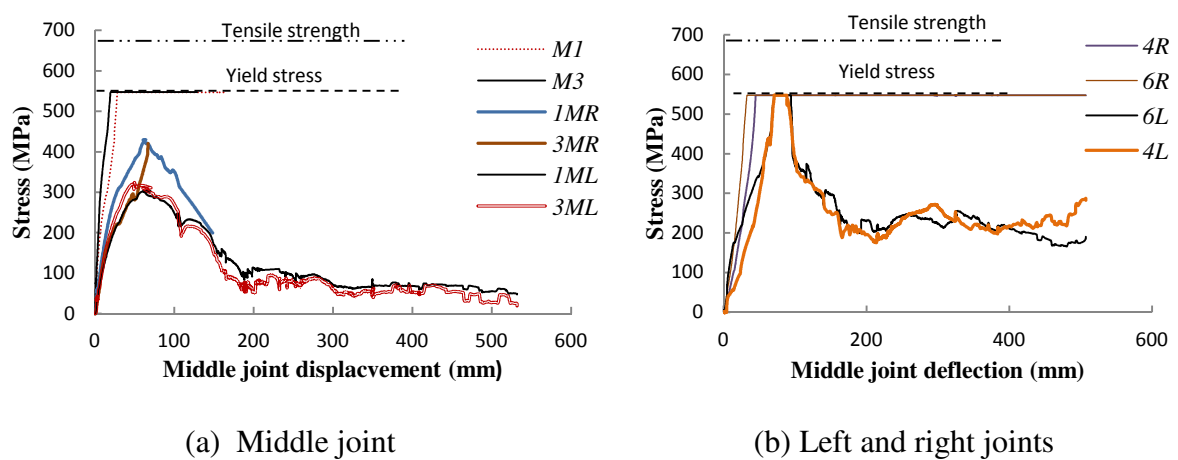


Figure 3.47 Stress versus vertical deflection (FT5)

Discussion

It is generally accepted that, through the catenary mechanism, the applied load is sustained by a tensile force along the elements. Although, to date, there is no clear definition for the onset of the catenary action, it can be defined as the point at which the axial force in the steel reinforcement at the compression zone turns from compression to tension (He et al., 2008). Alternatively, the point of the re-ascending phase has been defined by some researchers as the starting point of the catenary action (Jun, 2010). In the present study, the instance when two slabs at the middle joint are separated in the compression zone is defined as the point at which catenary action develops.

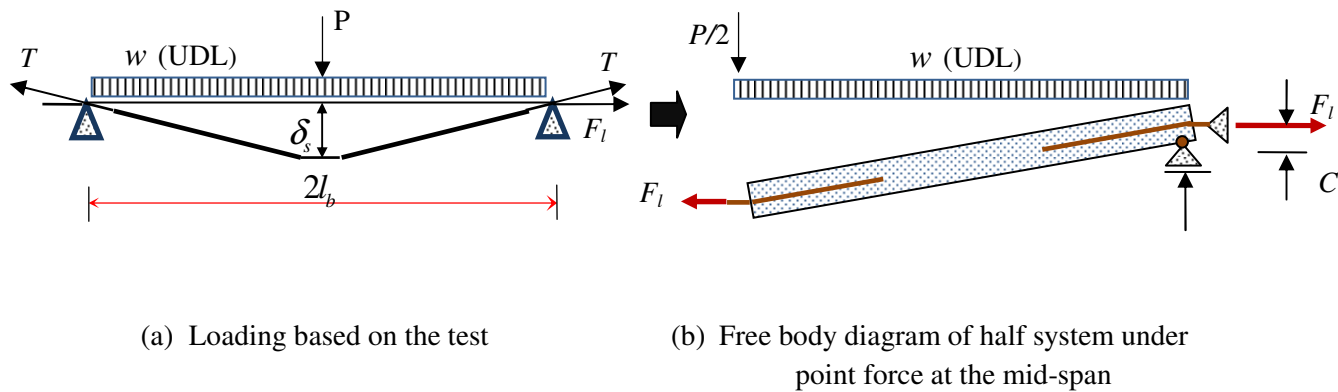


Figure 3.48 Calculation model for the catenary action mechanisms

In the bar fracture mode, the middle joint ties cannot contribute to the catenary action, as they have already fractured before the catenary action can develop; while the specimens with the pullout failure mode are capable of developing the catenary action mechanism. Based on their experimental results, Yi et al. (2008) and Su et al. (2009) argued that the bottom reinforcing bars in the middle joint of RC beams can contribute in the catenary action, while Yu et al. (2010) obtained the opposite results. In the case of RC beams, the beam ends are critical sections, the top bars at the middle joint can probably contribute in developing a

catenary action, while in precast cross wall structures, the most critical sections are at the middle joints, and fracture will start from these points (Fig. 3.38a, 3.41a). This can be considered as the main difference between RC and precast structures. Considering the catenary action, the relationship between tie force and vertical deflection using free body diagram in Fig. 3.48b gives

$$F_l = \frac{(wbl_b + P)l_b}{2n\delta} \quad (3.1)$$

where

- w = Uniformly distributed load (including permanent and variable loads)
- b = Slab width
- l_b = Floor span length
- F_l = Force in the longitudinal tie joining adjacent slabs
- δ_s = Vertical displacement at the middle wall support
- P = Line load exerted by screw jack
- n = Numbers of ties at the joints
- C = Distance between the side ties and the bottom surface of slab

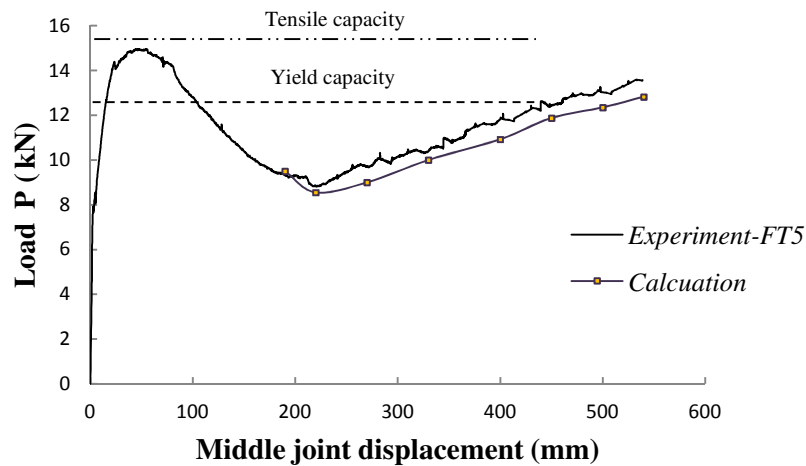


Figure 3.49 Load versus middle joint deflection based on test result of FT5

By using Equation (3.1), the applied force can be calculated from the tie force and the corresponding deflection. For instance, considering the tie force-deflection results of FT5 [Fig. 3.47(a)], the applied force P and the deflection relationship can be derived. Assuming proportional relationship of tie force with the embedment length, the modification factor of 2.0 was applied in Eq. (3.1) to calculate tie force at the loaded end. Fig. 3.49 presents such results, which agree with the experimental data reasonably well, particularly in the second ascending phase, where catenary action becomes dominant.

3.4.6 Summary

A total of five full scale tests were conducted to study the behaviour of specimens with two different failure modes. Group A specimens (FT1 and FT2) were tested to investigate the behaviour of systems considering the bar fracture failure mechanism and to examine the effect of the number of ties at the floor joints. Group B specimens (FT3, FT4 and FT5) were examined to investigate the behaviour of systems with respect to the pull-out failure mechanism.

In the specimens with the bar fracture failure mode, at the collapse, the longitudinal ties fractured at the mid joint, while the longitudinal ties at the side supports only experienced plastic deformation. This indicates that the middle joint is the most critical point in the floor joint system. Since the fracture occurs when the deflection is relatively small, the catenary behaviour is not well developed in this group of specimens.

In the second group, those specimens free of any concrete in the gaps, e.g. FT4, provide more measurable resistance than the other specimens, while the specimens with concrete at the joints e.g. FT3/FT5 can endure more deflection. All specimens in this group have a re-ascending phase in their tie force against deflection curves, indicating the occurrence of the

catenary action. Once the catenary action is developed, the loading resistance will continue to grow and it can provide more progressive collapse resistance for the floor slab system.

The comparison of the behaviour between these two groups of tests suggests that the key to inducing the catenary action is the introduction of an adequately large deflection before the system collapses. In this study, it was achieved as a result of the weak bond between the tie bars and the surrounding grout so that the bars fracture failure was suppressed.

3.5 OVERALL SUMMARY

To prevent progressive collapse of building structures, the establishment of the catenary action mechanism of beams or slabs is crucial so that adequate post-collapse resistance can be attained. It is believed that the joint design of precast floor system, e.g. the tie design, plays a key role in facilitating such a mechanism. An experimental investigation programme studying the pre- and post-bond failure performance of floor-to-floor connections with longitudinal ties is carried out. To develop reliable criteria for pullout and catenary behaviour two types of experimental tests are performed i.e. pullout tests and full-scale floor-to-floor tests.

The pullout experiments was carried out to study the behaviour of ribbed bar in grouted keyways of a precast slab, using actual embedment length and developing bond-slip criteria to design a floor-to-floor joint in precast concrete cross wall structures. The influences of concrete type, embedment length, bar size and slope of applied load were investigated. The specimens were designed based to meet pullout and bar fracture failure mode requirement. The result indicate that, pullout behaviour of tie bars into keyway of precast slab show relatively the same behaviour of tie bar with well condiment condition using prism.

Also, second set of experimental study has been undertaken to investigate the catenary behaviour of the precast concrete slab system following the removal of the intermediate wall supports. To this end, five full-scale concrete floor assembly tests have been devised and

carried out. Each test consisted of two standard hollow core floor slab units with various tie arrangements at the joints, which resembled a single storey floor structure supported by cross walls. The floor joint ties were placed on the pre-existing keyways where the grout was cast after the test assemblies were set up. The grout strength was specified to be 20 to 30 MPa and 10 or 12mm tie bars were used with an embedment length ranging from 250mm to 350mm. Test results indicated that specimens experiencing bar fracture failure patterns collapsed prior to the formation of the catenary action, but those specimens with the pullout failure pattern showed clear evidence of catenary behaviour. Furthermore, the difference in the post-collapse behaviour and the failure patterns indicated the characteristics of the catenary action. Test results reveal that for the ties designed with inadequate embedment length, the slip and the resulting large deflection will effectively trigger the catenary action. However, the full bond will limit the development deflection and lead to the fracture of tie bars before the catenary action is triggered.

Chapter 4

FINITE ELEMENT MODELLING

4.1 INTRODUCTION

To study the efficiency of reinforcement bars placed into keyways of precast slab to prevent progressive collapse, experimental, numerical and analytical analyses were carried out. This chapter presents a FE model for progressive analysis of a precast floor-to-floor system considering bar fracture and pullout failure mode. The problem is studied using nonlinear dynamic finite element simulations carried out following the DoD guidelines. The chapter focuses on developing a model for global analysis of precast structure subject to increasing vertical loading and notional removal wall support. To this end, detailed three-dimensional finite element models of the pullout behaviour of reinforcement bar in the keyway of precast concrete blocks to simulate pullout or bar fracture failure mode were developed. The same modelling method was then used in the subsequent three dimensional non-linear numerical analyses to simulate the ductility behaviour of precast concrete floor joints in the absence of underlying wall supports. The objective of the present study is to identify modelling parameters affecting the behaviour of system and proposes a model for progressive analysis of precast structure. The developed model in this chapter is used in the chapter 5 to analyse the floor-to-floor assembly considering both longitudinal and transverse ties and propose an improved TF method for progressive resistance of precast cross wall structures.

In this chapter a numerical simulation of pullout behaviour of steel bar into concrete and floor-to-floor system including two precast slabs and longitudinal reinforcement bars at the joints is discussed. A numerical simulation of a floor-to-floor system described in the

following sections is a highly non-linear problem with large vertical deflection, material and contact nonlinearities. For the numerical analyses of a precast concrete structure the well-established FE-programme ABAQUS is used. As far as possible, for the general material properties the default values defined by ABAQUS are applied. The influence of the remaining parameters to define the concrete model has been chosen according to test results conducted in the present study. The developed method given here can be used by other users in analyses of cross wall or RC structures, considering bar fracture and pullout failure mode.

Although ABAQUS has been used by many researchers (Josef et al., 2010; Marecek et al., 2006), but it is obvious that prior to starting the nonlinear simulation some basic questions need to be answered e.g. dynamic or static solution, mesh density, control parameters, boundary condition, applying load, concrete and reinforcement model, interface between steel and concrete parameters, friction coefficient between concrete and steel.

Due to high cost of a full scale experimental study, a reliable modelling of pullout behaviour using FE software packages is needed to extend the current knowledge about the behaviour of a floor-to-floor system, following removal of a wall support and improve the understanding of the effect of different components. The aim of this chapter is to develop a computer FE model which can be used for analyzing a floor-to-floor system using various loads, slab length, bar size, embedment length; and establish an accurate simulation of pullout and a floor-to-floor system without numerical difficulties. To this end, it requires a three dimensional analysis considering material, geometrical and steel-matrix interface nonlinearities.

The steel-concrete interface can be modelled using the connector element in ABAQUS. In this study, to simulate the steel-concrete interface a translator is used. The nonlinear relationship between the tie force and pullout displacement is used to simulate interface behaviour; as well as the geometric nonlinearities, due to large vertical deflection, which are

applied in the numerical model. A dynamic explicit solution strategy is employed to trace a stable post-peak response of the pullout and floor-to-floor system up to failure using ABAQUS. The pullout and full scale tests conducted in the present study is used to verify the developed FE model in the present study.

4.2 PROPERTIES OF REFERENCE TEST SPECIMENS

4.2.1 Pullout Test Specimens

To simulate pullout behaviour, a total of six pullout test results were used considering reinforcement into keyways of precast concrete under different bar sizes and embedment lengths (Fig. 4.1). The details and geometry properties of the specimens using reinforcement bars are given in Chapter 3 and summarized in Table 4.1.

Table 4-1 Specimens' properties for reinforcement bar into keyways

Specimens	Dimension (mm)	Steel Diameter (ϕ)	l_d/ϕ
ST42	250x300x150	12	20.83
ST43	300x300x150	12	25
ST44	350x300x150	12	29.2
ST54	350x300x150	16	21.8

* l_d = Embedment length of bars

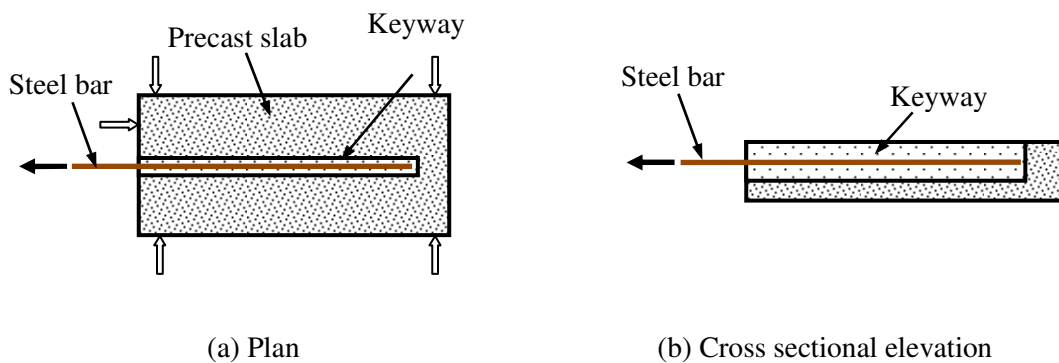


Figure 4.1 Illustrative diagram of the pullout test

The properties of the reinforcement bar in the keyways and precast slabs were chosen based on Bison Ltd's specification. The blocks were cut from the precast hollow core slabs and had the following dimensions: 400 mm in width, 150 mm in height and a variable length, with an aim to study the effect of the embedment length (Fig. 4.1). In the light of the fact that in actual use to meet progressive collapse requirements, the steel bars of $\phi 10$ and $\phi 12$ in the keyway of floor slabs are used, FE verification will be performed for these two reinforcement bars. Also, to show the efficiency of the developed method, a bar size of 16 mm is considered in the simulation.

4.2.2 Full Scale Floor Joint Test Specimens

Once the modelling for the grout-steel interface has been verified by the test results, it is then adopted in the modelling process to reproduce the full-scale floor-to-floor joint tests, also carried out via the present research program. In these experiments, the system consisting of two hollow core precast concrete slabs of full width, which were connected through two or three steel ties placed into two keyways (Fig. 4.2), was subjected to uniform and central line load to imitate the load exerted by the upper walls. All longitudinal ties were reinforcement bars, which were placed symmetrically into keyways in the middle and side joints.

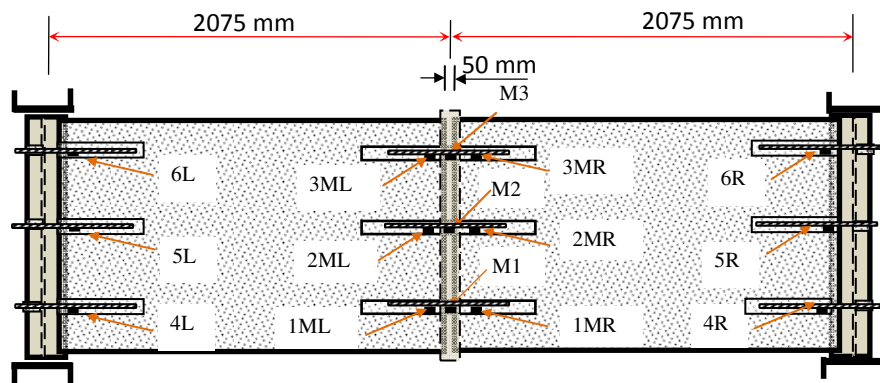


Figure 4.2 Illustrative diagram of the full scale floor joint tests with the layout of strain gauges

Table 4-2 Details of variables in the floor-to-floor system

Tests No.	Hollow core slab		l_d^*	Tie		Steel Type	f_c (MPa)	Number of Ties
	Length m	Weight kN/m ²		Bar diameter d_b (mm)	l_b/d_b			
FT1	2	1.95	350	$\phi 10$	35	Reinforcement	30	2
FT2	2	1.95	350	$\phi 10$	35	Reinforcement	32	3
FT3	2	1.95	200	$\phi 12$	16.7	Reinforcement	23	2
FT4	2	1.95	250	$\phi 12$	20.83	Reinforcement	18	2
FT5	2	1.95	250	$\phi 12$	20.83	Reinforcement	17	2

The five experimental tests on the floor joint systems conducted in the present study shown in Table 4.2, designated FT1, FT2, TF3, TF4, and FT5 are reproduced by numerical modelling to establish a verified model.

4.3 FINITE ELEMENT MODELS

Since bond is the key factor in the analysis and design of RC structures and it governs most RC performances, not just progressive collapse, seeking a technically reliable and economically viable bond modelling technique remains a challenging issue. To date, numerous research papers have been published which study the bond-slip behaviour between the tie and the surrounding grout; a large proportion of which were carried out by numerical modelling. To simulate reinforcement bar into keyways of precast slab either bond-slip or bar-steel interface need to be accurately defined.

4.3.1 Bond model

To simulate bond-slip behaviour, the first step is to select a method to develop a contact element between steel and concrete. To simulate bond various elements have been provided by ABAQUS (2006). Each element has been designed to simulate specific behaviour. A summary of these elements are introduced and discussed herein.

4.3.2 Embedded Element

To simulate the steel-concrete interface, an element or a group of elements in another “host” element forms an embedded element in ABAQUS can be used, where it embeds a region of the model within the whole or a “host” region of the model. Although ABAQUS specifies that this element technique can be used to model rebar reinforcement,; in reality, this technique only can model a perfect bond between concrete and rebar because the translational degree of freedom of all nodes in the embedded element (slave; rebar) are constrained to the corresponding degree of freedom of the host element (master; concrete). This element only can be used to simulate specimens with bar fracture failure mode.

4.3.3 Friction

A friction type of connector is defined in ABAQUS to model the behaviour of available components of relative motion or connecting surface. The principal concept of Coulomb friction between two contact surfaces is the relation between the maximum frictional stresses (force) on an interface with the normal force between two connecting surfaces. These two connecting bodies can sustain shear forces, F_t less or equal to a certain amount before sliding occurs at the interface between them, which it defines as sticking. This critical shear force can be defined as μF_N , where μ is the coefficient of friction and F_N is the normal force. The relation between sticking and sliding can be formalized as

$$\Phi = |F_t| - \mu F_N \leq 0 \quad (4.3)$$

Frictional sliding occurs if $\Phi = 0$, which in this case frictional force is μF_N and sticking occurs if $\Phi < 0$. Based on this definition, the behaviour of the frictional model in ABAQUS can be summarized in Figure 4.3 (ABAQUS, 2006).

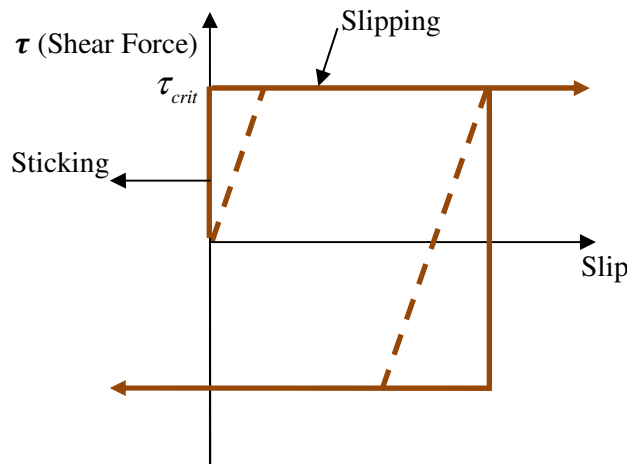


Figure 4.3 Frictional behaviour in ABAQUS (ABAQUS, 2006)

Due to the close similarity between bond exhibited across the interface of steel and concrete with frictional behaviour, only linear bond phenomenon and a fully debonding phase can be simulated by this model. As stated in literature review, the main shortcoming of the frictional method is that it can simulate neither degradation, nor the nonlinear phase of bond behaviour.

4.3.4 Spring Element

Spring elements in ABAQUS can be described through the terms of “force” and “displacement”. When the spring is related to translation degree of freedom, these variables are the relative displacement and force in the spring; also for rotational degree of freedom, they are the relative rotation and moment. In ABAQUS, an actual physical spring idealization

of torsional or axial components and restraints to prevent rigid body motion can be modelled by spring elements. The characteristic of a spring can be defined either linear by inputting a stiffness value, or nonlinear by employing pairs of force-relative displacement values (Fig. 4.4). It is important to note that the basic deficiency in this area is that the spring element cannot simulate the degradation portion of bond-slip behaviour. Moreover, nonlinear behaviour of the spring has not been supported in ABAQUS/CAE.

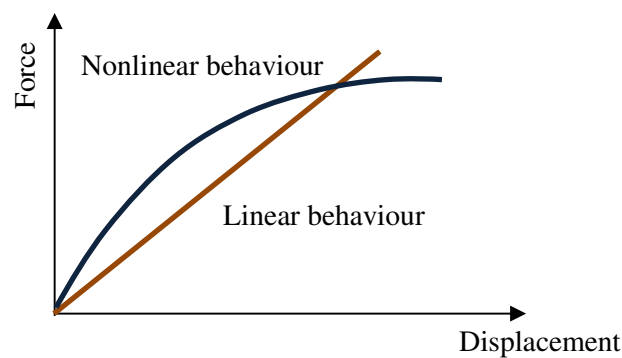


Figure 4.4 Linear and nonlinear spring element (ABAQUS 2006)

4.3.5 Translator

In ABAQUS various methods and elements to simulate this contact surface have been presented, such as contact, constraints, and connector elements. Since bond-slip is a function of the load versus relative displacement (slip), the elements which are able to couple a relative displacement with a force should be considered. The connectors may consist of a linear or nonlinear force versus displacement. Moreover, the connector can be used to specify damage mechanisms with different damage evolution laws.

A translator is a type of connector which provides a slot constraint between two nodes and aligns their local direction (Fig. 4.5). The translator element is a special type of FE element that has been built in the ABAQUS programme. It has two nodes, which can be attached to two substrates (see Fig. 4.5). Like other types of contact elements, it can be assigned a force

together with corresponding relative displacement between these two nodes. This connector dictates kinematic constraints by combining connection types with the options of SLOT and ALIGNS (ABAQUS 2006).

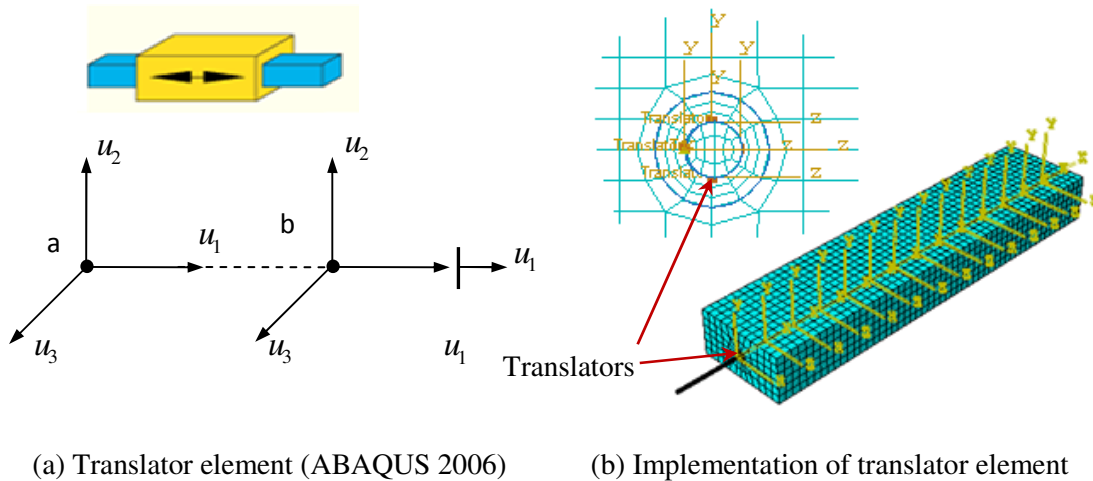


Figure 4.5 Translator type of connector (ABAQUS 2006)

As it can be seen clearly, the relationship between steel and concrete in the keyways of floor-to-floor joints is very similar to the relationship between the yellow and blue parts in Figure 4.5; in which the only degree of freedom is u_1 and it defines translation in the direction parallel to the axial axis of the blue bar. A translator connector allows the two parts to have relative displacement in this direction and interaction between parts in other directions is considered as a master-slave or a hard contact, i.e. all degree of freedom of node b to be the same as those for node a .

According to the analysis' requirement, different behaviour can be defined in a translator connector; thus relative motion; a spring-like elastic, plastic and damage behaviour can be introduced by the user. Two of these behaviours are quite crucial to simulate the bond model. The first is the ability of the connector to simulate damage, by defining the damage initiating

and degradation portion of the bond-slip relationship. The second is the elastic spring-like connector, which allows the translator to have the same behaviour as a spring element (ABAQUS 2006). Due to the capability of the translator to include multiple facets of connector behaviours and its connection type, it is well adapted with the contact between steel and concrete; hence a 3D reinforcement concrete model with a set of translator elements and a suitable bar-concrete interface appears to be the best approach after a number of different trials (Johnson S, 2006; Li, 2007).

4.4 MODELLING OF BAR-CONCRETE INTERFACE

The contact condition is considered as a specific class of discontinuous constraint in a finite element analysis, which allows the transmitting of stress or force from one part to another part of the model. ABAQUS/Explicit provides two algorithms to simulate contact between two parts: a general contact algorithm; and a contact pair algorithm. In this study the general contact algorithm is used. In both models the following settings are used:

- Mechanical constraint formulation: kinematic contact method
- Normal behaviour: hard contact for pressure-over closure and
constraint enforcement method: default
allow separation after contact
- Tangential behaviour: frictionless
- Contact pair: Master and Slave surface

To ensure perfect continuity between parts in the model, geometric kinematic constraints need to be applied into the model (Mahbuba 2007). In the full scale and pullout models the kinematic constraint method is applied by the translator's element to the model at the interfaces and it results in computational efficiency.

4.5 MESH DESCRIPTION

Both concrete and steel were modelled by the 8-node solid element i.e. C3D8 with linear reduced-integration. The fine mesh in reinforcement elements results in a smooth interaction at the interface between steel and concrete. In this study emphasis has been placed on the high level of reliability and accuracy of the model rather than efficiency of calculation.

According to ABAQUS documentation, a structured meshing technique is perfect for three-dimensional regions. Using this technique to mesh complex regions may require partitioning. Furthermore, for these types of elements, a structured meshing technique consisting of a hexahedral element is more efficient than a tetrahedral element. Regions with a hole (such as the present model), isolated face and vertices cannot be meshed using this technique. Accordingly, holes can be eliminated by partitioning their circumference into halves, quarters, etc. Figure 4.6 shows that the region with a hole needs to be converted to four regions without holes. On the other hand, using structured meshing near concave boundaries should be accompanied with caution. If in these regions the number of elements is decreased, a distorted mesh results near concave boundaries and nodes at this regions fall outside the region's geometry. Partitioning and refining mesh are able to resolve this problem (ABAQUS, 2006).

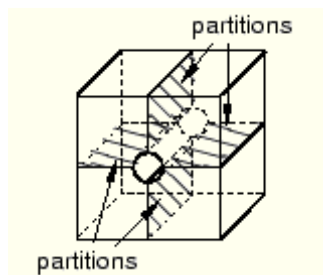


Figure 4.6 Partitions can make a part structured meshable (ABAQUS 6-10-1, 2006)

Due to the meshing technique and defining the translator's requirements, it is compulsory to divide the model around the circumference in both steel bars and concrete into at least four

elements every 50 mm for reinforcement bars along the embedment length. Accordingly, the minimum mesh size, which automatically is applied in a structured meshing technique, will be 4.71 mm around the circumference and 25 mm along the embedment length of the reinforcement. The model was discretised in such a way that the mesh density varied at different locations where the stress distributions were different. Three locations have been chosen to apply different mesh densities in the hollow core concrete slabs; these are the steel-grout interface, zones within the embedment length and the middle of the block (Fig. 4.7).

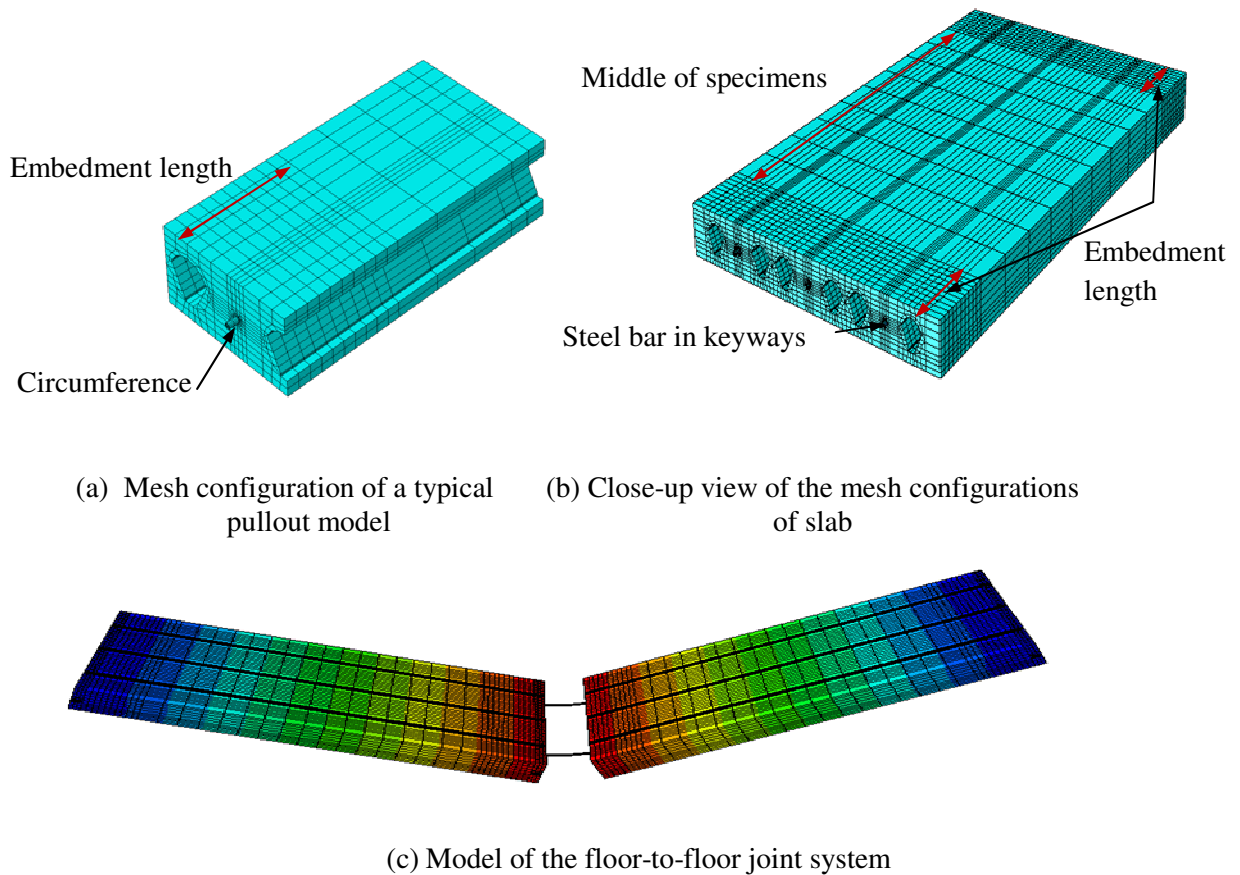


Figure 4.7 Finite element mesh pattern

A mesh size convergence analysis was carried out for pullout out analyses to determine the optimal meshing pattern. Table 4.4 presents three mesh trials with various mesh sizes at the circumference of the steel-grout interface, along the embedment length and the middle of the

block. The results of slip and tie-force were examined for the convergence check. Table 4.4 and Figure 4.8 indicate that meshing trials B and C yield very close results and hence trial B has been chosen for the following modelling work using reinforcement bars.

Table 4-3 Mesh properties for pullout models -reinforcement bars

Mesh trial	Number of element or mesh size			Pullout	
	Circumference at interface	Embedment length	Middle of block	Slip ratio	Tie force ratio
A	8 elements	25mm	150 mm	1	1
B	16 elements	25 mm	150 mm	0.99	0.96
C	32 elements	12.5 mm	50mm	0.99	0.96

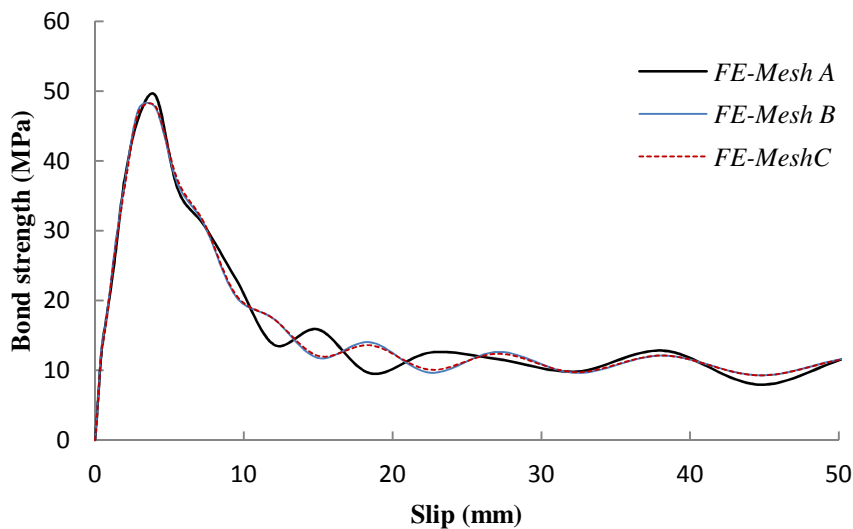


Figure 4.8 Convergences' analyses for pullout model; $\phi=12\text{mm}$, $L_d=250\text{ mm}$

To study the effect of the number of translators on the pullout behaviour of reinforcement into the keyways of precast slabs, using the optimum mesh, the specimens analysed using various translator patterns over the embedment length. The results of tie-force and slip were examined

for the convergence check. Figure 4.9 shows that translator trials 16TR and 24TR yielded very close results for the specimen with reinforcement bars and hence trial 24TR has been chosen for the proposed modelling work. It can be concluded that the optimum translator spacing and numbers over the embedment length for reinforcement bar modelling is 4TR/50mm. The results indicate that the proposed model is not highly sensitive to the number of translators and mesh pattern (Fig. 4.9).

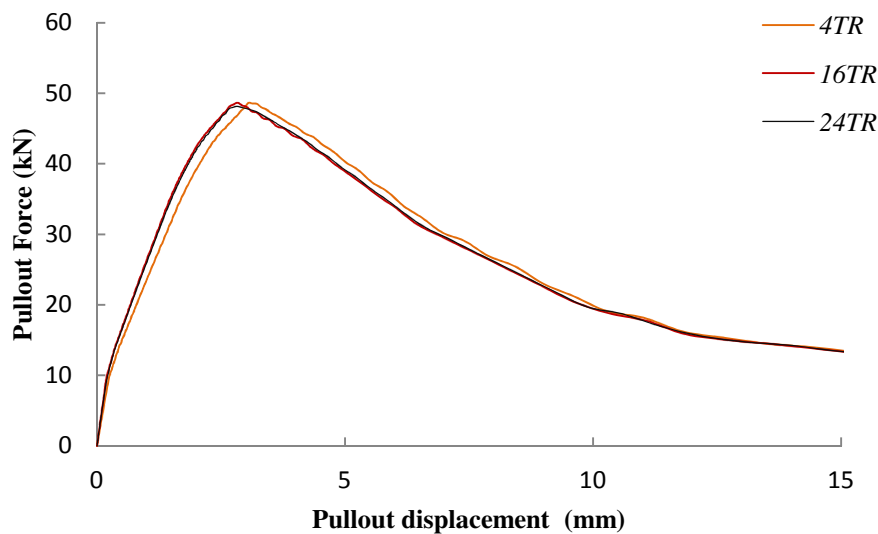


Figure 4.9 Effect of the translator pattern on the analyses result for pullout model; $s=12\text{mm}$, $L_d=250\text{ mm}$

The full scale floor joint system is constructed in several parts with different material properties and mesh patterns. To produce a full scale model (Fig 4.7) the parts are then assembled employing the “part”, “instance” and “assembly” options in ABAQUS. Most of the features of this model are similar to those of the pullout model. However, along the embedment length’s fine mesh and in the regions between two embedment lengths the number of elements is reduced to minimize the solution time; while maintaining a proper representation of the relative displacement of steel bar to concrete. Due to the special geometric property of the cross section, the concrete was divided into 40 and the steel bar into

10 segments. In summary, for dynamic analyses using ABAQUS/Explicit the numbers of the elements for the various parts in the full scale specimens i.e. FT1 are shown in Table 4.5:

Table 4-4 Mesh type for various parts in the full scale specimens

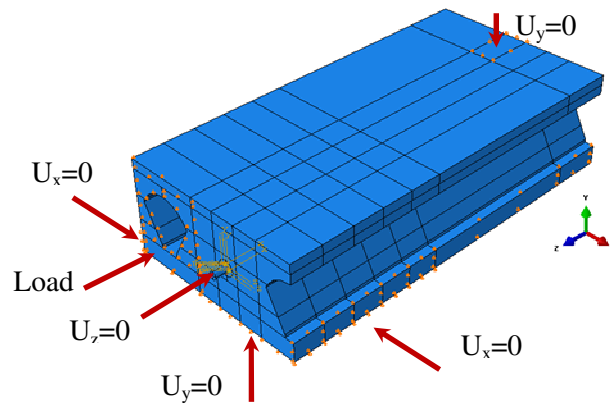
Part	Number of elements	Mesh type
Longitudinal ties	12060	C3D8R*
Precast slabs	59578	C3D8R
Gaps	9684	C3D8R
Reinforcement bars	-	T3D2**
Frame support	21251	C3D8R
Transverse ties	-	C3D8R
Total elements	102,573	

*C3D8R: 3D hexahedral (brick) element with linear approximation of displacements, reduced integration with hourglass control, 8 nodes/element, 3 translational DOFs/nodes.

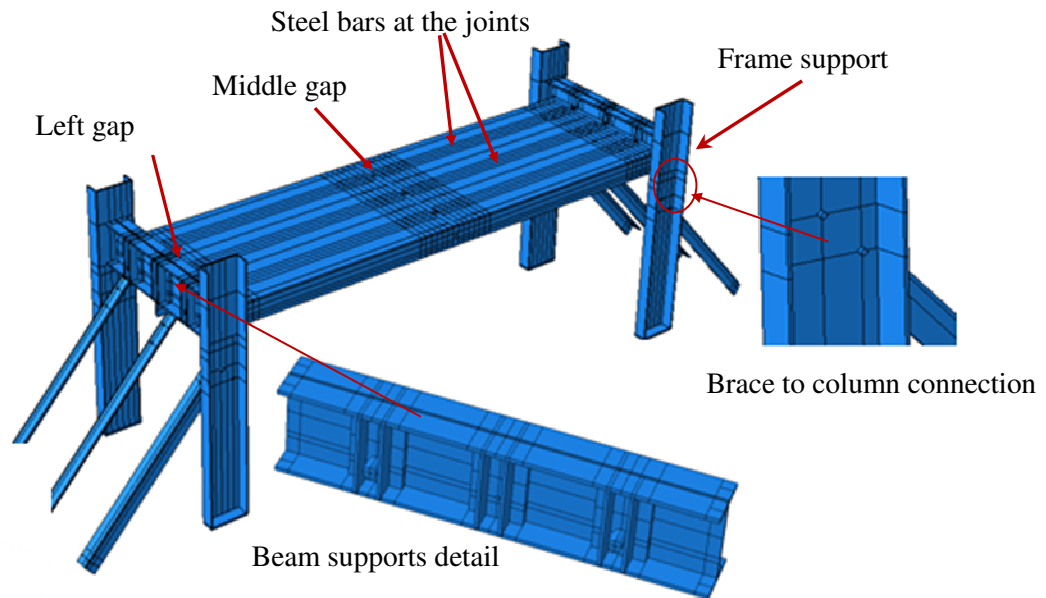
**T3D2: Truss element with linear approximation of displacements, 2 nodes/element, 3 translational DDOFs/node.

4.6 BOUNDARY CONDITIONS

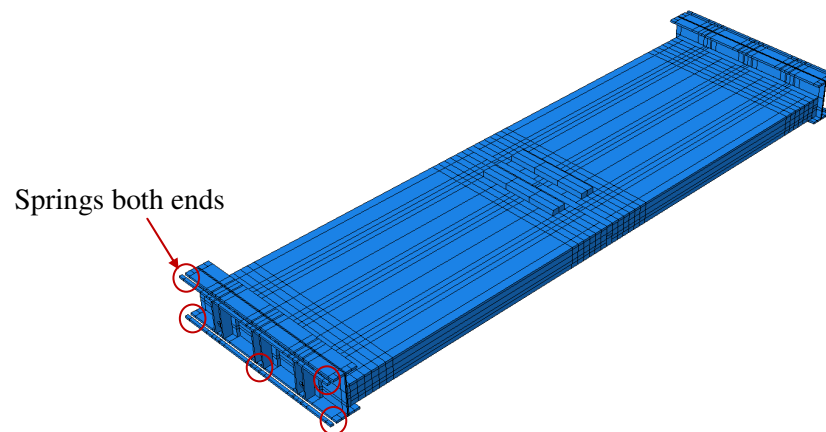
The boundary conditions applied in the concrete block and the floor-to-floor joint models are displayed in Figs. 4.10 (a) and (b). In the former case, only one degree of freedom of specimens remained free, i.e. the longitudinal movement. In the latter case, the preset slab sits on the beam support, which is a part of the very stiff frame. To reduce time of the analyses, the frame supports were replaced by five springs (Fig. 4.10c, and d).



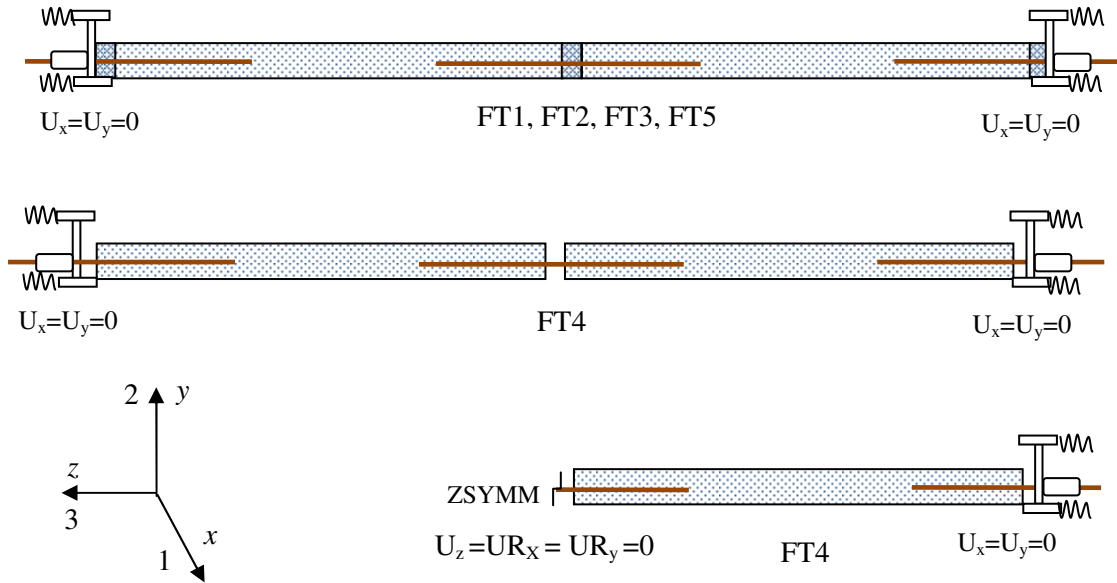
(a) Pullout model



(b) Full scale floor-to-floor model-full model



(c) Lateral elastic support



(d) Full scale model-simplified boundary condition

Figure 4.10 End boundary condition in finite element model for pullout and full scale model

Symmetry boundary conditions are only applied for full scale floor-to-floor at the middle of the model for specimens without grout in the gaps i.e. FT4. In the latter case, the right end node remains restrained but the middle point has been allocated a symmetry boundary condition, as only the right-hand side is included in the model. At this point, translations along 3 and rotation about 1 and 2 in the local coordinate system were fixed. At the right supports, both translations in 1 and 2 axes were fixed and rotation about them was released. In the axis 3, five springs were applied on the beam support to simulate bracing frame support (Fig. 4.10d).

4.7 MATERIAL PROPERTIES

4.7.1 Concrete and Steel

The elastic material properties of concrete and steel for the various specimens are shown in Table 4.6. For all specimens, stress-strain properties provided in the following sections are used to simulate the concrete damage plasticity model (CDP) at the joints and plastic behaviour of the steel bars. It is to be noted that nonlinearity was only applied in concrete gaps and the steel-concrete interface. The linear properties were allocated to the precast slabs.

Table 4-5 Materials' Properties

	Elastic Modulus E (N/m ²)	Specimen	Poisson's Ratio	Density (kg/m ³)
Concrete	30.5 E09	FT1, FT2	0.2	2400
	28.2 E09	FT3		
	26.2 E09	FT4, FT5		
Steel	210.0 E09	FT1, 2, 3, 4,5	0.30	7800
Precast slab	34.54E09	FT1, 2, 3, 4,5	0.2	2500

To analyse RC structures, for low confining pressure, three different concrete models has proposed by ABAQUS: (1) “Concrete smeared cracking” (2) “Concrete damaged plasticity” and (3) “Cracking model for concrete”. In this study Concrete Damage Plasticity (CDP) model is used and described in detail in the following sections and Appendix 4A.

4.7.2 Concrete Damage Plasticity (CDP)

Concrete Damage Plasticity (CDP) is available in ABAQUS/Explicit/Standard and is usable for both static and dynamic analyses. It is primarily designed to analyse RC structures subjected to monotonic, dynamic or cyclic loading under low confining pressure. This model can be used in all types of elements e.g. solids, shells, trusses and beams and “uses concepts

of isotropic damaged elasticity in combination with isotropic tensile and compressive plasticity to represent the inelastic behaviour of concrete” (ABAQUS, 2006).

Damage plasticity characterizes the uniaxial compressive and tensile response of concrete as a function of inelastic strain i.e. $\bar{\epsilon}_c^{in}$ (Appendix 4A) and cracking strain i.e. $\bar{\epsilon}_t^{ck}$ (Appendix 4A), respectively. In the analyses stress versus plastic strain i.e. $\bar{\epsilon}_c^{in}$ is used, which is automatically converted by ABAQUS from user defined stress-inelastic strain curve to stress-plastic strain. Furthermore, to define degradation of elastic stiffness, two damage variables of d_c and d_t have been introduced, which they are function of plastic strains.

4.7.3 Plotting Stress- Inelastic Strain Curve

According to uniaxial compressive test results and using the EC2 provision, the relationship between stress and strain for structural analyses can be established [Appendix 4A]. To define stress-strain curve two quantities of compressive strength i.e. strain and modulus of elasticity need to be defined. The average compressive strength of concrete can be obtained using a standard compressive strength test. The other quantity i.e. modulus of elasticity, is obtained using the EC2 regulation:

$$E_{cm} = 22(0.1f_{cm})^{0.3} \quad (4.1)$$

where

f_{cm} = Mean value of concrete cylinder compressive strength (MPa)

E_{cm} = Secant modulus of elasticity of concrete (MPa)

According to EC2 the relationship between stress and strain for short term loading can be expressed by Eq. (4.2).

$$\frac{\sigma_c}{f_{cm}} = \frac{k\eta - \eta^2}{1 + (k - 2)\eta} \quad (4.2)$$

Where

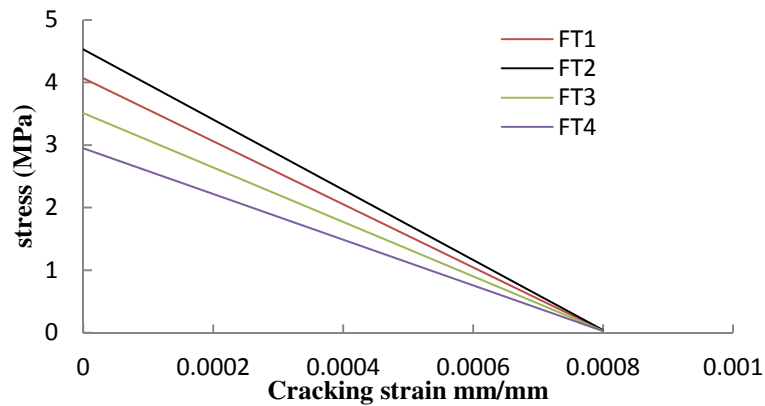
$$\eta = \varepsilon_c / \varepsilon_{c1}$$

$$k = 1.05E_{cm}(\varepsilon_{c1}) / f_{cm}$$

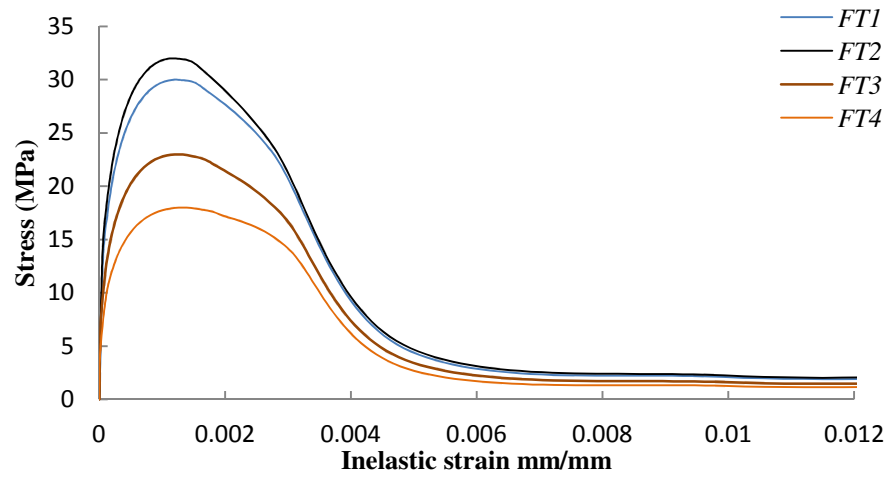
ε_{c1} = the strain at the peak compressive stress (EC2-Table 3.1)

f_{cm} (MPa)	16	20	25	30	35
ε_{c1} %	1.9	2.0	2.1	2.2	2.25

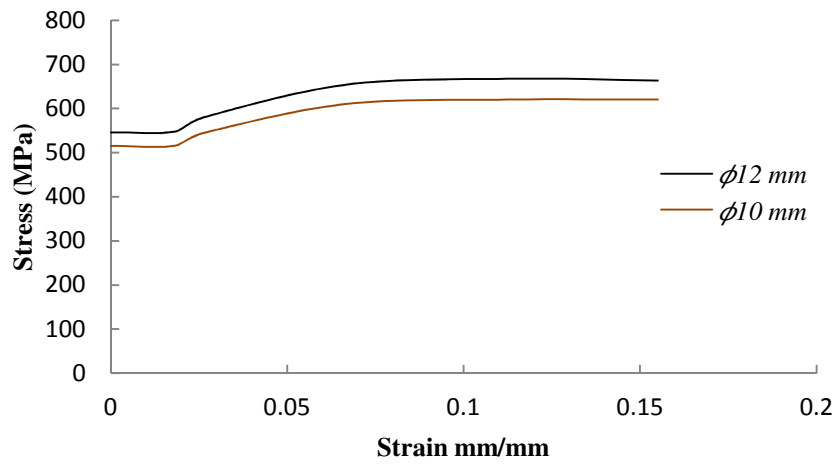
The input data for the CDP model in ABAQUS in the form of the stress-strain curve for tensile and compressive behaviour of concrete in different specimens is developed in Appendix 4A and displayed in Figure 4.11.



(a) Tension stiffening-CDP Model (Appendix 4A)



(b) Compressive hardening-CDP Model ((Appendix 4A)



(c) Plastic model-reinforcement bar

Figure 4.11 Properties of materials in CDP and plastic model

4.7.4 Damage Parameters of d_t and d_c

In the reinforced concrete model, the post failure behaviour is given as a function of cracking strain, $\bar{\epsilon}_t^{ck}$ [Appendix 4A]

$$\bar{\epsilon}_t^{ck} = \epsilon_t - \epsilon_{ot}^{el} \quad (4.3)$$

Where

ε_t = Total tensile strain

$\varepsilon_{ot}^{el} = \sigma_t / E_o$ Strain corresponding to undamaged material

To avoid numerical issues, ABAQUS requires that the lower limit of tensile stress needs to be equal to or more than one hundredth of the stress at the initial failure point i.e. $\sigma_t = \sigma_{to} / 100$. As stated, the input data for the tension softening regime needs to be provided in terms of the cracking strain and damage variable i.e., $d_t - \bar{\varepsilon}_t^{ck}$, and then plastic strain are automatically calculated by ABAQUS:

$$\bar{\varepsilon}_t^{pl} = \bar{\varepsilon}_t^{ck} - \frac{d_t}{(1-d_t)} \frac{\sigma_t}{E_o} \quad (4.4)$$

Where

$\bar{\varepsilon}_t^{pl}$ = Plastic strain

$\bar{\varepsilon}_t^{ck}$ = Cracking strain

d_t = Damage variable

σ_t = Stress at the failure point

E_o = Elastic stiffness of the concrete

It is to be noted that if the tensile damage parameter, d_t , is not introduced by the user ABAQUS assumes that $\bar{\varepsilon}_t^{pl} = \bar{\varepsilon}_t^{ck}$.

The behaviour of plain concrete under uniaxial compressive load is defined in terms of stress versus inelastic (or crushing) strain, $\bar{\varepsilon}_c^{in}$ instead of plastic strain $\bar{\varepsilon}_c^{pl}$ [Appendix 4A]. ABAQUS has defined inelastic strain as total compressive stress minus elastic strain corresponding to the undamaged stage (ABAUS 2006).

$$\bar{\varepsilon}_c^{in} = \varepsilon_c - \varepsilon_{oc}^{el} \quad (4.5)$$

where

$\bar{\epsilon}_c^{in}$ = inelastic strain

ϵ_c = total compressive strain

$\epsilon_{oc}^{el} = \sigma_c / E_o$ = elastic strain

To take into the unloading effect, ABAQUS provides unloading data based on the compressive damage curve i.e. $d_c - \bar{\epsilon}_c^{in}$. The inelastic strain is automatically converted to the plastic strain by ABAQUS

$$\bar{\epsilon}_c^{pl} = \bar{\epsilon}_c^{in} - \frac{d_c}{(1-d_c)} \frac{\sigma_c}{E_0} \quad (4.6)$$

The degradation variable of d_c , ranges from zero to one for undamaged and totally damaged material, respectively. So far, the explicit formulations for d_t and d_c are not available; hence, to define concrete compression damage, various methods have been introduced in the literature. Jankowiak and Lodygowski (2005) and Kmiecik and Kamiński (2011) imply that: d_c can be successfully defined using a uniaxial stress-strain test, by considering the ratio of stress in the descending stage over maximum compressive strength:

$$d_c = 1 - \frac{\sigma_c}{\sigma_{cmax}} \quad (\text{Model 1}) \quad (4.7)$$

Where

σ_c = Compressive stress in the descending phase

σ_{cmax} = Maximum compressive strength

Based on experimental data of (cyclic) uniaxial, biaxial or triaxial stress tests, Birtel and Mark (2006) conducted a comprehensive study to describe the nonlinear behaviour of concrete. An

efficient material parameter and function were derived and verified by experimental work. It was found that compressive damage variable d_c can be defined based on plastic strain, which is in proportion to the inelastic strain i.e. $\varepsilon_c^{pl} = 0.7\bar{\varepsilon}_c^{in}$, then

$$d_c = 1 - \frac{\sigma_c / E_c}{0.3\bar{\varepsilon}_c^{in} + \sigma_c / E_c} \quad (\text{Model 2}) \quad (4.8)$$

The result indicates that most of the inelastic strain remains after unloading. Similarly to the above definition, it was found that the damage parameter d_t also depends on ε_t^{pl} , which based on experimental data, was defined as $\varepsilon_t^{pl} = 0.1\bar{\varepsilon}_t^{in}$, Then

$$d_t = 1 - \frac{\sigma_t / E_c}{0.9\bar{\varepsilon}_t^{in} + \sigma_t / E_c} \quad (\text{Model 2}) \quad (4.9)$$

A new plastic-damage model was developed by Koh et al. (2008) and verified by experimental static and dynamic tests. Both damage variables d_c and d_t were used and calibrated. According to the work of Lee and Fenves (1998) and Lubliner et al. (1989), Koh et al. (2008) defined the above variables as

$$d_c = 1 - \exp(-a_c \varepsilon_c^{pl}) \quad (4.10)$$

$$d_t = 1 - \exp(-a_t \varepsilon_t^{pl}) \quad (4.11)$$

Where a_c and a_t can be calibrated using uniaxial tensile and compressive tests by considering the following boundary conditions:

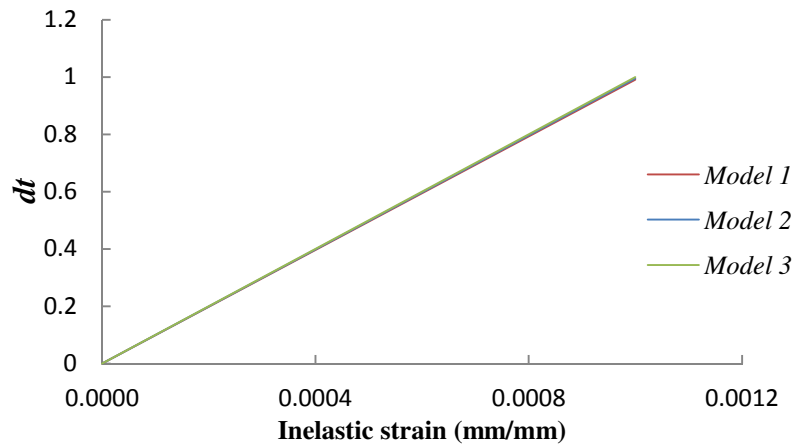
$$d_c \Big|_{\varepsilon_c^{pl} = \varepsilon_{c \max}^{pl}} = 1 \quad (4.12)$$

$$d_t \Big|_{\varepsilon_t^{pl} = \varepsilon_{t \max}^{pl}} = 1 \quad (4.13)$$

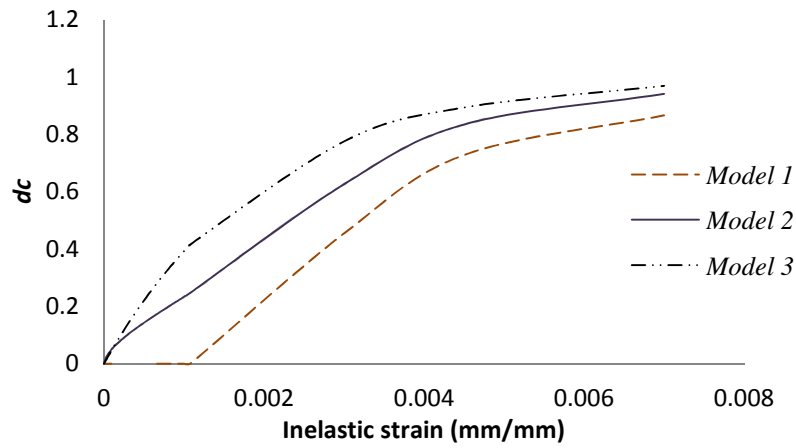
Replacing ε_c^{pl} by $0.7 \bar{\varepsilon}_c^{in}$ and ε_t^{pl} by $0.1 \bar{\varepsilon}_t^{in}$ in Eq. (4.10) and Eq. (4.11) and rearrangement gives

$$d_c = 1 - \exp(-0.7 a_c \bar{\varepsilon}_c^{in}) \quad (\text{Model 3}) \quad (4.14)$$

$$d_t = 1 - \exp(-0.1 a_t \bar{\varepsilon}_t^{in}) \quad (\text{Model 3}) \quad (4.15)$$

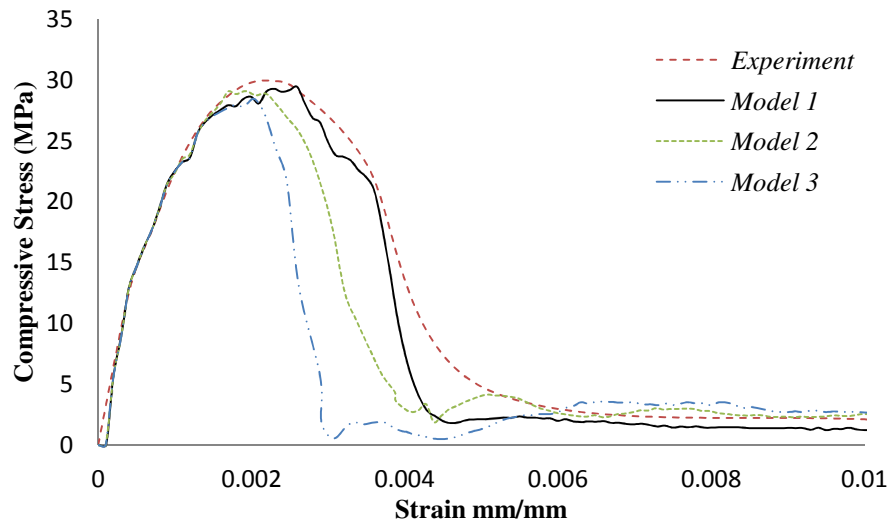


(a) Tension

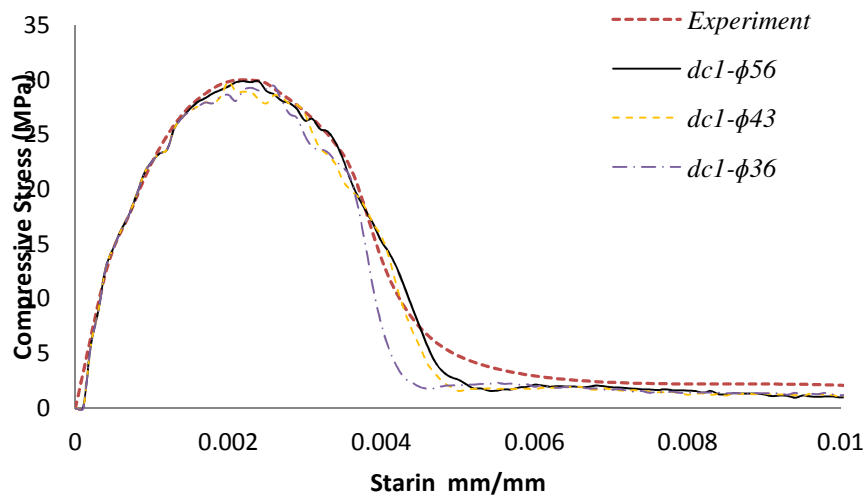


(b) Compression

Figure 4.12 Damage parameters for CDP model (Appendix 4A)



(a) Stress vs. strain for three different damage parameters- dilation angle=36°



(a) Stress vs. strain for three different dilation angle using model 1

Figure 4.13 Stress vs. strain using various damage parameter and dilation angle (Appendix 4A)

The calibration analyses developed in Appendix 4A using cube specimens indicate that, all three damage parameter provide same stress-strain relationship in ascending stage, while following peak stress the each damage parameter shows different trend compare to the original stress-strain data (Appendix 4A). The result indicate that, the strain-strain relationship using damage parameter of model 1 defined by Eq. (4.7) and dilation angle of 36 agrees well

with the original data compare to the other two models (Fig. 4.13a). To show the effect of dilation angle, the same cube specimens was reanalysed using dilation degree of 36, 43 and 56 (Appendix 4A). The results indicate that, the specimens with damage parameter of d_c defined by model 1 and dilation degree of 43/56 agree extremely well with the original stress-strain (Fig. 4.13).

The test results of FE analyses developed in the Appendix 4A indicate that, the failure strain can be assumed more than 1^{-4} , while cracking strain need to be less than 1^{-3} suggested by ABAQUS. The test and FE result indicates that the failure strain can be assumed 1.5^{-4} (Appendix 4A) and strain corresponding to zero stress should be assumed 0.8^{-3} (Appendix 4A).

4.7.5 Translator Property

One of the key challenges encountered in modelling is to define an appropriate and efficient bond-stress relationship. To determine the non-linear property of the translator elements, the pullout tests were used to derive the force-slip relationship. In the input data to define slip, the elongation of the ties needs to be deducted from pullout displacement. The measured results from the test were pullout force and overall displacement. It was assumed that the stiffness for the translator along the embedment length is uniform. According to the pullout test results, and using four translators at the interface and with an interval of 50 mm along the embedment length for the reinforcement bars, the translator properties were defined as shown in Figure 4.14. As the defined bond stress has been calibrated based on a compressive strength of 20 MPa (Chapter 3), to take in the effect of different compressive strengths, for any other compressive strength bond strength is modified by applying $\sqrt{f_c / 20}$ on the vertical axis in

Figure 4.14. The translator force is defined as $F_{TR} = psu / n$, where F_{TR} , p , s , and n are the translator force, the circumference of the bars, the translator spacing, the bond strength, and the number of translators in each section, respectively.

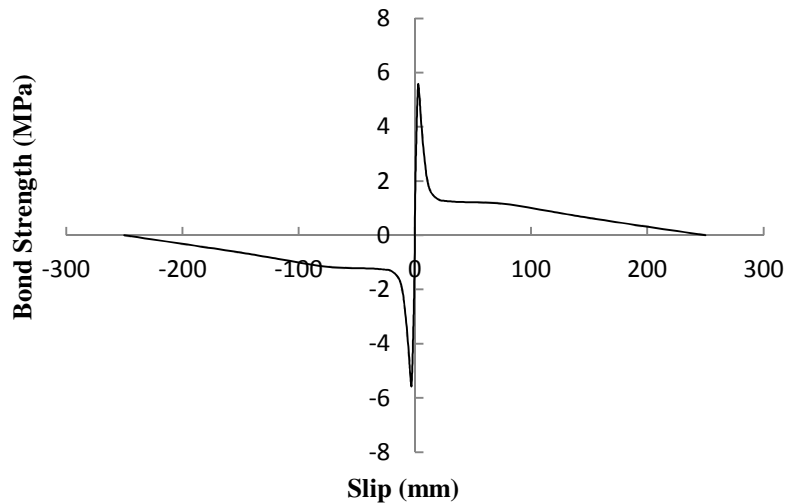


Figure 4.14 Translator properties used in the modelling process

4.8 ANALYSIS SOLUTION STRATEGY

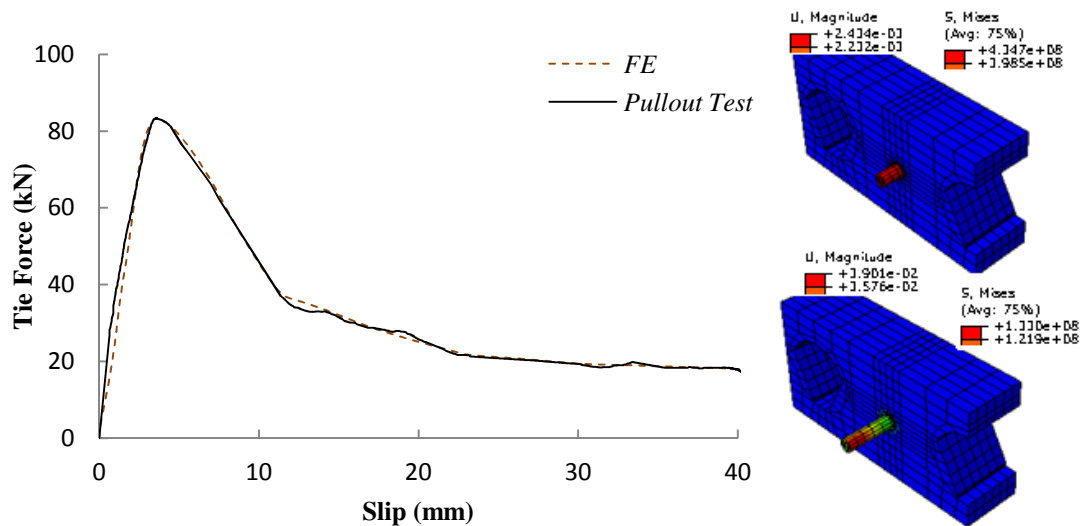
If the model contains highly discontinuous processes, such as the present work which contains contact sliding and translators, convergence may be not possible using an implicit method, especially after the peak point or in the descending zone. ABAQUS/Explicit is particularly well-suited for modelling the transient dynamic event in the structures that are subject to impact loads involving complex contact interaction between independent parts (ABAQUS, 2006). The contact condition and other discontinuous problems can be readily formulated in the explicit approach, which is enforced on a node-by-node basis without iteration. Furthermore, the translator element is only available in ABAQUS/Explicit. Hence it is used in this study to perform a non-linear quasi-dynamic analysis.

4.9 VERIFICATION OF MODELS

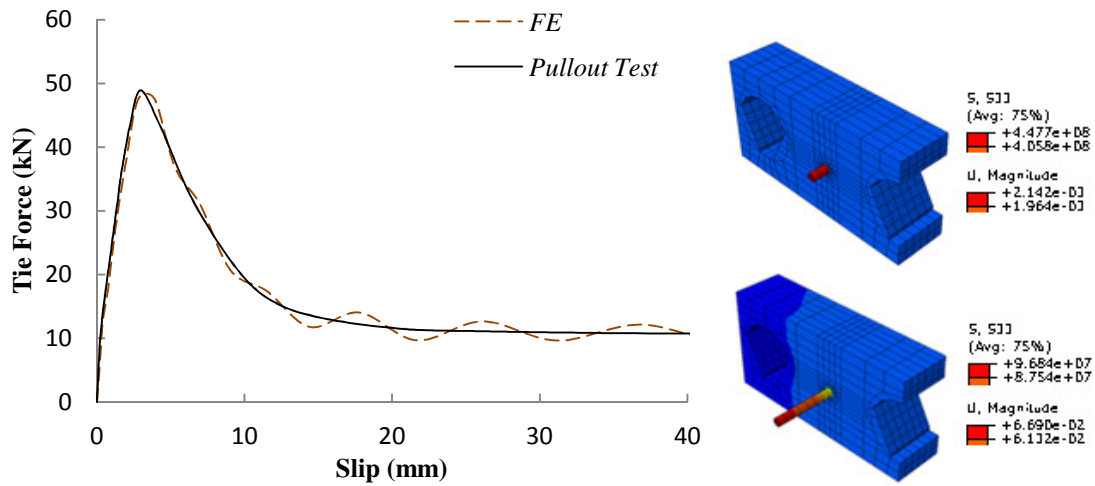
4.9.1 Performance of Pullout Models

The pullout model was developed at the initial phase of the FE study to investigate the suitability of the translator model and contact boundary condition to predict the pullout behaviour of the bar in concrete. The horizontally loaded pullout specimens were simulated using the pullout model conducted in the present study and by PCA (1979).

The ultimate pullout forces obtained from pullout models are compared with those which are derived from experimental study. For all specimens, the peak load and post-bond failure behaviour are found to be very close to those obtained from the pullout results. As it can be seen from Fig. 4.15, 4.16 and 4.17, all sets of results agree extremely well in the entire loading range, which indicates the accuracy of pullout model.



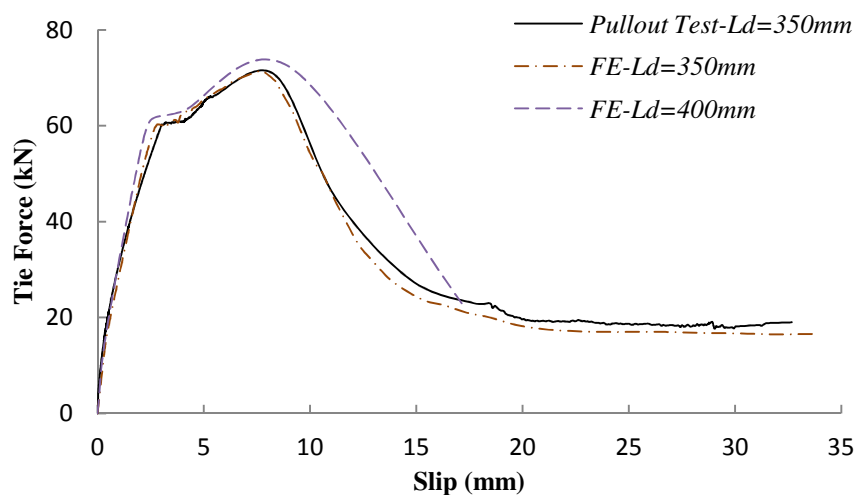
(a) ϕ 16mm, $L_d=350$ mm



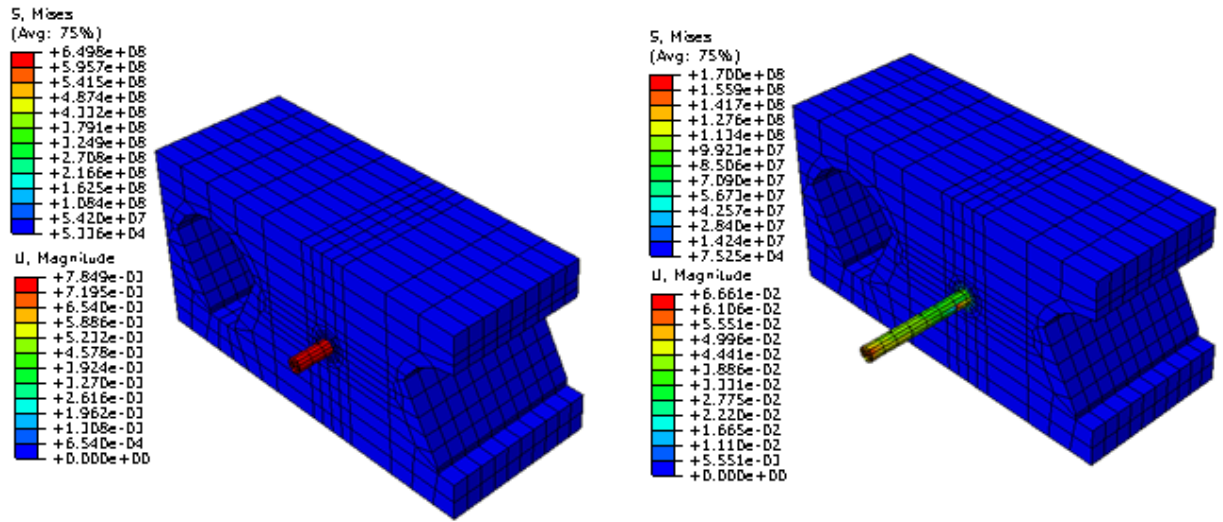
(b) ϕ 12mm, $L_d=250$ mm

Figure 4.15 Pullout load-displacement based on present experimental and FE results

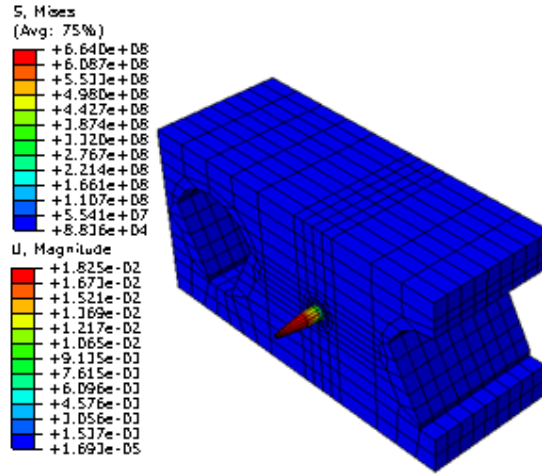
Figure 4.16 indicates that for specimens with embedment length slightly less than anchorage length prior to bar fracture and at the hardening stage, the response of the system turns from fracture to pullout failure mode. It can be concluded that the developed method is effectively able to simulate full pullout behaviour of reinforcement bars into keyways considering both bar fracture and pullout failure mode.



(a) Pullout load-displacement; ϕ 12mm, $L_d=350, 400$ mm



(b) ϕ 12mm, $L_d=350$ mm, Pullout failure mode following plastic stage



(c) ϕ 12mm $L_d=400$ mm, Bar fracture failure mode

Figure 4.16 Pullout and failure mode of specimen, ϕ 12mm $L_d=350, 400$ mm

The FE modelling also provides opportunities to investigate the bond behaviour along the entire embedment length of the tie. Figure 4.17 shows the pullout displacement along the reinforcement bar for the ST42 in the present study. Figures 4.17(a) present the result at two pullout force levels before reaching the ultimate value, i.e. the pre-bond-failure stage. The first curve corresponds to the case when the pullout force is less than the ultimate bond load, i.e. $P = 0.2P_{max}$, and no debonding along the entire steel occurs. The second curve is plotted when the pullout force is close to the ultimate load, i.e. $P = 0.97P_{max}$. At this level, the

reinforcement section near the loaded end is debonded while the rest remains unbonded. Figures 4.17(b) represent the post-bond-failure stage, i.e. the descending section in the pullout force against displacement curves. In this stage, the entire reinforcement has debonded and the pullout force has dropped to 40% of the ultimate value. At this level, all data points in the reinforcement experience excessive pullout displacement with a modest variation.

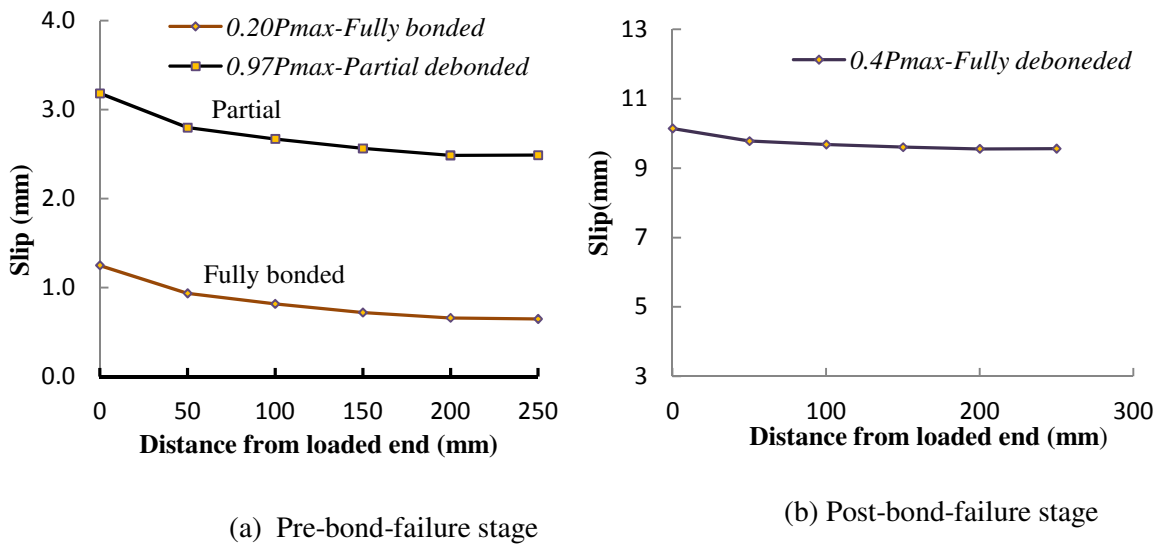


Figure 4.17 Slip over embedment length for reinforcement bars-ST42

Figure 4.18 shows the bond stress along the reinforcement under the same pullout force levels as indicated in Figures 4.17. If no debonding is found along the entire reinforcement, the shear stress distribution follows an exponentially decreasing pattern as is predicated by any conventional linear elastic analysis (Hodayoun and Denis, 1996, Naaman et. al., 1991, and the present analytical method in Chapter 5). Once a part of the steel bar is debonded, the bond stress in the debonded zone tends to be almost uniform, while in the bonded zone it still follows a similar pattern to the unbonded case. In the post-bond failure stage, when the pullout forces descend to $0.4P_{max}$, the shear stress shares a similar trend to the pullout displacement but with a smaller degree of variation.

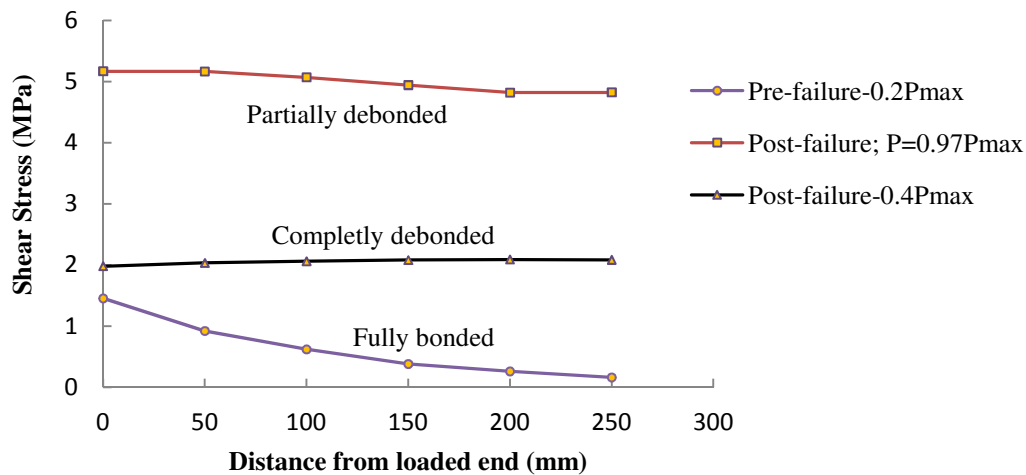


Figure 4.18 Bond stress over embedment length of steel into concrete

4.9.2 Performance of Floor-to-Floor Model

Test verifications are presented at two levels, i.e., at the floor units and the reinforcement bars.

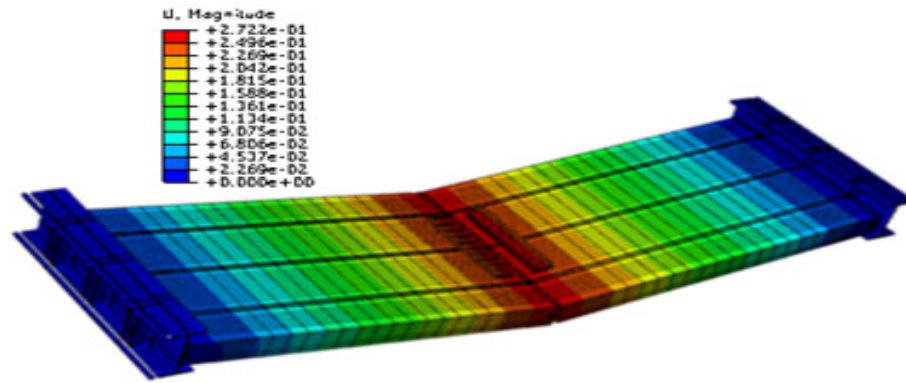
4.9.2.1 Verification at the floor units level

The full scale model was developed to predict the full scale floor-to-floor joint behaviour under uniform distributed load on the top of floors and line load at the joint. The characteristic of the full model is assumed to be similar to the pullout model in terms of steel-concrete interaction and connector element definition. The discrepancies are related to loading, slab dimension, and end boundary condition. The performance of the full floor-to-floor model was studied through the reproduction of a five floor-to-floor system tested in the present study.

It is important to note that, at the early stage of present study a comprehensive verification of the developed model was performed using cube, prism, and RC beam experiments which has been presented in Appendix 4A.

To define stiffness of the frame support a set of analyses have been carried out using SAP2000 software. It was assumed that lateral forces are applied at the location of tie bars. The stiffness of frame support without considering the effect of floor-to-floor system using

SAP 2000 was found to be $k = 180 \text{ kN/mm}$. To define actual stiffness of frame supports various levels of spring stiffness i.e. $k = 0, 150, 180, 200, 1250 \text{ kN/mm}$ applied and load-deflection of FE analyses were compared to the relevant experiment result. Due to the load-deflection relationship is not sensitive with a small variation of stiffness, the results with clear discrepancy is only presented herein. Figure 4.19 presents a comparison of numerical and experimental results for FT1 and FT2 specimen concerning bar fracture failure and indicates that the FE result using $k = 200 \text{ kN/mm}$ as stiffness of springs agree well with the corresponding stage in the ascending, peak load and descending stages in both specimen. The same stiffness was applied to analyse of other specimens.

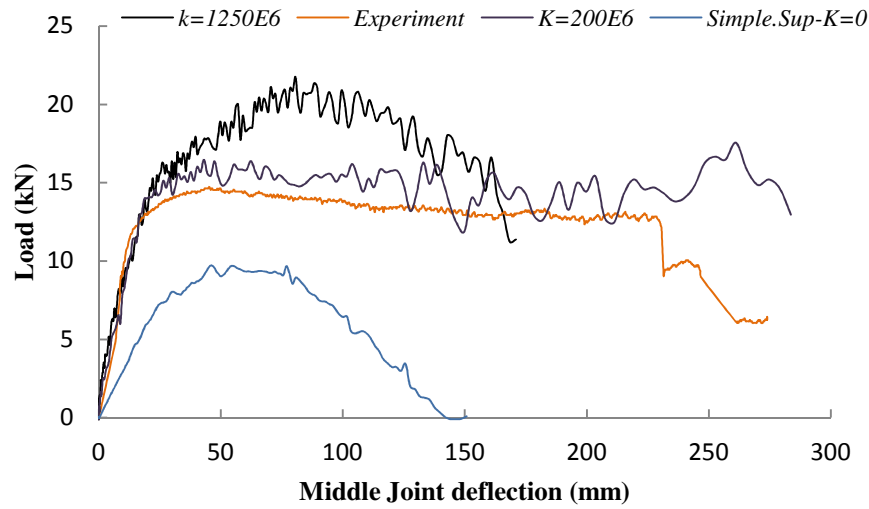


FE

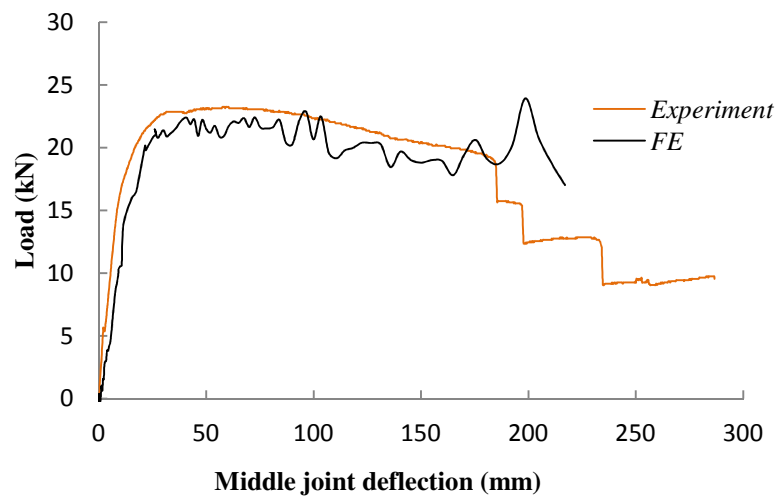


Test

(a) Failure mode-FT1-FT2



(b) FT1 using various stiffness

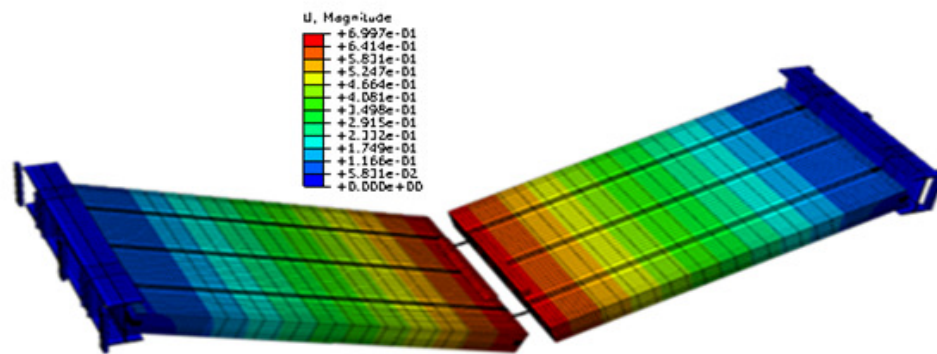


(c) FT2-K=200E6 N/m

Figure 4.19 Floor-to-floor behaviour for bar fracture failure mode

Figure 4.20 displays load versus middle joint deflection considering the experiment and FE results for FT3. The results indicate that the ascending, peak and descending stages of the FE analyses agree well with the full scale experiment; which confirms that this model is successfully capable to simulate both bar fracture and pullout failure mechanism. Unlike the

bar fracture failure mode, the results indicate that the pullout failure mode is capable of developing a catenary action mechanism with a considerable re-ascending phase. Comparing the results of the bar fracture failure and pullout failure mode indicate that assuming the same cross section of tie bars, pullout failure mode provides more ductility i.e. more than three times; while the strength is less than the specimens with bar fracture by 30% (Fig. 4.19b, 4.20). The literature on the robustness of structures (Chapter 2) clearly indicates that ductility can be taken into account as the most efficient parameter to prevent progressive collapse; hence it can be concluded that pullout failure mode will provide more robustness in the precast concrete structures.

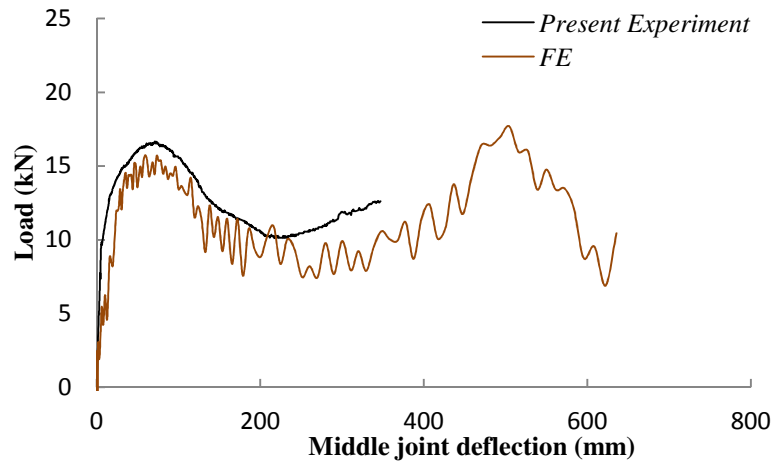


FE



Test

(a) Pullout failure mode-FT3



(b) Load-middle joint deflection relationship

Figure 4.20 Floor-to-floor joint behaviour for pullout failure mode-FT3

As stated in Chapter 3, due to specimens without concrete at the gap being capable of developing a relatively large deflection prior to peak capacity, hence the strength of the system was much more than other specimens. The same result was obtained using FE analysis (Fig. 4.21). Due to only tensile force being available at the joints of FT4 specimens, the catenary action mechanism is established from the beginning up to failure, which can be considered as the prominent difference to the other four specimens. On the other hand, the weak point of this specimen is that the descending stage is relatively steeper than in the other specimens. It is due to pullout behaviour dominating the total behaviour of the system without any membrane action. Also note that, prior to peak strength a transverse crack was observed at the end of embedment length in the keyway 4R, which can explain the reason of exceeding peak strength of FE analysis from the experiment result.

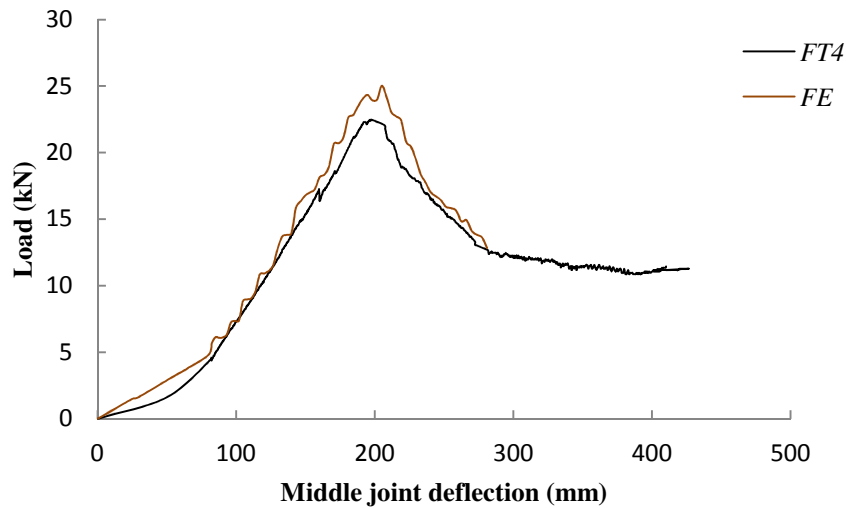
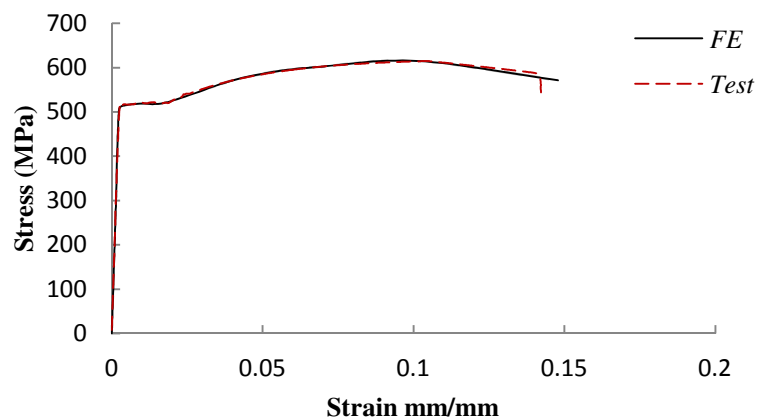


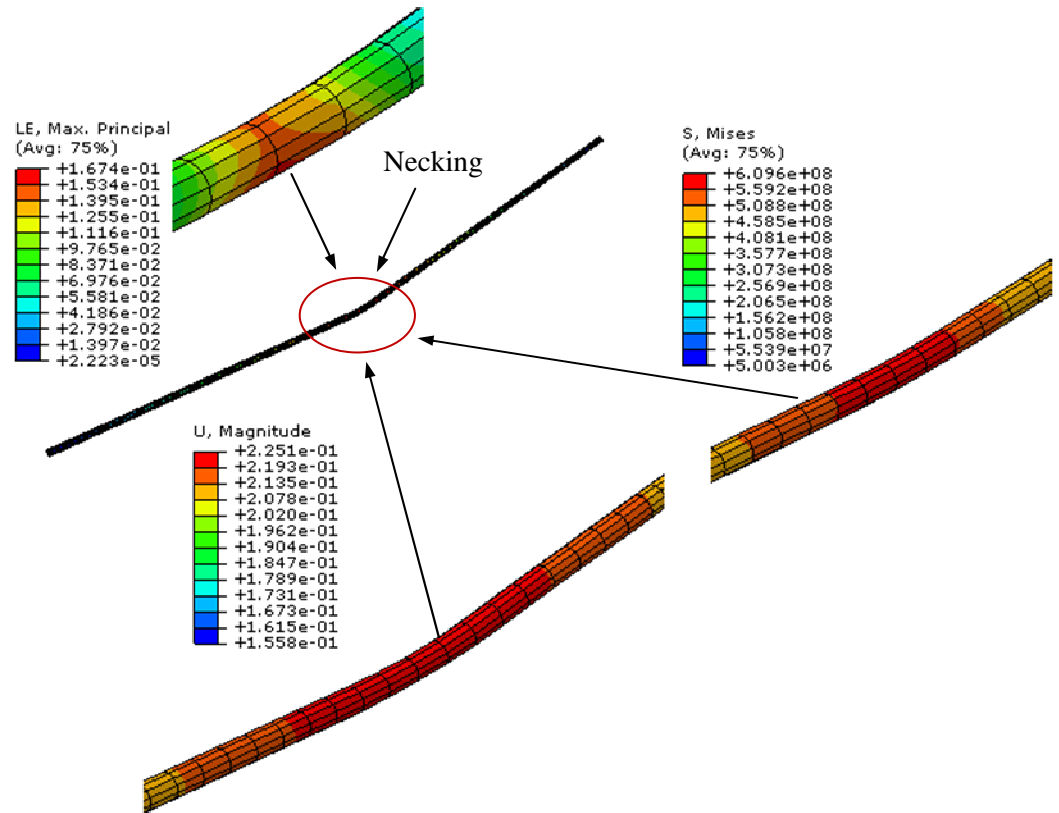
Figure 4.21 Load-middle joint deflection relationship for pullout failure mode-FT4

4.9.2.2 Verification at the reinforcement bar level

Bar fracture failure mode: Figure 4.22(a) shows that the stress strain curve for the critical element at the cracked area is very close to the standard tensile test for 10 mm bar diameter. The FE results indicate that the middle bars start necking at the strain around 14% and is fractured at the deflection between 190mm and 230 mm (Fig. 2.24b); which agrees extremely well with the both results of the full scale and tensile test (Chapter 3).



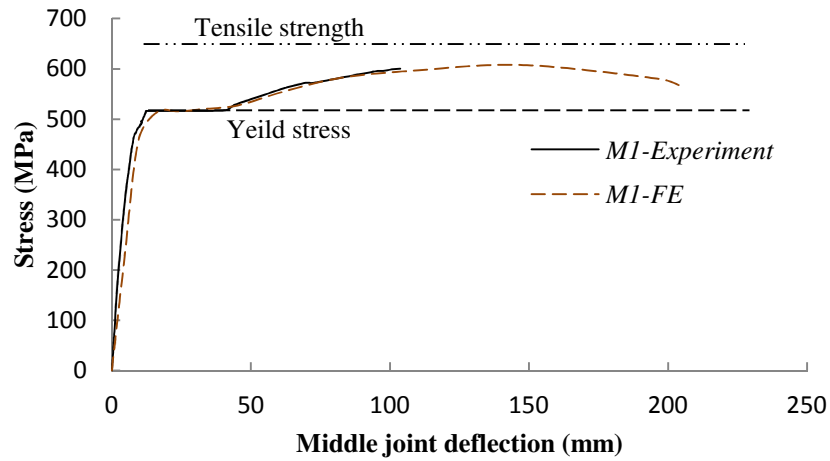
(a) Stress-strain curve



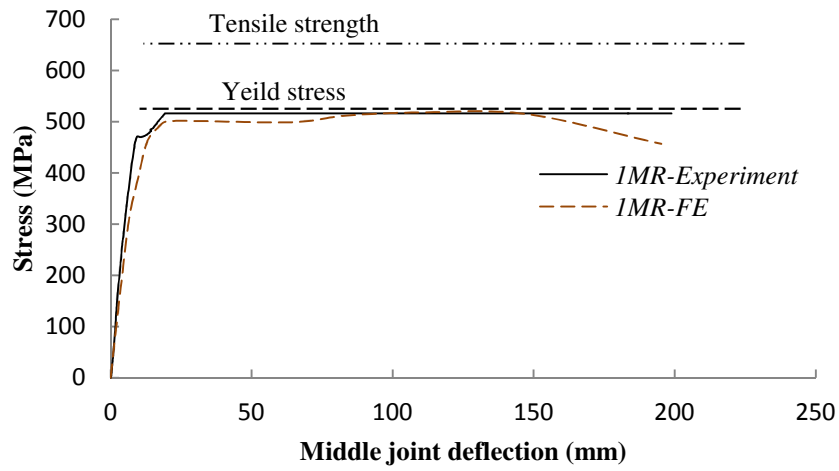
(b) Deflection, plastic strain, and stress at the middle bars at deflection of 225 mm

Figure 4.22 Behaviour of the middle bar at the cracked section-FT1

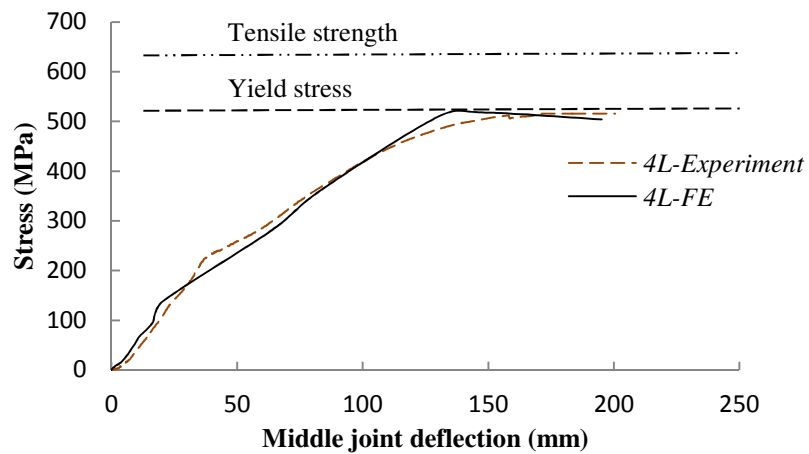
To show more capabilities of the developed model, the results of the stress-deflection relationship obtained from strain gauges and FE analyses for the same location are shown in Figure 4.23. The results indicate that the elastic, plastic and hardening stages of the FE analyses are very close to the test results. The same results can be obtained for the FT2 specimens; hence only the results of the side bars with a new strain gauge location are presented herein (Fig. 4.24). Comparing Figure 4.23 (a), (b) and 4.24 clearly shows that the rate of increasing stress in the middle bar is relatively quicker than in the side bars; which confirm the result obtained by experiments.



(a) Middle bar- gauge M1



(b) Middle bar- gauge 1MR



(c) Left bar-gauge 4L

Figure 4.23 Stress versus middle joint deflection at the location of strain gauges-FT1

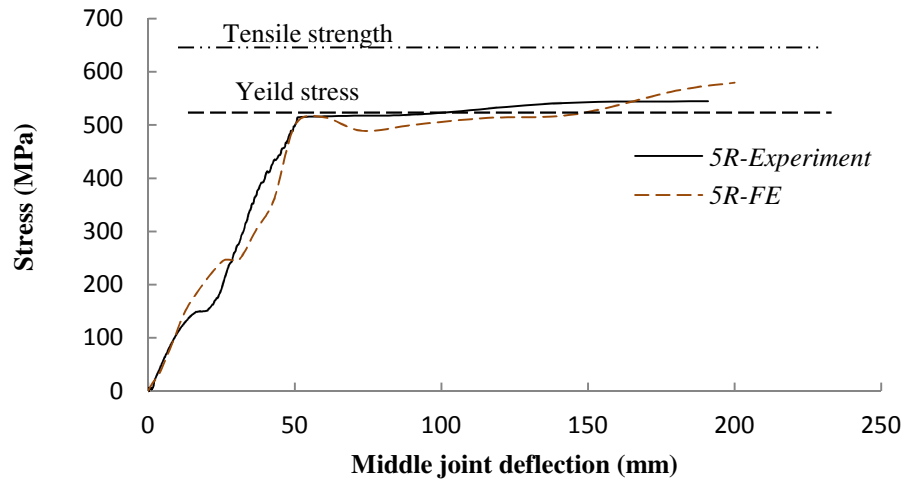


Figure 4.24 Stress-middle joint deflection at the location of strain gauges- Right bar-gauge 5R-FT2

As stated in Chapter 3, the maximum bar length which experiences either the yielding or hardening stage was around 145 and 100 mm for bars at the middle and side joints, respectively. The FE result for FT1 or FT2 shows that the post yielding length for the middle bars is around 145 mm; while it is slightly more than 100 mm for the side bars (Fig. 4.29).

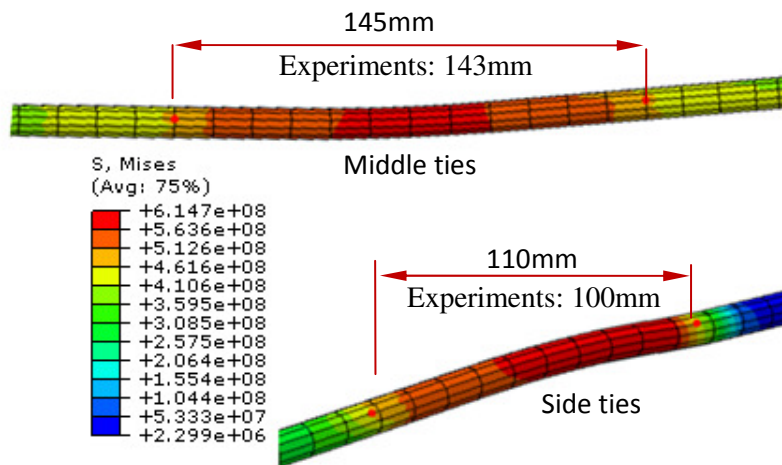
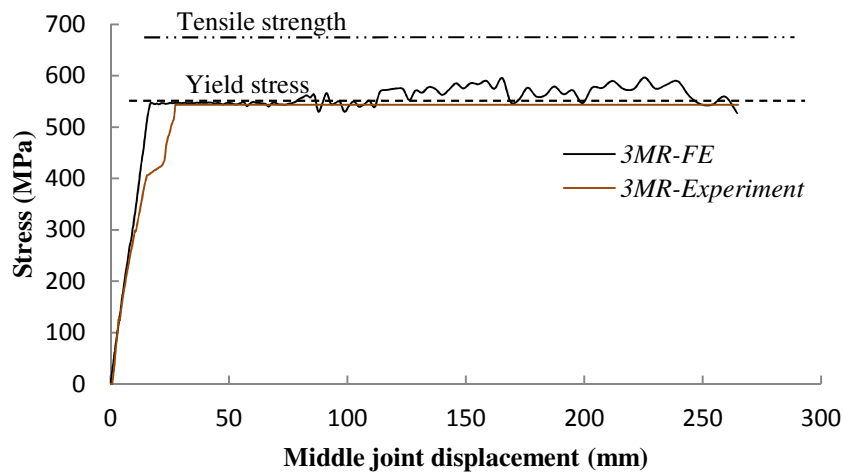
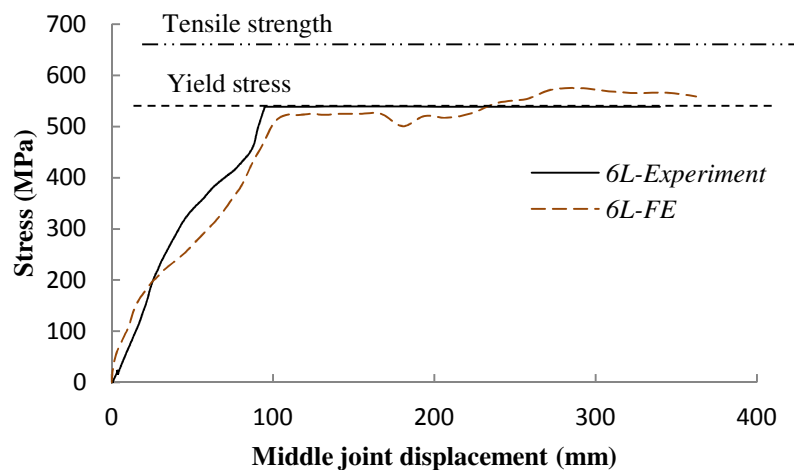


Figure 4.25 Post yielding length of ties for bar fracture failure mode-FT1 and FT2

Pullout failure mode: Figure 4.26 shows that the stress strain curve for the critical element at the cracked area is very close to the strain gauges' result in FT3 and indicates that the bottom of the bars at the middle joint reaches yielding point, even in pullout failure mode. This behaviour can be further confirmed by the FE and test results obtained from FT4 and FT5.



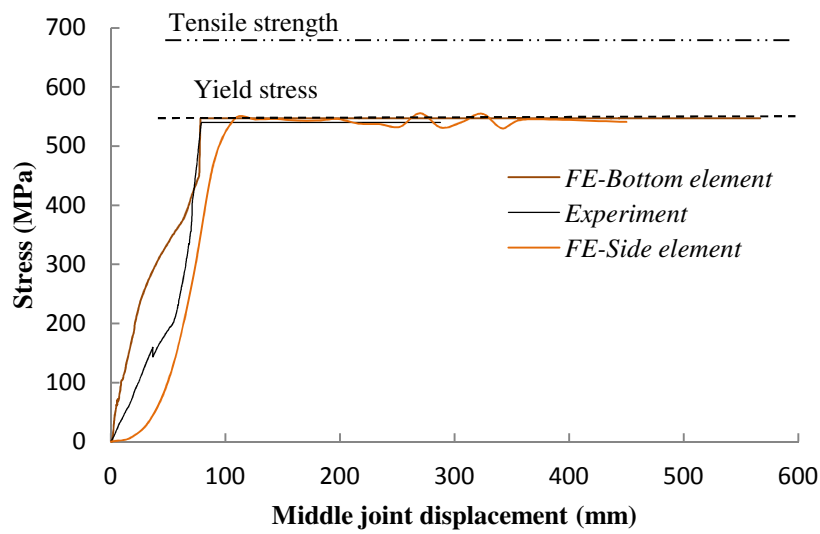
(a) Middle bar-gauge 3MR



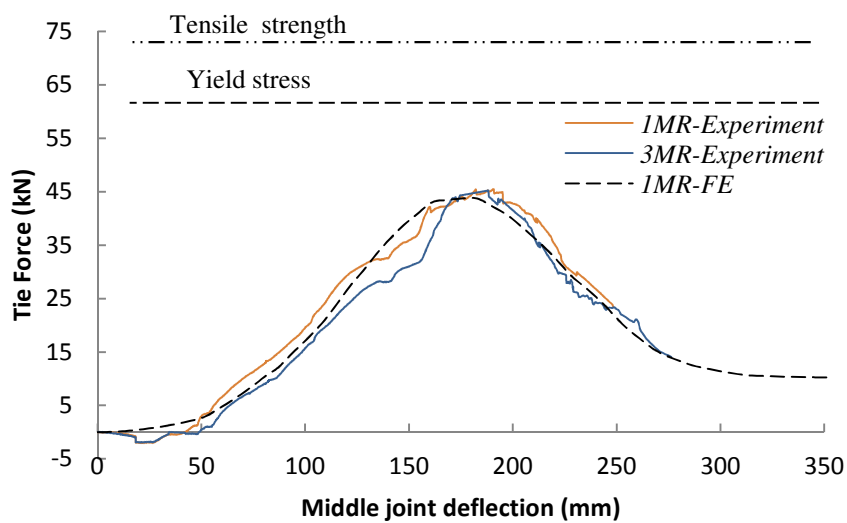
(b) Left bar-gauge 6L

Figure 4.26 Stress versus middle joint deflection at the location of strain gauges-FT3

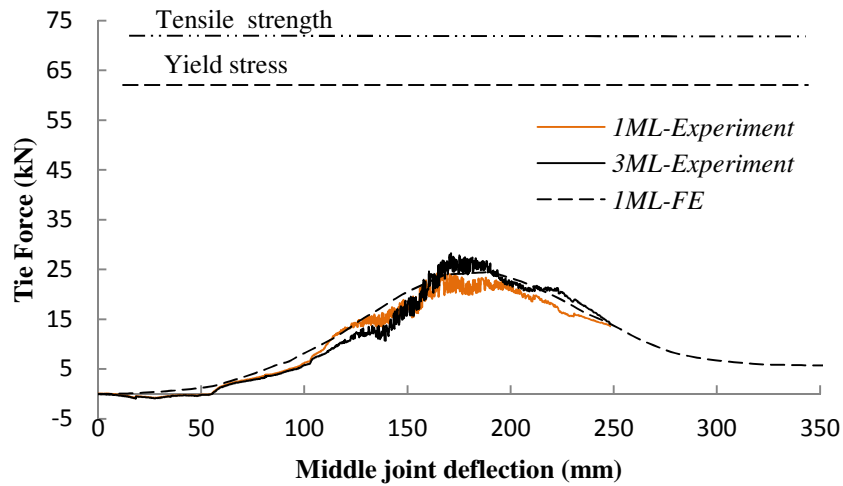
To show further ability of the developed method specifically pull-out behaviour, the relationship between tie force and middle joint deflection for pullout failure mode of specimen FT4 is presented in Figures 4.27. The results reveal that the FE modelling provides a good estimate in terms of peak load and the ascending or descending phase. Figure 4.27 shows that gauges on bottom of bar and at the cracked section experience yielding, while the gauges over embedment length results fully pullout behaviour.



(a) Middle bar-gauge M3



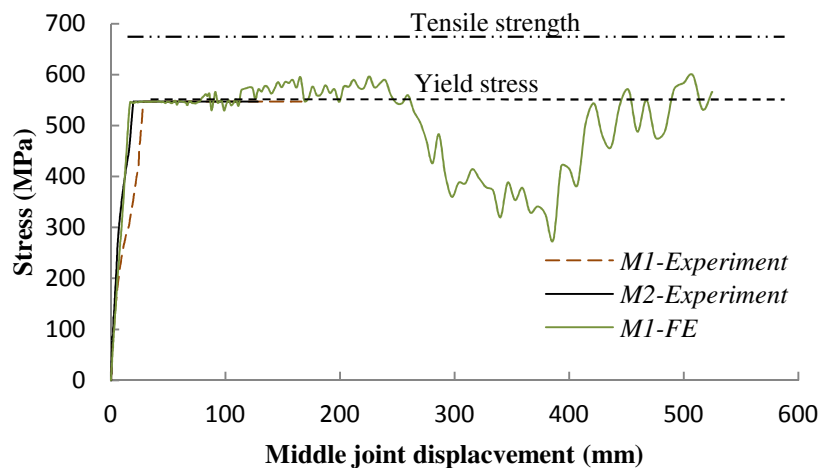
(b) Middle joint-gauges on the right side



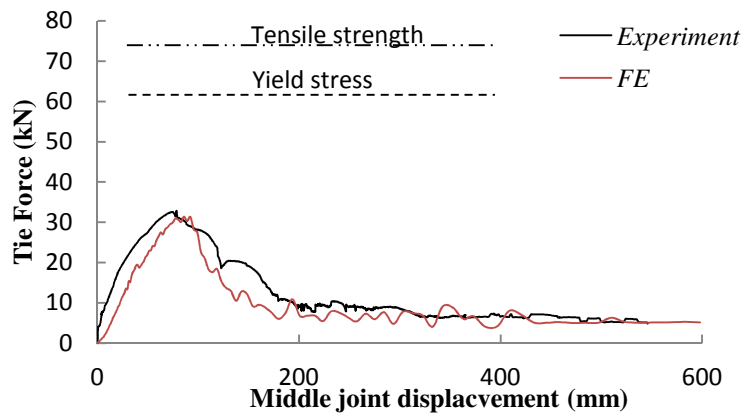
(c) Middle joint-gauges on the left side

Figure 4.27 Stress/pullout versus middle joint deflection at the location of strain gauges-FT4

Figure 4.28, also, shows that the stress-deflection relationship at the middle and over the embedment length agrees well with the test data of FT5. Comparison between Figure 4.28 (a) and (b) confirm that for the bar at the cracked section a combination of bending and pullout force induces stress at the bottom of the bars; while it is only pullout force which creates force in the bars over the embedment length.



(a) Middle bar-gauges on the gap

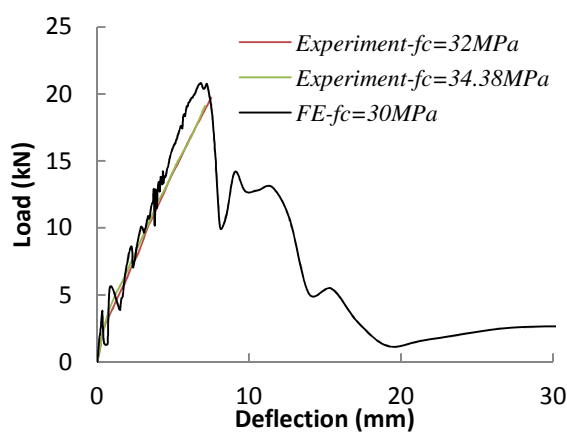


(b) Middle bar-gauge on the left keyway-1ML

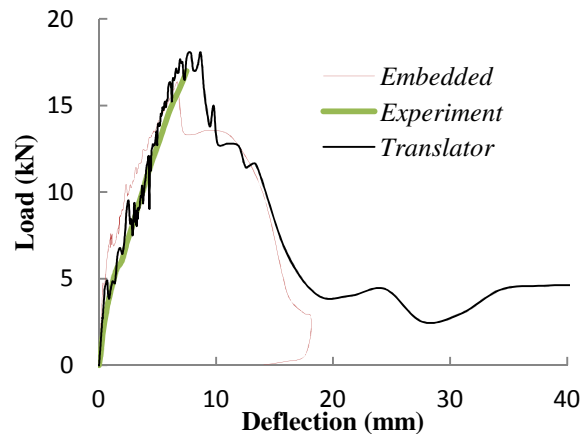
Figure 4.28 Stress versus middle joint deflection at the location of strain gauges-FT5

4.9.3 Performance of RC Beam Model

According to the detailed experimental result and FE analysis developed in the Appendix 4A, it was found that that the proposed FE model is also effectively able to predict the behaviour of RC beam. Figure 4.29 shows that, load vs. deflection of FE analyses is agree well with experimental study and embedded technique proposed by ABAQUS.



(a) Translator



(b) Embedded-Translator- $f_c=22\text{MPa}$

Fig. 4.29 Load vs. middle joint deflection for RC beam

4.10 SUMMARY

The developed model has been confirmed as being able to capture a complete tie force versus vertical deflection history with good accuracy for different bar sizes, embedment lengths and slab lengths. From both full-scale tests and FE modelling results, during the descending phase in the tie force versus deflection curves, ties undergo stable pullout damage until the pullout displacement becomes excessive.

The above results indicate that the developed model i.e. CDP model and TR element is capable of simulating both pullout failure and bar fracture mode. As these models provide further data regarding tie force, slip, yielding stress and elastic or plastic strain over the embedment length of the bar, they can be considered as new and the most efficient models for research proposes. According to the literature, CDP and CSC models together with truss element to simulate steel bars have been designed for fully bonded and also small slip can be considered by these two models; hence, the developed model can be considered as the third model to overcome the weak point of the two mentioned models. It is obvious that only the developed model can simulate pullout behaviour of bars into concrete. However, to show the further efficiency of the developed method to model full bonded bar into concrete, a simple support beam with two bar size of 8 mm and a length of one metre was analysed considering the embedded element and TR method; the result compared with the relevant test data. The most important result was that the model with the TR element was less mesh sensitive than the truss element and even the result is closer to the test result in the ascending, peak, and descending stages (Appendix 4A).

The outstanding result is that, in any RC structure any type of steel bars i.e. reinforcement, strand, and rock bolt can be easily simulated by this model.

Chapter 5

NUMERICAL PARAMETRIC STUDY

5.1 INTRODUCTION

Due to the high cost of large-scale experimental studies, FE modelling of a precast cross wall system using a computer-aided method is essential to broaden the experimental knowledge regarding the behaviour of floor-to-floor joints following removal of one wall support. It would also improve the understanding of different parameters which affect the behaviour of the system. Most of the early investigations on progressive collapse have been conducted on RC frame structures. As stated in the literature, some useful experimental and finite element studies on the behaviour of RC structures have been performed in the last decade. To the best knowledge of researchers, this is the first study to investigate the behaviour of floor-to-floor joints following removal of a wall support in typical precast cross wall structures. In this chapter, a floor-to-floor system is analyzed considering various parameters affecting the behaviour of the system. Although the main variables in the TF design method are slab length and load, based on pullout and full scale experimental study, embedment length, bar size, concrete strength, slab length, number of keyways and surface load can be considered as important variables which have a major effect on a floor-to-floor system's behaviour.

The developed model in Chapter 4 was found to be able to trace a complete and stable tie force-vertical deflection history with good accuracy and different bar size, embedment length, and slab length. Moreover, the results clearly confirm that both failure modes can be effectively simulated by the developed model. Due to the wide range of variables, to keep the experimental and FE study manageable the parametric study is limited to a floor-to-floor

system subjected to uniform surface load only, as this type of loading always occurs after removing wall supports due to an explosion.

The results obtained inform us of the adequacy and applicability of the code specifications; and will improve the understanding of the mechanism of how tie bars will contribute to the resistance of loads, for structures subjected to local damage. Discrepancies in the tie force between the numerical results and codified specifications have suggested an underestimate from the TF method, which may lead to an unsafe design.

5.2 DESCRIPTION OF THE SELECTED STRUCTURE

The designed precast slab by Bison Ltd was selected as the source of information for the subject of the feasibility study presented in this paper. This study uses the full scale finite element model developed in Chapter 4 to study the effect of different parameters on the behaviour of a floor-to-floor system. The studied specimens are a full-scale, realistic representation of simply supported concrete floor slabs in a precast concrete cross wall building. At the floor-to-floor joint, longitudinal ties are placed within the keyways. The section of the analyzed system consists of one full width of a precast concrete slab each containing two/three keyways/slab. The study is conducted assuming two different tie bars i.e. (1) specimens with longitudinal ties (Fig. 5.1); (2) specimens with longitudinal and transverse ties (Fig. 5.2).

As stated in Chapter 3, in a floor-to-floor joint in precast concrete cross wall buildings two types of collapse mechanism i.e. bar fracture and pullout failure mode govern the behaviour of this system. To show the behaviour of the system and develop a general analysis and design guide line, both failure modes are taken into account; considering various slab lengths and different numbers of longitudinal ties at the joints. As in actual use, transverse ties are used to develop a cantilever action; hence a series of 3D analyses considering both longitudinal and transverse ties at the joints is conducted with different slab lengths in

longitudinal and transverse directions. To study the effect of load exerted from upper floors, one specimen considering three storeys is analysed.

5.2.1 Floor-to-floor joint analysis using longitudinal ties

For the first case, at the floor-to-floor joint, longitudinal ties are placed within the keyways. The section of the analyzed system consists of one full width of a precast concrete slab each containing two/three keyways. A two-span slab system is modelled for different span lengths of 2, 4 and 6 using reinforcement bars in longitudinal direction (Fig. 5.1). The diameter of the reinforcement bars in all specimens is 12 mm. The embedment length of ties is 400 and 250mm for bar fracture and pullout failure mode, respectively. Also, the compressive strength of 30 and 20 MPa was assumed in specimen with bar fracture and pullout failure mode, respectively.

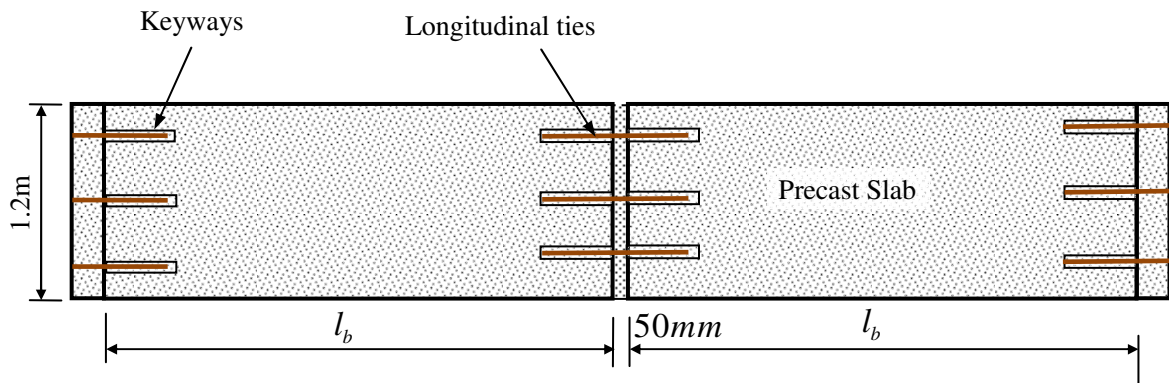


Figure 5.1 Floor-to-floor system facilitated by longitudinal ties.

5.2.2 Floor-to-floor system using longitudinal and transverse ties

Due to in actual use both alternate load paths will provide progressive collapse resistance, assuming 2D behaviour of structure considered in most of studies is not able to provide clear understanding about post-collapse and the mechanism of forming catenary action. To this end, in the second set of analyses both longitudinal and transverse ties are taken into account using

3D modelling (Fig. 5.2). The properties of the specimens for bar fracture and pullout failure mode are shown in the Tables 5.1 and 5.2, respectively.

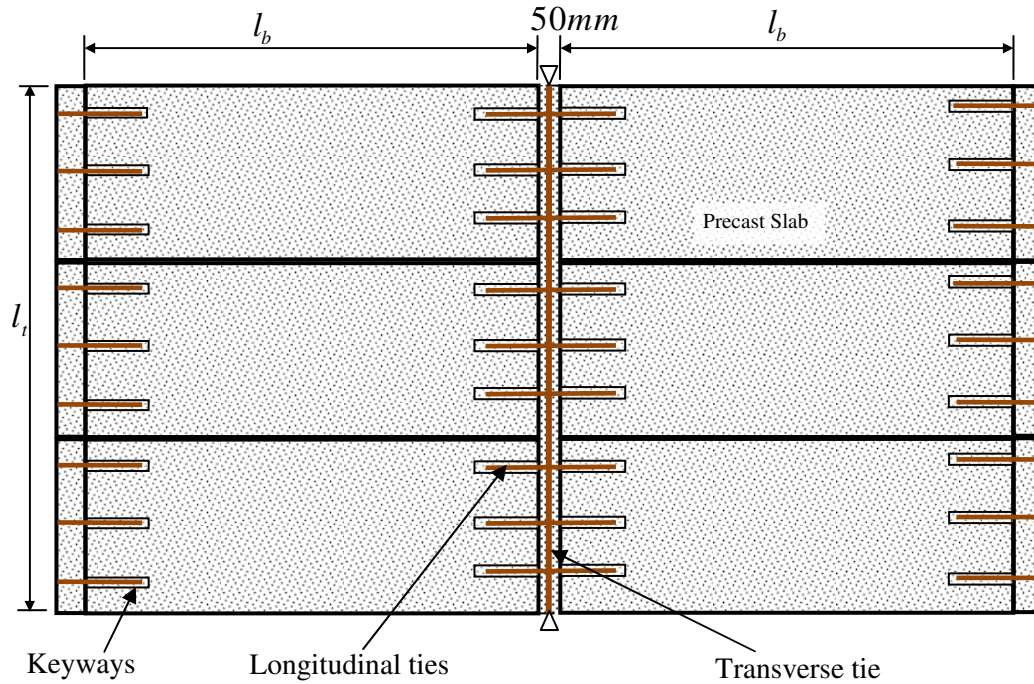


Figure 5.2 Floor-to-floor system facilitated by longitudinal and transverse ties.

Table 5-1 The properties of specimens for bar fracture failure mode

No.	Longitudinal Axis				Transverse Axis		f_{ck} (MPa)	f_t (MPa)
	Length (m)	Bar Diameter	Number of ties/slab	Embedment length (mm)	Length (m)	Bar Diameter		
LTF1	2	$\phi 12$	2	400	2.4	$\phi 18$	30	4.8
LTF2	4	$\phi 12$	2	400	2.4	$\phi 18$	30	4.8
LTF3	4	$\phi 12$	2	400	4.8	$\phi 24$	30	4.8
LTF4	6	$\phi 12$	3	400	4.8	$\phi 24$	30	4.8
LTF5	6	$\phi 12$	3	400	7.2	$\phi 36$	30	4.8

Table 5-2 The properties of specimens for pullout failure mode

No.	Longitudinal Axis				Transverse Axis		f_{α}	f_t
	Length (m)	Bar Diameter	Numbers of ties/slab	Embedment length (mm)	Length (m)	Bar Diameter	(MPa)	(MPa)
LTP1	2	$\phi 12$	2	250	2.4	$\phi 18$	20	3.5
LTP2	4	$\phi 12$	2	250	2.4	$\phi 18$	20	3.5
LTP3	4	$\phi 12$	2	250	4.8	$\phi 24$	20	3.5
LTP4	6	$\phi 12$	3	250	4.8	$\phi 24$	20	3.5
LTP5	6	$\phi 12$	3	250	7.2	$\phi 30$	20	3.5

5.3 FINITE ELEMENT MODELING TECHNIQUE

Fundamentals of developed numerical model in the chapter 4 are used to analyse of floor-to-floor system considering the same mesh pattern and bond modelling with the following boundary condition and material properties.

5.3.1 Boundary condition

The boundary conditions for both systems are shown in Fig. 5.3. The lateral stiffness of side supports is simulated using 6 springs/slab and the side reinforcement bars were assumed to be fully bonded to the supporting slabs (Fig. 5.3). It is assumed that the lateral forces due to arch action or catenary action are transferred directly to the adjacent shear walls parallel to the longitudinal axis. Due to symmetry boundary condition only one-fourth of specimens with longitudinal and transverse ties are taken into account.

To define lateral spring stiffness, it is, also, assumed that only the lateral wall directly close to the system provides the lateral support and the contribution of the other walls is neglected. According to SAP 2000 software, the stiffness of shear walls with a length of 2, 4 and 6 m is 691, 1925 and 3245 kN / mm (Fig 5.4). The thickness of the shear wall was assumed to be

250 mm. The lateral supports are simulated using six springs/slab at each support. Assuming cross wall of 2, 4 and 6 m as lateral support, corresponding spring stiffness will be 12E7, 16E7, and 18E7 N/m , respectively. As the response of the system was not considerably sensitive to a small alteration of spring stiffness, in the following analyses the average spring stiffness of 15E7 N/m was applied in all analyses.

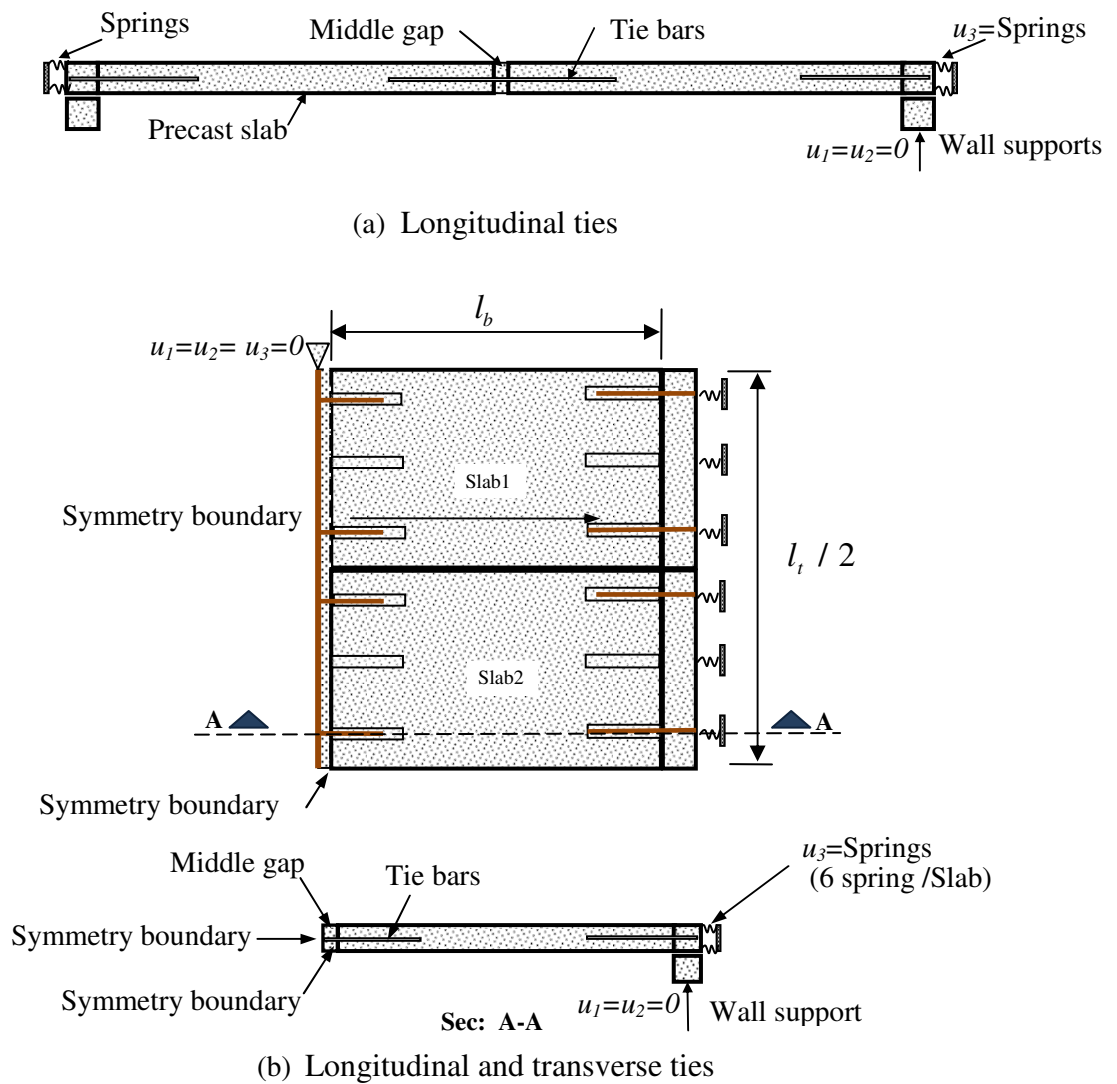


Figure 5.3 Boundary condition

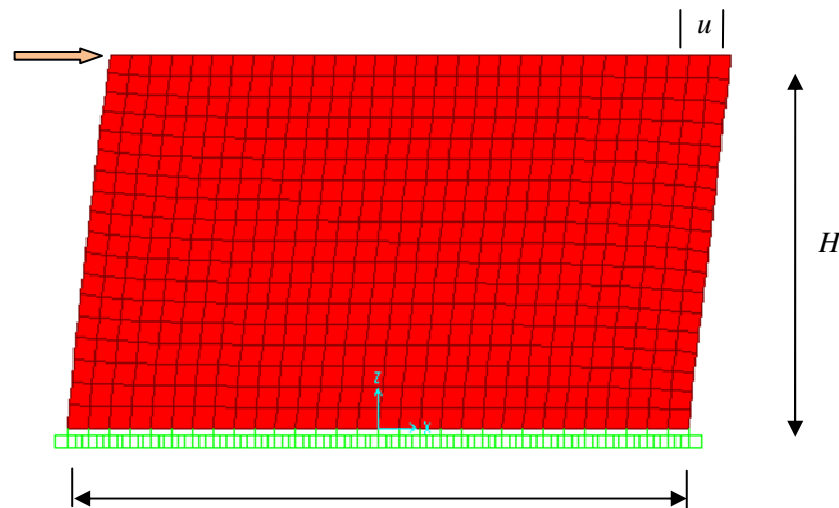
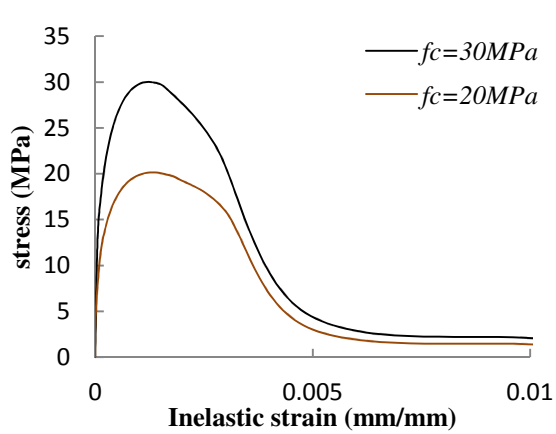


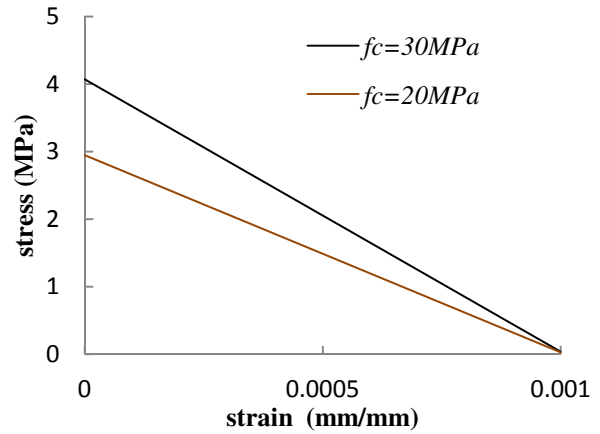
Figure 5.4 Stiffness of shear walls, $L=2, 4$ and 6 m - $H=3.5\text{ m}$

5.3.2 Material properties

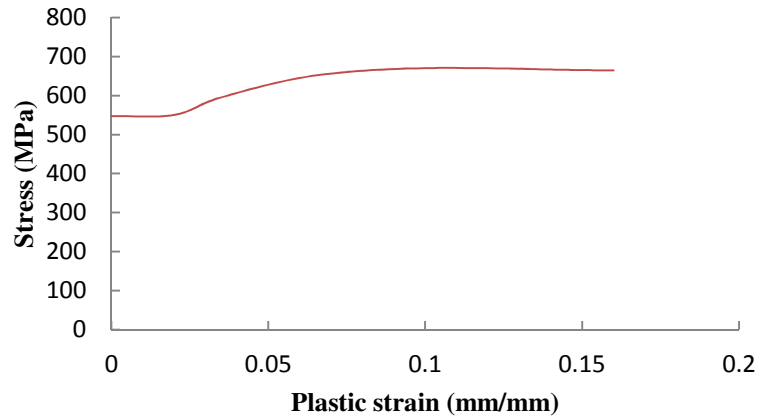
The concrete was modelled using concrete damage plasticity (CDP) available in ABAQUS, which can be used for both static and dynamic analyses and in all types of elements. Also, plastic model was used to model nonlinear behaviour of reinforcement bars. The input data for the CDP and plastic model in ABAQUS in the form of the stress-strain curve for tensile or compressive behaviour of concrete and reinforcement bar in different specimens is displayed in Figure 5.5 (Appendix 4A) and the relevant elastic material properties of specimens are shown in Table 5.3. The concrete with compressive strength of 30 and 20MPa was applied to introduce bar fracture and pullout failure model, respectively. The damage variables of d_c and d_t considering the compressive and tensile strength of various specimens are shown in Fig 5.6.



(d) Compressive hardening-CDP Model



(e) Tension stiffening-CDP Model



(f) Plastic model-reinforcement bar

Figure 5.5 Properties of materials in CDP and plastic model (Appendix 4A)

Table 5-3 Materials' Properties (Chapter 3)

	Elastic Modulus (GPa)	Failure mode	Poisson's Ratio	Density (kg/m ³)
Concrete	30.5	Bar fracture	0.2	2500
Concrete	27.08	Pull-out	0.2	2500
Precast slab	34.54	all	0.2	2500
Steel	210.0	all	0.30	7800

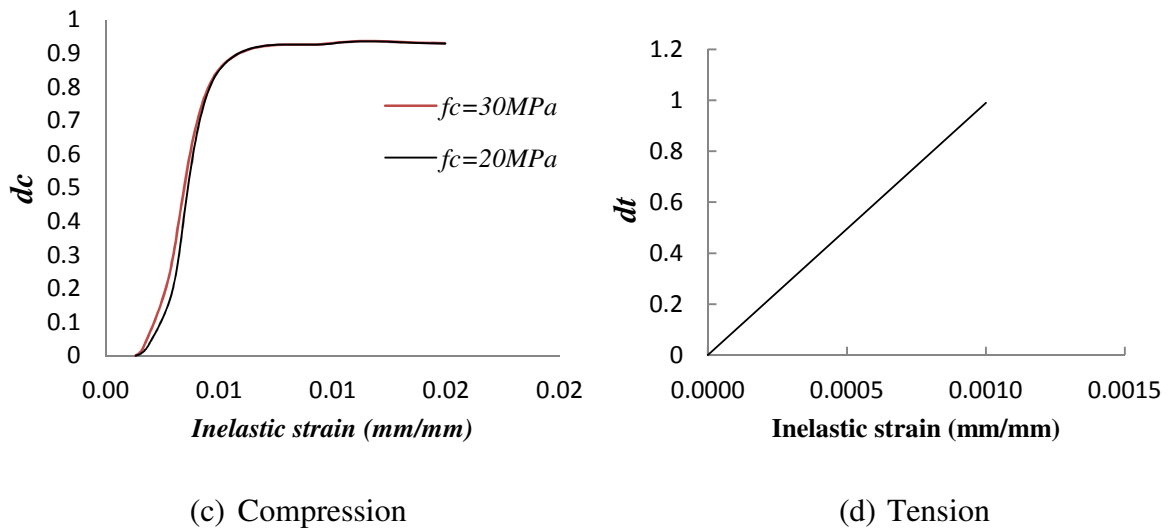


Figure 5.6 Damage parameters for CDP model

5.3.3 Translator properties

According to the pullout test results, the bond-slip relationship was defined as shown in Figure 5.7. The translator force is defined using the bond model (Fig. 5.7) as $F_{TR} = Csu / n$, where F_{TR} , C , s , and n are the translator force, the circumference of the bars, the translator spacing, the bond strength, and the number of translators in each section, respectively.

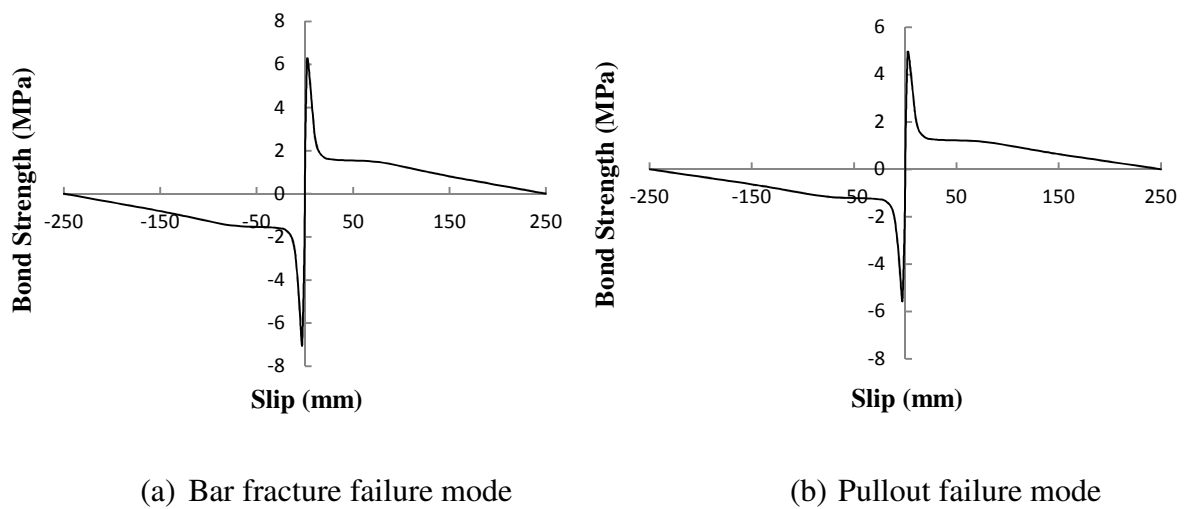


Figure 5.7 Bond-slip relationship to define translator property (Chapter 3 and 4)

5.3.4 Analysis solution strategy

As stated in Chapter 4, the translator element is only available in ABAQUS/Explicit, and the contact condition and other discontinuous problems can be readily formulated in the Explicit module. Hence it is used in this study to perform a non-linear quasi-dynamic analysis

5.4 WALL SUPPORT REMOVAL ANALYSIS

Due to simplicity of modelling and to provide initial data regarding floor-to-floor behaviour following removal wall support using static nonlinear analyses, at the early stage of present study the FE code of SPA 2000 was used to analyse of floor-to-floor system considering both longitudinal and transverse tie for the specimens without concrete at the gap. The results were used to design the main parameters which can affect the behaviour of system (Appendix 5A).

According to the embedment length of tie bars into keyways of precast slab, in a floor-to-floor joint two kinds of collapse mechanism i.e. bar fracture and pullout failure mode govern the behaviour of this system. To develop a generic analysis and design guide line, both failure modes are taken into account; considering various slab lengths and different numbers of longitudinal ties at the joints. In the first set of analyses only longitudinal ties into keyways of precast slabs is taken into account, followed by a series of 3D analyses considering both longitudinal and transverse ties at the joints with different slab lengths and bar sizes. Also, to study the effect of load exerted from upper floors, one specimen considering three storeys is analysed.

5.4.1 Floor-to-floor system using longitudinal ties

5.4.1.1 Bar Fracture Failure Mode

To study the behaviour of a floor-to-floor system and to provide initial data set about contribution of ties in progressive collapse resistance, three specimens with slab lengths of 2,

4 and 6 m are analysed. To make results manageable, in all specimens the translator's properties, bar size and embedment length are kept constant and only the slab length and load is taken into account as variable. Figure 5.8 shows the general failure mode and plastic strain of one element at the bottom of middle and top of side ties. The results indicate that, the collapse initiated by bar fracture at the middle bars (Fig. 5.8b), which shows the same behaviour with the experimental study.

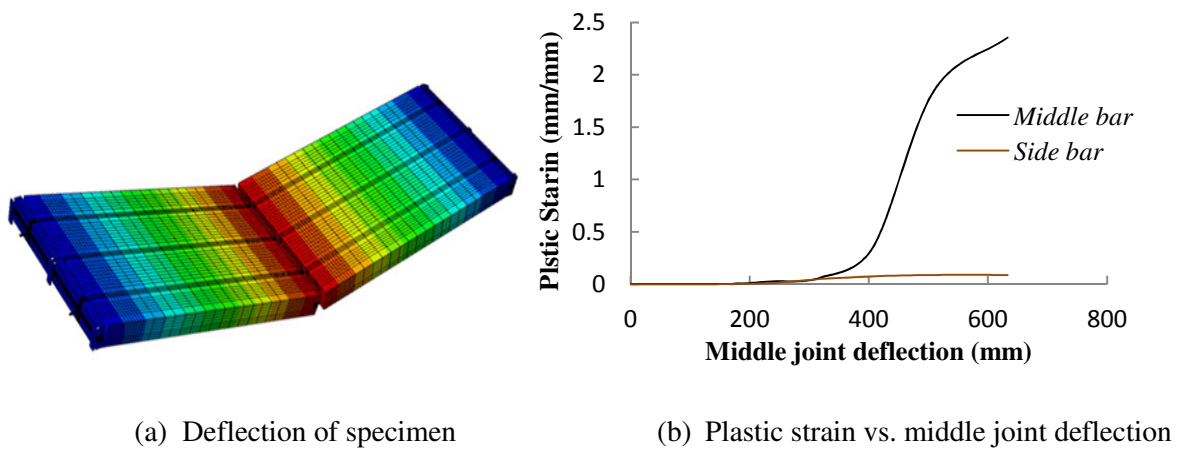


Figure 5.8 Bar fracture Failure mode

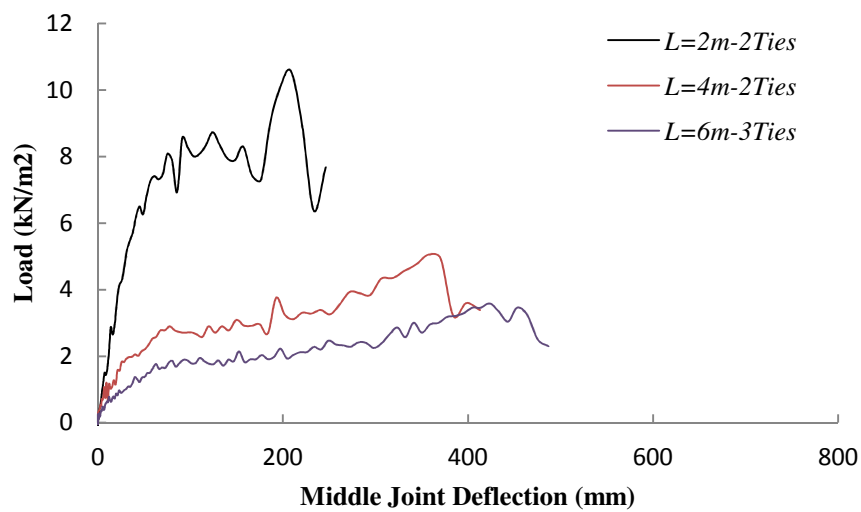


Figure 5.9 Load vs. middle joint deflection considering various slab lengths and ties at the joints

Figure 5.9 shows that, at the failure, the strength of the system is relatively in proportion to the slab length; which confirms the TF method's provision in this area. The result indicates that the system collapses by bar fracture of the tie bars at the middle joint and at a deflection/slab length ratio around 9% i.e. $\delta_s / l_b = 9\%$. Furthermore, Fig. 5.9 shows that, for the slab length of more than 2m the second peak strength to initial strength ratio is around 1.4 which less than reported experimental study on RC structures (Yi et al., 2008; Yu and Tan, 2010; Trung et al., 2010).

Figure 5.10 shows that, the strength of specimen with 3 ties is more than specimen with 2 ties by 67%; which is slightly more than the rate of increasing the numbers of ties. It is agree extremely well with the full scale test result (Chapter 3). In practical analysis and conservatively it can be assumed that the progressive collapse resistance of a floor-to-floor system is increased in proportion to the numbers of ties.

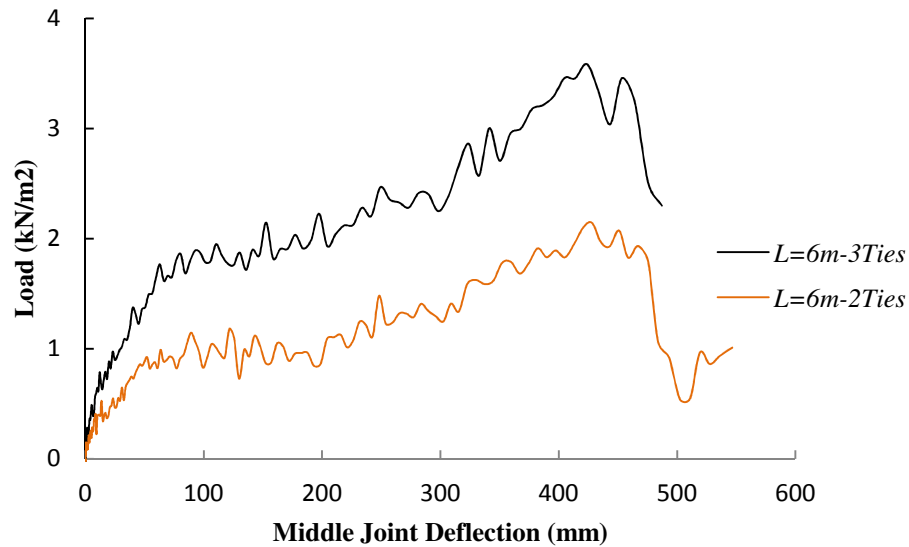


Figure 5.10 Load vs. middle joint deflection considering slab length of 6 m with 2 and 3 ties at the joints

Experimental studies indicate that in RC structures following column removal, prior to catenary action top bars at the middle joints and bottom bars at the supports are under compression, while following large deflection they are under tension and contribute in catenary action mechanism (Yi, et al. 2008, Su, et al. 2009). To investigate the contribution of top bars at middle joint and bottom bars at the supports, one specimen with a length of 2 m is analysed with a new arrangement of tie bars (Fig. 5.11). The result shows different behaviour with conventional RC structures.

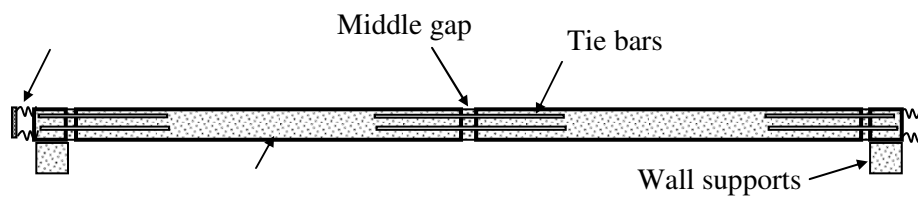


Figure 5.11 Floor-to-floor joint with top and bottom tie bars

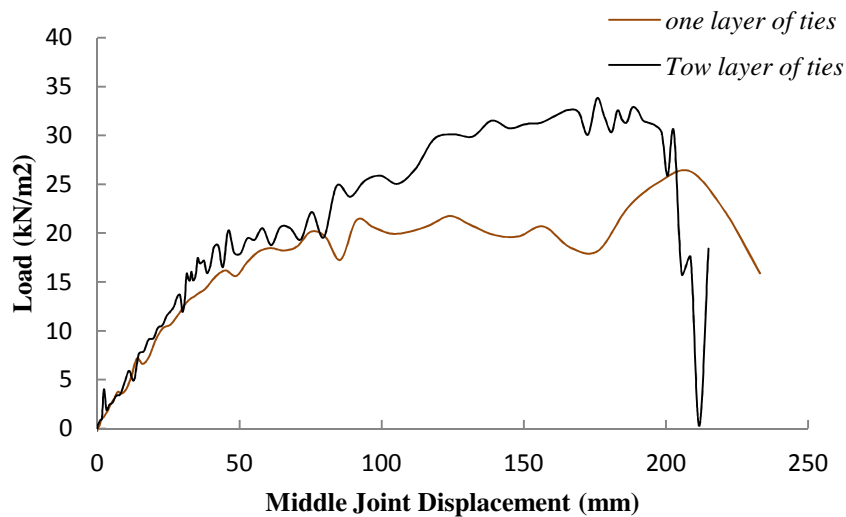


Figure 5.12 Load versus middle joint deflection for slab length of 2 m using tie bars at the top and bottom and only tie bar at the bottom of joints

Comparing Figures 5.9 and 5.12 indicates that the behaviour of the system with top and bottom bars is similar to the specimens with one bars layer at the joints up to the plastic stage,

followed by increasing the strength of the system up to failure by 50%. It can be explained based on the strain and stress distribution along the depth of the slab. Due to small cross section of reinforcements bars, the natural axis is relatively small i.e. <5mm. As the top bar is located 35mm from top of the slab, the top bars at the middle joints do not experience any compressive force; hence, similarly to the bottom bars, they are under tension up to failure although with different rates (Fig. 5.12). The result indicates that the system collapsed at $\delta_s / l_b = 11\%$, which is slightly more than specimens with bottom bars only

5.4.1.2 Pullout failure mode

To investigate the efficiency of failure mode on robustness of cross wall structures, the same specimens in section 5.4.1.1 are reanalysed considering pullout failure mode. Figure 5.13 illustrates that the strength of the specimen reached the initial peak at $\delta_s / l_b = 8\%$; followed by a descending phase up to $\delta_s / l_b = 12.5\%$. At this point the strength of the system is increased again up to $\delta_s / l_b = 20 - 25\%$; followed by a steady descending stage up to failure at around $\delta_s / l_b = 60\%$. The results agree extremely well with the experimental studies (Chapter 3). Figure 5.13 clearly indicates that catenary action is established for the specimens concerning pullout failure mode. Comparing Fig. 5.9 and 5.13 illustrate that, the strength-deflection relationship of specimens with bar fracture and pullout failure mode is relatively similar in the ascending stage up to the first peak load. Furthermore, although the strength of the specimens with bars' fracture failure mode is slightly more than the specimen considering pullout failure, but the ductility of specimens with pullout failure mode is significantly higher than specimens with bar fracture failure mode i.e. more than two times; the characteristic which can be considered as the key parameter influencing the robustness of structures. The results clearly indicate that to provide a required progressive resistance, the number of ties needs to increase in proportion to the increase in the slab length (Fig. 5.13a).

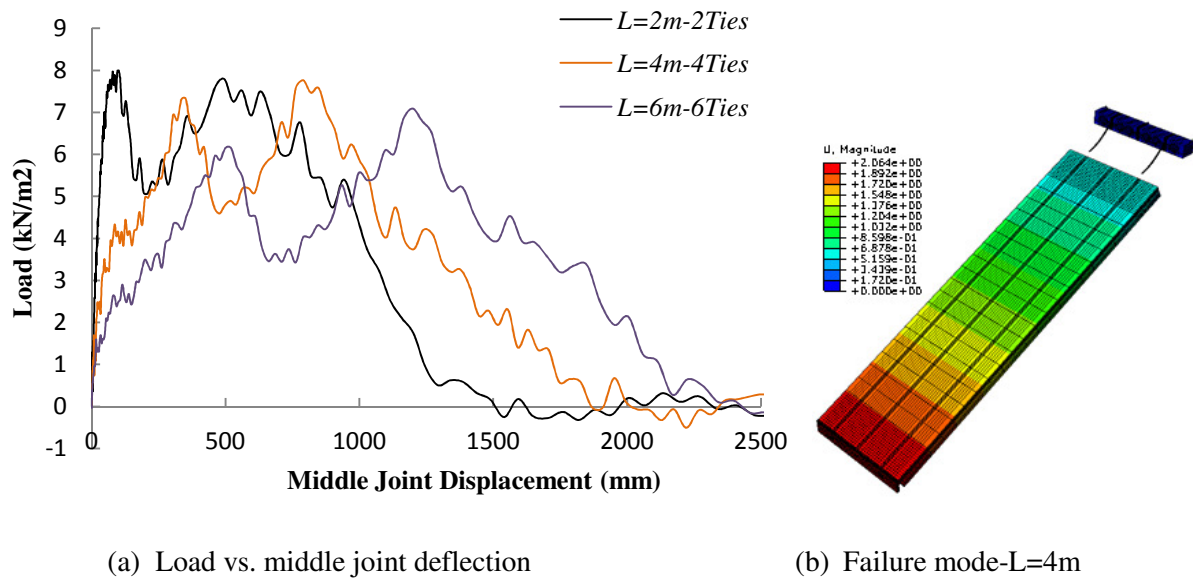


Figure 5.13 pullout failure mode behaviour of floor-to-floor system for various slab lengths and ties at the joints

5.4.2 Floor-to-floor joint analysis using longitudinal and transverse ties

The main aim of present study was to study the behaviour of a floor-to-floor system considering longitudinal ties at the joint following the removal wall support, but as in practice both longitudinal and transverse ties are used, the aim was extended and the effect of both longitudinal and transverse ties was taken into account to improve understanding real behaviour of cross wall structure during the progressive collapse. To make the results manageable, in all analyses the cross section area of the reinforcement bars in the longitudinal and transverse directions is assumed to be relatively identical. Furthermore, the translator property, embedment length and compressive strength of the specimens are kept constant same as the specimens with longitudinal ties. Prior to removing the wall support, the floor-to-floor system acts as a one way slab; while following removal wall support the behaviour of the system considering longitudinal and transverse ties approximately represents two way slab behaviour.

5.4.2.1 Bar Fracture Failure Mode

In the first specimens the span length in the longitudinal and transverse direction is 4.05 and 2.4 m, respectively with two longitudinal ties at the middle and side joints and one transverse tie at the middle gap (Table 5.1). Figure 5.14 shows failure mode of specimen LFT1 and strength of system versus middle joint deflection is shown in the Figure 5.15. The result indicates that the progressive collapse resistance is increased more than 2 times compared to the specimens with longitudinal ties only. It can be explained based on assuming the transverse tie as a middle support. For a one way slab and the rigid support, following the application of a middle support, the strength is increased in proportion to the length squared i.e. l_b^2 . However, as the transverse tie at the middle joint acts as an elastic support, hence it is expected that the strength of the system will be increased by less than four times.

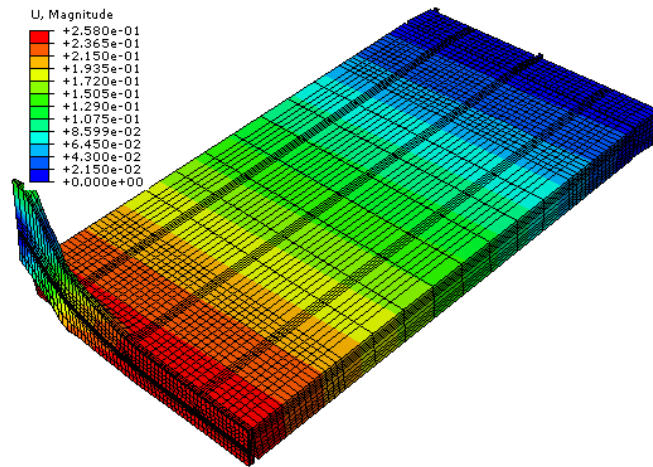


Figure 5.14 Failure mode of specimen-LFT1

Figure 5.15 indicate that, system reached maximum capacity at $\delta_s / l_b = 10\%$. The result, also, shows that at the deflection around 200 mm the strain is more than the yield or fracture strain in middle and transverse bars. Furthermore, it can be shown that most of the tie bars experience fracture strain prior to deflection of 300 mm i.e. $\delta_s / l_b = 15\%$, and $\delta_s / l_t = 12.5\%$.

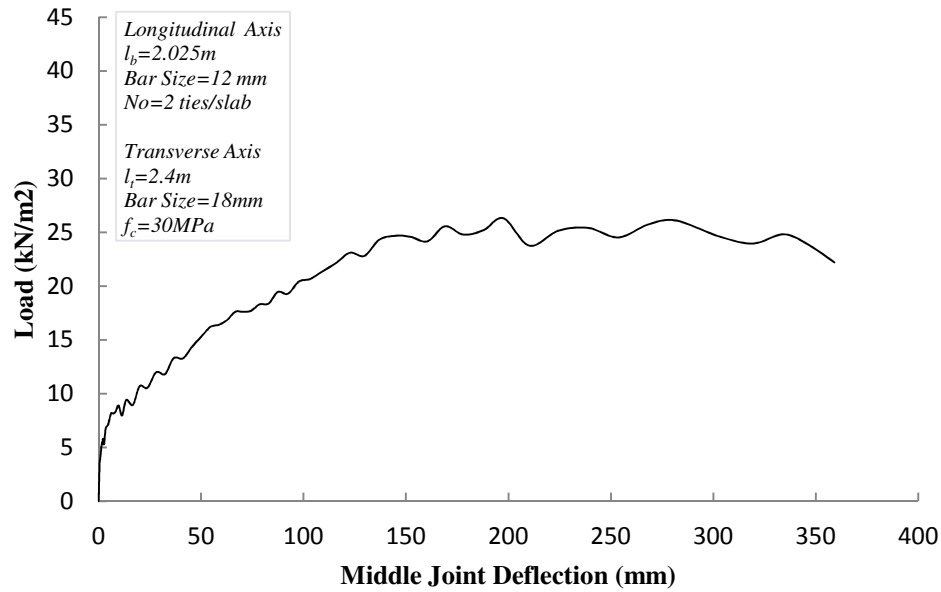


Figure 5.15 Load versus middle joint deflection using longitudinal and transverse ties - LTF1.

The results show that prior to the collapse and in the ascending stage, the load sustained by the longitudinal ties is more than the load sustained by the transverse tie; but prior to failure, the load is redistributed and both ties sustain a relatively identical load (Fig. 5.16). Figure 5.17 display the progressive failure of the system at various locations. The results illustrate that the failure is initiated at the middle longitudinal ties followed by transverse and side ties, respectively (Fig. 5.17).

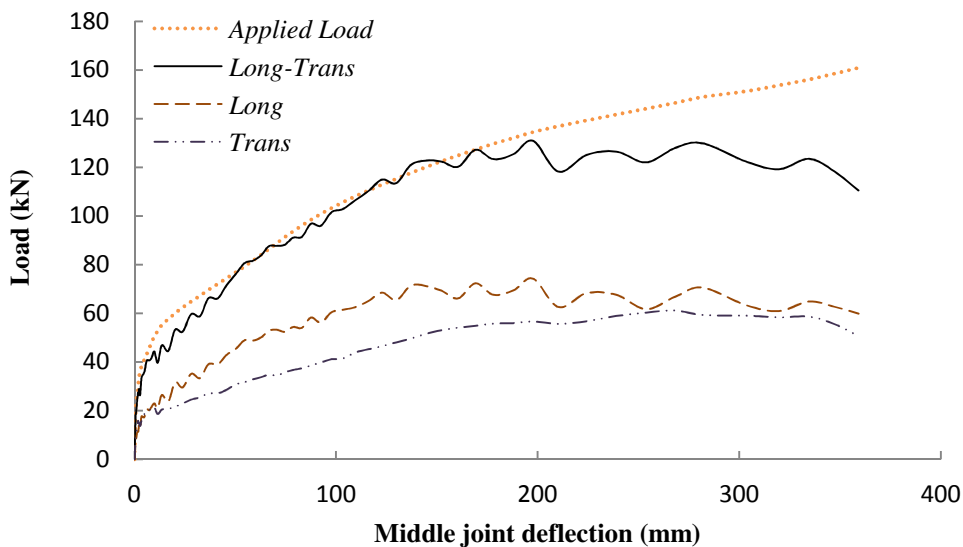


Figure 5.16 Reaction supports versus middle joint deflection - LTF1

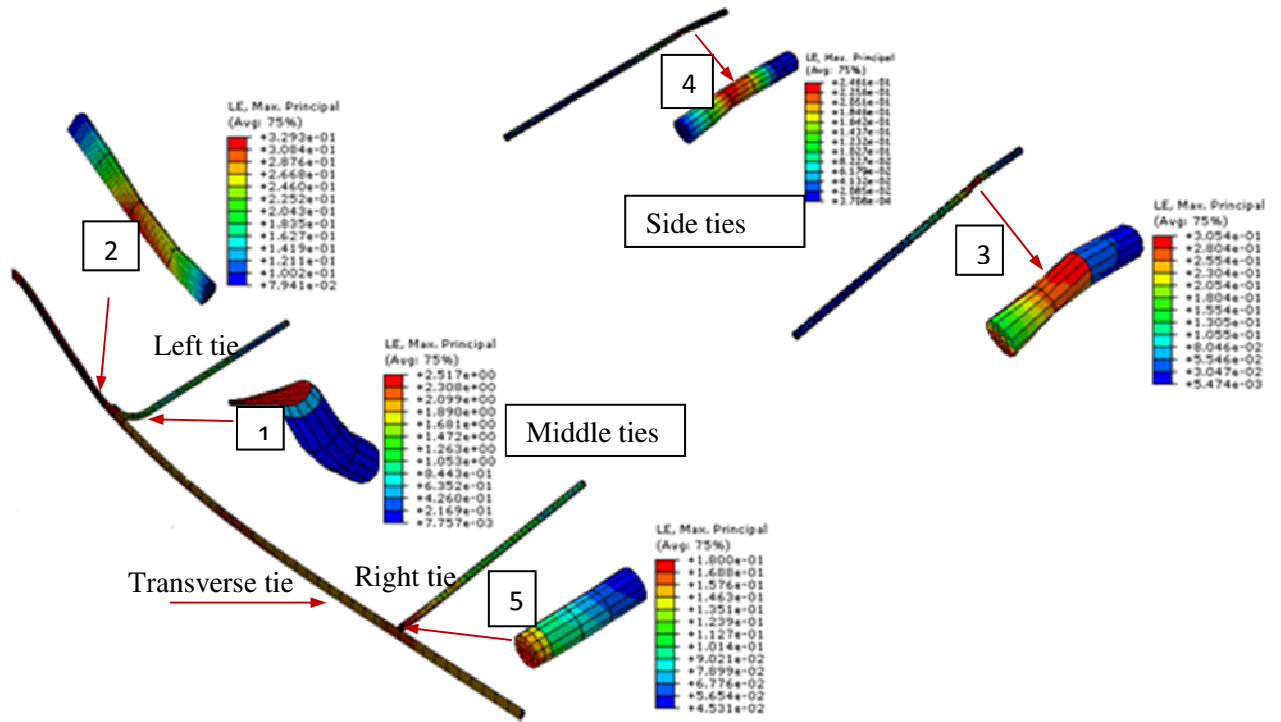


Figure 5.17 Failure procedure in the longitudinal and transverse ties; strain in different ties at middle joint deflection of 365-LFT1

The strength of the specimen with a slab length of 4 m and width of 2.4 m is shown in Figure 5.18. The tie properties remain the same as specimen LFT1. The results indicate that the failure process follows the same failure mechanism of LFT1 (Fig. 5.17). The result indicates that system reaches its maximum capacity at $\delta_s / l_t = 10\%$ and also, middle and transverse ties reaches the failure strain at the same deflection. Furthermore, the result shows that most of ties reaches fracture strain at the deflection around 385 mm i.e. $\delta_s / l_b = 9.6\%$ or $\delta_s / l_t = 16.05\%$. Comparing Figures 5.15 and 5.18 indicates that the progressive collapse resistance of specimen LFT2 is approximately half of that of LFT1. As the same property in the transverse direction was applied in both specimens, it can be concluded that the strength of the system is in proportion inversely to the slab length in the longitudinal direction. Furthermore, the yielding capacity for both LFT1 and LFT2 specimens occurs at approximately the same middle joint deflection/span ratio. Figure 5.19 shows that load

sustained by longitudinal ties are closer to the transverse ties rather than the specimen LFT1. It can be attributed to the more stiffness provided by the transverse tie compared to LFT1

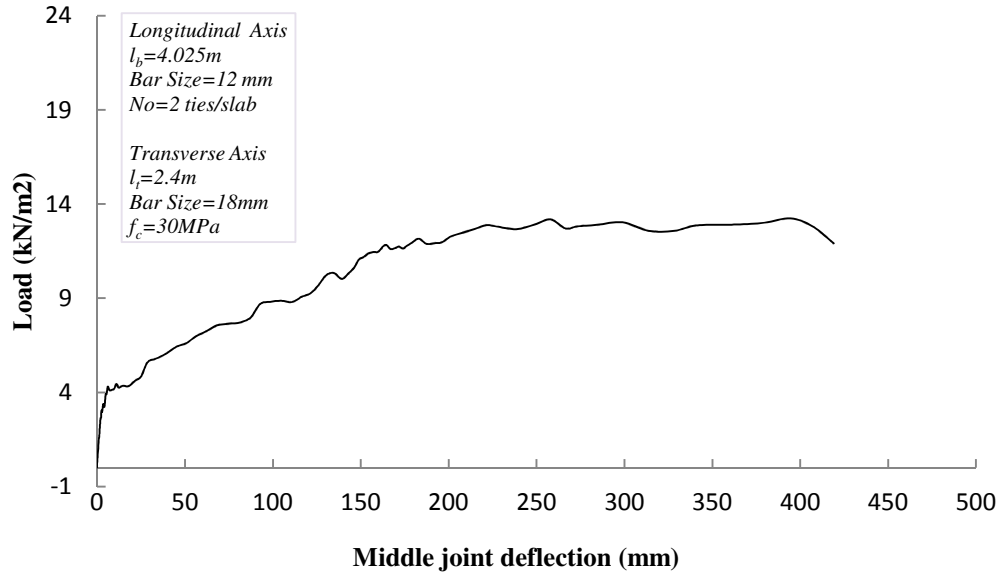


Figure 5.18 Load versus middle joint deflection using longitudinal and transverse ties - LTF2

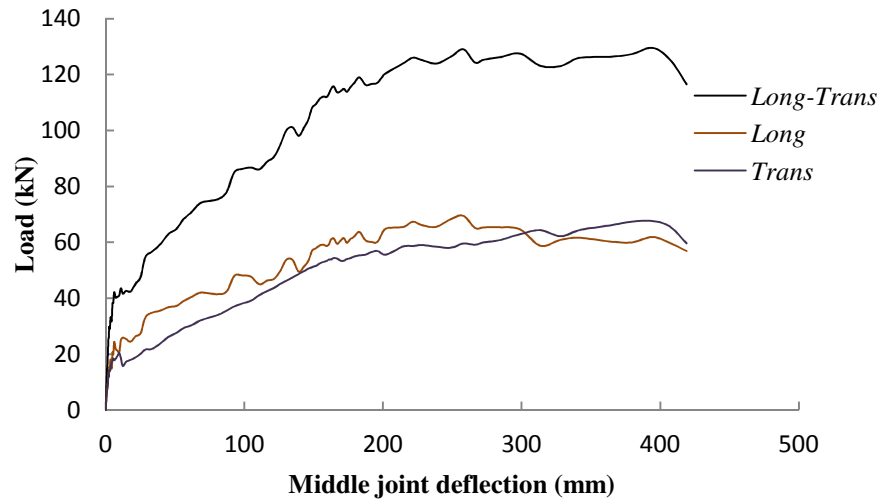


Figure 5.19 Reaction supports versus middle joint deflection - LTF2

To study the effect of the properties of the transverse tie on the behaviour of the system, in specimen LFT3, the tie with a length of 4.8 m and bar size of 24 mm was used; while the properties of the longitudinal ties remain the same as LFT2. The failure mode of the specimen

is shown in Figure 5.20, which indicates that at the collapse maximum deflection of the middle slab is more than four times of the maximum deflection in the side slabs.

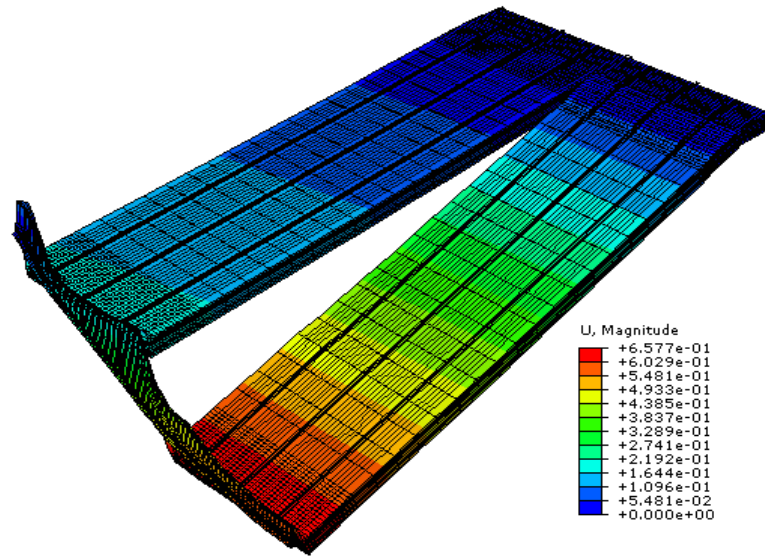


Figure 5.20 Failure mode of LFT3 specimen

Figure 5.21 shows that the strength of the system is less than specimen LFT2 by 23% and maximum capacity is induced at $\delta_s / l_b = 10\%$, which is similar to the specimen LFT1. The result indicates that to provide the same strength, the cross section of the tie needs to be increased in proportion to the length of the specimens in the corresponding directions. The result of the strain-deflection relationship indicates that the system collapses at the deflection around 580 mm i.e. $\delta_s / l_b = 14.6\%$ and $\delta_s / l_t = 12.01\%$ which is more than specimen LFT2 but similar to LFT1 (Figure 5.21). The collapse limit was defined considering strain fracture in the tie at the middle slab (Fig. 5.22).

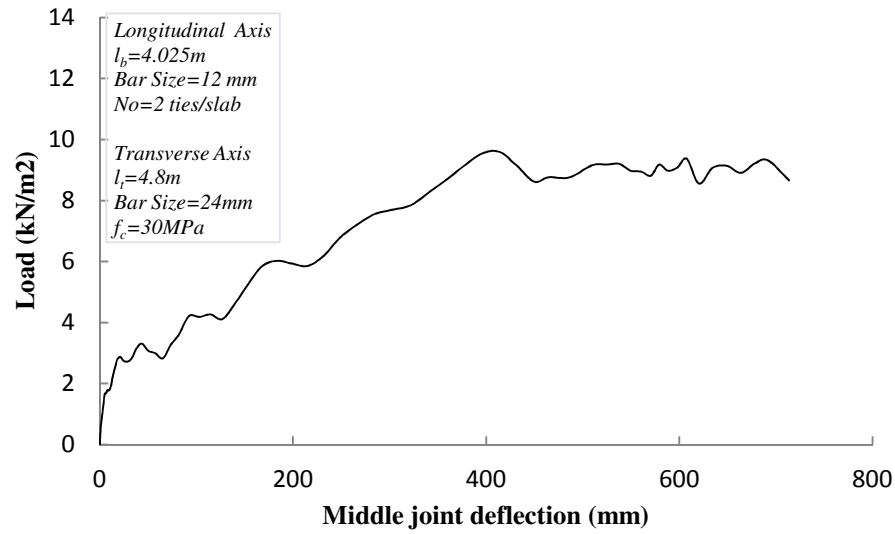
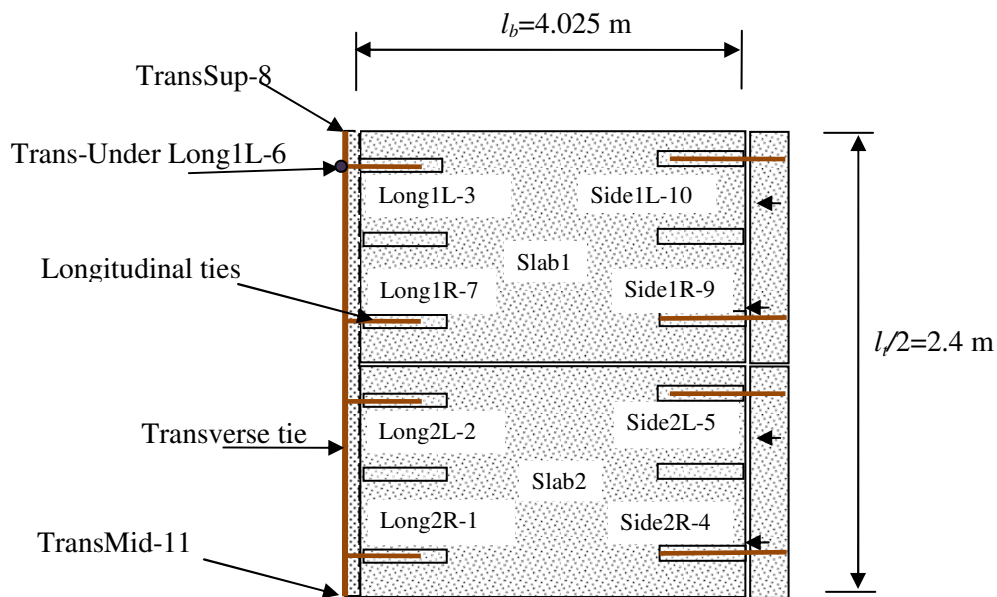
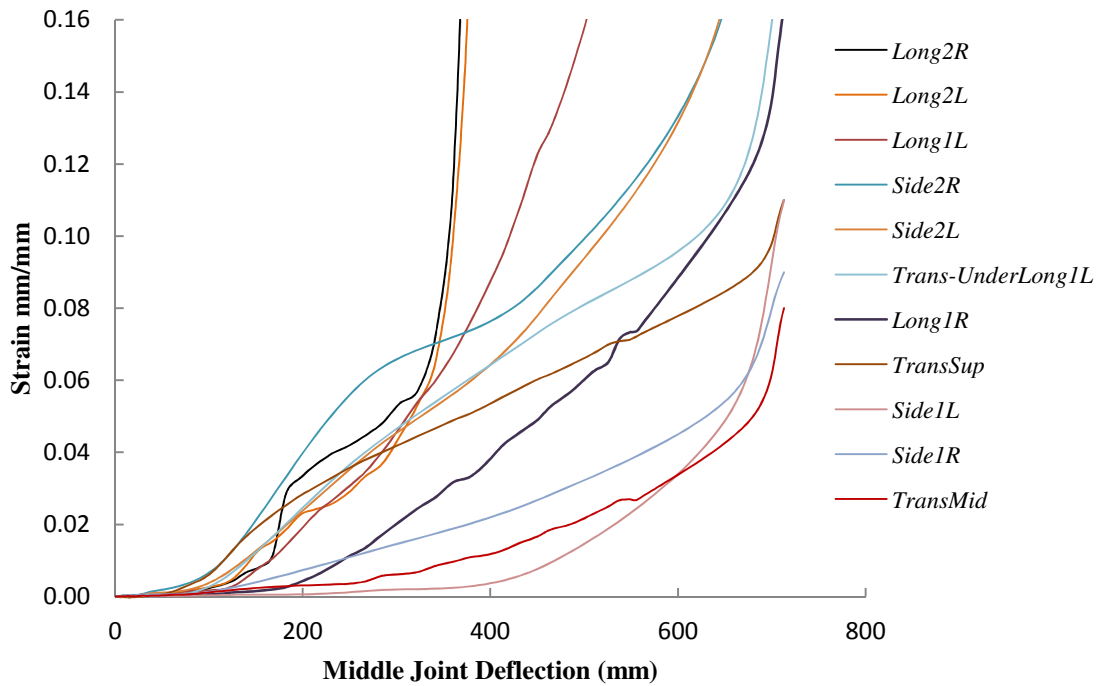


Figure 5.21 Load versus middle joint deflection using longitudinal and transverse ties - bar fracture failure mode - LTF3

Although the longitudinal span in LFT2 is two times of LFT1, the specimens LFT1 and LFT2 experience collapse at the same deflection/span ratio $\delta_s / l_{\min} = 10\%$, while specimen LFT3 collapsed at $\delta_s / l_b = 13.67\%$ which is slightly more than other specimens.



(a) Layout of longitudinal/transverse tie and failure process



(b) Strain versus middle joint deflection in the longitudinal and transverse ties

Figure 5.22 Failure process of LFT3

Figure 5.22 shows the strain in the critical section of various longitudinal and transverse ties. The collapse mechanism is initiated from the longitudinal tie at the right hand side of the middle gap and propagates to the longitudinal ties at the left side of the gap, followed by bar fracture at the transverse tie underneath of 1L's longitudinal ties. It obviously indicates that, similar to the experimental study, for the specimens with longitudinal and transverse ties the collapse of the system is initiated by bar fracture at the middle joint

According to the TF method in DoD 2013, the tie forces are increased in proportional to the span length; hence in specimen LFT4 with a longitudinal length of 6 m the numbers of ties are increased by 50% compared to LFT3.e. 3 ties/slab, but the same cross section of the

transverse tie was applied, which is 50% less than the cross section of the longitudinal ties (Fig. 5.23). Figure 5.23 displays the layout of the ties showing the progressive failure of ties from 1 to 12 using the strain-deflection relationship provided in Figure 5.24. The result indicates that LFT3 and LFT4 exhibit slightly different progressive failure procedure.

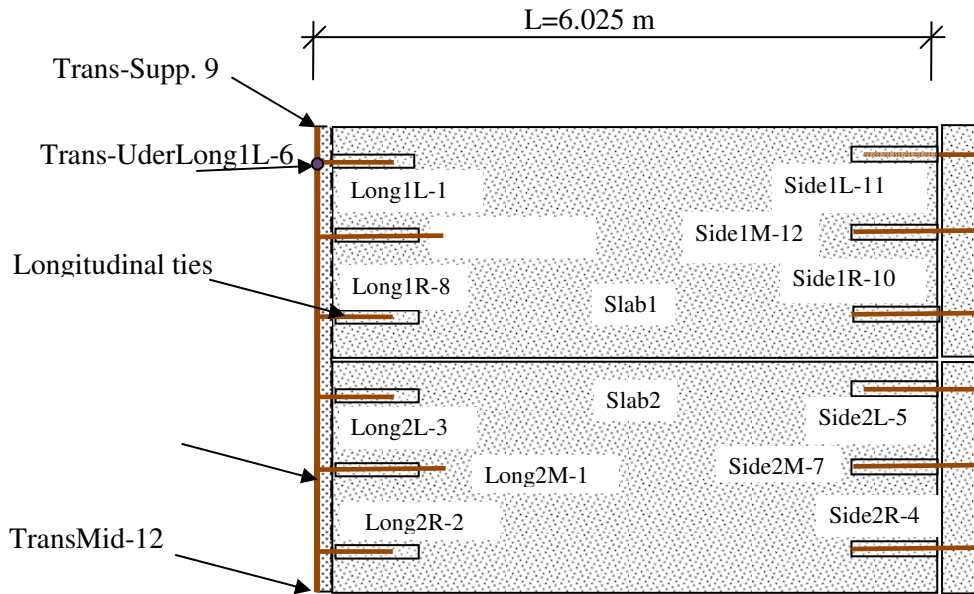


Figure 5.23 The layout of longitudinal and transverse ties indicating progressive failure procedure

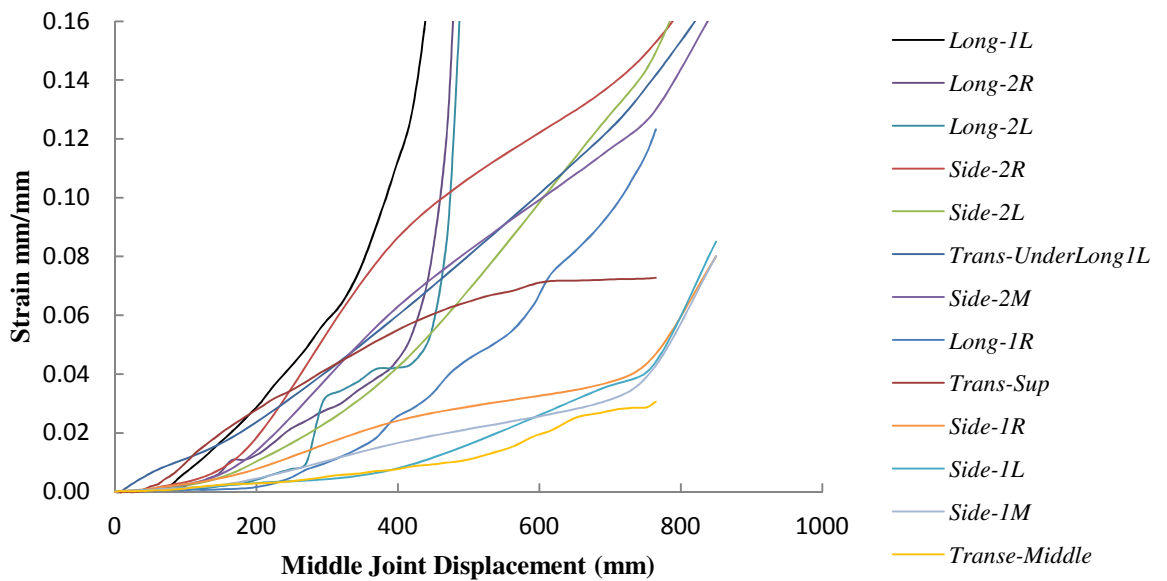


Figure 5.24 Strain versus middle joint deflection-LFT4

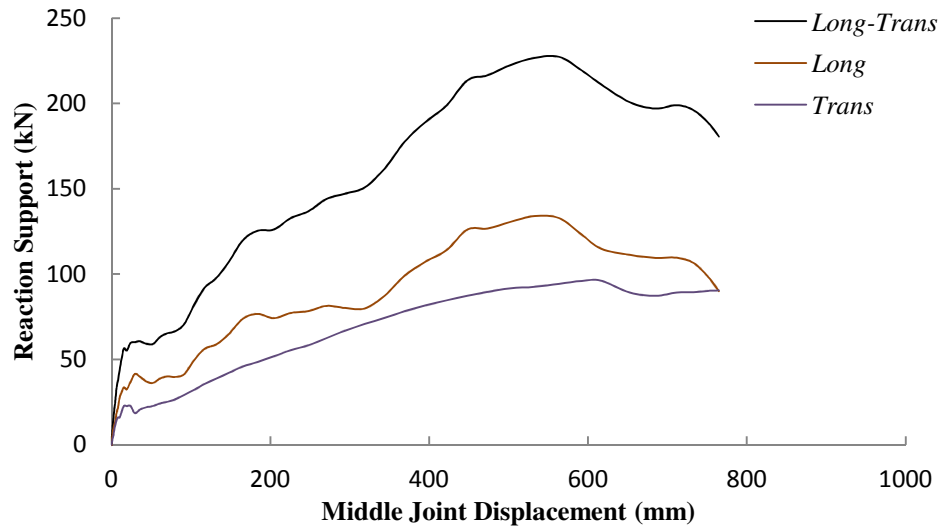


Figure 5.25 Reaction supports versus middle joint deflection - bar fracture failure mode - LTF4

Figure 5.25 indicates that similar to other specimens at the yielding stage the load sustained by the longitudinal ties is more than the transverse ties by more than 50 %, while at the certain deflection ties in both directions carry the same load. Figure 5.26 indicate that system reached maximum capacity at $\delta_s / l_t = 11\%$ and collapsed at $\delta_s / l_b = 13.61\%$ and $\delta_s / l_t = 17.08\%$, which shows slightly more ductility than specimen LFT2.

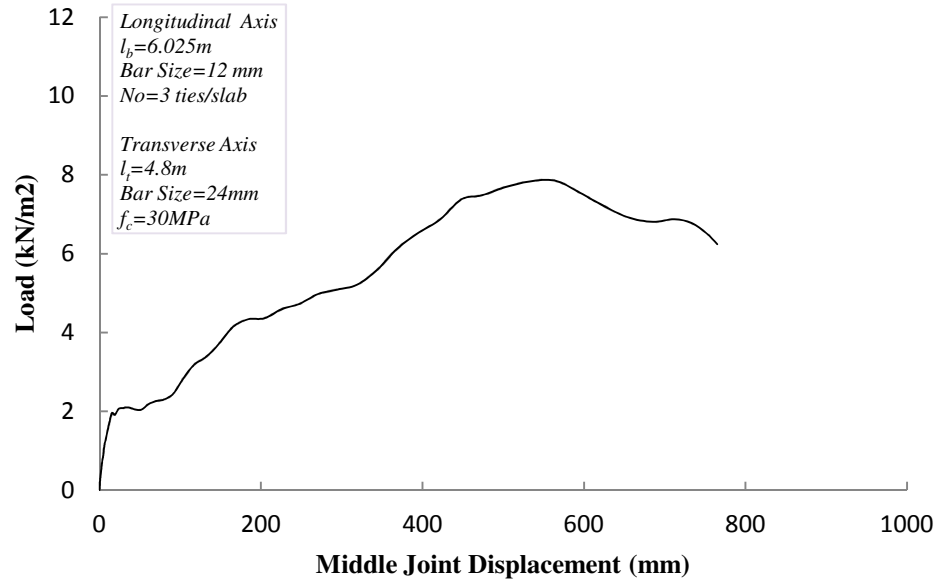


Figure 5.26 Load versus middle joint deflection for using longitudinal and transverse ties - bar fracture failure mode - LTF4

Comparing results between LTF3 and LTF4 indicate that, with the same properties of transverse ties, although the cross section of the longitudinal tie is increased in proportion to the increase in the length of the slab in the longitudinal axis, the strength of the system is decreased by 25%; (Fig. 5.26). It indicates that to provide the same level of progressive resistance, the cross section of both longitudinal and transverse tie need to be increased.

In specimen LTF5, the span in the transverse direction is increased by 50% compared to LTF4, hence to provide relatively the same tie cross section/span length ratio the bar size of 36 mm is used as a transverse tie. Figure 5.27 shows that the progressive collapse resistance of specimens reaches to its maximum capacity at a deflection/length ratio around $\delta_s / l_b = 10\%$ and collapses at $\delta_s / l_b = 13.27\%$ and $\delta_s / l_t = 11.05\%$. Figures 5.26 and 5.27 again confirm that, as long as the cross section of the tie is increased in proportion to the

length of the specimens in the relevant direction, the specimens are capable of providing the same capacity.

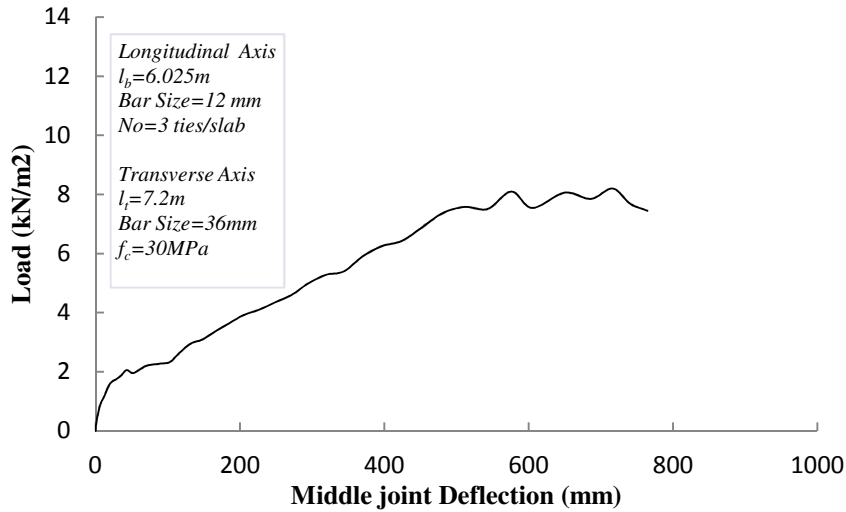


Figure 5.27 Load versus middle joint deflection for various slab lengths using longitudinal and transverse ties - bar fracture failure mode - LTF5

The reaction support-deflection relationship follows the same behaviour of the previous specimens. Figure 5.28 shows that, although at $\delta_s / l_b = 8.1\%$ the load sustained by the longitudinal ties is more than the transverse tie by 40%, but at the $\delta_s / l_b = 12.5\%$, both longitudinal and transverse ties sustain the same load; which again confirm that following yielding in longitudinal ties, the load is redistributed from the longitudinal ties to the transverse ties.

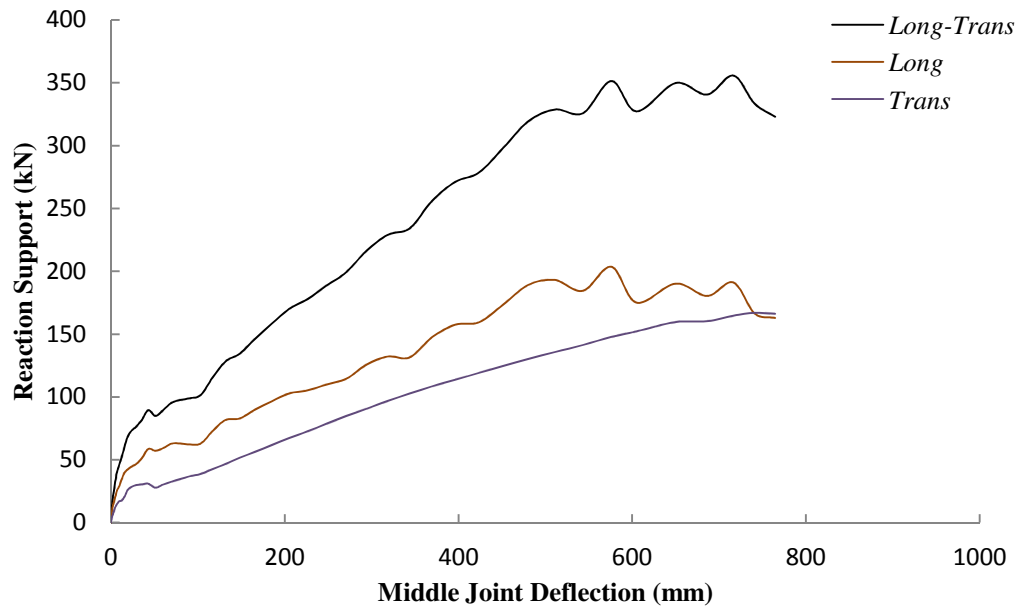


Figure 5.28 Reaction supports versus middle joint deflection -LTF5

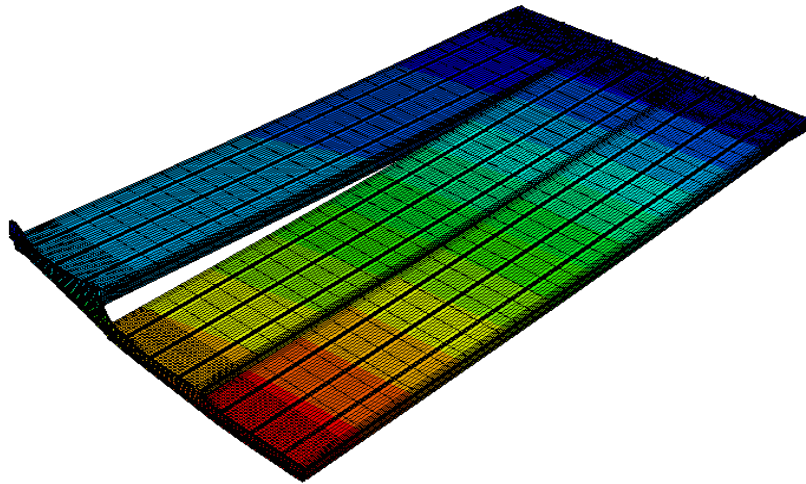
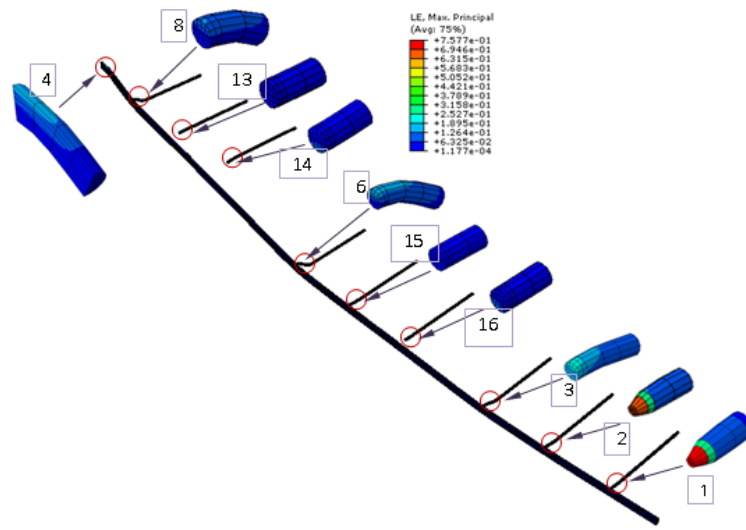


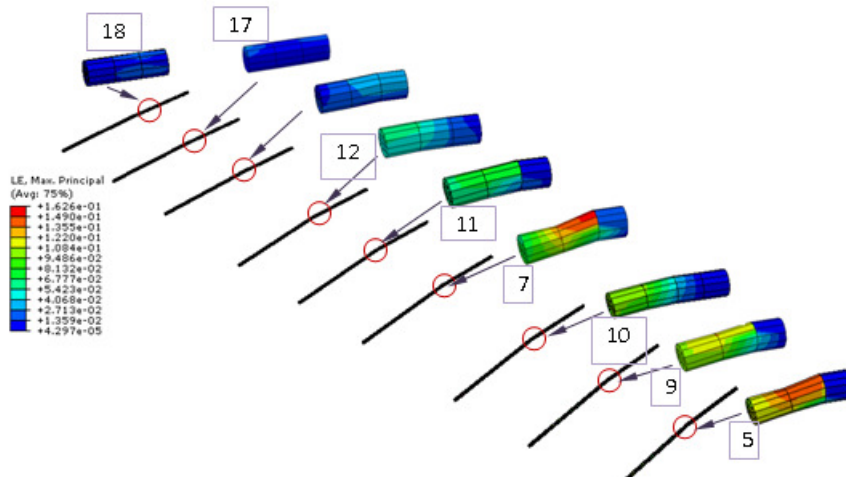
Figure 5.29 Failure mode of LFT3 specimen, $\delta_s / l_b = 8\%$

The overall failure mode of the specimen at the collapse is shown in Figure 5.29 and detailed in Figure 5.30. The result indicates that the failure mechanism is initiated by yielding in the middle longitudinal tie at the right hand side of the middle gap. Also, note that in the specimen LFT1 the transverse tie starts yielding underneath the longitudinal tie close to the

side transverse tie support, while in this specimen the yielding in the transverse tie is initiated at the top of the bar at the left support. The result indicates that the specimens with different slab length shows slightly different failure procedure, but generally it is initiated from longitudinal at the middle joint, followed by bar fracture of transverse and side ties (5.30).



(a) Middle ties



(a) Side ties

Figure 5.30 Failure mechanism of specimen, $\delta_s / l_b = 8\%$ -LFT5

Considering the maximum failure force corresponding to a strain fracture of 16%, the relationships between the tie force with load and slab lengths for each specimens is summarised in Table 5.4 following applying over strength factor of 1.25.

Table 5-4 Longitudinal and transverse tie force with relevant maximum strength

	LTF1	LTF2	LTF3	LTF4	LTF5
$P_l (kN / m)$	$1.95wl_b$	$1.92wl_b$	$2.6wl_b$	$3.2wl_b$	$3.16wl_b$
$P_t (kN)$	$1.37wl_t l_b$	$1.36wl_t l_b$	$1.65wl_t l_b$	$1.33wl_t l_b$	$1.99wl_t l_b$

Where

P_l = Required longitudinal tie force at joints (kN)

W = UDL load on the floor i.e. (DL+0.5L, DoD 2013), kN / m^2

l_b = Longitudinal span length (m)

P_t = Required transverse tie force at joints (kN)

l_t = Length of transverse tie (m)

5.4.2.2 Stiffness Analyses

To study the effect of lateral stiffness, two specimens e.g. LFT3 and LFT5 were reanalyzed with fixed support (Fig. 5.31). The results indicate that prior to plastic capacity the lateral stiffness has a remarkable effect on the behaviour of the specimens; while at the collapse, the progressive resistance of specimens with fixed support is increase by 20%. It is obvious that the side support experiences a small lateral movement due to the arch or catenary action, hence assuming fixed support might result in relatively conservative progressive collapse resistance.

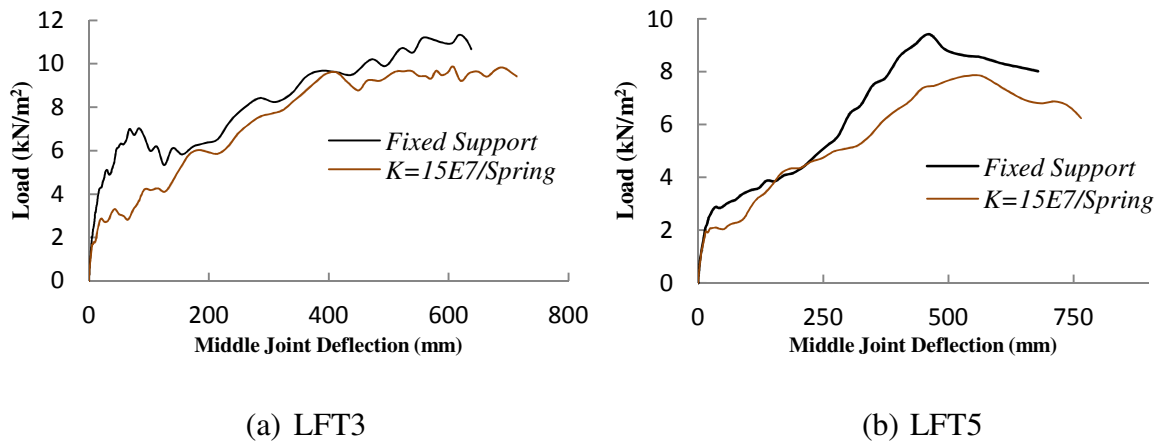


Figure 5.31 Load versus deflection for different stiffness

5.4.2.3 Pullout Failure Mode

The specimens with bar fracture failure mode indicate that the failure is initiated by yielding in the middle joint ties, followed by yielding in the transverse and longitudinal ties at the side joints. To improve behaviour of a floor-to-floor system and increase ductility of the specimens by avoiding yielding in the longitudinal ties at the small deflection, the length of the longitudinal ties is decreased to change the failure mechanism from bar fracture to pullout failure mode. In the following specimens the bar size of 12 mm with an embedment length of 250 mm is used as longitudinal ties and the other properties remain the same as the specimens with bar fracture failure mode. It is important to note that, in pullout failure mode, the compressive strength of concrete is assumed to be 20MPa in all the specimens.

The failure mode of specimen LFP1 is shown in Figure 5.32, which indicates an obvious discrepancy in the progressive failure mechanism compare to the bar fracture failure mode (Fig.5.14). Due to pullout governing the behaviour of bars in the keyway, in this type of specimen the longitudinal tie at the joints prior to peak capacity does not fracture. The system collapses by yielding in the transverse tie, followed by pullout failure of the side ties (Fig. 5.33). In this case, it is transverse ties which govern the failure of the specimen. Figure 5.34

shows that the transverse tie at the location of the left longitudinal tie at the middle joint is fractured at the deflection of 200 mm; while due to pullout behaviour; strain in all other longitudinal ties is less than the fracture strain.

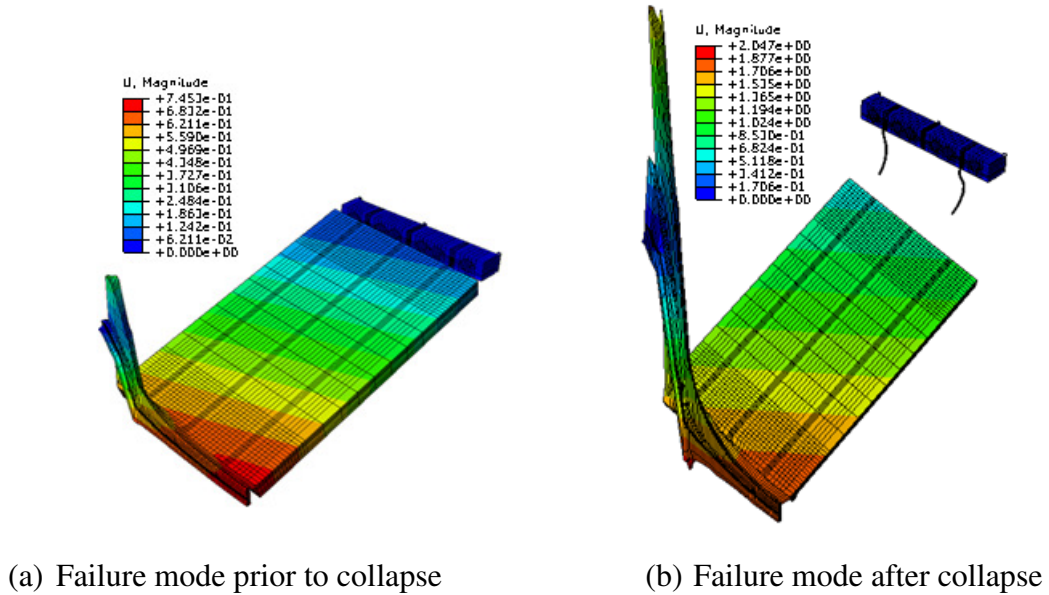


Figure 5.32 Failure mode of specimen

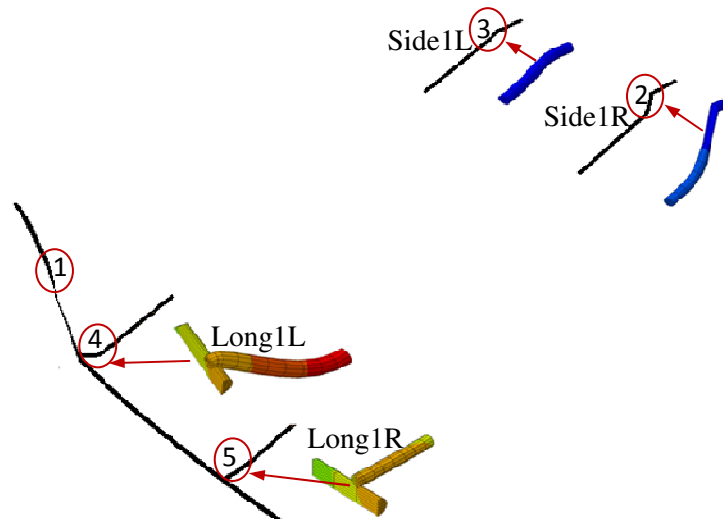


Figure 5.33 Failure process of longitudinal and transverse tie at deflection of 745 mm

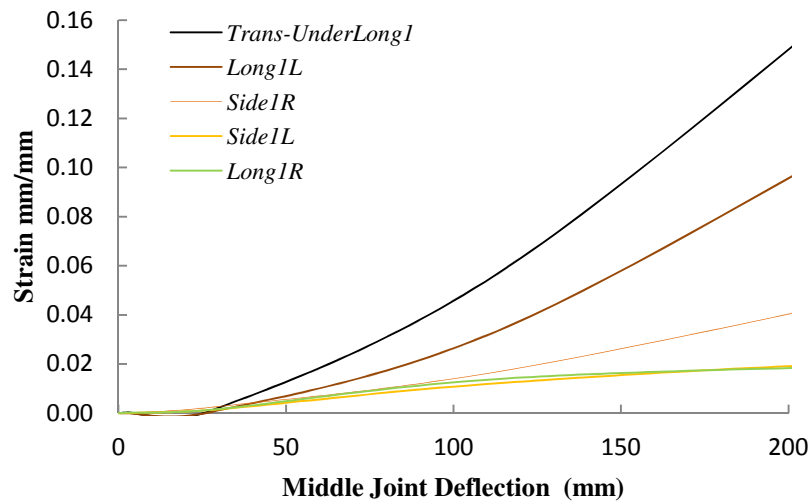


Figure 5.34 Strain versus deflection in longitudinal and transverse ties-LFP1

The result indicates that the specimen with pullout failure mode relatively enhances the ductility of the system; which is considered as a key influence parameter in robust structures (Fig. 5.35). Comparing Figure 5.15 and 5.35 shows that in the specimen with bar fracture failure mode i.e. LFT1, the system reaches its maximum progressive collapse capacity at deflection of 200 mm i.e. $\delta_s / l_b = 10\%$; while LFP1 is capable of sustaining relatively the same load up to a deflection of 275 mm i.e. $\delta_s / l_b = 13.5\%$, followed by a relatively steady descending phase without any abrupt failure as bar fracture failure mode. It can be attributed to that fact that following the initial yielding of the transverse tie, the load is redistributed to the longitudinal ties which capable to sustain more load due to catenary action and being in the elastic phase; hence a combination of transverse ties in the plastic or hardening stage and catenary behaviour of longitudinal ties is capable of providing more strength up to $\delta_s / l_b = 13.5\%$ (Fig. 5.36).

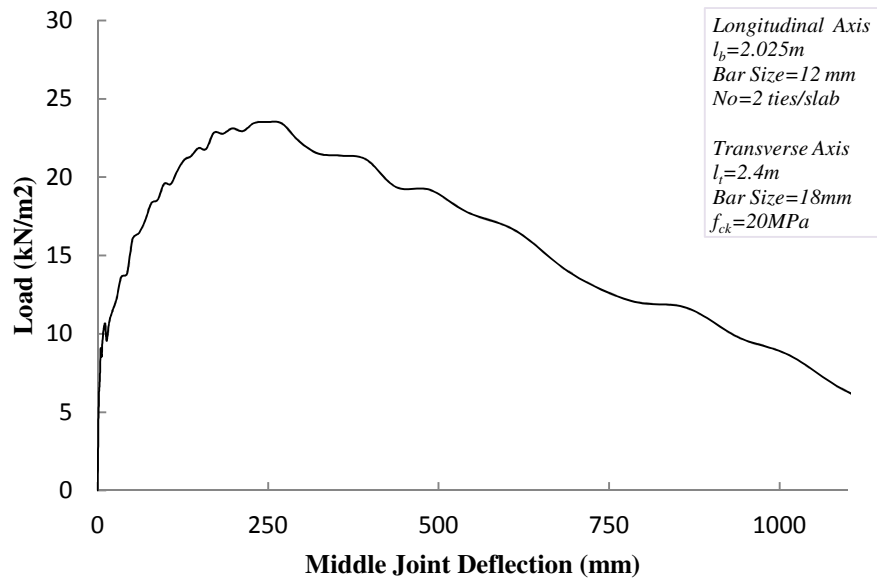
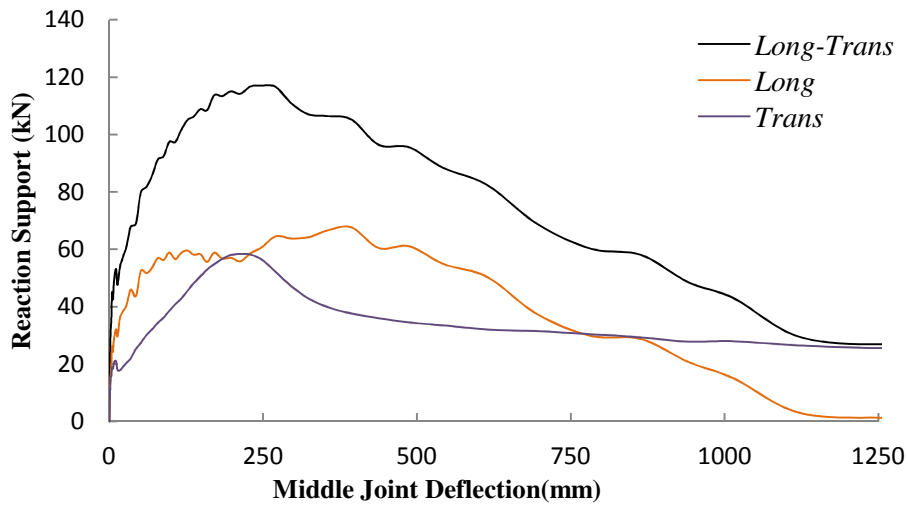


Figure 5.35 Load versus middle joint deflection for various slab lengths using longitudinal and transverse ties - bar fracture failure mode – LTP1



(a) Reaction support

Figure 5.36 Load versus middle joint deflection using longitudinal and transverse ties - bar fracture failure mode - LTP1

Unlike to bar fracture failure mode, the peak pullout capacity of bar into keyways is induced at relatively large deflection (Fig. 5.37), which can explain why the peak strength is induced

at larger middle joint deflection. Also, Figure 5.36 indicates that, longitudinal ties are capable to provide second peak strength similar to specimens with only longitudinal ties.

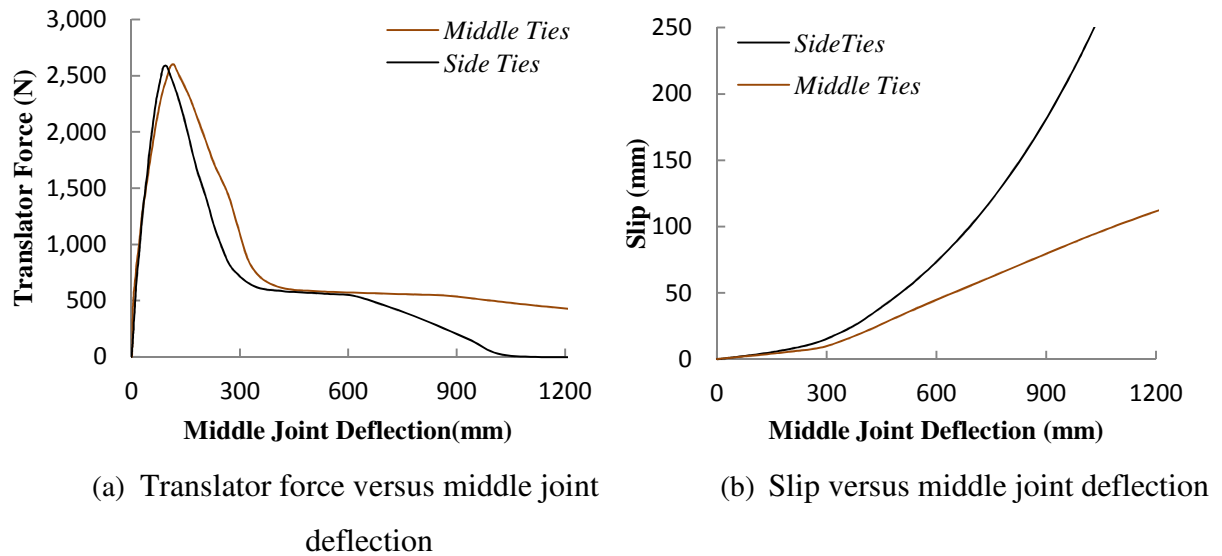


Figure 5.37 Bond behaviour of tie bars-LFP1

Figure 5.37 indicates that the longitudinal ties at the middle joint and side supports experience relatively the same bond stress and slip up to peak strength at a deflection of 247 mm; followed by a dramatic decrease in bond strength in longitudinal ties at the side supports. It can be attributed to this fact that, the gravity load pushing the slab towards the middle joint at a large deflection, hence the ties at the middle joints do not experience further slip; accordingly constant bond strength exists up to failure. Figure 5.37(b) shows that at a deflection of 1000 mm, slip at the side tie is 250 mm and equal to the embedment length of ties, which indicates the zero capacity of the system. Furthermore, it shows that the system collapses by the pulling out of bars at the side supports (5.37b).

Figure 5.38 shows that although the longitudinal span length of LFP2 is increased two times compared to LFP1; the strength of the specimen is decreased only by 30% which is less than rate of increasing of the length of specimen in longitudinal direction. It is due to the transverse tie provides the same strength as LFT1 and decrease of capacity of system is only related to

longitudinal ties. The result, also, indicates that the system reaches its capacity at $\delta_s / l_b = 10.2\%$ $\delta_s / l_t = 17.5\%$ and collapses at $\delta_s / l_b = 40\%$ and $\delta_s / l_t = 68.75\%$ (Fig. 38). Furthermore, comparing Fig. 5.18 and 5.38 indicates that for the same ties and span lengths, the progressive resistance and ductility of specimens with pullout failure mode is relatively more than specimens with bar fracture failure mode.

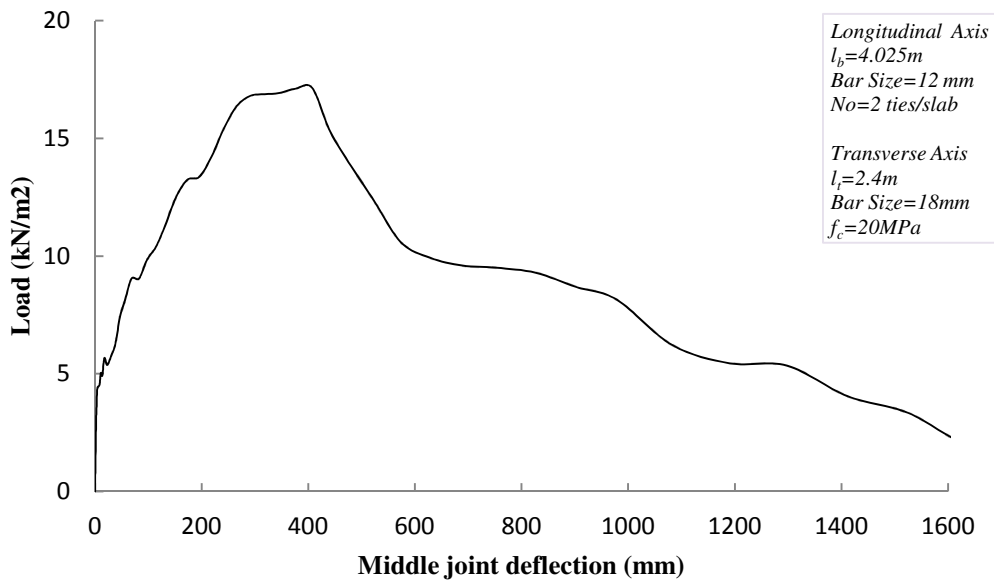


Figure 5.38 Load versus middle joint deflection using longitudinal and transverse ties - bar fracture failure mode - LTP2

The failure mode of the specimen LFP3 at the middle joint deflection of 1.48 m is displayed in Figure 5.39. It shows that the middle precast slabs are more susceptible to failure rather than the side slabs. Figure 5.40 indicate that the transverse tie yielded at $\delta_s / l_b = 11.86\%$; while at this deflection the longitudinal ties remain in the elastic zone due to pullout governing the behaviour of the ties.

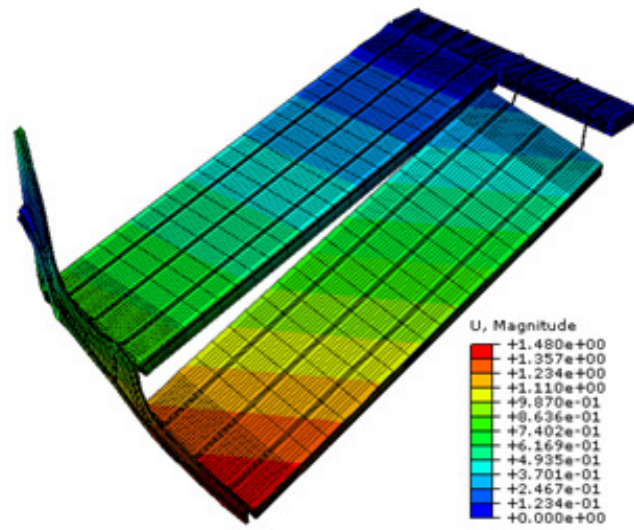
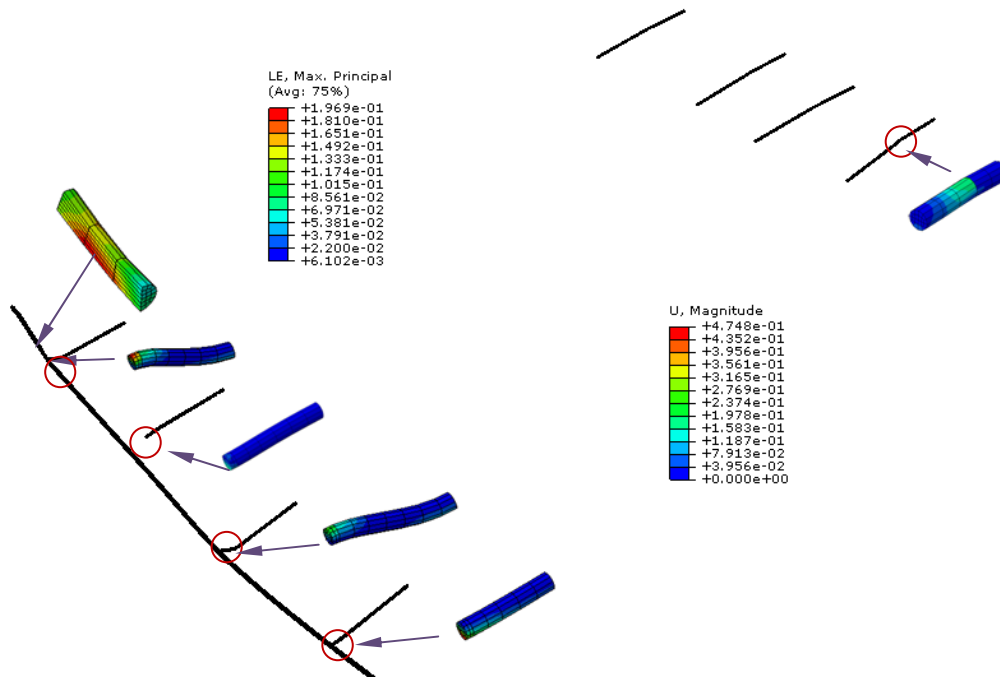
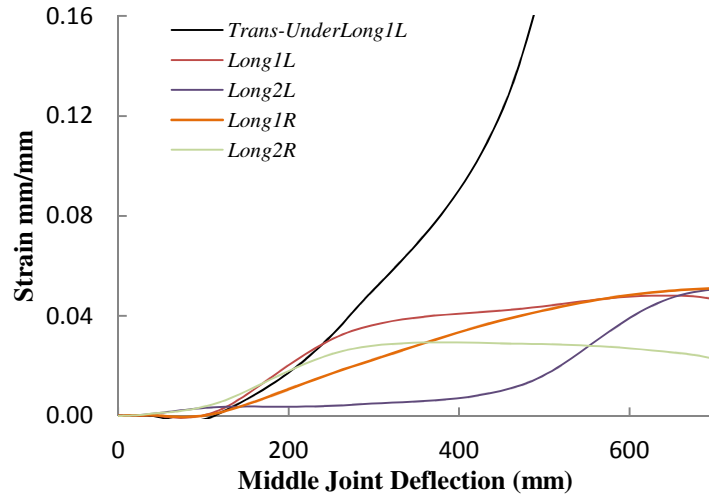


Figure 5.39 Failure mode of specimen LFP3



(a) Failure process of longitudinal and transverse tie



(b) Strain versus middle joint deflection

Figure 5.40 Failure mechanism of specimen LFP3 at deflection of 475mm

Figure 5.41 shows that compared to LFP2, the strength of LFP3 decreased by 40%; which is slightly less than the rate of increase in the span length in transverse direction. The system reaches its maximum capacity at $\delta_s / l_b = 17.4\%$.

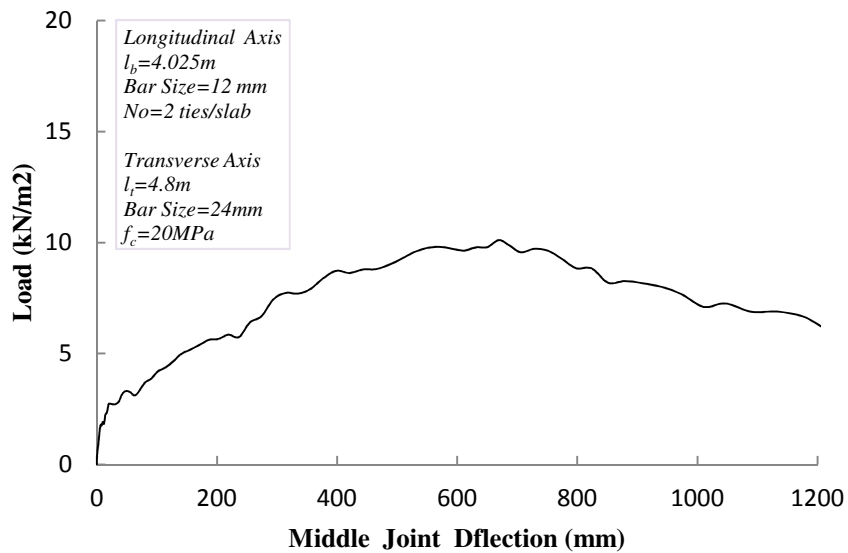


Figure 5.41 Load versus middle joint deflection using longitudinal and transverse ties - bar fracture failure mode - LFP3

In specimen LFP4, the length of the specimen and the number of ties in longitudinal direction increased by 50%, while the other properties remained the same as LFP3. The result indicates that compared to LFP3, the strength of LFP4 decreased by 20% (Fig. 5.42), which again indicates that to provide relatively the same capacity the numbers of ties or cross section of ties need to be increased proportional to the relevant span length. Comparing Figures 5.41 and 5.42 reveals that both specimens provide the same ductility at maximum progressive collapse resistance.

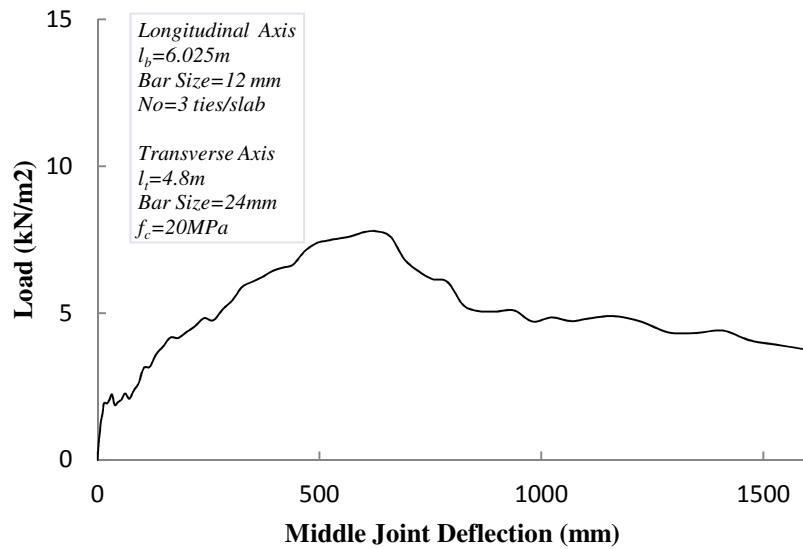


Figure 5.42 Load versus middle joint deflection using longitudinal and transverse ties - bar fracture failure mode - LTP4

In order to study the effect of the length of the specimens in longitudinal and transverse directions on the behaviour of the system, in LTP5 the length of the specimen in transverse axis is increased by 50% with a bar size of 30 mm, while all other parameters remain the same as LFP4. In this specimen the cross section of the tie in the longitudinal axis is more than the transverse direction by 50%. Figure 5.43 shows the failure mode of the specimen at a deflection of 1380 mm i.e. $\delta_s / l_b = 23\%$. Similarly to the bar fracture failure mode, the two middle slabs experience much more deflection compared to the side slab. Figure 5.44 indicates that following the initial peak strength $\delta_s / l_b = 9\%$, the strength provided by

longitudinal ties is relatively increased again up to $\delta_s / l_b = 20\%$, which result more robustness. The results indicate that the system reaches maximum strength at $\delta_s / l_b = 16.6\%$, $\delta_s / l_t = 13.9\%$, followed by steady decrease of capacity up to total failure, which exhibits relatively similar behaviour to other specimens (Fig. 5.45).

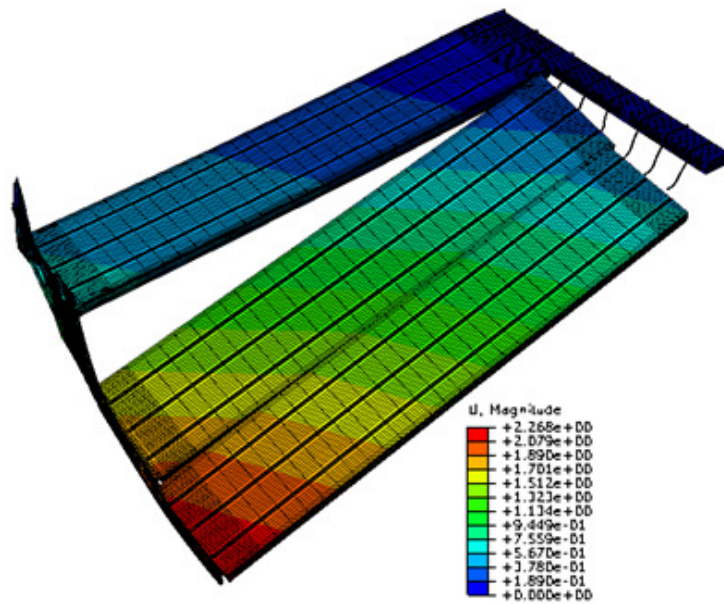


Figure 5.43 Failure mode of specimen LFP5

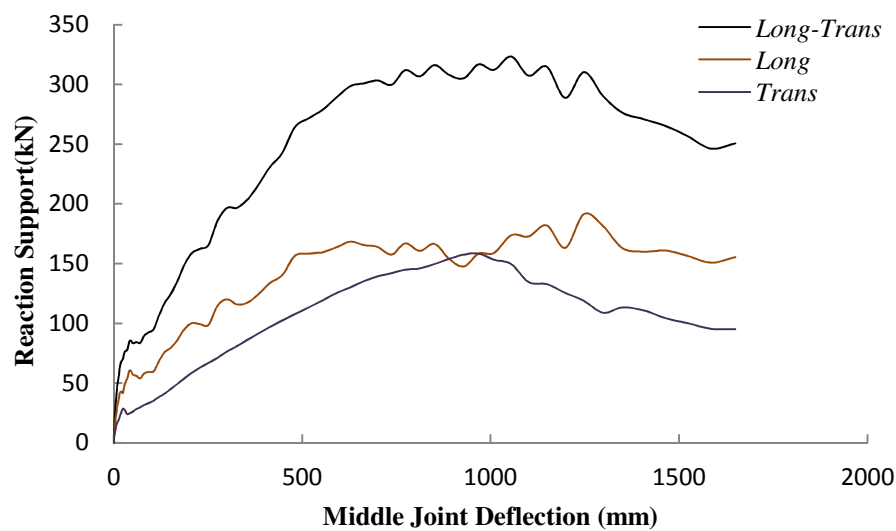


Figure 5.44 Reaction support versus middle joint deflection using longitudinal and transverse ties - pullout failure mode - LFP5

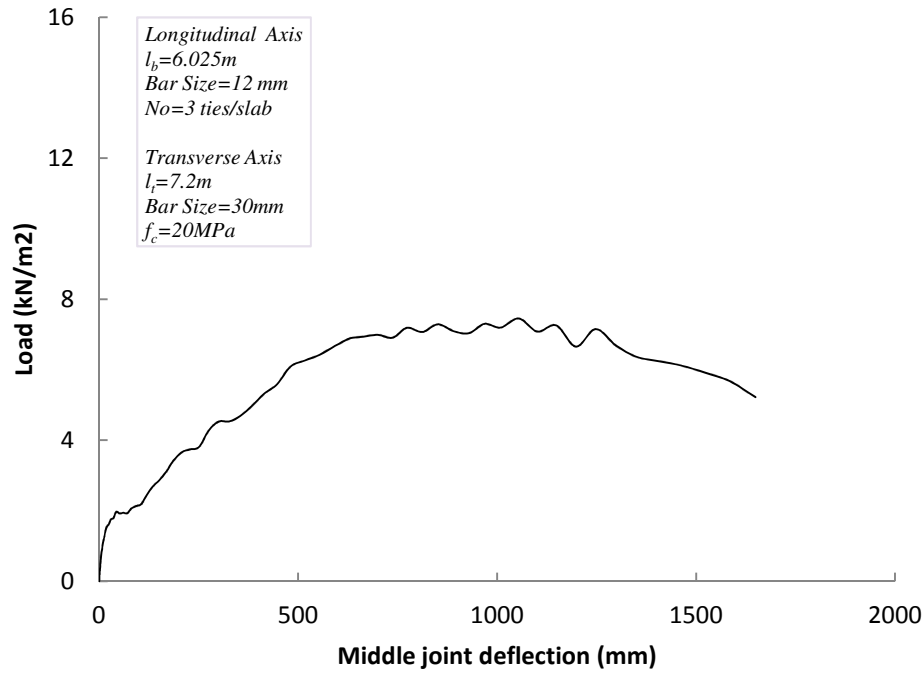


Figure 5.45 Load versus middle joint deflection using longitudinal and transverse ties - LTP5

Considering maximum failure force corresponding to fracture strain in the transverse tie and maximum pullout force (Table 3.3), the relationships between tie force with load and slab lengths for different specimens are shown in Table 5.5.

Table 5-5 Tie force based on pullout failure mode

	LTP1	LTP2	LTP3	LTP4	LTP5
P_l (kN / m)	$1.85wl_b$	$1.3wl_b$	$2.18wl_b$	$2.27wl_b$	$3.55wl_b$
P_t (kN)	$1.48wl_t l_b$	$1.04wl_t l_b$	$1.55wl_t l_b$	$1.34wl_t l_b$	$1.49wl_t l_b$

To show dynamic behaviour of the floor-to-floor joint following applying an actual load, the specimen LFP3 reanalysed under instantaneous load of 75% of maximum strength of the system assuming default damping provided by ABAQUS (Fig. 5.46). The result indicates

that, by increasing nonlinearity the impact factor due to dynamic behaviour is decreased. Fig. 5.46b shows the history of the deflection of the floor just above the removed wall. As seen, the floor exhibited a sudden deflection of 265 mm but then vibrates up and down around a residual deflection of 250 mm, which represents a final stable state for the floor.

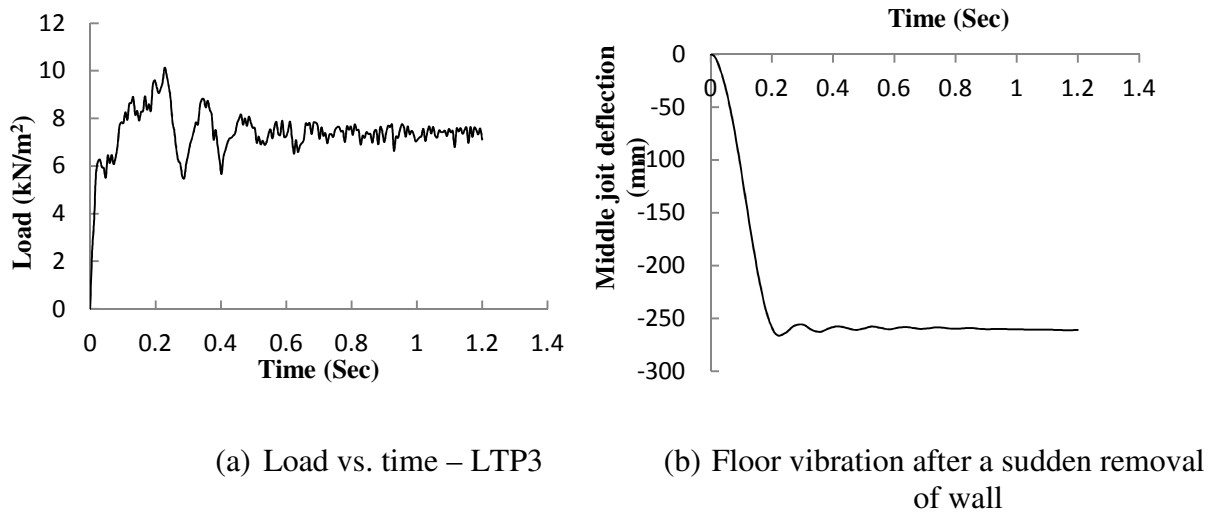


Figure 5.46 Behaviour of specimen LFP3 under instantaneous load of $7.5 \text{ kN} / \text{m}^2$

5.5 SUMMARY

The overall behaviour of specimens in bar fracture failure clearly indicates that up to yield capacity, the load sustained by longitudinal ties is more than transverse ties by around 35-50%; while at the collapsing stage both longitudinal and transverse ties carry the same load which indicates the redistribution of loads prior to collapse. The results show that, the systems reach yield capacity at $\delta_s / l_b \approx 2\%$ and maximum strength at $\delta_s / \min(l_b, l_t) \approx 10\%$, followed by sudden collapse at $\delta_s / \min(l_b, l_t) \approx 13-17\%$ and $\delta_s / \max(l_b, l_t) \approx 9.6-13.61\%$. The results indicate that, for specimens with the same length, precast floor-to-floor system assuming bar fracture failure mode exhibits relatively less ductility compare to the

conventional RC structure, while specimens with pullout failure mode provides relatively the same ductility.

The results show that, for the specimens with bar fracture failure mode, although the failure mechanism varies with the number of slabs in the direction of the transverse tie, generally the failure is initiated from the middle longitudinal ties followed by the side longitudinal ties at the middle joint. Subsequently, the transverse tie reaches its capacity followed by failure in the longitudinal ties at the side supports, which is in contrast to progressive mechanism of RC structures. The strength analysis of the specimens clearly indicates that, following maximum capacity the progressive collapse resistance remains relatively constant up to overall collapse of the system, which shows redistribution mechanism. The result of load versus middle joint deflection indicates that the floor-to-floor joint exhibits similar behaviour as that of an RC structure with non-seismic detailing and low compressive strength (Trung et al. 2010). The results, also, indicate that the strength of system is in proportion to cross section area of longitudinal and transverse ties.

In the specimens with pullout failure mode, prior to peak pullout force, longitudinal ties at the middle and side joints show the same behaviour; afterwards the tie force in the middle bar remains constant while the side bars experience the same behaviour as tie bars in concrete under pullout force. In these specimens, failure will be initiated by yielding in the transverse ties followed by pullout failure of the tie bars at the side joints. The results indicate that, following initial yielding at the transverse tie a combination of longitudinal tie at partial debonding and transverse tie at plastic/hardening stage increases the strength of system up to $\delta_s / l_b \approx 13.5-17.4\%$, followed by a steady decrease up to pulling out of side bars. Comparing the two failure modes shows that, the specimens with pullout failure mode provide more strength and ductility rather than bar fracture failure mode, which can be considered as the outstanding outcome of this study.

Chapter 6

GENERAL ANALYSIS AND DESIGN GUIDELINE

6.1 INTRODUCTION

The aim of this chapter is to provide an improved tie force (TF) method to analyze precast structures for progressive collapse using the numerical analyses carried out in the chapter 5. The proposed TF method is presented for both bar fracture and pullout failure mode separately. Also, a detailed method using conventional alternate load pad (ALP) is presented to provide a basis for an advanced analysis.

6.2 DESIGNS FOR PROGRESSIVE COLLAPSE

According to the code regulations, this section summarises the required steps to design robust structures to prevent progressive collapse. The strategy to achieve robustness and prevent progressive collapse relies mostly on good building practice, codified regulations and the design team. It has to be emphasised that notwithstanding the UK rules being mostly based on Ronan Point, where the initiating event is completely notional, while in BS EN 1991-1-7:2006 the buildings should be designed for a specific action (Mann et al. 2010). Since progressive collapse can affect a considerable part or even the entire structure with different probabilities of the state of the collapse, a specific design method may not to be reached.

However, to design structures for progressive collapse, robustness should be considered at two levels; the overall structural integrity and detailed regulation.

6.2.1 Overall Structural Concept

The overall structural form will remarkably affect the robustness of buildings. In structures with several load bearing walls, loss of one wall support does not result in the collapse of a large part of the structures; thus in comparison with buildings with large spans a degree of robustness can be established so that failure of a single element does not progress to widespread collapse. Current experiences have indicated that transfer beams, significant cantilevers, long span and simple supported beams or slabs are considerably vulnerable. Accordingly, for all structures a clear load path in horizontal and vertical directions must be provided.

6.2.2 Detailed Provisions

The principle design approaches adopted in the codes and standards can be classified in the three following methods:

1. **Indirect method:** prescriptive design rules, which rely on providing a minimum level of strength, continuity and ductility through the horizontal and vertical ties (Tie Force method). The TF method is a quantitative approach to design structures for progressive collapse. In this method ties in all connections must provide sufficient strength to establish structural integrity and redundancy. This technique considers an indeterminate structure as determinate by assuming a hinge in the connections, whereby a minimum tie force can be calculated and complicated analysis is avoided.
2. **The alternate load path (ALP) method** (design for load case “local failure”) in which a degree of local failure is acceptable, but by providing redundant and alternate load paths to bridge over the failed members, progressive collapse will be prevented. In this method

following removal of a critical element from the structure due to an abnormal loading, the structure should be capable to redistribute the *gravity* loads to the remaining undamaged structural elements. In this approach to analyze structures, linear elastic static, linear elastic dynamic, nonlinear static and nonlinear dynamic approaches can be used.

3. **The specific local resistance method (high safety against local failure)** in which key elements will be designed against specific loads by providing sufficient strength to resist failure.

Currently most standards have recommended as a first approach, the tie force (TF) method or minimum detailing for the designing of LP structures. The minimum detailing was proposed to establish a rational structural integrity through an indirect method. Due to the variety of construction systems and different types of local damage, developing regulations to provide general structural integrity is more difficult. Perhaps a minimum level of continuity and ductility might be the easiest type of provision to connect different elements in LP structures (Ned, 2007). This approach is relatively inexpensive to implement, avoids the need to specify tolerable damage and does not depend on a specific threat or abnormal load. It is acceptable that the preventing of progressive collapse should be imperative in all structures, but in fact, the main concern should be disproportionate collapse not progressive collapse.

6.3 IMPROVED TF METHOD

The results of the FE analyses indicate that for the pullout failure mode, maximum strength occurs at $\delta_s / \min(l_b, l_t) \approx 13.5 - 17.4\%$, followed by a steady decrease in the strength of the system up to total collapse at $\delta_s / \min(l_b, l_t) \approx 50\%$. While in bar fracture failure mode, the specimens reach to their maximum strength at $\delta_s / \min(l_b, l_t) \approx 10\%$, followed by sudden

collapse at $\delta_s / \min(l_b, l_t) \approx 13.5 - 17\%$. It can be concluded that specimens with pullout failure mode significantly improve the robustness of precast cross wall structures compared to the specimens with the bar fracture failure mode.

The result shows that for the pullout failure mode following initial yielding in transverse ties and peak pullout force in the longitudinal ties, the longitudinal ties provide more ductility and strength, hence maximum capacity occurs at the deflection slightly more than the deflection representing fracture of the transverse tie. For both failure modes, the improved TF method is presented herein.

6.3.1 Bar Fracture Failure Mode

The result of the tie force in the longitudinal and transverse ties based on the present study, BS Standard, and DoD 2013 is shown in Figure 6.1. The dead and live loads are assumed to be 6.5 and 3.5 kN/m^2 , respectively. The relationship between tie force with load and slab length assuming bar fracture failure mode is shown in Table 6.1 (Chapter 5). Figure 6.1 shows that compare to the TF proposed by DoD 2013 the results of the present study provide the less force for the specimens with a length of less than 5m and a significant discrepancy exists for the specimens with a slab length of more than 6m . Also, the result indicates that the current BS Standard and EC1 code underestimate the tie force requirement.

Table 6-1 Tie force based on bar fracture failure mode

	LTF1	LTF2	LTF3	LTF4	LTF5
$P_l \text{ (kN / m)}$	$1.95wl_b$	$1.92wl_b$	$2.6wl_b$	$3.2wl_b$	$3.16wl_b$
$P_t \text{ (kN)}$	$1.37wl_t l_b$	$1.36wl_t l_b$	$1.65wl_t l_b$	$1.33wl_t l_b$	$1.99wl_t l_b$

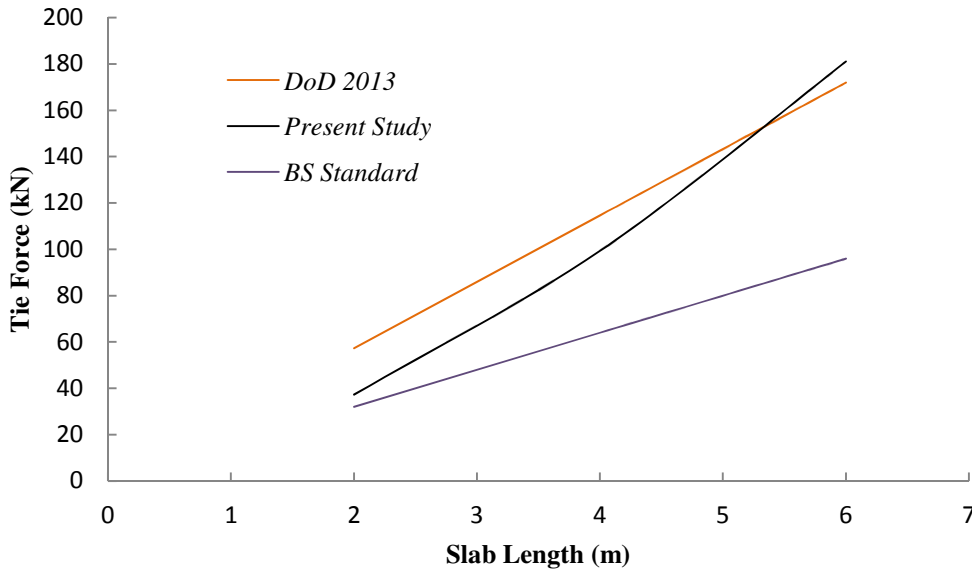


Figure 6.1 Tie-Force versus slab length

According to the results, a nonlinear relationship between tie force and slab length for bar fracture failure mode can be defined:

$$P_l = 1.39wl_b^{1.46} \quad (6.1)$$

Where

P_l = Longitudinal tie force (kN/m)

w = Load combination according to DoD 2013, kN/m^2 ; $w = 1.2D + 0.5L$

D = Dead load (kN/m^2)

L = Live load (kN/m^2)

l_b = Slab length in the direction of longitudinal ties (m)

The result of the analysis for bar fracture failure indicate that the relationship between tie force, load and slab length in the longitudinal tie can be considered linear up to a slab length of 4m; while a high level of nonlinearity exists with the increasing of the slab length (Figure

6.1). Figure 6.2 shows that the tie force versus slab length based on the proposed method i.e. Eq. (6.1) agrees extremely well with the FE results conducted in the present study.

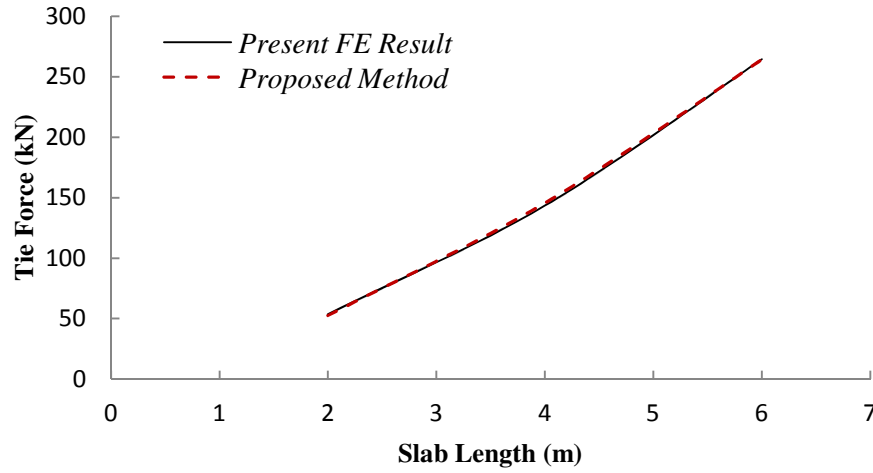


Figure 6.2 Axial force in longitudinal ties based on the proposed method and the FE method

According to the FE result (Table 6.1), the relationship of force in the transverse tie with load, slab length and span length in the transverse direction can be proposed as follows:

$$P_t = 1.1wl_b l_t^{1.32} \quad (6.2)$$

Where

P_t = Transverse tie force (kN)

l_t = Span length in the direction of transverse ties (m)

Figure 6.3 indicates that similarly to the longitudinal ties, a linear relationship exists for a span length of less than 5m; while the tie force is rapidly increased for higher span lengths which indicates that the tie force in both directions follows the same behaviour.

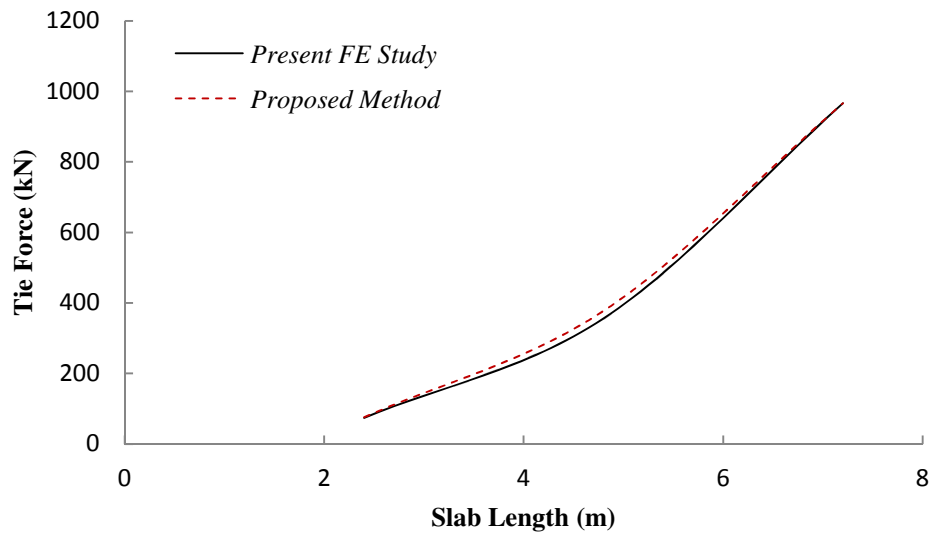


Figure 6.3 Axial force in transverse ties based on the proposed method and an FE approach

The result of the analysis for the tie force in the transverse tie indicates that the equation developed in the present study is significantly less than DoD 2013. It can be attributed to the fact that in practice transverse ties carry the load due to the cantilever and catenary action; while in the present study the effect of cantilever action is ignored.

Table 6-2 Tie force based on pullout failure mode

	LTP1	LTP2	LTP3	LTP4	LTP5
$P_t \text{ (kN / m)}$	$1.85wl_b$	$1.3wl_b$	$2.18wl_b$	$2.27wl_b$	$3.55wl_b$
$P_t \text{ (kN)}$	$1.48wl_t l_b$	$1.04wl_t l_b$	$1.55wl_t l_b$	$1.34wl_t l_b$	$1.49wl_t l_b$

6.3.2 Pullout Failure Mode

Applying the same procedure discussed in section 6.3.1 and using the FE result (Table 6.2), the relationship between force in the longitudinal tie with load and slab length can be proposed as follows:

$$P_t = 0.85wl_b^{1.82} \quad (6.3)$$

In the pullout failure mode, the maximum tie strength sustained by the longitudinal ties is dominated by pullout force; hence to design the required reinforcement bars, the tie force in the longitudinal ties needs to be less than the maximum pullout force obtained in the experimental study (Table 6.3). Furthermore, the embedment length of tie into keyways needs to be less than the values specified in Table 6.3. Furthermore, the compressive strength of the concrete needs to be around 20MPa.

Table 6-3 Pullout specification of different reinforcement bars

Bar size (mm)	Embedment length (mm)	f_c (MPa)	P_{max} (kN)
16	350	20	100
12	250	20	54
10	200	20	34
8	160	20	17.4

According to the FE result, the relationship of force in the transverse ties with load, slab length and span length in the transverse direction can be proposed as follows:

$$P_t = 1.16w l_b l_t^{1.12} \quad (6.4)$$

6.4 ALTERNATE LOAD PATH METHOD (ALP)

As progressive collapse take places in a very short time, it is a dynamic and nonlinear phenomenon and structural elements sustain large nonlinear deformation before collapse. Although to account for energy dissipation, material yielding, large inelastic deformation, cracking and fracture, nonlinear dynamic analysis should be used; but due to lack of structural behaviour data and it being time consuming, evaluation of the results might be quite difficult. Accordingly, for low and mid-rise structures most codes and standards recommend the alternate load path method.

The DoD 2013 states: “the Alternate Load Path (ALP) method is used in two situations: 1) when a vertical structural element cannot provide the required tie strength, the designer may use the ALP method to determine if the structure can bridge over the deficient element after it has been notionally removed, and 2) for Occupancy Category II Option 2, Occupancy Category III (UFC 4-023-03 14 July 2009 Including Change 2 – 1 June 2013), and Occupancy Category IV, the AP method must be applied for the removal of specific vertical load-bearing element”.

In this approach a critical element notionally is removed and then the remaining structure must be capable of transferring load to the undamaged parts through a safe load path and the structure as a whole should be stable. If this element removal cannot be tolerated, the element should be designed as a key element. The British Standard does not provide any provision to consider the dynamic effect of the element removal. It is important to note that in this approach the wall support should be notionally removed one at a time in different locations and storeys.

BS EN 1991-1-7 provides guidance for elements which should be removed and the maximum area which collapse is permitted. The member which ought to be removed one at a time is each load bearing wall, column, or transfer beam. In cross wall structures the nominal removal length for an internal wall is $2.25H$ and for a wall at the corner is H , in which H is the storey height (Fig 6.4). An alternate load path is examined for each removal element on each floor one at a time.

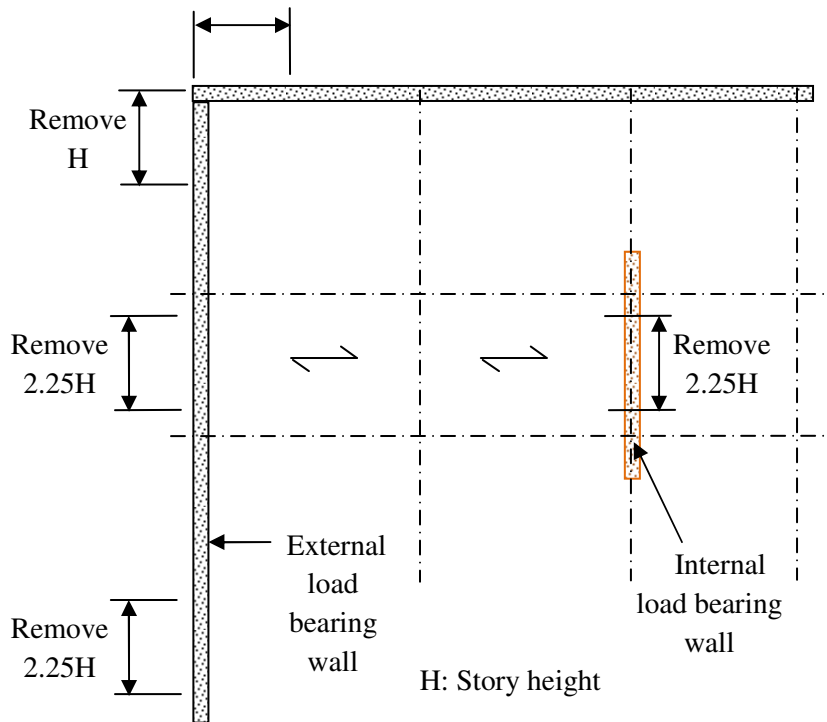


Figure 6.4 Location of external and internal load bearing wall removal (BS EN 1991-1-7:2006)

The procedure and analysis details leading to the numerical method are outlined as follows:

1. An isolated substructure floor-to-floor system is established,
2. A uniformly surface load Q is applied on slabs i.e. $Q = 2(1.2D + 0.5L)$ for static or $Q = 1.2D + 0.5L$ for dynamic analysis, and a line load exerted from an upper floor is considered on the middle gap of the slabs using BS EN1991-1-7 (2006),
3. Translator property is used to define bond strength between ties and concrete as discussed in Chapter 4 and 5,
4. To introduce either bar fracture or pullout failure mode the relevant embedment length according to Table 3.1-3.4 need to be applied,
5. To define boundary condition a stiffness of $90E7 (N / mm) / slab$ is introduced using spring element in ABAQUS,

6. To define material properties of the steel, plastic and for the concrete CDP model as discussed in Chapter 4 and 5 is used,
7. For the initial try, the numbers of ties in longitudinal direction is assumed to be equal to the value of slab length, and cross section of tie in transverse direction is assumed to be equal to cross section of longitudinal ties,
8. The structure is analyzed based on loading type and for each removal element on each floor one at time.
9. The tie forces assess only through catenary action mechanism. For catenary action, tie demand should satisfy Eqs. (2.2), and
10. To prevent progressive collapse structures should provide tie strength and vertical deflection demand in a safe region according to test results of full scale specimens i.e.
 $\delta_s / l_b \geq 10\%$.

Chapter 7

APPROXIMATE ANALYTICAL APPROACH

7.1 INTRODUCTION

Progressive collapse of buildings typically occurs when abnormal loading conditions cause the loss of the structural capacity (not necessarily removal) of one or more critical members, which leads to a chain reaction of failure and ultimately catastrophic collapse. The tensile tie force (TF) method is one of main design approaches for progressive collapse; whereby an indeterminate structure is analyzed statically by assuming a specific failure mode for a partial structure that has been simplified into a determinate structure. As the TF method does not taken into account the effect of bond behaviour and its inherent influencing factors, such as steel-concrete interfacial behaviour; the size and the embedment length of the tie bars; thus it can only give a rough estimation. This has naturally led to a pressing need for a better understanding of bond behaviour; in particular, the post bond-failure behaviour of tie bars in floor-to-floor joints and also to evaluate the adequacy of the TF method.

The main aim of this chapter is to introduce an analytical model to predict behaviour of floor-to-floor system following wall removal concerning pull-out failure mode. The proposed model is then extended to predict capacity of specimens with the bar fracture failure mode. It is to be noted that, the developed model is able to predict accurate behaviour of system in catenary action stage for the specimens with pull-out failure mode while it provide approximate analysis for the plastic stage or small deflection.

In this chapter, the pullout behaviour of reinforcement in grout is firstly analyzed. Then by considering the tie force-pullout displacement relationship with the catenary action mechanism, a comprehensive analytical method to analyze the robustness behaviour of the floor-to-floor joint, containing longitudinal ties in a precast cross-wall structure following the removal of a wall support and for pull-out failure mode, is developed. The proposed approach can be used to analyze floor-to-floor systems with various design loads, slab configurations (equal or unequal span), steel diameters, embedment lengths, the types of ties, and the concrete with different elastic modulus. The reliability of this approach is verified by the experimental results of pullout and full scale floor-to-floor tests undertaken during the present study. The developed model, also, extended to predict approximate progressive collapse resistance of the system using longitudinal and transverse ties.

7.2 MODELLING OF FLOOR-TO-FLOOR SYSTEM UNDER CATENARY ACTION

As stated in the literature, the relationship between tie force and vertical deflection in a catenary action mechanism (Fig. 7.1) considering gravity and line load is given by Eq. (7.1).

$$F_l = \frac{(wl_b + \alpha q)bl_b}{2\delta_s} \quad (7.1a)$$

$$\text{Let } q = wl_b, F_l = (1 + \alpha) \frac{wl_b^2}{2\delta_s} \quad (7.1b)$$

The variables in Eq. (7.1) have been defined in the Chapter 2. Using a free-body diagram of the half system (Fig. 7.1b), for gravity and point load at the middle joint, Eq. (7.1a) is modified as follows:

$$F_l = \frac{(wbl_b + P)l_b}{2n\delta_s} \quad (7.1c)$$

Where P is the point load at the middle joint applied by a screw jack in the test specimen or load from an upper floor; b is the width of the slab and n is the numbers of ties at the joints. For the small deflection (Fig. 7.1c) leads to

$$F_l = \frac{(wbl_b + P)l_b}{2n(d + C)} \quad (7.1d)$$

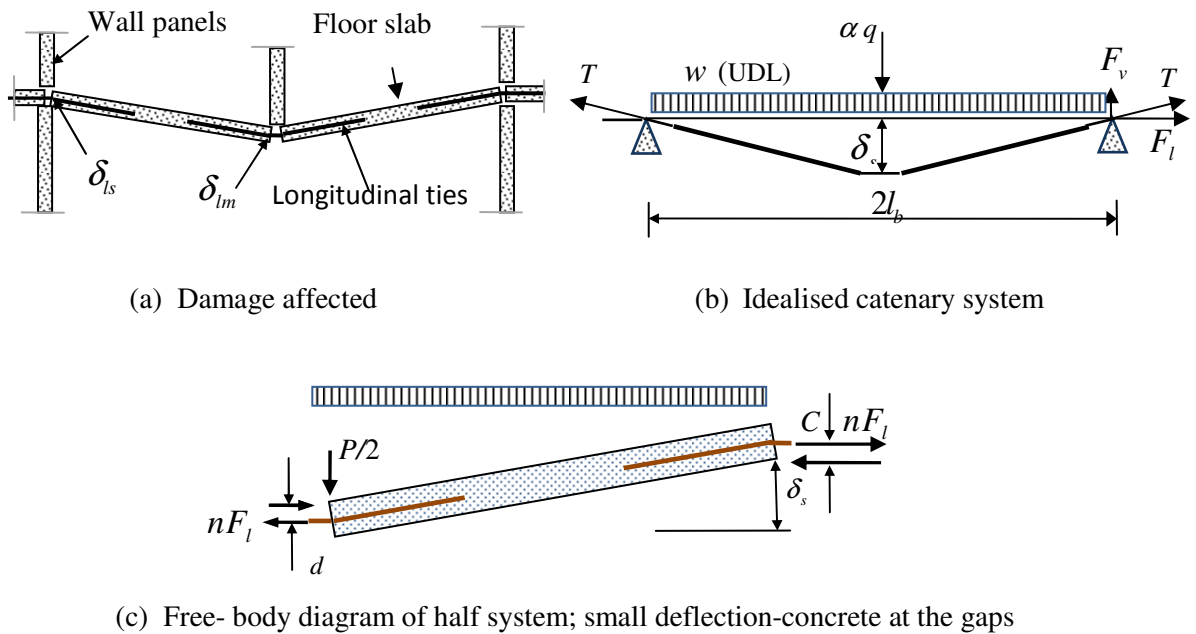


Figure 7.1 Catenary action facilitated by longitudinal ties

Where C=distance between the centre of the reinforcement bar to the bottom of the slab. Based on the compatibility condition of deformation in Fig. 7.1 (b) (PCA, 1979; Moreal, 2009):

$$\delta_l = \sqrt{l_b^2 + \delta_s^2} - l_b \quad (7.2)$$

$$\delta_l = l_b \left(\sqrt{1 + \left(\frac{\delta_s}{\delta_b} \right)^2} - 1 \right) \quad (7.3)$$

$$\frac{\delta_l}{l_b} = \frac{1}{2} \left(\frac{\delta_s}{l_b} \right)^2 \quad \text{if } \left(\frac{\delta_l}{l_b} \right) \ll 1 \quad (7.4)$$

Where δ_l represents the increase in the length of each floor slab, which consists of the extension at both ends of the floor slab. Assuming δ_{ls} and δ_{lm} as the extension at the side and middle joint of one of the affected floor slabs, we have:

$$\delta_l = \delta_{ls} + \delta_{lm} \quad \text{or} \quad \delta_{ls} = \delta_{lm} = \delta_l / 2 \quad (7.5)$$

The failure of the catenary system occurs when the extension reaches a certain level. The corresponding deflection at the joint has often been set as the failure criteria. In pullout failure mode, the tensile force in the tie is usually reduced below the yield stress and therefore most extension is provided by the slip due to the pullout action. It is noted that to satisfy the large deflection requirement for the catenary action mechanism, according to Eqs. (7.1a) and (7.1b), a large extension should be provided at each joint. As a result, it is anticipated that the catenary action will occur in the post-bond-failure stage.

By employing the same process and taking moment around middle joint, tie force for unequal spans (Fig. 7.2) in catenary action can be derived as follows:

$$F_l = (wb_p l_1 l_2 / 2 + \alpha q b_p l_1 l_2 / (l_1 + l_2)) / \delta_s \quad (7.6a)$$

$$\text{Let } q = w(l_1 + l_2) / 2, \quad F_l = (1 + \alpha) \frac{wb_p l_1 l_2}{2\delta_s} \quad (7.6b)$$

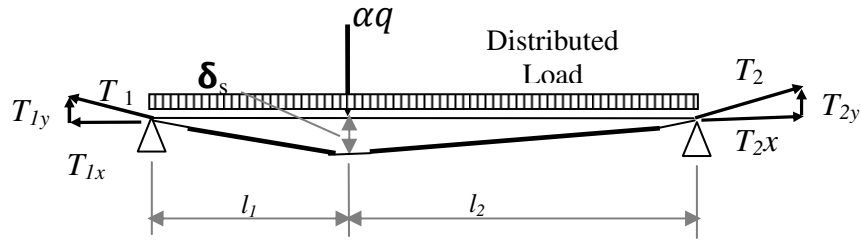


Figure 7.2 Catenary mechanism for unequal span

where l_1, l_2 = Floor span length in the first and second span, respectively. Li et al. (2011) assumed that the tie force of both sides is equal and the entire vertical reaction support is induced only by the vertical component of tie force; hence without considering load exerted from the upper floor the tie force was obtained as follows:

$$F_l = wb_p l_1 l_2 / \delta_s \quad (7.7)$$

It is obvious that only the horizontal components of support reactions are equal and due to the unequal vertical components, the tie force at both ends will be unequal. To verify the two above tie forces i.e. Eq. (7.6), and (7.7), a series numerical analyses with geometrical nonlinearity were conducted, which confirmed the adequacy of Eq. (7.6). Moreover, in the case of $l_1 = l_2$, Eq. (7.7) will be two times of the basic tie force in the catenary mechanism i.e. Eq. (7.1), while Eq. (7.6) provides the same result.

7.3 ULTIMATE DEFORMATION FOR CATENARY ACTION FOR THE TF METHOD

To prevent the failure of a damaged floor onto the lower floors, deflection should be less than a storey height, i.e. around 3m. The limitation on deflection can be theoretically defined based

on BS 8110-1:1997, BS EN 1991-1-7:2006, and DoD (2005) rules with reference to internal ties. The internal ties must sustain a tensile force of P (Chapter 2; Section 2.4.1). It can be seen that in these equations $P_1 > P_2$ if:

$$\frac{(g_k + q_k) l_b}{7.5} > 1 \quad (7.8)$$

$$(g_k + q_k) > \frac{37.5}{l_b} \quad (7.9)$$

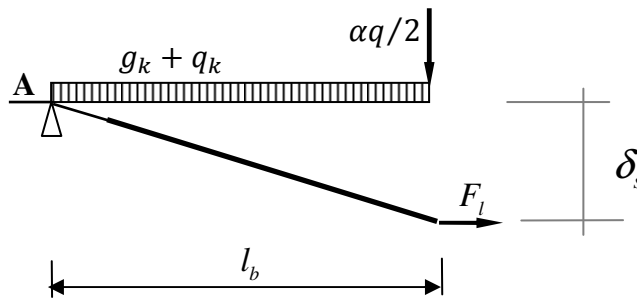


Figure 7.3 Catenary system idealized as a free body

In Figure 7.3, the equilibrium requires that $M_A = 0$, which gives:

$$F_l \delta_s - (g_k + q_k) b l_b \frac{l_b}{2} - \frac{\alpha q b}{2} l_b = 0 \quad (7.10)$$

Where F_l is the tie force at the mid-support; then

$$\delta_s = (g_k + q_k) b \frac{l_b^2}{2F_l} + \frac{\alpha q b l_b}{2F_l} \quad (7.11)$$

By substituting Eq. (2.3a) in Eq. (7.11) assuming that the condition in Eq. (7.9) is valid, gives

$$\delta_s = (g_k + q_k) b \frac{l_b^2}{2(g_k + q_k) b l_b F_t} 37.5 + \frac{\alpha q b l_b}{2(g_k + q_k) b l_b F_t} 37.5 \quad (7.12)$$

The line load exerting from the upper load i.e. q can be defined as follows:

$$q=(g_k+q_k)l_b \quad (7.13)$$

Substituting Eq. (7.13) in Eq. (7.12) and with some re-arrangement gives

$$\delta_s = 18.75(1+\alpha) \frac{l_b}{F_t} \quad (7.14)$$

Assuming α between 0 and 1.5 (Table 2.1) and setting $F_t = 24$, and 60 kN/m for one and 10 storey building, respectively; from Eq. (7.14) the maximum deflection can be defined

$$\delta_s \leq \frac{l_b}{1.28} \quad (7.15a)$$

Using the same procedure for DoD (2013) leads to:

$$\delta_s = \frac{l_b}{6} \quad (7.15b)$$

Equation (7.15a) has provided the upper bounds for the vertical deflection. Based on the results from the pullout and the full scale floor-to-floor joint tests carried out by PCA (1975-1979), it is implied that the catenary action will stop at a deflection greater than $l_r/6.67$ which is agree well with the DoD (2013) requirements and other research study on RC structures (Li et al., 2011; Yi et al., 2008; Jun and Kang, 201; Sasani and Kropelnicki, 2007; He, 2008; Trung, 2010). Furthermore, the present experimental study indicates that in bar fracture failure mode the system is collapsed at $\delta_s \approx l_b/10$. It appears that the discrepancy in the deflection limit between the BS standard with other researches or code prevision is remarkable and BS standard is more relaxed.

7.4 PULLOUT LOAD-DISPLACEMENT SIMULATION

To develop real bond stress distribution along the embedment length of steel bar in concrete, many studies have been conducted in last decades (CEB-FIP, 2000; Abrishami, and Mitchell, 1996; Yankelevski, 1985; Eligehausen et al., 1983; and Nilson, 1972). Due to non-uniformity

of bond stress distribution, to date no comprehensive analytical simulation of bond distribution exists; hence “average bond strength” is used by codes of practice (Abrishami, and Mitchell, 1996). According to current studies, it can be seen clearly that maximum bond stress is much greater than average bond stress. Furthermore, the studies have shown that bond stress distribution greatly changes as pullout displacement develops (Feldman and Bartlett, 2007; Abrishami and Mitchell, 1996; Bertero and Besler, 1968). It has also been shown that average bond stress cannot predict maximum pullout load and it is not suitable for developing a finite-element model (Keuser and Mehlhorn, 1987). According to the result of these studies, Abrishami and Mitchell (1996) developed an analytical method to simulate uniform bond stress distribution using a pullout test, a push-in test and a combination of both.

As a part of this research programme, a close-form solution to predict mechanical and pullout behaviour of reinforcement in concrete is developed. In this solution, a realistic bond-model is used to accurately simulate pullout load-displacement of steel bar under tension. In the bond model, three stages are identified as interfacial bond stress: bonded, partial debonding and fully debonding (frictional) stage (Fig. 7.4). Based on force equilibrium and strain compatibility, pullout load-displacement and bond stress distribution is derived at each stage and the close-form solutions are developed. This study uses a four/five-linear bond slip model; hence the analytical solution would be more complicated (Fig. 7.4).

7.4.1 Four/Five-Linear Bond-slip Model

This analytical solution closely follows the procedure detailed by Ren et al. (2010), Abrishami, H. H. & Mitchell, D (1996), Stocker and Sozen, (1970), and Naaman, et al. (1991); in which the pullout behaviour of rock-bolt, reinforcement bar, strand and plain bar in concrete were derived. However, two main differences exist between the first two studies and the present work: (i) the pullout load-slip relationship of rock bolts is totally different from ribbed bar, (ii) to better simulate the descending stage in load-displacement, the descending

branch of the bond model was divided into three stages (Fig. 7.4); while only one stage was considered by Abrisham and Mitchell (1996), (iii) for the pullout specimen with inclined load, the ascending stage needed to be divided at least into two phases which has not been taken into account in the literature. The proposed model in this paper can be considered as the most comprehensive and generic pullout load-slip simulation to date.

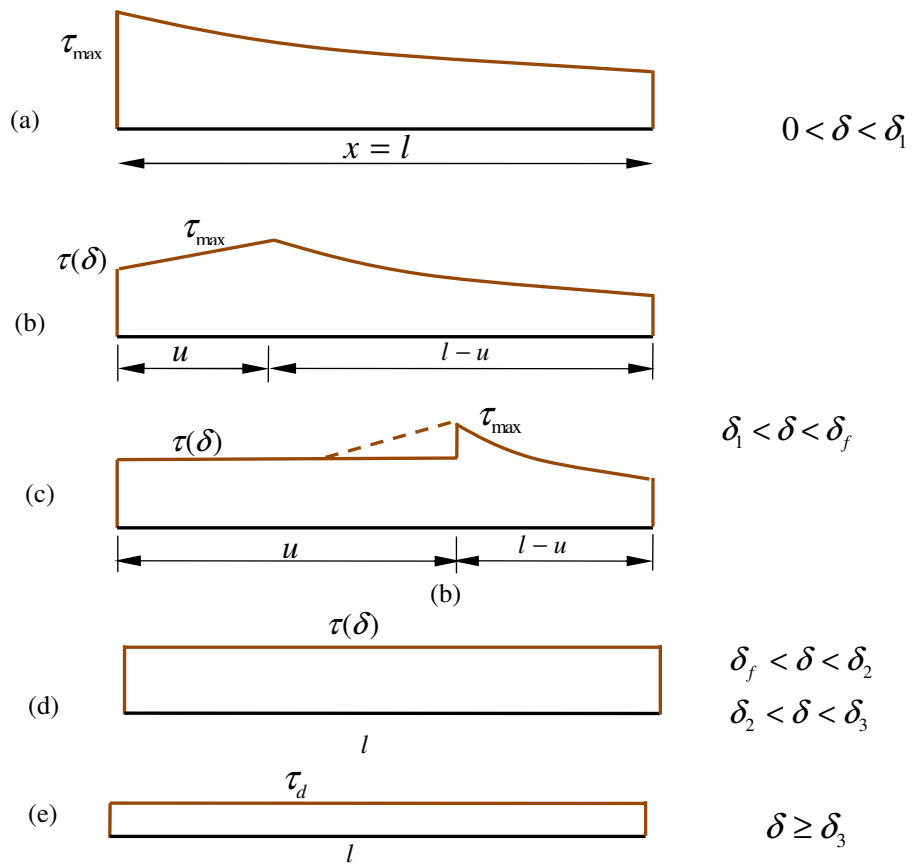


Figure 7.4 Interfacial bond stress distribution along embedment length. (a) Bonded phase; (b, c) elastic–softening phase; (d) elastic–debonding phase; (e) debonding phase

To simplify the bond-slip mechanism and for better use in practical analysis, a linear or bilinear relationship has been suggested by most researchers e.g. the three segments model (Nilson, 1972); the five segments model (Guo and Shi, 2003); and the six segments model (Tassios, 1982). Figure 7.5 demonstrates a mathematical relationship between bond stress and

slip in the present study. This model consists of an ascending stage up to maximum bond stress at (τ_{\max}, δ_1) , followed by a descending (softening) stage down to (τ_f, δ_2) or (τ_d, δ_3) , and finally frictional stage. The four-linear bond-slip model can be assumed as a material property and all the parameters are calibrated from the pullout test results, which will be discussed later in this section.

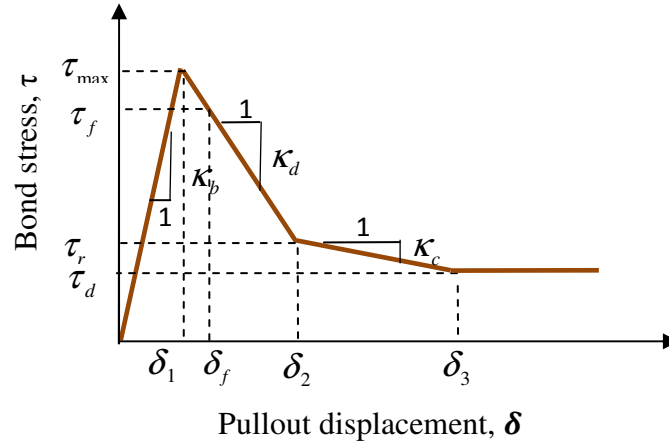


Figure 7.5 Analytical bond-slip model

Let κ_b , κ_d , and κ_c be the slop of the ascending and descending branches, then the four-linear model as shown in Figure 7.5 can be mathematically defined as:

$$\tau = \kappa_b \delta \quad 0 < \delta < \delta_1 \quad (7.16a)$$

$$\tau = \kappa_d \delta + (\kappa_b - \kappa_d) \delta_1 \quad \delta_1 < \delta < \delta_2 \quad (7.16b)$$

$$\tau = \kappa_c \delta + (\kappa_b - \kappa_d) \delta_1 + (\kappa_d - \kappa_c) \delta_2 \quad \delta_2 \leq \delta \leq \delta_3 \quad (7.16c)$$

$$\tau = \tau_d \quad \delta \geq \delta_3 \quad (7.16d)$$

where $\kappa_b = \tau_{\max} / \delta_1$, and $\kappa_d = (\tau_r - \tau_{\max}) / (\delta_2 - \delta_1)$, and $\kappa_c = (\tau_d - \tau_r) / (\delta_3 - \delta_2)$.

7.4.2 Governing Equations for Bond

Since the 1970s, much experimental research has been conducted to predict bond stress along the embedment length of steel bar in concrete; but most test results were reported based on

average bond stress versus slip at the loaded end of specimens (Ren et al, 2010). To develop a generic pullout load versus pullout displacement, the relationship between bond stress and slip between concrete and steel bars at the interface, can be considered as the most fundamental and challenging issue. The mechanics-based relationship between pullout force, bond stress and pullout displacement at the loaded end of the steel bar is necessary in order to understand pullout behaviour of ribbed bars in concrete. In this section, the bond stress distribution along the embedment length will be derived as a function of the applied load and then pullout load versus slip will be developed.

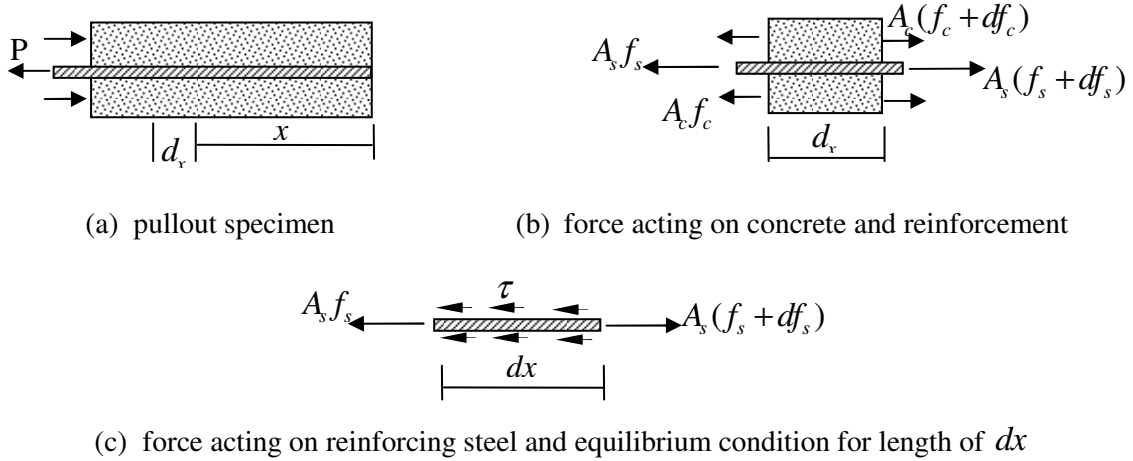


Figure 7.6 Free-body diagrams of pullout specimen

Figure 7.6 illustrates a free-body diagram for a standard pullout specimen and shows applied pullout load P at the loaded end; which is equilibrated by reaction supports on the concrete. The horizontal equilibrium of forces acting on the concrete and steel bar shown in Figure 7.6 (b and c) requires

$$A_c df_c + A_s df_s = 0 \quad (7.17)$$

$$\tau(\pi d_b dx) = A_s (f_s + df_s) - A_s f_s \quad (7.18a)$$

$$\text{or} \quad \frac{df_s}{dx} - \frac{4\tau}{d_b} = 0 \quad (7.18b)$$

where A_c and A_s is area of concrete and steel bar, and f_c and f_s are stress in concrete and steel, respectively; τ =shear stress at the interface, and d_b =bar diameter. Assuming that through the pullout test the steel bar remains linear elastic, the fundamental equation for the reinforcement bar and the interface are

$$\tau = \tau(\delta) \quad (7.19)$$

$$f_s = E_s \frac{du_b}{dx} \quad (7.20)$$

where $\tau(\delta)$ represents the relationship between bond stress τ and local slip δ as shown in Eq. (7.16), and E_s is the Young's modulus of the reinforcement bar. The shear slip δ = relative displacement between steel and concrete at the interface. It is assumed that the shear slip is equal to the displacement of steel at point of x i.e. $u_b = \delta$ (Abrisham and Mitchell, 1996). Substituting Eq. (7.19) and Eq. (7.20) in Eq. (7.18b) gives:

$$\frac{d^2\delta}{dx^2} - k_s \tau = 0 \quad (7.21)$$

Where $k_s = 4/d_b E_s$. Eq. (7.21) is a generic differential equation for bond slip relationship as a function of x . This equation can be separately solved for different branches defined by Eq. (7.16). The slip and bond stress distribution along the embedment length, the axial stress in reinforcement and finally, pullout load-displacement, can be derived using the four-linear model bond-slip defined in Eq. (7.16).

7.4.3 Bonded (Elastic) Stage

For the small pullout load or low bond-stress, perfect bond exists at the interface and thus the behaviour can be considered elastic. This is valid until bond stress reaches τ_{\max} at $x = l$.

Substituting Eq. (7.16a) in Eq. (7.21), the differential equation for the case of $0 \leq \delta \leq \delta_1$ in the elastic stage can be derived

$$\frac{d^2 \delta}{dx^2} - \lambda_1^2 \delta = 0 \quad (7.22)$$

Where $\lambda_1^2 = k_s \kappa_b$. Equation (7.22) is a second-order differential equation in terms of δ . The solution for this type of differential equation is as follows:

$$\delta = A \sinh \lambda_1 x + B \cosh \lambda_1 x \quad (7.23)$$

$$\tau = \kappa_b (A \sinh \lambda_1 x + B \cosh \lambda_1 x) \quad (7.24)$$

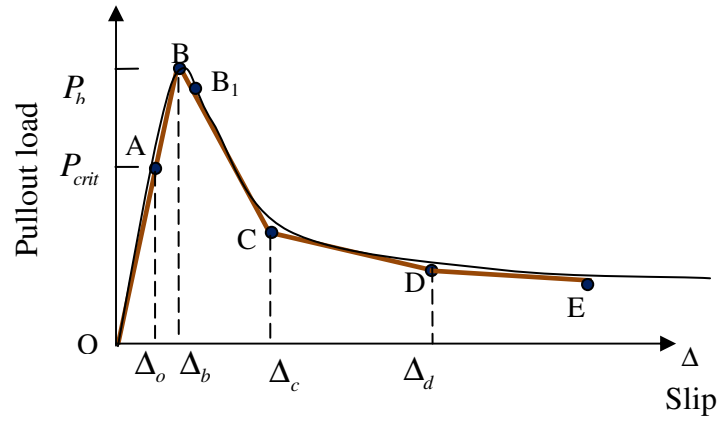


Figure 7.7 Typical non-dimensional pullout load-slip cure

According to the standard pullout test Fig. (7. 6a), the following boundary condition can be considered

$$f_s = 0 \quad \text{at } x = 0 \quad (7.25)$$

$$f_s = \frac{P}{A_s} \quad \text{at } x = l \quad (7.26)$$

Using Eq. (7.20) and applying boundary conditions gives

$$A=0, \quad B = \frac{P}{A_s E_s \lambda_1 \sinh \lambda_1 l} \quad (7.27)$$

By substituting Eq. (7.27) into Eqs. (7.23 and 7.24) the interfacial slip, bond stress and axial stress in the reinforcement bar can be obtained as:

$$\delta = \frac{P}{A_s E_s \lambda_1 \sinh \lambda_1 l} \cosh \lambda_1 x \quad (7.28)$$

$$\tau = \frac{P \kappa_b}{A_s E_s \lambda_1 \sinh \lambda_1 l} \cosh \lambda_1 x \quad (7.29)$$

$$f_s = \frac{P}{A_s \sinh \lambda_1 l} \sinh \lambda_1 x \quad (7.30a)$$

$$F_x = \frac{P}{\sinh \lambda_1 l} \sinh \lambda_1 x \quad (7.30b)$$

As in a common pullout test, pullout displacement at the loaded end is measured and the shear slip at $x = l$ is defined as pullout displacement Δ , Hence the following pullout load-displacement for the bonded stage can be derived as

$$P = A_s E_s \lambda_1 \tanh(\lambda_1 l) \Delta \quad (7.31)$$

The bonded stage is true, while shear stress is less than bond strength τ_{\max} at $x = l$; hence the force at the initiating of the partial debonding stage which induces τ_{\max} is defined as critical force P_{crit} , and it is found to be

$$P_{crit} = \frac{\tau_{\max} A_s E_s \lambda_1}{\kappa_b} \tanh \lambda_1 l \quad (7.32)$$

7.4.4 Elastic-softening Stage

7.4.4.1 Bonded Zone

Substituting Eq. (7.16b) in Eq. (7.21), the differential equation for the case of $0 \leq \delta \leq \delta_1$ can be derived

$$\frac{d^2 \delta}{dx^2} - \lambda_1^2 \delta = 0 \quad (5.33)$$

The solution for this type of differential equation is the same as Eq. (7.23, and 7.24), considering the following boundary condition

$$f_s = 0 \quad \text{at } x = 0 \quad (7.34)$$

$$\delta = \delta_1 \quad \text{at } x = l - u \quad (7.35)$$

Using Eq. (7.20) and applying the above boundary conditions, gives:

$$A=0, \quad B = \frac{\delta_1}{\cosh \lambda_1 (l - u)} \quad (7.36)$$

Substituting Eq. (7.36) in Eqs.(7.23, 7.24) leads

$$\delta = \frac{\delta_1}{\cosh \lambda_1 (l - u)} \cosh \lambda_1 x \quad (7.37)$$

$$\tau = \frac{\kappa_b \delta_1}{\cosh \lambda_1 (l - u)} \cosh \lambda_1 x \quad (7.38)$$

$$f_s = E_s \frac{\delta_1 \lambda_1}{\cosh \lambda_1 (l - u)} \sinh \lambda_1 x \quad (7.39)$$

$$P_e = A_s E_s \frac{\delta_1 \lambda_1}{\cosh \lambda_1 (l - u)} \sinh \lambda_1 x \quad (7.39)$$

7.4.4.2 Softening Zone

$$\frac{d^2 \delta}{dx^2} + \lambda_2^2 \delta = k_s \kappa_d \left(\frac{\kappa_b}{\kappa_d} - 1 \right) \delta_1 \quad \delta_1 < \delta < \delta_f \quad (7.40)$$

Where $\kappa_d = (\tau_f - \tau_{\max}) / (\delta_f - \delta_1)$, and $\lambda_2 = \sqrt{-k_s \kappa_d}$. The solution for this type of differential equation with $\delta_1 < \delta < \delta_f$ is as follows:

$$\delta = C \sin \lambda_2 x + D \cos \lambda_2 x - m \quad (7.41)$$

$$\tau = \kappa_d (C \sin \lambda_2 x + D \cos \lambda_2 x) \quad (7.42)$$

where $m = (\frac{\kappa_b}{\kappa_d} - 1)\delta_1$. According to the standard pullout specimen and considering bond stress distribution (Figs. 7.4c, and 7.5), the following boundary condition can be considered:

$$\delta = \delta_1 \quad \text{at } x = l - u \quad (7.43)$$

$$\delta_1 = C \sin \lambda_2 (l - u) + D \cos \lambda_2 (l - u) - m \quad (7.44)$$

$$f_s = \frac{P}{A_s} \quad \text{at } x = l \quad (7.45)$$

$$\frac{P}{E_s A_s} = C \lambda_2 \cos \lambda_2 l - D \lambda_2 \sin \lambda_2 l \quad (7.46)$$

Solving Eq. (7.44) and Eq. (7.46) gives:

$$C = \left(\frac{\delta_1 + m}{\cos \lambda_2 (l - u)} + \frac{P}{\lambda_2 A_s E_s \sin \lambda_2 l} \right) / (\tan \lambda_2 (l - u) + \cot \lambda_2 l) \quad (7.47)$$

$$D = \left\{ \left(\frac{\delta_1 + m}{\cos \lambda_2 (l - u)} + \frac{P}{\lambda_2 A_s E_s \sin \lambda_2 l} \right) / (\tan \lambda_2 (l - u) + \cot \lambda_2 l) \right\} \cot \lambda_2 l - \frac{P}{\lambda_2 A_s E_s \sin \lambda_2 l} \quad (5.48)$$

By substituting C and D in Eqs. (7.41) and for $x = l$, the load-displacement relationship can be obtained:

$$\Delta = C \sin \lambda_2 l + D \cos \lambda_2 l - m \quad (7.49)$$

The pullout force representing softening zone is obtained using Eq. (5.46)

$$P = E_s A_s [C \lambda_2 \cos \lambda_2 l - D \lambda_2 \sin \lambda_2 l] \quad (7.50)$$

Eq. (7.49) is used to predict pullout load-displacement in the softening stage i.e. ABB₁ branch in Figure 7.7. In the Eq. (7.49) four unknowns i.e. λ_1 , δ_1 , u_b and λ_2 need to be defined. The value of λ_1 can be determined by P / Δ of the pullout load-displacement curve in the bonded stage. Furthermore, once λ is known, κ_b can be found. In the next step δ_1 , u_b and λ_2 should be calculated. They are calibrated using pullout load-displacement of reinforcement bar in grout undertaken in the present study by substituting $P = P_b$ in Eq. (7.50) and (P_b, Δ_b) in Eq. (7.49) at point B. The quantity of u corresponding to the peak load is the value of u that would maximize P based on Eq. (7.50). Thus, for $u = u_b$, we have $(dP / du)_{u=u_b} = 0$.

The above boundary condition results in a nonlinear system of three equations with three unknown variables δ_1 , u_b and λ_2 . To find the quantities of the three unknowns the equation system needs to be solved using an optimization programme named MATLAB.

$$E_s A_s [C \lambda_2 \cos \lambda_2 l - D \lambda_2 \sin \lambda_2 l] - P_b = 0 \quad (7.51a)$$

$$C \sin \lambda_2 l + D \cos \lambda_2 l - m - \Delta_b = 0 \quad (7.51b)$$

$$(dP / du)_{u=u_b} = 0, \quad P = E_s A_s [C \lambda_2 \cos \lambda_2 l - D \lambda_2 \sin \lambda_2 l] \quad \text{and} \quad u = u_b \quad (7.51c)$$

As a control the value of u_b must be between zero and l . Eventually with four parameters λ_1 , δ_1 , u_b and λ_2 the whole bond-shear-stress-slip relationship can be derived and drawn. As it can be seen from above calculation, defining the elastic-softening stage considering partial debonding, leads to a complex analysis. Due to wide range of parameters affecting the progressive collapse resistance, hence the accuracy obtained from the above complex calculation will not lead more safety. Furthermore, Abrishami and Mitchell (1996) suggested that the slop of pullout force-slip relationship in the ascending stage can be assumed constant

up to the peak pullout load; accordingly, to simulated the entire ascending phase in the proposed model Eq. (7.31) is used.

7.4.5 Elastic- debonding Stage

As stated, debonding occurs once $P \geq P_{crit}$ and propagates with the increasing of the applied load of P followed by decreasing of the bond stress. The maximum shear stress is moving towards to the end of the embedment length. With the development of the debonding zone u , the load P is increased due to more interface between steel and concrete, which contributes to resistance against the axial force. Hence, two types of bond stress will exist: a bonded and debonded zone as shown in Figure 7.4. The force in the bonded zone and the debonded zone is defined as P_e and P_d , respectively. Although using the above procedure developed in the elastic-softening stage, pullout load and displacement can be derived as a function of u ; however, as Eq. (7.31) is true for the whole ascending branch, the load-displacement is only developed for the descending branch of bond stress-slip. The governing differential equation for bond in the descending zone is:

$$\frac{d^2 \delta}{dx^2} + \lambda_2^2 \delta = k_s \kappa_d \left(\frac{\kappa_b}{\kappa_d} - 1 \right) \delta_1 \quad \delta_1 < \delta < \delta_2 \quad (7.52)$$

where $\kappa_d = (\tau_r - \tau_{max}) / (\delta_2 - \delta_1)$, and $\lambda_2 = \sqrt{-k_s \kappa_d}$. The solution for this type of differential equation is as follows

$$\delta = C \sin \lambda_2 x + D \cos \lambda_2 x - m \quad (7.53)$$

$$\tau = \kappa_d (C \sin \lambda_2 x + D \cos \lambda_2 x) \quad (7.54)$$

where $m_d = (\frac{\kappa_b}{\kappa_d} - 1)\delta_1$. According to the standard pullout specimen (Fig. 7.4a), the following

boundary condition can be considered:

$$f_s = 0 \quad \text{at } x = 0 \quad (7.55)$$

$$f_s = \frac{P}{A_s} \quad \text{at } x = l \quad (7.56)$$

Using Eq. (7.20) and applying the boundary conditions leads:

$$C = 0, \quad D = -\frac{P}{\lambda_2 A_s E_s \sin \lambda_2 l} \quad (7.57)$$

By substituting Eq. (7.57) into Eqs. (7.53), and (54) the interfacial slip, bond stress, and axial stress in the reinforcement bar can be obtained

$$\delta = -\frac{P}{\lambda_2 A_s E_s \sin \lambda_2 l} \cos \lambda_2 x - m \quad (7.58)$$

$$\tau = -\frac{P \kappa_d}{\lambda_2 A_s E_s \sin \lambda_2 l} \cos \lambda_2 x \quad (7.59)$$

$$f_s = \frac{P}{A_s \sin \lambda_2 l} \sin \lambda_2 x \quad (7.60)$$

Using Eq. (7.58) and $\delta = \Delta$, the following pullout load-displacement for the debonded stage in branch BC can be derived

$$P = -A_s E_s \lambda_2 \tan(\lambda_2 l) [\Delta + m] \quad (7.61)$$

Using the same procedure for the branch CD in Figure 7.7 gives

$$\frac{d^2 \delta}{dx^2} + \lambda_3^2 \delta = k_s \kappa_c [(\frac{\kappa_d}{\kappa_c} - 1)\delta_2 + \frac{\kappa_b - \kappa_d}{\kappa_c} \delta_1] \quad \delta_2 < \delta < \delta_3 \quad (7.62)$$

Where $\kappa_c = (\tau_d - \tau_r) / (\delta_3 - \delta_2)$, and $\lambda_3 = \sqrt{-k_s \kappa_c}$, and $m_c = (\frac{\kappa_d}{\kappa_c} - 1)\delta_2 + \frac{\kappa_b - \kappa_d}{\kappa_c} \delta_1$.

By substituting λ_3 and m_2 , Eq. (7.61) can be used to simulate the pullout force-slip relationship in branch CD.

7.4.6 Debonding Stage

If u reaches the entire length of the embedment length, the softening zone disappears and the fully debonding phase develops. In the branch CD, purely frictional bond shear stress at the interface between the reinforcement bar and the concrete is presented and load is solely carried by the interface friction. The pullout displacement at the point D (Fig. 7.7) can be calculated from Eq. (7.58) at the end of softening-debonding phase, the governing differential equation for bond in this zone is:

$$\frac{d^2 \delta}{dx^2} - k_s \tau_f = 0 \quad (7.63)$$

Solving differential Eq. (7.63) leads

$$\delta = \frac{1}{2} k_s \tau_d x^2 + ax + b \quad (7.64)$$

According to the standard pullout test Fig. 7.6a, the following boundary condition can be applied

$$f_s = 0 \quad \text{at } x = 0 \quad (7.65)$$

$$f_s = \frac{P}{A_s} \quad \text{at } x = l - \Delta \quad (7.66)$$

Using Eq. (7.20) and applying the boundary conditions leads

$$a = 0, \quad \frac{P}{A_s} = E_s k_s t_d (l - \Delta) \quad (7.67)$$

Substituting $k_s = 4 / (E_s d_b)$ in Eq. (7.67) gives

$$P = \pi d_b \tau_d [l - \Delta] \quad , \quad \Delta \geq \Delta_0 \quad (7.68)$$

The displacement at the beginning of the frictional zone, denoted by Δ_o , can be assumed as slip at the end of previous phase

$$\Delta_o = \delta_3 \quad (7.69)$$

At the frictional stage, the pullout-displacement Δ varies from Δ_0 to l when the reinforcement bar is entirely pulled out. In the case of increasing another branch before the fully frictional stage i.e. DE, Eqs. (7.58-7.61) can be used by assuming

$m_e = (\frac{\kappa_c}{\kappa_e} - 1)\delta_3 + \frac{\kappa_b - \kappa_d}{\kappa_e}\delta_1 + \frac{\kappa_d - \kappa_c}{\kappa_e}\delta_2$. Furthermore, in the case of using two branches in the ascending stage (Fig. 7.8) the bond slip can be defined as follows:

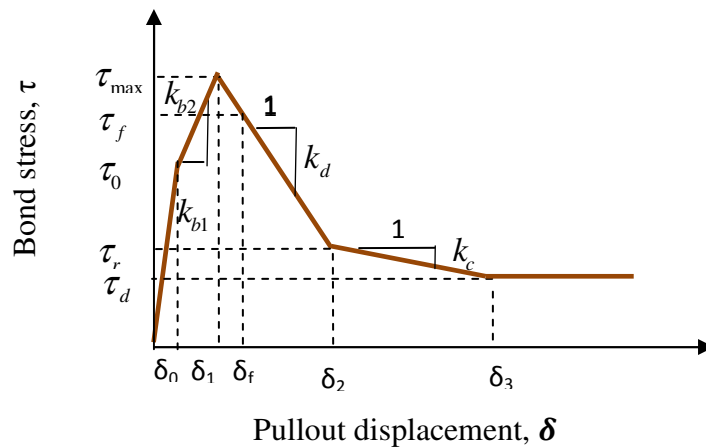


Figure 7.8 Analytical bond-slip model-two branch in the ascending stage

$$\tau = \kappa_{b1} \delta \quad 0 < \delta < \delta_0 \quad (7.70a)$$

$$\tau = \kappa_{b_2} \delta + (\kappa_{b_1} - \kappa_{b_2}) \delta_o \quad \delta_0 < \delta < \delta_1 \quad (7.70b)$$

$$\tau = \kappa_d \delta + (\kappa_{b1} - \kappa_{b2}) \delta_0 + (\kappa_{b2} - \kappa_d) \delta_1 \quad \delta_1 \leq \delta \leq \delta_2 \quad (7.70c)$$

$$\tau = \kappa_c \delta + (\kappa_{b_2} - \kappa_d) \delta_1 + (\kappa_d - \kappa_c) \delta_2 \quad \delta_2 \leq \delta \leq \delta_3 \quad (7.70d)$$

$$\tau = \tau_d \quad \delta \geq \delta_3 \quad (7.70e)$$

Where $\kappa_{b1} = \tau_0 / \delta_0$ and $\kappa_{b2} = (\tau_{\max} - \tau_0) / (\delta_1 - \delta_0)$, $\kappa_d = (\tau_r - \tau_{\max}) / (\delta_2 - \delta_1)$ and

$$\kappa_c = (\tau_d - \tau_r) / (\delta_3 - \delta_2), m_{b2} = \left(\frac{\kappa_{b1}}{\kappa_{b2}} - 1 \right) \delta_0, m_d = \left(\frac{\kappa_{b2}}{\kappa_d} - 1 \right) \delta_1, m_c = \left(\frac{\kappa_d}{\kappa_c} - 1 \right) \delta_2 + \frac{\kappa_{b2} - \kappa_d}{\kappa_c} \delta_1.$$

Using the same procedure of branch BC, the pullout-slip relationship in the second ascending stage in Figure 7.8 can be obtained

$$P = A_s E_s \lambda_2 \tan(\lambda_2 l) [\Delta + m] \quad (7.71)$$

The outstanding of the developed model is that, it explicitly defines the pullout-slip relationship in the various stages and it can be applied for any number of branches in the bond stress-slip model, which shows significant discrepancies with the current model in the literature.

7.4.7 Pullout Load-Slip Calibration

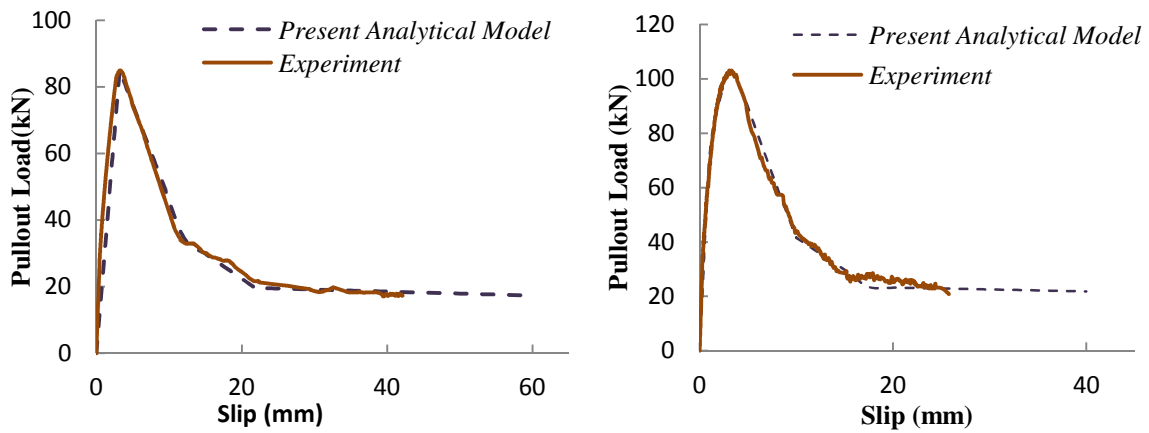
The load-displacement relationship is calibrated using the experimental pullout test results at control point B (P_b, Δ_b), C (P_c, Δ_c) and D (P_d, Δ_d) in Figure 7.7. According to the pullout test results, the ascending branch can be assumed linear with the slope of

$$\frac{P}{\Delta} = A_s E_s \lambda_1 \tanh(\lambda_1 l) \quad (7.72)$$

P/Δ can be obtained from the load-displacement curve at the point B (P_b, Δ_b); hence using Eq. (7.72) λ_1 and then κ_b can be obtained. Substituting P_b, Δ_b and P_c, Δ_c in Eq. (7.61), results in a nonlinear system of two equations with the two unknown variables δ_1 and κ_d . Following the same procedure, by substituting P_c, Δ_c and P_d, Δ_d in Eq. (7.61), δ_2, κ_c can be obtained. If

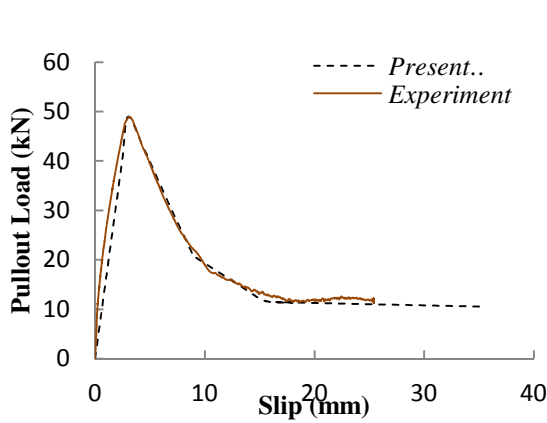
the bond stress model is to be divided into more branches, a similar procedure can be applied to calculate δ_i and κ_i . Maximum bond stress, τ_{\max} , can be obtained by substituting k_b and δ_1 in Eq.(7.16a) and then P_{crit} , which represents pullout load when $\tau = \tau_{\max}$ can be obtained. Pullout displacement at the beginning of the flat branch δ_3 can be obtained using the bond stiffness of the previous branch of the bond stress model. The bond stress at the beginning of the flat branch is calculated by $\tau_d = P / \pi d_b (l - \Delta_o)$.

In this section, the above calibration procedure is used to simulate pullout load-displacement and the bond-displacement relationship for the three pullout tests using bar size of 16 mm, 12 mm and 10 mm into grouted keyways of precast concrete, conducted in the present study. The material and geometrical properties of the specimens with the relevant experimental result are given in Chapter 3. The developed method can be used to predict the pullout behaviour of steel bar and bond stress distribution along the embedment length. The pullout force-displacement for the test results and analytical simulation is shown in Figure 5.9. The analytical results were found to be very close to those of the pullout test result for all specimens. The results clearly indicate that, for the bond-slip with 5 branches the pullout-slip simulation is closer to the pullout test results of specimens with inclined angle of load (Fig. 7.9b).

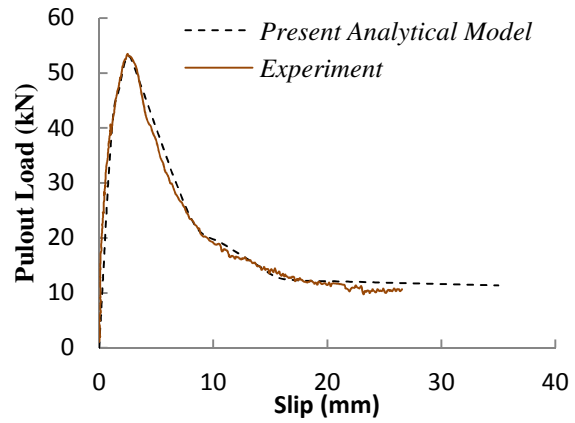


(a) $\phi 16$ mm, $L_d=350$ mm- $\alpha=0$ -using four segments bond slip

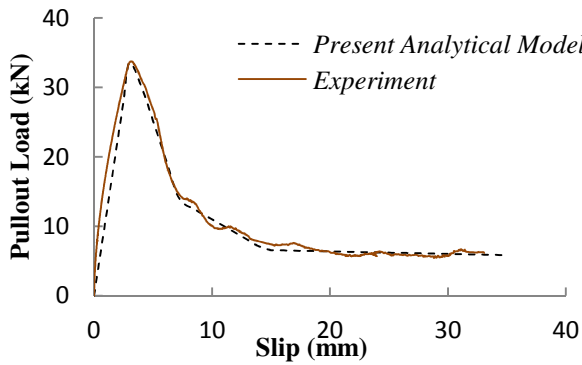
(b) $\phi 16$ mm, $L_d=350$ mm, $\alpha=9^\circ$ - using five segments bond slip



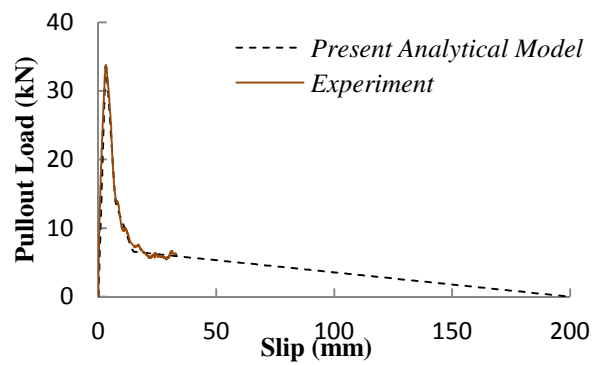
(c) $\phi 12$ mm, $L_d=250$ mm- using four segments bond slip



(d) $\phi 12$ mm, $L_d=250$ mm, $\alpha=90^\circ$ - using five segments bond slip



(a) $\phi 10$ mm, $L_d=200$ mm- using four segments bond slip-large scale



(b) $\phi 10$ mm, $L_d=200$ mm- using four segments bond slip-full scale

Figure 7.9 Comparison between pullout load-displacement based on analytical and pullout test results

The bond-slip parameters using the above simulation are shown in Table 7.1 and the bond stress-slip relationship for all three bars is shown in Figure 7.10. Figure 7.10 indicate that, a generic bond-displacement relationship can be developed which can be used to predict the pullout behaviour of reinforcement bar with different embedment lengths and bar sizes, when the embedment length is less than the anchorage length.

Table 7-1 Bond stress-slip properties for three different specimens, $f_c = 20\text{MPa}$, $\alpha = 0$

Bar Size (mm)	Displacement (mm)			Bond stress (MPa)			Bond Stiffness (MPa/mm)			λ_i		
	δ_1	δ_2	δ_3	τ_{\max}	τ_r	τ_d	κ_b	κ_d	κ_c	λ_b	λ_d	λ_c
$\phi 10$ mm	2.86	7.2	15	5.60	2.27	1.13	1.87	-0.79	-0.155	0.00193	0.0012	0.0006
$\phi 12$ mm	2.8	9.5	16	5.43	2.18	1.3	1.84	-0.51	-0.19	0.00175	0.00089	0.00050
$\phi 16$ mm	2.97	12	23	5.23	1.99	1.1	1.63	-0.32	-0.085	0.00142	0.00063	0.00033

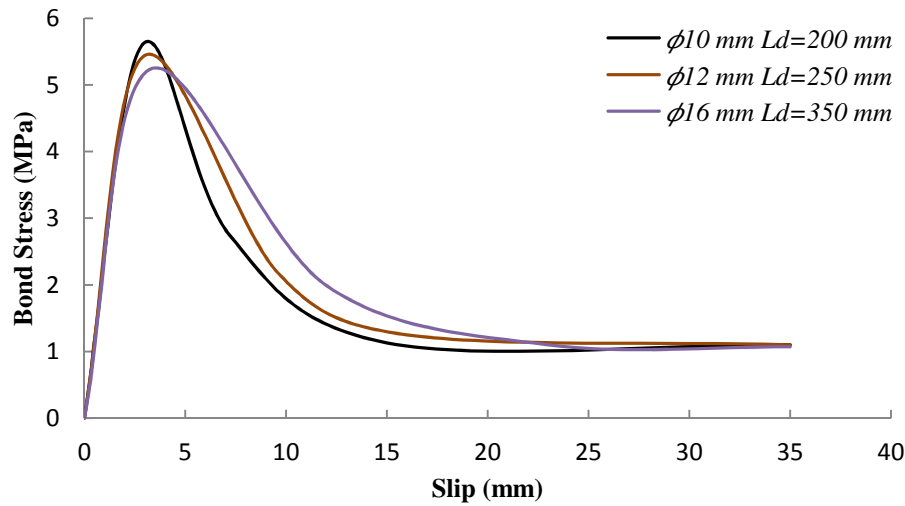


Figure 7.10 Bond stress versus pullout displacement for three specimens

Furthermore, the developed model is able to calculate the anchorage length of bar in concrete by substituting pullout load with $P_y = A_s f_y$ in an ascending branch.

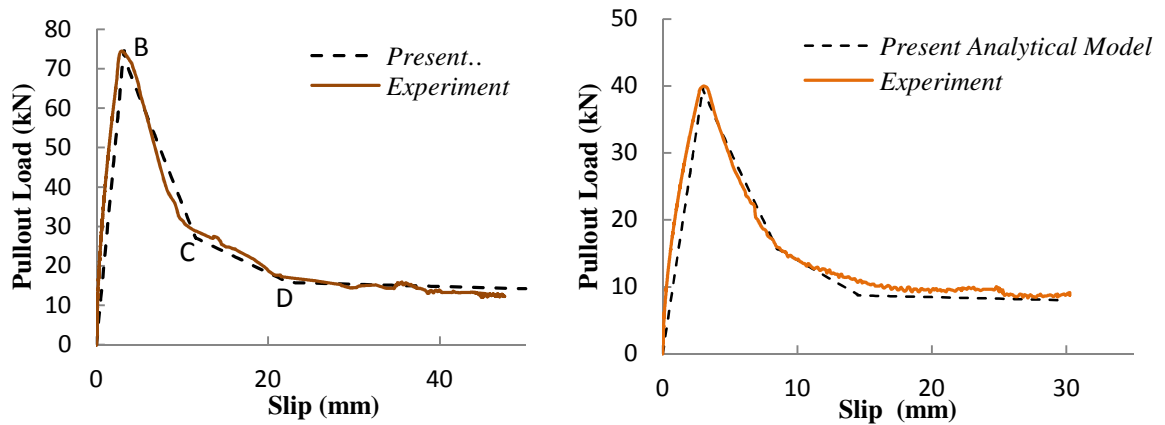
$$l_{db} = \frac{1}{\lambda_1} \tanh^{-1} \left(\frac{f_y}{E \lambda_1 \Delta} \right) \quad (7.73a)$$

As Eq. (7.73) obtained based on compressive strength of 20MPa, for concrete with the other compressive strengths, it should be modified

$$l_{db} = \frac{1}{\lambda_1} \tanh^{-1} \left(\frac{f_y}{E \lambda_1 \Delta} \right) / \sqrt{f_c / 20} \quad (7.73b)$$

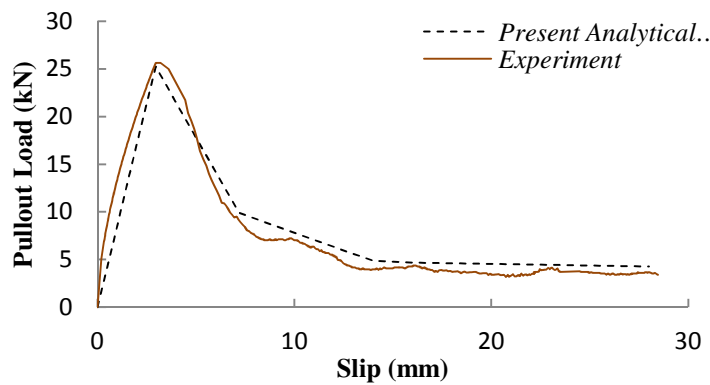
According to Eq. (7.73) and the pullout test results, the anchorage length l_{db} for the bar size of 10mm, 12mm, and 16 mm are 261.56 mm, 369.43 mm, and 512.74 mm, respectively. According to the tensile test conducted in the present study, the average yield stress of three specimens was 515, 547, and 555 MPa, respectively. To show the efficiency of Eq. (7.73), a comparison has been made with the pullout test results in Chapter 3. The experimental results show that the bars fractured when the embedment length for the same bar size of 10, 12 and 16 mm was 250 mm, 400 mm, and 500 mm, respectively. According to EC2 the ultimate anchorage bond length in a good condition and concrete with $f_c = 20\text{MPa}$, for bar sizes of 10mm, 12mm and 16 mm are 371mm, 475 mm and 696 mm, respectively. The experiment results show a safety factor of 1.3 on the anchorage length. Hence, to provide sufficient pullout displacement in the catenary action mechanism, the embedment length needs to be less than the anchorage length of EC2 e.g. $L_d \leq 0.6l_{db}$; where l_{db} is the basic anchorage length for good conditions.

It is obvious that calibrated bond parameters can be used for different bar sizes with various embedment lengths. In the other word, bond parameters such as δ_1 , δ_2 , δ_3 , κ_b , κ_d and κ_c can be applied for steel bars with different embedment lengths. To show the applicability of the proposed method, the developed bond-slip was used to predict the pullout behaviour of reinforcement bars with different embedment lengths. As a result, by adjusting pullout displacement at the control points of B, C and D, the pullout load-displacement of the reinforcement bar with various embedment lengths was obtained. Figure (7.11) indicates that the results of analytical model agree well with experimental study using the various embedment lengths. It can be concluded that this method is capable of studying the entire pullout behaviour of different bar sizes with various embedment lengths.



(a) $\phi 16$ mm, $L_d=300$ mm- using four segments
bond slip

(b) $\phi 12$ mm, $L_d=200$ mm- using four segments
bond slip



(c) $\phi 10$ mm, $L_d=150$ mm- using four segments bond slip

Figure 7.11 Comparison of pullout load-displacement between analytical and pullout test results

The pullout load-slip for different bar sizes and bar size of 12 mm with various embedment lengths are shown in the Figures 7.12 and 7.13, respectively.

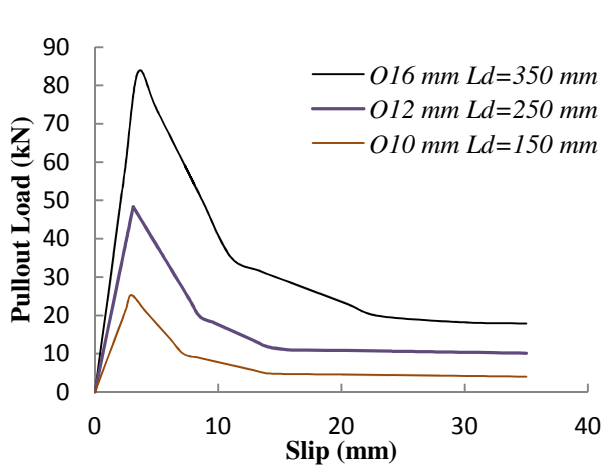


Figure 7.12 Pullout load-displacement relationship for three different reinforcement bars based on an analytical model

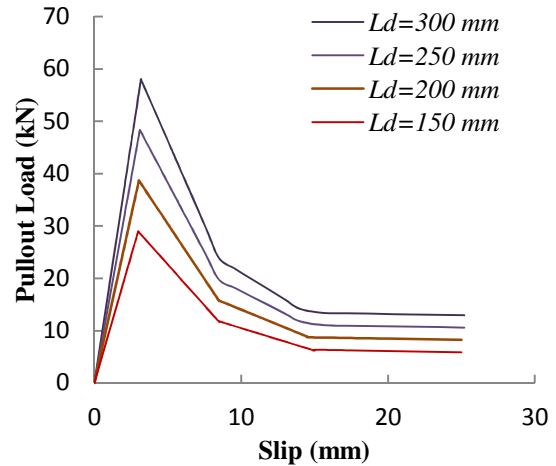


Figure 7.13 Pullout load-displacement relationship for bar size of 12 mm with different embedment lengths based on an analytical model

7.5 ANALYSIS OF FLOOR-TO-FLOOR SYSTEM WITH LONGITUDINAL TIES

The assembly was considered to represent a portion of floor system that is affected by the loss of wall support. It includes one pair of floor units spanning on two adjacent spans in the longitudinal direction (Fig. 7.14), which consists of two hollow-core planks with the dimension of $l_b \times 1200 \times 150\text{mm}$. This assembly provides two or three keyways, where straight steel bars can be placed as longitudinal ties (Fig. 7.14).

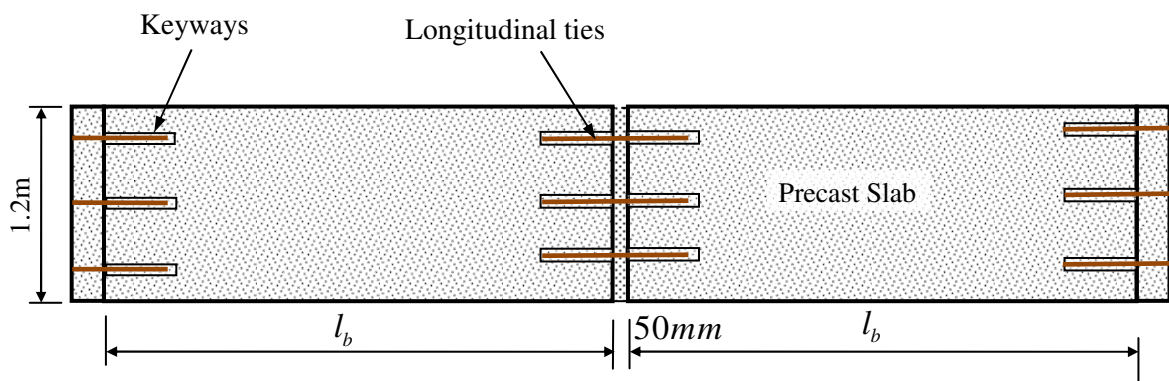


Figure 7.14 Floor-to-floor system facilitated by longitudinal ties.

Experimental and FE studies conducted in the present study clearly indicates that, following the initial crack at the middle joint and from the very beginning i.e. at $\delta_s/l_b=0.15$, floor slabs act as two totally rigid bodies connected by longitudinal tie bars at the joints (Fig. 7.14); hence it can be concluded that, following wall removal at the middle joint, it is pullout behaviour of longitudinal ties which governs the behaviour of floor-to-floor joint.

By considering the tie force-slip relationship developed in the first part together with the catenary action mechanism, for the first time, a comprehensive analytical method is developed considering both pullout and bar fracture failure mode. In this study, two possible failure modes of tie bars are expected to attain, i.e. the pull-out failure (group A) and the bar fracture (group B); both group shows the same failure mode (Chapter 3). Also, to investigate the contribution of concrete at the joints the analytical model is developed for both cases of specimens with and without concrete at the gaps.

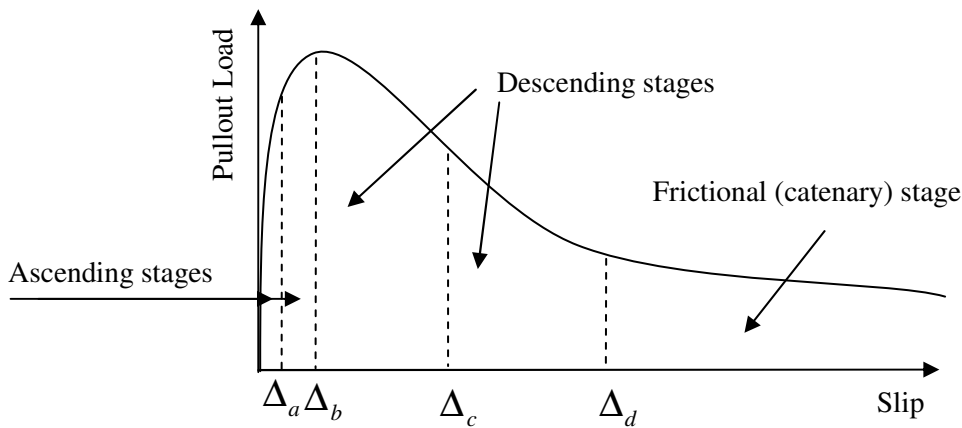


Figure 7.15 Assumed tie force-deflection relationship

7.5.1 Pullout failure mode (group A)

Experimental study (Chapter 3) indicates that, pullout behaviour of steel bars into concrete experiences three different stages i.e. ascending, descending and frictional stage (Fig. 7.15). To analyze a floor-to-floor system when a support wall is removed (Fig 7.1), all three

different stages are taken into consideration. Figure 7.15 shows a typical load-middle joint deflection corresponding to the different stages.

7.5.1.1 Cast-in-suit concrete grout in the gap and keyways

Ascending stages: For the ascending stages it is assumed that two slab at the joint are connecting to each other at the middle gap while the system undergoing small deflection or prior to yielding or peak pullout force of tie bars. Replacing tie force in Eq. (7.1d) by pullout force in the first ascending stage i.e. $P = A_s E_s \lambda_1 \tanh(\lambda_1 l) \Delta$ gives

$$A_s E_s \lambda_1 \tanh(\lambda_1 l) \Delta = \frac{(wbl_b + P)l_b}{2n(d + C)} \quad 0 \leq \Delta \leq \Delta_a \quad (7.74)$$

Rearrangement in Eq. (7.74) leads to

$$(wbl_b + P) = \frac{2n(d + C)A_s E_s \lambda_1 \tanh(\lambda_1 l) \Delta}{l_b} \quad 0 \leq \Delta \leq \Delta_a \quad (7.75)$$

Also, substituting pullout force in the second ascending stage i.e.

$P = F_l = A_s E_s \lambda_2 \tanh(\lambda_2 l) [\Delta + m_2]$ in Eq. (7.1d) gives

$$(wbl_b + P) = \frac{2n(d + C)A_s E_s \lambda_2 \tanh(\lambda_2 l) [\Delta + m_2]}{l_b} \quad \Delta_a \leq \Delta \leq \Delta_b \quad (7.76)$$

Deflection prior catenary stage: For the specimen with concrete at the gap, the middle joint deflection is induced by slip of tie bars placed into the keyways of slabs. According to full scale test result, the deflection mode of full scale test is taken into account to propose a simple but reliable relationship between slip and deflection using Fig. 7.77. The reliability of Eq. (7.77) was verified by the full scale test results (Appendix 3C).

$$\frac{\delta_s}{l_b} = \frac{\Delta}{d} \quad (7.77)$$

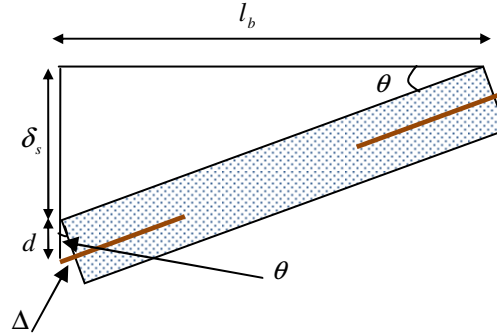


Figure 7.16 Deflection mode of full scale tests

Descending stage: Experimental study (Chapter 3) indicates that, for the specimens with concrete at the joints the catenary action is established at $\delta_s = 0.12l_b$, which is corresponding to slip of 8-10 mm. The analytical model developed in the section 7.4 indicated that, approximately for all bar sizes the frictional stage is started at slip of more than 9-10mm. It can be concluded that, the catenary action mechanism is approximately induced slightly prior to the frictional stage; hence to define behaviour of floor-to-floor system corresponding to the descending stage the same method of small deflection should be applied for both descending stages. Substituting pullout force in the descending stages developed in the section 7.4 i.e. $P = F_l = -A_s E_s \lambda_i \tan(\lambda_i l) [\Delta + m_i]$ in Eq. (7.1d) gives

$$(wbl_b + P) = \frac{-2n(d + C)A_s E_s \lambda_i \tan(\lambda_i l) [\Delta + m_i]}{l_b} \quad i = 2, 3 \quad \Delta_b \leq \Delta \leq \Delta_d \quad (7.78)$$

Ctenary action (frictional) stage: For the specimens with pullout failure mode at the large deflection, the load is sustained through catenary action mechanism. As stated catenary action

is induced in frictional stage, hence replacing F_l in Eq. (7.1a) by pullout force in frictional stage $P = n\pi d_b \tau_f [l - \Delta]$ leads

$$(wbl_b + P) = \frac{2n\pi d_b \tau_d [l - \Delta]}{l_b} (\delta_s) \quad \Delta \geq \Delta_d \quad (7.79)$$

Substituting $\Delta = \frac{\delta_l}{2} = \frac{l_b}{4} \left(\frac{\delta_s}{l_b} \right)^2$ in Eq. (7.79) and rearranges leads to

$$\delta_s^3 - 4l_b^3 \delta_s + \frac{2(wbl_b + P)l_b^3}{n\pi d_b \tau_f} = 0 \quad (7.80)$$

7.5.1.2 Cast-in-suit concrete grout in the keyways only

Ascending stages: for the specimen without concrete at the gap i.e. FT4, the catenary action mechanism governs the behaviour of system in all ascending, descending, and frictional stages. Substituting pullout force model i.e. $P = A_s E_s \lambda_1 \tanh(\lambda_1 l) \Delta$ in Eq. (7.1c) gives:

$$A_s E_s \lambda_1 \tanh(\lambda_1 l) \Delta = \frac{(wbl_b + P)l_b}{2n\delta_s} \quad (7.81)$$

$$\text{Let } \frac{\Delta}{l_b} = \frac{1}{4} \left(\frac{\delta_s}{l_b} \right)^2, \quad (wbl_b + P) = \frac{nA_s E_s \lambda_1 \tanh(\lambda_1 l) \delta_s^3}{2l_b^2} \quad (7.82)$$

A rearrangement in Eq. (7.82) leads to:

$$\delta_s = \sqrt[3]{\frac{2wbl_b^3}{nA_s E_s \lambda_1 \tanh(\lambda_1 l)}} \quad 0 \leq \Delta \leq \Delta_a \quad (7.83)$$

Also, substituting pullout force in the second ascending stage i.e. $P = F_l = A_s E_s \lambda_2 \tanh(\lambda_2 l) [\Delta + m_2]$ in Eq. (7.1c) gives

$$A_s E_s \lambda_i \tan(\lambda_i l) [\Delta + m_2] = \frac{(wbl_b + P)l_b}{2n\delta_s} \quad \Delta_a \leq \delta_s \leq \Delta_b \quad (7.84)$$

Replacing slip with deflection using Eq. (7.4) i.e. $\Delta = \delta_l / 2$

$$(\delta_s) \left[\frac{l_b}{4} \left(\frac{\delta_s}{l_b} \right)^2 + m_2 \right] = \frac{(wbl_b + P)l_b}{2nA_s E_s \lambda_2 \tan(\lambda_2 l)} \quad (7.85)$$

$$(wbl_b + P) = \frac{2nA_s E_s \lambda_2 \tan(\lambda_2 l)}{l_b} (\delta_s) \left[\frac{l_b}{4} \left(\frac{\delta_s}{l_b} \right)^2 + m_2 \right] \quad (7.86)$$

For gravity load only, Eq. (7.86) can be simplified

$$\delta_s^3 + m_2 4l_b \delta_s - \frac{2wbl_b^3}{nA_s E_s \lambda_2 \tanh(\lambda_2 l)} = 0 \quad (7.87)$$

Descending stage: For all descending stages, replacing the relevant pullout force i.e.

$P = -A_s E_s \lambda_i \tan(\lambda_i l) [\Delta + m_i]$ by F_l in Eq. (7.1c) leads to

$$-A_s E_s \lambda_i \tan(\lambda_i l) [\Delta + m_i] = \frac{(wbl_b + P)l_b}{2n\delta_s}, i = 3, 4 \quad (7.88)$$

Substituting Eq. (7.4) i.e. $\Delta = \delta_l / 2$ in Eq. (7.88) gives

$$\delta_s \left[\frac{l_b}{4} \left(\frac{\delta_s}{l_b} \right)^2 + m_i \right] = -\frac{(wbl_b + P)l_b}{2nA_s E_s \lambda_i \tan(\lambda_i l)}, i = 3, 4 \quad (7.89)$$

For only gravity load, Eq. (7.89) can be simplified as

$$\delta_s^3 + m_i 4l_b \delta_s + \frac{2wbl_b^3}{nA_s E_s \lambda_i \tan(\lambda_i l)} = 0, i = 3, 4 \quad (7.90)$$

Eq. (7.90) is used for all descending branches by applying relevant λ and m .

Ctenary action (frictional stage): in the catenary stage both cases shows the same behaviour, hence Eq. (7.79-7.80) can be directly applied.

7.5.2 Bar fracture failure mode (group B)

The developed method for ascending stage Eqs.(7.74) can be used to analyse floor-to-floor system assuming bar fracture failure mode. In this case the relevant bond properties need to be used.

$$(wbl_b + P) = \frac{2n(d + C)A_s E_s \lambda_f \tanh(\lambda_f l) \Delta}{l_b}, \quad \frac{\delta_s}{l_b} = \frac{\Delta}{d} \quad 0 \leq \Delta \leq \Delta_a \quad (7.91)$$

However, assuming tie force at the plastic and fracture stage as $F_l = A_s f_y$ and $F_l = A_s f_u$, respectively; the maximum strength of system corresponding to the plastic and collapse stage using Figure 7.1c can be obtained

$$(w_i bl_b + P_i) = \frac{2nA_s f_s (d + c)}{l_b} \quad (7.92)$$

7.5.3 Effect of compressive membrane action

Considering the effect of compressive membrane action using the developed model by Rankin and Long (1997), the total load capacity is obtained by adding the strength due to arch action to the relevant strength due mechanism load

7.5.3.1 Pull-out failure mode

$$(wbl_b + P) = \frac{2n(d + C)A_s E_s \lambda_2 \tanh(\lambda_2 l) [\Delta + m_2]}{l_b} + \frac{2M_a}{l_b} \quad 0 \leq \Delta \leq \Delta_a \quad (7.93)$$

7.5.3.2 Bar fracture failure mode

$$(wbl_b + P) = \frac{2n(d + C)A_s E_s \lambda_f \tanh(\lambda_f l) \Delta}{l_b} + \frac{2M_a}{l_b} \quad 0 \leq \Delta \leq \Delta_a \quad (7.94)$$

$$(w_i bl_b + P_i) = \frac{2nA_s f_y (d + c)}{l_b} + \frac{2M_a}{l_b} \quad (7.95)$$

Where M_a is given by Eq. (2.43) (Chapter 2). The effect of compressive membrane action is decreased following the peak strength; hence it is assumed that, it decreases from maximum at the peak strength to zero at the beginning of the catenary action stage.

7.5.4 Verification

To verify the adequacy of the proposed method to analyze the catenary system, a comparison is performed with the result of the full scale floor-to-floor test conducted in the present study. In this section, the calibrated parameters following the pullout simulation procedure are used to analyze the floor-to-floor system. The comparison between analytical models with experimental study at the key points is presented in Table 7.2. The tie force in group B with pullout failure mode is taken from Table 3.1-3.4.

Table 7-2 Comparison between experimental study and analytical model

Group	Tests No.	Steel Ties			Tie Force (kN)			Strength (kN)	
		d_b (mm)	Yield stress (MPa)	Tensile strength (MPa)	Yield/ peak pullout force	Tensile strength	Tie No.	Experimental study	Proposed Analytical model
A	FT3	$\phi 12$	545	677	57.4	-	2	16.65	18.60
	FT4	$\phi 12$	545	677	50.65	-	2	22.47	20.1
	FT5	$\phi 12$	545	677	49.23	-	2	14.9	14.03
B	FT1	$\phi 10$	515	645	40.42	50.63	2	15.7	17.9
	FT2	$\phi 10$	515	645	40.42	50.63	3	24.15	23.76

7.5.4.1 Pullout failure mode

To show further efficacy of the developed model, the results of the tie force versus vertical deflection at mid joint for the specimen FT4 based on analytical model and tests result is presented in Figure 7.17. The discrepancy between analytical and experiential is attributed to different location of tie force, in which tie force in experimental study is based stress in the strain gauges 50 mm away from loaded end of ties and over embedment length while analytical model presents tie force at the loaded end.

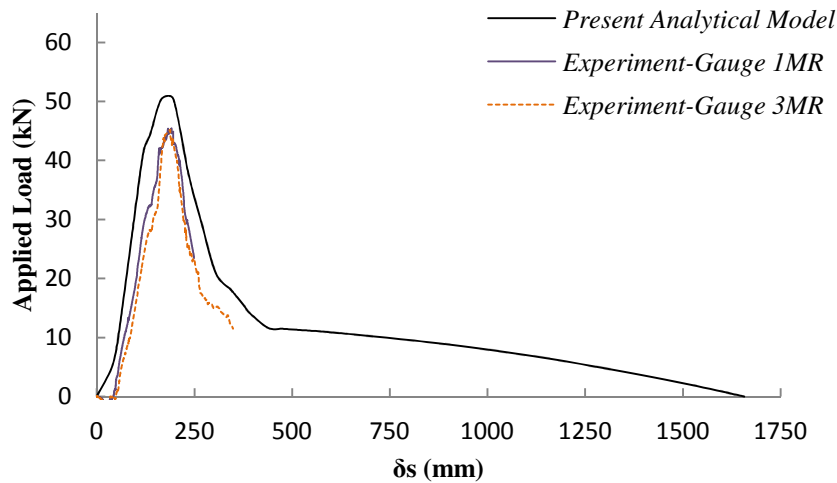


Figure 7.17 Tie force-deflection relationship based on analytical and experimental study

Figure 7.18 indicates that, applied load versus vertical deflection based on analytical method are approximately agree well to the experimental work. The results illustrate that load-deflection based on pullout simulation using pullout specimens with 9° against to horizontal axis; provide the relatively same peak load (Fig. 7.18). The difference between peak loads is attributed to the actual boundary condition with the simplified boundary condition in the analytical model, simplification in the pullout simulation of the reinforcement bar in the concrete and small lateral displacement of the supports during the test. Numerical analyses show that the deflection of the actual model is more than the model with fixed support, by 21.72 mm (Fig. 7.19).

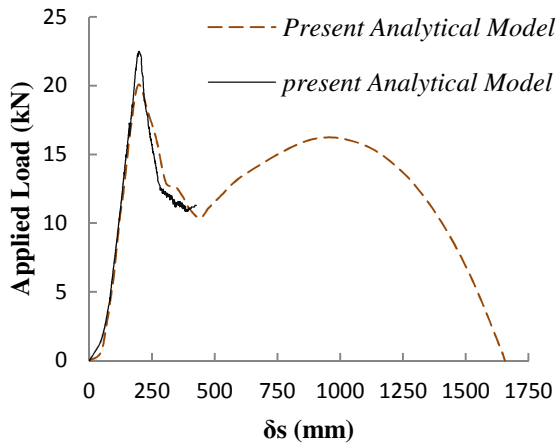


Figure 7.18 Applied line load – displacement relationship according to experimental and analytical study-FT4

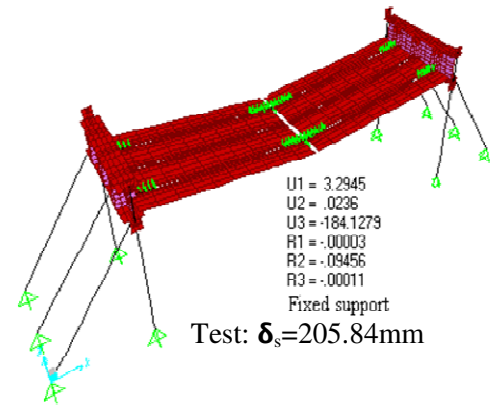


Figure 7.19 Tie force and vertical deflection-FT4; $w=2.35 \text{ kN/m}^2$, $P=17.1 \text{ kN}$

The comparison in Fig. 7.18 reveals that the analytical modelling provides a good estimate in terms of both peak load and ascending or descending phases. Also, the slight discrepancy can be attributed to the measuring errors from the full scale test procedure and inherent errors associated with the assumptions introduced in the modelling process. Furthermore, according to test results the tie force versus vertical deflection in the middle and sides of the floor-to-floor system follows a different trend; while in the analytical approach the same behaviour is assumed. The other source of error might be the difference in the key influence factors e.g. compressive strength, embedment length and boundary condition.

In the specimens with concrete at the gaps, Eqs. (7.75-7.80 and 7.93) are used to define load-deflection relationship corresponding to the ascending, descending, and catenary action stage, respectively. Figure 7.20 shows that the proposed analytical model provide a good estimate in the terms of peak load ,ascending, descending, and catenary stages. The results indicate that the specimens with pullout behaviour are capable to developed effective catenary action and provide considerably more ductility compared to the specimens with bar fracture failure mode. For the specimens with concrete at the gap, following the initial failure, the progressive

collapse resistance reaches to the second maximum at $\delta_s / l_b = 35\%$; which is approximately 3 times that of specimens with bar fracture failure. Figure 7.17, 7.18 and 7.20 indicate that the present analytical method is successfully capable of predicting the behaviour of the floor-to-floor system in the all stages. Furthermore, Fig. 7.18 shows that unlike the specimens with concrete at the gaps, maximum strength is induced at relatively large deflection in the specimens without concrete at the gaps.

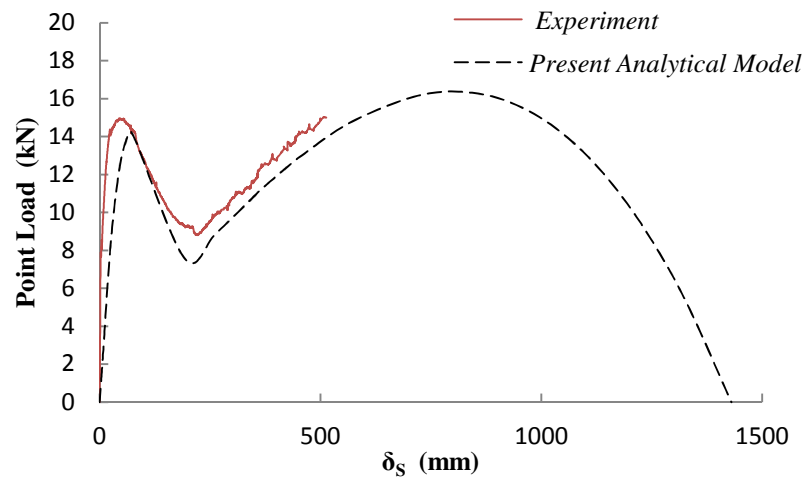


Figure 7.20 Load vs. middle joint deflection -FT5

7.5.4.2 Bar fracture failure mode

The relationship between load and middle joint using Eq. (7.94-7.95) is shown in Figure 7.21. The strength of system at the plastic and collapse stage can be obtained using Eq. (7.95). The deflection of middle joint is calculated using Eq. (7.77) considering relevant displacement i.e. Δ . The pull-out experiments (Chapter 3) indicate that, in the specimens with the bar the fracture failure mode, the displacement corresponding to the plastic and collapse stage is 0.8 and 8.5 mm, respectively. Also, measurements following performing tests indicated that the effective depth for specimens FT1 and FT2 was 90 mm. The stiffness of frame support i.e. S using SAP2000 software is 180 kN/mm. The result indicates that, the peak strength obtained from analytical model is slightly more than experimental results for FT1, while there is good agreement between analytical and test result for FT2. It can be attributed to that fact that, due

to some slack in the connections actual stiffness of frame support for the first test is less than the stiffness obtained by SAP 2000. It can be concluded that, the developed approximate analytical model is able to predict the maximum capacity and load-deflection relationship of specimens with both pullout and bar fracture failure mode.

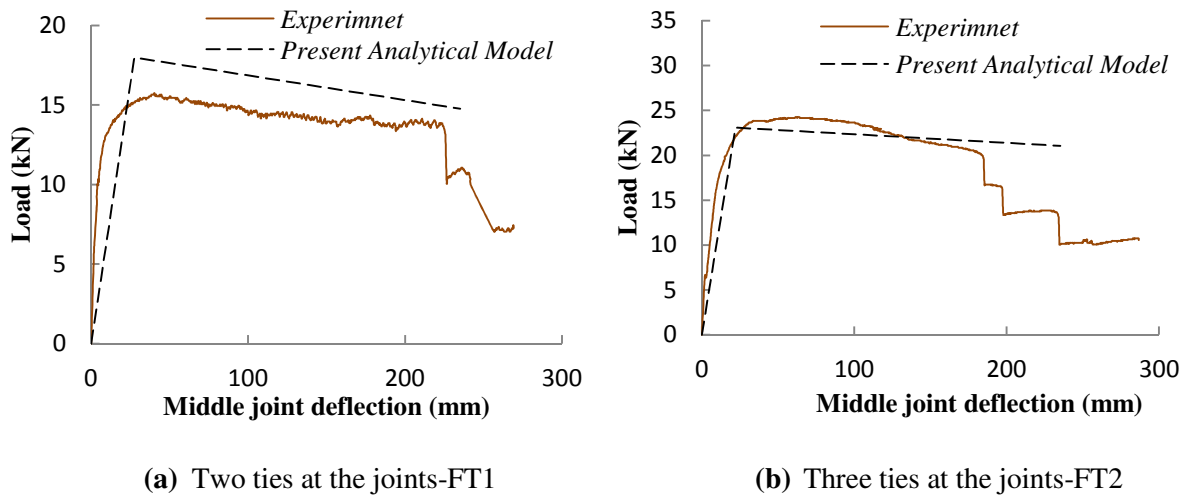


Figure 7.21 Load vs. middle joint deflection relationship-bar fracture failure mode

7.6 APPROXIMATE ANALYSIS OF FLOOR-TO-FLOOR SYSTEM USING LONGITUDINAL AND TRANSVERSE TIES

It is obvious that, assuming 2D behaviour of structure considered in most of studies is not able to provide clear understanding about post-collapse and the mechanism of forming catenary action. To end this, in the second set of analyses both longitudinal and transverse ties are taken into account using 3D modelling (Fig. 7.22). The contribution of longitudinal tie in progressive collapse resistance have been proposed and verified in the first part of this paper. In this section a model to simulate the contribution of longitudinal and transverse ties is developed.

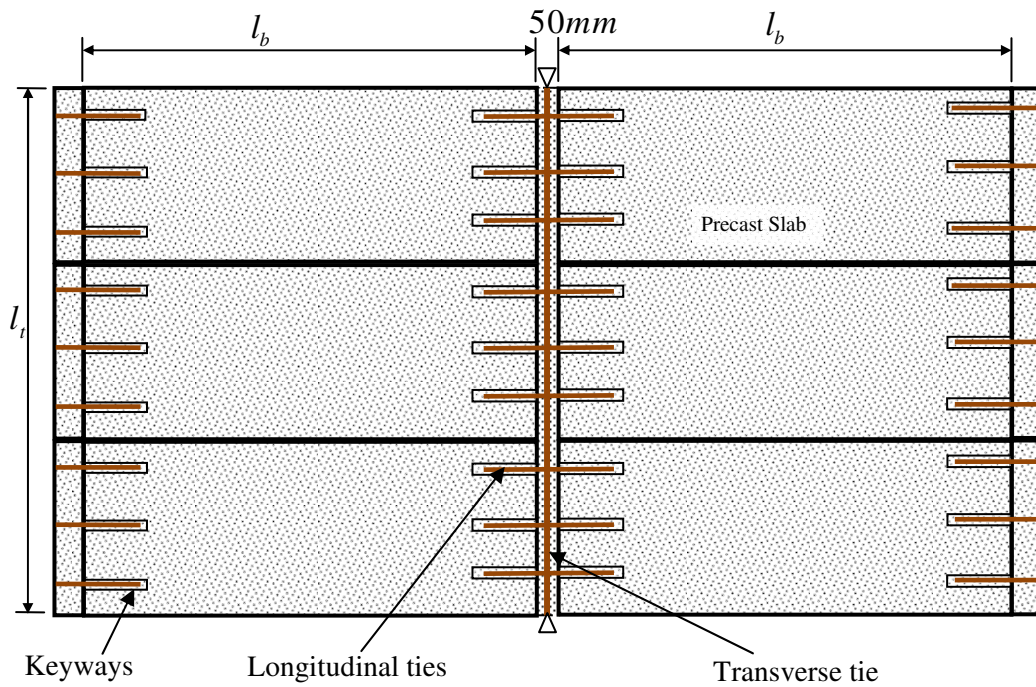


Figure 7.22 Floor-to-floor system facilitated by longitudinal and transverse ties

7.6.1 Strength of system provided by transverse ties

The catenary behaviour of transverse ties can be developed by applying the catenary equation introduced by Popov (1990), which included the relation between applied load, catenary tension force and vertical deflection. According to Figure 7.23, a rational estimation of the catenary tension forces given by Popov (1990) is presented

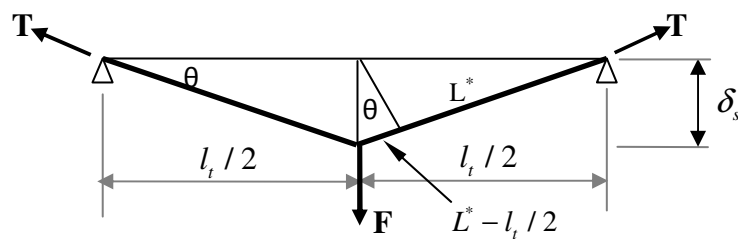


Figure 7.23 Catenary action behaviour of transverse ties (Astaneh et al., 2001)

$$\delta_s = l_t / 2 \tan \theta \text{ , and } L^* = l_t / (2 \cos \theta) \quad (7.96)$$

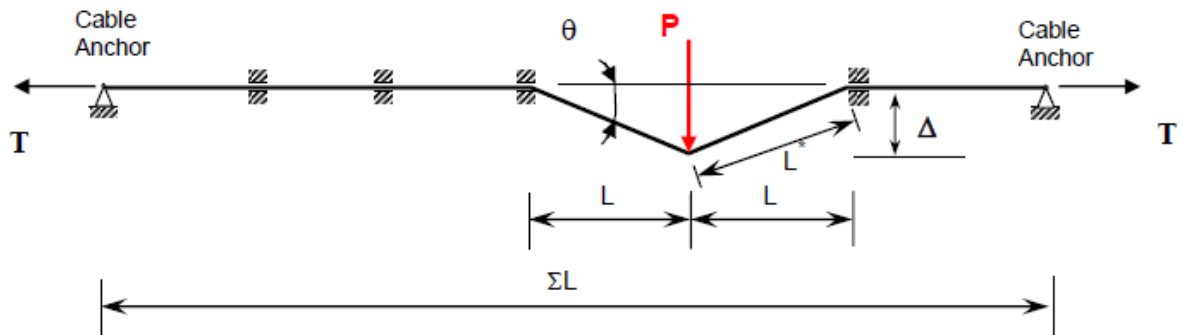
$$T = \frac{AE}{L^*} (L^* - l_t / 2) , \text{ and } (L^* - l_t / 2) = \delta_s \sin \theta \quad (7.97)$$

$$F = 2T \sin \theta \quad (7.98)$$

Using the same approach presented by Popov (1990) and applying Catigliano's first theorem, Astaneh et al. (2001) developed some equations to calculate tie force and deflection to simulate the catenary behaviour of strand in composite structure (Figure 7.24). It is important to note that, due to considering all parameters which affect the behaviour of the system results in a very complex method, the contribution of the deck, reinforcement bars in the slab, connection and shear studs were not included in developing this method (Astaneh et al., 2001). It was assumed that load P is representing the force in the removed support.



(a) Layout of test specimen



(b) Catenary model of strand in composite structure

Figure 7.24 Model of the cables laced in the floor slab of a typical structure (Astaneh et al., 2001)

According to the model displayed in Figure 7.24b and considering cable only, the relation between various parameters with reference to Popov's (1990) method was developed by Astanek et al. (2001)

$$T = \frac{2LAE(1 - \cos \theta)}{\cos \theta(\Sigma L)} \quad (7.99)$$

$$F = \sqrt{\frac{4T^3(\Sigma L)}{AEL}} \quad (7.100)$$

$$\delta_s = \sqrt[3]{\frac{F(\Sigma L)L^2}{2AE}} \quad (7.101)$$

$$T = \sqrt[3]{\frac{F^2 AEL}{4(\Sigma L)}} \quad (7.102)$$

The reliability of the developed method is verified using non-linear analysis by SAP2000 considering geometric nonlinearity (Fig. 7.25). The result of analytical analysis indicates that tie force i.e. T and deflection i.e. δ_s for an applied load of 90,000 N is 386331 N and 731 mm, respectively; which is very close to the FE analysis (Fig. 7.25). In this model it is assumed that during progressive collapse no bond strength exists between the strand and concrete in all spans, which results in relatively more ductility and strength.

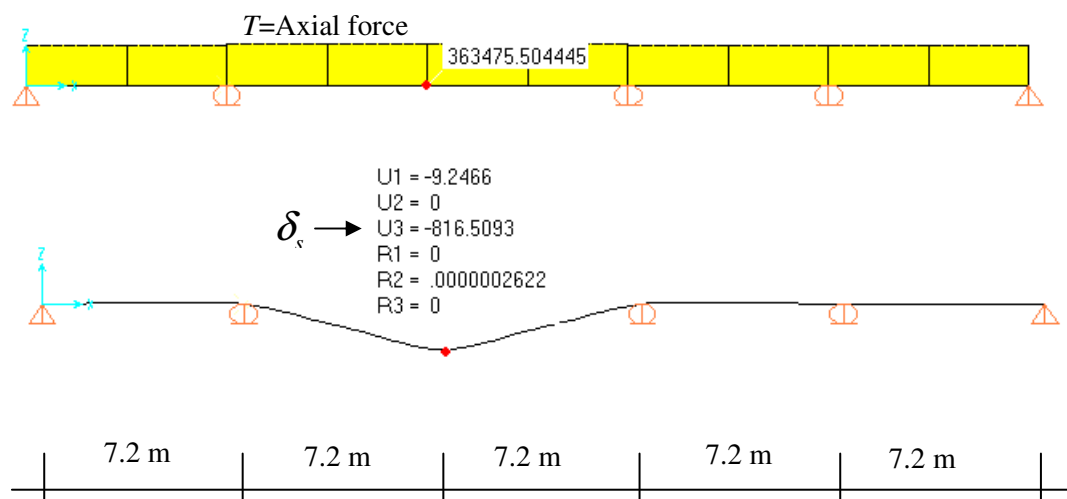


Figure 7.25 FE analysis of a specimen with 5 span lengths of 7.2 m and bar size of 30mm

It is obvious that in a precast structure, due to the concrete in the spans without the removed walls being intact, the fixed support needs to be applied to the strand at both ends of the strand in the removed span. The FE analysis indicates that the above analytical model is still valid assuming $\Sigma L = 2L$ (Fig. 7.24). For the specimen with a fixed boundary condition using the analytical model, tie force T and vertical deflection δ_s is 386455 N and 500.1mm, respectively. For the same specimen discussed in Figure 7.24 with a fixed boundary condition at the both sides of the strand, the result of the analytical model is found to be very close to the FE analysis (Fig. 7.26).

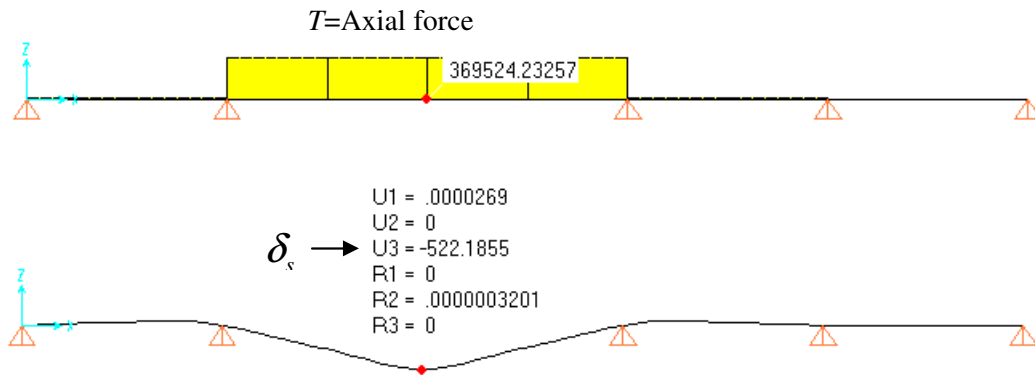


Figure 7.26 FE analysis of a specimen with 5 spans lengths of 7.2 m, bar size of 30mm with fixed boundary condition at side supports

To obtain capacity of system due to transverse ties two models are presented:

Model 1: As in a floor-to-floor system, the transverse ties sustain the load from several longitudinal ties; modelling a transverse tie as shown in Fig. 7.23 results less stiffness and overall capacity of the system. According to the standard tensile test on ribbed bars, the yield and fracture strain is around 0.0028 and 16% respectively; hence the maximum deflection/span length ratio corresponding to yielding and the bar fracture point in transverse ties is 3.7% and 29% i.e. $\delta_s = 0.037l_t$ and $\delta_s = 0.29l_t$. According to Figure 7.23 and using Eq. (7.96-7.98), the stiffness of the transverse tie at the middle joint can be defined

$$F = 2T \sin \theta = \frac{4E_s A_{st}}{l_t} (L^* - l_t / 2) \cos \theta = \frac{4E_s A_{st}}{l_t} (\delta_s \sin \theta) * \sin \theta \cos \theta \quad (7.103)$$

$$k_s = \frac{4E_s A_{st}}{l_t} \sin^2 \theta \cos \theta \quad \delta_s < 0.037l_t \quad (7.104)$$

At the yielding point

$$k_{sp} = \frac{0.022E_s A_{st}}{l_t} \quad \delta_s = 0.037l_t \quad (7.105)$$

It is to be noted that, as a high level of nonlinearity occurs during the progressive collapse, the contribution of the concrete gap is not included. Furthermore, with considering concrete at the gap, a simple and reliable mathematical method could not be established or it would be relatively very complex. The transverse ties are performed perpendicular to the longitudinal ties at the gaps between the precast slabs; hence they provide an elastic support for the longitudinal ties following removal of a wall support (Fig. 20).

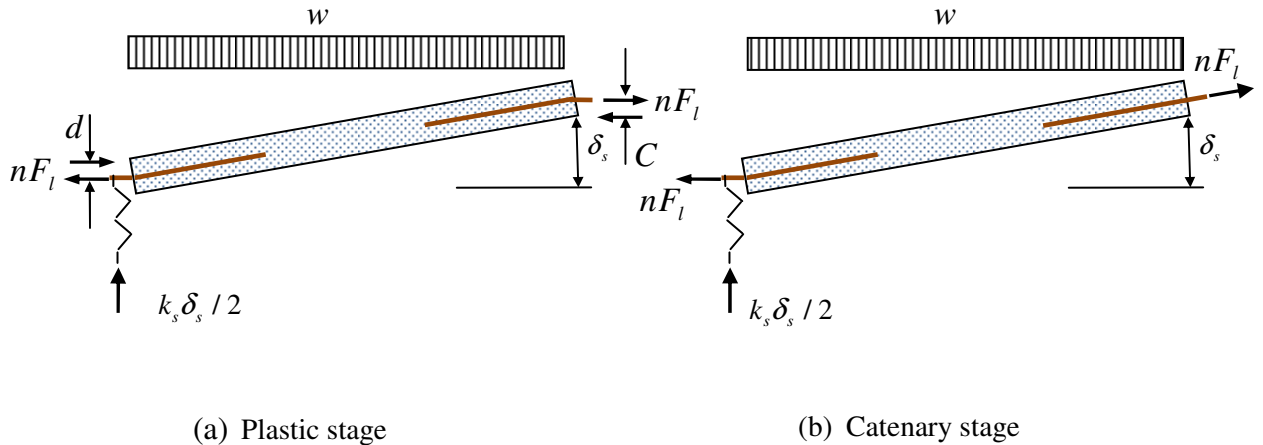


Figure 7.27 Floor-to-floor joint facilitated by longitudinal ties and transverse ties-free body diagram of half system

According to Figure 7.27a, the equilibrium of the free body diagram gives:

$$wbl_b^2 / 2 - nF_l(d + C) - \delta_s k_s / 2l_b = 0 \quad (7.106)$$

Substituting Eq. (7.105) in Eq. (7.106) and rearrangement leads to

$$w = \frac{2n(d + C)F_l + 0.022E_s A_{st} \frac{l_b}{l_t} \delta_s}{bl_b^2} \quad \delta_s \leq 0.037l_t \quad (7.107)$$

Model 2: Furthermore, it can be assumed that, the strength of system is sum of strengths provided by longitudinal and transverse ties separately. The strength of system with longitudinal tie was developed in section 7.5 and a simple model to define strength provided by transverse ties is presented herein. Figure 7.28 shows the free body diagram of half transverse tie. At the large deflection, the tie force in the transverse tie can be calculated based on catenary mechanism subjected to the uniform load of $w_t l_b$ (Fig. 7.28).

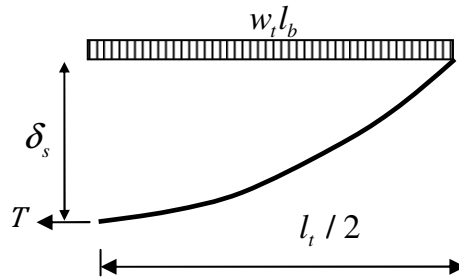


Figure 7.28 Free body diagram of half transverse tie

Equilibrium in Figure 7.28 gives:

$$T = \frac{w_t l_b l_t^2}{8\delta_s} \quad (7.108)$$

$$\text{Let } T = A_{st} f_s ; \quad w_t = \frac{8A_{st} f_s}{l_b l_t^2} \delta_s \quad (7.109)$$

Considering contribution of longitudinal and transverse ties, the strength of system can be summarized as follow

$$w = \frac{2n(d + C)F_l}{bl_b^2} + \frac{8A_{st} f_s}{l_b l_t^2} \delta_s \quad (7.110)$$

Due to simplicity Eq. (7.110) is used to propose generic analysis and design model for both pullout and bar fracture failure mode.

7.6.2 Pull-out failure mode

For the ascending stages of pullout behaviour, replacing F_l in Eq. (7.110) by the relevant pullout load model, the relationship between the applied load with the properties of the longitudinal and transverse ties corresponding to the ascending stages can be obtained

$$w = \frac{2n(d+C)A_s E_s \lambda_1 \tanh(\lambda_1 l) \frac{d}{l_b} \delta_s}{b l_b^2} + \frac{8A_{st} f_s}{l_b l_t^2} \delta_s \quad \delta_s < 0.02l_b \quad (7.111)$$

$$w = \frac{2n(d+C)A_s E_s \lambda_2 \tanh(\lambda_2 l) [\frac{d}{l_b} \delta_s + m_2]}{b l_b^2} + \frac{8A_{st} f_s}{l_b l_t^2} \delta_s \quad \delta_s < 0.033l_b \quad (7.112)$$

At the slip corresponding to peak pullout load i.e. $\Delta = 2.5mm$, $\delta_s = 0.033l_b$. Comparing this deflection with deflection corresponding to yield point in the transverses tie i.e. $\delta_s = 0.037l_t$ indicate that that, transverse ties experience yielding at the peak pullout force, hence at this deflection f_s in Eq. (7.112) can be replaced by yield stress i.e. f_y . For the all descending stages, replacing F_l by the relevant pullout force model leads to

$$w = -\frac{2n(d+C)A_s E_s \lambda_2 \tanh(\lambda_2 l) [\frac{d}{l_b} \delta_s + m_i]}{b l_b^2} + \frac{8A_{st} f_y}{l_b l_t^2} \delta_s, \quad i = 3, 4 \quad 0.033l_b < \delta_s < 0.1l_b \quad (7.113)$$

According to the test result, at the large deflection i.e. $\delta_s > 0.11l_b$ catenary action governs the behaviour of the system. The corresponding slip to this deflection i.e. $\Delta = 8-10mm$ indicates that longitudinal ties experience a frictional or fully debonded stage while the transverse tie is still in the plastic zone e.g. $\epsilon \leq 0.0239$. Assuming catenary behaviour for the longitudinal

ties, replacing F_l by pullout force in frictional stage i.e. $n\pi d_b \tau_f [l - \Delta]$, assuming tensile strength for transverse ties i.e. $f_s = f_u$ and $\Delta = \delta_s^2 / 4l_b$ in Eq. (7.110) leads to

$$w = \frac{n\pi d_b \tau_d [l - (\frac{\delta_s^2}{4l_b})]}{bl_b^2} + \frac{8A_{st}f_u}{l_b l_t^2} \delta_s \quad \delta_s > 0.11l_b \quad (7.114)$$

7.6.3 Bar fracture failure mode

The developed method for ascending stage Eqs.(7.111) can be used to analyse floor-to-floor system assuming bar fracture failure mode. In this case the relevant bond properties need to be used. However, assuming tie force at the plastic and fracture stage as $F_l = A_s f_y$ and $F_l = A_s f_u$, respectively; the maximum strength of system corresponding to the plastic and collapse stage can be obtained

$$w_p = \frac{2nA_s f_s (d + c)}{bl_b^2} + \frac{8A_{st}f_y}{l_b l_t^2} \delta_s \quad \delta_s < 0.013l_b \quad (7.115)$$

$$w_c = \frac{2n(d + C)A_s f_u}{bl_b^2} + \frac{0.8A_{st}f_u}{l_t^2} \delta \quad \delta = 0.1l_b \quad (7.116)$$

Where

w = Progressive resistance of system corresponding to plastic and collapse ((kN / m²))

n = Longitudinal ties at the joint

d = The effective depth of slab (mm)

A_s = The cross section of one longitudinal tie (mm²)

E_s = Elastic modulus of ties (N/mm²)

λ_1 = Bond parameter defined in Chapter 2

l = Embedment length of longitudinal ties into keyway of precast slab (mm)

δ_s = Middle joint deflection (mm)

l_b = Slab length (mm)

A_{st} = The cross section of transverse ties (mm²)

l_t = Span length in transverse direction (mm)

Table 7-3 The property and strength of a floor-to-floor system with longitudinal and transverse ties

No.	Longitudinal Axis			Transverse Axis			W (kN/m2)	
	Length (m)	Bar Diameter (mm)	Numbers of Ties/Slab	Length (m)	Bar Diameter (mm)	Yielding Strain	Yielding Level	Tensile Strength level
LTF1	2	$\phi 12$	2	2.4	$\phi 18$	0.0028	11.27	21.28
LTF2	4	$\phi 12$	2	2.4	$\phi 18$	0.0028	5.47	14.18
LTF3	4	$\phi 12$	2	4.8	$\phi 24$	0.0028	5.44	9.99
LTF4	6	$\phi 12$	3	4.8	$\phi 24$	0.0028	4.15	8.41
LTF5	6	$\phi 12$	3	7.2	$\phi 36$	0.0028	4.44	9.99
LTF6	8	$\phi 12$	4	7.2	$\phi 36$	0.0028	4.47	8.81
LTF7	8	$\phi 12$	4	9.6	$\phi 44$	0.0028	5.1	9.15

The above process indicates that the relationship between the strength of the system with various bond and geometrical properties can be established. For the pullout failure mode, the strength corresponding to the peak pullout force is assumed to be the maximum capacity of the system. The results of strength analysis for specimens with various longitudinal/transverse lengths and bar sizes for bar fracture failure mode are shown in Table 7.3. The longitudinal and transverse tie forces for the different specimens with the relevant average strength of each specimen are shown in the Table 7.4. The over strength of 1.25 (DoD, 2013) was applied to calculate tie forces.

Table 7-4 Longitudinal and transverse tie force with relevant average strength-bar fracture failure mode

	LTF1	LTF2	LTF3	LTF4	LTF5	LTF6	LTF7
$w_{\max} (kN / m^2)$	21.28	14.18	9.99	8.41	9.99	8.81	9.15
$P_l (kN / m)$	$2.25wl_b$	$1.71wl_b$	$2.43wl_b$	$2.91wl_b$	$2.44wl_b$	$2.45wl_b$	$2.68wl_b$
$P_t (kN)$	$1.66wl_t l_b$	$1.25wl_t l_b$	$1.58wl_t l_b$	$1.25wl_t l_b$	$1.57wl_t l_b$	$1.34wl_t l_b$	$1.44wl_t l_b$

Comparing tie force from analytical analyses (Table 7.3) with the result of FE analyses (Table 5.4) indicates that, the analytical model provide more strength for the specimens with slab length of more than 2m. It is to be noted that, maximum discrepancy is less than 17%.

7.7 SUMMARY

The tie force (TF) method is one of the main methods in designing concrete structures for progressive collapse. Due to the many simplifications, this method is easy in calculation as compared to the alternate load path or the proposed analytical methods. Despite these advantages, the TF method is not appropriate to analyze a floor-to-floor joint in cross wall structures.

In the first part, the tie force-slip relationship was developed to reproduce laboratory tests. The model is also used to derive, for the first time, explicit simulation of ascending and descending phase especially the post-bond-behaviour of steel into concrete. An analytical method is subsequently proposed, taking into account such important factors as bar size, embedment length, elastic module, and compressive strength of concrete. The analytical method proposed in this study, is reliable for a realistic analysis and better understanding of the pullout behaviour of steel bars into concrete. The developed model is, then, used to analyse of floor-to-floor joint in the precast cross wall structures, which is presented in the second part.

It is demonstrated in this paper that close agreement was observed between experimental study and the analytical model, for pullout behaviour of bar in grout using various bar size and embedment length. The results of the experimental and analytical model indicate that the ascending branch of the curve plays a minor role in energy absorption in comparison to the contribution of the descending stage; hence special attention must be given to pullout

behaviour of steel bars in the frictional stage to enable floor-to-floor joint bridge over loads following removal wall supports due to any abnormal loads.

The novelty of this study is that, from analysis and design perspective, the developed model can be considered as a generic model to simulate pullout behaviour of various type of steels i.e. ribbed bar, strand and rock bolt in concrete. Furthermore, the developed model is able to be extended for n-linear bond-slip model with minor modification

The developed model to simulate pullout behaviour of bars into keyways of precast slabs was used to propose an approximate analysis of floor-to-floor joint in absence of a supporting wall. In the second part of this chapter, a generic method to analyse the floor-to-floor joint with longitudinal and transverse ties for both pullout and bar fracture failure mode was developed. The validation of this technique developed in this chapter is verified by experimental study on full scale floor-to-floor joints and pullout tests. It is demonstrated in this chapter that close agreement was observed between experimental study and the analytical model for both pullout and floor-to-floor simulation.

It is obvious that as in the larger part of the plastic zone of transverse ties, longitudinal bars experience pullout behaviour and they can even provide more strength at the catenary stage, hence the specimens with pullout failure mode are able to provide more ductility than specimens with bar fracture failure mode. Also, the analytical method purposed in this study, is reliable for better understanding of the behaviour of the full scale floor-to-floor joints following removal wall support.

.

Chapter 8

CONCLUSION AND RECOMMENDATIONS FOR FUTURE WORK

8.1 INTRODUCTION

The main aims of this study was to investigate the post collapse behaviours of precast floor-to-floor joint following wall removal due to any abnormal load, developing a FE and analytical model to analyse and design of floor-to-floor joint, and study the efficiency of current TF method to design of precast structures for progressive collapse. Particular attention was given to the efficiency of the longitudinal and transverse tie to establish alternate load path to bridge load over removed wall support to the undammed parts of buildings.

The principal conclusion of this research is listed in the Section 8.2 to 8.7. Recommendations for further works and applications in the relevant areas are presented in 8.8 and 8.9.

8.2 PULL-OUT EXPERIMENTAL STUDY

The present experiment study was carried out with the aim of studying the behaviour of ribbed bar in grouted keyways of a precast slab and developing the bond-slip criteria to design a floor-to-floor joint in precast concrete cross wall structures. The influences of concrete type, embedment length, bar size and slope of applied load were examined through performing 57 pullout tests.

For the bars placed in the keyways of short precast slab specimens, three different modes of failure were observed. For the specimens with a small embedment length of bars in the keyways i.e. $l_d / \phi \leq 20$ and in low compressive strength i.e. $f_c \leq 20\text{MPa}$, pullout failure mode occurred. For the same compressive strength, specimens with higher embedment lengths i.e. $l_d / \phi = 30$, the stress in the steel bar exceeded the yield stress and the reinforcement bars fractured. For the intermediate embedment length i.e. $l_d / \phi = 25$, in some specimens the yield stress of the reinforcements is reached, but at the hardening stage pullout failure mode occurred with considerable plastic deformation experienced by the steel bars.

In the pullout failure mode, it was observed that reinforcement bars slid in a cracked circular plan around the steel bars and concrete was left between the ribs. For the well confined specimens no splitting crack was observed; while a cone failure at the loaded end of the bars was formed. It was found that, the average depth of cone failure can be defined as 1.75 times the bar diameter.

It was found that on considering actual embedment length, the relationship between the average bond strength and the square root of compressive strength can be assumed approximately linear. The average bond strength was found to be $\tau_{ave} = 1.45\sqrt{f_{ck}}$ or $\tau_{ave} = 0.29f_{ck}$.

8.3 FULL SCALE EXPERIMENTAL STUDY

A total of five full scale tests were conducted to study the behaviour of specimens considering two different failure modes. Group A specimens (FT1 and FT2) were tested to investigate the behaviour of systems considering the bar fracture failure mechanism and to examine the effect of the number of ties at the floor joints. Group B specimens (FT3, FT4 and FT5) were

examined to investigate the behaviour of systems with respect to the pull-out failure mechanism.

In the specimens with the bar fracture failure mode, at the collapse, the longitudinal ties fractured at the mid joint, while the longitudinal ties at the side supports only experienced plastic deformation. This indicates that the middle joint is the most critical point in the floor joint system. Since the fracture occurs when the deflection is relatively small, the catenary behaviour is not well developed in this group of specimens.

In the second group, those specimens free of any concrete in the gaps, e.g. FT4, provide more measurable resistance than the other specimens, while the specimens with concrete at the joints e.g. FT3/FT5 can endure more deflection. All specimens in this group have a re-ascending phase in their tie force against deflection curves, indicating the occurrence of the catenary action. Once the catenary action is developed, the loading resistance will continue to grow and it can provide more progressive collapse resistance for the floor slab system.

The comparison of the behaviour between these two groups of tests suggests that the key to inducing the catenary action is the introduction of an adequately large deflection before the system collapses. In this study, it was achieved as a result of the weak bond between the tie bars and the surrounding grout so that the bars fracture failure was suppressed.

8.4 FINITE ELEMENT SIMULATION

A FE model for progressive analysis of a precast floor-to-floor system considering bar fracture and pullout failure mode was developed using nonlinear dynamic finite element simulations carried out following the DoD guidelines. To this end, detailed three-dimensional finite element models of the pullout behaviour of reinforcement bar in the keyway of precast

concrete blocks to simulate pullout or bar fracture failure mode were developed. The same modelling method was then used in the subsequent three dimensional non-linear numerical analyses to simulate the ductility behaviour of precast concrete floor joints in the absence of underlying wall supports. Finally a comprehensive model for global analysis of precast structure subject to increasing vertical loading and notional removal wall support was proposed.

The developed model has been confirmed as being able to capture a complete tie force versus vertical deflection history with good accuracy for different bar sizes, embedment lengths and slab lengths. The results indicate that the developed model i.e. CDP model together with TR element is capable of simulating both pullout failure and bar fracture mode. As these models provide further data regarding tie force, slip, yielding stress and elastic or plastic strain over the embedment length of the bar, they can be considered as new and the most efficient models for research proposes. According to the literature, CDP and CSC models together with truss element as steel bars have been designed for fully bonded and also small slip can be considered by these two models; hence, the developed model can be considered as the third model to overcome the weak point of the two mentioned models.

8.5 NUMERICAL PARAMETRIC STUDY

Due to in actual use both alternate load paths will provide progressive collapse resistance, assuming 2D behaviour of structure considered in most of studies is not able to provide clear understanding about post-collapse and the mechanism of forming catenary action, hence to investigate actual behaviour of floor-to-floor system following wall removal both longitudinal and transverse ties are taken into account using 3D modelling.

For the specimens with bar fracture failure mode, the results show that, the systems reach yield capacity at $\delta_s / l_b \approx 2\%$ and maximum strength at $\delta_s / \min(l_b, l_t) \approx 10\%$, followed by sudden collapse at $\delta_s / \min(l_b, l_t) \approx 13-17\%$ and $\delta_s / \max(l_b, l_t) \approx 9.6-13.61\%$. The results indicate that, for specimens with the same length, precast floor-to-floor system assuming bar fracture failure mode exhibits relatively less ductility compare to the conventional RC structure, while specimens with pullout failure mode provides relatively the same ductility.

The results show that, for the specimens with bar fracture failure mode, although the failure mechanism varies with the number of slabs in the direction of the transverse tie, generally the failure is initiated from the middle longitudinal ties followed by the side longitudinal ties at the middle joint. Subsequently, the transverse tie reaches its capacity followed by failure in the longitudinal ties at the side supports, which is in contrast to progressive mechanism of RC structures.

In the specimens with pullout failure mode, prior to peak pullout force, longitudinal ties at the middle and side joints show the same behaviour; afterwards the tie force in the middle bar remains constant while the side bars experience the same behaviour as tie bars in concrete under pullout force. In these specimens, failure will be initiated by yielding in the transverse ties followed by pullout failure of the tie bars at the side joints. The results indicate that, following initial yielding at the transverse tie a combination of longitudinal tie at partial debonding and transverse tie at plastic/hardening stage increases the strength of system up to $\delta_s / l_b \approx 13.5-17.4\%$, followed by a steady decrease up to pulling out of side bars. Comparing the two failure modes shows that, the specimens with pullout failure mode provide more strength and ductility rather than bar fracture failure mode, which can be considered as the outstanding outcome of this study.

8.6 GENERAL ANALYSIS AND DESIGN GUIDELINE

According to parametric study, an improved tie force (TF) method to analyze precast structures for progressive collapse using the numerical analyses was proposed. The proposed TF method is presented for both bar fracture and pullout failure mode separately. Also, a step by step procedure using alternate load pad (ALP) is presented to provide a basis for an advanced analysis.

8.7 APPROXIMATE ANALYTICAL APPROACH

In this method, first the pullout force-slip relationship was developed to reproduce laboratory tests. The model is also used to derive, for the first time, explicit simulation of ascending and descending phase especially the post-bond-behaviour of steel into concrete. An analytical method is subsequently proposed, taking into account such important factors as bar size, embedment length, elastic module, and compressive strength of concrete. The analytical method proposed in this study, is reliable for a realistic analysis and better understanding of the pullout behaviour of steel bars into concrete. The developed model is, then, used to analyse of floor-to-floor joint in the precast cross wall structures, which is presented in the second part.

It is important to note that, from analysis and design perspective, the developed model can be considered as a generic model to simulate pullout behaviour of various type of steels i.e. ribbed bar, strand and rock bolt in concrete. Furthermore, the developed model is able to be extended for n-linear bond-slip model with minor modification.

8.8 RECOMENDATION FOR EXPERIMENTAL STUDIES

8.8.1 Using longitudinal, transverse, vertical, and peripheral ties

The post collapse behaviour of floor-to-floor joint using longitudinal ties was investigated in the present study. To establish reliable data set for the global analysis of precast structure using proposed FE model in the present study, a series of full scale experimental study need to be carried out considering longitudinal, transverse, vertical, and peripheral ties with minimum span length of 3 m in both sides and 3 storey building.

8.8.2 Using modified pullout failure mode

The result of experimental and FE studies indicate that, in the specimens concerning pull-out failure mode following peak pullout force the tie bars experience large slip which result large deflection while the stress is relatively less than yielding stress. Providing a stud on the bars beyond the designed embedment length can change pullout failure mode to bar fracture failure mode, which leads relatively higher progressive resistance at large deflection than specimens with the bar fracture failure mode. The efficiency of this approach need to be investigated by pullout test (Fig. 8.1).

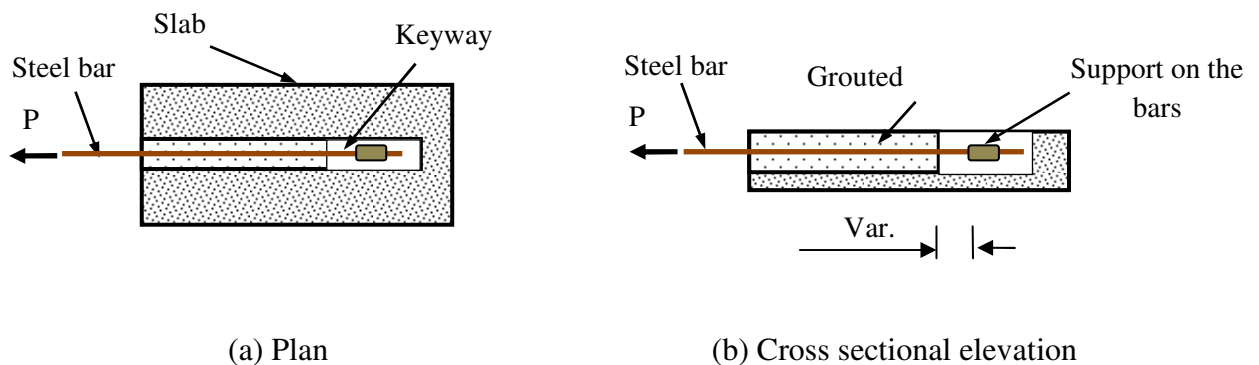
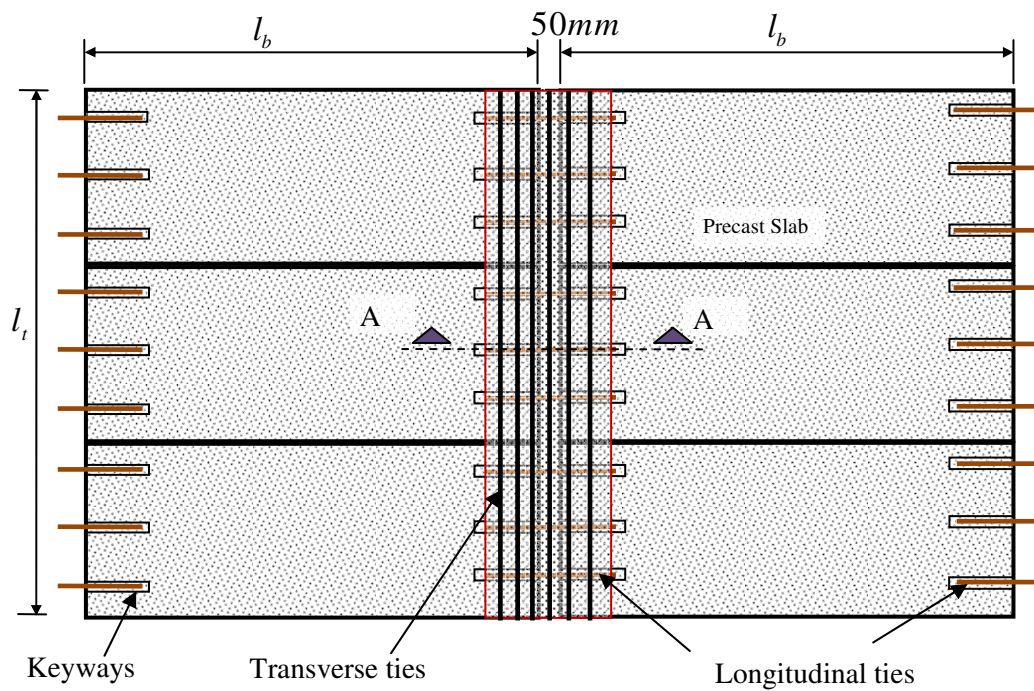
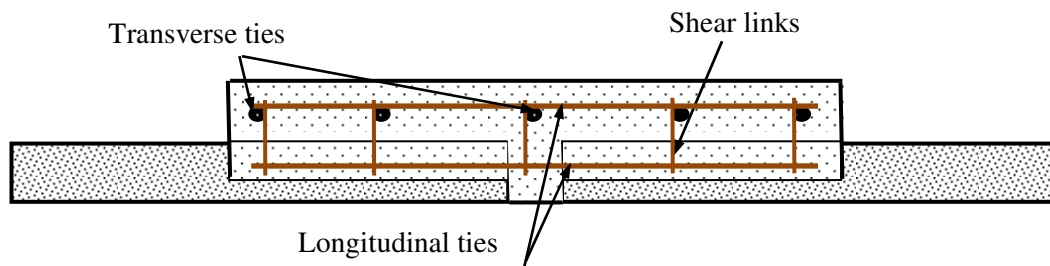


Figure 8.1 Illustrative diagram of the modified pullout test with a support outside of grouted keyway



(a) Plan view



(b) Cross section A-A

Figure 0.2 Proposed alternative for transverse and longitudinal ties

8.8.3 Using distributed transverse ties

According current regulation in the UK, to provide cantilever action one transverse tie is placed at the bottom of gaps. For this type of construction, compare to the longitudinal ties a tie with relatively high bar size need to be used. To provide more alternative load path and robustness, the transverse ties need to distributed at top of the gaps perpendicular to the

longitudinal ties. The higher the depth of section results more progressive collapse resistance and distributed transverse tie results more load paths compare to the conventional application of the transverse ties. The efficiency of this model and effective depth of width which the transverse ties are distributed need to be underpinned by full scale experiments (Fig. 8.2).

8.9 RECOMENDATION FOR FE STUDIES

8.9.1 Applied element method (AEM)

As stated in Chapter 4, the developed FE modelling require very fine mesh at the gaps and over embedment length in both steel and concrete which lead to relatively long-time analysis, hence using the same process to study the behaviour of structure as a whole would be out of reach. Furthermore, the maximum collapsed area is one of the main limitations in design for progressive collapse of structures, which cannot be obtained through conventional FE models. To simulate the actual progressive collapse behaviours of precast structures following removal wall support, the separation between elements would be the key factor, which also cannot be obtained using conventional FE analyses.

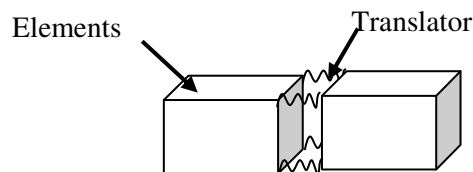


Figure 0.3 Applied element model (AEM)

Failure mechanism of specimens concerning bar fracture failure indicates that, the failure is initiated by bar fracture only in a few specific sections on the reinforcement bars which are

approximately similar for all specimens, while steel bars in other parts are fully bonded to the surrounded concrete. It can be concluded that, to simulate the real progressive behaviour of cross wall structures, the fracture failure property can be only applied to the critical sections. It is found that, using Applied Element Method (AEM) (Fig. 8.1), the nonlinear modelling is reduced to define fracture behaviours of reinforcement bars at the critical sections along with compressive and tensile behaviour of concrete at the interface between gap and precast slab at the joints, hence coarse mesh can be applied to the other parts of structures.

It is obvious that, the analysis time is significantly reduced due to using coarse mesh compare to the developed method in Chapter 4 and 5. The outstanding result of using this method is that, the total separation of elements allows simulation of actual failure mechanism following removal a wall supports.

To simulate total separation, concrete and steel bars need to be divided in some parts and each part is connecting by Translator element defined in chapter 4. The properties and location of Translator need to be investigated using pullout experimental study and FE analyses.

8.9.2 Modified Pull-out failure mode

As stated in Section 8.8.2 using a stud slightly beyond the designed embedment length, changes the failure mode from pullout failure mode to bar fracture failure mode which result more progressive resistance and energy absorption. As in practice the failure of longitudinal and transverse ties induces in the different stages, the optimum location of the stud need to be investigated in which the both failure induces at the same time.

APPENDIX 3A: GAUGE PREPARATION AND VALIDATION

3A.1 Strain Gauges

Strain gauges are attached to the reinforcement bars at the loaded end and over embedment length. In each specimen six to nine strain gauges were placed on six or nine longitudinal bars into keyways. The main aim of using these gauges was to detect stress while the floor-to-floor system is slowly lowering. All gauges are linear horizontal and were used for all full scale testes.

To detect accurate result each gauge need a high preparation before application. Before placing bar into keyways, it is glued along their length at the proscribed locations on the rebar. To remove the mill-scale from the bars, a coarse sand grinder is used. To smooth the surface further and remove any excess scale sanding wheel is used until steel bar had shiny and very smooth surface. In this phase, surface is smoothed further using 240-grit followed by 400-grit sandpaper and it can be considered as the final smoothing step.

Figure 3A.1 shows strain gauges preparation sequence. There is no specific recommendation for physical form of specimen and location of the gauges thereon, but may it varies with special requirement for each tests. As the deflection of any loaded member within the elastic region is proportional to strain, it can be derived directly by accomplishing strain gauges result. The procedure to measure force with stain gauges is quite similar to that for displacement. If the stresses are in elastic limit, the force is proportional to strain in transducer and then output signal. In case of extra precision, a calibration between strain and force must be accomplished to obtain the constant between strain and force. Otherwise, they may produce an error about 5 percent or greater.

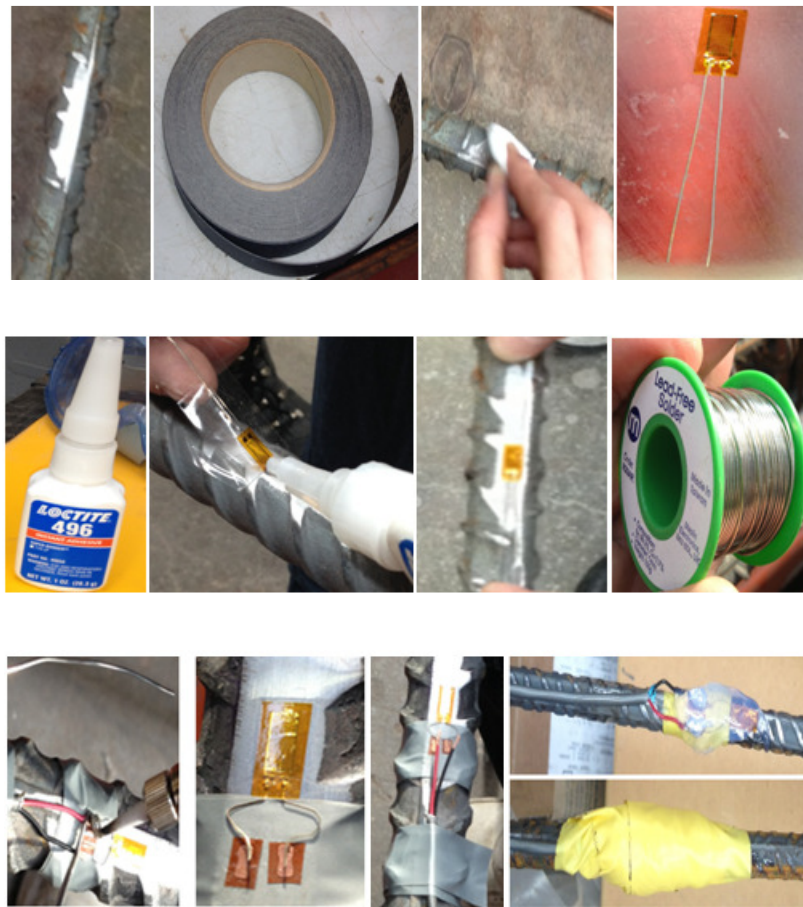


Fig. 3A.1 Strain gauges preparation sequence

3A.2 Data Acquisition

Following proper placement of strain gauges, load cells and LVDTs, the relative wires were connected to the data acquisition machine. The acquisition system is called data logger. It has maximum capacity of 11 channels, and capable to record 19 data per 4 second. Due to reasonable speed of the data logger, this system was optimal for the present study. This machine capable to record all data as the test proceeds. In addition, a separate amplifier (AC) was used to take reading from LVDT.

3A.3 Initial Measurements

To provide required accuracy, prior to performance of each test all instruments were tested and the dimension of specimens was measured. As stated earlier, all the rig and loading system was designed and fabricated in the laboratory, so before installation all members, holes and plates measured out with the relevant accuracy.

According to load cell and LVDT manual, they need to be calibrated following any disconnecting from data logger. However, before full scale tests all instruments were calibrated. The load cell was calibrated with aid of SANS machine using seven data reading voltages from data logger and loads from the SANS machine (Fig. 3A.2). To calibrate LVDT, first the relevant amplifier needs to be calibrated using factory constriction manual. The amplifier was calibrated so that zero volts represented zero displacement and 10 volts represented 300 mm displacement. The LVDT was calibrated with aid of special tool with accuracy of 2 dismal points in mm. Finally, using voltages reading (5 reading) from data logger and especial tool to measure displacement the required equation for load cell and LVDT was derived and applied in the data logger.



Fig. 3A.2 Load cell calibration

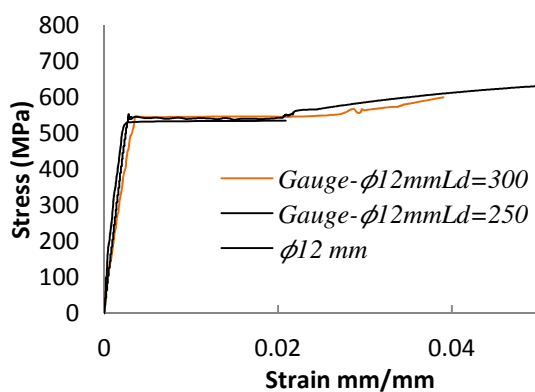
3A.4 Gauges Verification

To show efficiency of strain gauges setup, prior the full scale tests 6 strain gauges attached on the 12 mm and 10 mm reinforcement bar in a standard pullout test considering pullout and bar fracture failure mode. The pullout force calculated using strain gauges attached to 12 mm bars, was found to be very close to pullout load from load cell using screw jack for both pullout and bar fracture behaviour (Fig. 3A.3 and 3A.4). In both pullout and bar fracture failure mode, the pullout load or stress calculated from strain gauges is found to be very close to that observed using load cell results. The discrepancy is started while visible crash at the loaded end observed following pullout behaviour.

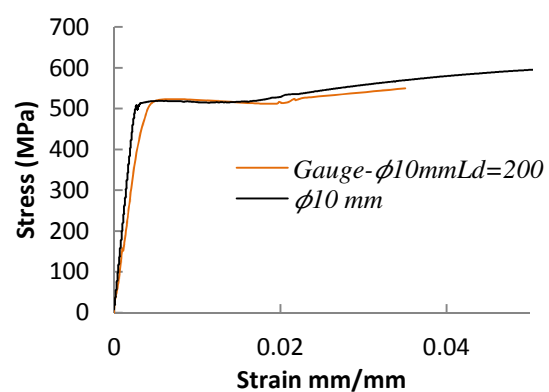


(a) Pullout specimen

(b) Strain gauges on the bars

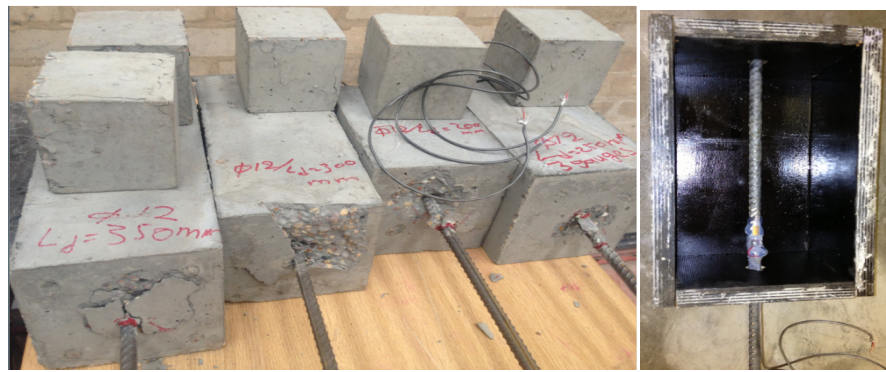


(c) $\phi 12\text{ mm}$

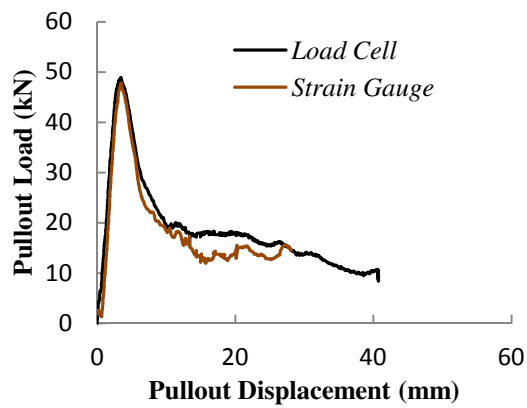


(d) $\phi 10\text{ mm}$

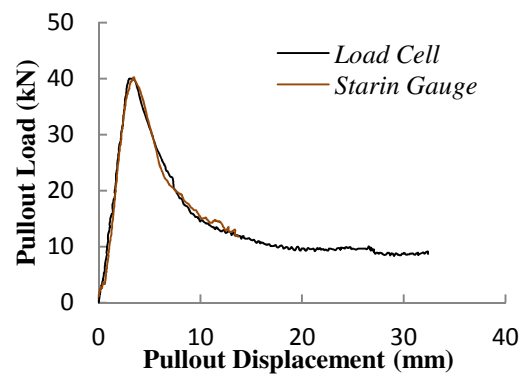
Fig. 3A. 3 Stress-stain curve based on strain gauge and load cell result-bar fracture failure mode



(a) Pullout specimens with strain gauges



(b) $\phi 12$ mm $L_d=250$ mm



(c) $\phi 12$ mm $L_d=200$ mm

Fig. 3A. 4 Pullout force-displacement curve based on strain gauge and load cell result

APPENDIX 3B: DETAILS OF THE FULL SCALE TEST STRUCTURE

The full scale test specimen is a full scale of a typical simply supported precast concrete hallow core slab with ties arrangement at the joints based on the standard specifications by the manufacturer, Bison. The test frame is constructed with steel columns, beams and bracings (Fig. 3B.1). For safety reason and to ensure enough space for high vertical deflection of slab at the middle joints, the distance between upper level of slab and ground was chosen to be 1.47 m (Fig. 3B. 2). Beams are connected to column by two angle cleats placed at both top and bottom. Two side bracings were bolted directly to the columns and the middle bracing was connected to the centre of the beam through a plate welded onto the bottom of the beam (Fig. 3B.2).

3B.1 Frame details

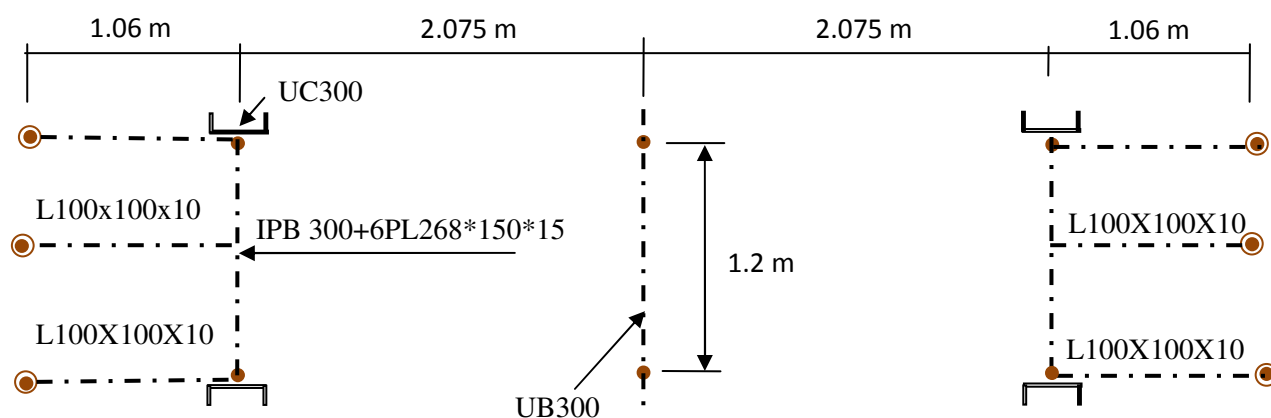


Fig. 3B.1 Plan view of test rig

Each column was seated on a 15 mm plate and bolted to the strong laboratory floor by a single 40 mm rod. Although the gravity and applied load by screw jack was not relatively big, but according to initial analysis using SAP 2000 the horizontal load on the supported beams



3B.3 Loading Device Used in the Test

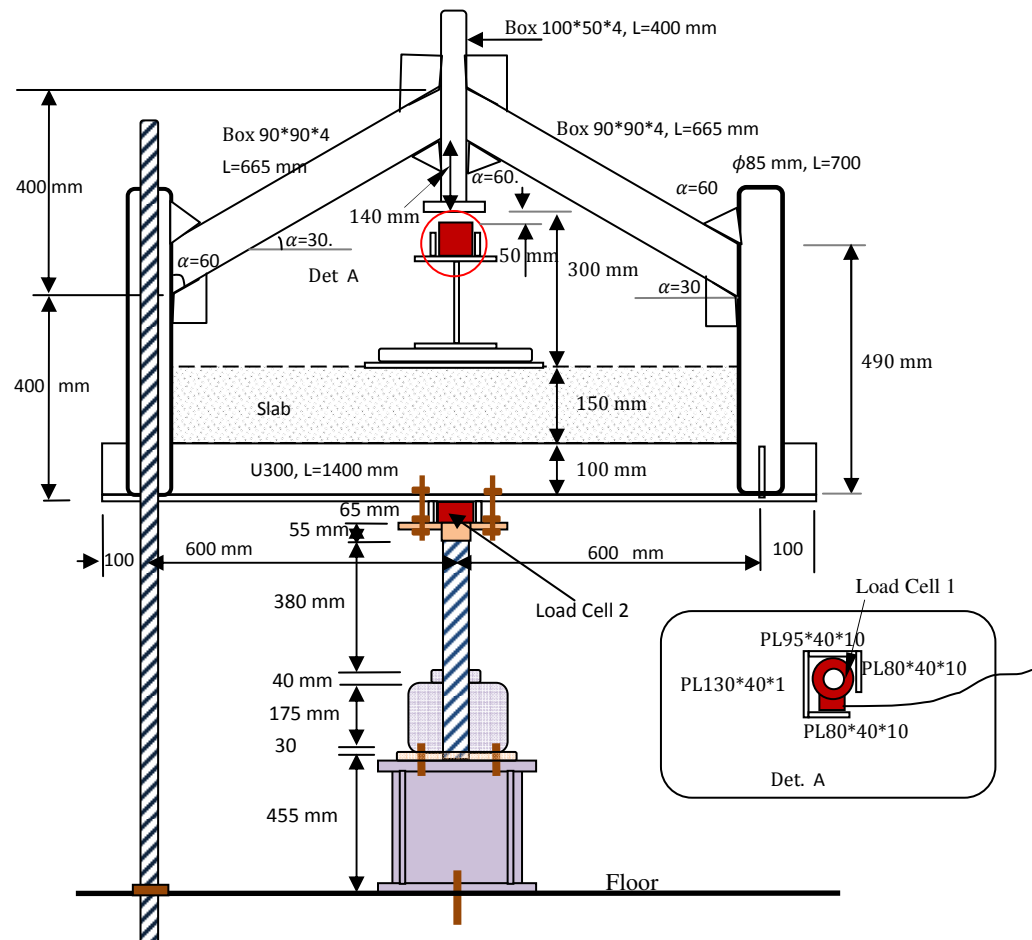


Fig. 3B. 3 Elevation of loading details at floor-to-floor joint

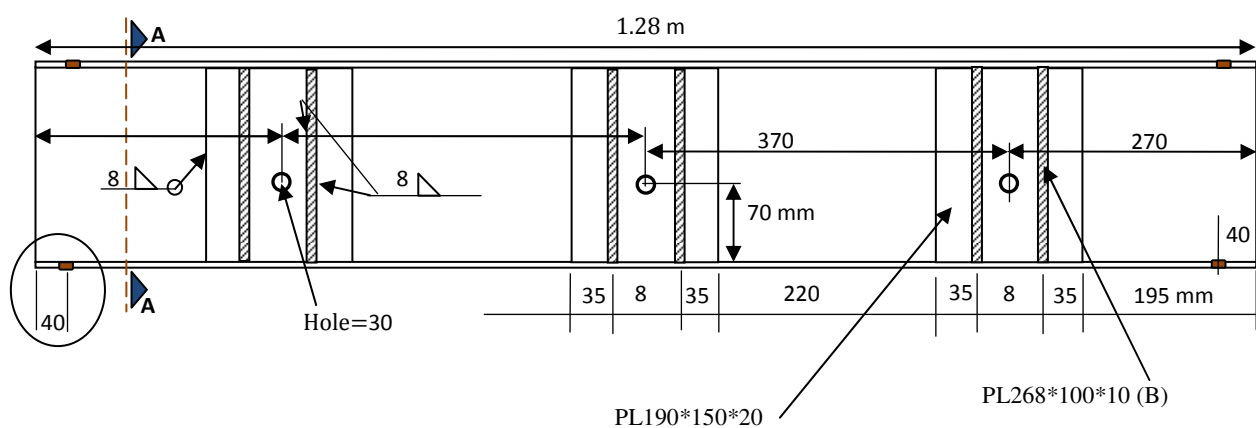


Fig. 3B.4 Detail of supporting beam at the both end

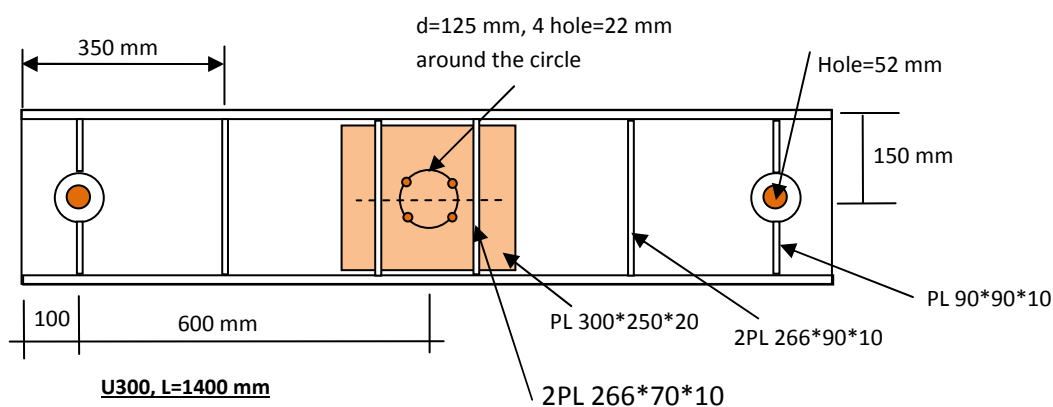


Fig. 3B. 5 Detail of supporting beam at the middle joint and top of screw jack

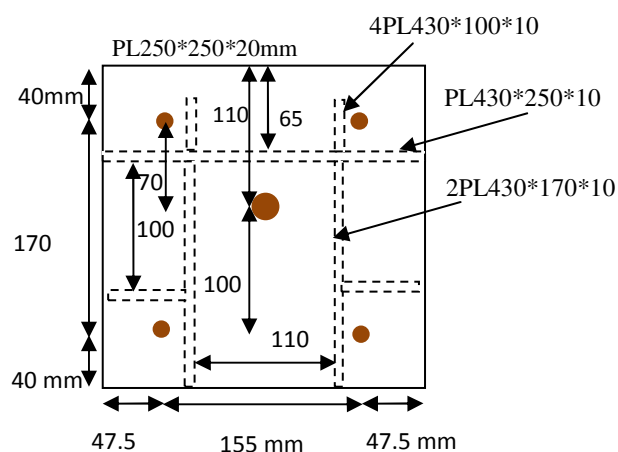


Fig. 3B. 6 Detail of supporting box for screw jack

3B.4 Design of the rig

Structural analysis indicated that during arch and catenar action the tie bars at the side joint exert significant horizontal load to the lateral support, which results considerable uplift reaction in the pinned supports of side bracing. Prior to design of the full scale test rig, I have been informed that, maximum tensile force transferred through the anchor bolts to the strong floor need to less than 80 kN. Accordingly, the properties of specimens has been designed, in which maximum uplift meet this requirement. To meet to this requirement, a comprehensive analysis has been conducted to prevent any damage to rig and especially to the strong floor using SAP 2000 (Fig. 3B. 7 and 8).

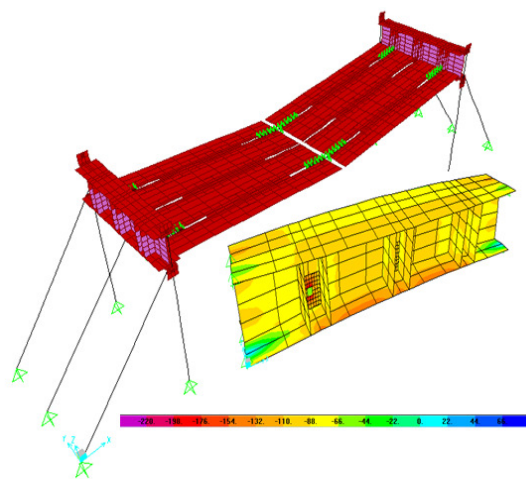


Fig. 3B. 7 Full scale simulation of test rig using SPA 2000

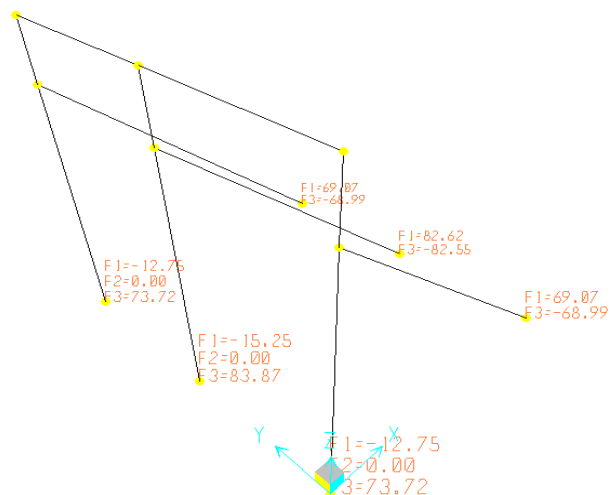
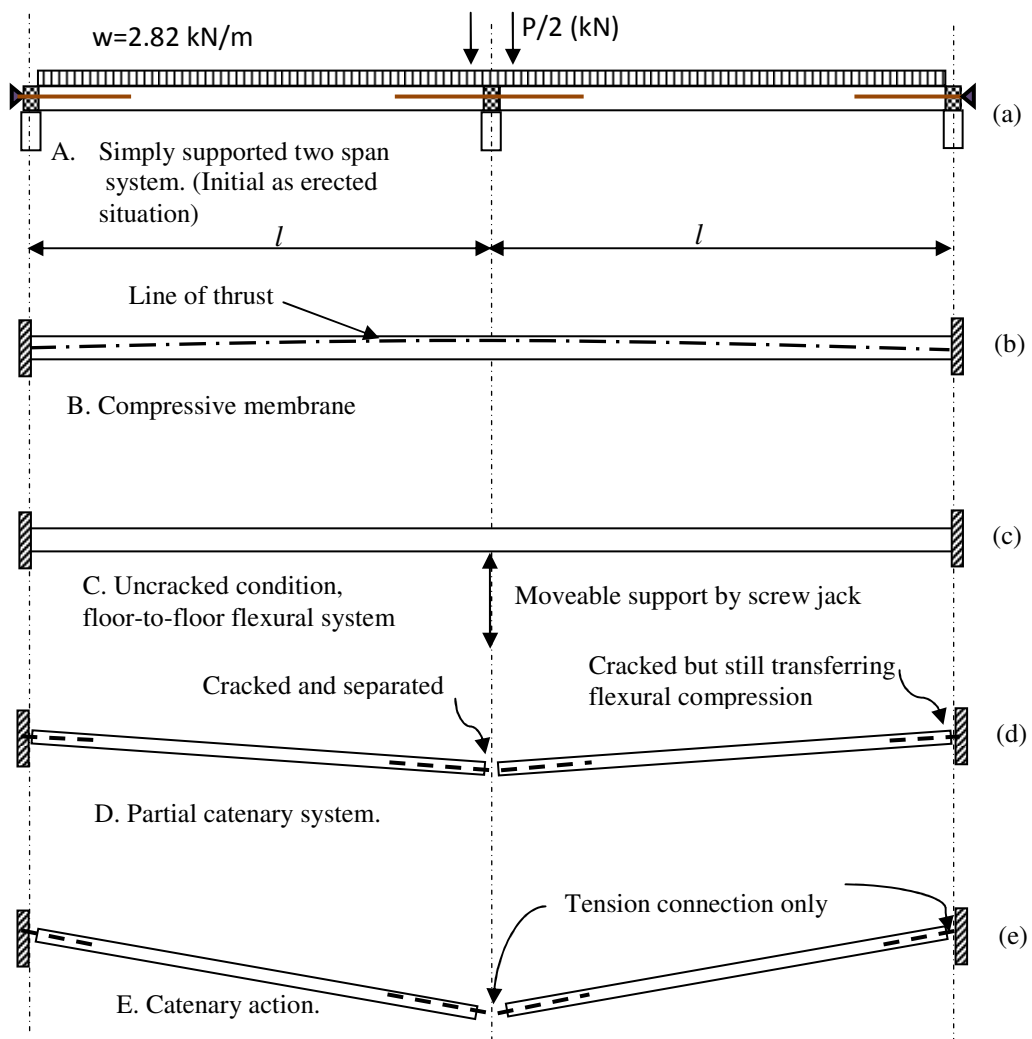


Fig. 3B. 8 Reaction supports

APPENDIX 3C: BEHAVIOUR OF THE FULL SCALE SPECIMENS

A total of five full scale tests were performed considering different bar size, embedment length, and number of tie at the joints. The first two tests were conducted to investigate the behaviour of system using embedment length more than anchorage length to develop bar fracture mechanism at the failure point and considering the effect of number of tie at the floor-to-floor joints. Specimen FT3, FT4, and FT5 were conducted to investigate the behaviour of system considering pullout mechanism using different bar size and embedment length.

The entire behaviour of floor-to-floor system immediately following removing wall support at the middle joint is shown in Figure 3C.1. Reducing reaction support with slowly lowering of the midsupport can be related to transition mechanism from assumed simply support condition to actual support condition. For the small vertical deflection due to flexural behaviour, load is redistributed from midsupport to the end supports. In this stage a combination of flexural and compressive membrane action governs the behaviour of system. As expected this phase was short-lived and ended following the visible crack at the mid and side supports (Fig. 3C.1). For the small bending moment, the maximum tensile stress is less than modulus of rupture, hence no crack is observed and whole cross section will be under tensile or compressive stress (Fig. 3C.1b).



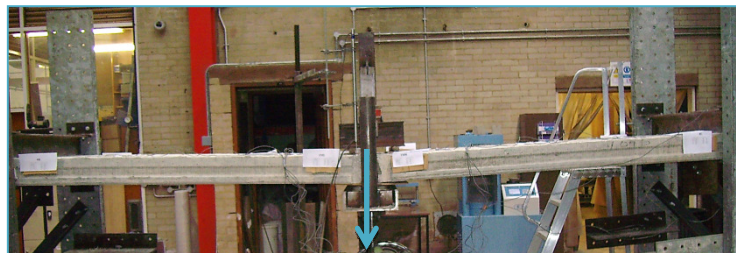
(f)

Fig. 3C. 1 Behaviour of floor-to-floor system after removing wall support at the middle

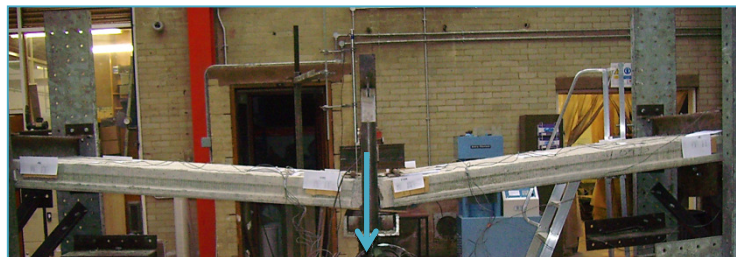


(g)

1. Initial state



2. During loading



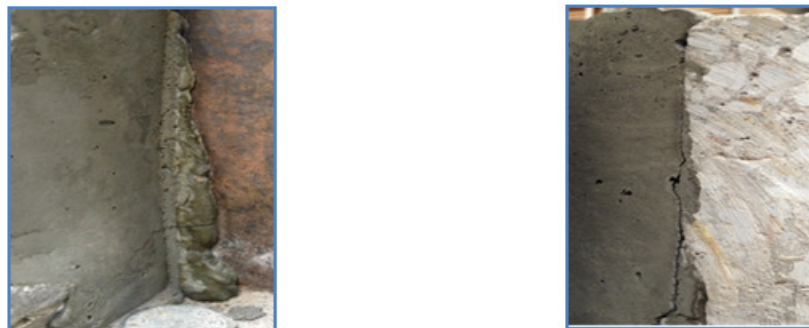
3. Final state



(h)

Fig. 3C. 1 Behaviour of floor-to-floor system after removing wall support at the middle (cont.)

Transition from flexural to catenary action mechanism is not clear, but can be shown through Figure 3C.1 b, c, and d. However, while the flexural cracks at the middle joint and supports were widened a small part of concrete gap i.e. less 4 mm at the compressive zone was crashed (Fig. 3C.2 – 3C. 3) and separated at the vertical deflection around 200 mm i.e. 10% of slab length in the specimens FT1/FT2 (Fig. 3C. 1). This stage is defined as “d” in Figure 3C.1. Following this stage, the fully catenary mechanism is developed in the specimens with pullout behaviour (Fig. 3C.1e).



(a) Crack at right support, $\delta_s / l_b = 0.15\%$ (b) Crack at mid support $\delta_s / l_b = 0.150\%$

Fig. 3C. 2 Initial crack at right support and middle joint



(a) Side view of middle gap support (b) Top view of middle gap (c) Side view of right gap

Fig. 3C. 3 Concrete crash at the middle gap and widened crack at the right support,

FT1, $\delta_s / l_b = 3.96\%$

The required elongation is provided by relative displacement between tie against to concrete at the interface and elastic or inelastic displacement in the reinforcement bars. This elongation accrued at the cracks at the middle joint or side joints.

Due to the small cross section of reinforcement, they can be ignored in stress calculation in uncracked section analyses. For uncracked section, the tensile stress can be calculated using the standard equation to calculate stress in beams:

$$f = \frac{My}{I_g} \quad (3C.1)$$

Where

M = bending moment

y = distance between a specific point to the natural axis of section

I_g = moment of inertia of the uncracked section

f = stress at the point with distance y from natural axis

This equation is valid while the maximum tensile stress is less than tensile strength. Following the first crack, entire tensile force is sustained by reinforcement bars at the tensile zone and concrete at the top carries compressive force (Fig. 3C. 4). To calculate the stress in steel bars and concrete the following equations developed based on Figure 3C. 4 are used.

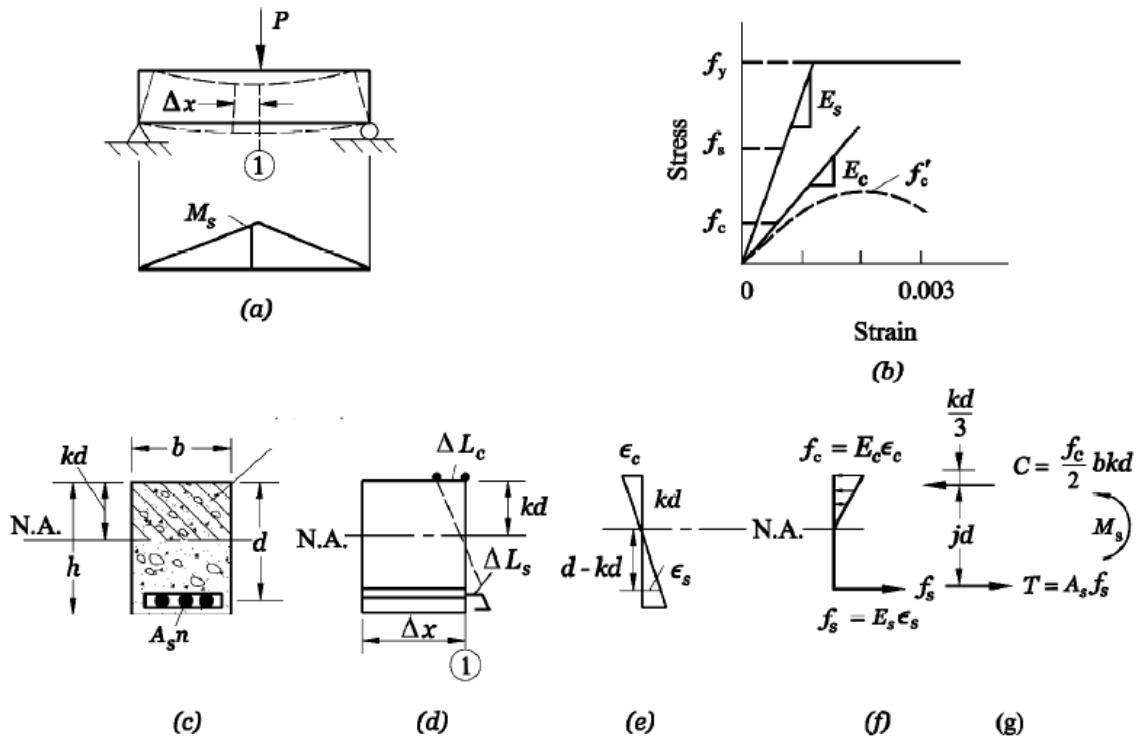


Fig. 3C. 4 Stress and strain for cracked section (a) simple support beam under point load, (b) stress-strain curve, (c) cross section of slab, (d) deflection due to moment, (e) strain distribution, (f) stress distribution, (g) internal couple (Tohidi, 2008, Leet, 1997)

To calculate tensile stress in the concrete and bars the following equations are used

$$f_s = \frac{M}{A_s \cdot jd} \quad f_c = \frac{2M}{jkb d^2} \quad (3C.2)$$

$$(3C.3)$$

where

$$jd = d - \frac{kd}{3} \quad \text{and} \quad j = 1 - \frac{k}{3} \quad (3C.4)$$

$$k = -\rho n + \sqrt{(\rho n)^2 + 2(\rho n)} \quad \rho = \frac{A_s}{bd} \quad \text{and} \quad n = \frac{E_s}{E_c} \quad (3C.5)$$

Due to equilibrium condition, the tensile force in the tie bars need to equal to compressive force at the top of section

$$A_s f_s = \frac{f_c}{2} b(kd) \quad (3C.6)$$

As the section of precast slabs at the joints for all specimens are identical, reinforcement bar in the cross sections is the only variable in concrete crack analyses. Following cracks as the tie force is dramatically increased; hence tie force at the supports will provide an extra bending resistance around support provided under the slabs. Considering tie force developed in Chapter 2, the maximum stress at the tie bars can be obtained

$$f_s = \frac{(wbl_b + P)}{2nA_s(d + c)} l_b \quad (3C.7)$$

According to test result for FT1/FT2 the first crack was absorbed corresponding to the load of 3.7 kN, while the first crack in FT3 was observed prior applying line load by screw jack. Considering self-weight of slab and line load (Table 3C. 1); the first crack is induced at tensile stress of 0.8 and 0.35 MPa for specimens FT1/FT2 and FT3 respectively, which relatively less than tensile strength of concrete at the gaps. This crack was propagated from the bottom to the top at $\delta_s / l_b = 0.150\%$. Using test result data, the stress analysis is shown in the Table 3C.1.

Table 3C. 1 The cracked section analysis results for the specimens FT1, FT2, and FT3

Test	Bras	A_s (mm ²)	Tensile stress	Cracked section						
			f_{ct} MPa	ρ	n	k	j	kd mm	f_c MPa	f_s MPa
FT1	2 ϕ 10	157	1.23	0.0017	6.54	0.14	0.954	11.55	6.49	332.57
FT2	3 ϕ 10	235.5	1.23	0.0026	6.54	0.17	0.945	13.9	5.42	221.71
FT3	2 ϕ 12	226.08	0.6	0.0012	7.09	0.12	0.94	10.29	3.03	125.83

According to the test results the deflection at the cracked stage for FT1 and FT2 was 4.07 mm which propagate quickly to 40.22 mm and 30.64 mm corresponding to the maximum applied load on FT1, and FT2 respectively. In the specimen FT3, deflection corresponding to the first

crack was 3.25 mm. Unlike to the first two specimens crack induced prior to applying load at the middle joint by screw jack. It can be attributed that, tensile stress in FT3 specimens is less than other two specimens. However, the stress following first crack increases relatively smoother than FT1 and FT2 up to maximum line load at the middle.

The above analytical analyses show that compressive stress at the top of concrete gap at the middle joint corresponding first cracks was relatively less than compressive strength of specimens. Also, the tensile stress in the reinforcement bars at the cracked section is less than the yielding stress i.e. $f_y = 515$ MPa (Table 3C. 1).

Table 3C. 2 indicate that, stress in the tie bars corresponding to the peak load is slightly more than yield stress of ties for FT1 and FT2 i.e. $f_y = 515$ MPa. It can be attributed to the effect of boundary condition, real position of tie bars, and actual strength of either steel or concrete. Also, as expected the stress corresponding to the peak load for the specimens with pullout failure mode is less than yield stress. The stress-deflection relationships of the five full scale tests clearly confirm the above conclusions.

Table. 3C. 2 Stress at the plastic stage for the specimens FT1, FT2, and FT3

Test	Bras	A_s (mm ²)	Cracked section						
			ρ	n	k	j	kd mm	f_c MPa	f_s MPa
FT1	2 ϕ 10	157	0.0017	6.54	0.14	0.954	11.55	11.66	569.69
FT2	3 ϕ 10	235.5	0.0026	6.54	0.17	0.945	13.97	14.47	566.38
FT3	2 ϕ 12	226.08	0.0012	7.09	0.12	0.94	10.29	10.97	431.62

Eq. (3C.6) indicates that, beyond the yielding point the tensile force is constant; hence more applied load is sustained by increasing lever arm or decreasing compressive zone at top of the concrete section. According to EU Code, at the ultimate state the neutral axis, x , and moment resistance, M , for singly reinforced beam is

$$x = A_s f_s / 0.8 f_c b \quad (3C.8)$$

$$M = A_s f_s (d - 0.4x) \quad (3C.9)$$

The neutral axis at the yield stage for FT1, FT2, and FT3 is 2.81 mm, 4.21 mm, and 4.41 mm, respectively. The test results indicate that the depth of crashed concrete at the top of middle gap and at the collapse is less than 5.0 mm.

Deflection prior to catenary stage

For the specimen with concrete at the gap, the middle joint deflection is induced by slip of tie bars into the keyways of slabs. According to full scale test result, the deflection mode of full scale test is taken into account to propose a simple but reliable relationship between slip and deflection (Fig. 3C. 5). The five experiments clearly indicate that the precast slabs can be assumed as a rigid body; hence by using similarity between triangles in Figure 3C. 5 the relationship between slip and deflection can be obtained

$$\frac{\delta_s}{l_b} = \frac{\Delta}{d} \quad (3C. 10)$$

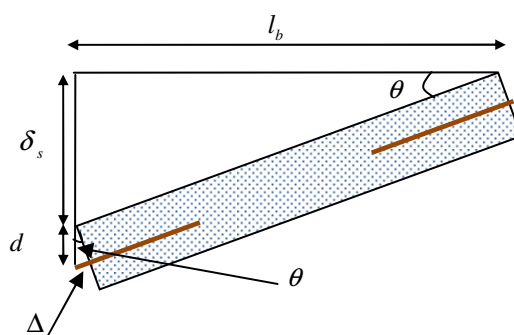


Fig. 3C. 5 Deflection mode of full scale tests

The reliability of Eq. (3C. 10) was verified by comparing the load-deflection of full scale test results and pullout force-deflection using Eq. (3c. 10). Figure 3C. 6 indicates that deflection corresponding to maximum strength of floor-to-floor system is approximately equal to calculated deflection using Eq. (3C. 10) corresponding to peak pullout force. As maximum strength of full scale system is occurred at the peak pullout force, it reveals that Eq. (3C. 10) is able to predicted deflection of floor-to-floor system prior to developing catenary action mechanism.

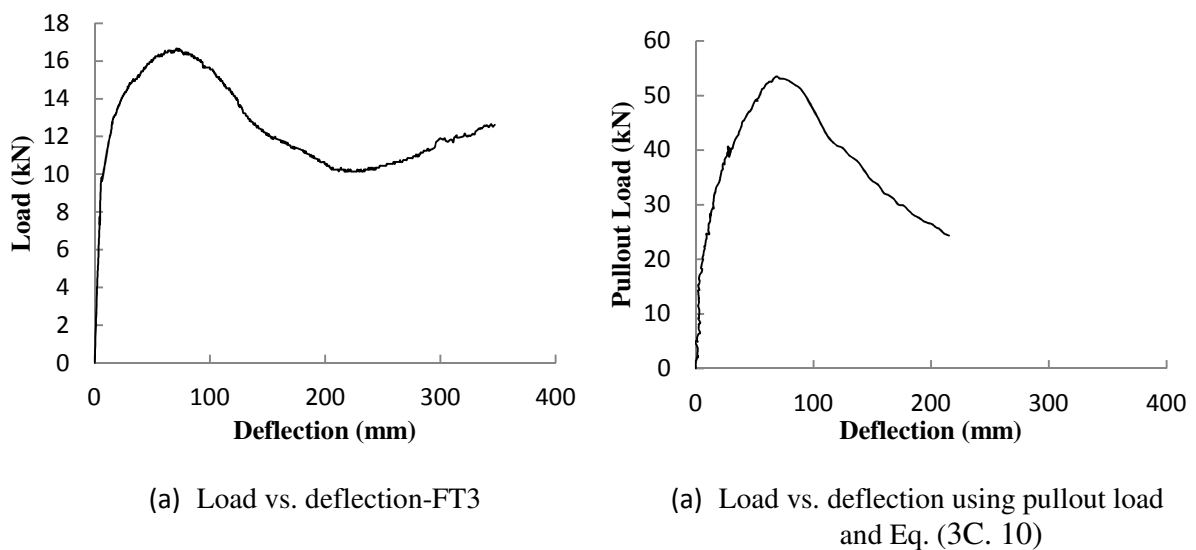


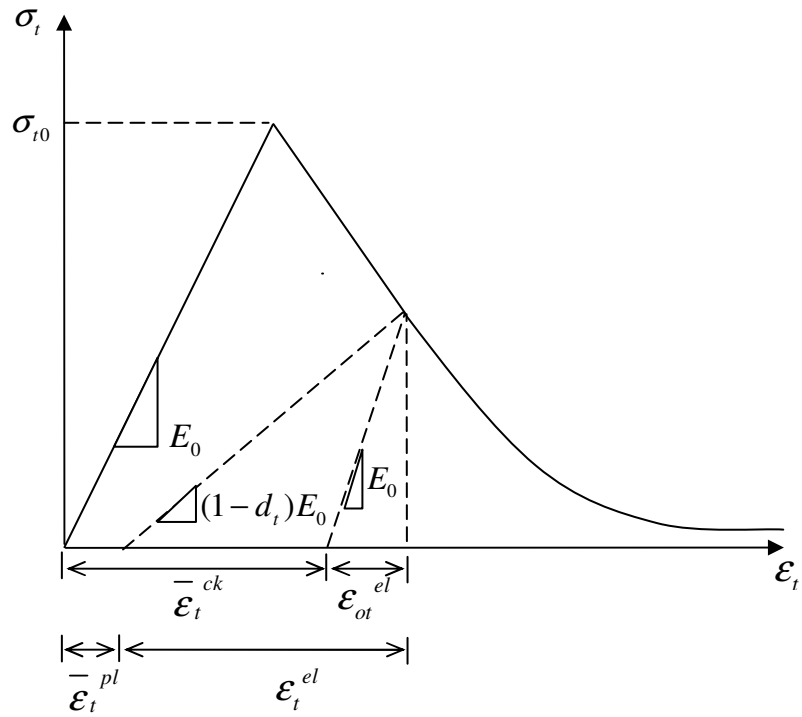
Fig. 3C. 6 Verification of Eq. (3C. 6) using full scale and pullout test result

APPENDIX 4A: CONCRETE MODELLING

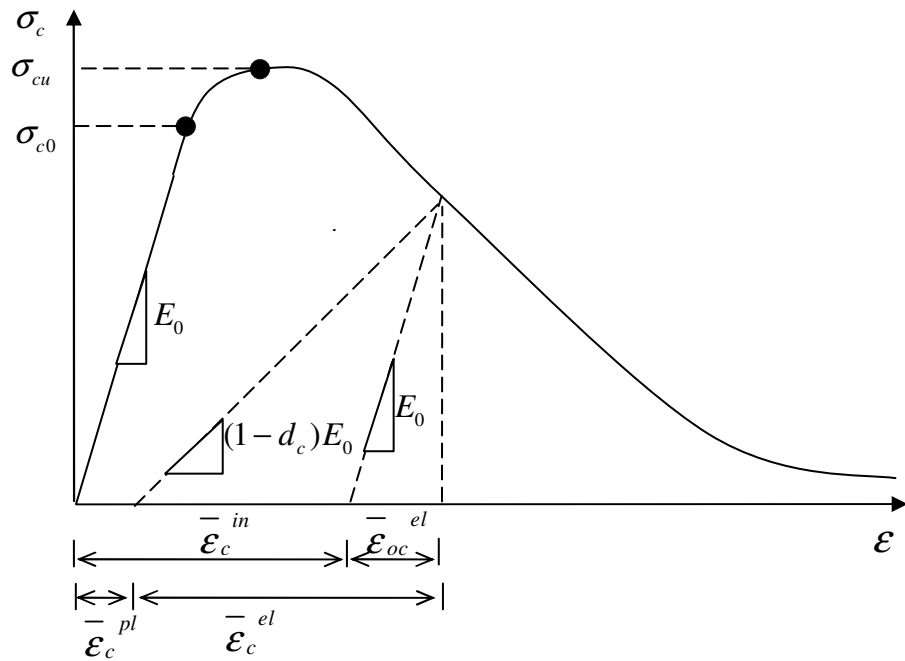
To analyse RC structures, for low confining pressure, ABAQUS has provided three different concrete models: (1) “Concrete smeared cracking” (2) “Concrete damaged plasticity” and (3) “Cracking model for concrete”. In this study Concrete Damage Plasticity (CDP) model is used, but CDP model is described in detail in the following sections.

4A.1 Concrete Damage Plasticity (CDP)

Concrete Damage Plasticity (CDP) is available in ABAQUS/Explicit/Standard usable for both static and dynamic analyses. It is primarily designed to analyse of RC structures subjected to monotonic, dynamic or cyclic loading under low confining pressure. This model can be used in all types of elements e.g. solids, shells, trusses, and beams and “uses concepts of isotropic damaged elasticity in combination with isotropic tensile and compressive plasticity to represent the inelastic behaviour of concrete” (ABAQUS, 2006). This model can be used to model plain concrete and it can be extended to RC elements by introducing one-dimensional rebar element in one or more layer embedded in concrete. In this model compressive crushing and tensile cracking are the main two failure mechanism of concrete material. The yield failure is defined by two hardening parameters, $\bar{\epsilon}_c^{pl}$ and $\bar{\epsilon}_t^{pl}$ corresponding to failure mechanism under plastic compression and tension loading, respectively (Fig. 4A. 1).



(a) Tension response of concrete and definition of cracking strain $\bar{\epsilon}_t^{ck}$ to define tension stiffening data



(b) Compression response of concrete and definition of inelastic strain

Fig. 4A. 1 schematic stresses versus strain curve for concrete under uniaxial loading

4A. 2 Concrete properties

The concrete mix was designed for standard compressive strength of 20 and 30MPa at 28 days. The relevant compressive strength for the different full scale test specimens is shown in the Fig. 4A. 2. Average compressive strength of cube or cylinder, and tensile strength of prism were calculated based on the three specimens on the days of tests. The slump of concrete was between 90-110 mm on the day of placements. For each tests, strain-stress were provided using three cylinder/cube specimens.

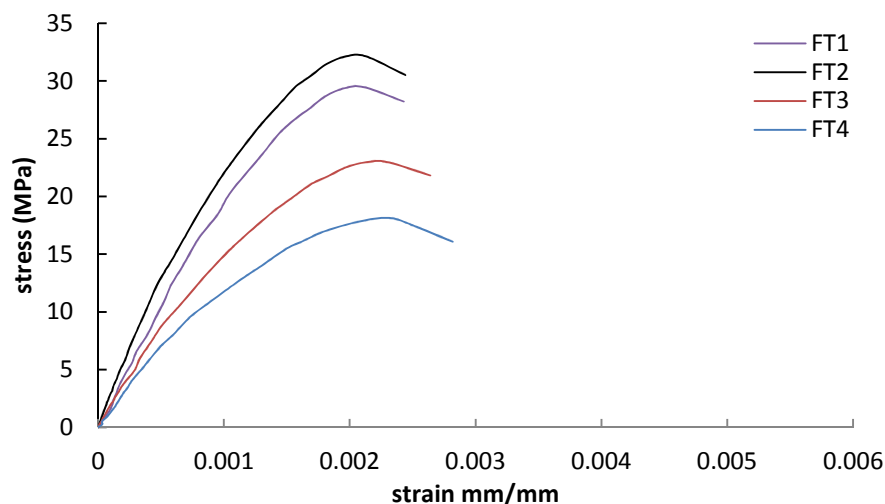


Fig. 4A. 2 Stress-Strain curves used in the concrete gap of specimens

Due to the test procedure discussed in Chapter 3 is only able to provide a small part of descending stage, hence the second set of test programme was conducted to define total descending stage (Fig. 4A.3). Furthermore, the model provided by EC2 is not be able to define stress-strain beyond the strain of 0.0035, hence to define input data for CDP model, a combination of EC2 regulation and test result was used.



Fig. 4A. 3 Compressive test rig to define descending stage- series 2

The results of strain-stress relationship for various compressive strengths are displayed in Figure (4A. 4). In these set of tests cube specimens with dimensions of 50x50x50 mm is used. The results indicate that in the both sets of experiments, the result provide more strain corresponding to peak stress and less modulus of elasticity compare to the EC2 regulation, while the descending stage shows acceptable agreement with EC2. Due to these deficiencies, in this study for the input date CE2 concrete model is used with a minor modification (Fig. 4A. 5 and 6).

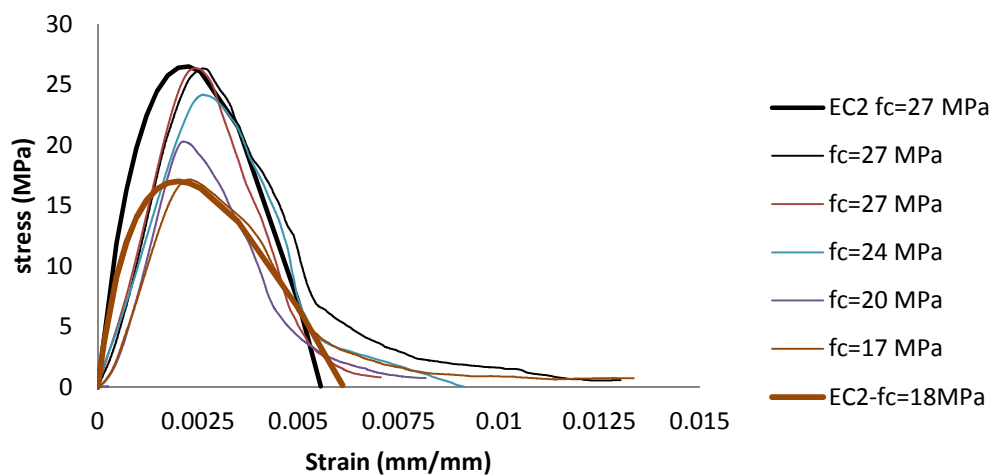


Fig. 4A. 4 Stress-Strain curves for various compressive strengths

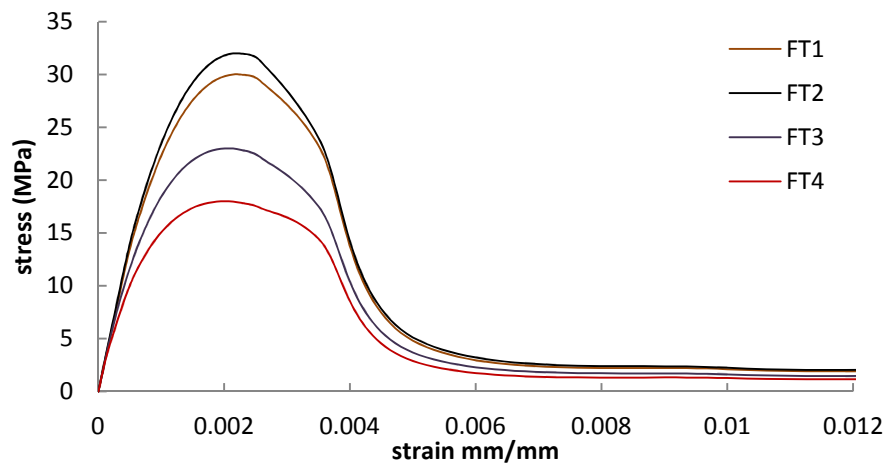
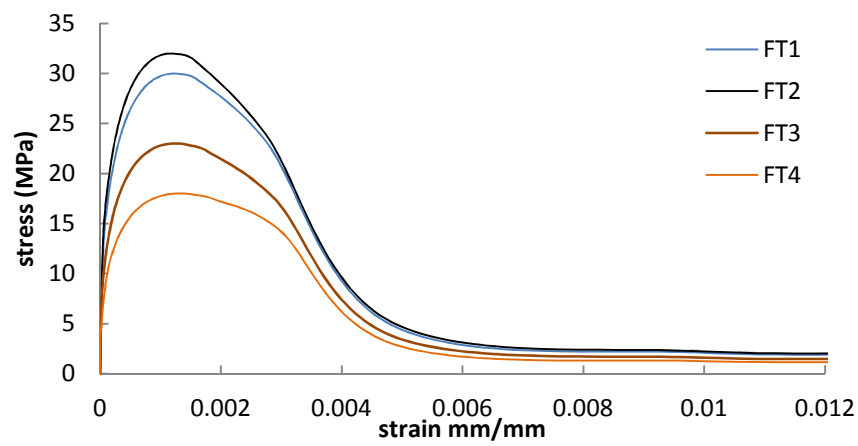
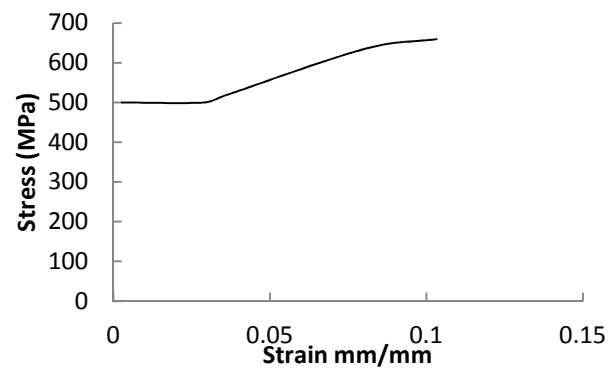
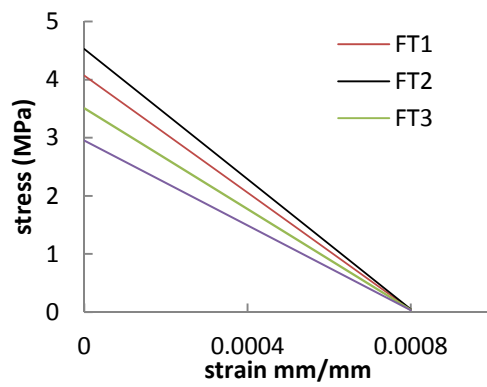


Fig. 4A. 5 Final stress-strain curves used in CDP model



(a) Compressive hardening



(b) Tension stiffening

(c) Steel

Fig. 4A. 6 Stress-strain data for CDP model

4A. 3 Calibration/verification of the CDP model

4A. 3.1 Cube model

To calibrate the CDP model, a series of FE analyses on cube model (Fig. 4A. 7) are performed using the strain-strain relationship based on compressive test results on cube specimens conducted at the same days of the full scale tests.

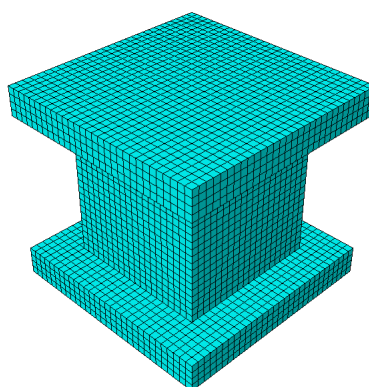


Fig. 4A. 7 Cube model

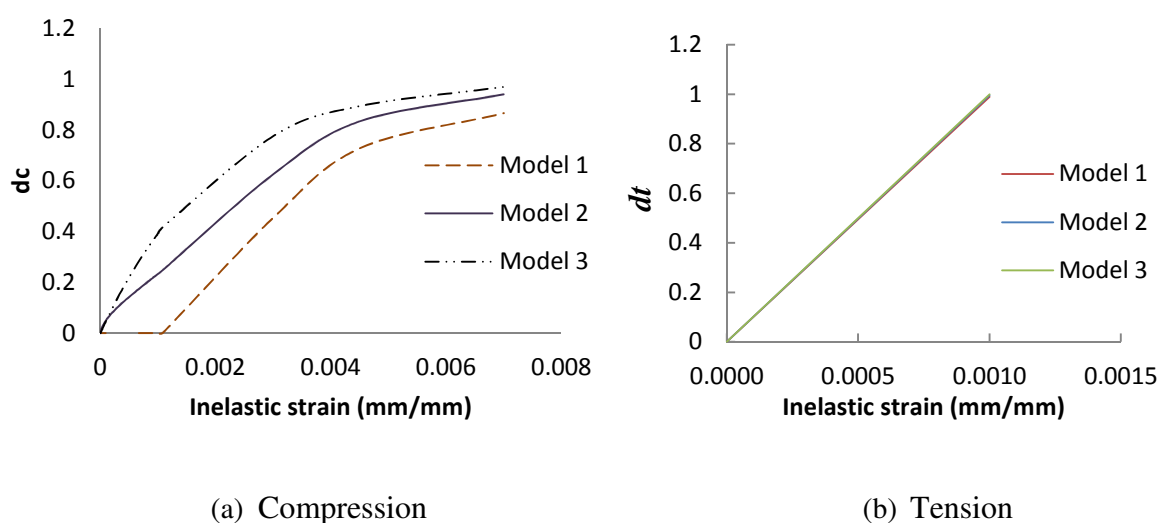
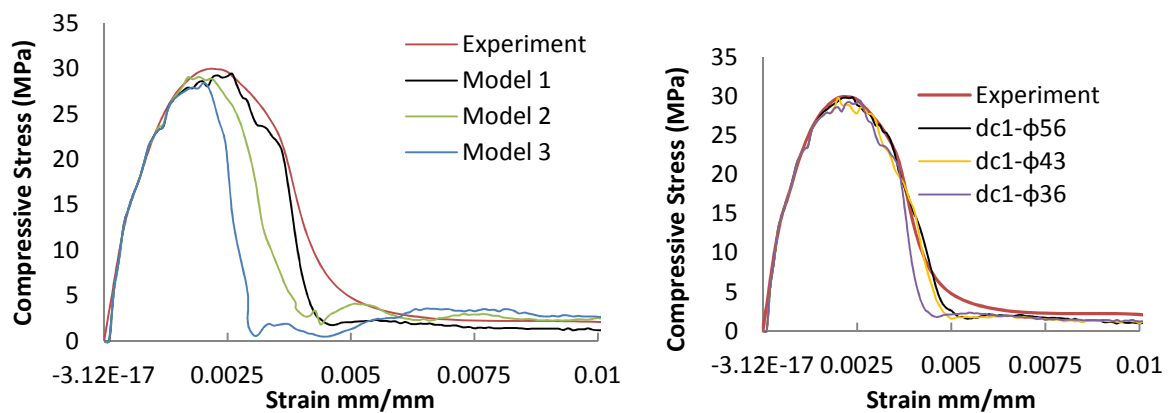


Fig. 4A. 8 Damage parameters for CDP model

To define valid CDP model three parameters of stress-inelastic strain, d_c , and d_t need to be defined. The stress-inelastic strain is defined using Fig. 4A. 6. The relevant damage parameters of d_c , and d_t are shown in Figure 4A. 8. To define optimum d_c the specimens analyzed using three models discussed in the Chapter 4. In these analyses only d_c were variable and all other CDP parameters assumed to be constant. The dilation angle, eccentricity, f_{b0} / f_{co} , and k was assumed to be 36° , 0.1, 1.1, and 0.667, respectively.

Figure 4A. 9a indicate that, all three damage parameter provide same stress-strain relationship in ascending stage, while following peak stress the each damage parameter shows different trend compare to the original stress-strain data. The result indicates that, the strain-strain relationship using damage parameter of model 1 defined in Chapter 4 is agreeing well with the original data compare to the other two models (Fig. 4A. 9a). To show the effect of dilation angle, the same cube specimens was reanalysed using dilation degree of 43 and 56 (Fig. 4A. 9b). The results indicate that, the specimens with damage parameter of d_c defined by model 1 and dilation degree of 43/56 agree extremely well with the stress-strain defined in section 4A. 3. The same result can be obtained using specimens with other compressive strength. The results of stress and strain for the cubes in the different stages are shown in Fig. 4A. 10.



(a) Stress vs. strain for three different damage

(b) Stress vs. strain for three different dilation

parameters

angle

Fig. 4A. 9 stress vs. strain using various damage parameter and dilation angle

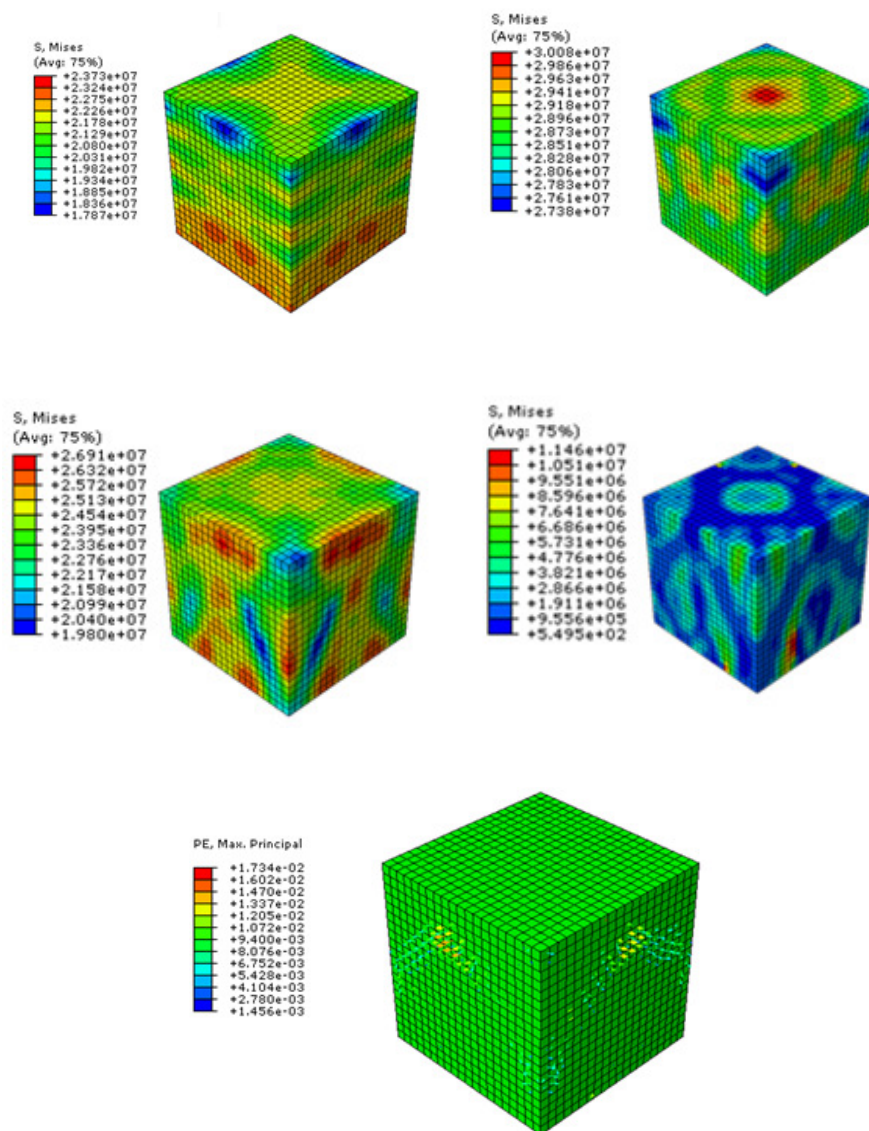


Fig. 4A. 10 Stress and strain pattern on the cube

To show more efficiency of the calibrated CDP model, the crack pattern of specimens using FE analyses was compared to the experimental test results. Figure 4A. 11 shows that crack pattern of FE analyses shows relatively the same configuration of crack pattern of cube test result

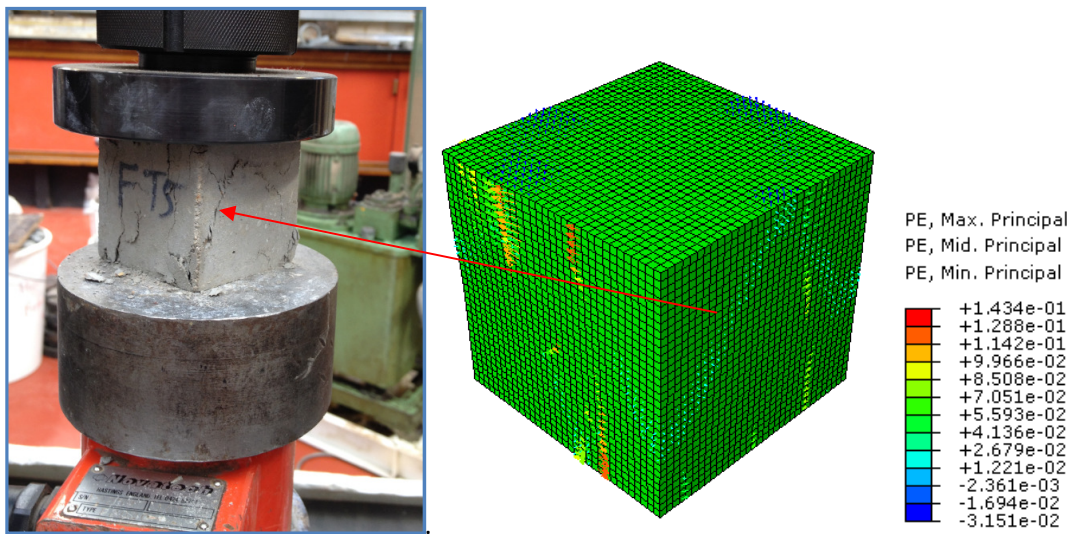


Fig. 4A. 11Crack pattern in FE analysis and cube test specimens

4A. 3.2 Prism model

To show the efficiency of the developed CDP model, the results of FE analyses was compared with short beam test on plain concrete. To verify the developed model ten experimental studies was conducted on simple support beams with length of 500 mm and width and height of 100 mm (Fig. 4A. 12). For all specimens to define the tensile strength both beam and splinting test was performed. The results are shown in Table 4A. 1.

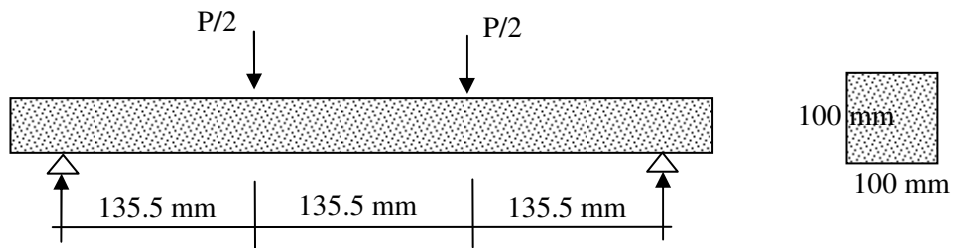
Table 4A.1 Tensile stress based on short and cylinder splitting test

Test No	Fcm (MPa)	Beam		Cylinder	
		P (kN)	Fct (MPa)	P (kN)	Fct (MPa)
1	28.25	11.6	4.7	65.8	1.39
2	22.3	9.49	3.8	62.5	1.32
3	31.4	12.7	5.15	111	2.36
4	28	10.7	4.33	71.5	1.5
5	22.1	10.1	4.09	75.3	1.6
6	23.4	11.1	4.4	71.7	1.52



(a) Short beam

(b) Cylinder splitting



(c) Short beam dimensions

Fig. 4A. 12 Bending test on short beam and cylinder splitting

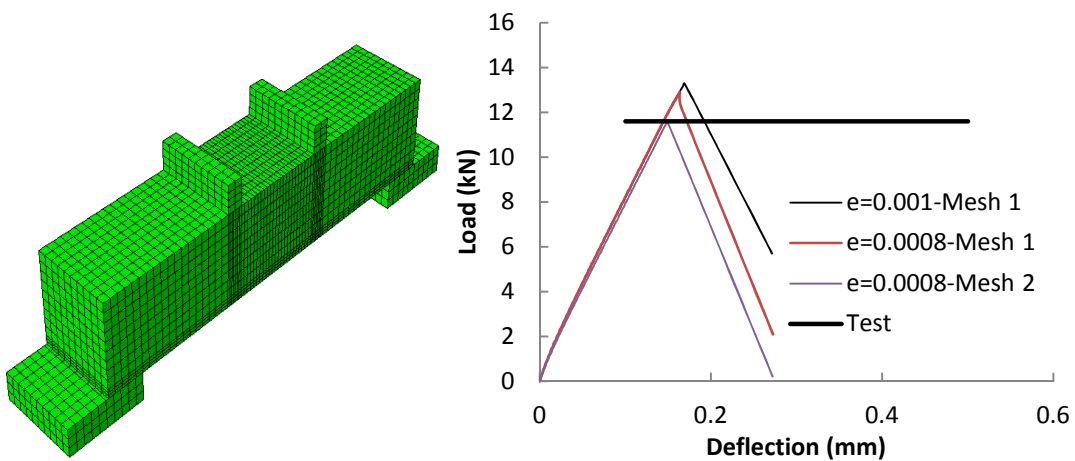


Fig. 4A. 13 Prism model

Fig. 4A. 14 Load vs. deflection using prism model

To reproduce experiment test result, the same prism of experimental study is modelled using ABAQUS (Fig. 4A. 13). The prism is analysed using various mesh pattern and cracking stain. Figure 4A. 14 indicate that, the mesh pattern has significant effect on the strength of short

beam. For the first mesh pattern, the mesh size is assumed to be 10 mm, while in the second mesh pattern the mesh size at the bottom and loading area is assumed to be 5 mm and the rest is set on 10 mm.

Figure 4A. 15 shows the tensile stress prior initial crack for mesh pattern 2. The result indicates that, the mesh pattern trail 2 provide the exactly the same tensile stress as that of experiment. The test results indicate that, the failure strain can be assumed more than 1^{-4} , while cracking strain need to be less than 1^{-3} suggested by ABAQUS. The test and FE result indicates that the failure strain can be assumed 1.5^{-4} (Fig. 4A. 16) and strain corresponding to zero stress can be assumed 0.8^{-3} (Fig. 4A. 14).

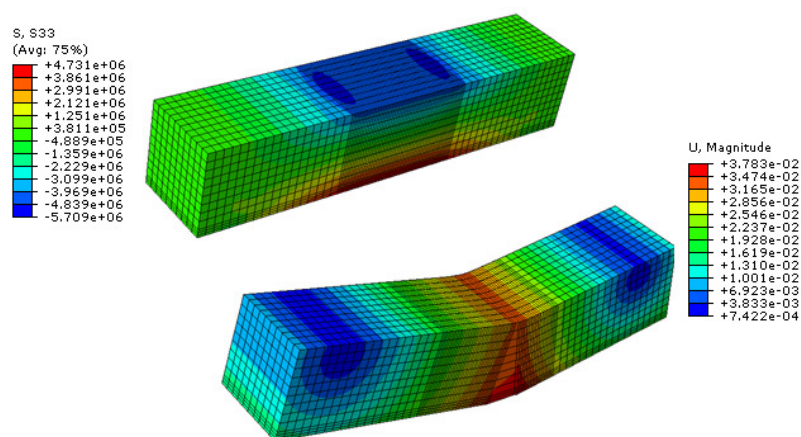


Fig. 4A. 15 Stress and deflection in the prism model - $f_{ct} = 4.73 \text{ MPa}$ MPa

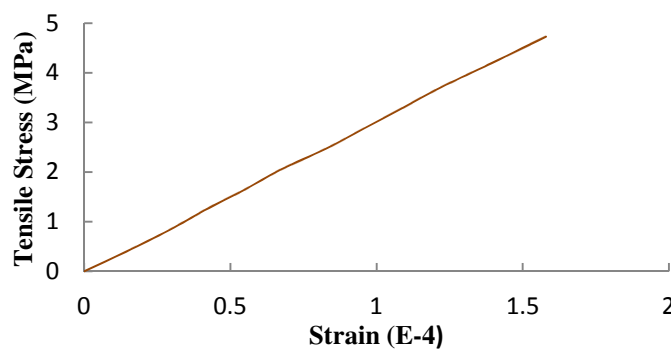


Fig. 4A. 16 Maximum failure strain



(a) Test specimen

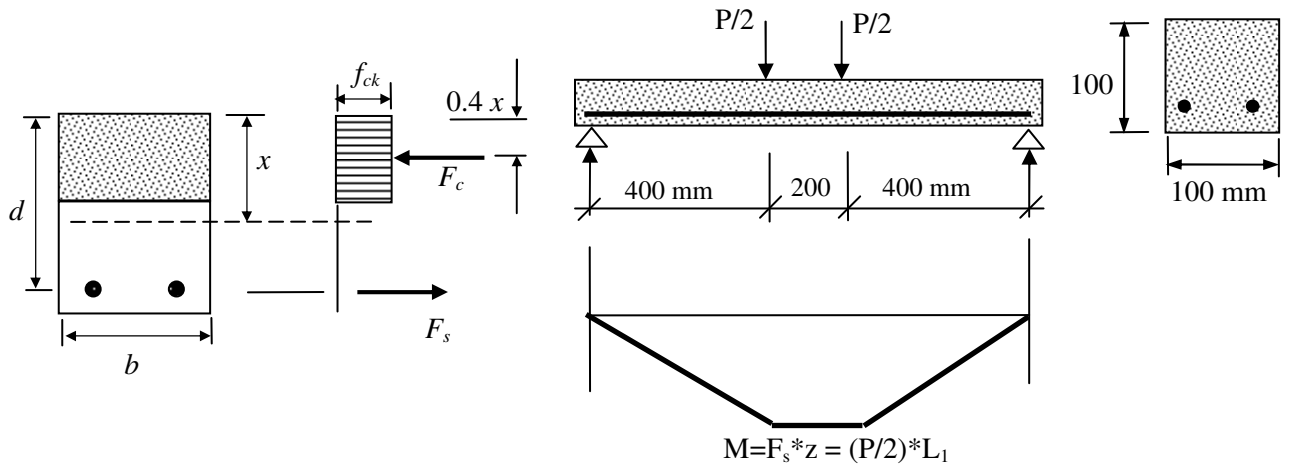


Fig. 4A. 17 Theoretical strength of the beam

4A. 3.3 RC beam model

To show more efficiency of the CDP/Translator model developed in the Chapter 4, 8 experiments have been conducted on RC beam with length of one meter. The width and height of beam section is 100x100 mm with two bar size of 8 mm at 15 mm from the bottom of beam (Fig. 4A. 17). The load increment of 1 kN applied on the middle of beam and relevant deflection was recorded at each stages. Also, the load corresponding to the first crack and collapse was recorded. The propagation of crack was marked for each load increment. For the each tests the theoretical capacity of beam obtained using EC2 provision. To calculate the

strength of the beam, stress distribution and bending moment diagram shown in Figure 4A. 17 and the following procedure are used

$$M = F_s Z \quad (4A. 10)$$

Where $Z = d - 0.4x$, $x = \frac{f_{yk} A_s}{0.64 f_{cu} b}$ and $F_s = f_{yk} A_s$.

$$P = \frac{2M}{0.4} \quad (\text{Fig. 4A. 17}) \quad (4A. 12)$$

The results of load vs. deflection for three specimens are shown in Figure 4A. 18. The result indicates that, maximum load sustained by RC beams using theoretical method is agreed well with experimental study (Table 4A. 2).

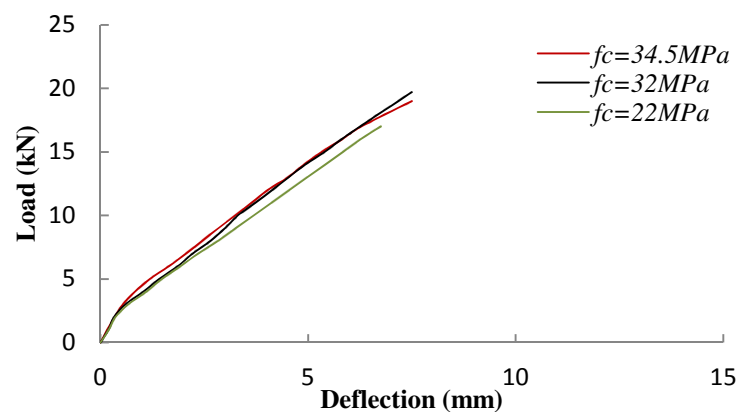


Fig. 4A. 18 Load vs. deflection based on experimental study

Table 4A. 2 Strength of RC beam based on experimental and theoretical method (EC2)

Test	f_{cm}	f_{ct}	P_{theory}	P_{test}
B1	34.38	5.15	20.1	19.1
B2	32	4.71	19.9	19.7
B3	30	4.8	19.8	18.0
B4	22	3.7	19.2	18.3

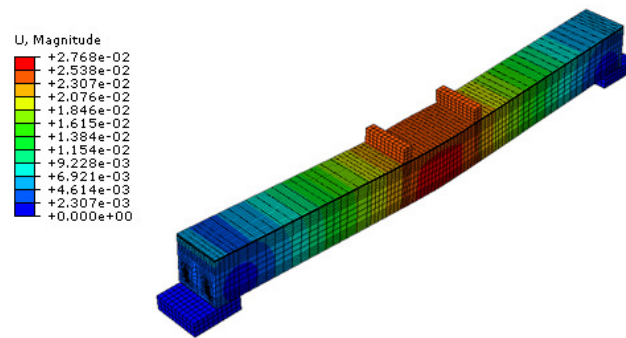


Fig. 4A. 19 FE model of RC beam - deflection following the peak strength

To show the efficiency of the developed CDP model in Chapter 4, two RC beams with compressive strength 30 MPa and 20 MPa is analysed and compared with the result of experiment and theoretical method and displayed in the Chapter 4 (Fig. 4.29). The deflection of the RC beam is shown in the Figure 4A. 19. In this model reinforcement bars and concrete was modelled using solid element i.e. C3D8R and to define bond stress at the interface between concrete and steel translator as a special connector in ABAQUS is used. Figure 4A. 20 indicates that stress-strain at a critical point at the middle of the beam in ascending, peak, and descending stage are agree extreme well with the strain-strain defined as input data.

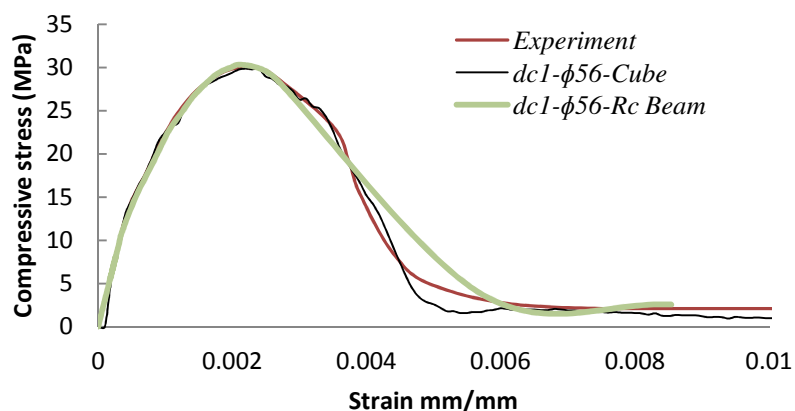
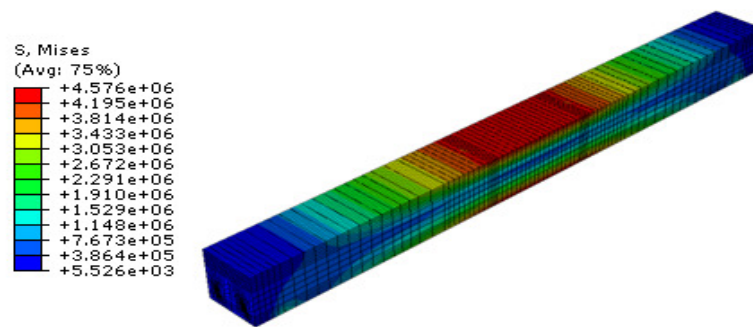
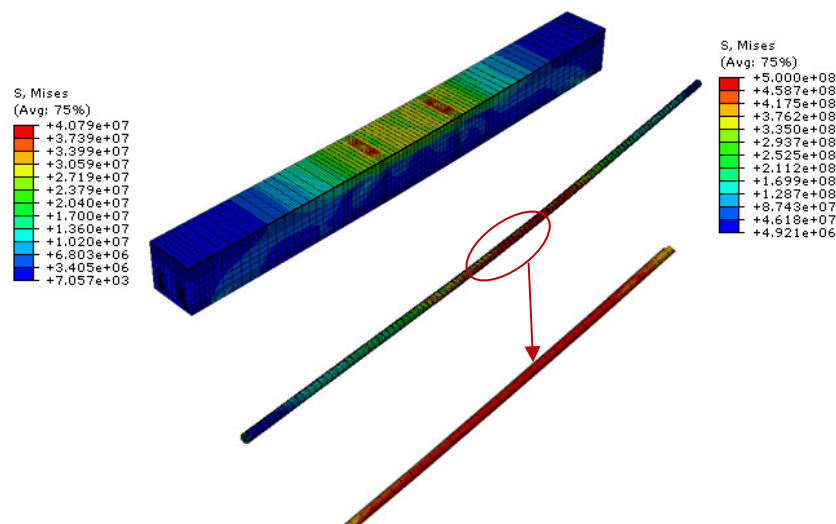


Fig. 4A. 20 stress vs. strain using various damage parameter and dilation angle for critical element at the middle joint of RC beam- $f_c=30$ MPa

The failure procedure of RC beam is shown in Figure 4A. 21. Figure 4A. 21a indicates that maximum tensile stress prior to the first crack is 4.57MPa which is slightly less than tensile strength obtained by experimental study i.e. 4.8MPa ($f_c=30\text{MPa}$). The result shows that, following the first crack the stress at the top of cross section increased by 2.7 times. As expected the reinforcement bars experiences yielding while the compressive stress at the top of section reaches the maximum compressive strength. From the above results and comprehensive simulation provided in the Chapter 4, It can be clearly concluded that the developed CDP model is successfully able to model any RC beam elements.



(a) Tensile stress prior to the initial crack



(b) Compressive stress in concrete and bars prior to the failure

Fig. 4A. 21 Failure mechanisms

APPENDIX 5A SAP 2000 MODELLING

Due to simplicity of modelling and to provide initial data regarding floor-to-floor behaviour following removal wall support using static nonlinear analyses, at the early stage of present study the FE code of SPA 2000 is used.

5A. 1 Bond Slip simulation

To simulate steel-grout interfacial behaviour, NLLink element was used (Fig. 5A. 1). The property of the NLLink element was calibrated using average bond stress-slip relationship result from pullout tests considering bar size 12 mm into concrete with the embedment length of 250 mm. The stiffness of the NLLink element can be defined as $k = \frac{usC}{n\Delta}$. All variables are the same as variables in Chapter 4. To show the validity of the simulation, pullout and full scale floor-to-floor experimental study in the present study was used.

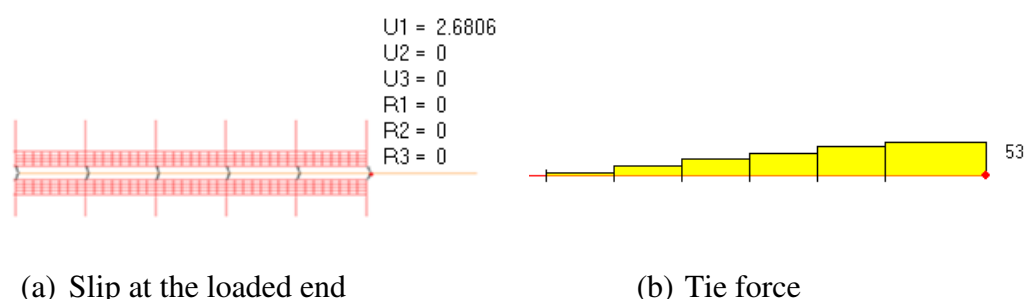


Fig. 5A. 1 Pullout simulation using NLink element-P=53kN, K=2.13kN/mm

5A.2 NUMERICAL CASE STUDY

A three dimensional full model was created by using a general purpose FEA software SAP 2000. For this propose, the specimen with the same properties of FT4 described in Chapter 3

is used. In this model, slabs and steel bars have been modelled as shell and frame element, respectively.

5A.3 Verification

The proposed method is verified using FT4 specimen conducted in the present study. According to pullout test results, the stiffness of NLLink spring for bar size 12 mm with 250 mm embedment length is 2.13 kN/mm and 1.06 kN/mm for the middle and side stiffness, respectively. Gravity load due to slab weight and extra point load applied by screw jack was applied on the top of the slab and middle joint, respectively. The results show that, both vertical deflection and tie force agree extremely with the present experimental study i.e. FT4 (Fig.5A. 2). The slight discrepancy is related to considering average bond slip to define NLLink spring properties

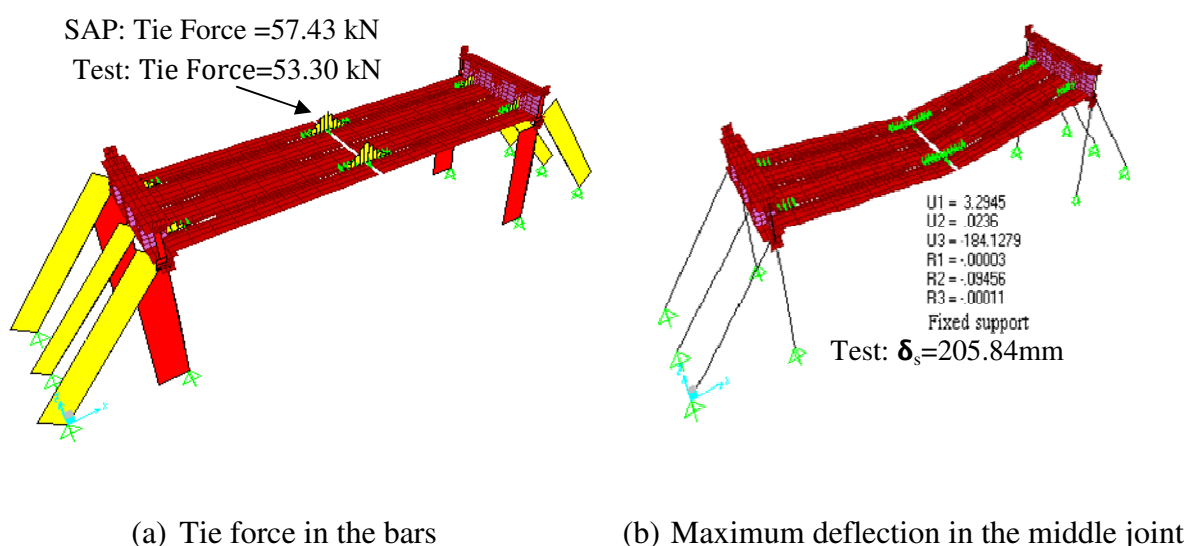


Fig. 5A. 2 Tie force and maximum vertical deflection-FT4; $w=2.35 \text{ kN/m}^2$, $P=14.5 \text{ kN}$, $k_m = 2.13 \text{ kN/mm}$, $k_s = 1.06 \text{ kN/mm}$

5A. 4 ANALYSIS RESULTS

Longitudinal Ties: A series of full scale floor-to-floor joint with various floor span lengths were analyzed (Fig. 5A. 3). The analyses are conducted for three different span lengths and uniform load of 6.25kN/m^2 . The result of analyses are summarised in the Table 5A. 1.

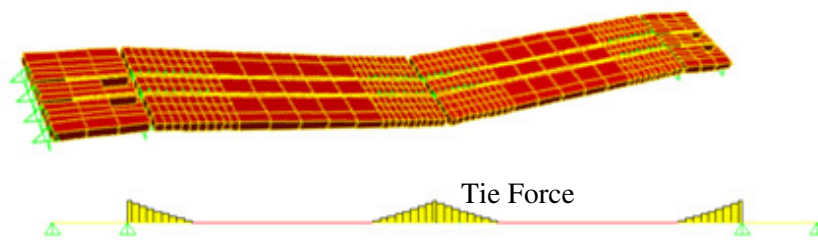


Fig. 5A. 3 Floor-to-floor model using longitudinal ties

Table 5A.1 Tie force and deflation using longitudinal ties at the joints

L (m)	F (kN)	δs (mm)	$P = \alpha w l$
4.075	108.3	289	$P = 4.2 w l$
6.075	181.8	583	$P = 4.8 w l$
8.075	239.4	793	$P = 4.7 w l$

Longitudinal and Transverse ties: The developed model for longitudinal ties is used to analyse of floor-to-floor system using longitudinal and transverse ties (Fig. 5A. 4). In these set of analyses the applied load was assumed to be two times of applied load on model with longitudinal ties i.e. 12.5 kN/m^2 . The results of tie force in longitudinal and transverse ties are shown in Table 5A.2. The results indicate that tie force in the all longitudinal ties is more than transverse ties, which shows the result of ABAQUS modelling. Furthermore, Figure 5A. 4 clearly shows the same deflection pattern obtained by ABAQUS.

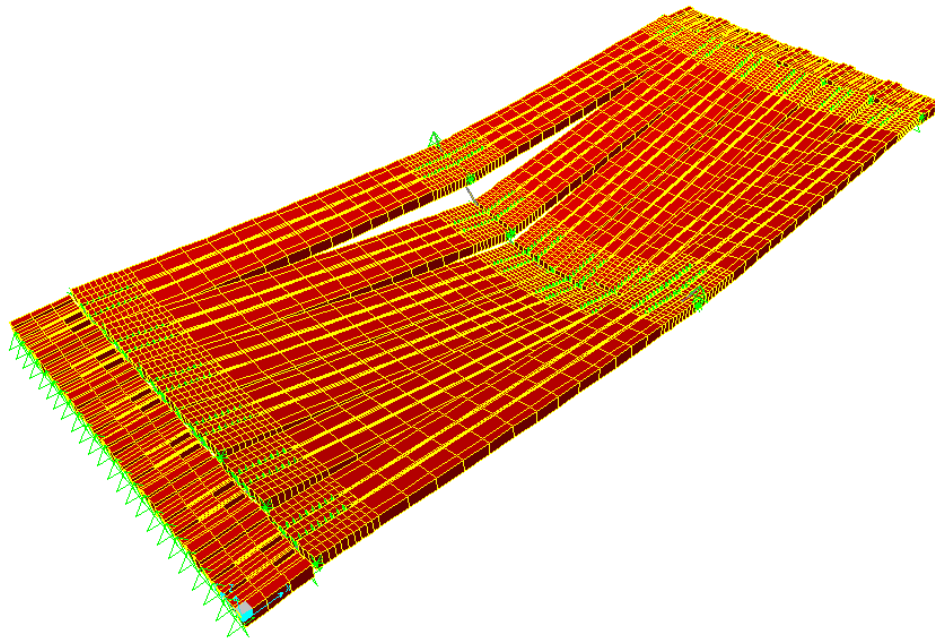


Fig. 5A. 4 Floor-to-floor model using longitudinal and transverse ties

Table 4A.1 Tie force in longitudinal and transverse ties

No.	Longitudinal Axis			Transverse Axis		Tie forces		TF Method	
	Length (m)	Bar Diameter (mm)	Numbers of Ties/Slab	Length (m)	Bar Diameter (mm)	P_l /Slab kN/m	P_t kN	$P_l = \alpha w l_b$	$P_t = \alpha w l_b l_t$
LTF1	4.075	$\phi 12$	2	3.75	$\phi 18$	62.51	269	$1.23 w l_b$	$1.41 w l_b l_t$
LTF2	4.075	$\phi 12$	2	4.7	$\phi 18$	88.52	295.9	$1.70 w l_b$	$1.23 w l_b l_t$
LTF3	4.075	$\phi 12$	2	5.65	$\phi 24$	112.63	304	$2.20 w l_b$	$1.06 w l_b l_t$
LTF4	6.075	$\phi 12$	3	3.75	$\phi 24$	143.22	459	$1.86 w l_b$	$1.61 w l_b l_t$
LTF5	6.075	$\phi 12$	3	5.65	$\phi 36$	114.26	568.	$1.51 w l_b$	$1.32 w l_b l_t$
LTF6	8.075	$\phi 12$	4	3.75	$\phi 36$	152.75	686	$1.51 w l$	$1.81 w l_b l_t$
LTF7	8.075	$\phi 12$	4	5.65	$\phi 44$	161.29	880	$1.60 w l_b$	$1.54 w l_b l_t$

REFERENCES

American Society of Civil Engineers (ASCE 7-05). (2006). Minimum Design Loads for Buildings and Other Structures.

Abruzzo, J. and Matta, A. and Panariello, G. (2006). Study of Mitigation Strategies for Progressive Collapse of a Reinforced Concrete Commercial Building. *Journal of Performance of Constructed Facilities*. ASCE, November, pp. 384-390

Abrishami, H. H. and Mitchell, D. (1992). Simulation of Uniform Bond stress. *ACI Material Journal*, V.89, No.2, March-April,-pp 161-168.

ACI Committee 408. (1992). Bond Under Cyclic Loads. *Journal of the American concrete Institute*.

Abrishami H.H, Mitchel D. (1996). Analysis of bond stress distributions in pullout specimens. *Journal of structural engineering*, Vol. 122, pp.255-261.

American Concrete Institute (ACI) Committee.318. (1995-2008). Building Code Requirements for Structural Concrete (ACI 318-95) and Commentary (ACI318R-95). Detroit, MI: ACI

ABAQUS theory manual (2003). Version 6.7 Hibbitt. Pawtucket (RI): Karlsson and Sorensen, Inc.; 2003.

ABAQUS. (2006). Benchmark Manual: Version 6.6-1. ABAQUS, Inc., Providence, RI.

Amleh, L., and Ghosh, A. (2006). Modeling the Effect of Corrosion on Bond Strength at the Steel Concrete Interface with Finite-Element Analysis. *Canadian Journal of Civil Engineering*, Vol.33, No. 6, pp. 673-682

Breen, J. (1975). Progressive Collapse Building Structures. Proceedings of a Research Workshop Held at the University of Texas at Austin, 18-19 November 1975, pp.

Burnet, E.F.P and Hanson, N.W. (1977). Experimental Slab Suspension Tests, Design and Construction of Large Panel Concrete Structure, prepared for Office of Policy Development and Concrete Department of Housing and Urban Development, by Portland Cement Association, (PCA).

British Standard BS 8110-11. (1997). The structural use of concrete in building — Part 1: Code of practice for design and construction. London, U.K.

BS EN1991-1-7. (2006). Action on Structures - Part 1-7: General Actions- Accidental Action. London, UK.

Banu, O.M (2011). Structural robustness provisions in modern design codes and regulations. Bul. Inst. Polit. Iași, t. LVII (LXI), f. 4. pp.54-63.

Beeby, A. W. (1997). Ductility Tests for ASW Ltd. Unpublished Report for Allied Steel and Wire Ltd, University of Leeds.

Brooker O (2008). How to design concrete buildings to satisfy disproportionate collapse requirements. Ref: TCC/03/45 ISBN 978-1-904818-66-3. The Concrete Centre, UK

Burnett E. F. P (1975). The avoidance of progressive collapse: Regulatory approaches to the problem. Center for Building Technology, Institute for Applied Technology, Natinal Bureau of Standards, Washington.

Bae SW, LaBoube RA, Belarbi A, Ayoub A. (2008). Progressive collapse of cold-formed steel framed structures. *Thin-Walled Struct*;46:706_19.

Bertero, V. V., and Bresler, B. (1968). Behaviour of reinforced concrete under repeated loading. *J. Struct. Div., ASCE*, 94(6), 1567-1590.

Birtel, V, Mark P (2006). Parameterised Finite Element Modelling of RC Beam Shear Failure, AQAQUS users' conference, Ruhar- University Bochum. Institute for reinforced and prestressed concrete structures.

Astaneh-Asl, A. (2000). "Use of catenary cables to prevent progressive collapse of buildings". Report to the General Services Administration and Skilling Ward Magnusson arkshire. Report number: UCB/CEE-STEEL-01/02. September.

CEB-FIP. (2000). State-of-the-Art Report on Bond of Reinforcement in Concrete. State- of-Art Report Prepared by Task Group Bond Models (former CEB Task Group 2.5) FIB - Féd. Int. du Béton: 1-97.

CEB-FIP, "CEB-FIP Model Code (MC-90). (1990). Comité Euro-International du Béton (CEB), Thomas Telford Ltd., London, UK, 437 pp.

Cairns J., Abdollah R.B. (1996). Bond strength of black and epoxy-coated reinforcement-a theoretical approach, *ACI Materials*, 93(4):pp. 362-369.

Girard, C. and Bastien, J. (2002). Finite-Element Bond-Slip Model for Concrete Columns under Cyclic Loads. *J. Struct. Eng.*,128(12), 1502–1510.

Colin B.B (1966). Colin B.B. (1966). Bond Failure Between Steel and Concrete. *Journal of The Franklin Institute*, 282, pp. 271-290.

Department of Defense (DoD) Unified Facilities Criteria (UFC-04-023-03) (2005). Design Building to Resist Progressive Collapse. Washington, D.C.

Department of Defense (DoD) Unified Facilities Criteria (UFC-04-023-03) (2013). Design Building to Resist Progressive Collapse. Washington, D.C

Dusenberry D (2002). Review of existing guidelines and provisions related to progressive collapse. Workshop on prevention of progressive collapse, National Institute of Building Sciences, Washington (DC), USA.

Darwin D, McCabe S.L, Brown C.J. (1994). Fracture analysis of steel-concrete bond, Proc. Europe-US Workshop on fracture and damage in quasi brittle structure. Ed. by Bittnar, Z. Jirasek M.and Mazars J., Pregue, Czech Republic, pp. 557-566.

Eurocode 1-Action on Structures-Part 1-7:General action- accidental Action, BS EN 1991-1-7:2006.

Ellingwood, B. R, Smilowit R, Donald O. D, Duthinh D, Nicholas J. C. (2007). Best Practices for Reducing the Potential for Progressive Collapse in Buildings. U.S. Department of Commerce, Technology Administration, National Institute of Standards and Technology.

Ettouney M, Smilowitz R, Tang M, Hapij A. (2006). Global system considerations for progressive collapse with extensions to other natural and man-made hazards. ASCE Journal of performance of constructed facilities, pp.403–417.

Eligehausen R. (1979). Bond in Tensile Lapped Splices of Ribbed Bars with Straight Anchorages”, Publication 301, German Institute for Reinforced Concrete, Berlin, German, 118 pp.

Edwards, A. D., and Yannopoulos, P. J. (1979). Local bond stress to slip relationships for hot rolled deformed bars and mild steel plain bars. *ACI J.*, 76(3), 405-420.

Eligehausen, R., Popov, E. P., and Bertero, V. V. (1983). Local bond stress-slip relationships of deformed bars under generalized excitations. Rep. No. UCBIEERC 83-23, Earthquake Engrg. Res. Ctr., Univ. of California, Berkeley, Calif.

Engstrom B, Magnusson J, Huang, Z (1998). Experimental and analytical studies of the bond behaviour of deformed bars in high strength concrete. 4th International Symposium of High-strength/High performance concrete, Paris pp. 1115-1124.

Engstrom B, Magnusson J, Huang, Z (1996). Pullout bond behaviour of riddled bars in normal and high-strength concrete with various confinements. State-of-the-art in bond research, ACI convention/ACI Committee 408-SP-180.

Edwards A.D, Picard A (1972). Bonding properties of ½ in. diameter strand. *ACI Journal*, proceeding, V.69, No. 11, pp.684-689.

Eyre, J. R. (1997). Direct Assessment of Safe Strengths of RC Slabs Under Membrane Action. *Journal of Structural Engineering*, ASCE, Vol. 123, No. 10, pp. 1331-1338.

Eyre, J. R. (1990). Flow Rule in Elastically Restrained One-Way Spanning RC Slabs. *Journal of Structural Engineering*, ASCE, Vol. 116, No. 12, pp. 3251-3267.

Franz K, Thomas V. (2009). Design for robustness. McGill College, Montreal, QC, Canada. Institute of structural engineering (IBK). ETH Zurich CH-8093 Zurich.

He Q, F, Yi W. J. (2008). Experimental Study on Collapse-Resistant Behavior of RC Beam-Column Sub-structure considering Catenary Action. The 14th World Conference on Earthquake Engineering October 12-17, Beijing, China.

Fu F. (2009). Progressive collapse analysis of high-rise building with 3-D finite element modelling method. WSP Group, WSP House, 70 Chancery Lane London WC2A 1AF, United Kingdom

Ferguson P. M., Breen, J. E., and Jirsa, J. O., (1988). Reinforced Concrete Fundamentals. 5th edition, John Wiley, New York, USA.

Feldman, L. R. and Bartlett, F.M. (2007). Bond Stresses Along Plain Steel Reinforcing Bars in Pullout Specimens. ACI Structural Journal, V. 104, No. 6, November-December, pp 685-692.

Griffiths, H., Pugsley, A. G. and Saunders, O. (1968). "Report of the Inquiry Into the Collapse of Flats at the Ronan Point, Canning Town". HMSO, London.

General Service Administration (GSA). (2003.). Progressive collapse analysis and design guidelines for new federal office buildings and major modernization projects. Washington (DC).

Guo, Zhenhai, and Shi Xudong. (2003). Reinforced Concrete Theory and Analysis. Super Star Digital Library. Qing Hua Da Xue Chu Ban She: Beijing, China.

Hemmaty Y, De Roeck G, Vandewalle L. (1991). Finite element modelling of reinforced concrete taking into consideration bond-slip, 5th ANSYS Int. Conf. Pittsburg Penn, USA.

HMSO. (1976). Statutory Instrument, No. 1676 'Building and Buildings', London

Hartmann D, Breidt M, Nguyen V, Stangenberg F, Höhler S, Schweizerhof K, et al. (2008). Structural collapse simulation under consideration of uncertainty -Fundamental concept and results. Comput Struct;86:2064-78.

Institution of Structural Engineers. (2002). Safety in Tall Buildings. The Institution of Structural Engineers, London, pp. 55

Izzuddin BA, Vlassis AG, Elghazouli AY, Nethercot DA. (2008). Progressive collapse of multi-storey buildings due to sudden column loss - Part I: Simplified assessment framework. Eng Struct;30:1308-18

Jefferson A.D, Bennett T, Hee S.C. (2005). Fracture mechanics based problem for the analysis of dam concrete, NW-IALAD-Final Technical report-Task Group 2.4, Cardiff University (UWC), 15.

Johnson S. (2006). Comparison of Nonlinear Finite Element Modelling Tools for Structural Concrete, CEE561 Project, the University of Illinois, Department of Civil and Environmental Engineering College of Engineering

Jankowiak T, Lodygowski, T. (2005). Identification of parameters of concrete damage plasticity constitutive model. Foundation of civil and environment engineering, No.6, Poznan University of Technology, Institute of Structural Engineering (ISE)

Josef F., Thomas P., Lubomir O. (2010). Push-out Test Parameter Simulation Study of a New Sheet-Type Shear Connector. Institute of steel structure, TU Vienna, Karlsplatz 13/212, A-1040, Vienna/Austria.

Knoll, F. and Vogel, T. (2009). Design for Robustness, Structural Engineering Documents 11, IABSE, Zurich

Koncz, T. (1995). New Technology for Large Panel Precast Concrete Buildings. PCI Journal. January-February.

Khandelwala K, El-Tawila S, Sadekb F. (2009). Progressive collapse analysis of seismically designed steel braced frames. *J Constr Steel Res*; 65:699-708.

Kwasniewski L (2010). Nonlinear dynamic simulations of progressive collapse for a multi-storey building. *Engineering Structures* 32, pp.1223-1235

Kmiecik P, Kamiński M. (2011). Modelling of reinforced concrete structures and composite structures with concrete strength degradation taken into consideration. *ARCHIVES OF CIVIL AND MECHANICAL ENGINEERING*, No.3 Vol.XI.

Koh C. G., Teng M. Q., Wee T. H. (2008). A Plastic-Damage Model for Lightweight Concrete and Normal Weight Concrete, *International Journal of Concrete Structures and Materials* Vol.2, No.2, pp. 123~136.

Keuser M, Mehlhorn G. (1987). Finite element model for bond problem. *Journal of Structural Engineering*, (ASCE), 113(10), pp. 2160-2173.

Li, Y., Lu, X., Guan, H., and Ye, L. (2011). An Improved Tie Force Method for progressive Collapse Resistance Design of Reinforced Concrete Frame Structures. *Engineering Structure*, Elsevier Ltd 33, pp 2931-2942.

Li, X. (2007). Finite Element Modeling of Skewed Reinforced Concrete Bridges and the Bond-slip Relationship between Concrete and Reinforcement, Auburn University, Alabama.

Lee, J. and Fenves, G. L., (1988). Plastic-Damage Model for Cyclic Loading of Concrete Structures. *Journal of Engineering Mechanics*, ASCE, Vol.124, No.8, pp. 892~900.

Leet k, Bernal D. (1997). Reinforced Concrete Design, Third edition- Mc Graw -Hill, Newyor.
Lubliner, J., Oliver, J., Oller, S., and Onate, E. (1989). A Plastic damage Model for Concrete. *International Journal of Solids and Structures*, Vol.25, No.3, 1989, pp. 299~326

Lee CH, Kim S, Han KH, Lee K. (2009). Simplified nonlinear progressive collapse analysis of welded steel moment frames. *J Constr Steel Res*; 65:113_1137.

Meacham, B. J. and Matthew, A. J. (2006). *Extreme Event Mitigation In Building; Analysis And Design*. National Fire Protection Association, pp. 559.

Mann A P et al. (2010). *Practical guide to structural robustness and disproportionate collapse in buildings*. Published by the Institution of Structural Engineers, UK.

Moore DB (2002). The UK and European regulations for accidental actions. In: *Proc. workshop on prevention of progressive collapse*. National Institute of Building Sciences. Washington (DC).

Mcnamara, R. J. and Salvia, M. (2003). *Conventionally Design Building: Blast and Progressive Collapse Resistance*. Blast Symposium Proceeding. American Institute of Steel Construction (AISC), New York, December.

Merola R. (2009). *Ductility and Robustness of Concrete Structures under Accident and Malicious Load Cases*. PhD Thesis. School of Civil Engineering, University of Birmingham, U.K.

Marjanishvili SM. (2004). Progressive analysis procedure for progressive collapse. *J Perform Constr Facilities ASCE*;18(2):79_85.

Möller B, Liebscher M, Schweizerhof K, Mattern S, Blankenhorn G. Structural collapse simulation under consideration of uncertainty _ Improvement of numerical efficiency. *Comput Struct* 2008;86:1875_84.

Meguro K, Tagel-Din H. (2002). Applied Element Method used for large displacement structure analysis. *J Natural Disaster Sci*;24(1):25–34.

Meguro K, Tagel-Din H. (2001). Applied element simulation of RC structures under cyclic loading. *ASCE*;127(11):1295–305.

MacGregor, J.G. (1997), “Reinforced Concrete: Mechanics and Design”, Third Edition, Prentice Hall, Upper Saddle River, New Jersey, USA.

Marecek j., Chromiak P., Studnicka J. (2006). Numerical model of perforated shear conector, in Gizejowski, Kozlowski, Slecza, Ziolk: Progress in Steel, Composite and Aluminium Structure, Taylor&Francis Group, London, 2006, ISBN 0-415-40120-8

Mahbuba Begum, et al. (2007). “Numerical Simulation of the Behaviour of Partially Encased Composite Columns”. Structural Engineering Report 269, Department of Civil and Environmental Engineering, University of Alberta, Edmonton, Alberta, Canada.

McCabe S.L., Pantazopoulou S.J. (1998). Evaluation of bond performance in reinforced concrete structures, State-of-the-art in bond research, ACI convention/ACI Committee 408-SP-180.

Ned M. (2008). Structural Integrity and Progressive Collapse in Large-Panel Concrete Structural system. *PCI Journal*, July- August-pp. 55-61.

Ned M. (2007). Containing Progressive Collapse in Precast Concrete Systems. *ASCE, SUMMER*: PP. 26-29.

Nair, R.S. (2003). Progressive Collapse Basics. Blast Symposium Proceeding. American Institute of Steel Construction (AISC), New York.

Nawy, E. G. (1996), "Reinforced Concrete: A Fundamental Approach", 3rd Edition, Prentice Hall Canada Inc., Toronto, Canada, pg. 415.

Nilson, A. H. (1972). "Internal measurement of bond slip." ACI J., 69(7), 439-441.

Nilson H. (1968). Nonlinear analysis of reinforced concrete by the finite element method. ACI Journal proceeding, 65, pp. 757-766.

Naaman, E. (1991). Fibre pullout and bond slip. I. Journal of Structural Engineering", Vol. 117, No. 9, September, pp. 2791-2800.

Naaman, et al. (1991). Fibre pullout and bond slip. II. Journal of Structural Engineering, Vol.117, No. 9, September, pp. 2769-2790.

Ngo D, Scordelis A.C. (1968). Finite element analysis of reinforced concrete beams, ACI Journal 64(3), pp. 152-163.

Nardin D. S, Filho A, Fillo O. J, Haach V.G, Debs E.A.L.H.C. (2005). Non-linear analysis of the bond strength behavior on the steel-concrete interface by numerical models and pull-out tests. Structures Congress, ASCE.

Orton S. (2007). Development of a CFRP System to Provide Continuity in Existing Reinforced Concrete Buildings Vulnerable to Progressive Collapse. PhD Thesis. The University of Texas at Austin .

Ockleston, A. J. (1955). Load Test on a Three-storey Reinforced Concrete Building in Johannesburg. Structural Engineer, Vol. 33, pp. 304-322.

Ockleston, A. J. (1958). Arching Action in Reinforced Concrete Slabs. Structural Engineer, Vol. 36, No. 6, pp. 197-201.

Portland Cement Association (PCA). (1975). Loading Conditions. Design and Construction of Large-Panel Concrete Structures, report 1.

Portland Cement Association (PCA). (1976). Philosophy of Structural Response to Normal and Abnormal Loads. Design and Construction of Large-Panel Concrete Structures, report 2.

Portland Cement Association (PCA). (1976). Wall Panels: Analysis and Design Criteria. Design and Construction of Large-Panel Concrete Structures, report 3.

Portland Cement Association (PCA). (1977). A Design Approach to General Structural Integrity. Design and Construction of Large-Panel Concrete Structures, report 4.

Portland Cement Association (PCA). (1979). Special Topics. Design and Construction of Large-Panel Concrete Structures, report 5.

Portland Cement Association (PCA). (1979). Design Methodology. Design and Construction of Large-Panel Concrete Structures, report 6.

Portland Cement Association (PCA). (1978). Wall Cantilever and Slab Suspension Tests. Design and Construction of Large-Panel Concrete Structures, report A.

Portland Cement Association (PCA) (1978). Horizontal Joint Tests. Design and Construction of Large-Panel Concrete Structures, supplemental report B.

Portland Cement Association (PCA). (1979). Seismic Tests of Horizontal Joints. Design and Construction of Large Panel Concrete Structures, Supplementary report C.

Park, R. (1964a). "Ultimate Strength of Rectangular Concrete Slabs Under Short-term Uniform Loading With Edges Restrained Against Lateral Movement". Proceedings of the Institution of Civil Engineers, Vol. 28, June 1964, pp. 125-150.

Park, R. (1964b). "The Ultimate Strength and Long-term Behaviour of Uniformly Loaded, Two-way concrete Slabs with Partial Lateral Restraint at all Edges". Magazine of Concrete Research, Vol. 16, No. 48, September 1964, pp. 139-152.

Pearson C, Delatte N. (2005). Ronan point apartment tower collapse and its effect on building codes. J Perform Constr Facil, ASCE: 19(5):172–7.

Pekau O., Cui Y. (2006). Progressive collapse simulations of precast panel shear walls during earthquakes. Computers & structures, Vol. 84, pp.400-412.

Powell (2003). Simple nonlinear static analysis procedure for progressive collapse evaluation. Blast Symposium Proceeding. American Institute of Steel Construction (AISC), New York.

Park, R., and Paulay, T. (1975). Reinforced Concrete Structures. John Wiley & Sons, Inc. New York, USA.

Park, R. and Gamble, W. L. (1980). Reinforced Concrete Slabs, John Wiley and Sons, New York, pp. 618.

Regan, P.E. (1975). Catenary Action in Damaged Concrete Structures. Industrialization in Concrete Building Construction ACI SP-48, pp191-225.

Rahmani A., Moazami K. (2003). Non-linear structural integrity analysis. Blast Symposium Proceeding. American Institute of Steel Construction (AISC), New York.

Radloff B., M. Kreger (1991). Bonding of external tendons at deviators. Centre for Transportation research, The University of Texas at Austin.

Rehm, G. (1968). The Basic Principles of the Bond between Steel and Concrete, Translation No. 134, Cement and Concrete association, London, UK, pp. 66.

Ren, F.F., Yang b, Z.J. and Chen, J.F. and Chen a, W. W. (2010). An analytical analysis of the full-range behaviour of grouted rock bolts based on a tri-linear bond-slip model. *Construction and Building Materials* 24, pp 361-370.

Reinhardt H.W, Blaauwendraad J, Vos E (1984). Prediction of bond between steel and concrete by numerical analysis, *RLLEM Materials and Structures* 17(100), pp.311-320.

Rankin, G. I. B. and Long, A. E. (1997). Arching Action Strength Enhancement in Laterally-Restrained Slab Strips. *Proceedings of the Institution of Civil Engineers, Structures & Buildings* 122, November 1997, Issue 4, pp. 461-467.

Spyridaki A, Gerasimidis S, Deodatis G, Ettouney M. (2013). A new analytical method on the comparison of progressive collapse mechanism of steel frames under corner column removal. In: Ellingwood, Frangopol (Eds). *Safety, reliability, risk and life-cycle performance of structure & infrastructures – Deodatis*. London: Taylor & Francis Group. ISBN 978-1-138-00086-5.

Starossek, U. (2007). Typology Of Progressive Collapse. *Engineering Structures* Vol. 29, No. 9, pp. 2302-2307.

Starossek, U. (2007b). Disproportionate Collapse: A Pragmatic Approach. *Proceedings of the Institution of Civil Engineers, Structures & Buildings* 160, Issue SB6, pp. 317-325.

Sasani, M., Kropelnicki, J. (2007). Progressive collapse analysis of an RC structure. *The Structural Design of Tall and Special Buildings*. V.17, No.4, 2007, pp. 757-771

Scanlon, A. Kianoush, M. R. (1988). Behaviour of large panel precast coupled wall systems subject to earthquake loading. *PCI journal*, September-October, pp. 124-1373

Shi Y., Li Z.X., Hao h. (2010). A new method for progressive collapse analysis of RC frames under blast loading. *Engineering Structures* 32, pp.1691-1703

Salem H.M, El-Fouly A.K, Tagel-Din H.S (2011). Toward an economic design of reinforced concrete structures against progressive collapse. *Engineering Structures* 33 (2011) 3341–3350.

Sasani M. (2008). Response of a reinforced concrete infilled-frame structure to removal of two adjacent columns. *Eng Struct*;30:2478–91.

Salmons, J. R. and T. E. McCrate (1977). Bond characteristics of untensioned prestressing strand. *PCI Journal* 22(1): 52-65.

Stocker, M.F., and Sozen, M.A., (1970). Investigation of Prestressed Reinforced Highway Bridge, Part V: Bond Characteristic of Prestressing Strand, *Engineering Experimental Station, Bulletin 503*, University of Illinois, College of Engineering.

Tepfers, R. A., (1979). Cracking of Concrete Cover along Anchored Deformed Reinforcing Bars. *Magazine of Concrete Research*, Vol. 31, No. 106, pp. 3-12

Tassios, T. P., Koroneos, E. G. (1984). Local bond-slip relationships by means of the Moire method. *ACI J.*, 81(1), 27-34

Tohid Mosleh. (2009). Design of reinforced concrete structures. Azad University of Sanandaj, ISBN:978-964-223-420-2

Teychenné D C., Franklin R E., Erntröy H C. (1997). Design of normal concrete mixes. Second edition. Building Research, Establishment Ltd, Garston, Watford

Taylor, S. E., Rankin, G. I. B. and Cleland, D. J. (2001). Arching Action in High-Strength Concrete Slabs. Proceedings of the Institution of Civil Engineers, Structures & Buildings 146, November 2001, Issue 4, pp. 353-363.

Trung C. H., Park J., Kim J (2010). Progressive collapse resisting capacity of reinforced concrete beam-column sub-structures. Dept. Architectural Eng., Sungkyunkwan Univ., Suwon, Korea. Research Institute of Technology, Samsung Engineering & Construction, Seoul, Korea.

Usmani AS, Chung YC, Torero JL. (2003). How the WTC did towers collapse: A new theory. Fire Safety J 2003;38:501_33.

Vlassis AG, Izzuddin BA, Elghazouli AY, Nethercot DA. (2008). Progressive collapse of multi-storey buildings due to sudden column loss Part II: Application. Eng Struct;30:1424-38.

Van D. V. C (1990). Theoretical and experimental determination of crack width in reinforced concrete at very low temperature. Heron Vol. 35, No. 2, pp.104.

Xue, C. and Wang, X. and Zhang, S. (2008). Bond Properties of High-Strength Carbon Fiber-Reinforced Polymer Strands. ACI Materials Journal, V. 105, No. 1, January-February. pp. 11-19.

Yan Y, Gerasimidis S, Deodatis G, Ettouney M. (2013). A study on the global loss of stability progressive collapse mechanisms of steel moment frames. In: Ellingwood,

Frangopol, editors. Safety, reliability, risk and life-cycle performance of structure & infrastructures – Deodatis. London: Taylor & Francis Group. ISBN 978-1-138-00086-5.

Yun J., Tan H. k (2010). Experimental study on catenary action of RC beam-column sub assemblages. 3rd fib International Congress.

Yan Y, Gerasimidis S, Deodatis G, Ettouney M (2013). A study on the global loss of stability progressive collapse mechanisms of steel moment frames. Safety, Reliability, Risk and Life-Cycle

Yi Wei-Jian, He Qing-Feng, Xiao Yan, Kunnath SashiK. (2008). Experimental study on progressive collapse-resistant behaviour of reinforced concrete frame structures. ACI Struct J;105(4):433–9.